

FINGER EXERCISES WITH ANATOMICAL CONSTRAINTS

**A METHODOLOGICAL ANALYSIS OF NON-PATHOLOGICAL
ANATOMICAL VARIATIONS AS CAUSES OF HAND PROBLEMS IN
MUSICIANS**

VINGEROEFENINGEN MET ANATOMISCHE BEPERKINGEN

**EEN METHODOLOGISCHE ANALYSE VAN NIET-PATHOLOGISCHE
ANATOMISCHE VARIATIES ALS OORZAKEN VAN HANDPROBLEMEN BIJ
DE MUSICUS**

PROEFSCHRIFT

Ter verkrijging van de graad van Doctor aan de Erasmus Universiteit Rotterdam
op gezag van de Rector Magnificus Prof.Dr. P.W.C Akkermans M.A.,
en volgens het besluit van het College voor Promoties.
De openbare verdediging zal plaatsvinden op
woensdag 6 december 1995 om 13.45 uur.

door

Joris Nicolaas Anna Leon LEIJNSE

Geboren te Aalst, België

Promotiecommissie:

Promotoren:

Prof.Dr.Ir. C.J. Sijnders
Prof.Dr. J.C.H. van der Meulen

Leden:

Prof.Dr.Ir. J.J. Kalker
Prof.Dr. J. Voogd
Dr. S.E.R. Hovius

To my parents, who created me,
to my surgeon, Dr. Bonte, who recreated me,
to Prof. van der Meulen, who put me on tenure track,
to my PC, without which this could not have been written.

Printed by Optima Druk, Molenaarsgraaf, The Netherlands.

ISBN 90-9009076-2

CONTENTS

PREFACE

INTRODUCTION

CHAPTER I KINEMATIC MODELS

- (i) Biomechanics of the finger with anatomical restrictions - the significance for the exercising hand of the musician

J.N.A.L. Leijnse, J.E. Bonte, J.M.F. Landsmeer, J.J. Kalker, J.C. van der Meulen, C.J. Snijders

- (ii) The hand of the musician: the kinematics of the bidigital finger system with anatomical restrictions

J.N.A.L. Leijnse, C.J. Snijders, J.E. Bonte, J.M.F. Landsmeer, J.J. Kalker, J.C. van der Meulen, G.J. Sonneveld, S.E.R. Hovius

- (iii) A two dimensional kinematic model of the lumbrical in the human finger

J.N.A.L. Leijnse, and J.J. Kalker

CHAPTER II FORCE MODELS AND INDETERMINATE PROBLEMS

- (i) A graphic analysis of the biomechanics of the massless bi-articular chain

J.N.A.L. Leijnse

- (ii) The controllability of the unloaded finger with superficial or deep flexor

J.N.A.L. Leijnse

- (iii) Why the lumbrical muscle should not be bigger - a force model of the lumbrical muscle in the unloaded human finger

J.N.A.L. Leijnse

CHAPTER III MEASURING FORCE TRANSFERS IN THE M. FLEXOR DIGITORUM PROFUNDUS

- (i) Measuring force transfers in the deep flexors of the musician's hand - theoretical analysis, clinical examples

J.N.A.L. Leijnse

- (ii) Measuring force transfers in the deep flexors of the musician's hand - device and systematic measuring errors

J.N.A.L. Leijnse

CHAPTER IV ANATOMIC FACTORS PREDISPOSING TO FOCAL DYSTONIA IN THE MUSICIAN'S HAND

Anatomic factors predisposing to focal dystonia in the musician's hand

J.N.A.L. Leijnse

CHAPTER V MODELS OF MUSCLES AND APONEUROSES

(i) A generic model of a muscle group - application to the muscles of the forearm

J.N.A.L. Leijnse

(ii) The morphology of holes in aponeuroses caused by perforating nerves or vessels at the medial epicondyle of the elbow

J.N.A.L. Leijnse

CHAPTER VI MODELLING THE MORPHOLOGY OF ANATOMICAL INTERCONNECTIONS IN THE M. FLEXOR DIGITORUM PROFUNDUS

(i) Anatomical interconnections within the M. flexor digitorum profundus - the significance for the hand of the musician

J.N.A.L. Leijnse, E.T. Walbeehm, G.J. Sonneveld, S.E.R. Hovius

(ii) Connections between the tendons of the M. flexor digitorum profundus formed by the synovial sheaths in the carpal tunnel

J.N.A.L. Leijnse, E.T. Walbeehm, G.J. Sonneveld, S.E.R. Hovius, J.M.G. Kauer

(iii) A generic model of the anatomic variability in the M. flexor digitorum profundus, M. flexor pollicis longus, and Mm. lumbricales complex - the significance for the musician

J.N.A.L. Leijnse

CHAPTER VII SURGICAL CLEARANCE OF INTERTENDINOUS CONNECTIONS - A CASE STUDY

Total surgical clearance of intertendinous connections in a musician's hands, including cleavage of bitendinous lumbrical origins - a case study

J.N.A.L. Leijnse, and J.E. Bonte

CHAPTER VIII SUMMARY AND CONCLUSIONS

Samenvatting en conclusies

ACKNOWLEDGEMENTS

CURRICULUM VITAE

PREFACE

Consider a group of men, selected from many for their exceptional ability to hammer tiny nails in regular arrays in endless walls. Assume their future will be to daily hammer a fixed number of such nails into artistic patterns, to the amusement of a public which esteems this greatly. At the onset of this task each receives a small hammer of superb quality, which, like a fountain pen, is never to be held by others. All hammers look alike exactly, but there is a snag: one is made from outlandish material more than five times as heavy as the normal steel. Day by day the men hammer away producing great events, but as time proceeds the man with the heavy hammer becomes a little tired and sometimes hits the little nails not quite on their little head. Moreover, as more nails are wrongly hit, more time is spent hitting them rightly. Others notice, and give advice in sympathy, but eventually he is a liability and hammers alone. Then the pain starts, his hand starts shaking, he tries strange hammering positions in despair, on a ladder bent over upside down, but hammering becomes ever so difficult and finally impossible. He seeks professional help. Someone looks at him and says: your back is crooked, your posture bad. So they work until he is erecter than the homo erectus ever was, but hammering remains a problem. Then electrodes reveal unexpected muscle activity, and he learns to relax until he is a jelly pudding, but the hammer still trembles. Then someone gets smart and says: there is an antagonistic disbalance, and fills him up with botulinum toxin (type A). Now he cannot hammer, but for good cause: his muscles are paralysed. However, the pain disappears, and when he finally hammers again, at first all goes well, until the problem returns. And so it goes on, and on, and on. Clearly, this man is doomed, and will never hammer again, unless given a normal hammer. Moreover, barring meanwhile permanent damage, the mere exchange of hammers will make this man a normal hammerman. The basic question, however, remains: how does one find out the weight of this hammer - when the man never gives it to you to weigh?

This imaginary set-up describes an overuse situation, as conceived in the present thesis. The variables may be changed: our hapless hammerman may be a musician, the weight of his hammer a mysterious property in his hand, and the name of his complaint "focal dystonia". However, the structure of the situation remains. It is, by present hypothesis, a complaint in which nothing is basically wrong with anything, except that the constellation of the factors leads to conflict. The example clearly outlines the possible cures: diminishing hammering time may resolve the clinical complaint, but perhaps performance may remain dissatisfactory; different posture and technique may lead to better results, but when the hammer is too heavy they will not resolve the problem, while changing the hammer resolves the conflict forever. For proper diagnosis, the hammer's weight must be quantified, for other causes may produce similar symptoms. This then is the aim of the present thesis: to quantify why hands to one musician may be almost weightless, and to another may be more than he can pull.

INTRODUCTION

INTRODUCTION

Recently, hand problems in musicians have been recognised as systematic events. Numerous papers and statistics have been published (see Chapter IV); even, a journal exclusively devoted to such and similar problems in performing artists exists¹. The present thesis defends the hypothesis that many hand complaints, such as focal dystonia, are caused by non-pathological anatomical variations in the hand. It is good habit to introduce such thesis by profiling it against the historic and current state of affairs. Instead, however, I would like to present an account of the events which led to this thesis, which is, to a degree, an autobiography.

A short auto-biography

I started as a violin player, studying at a special high school for musicians, and subsequently at the conservatory of Brussels (1974-1976). There, I soon developed hand coordination problems which terminated this career. With some talent to burn, I studied graphic arts. However, in the process of long hours of drawing and engraving, I gradually lost the very fine motor control required for high quality work, and quit this career with hands feeling like wood. Unabashed, I took a prep year of mathematics and subsequently studied civil engineering with a major in applied mathematics, only soon to develop problems with hand-writing. As the formulas grew longer, handwriting grew worse, and a third career became jeopardised by basically the same problem. The regular route for professional help of the overuse patient is the general physician, the music therapist, the hand surgeon, the neurologist, or the alternative medicine man, or all of them in some order (Tubiana, 1993). Some cases respond to therapy, but many remain untreatable, and patients will seek help until they run out of advise, money or motivation. I took a different route. In art school I studied the musculo-skeletal system from the medicine courses. There I found a little remark on the effect of the juncturae tendinum on extensor independence. These jucturae were exceptionally developed in my hands, as could be verified by superficial observation. The removal of the connections took some effort, because at first, and despite vigorous mobilisation they tended to regenerate. Although the effect was beneficial, it turned out that many other extremely strong intertendinous connections were present. I became expert in localising them by hand tests, my surgeon in removing them. The left hand, which was treated for violinistic reasons, was used as a model for the right hand, where the later writing problem was treated. During the period of 1979-1988, all connections between all finger tendons were systematically removed in both hands: between the extensors, between the superficial flexors, between the deep flexors, and between the lumbricals. Collateral damage was caused to the flexor retinacula which resulted in thumb weakness in both hands; this was resolved to a large degree by the reconstruction of the ligaments (1989). The final result was a new pair of hands, with enormously improved dexterity and tactile abilities, without loss of basic strength except for the thumbs. The original hand coordination problems had completely disappeared. Although I can now easily type at great speed, I never returned to the violin, for the reasons given in Chapter VII, which presents the case-study. Considering the novelty of these surgical procedures and their

Introduction

number, this relative success is a miracle in itself, in which good surgery and my mobilisation efforts were at par. In 1989 I had a memorable meeting with prof. Landsmeer, and with his support applied for a research position at the Dept. of Hand Surgery at the Erasmus University of Rotterdam. Such a position was created by Prof. van der Meulen, head of the department, with the valuable support of prof. Snijders, head of the Dept. of Biomedical Technology (1990).

The methods of the present thesis

The above history motivates the approach taken in present thesis. Most noticeable is the almost total lack of experimental data. The quantification of the surgical model assumptions by e.g. comparing normal and diseased hands would have required massive equipment and organisation, for which there was no allocated money. Therefore, I chose to minimise measuring attempts, and to present the therapeutic models as clearly as possible for further validation by the scientific community. As a result, the present thesis is foremost a study of method; i.e. the theoretical proof that anatomical variations are important and may harm hand function. Nevertheless, a measuring device was built to quantify the force transfers between the deep flexors. This instrument now serves for diagnosis and prognosis of clearance of anatomical connections in this muscle group. The thesis analyses the effects of anatomic intertendinous connections at different levels. In Chapter I, the kinematics of fingers with intertendinous connections are addressed. In Chapter II, the indeterminates in finger motor function in the unconstrained normal finger are analysed. In Chapter III, the force transfers within the deep flexors are modelled, and validated by means of mentioned measuring device, and the systematic problems with these measurements are discussed. In Chapter IV, the muscle load increases due to intermuscular force transfers are discussed, both generally, and by means of a simple example of pianist's hand with a connection between the long thumb flexor and the deep flexor of the index. By way of examples a number of important biomechanical elements which concern diagnosis are illustrated. An anatomic section is included. This discusses as a general introduction a basic muscle model used throughout this text (Chapter V), and further models the systematic anatomical variations in the deep flexor group (Chapter VI). Lastly, the post-op results of the surgery in my own hands are presented.

The kinematic finger model

The choice of a model is an important research decision. Given the complexity of the subject matter, the model had to be as simple as possible, yet comprehensive. This simplicity was found in Landsmeer's models, in the formulation of Spoor and Landsmeer (1976). However, this paper describes model elements, rather than a holistic model. Moreover, in some finger movements tendon parts become slack, a property I found difficult to implement into a general formulation. This problem was solved by Prof.Dr.Ir J.J. Kalker, from the Delft University of Technology. Prof. Kalker is a tribologist, who normally solves problems of friction and vibrations in wheels of trains. Contact forces and muscle forces share the property of being unidirectional, and with his vast experience with such systems prof. Kalker effortlessly wrote out a general concept incorporating the tendon slacks (Kalker, 1990). However, he formulated it in terms of inequalities, which are mathematically tedious. This I resolved by quantifying the tendon slack by

Introduction

non-negative slack variables, as are used in linear programming to reduce inequality constraints to equalities. The result was the simple, comprehensive model of Chapter I.i, in which the lumbrical was implemented in Chapter I.iii, and which is used for calculations throughout the text. In practical terms, the slack variables proved their usefulness by allowing concise indications of the different states of model functioning. In the text models moment arms are assumed constant, except for the lateral slips of the extensor assembly at the PIP joint. Yet, in other models considerable effort is made of implementing the relatively small changes of the other motor moment arms with joint rotations. For the present applications this additional complexity seemed useless, besides, it would distract the attention from the systemically important PIP-DIP coupling mechanism resulting from the shifting of the lateral slips of the extensor assembly at the PIP.

Cracking the Landsmeer model

In 1955, Landsmeer provided a displacement model to explain the mechanisms of claw and swan-neck formation. Although recognised as a fundamental contribution, it was perceived as somewhat enigmatic and remained basically unchanged for the past forty years. When tackling the problem of flexor redundancy and finger control (Chapter 6), which to my intuition is basic to the deeper understanding of hand function in the musician, I started from the Landsmeer model, but soon became entangled in certain particularities of its original formulation. These I could not resolve in the original displacement model, but they proved well treatable in the equivalent force model. This resulted in the general formulation of the statics of the bi-articular chain in Chapter II.i, which confirms Landsmeer's model principles while making them more accessible. Anecdotically, this paper has the extra dimension of an expected publication exactly forty years after Landsmeer's, while it was born accompanied by his encouragements.

A clinic for musicians

Over the past decades, a consultive cooperation developed between a music therapist, Mr. van de Klashorst and Prof. van der Meulen, who, with his successor, Dr. Hovius, contemplated the establishment of a proper clinic for musicians. The present study provided a theoretical background for surgical treatment of otherwise hopeless cases. The clinic took a definite form when Dr. Sonneveld took charge. Musicians are not the usual patients and they require a physician with both skill and patience. Today, a few musicians have already been surgically treated, and all have resumed their activities, even reporting improved technical abilities.

¹Medical problems of performing artists. Hanley and Belfus, Inc., Medical publishers, Philadelphia

Tubiana R., (1993) *The Hand*, pp. 873-885, W.B. Saunders Company.

Kalker, J.J. (1990) An inequality calculus for the tendons of the hand. Private communication.

CHAPTER I

KINEMATIC MODELS

Biomechanics of the finger with anatomical restrictions - the significance for the exercising hand of the musician

J.N.A.L. Leijnse, J.E. Bonte, J.M.F. Landsmeer, J.J. Kalker, J.C. van der Meulen, C.J. Snijders

Reprinted from *J. Biomechanics*, Vol. 25, 1253-1264, Copyright 1992*

The hand of the musician: the kinematics of the bidigital finger system with anatomical restrictions

J.N.A.L. Leijnse, C.J. Snijders, J.E. Bonte, J.M.F. Landsmeer, J.J. Kalker, J.C. van der Meulen, G.J. Sonneveld, S.E.R. Hovius

Reprinted from *J. Biomechanics*, Vol. 26, 1169-1179, Copyright 1993*

A two dimensional kinematic model of the lumbrical in the human finger

J.N.A.L. Leijnse, and J.J. Kalker

Reprinted from *J. Biomechanics*, Vol. 28, 237-249, Copyright 1995*

*with kind permission from Elsevier Science Ltd,
The Boulevard, Langford Lane, Kidlington OX5 1GB, UK
Not to be copied without the publisher's specific permission.

BIOMECHANICS OF THE FINGER WITH ANATOMICAL RESTRICTIONS—THE SIGNIFICANCE FOR THE EXERCISING HAND OF THE MUSICIAN

J. N. A. L. LEIJNSE,*†† J. E. BONTE,§ J. M. F. LANDSMEER,|| J. J. KALKER,‡
J. C. VAN DER MEULEN† and C. J. SNIJDERS*

Departments of *Biomedical Physics and Technology and †Plastic and Reconstructive Surgery, Erasmus University, Burgemeester Oudlaan 50, P.O.B. 1738, 3000 DR, Rotterdam, The Netherlands, ‡Department of Technical Mathematics, Technical University Delft, The Netherlands, §Emmanuel Hospital, Wetteren, Belgium and ||Professor Emeritus, Department of Anatomy, Leiden, The Netherlands

Abstract—Exercise and teaching of musicians presupposes in the individual the constitutive ability to freely execute the finger movements required in the playing of the instrument. However, in the hand anatomical restrictions may exist that limit the mobility of the fingers and, thereby, the possibility to determine their movements voluntarily. In this article we investigate the kinematics of a monodigital system in which restrictions are present.

NOMENCLATURE

MCP	metacarpophalangeal joint
PIP	proximal interphalangeal joint
DIP	distal interphalangeal joint
FP	flexor digitorum profundus
FS	flexor digitorum superficialis
ED	extensor digitorum
IO	interosseus
MB	common medial band of extensor and interosseus
LB	common lateral band of extensor and interosseus
r_{ij}	moment arms of the tendons over the respective joints. The first index denotes the motor: P=FP, S=FS, E=ED, I=IO, M=MB, L=LB. The second index numbers the joint: MCP=1, PIP=2, DIP=3 (see Table 1)
$d\epsilon_T$	infinitesimal displacement of a tendon T
$d\theta_j$	infinitesimal joint displacements of joint j
$d\sigma_T$	infinitesimal accumulation of slack in tendon T

INTRODUCTION

The tendons of the fingers are often thought of as rope-like structures running independent from each other. In reality, however, anatomical interconnections between the finger tendons may exist that considerably limit the displacements of the tendons relative to each other. Such interconnections appear almost systematically between the individual tendons of the respective finger motor groups. For example, in the extensor digitorum there are the connexus intertendinei coupling the extensor tendons proximal to the MCP joints (Kaplan, 1965; von Schroeder *et al.*, 1990). In the flexor digitorum profundus there is the well-known phenomenon of the quadriga, i.e. the interdependence of the tendons of the digits d3, d4 and d5 (Fahrer, 1971; Verdan, 1960). The flexor digitorum superficialis presents frequent couplings of digits d4 and d5 (Baker

et al., 1981; Austin *et al.*, 1989). More generally, case studies abound of other more or less functionally limiting anatomical aberrations (Linburg and Comstock, 1979; Culver, 1980; Blair and Omer, 1981 etc.). The interconnections are generally strong tendinous or fascia-like structures which are not likely to be significantly stretched or lengthened by exercise.

One of the fundamental axioms in the teaching of a musical instrument is that exercise increases the independence of the fingers. The present study is initiated by the assumption that this axiom does not fully apply to hands in which anatomical interconnections between tendons are present. The question then arises as to how these hands behave when exercised.

In this article we limit ourselves to the modelling of the kinematic implications of anatomical interconnections that do not allow any relative movement at all of the tendons they connect.

METHODS

From the point of view of kinematics, movement in the body is the transformation of tendon displacements into joint displacements. Anatomical interconnections between tendons limit the displacements of the coupled tendons in relation to one another. They thus reduce the domain of tendon displacements that can be transformed into joint displacements. The result is a limitation of the movements possible in the connected system as compared with the unconnected one (Fig. 1).

In this paper we illustrate this phenomenon in a monodigital finger model. Anatomical interconnections are simulated by mathematical constraints. The fingers thus constrained are required to perform a simple task. Our interest is to show how, at the kinematic level, the execution of this task is affected by the constraints.

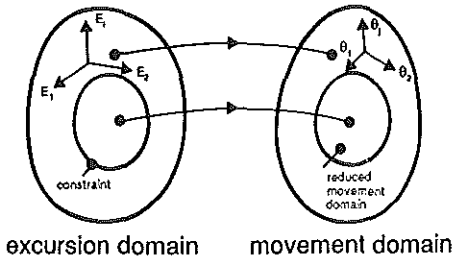


Fig. 1. Constraints on tendon displacements result in reduced possibilities of movement.

The following terminology will be used throughout the text. The kinematic transformation of tendon displacements into joint displacements is called the 'displacement model'. A curve in the tendon displacement domain or 'excursion domain' is an 'excursion pattern' (excursion is a clinical term indicating displacement); its image is a curve of joint displacements in the 'joint angle domain' and is called a 'movement'. The task to be performed is called a 'functional problem'. Note that a functional problem presents a condition in the movement domain. A 'solution' is any coordinated joint action that 'solves' the functional problem. A solution is 'feasible' if it can be realised by manipulation of the tendons alone. The 'set of feasible solutions' ('feasible set') consists of all feasible solutions to the functional problem.

In the defined terminology, the aim of this article is to investigate in a monodigital finger model, and for a single functional problem, how the set of feasible solutions changes as a function of the constraints on the tendon displacements.

MATERIALS

The displacement model

The displacement model of the finger presented here is essentially the Landsmeer model (Landsmeer, 1955; Spoor and Landsmeer, 1976), which is derived from the simplified representation of the finger given in Fig. 2. The motors are the flexor digitorum profundus (FP), the flexor digitorum superficialis (FS), the extensor digitorum (ED) and the interosseus (IO). The lumbricalis is ignored. Both the ED and the IO are present with medial and lateral bands (ED_M , ED_L , IO_M , IO_L), inserting in the bases of the middle and end phalanges, respectively. The parameters are the lengths of the moment arms of the motors over the respective joints (r_{ij}), and the lengths of the phalanges as measured between successive joint axes (see Table 1). The tendon displacements $d\epsilon_{Tj} = (+/-)r_{Tj} \cdot d\theta_j$ over the individual joints are defined as positive when corresponding to muscle contraction, while the joint rotations $d\theta_j$ are positive when corresponding to flexion. When the moment arms of extension are given a negative sign, the convention holds: positive joint displacements produce positive displacements in the flexors and negative displacements in the extensors. The total displacement c_T of a tendon T is the displacement of the tendon when measured proximal to the MCP.

A tendon in the model can be taut or slack. The slack in a tendon T is quantified by the use of the non-negative slack variables σ_T . At any time, the value of these variables is equal to the proximal displacement needed to tauten the tendon, with the joints remaining fixed in their momentary position. Thus, when the tendon is taut the slack variable is zero, and when the tendon is slack the slack variable is positive. During a movement, the total slack in the tendon is the sum of the initial slack, and the differential accumulation of

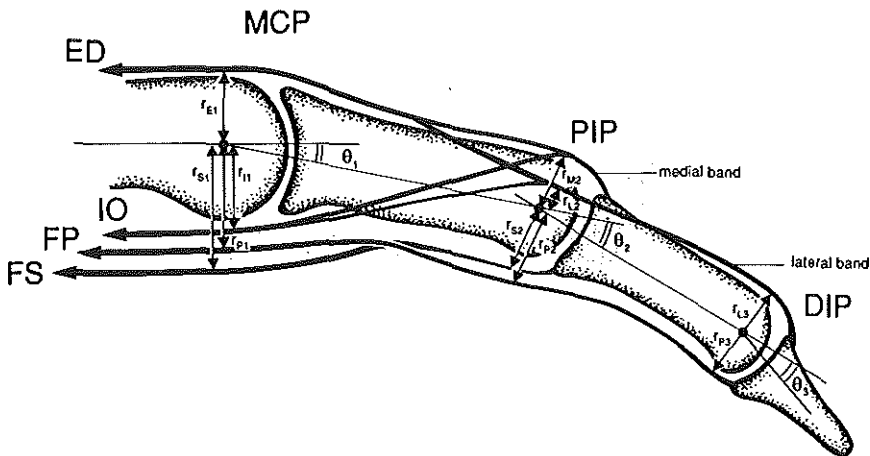


Fig. 2. Model of the human finger.

Table 1. Moment arms of the tendons

Motor/Joint	MCP			PIP			DIP		
	Symbol*			Value†					
FP	r_{P1}	r_{P2}	r_{P3}	11	10.5	6			
FS	r_{S1}	r_{S2}	/	13	8.5	/			
ED _{MB}	r_{E1}	r_{M2}	/	9	5	/			
IO _{MB}	r_{I1}	r_{M2}	/	6	5	/			
ED _{LB}	r_{E1}	r_{L2}	r_{L3}	9	‡	4			
IO _{LB}	r_{I1}	r_{L2}	r_{L3}	6	‡	4			

*Notations used in the text.

†Real values (in mm) used to calculate the results (Spoor, 1983).

$$\ddagger r_{L2} = r_{M2} - r_{L3} \left(0.25 + \frac{0.55}{\pi/2} \cdot \theta_2 \right).$$

(/) indicates that the tendon does not cross this joint.
Proximal, middle, distal Phalanx: 50, 34, 17.

slack, which is defined as

$$d\sigma_T = \sum_{j=1}^{n_T} (+/-) r_{Tj} \cdot d\theta_j - d\epsilon_T, \quad (1)$$

where n_T is the number of joints the tendon spans. The differential $d\sigma_T$ can take any value, but the total slack is at all times non-negative

$$\sigma_T = \sigma_{T_0} + \int d\sigma_T \geq 0. \quad (2)$$

The finger actions studied are balanced movements of the unloaded finger. A balanced movement is, by definition, a movement which the motors should be able to check at any time, to bring about a balanced finger position. The condition for this is that at any time during the movement all joints remain balanceable. In the following, this condition will be implemented in the displacement model. We hereby start from the plain displacement equations of the individual tendon parts

$$d\epsilon_{FP} = r_{P1} \cdot d\theta_1 + r_{P2} \cdot d\theta_2 + r_{P3} \cdot d\theta_3 - d\sigma_P, \quad (3a)$$

$$d\epsilon_{FS} = r_{S1} \cdot d\theta_1 + r_{S2} \cdot d\theta_2 - d\sigma_S, \quad (3b)$$

$$d\epsilon_{EDM} = -r_{E1} \cdot d\theta_1 - r_{M2} \cdot d\theta_2 - d\sigma_{EM}, \quad (3c)$$

$$d\epsilon_{IOM} = r_{I1} \cdot d\theta_1 - r_{M2} \cdot d\theta_2 - d\sigma_{IM}, \quad (3d)$$

$$d\epsilon_{EDL} = -r_{E1} \cdot d\theta_1 - r_{L2} \cdot d\theta_2 - r_{L3} \cdot d\theta_3 - d\sigma_{EL}, \quad (3e)$$

$$d\epsilon_{IOL} = r_{I1} \cdot d\theta_1 - r_{L2} \cdot d\theta_2 - r_{L3} \cdot d\theta_3 - d\sigma_{IL}. \quad (3f)$$

Not all the displacements in equations (3a)–(3f) are independent. The medial and lateral bands of the same motor originate from a single tendon, so their displacements proximal of the MCP are equal to the displacement of this tendon:

$$\begin{aligned} d\epsilon_{EDM} &= d\epsilon_{EDL} = d\epsilon_{ED}, \\ d\epsilon_{IOM} &= d\epsilon_{IOL} = d\epsilon_{IO}, \end{aligned} \quad (4)$$

which leads to

$$d\theta_3 = \frac{r_{M2} - r_{L2}}{r_{L3}} \cdot d\theta_2 - \frac{d\sigma_{EL} - d\sigma_{EM}}{r_{L3}}, \quad (5a)$$

$$d\theta_3 = \frac{r_{M2} - r_{L2}}{r_{L3}} \cdot d\theta_2 - \frac{d\sigma_{IL} - d\sigma_{IM}}{r_{L3}}. \quad (5b)$$

In the unloaded finger, balanced movements imply the following conditions on the tautness of the tendons:

$$\sigma_{ED} = 0 = \sigma_{EM} * \sigma_{EL}, \quad (6a)$$

$$\sigma_{IO} = 0 = \sigma_{IM} * \sigma_{IL}, \quad (6b)$$

$$\sigma_P * \sigma_S = 0, \quad (6c)$$

$$\sigma_{IM} = \sigma_{EM} (= \sigma_M), \quad (6d)$$

$$\sigma_{IL} = \sigma_{EL} (= \sigma_L), \quad (6e)$$

$$\sigma_M = 0. \quad (6f)$$

The conditions (6a)–(6c) regard the tautness of the main tendons, i.e. the motors themselves, while the conditions (6d)–(6f) regard the tautness of the medial and lateral bands. For further use, we say that a motor is active when its main tendon is taut, and inactive when it is slack. The conditions are discussed one by one.

Condition (6a) expresses that the main tendon of the ED must always be taut, which is equivalent to the condition that either the ED_M or the ED_L or both must be taut. The condition is necessary because the ED is the only extensor of the MCP. If this extensor became slack, the MCP would be unbalanced, and the finger would drop immediately.

Condition (6b) states that the IO must also be always taut. This is because the IO must at any time prevent the 'collapse' (van der Meulen, 1972) of the proximal finger (MCP, PIP). This collapse is the natural zigzagging of the finger into the 'intrinsic minus' or 'claw hand' position under the unopposed forces of the extrinsics (FP, FS, ED) (Landsmeer, 1955).

Condition (6c) states that at least one of the flexors (FP or FS) must always be taut. This is because the MCP and PIP joints must remain balanced on the flexion side (the PIP can only be balanced by these flexors). Strict balancing of the DIP is not a condition (the FP may be slack). This is because the range of movement of the DIP is checked by the coupling mechanism [see the text following equation (7)].

Condition (6d) states that the slack in the medial bands of the IO and the ED is equal, while condition (6e) states the same for the lateral bands. This can be shown as follows. In the model, the moment arms of the medial bands for the PIP are equal to each other (r_{M2}); the same holds for the moment arms of the lateral bands for the PIP and the DIP (r_{L2} , r_{L3}). Further, by definition, a balanced finger position exists in which all tendon parts are taut. From this

position, any feasible finger position can be achieved by manipulation of the tendons. Now, slack in the medial and lateral bands cannot be caused by displacements of the MCP (for which the moment arms of the ED and the IO differ), because the main tendons of the IO and the ED must remain taut. It can, therefore, only result from displacements of the distal two joints. Since in the initial position all slacks are zero, and the displacements of the medial and lateral bands, respectively, over the distal joints are equal, in any feasible finger position the slack in the corresponding bands of the ED and the IO must be equal. We can, therefore, fuse the medial bands of the ED and the IO over the PIP into a single medial band (MB), and the lateral bands over the PIP and the DIP into a single lateral band (LB).

Condition (6f) expresses that the MB must always be taut. Two situations are to be distinguished here. (i) If the FP and the LB are slack, the MB is taut because of conditions (6a) and (6b): σ_{EM} and σ_{IM} must be zero since σ_{EL} and σ_{IL} are not. (ii) If the FP and the LB are taut, the MB must be taut to prevent the collapse of the distal finger (PIP, DIP) under the forces of the FP and the LB.

To summarise, in the unloaded, free moving finger the medial bands are always taut, while the lateral bands may be taut or slack. From this and equation (4) it follows that the displacements of the main tendons of the ED and the IO are always equal to the displacements of their medial bands:

$$\begin{aligned} d\epsilon_{ED} &= d\epsilon_{EDM}, \\ d\epsilon_{IO} &= d\epsilon_{IOM}. \end{aligned} \quad (7)$$

Substituting conditions (6d)–(6f) into equations (5a) and (5b) results, for both equations, in one and the same condition, which will be called the *coupling mechanism* (CM):

$$d\theta_3 = \frac{r_{M2} - r_{L2}}{r_{L3}} \cdot d\theta_2 - \frac{d\sigma_L}{r_{L3}} = K \cdot d\theta_2 - \frac{d\sigma_L}{r_{L3}}. \quad (8)$$

The CM quantifies the coupling of the actions of the PIP and the DIP due to the division of the extensor apparatus in the medial and the lateral bands. When the lateral bands are taut, the CM is called *active*, and *vice versa*; when the lateral bands are slack, it is called *inactive*:

$$\sigma_L = 0 \Leftrightarrow \text{CM active}. \quad (9)$$

The working of the CM is as follows:

- (1) $\sigma_L > 0$ (CM inactive).

When the coupling mechanism is inactive, the DIP can be freely moved by an external force from the limit of extension to the position in which the CM becomes active, i.e. the lateral bands become taut. The limit of extension of the DIP is either the position in which the FP becomes taut, or the limit of hyperextension of the joint itself.

- (2) $\sigma_L = 0$ (CM active).

When the CM is active, the distal two joints move in a coordinated way, as a mechanism. The working of this mechanism depends primarily on the sign of the factor $K = (r_{M2} - r_{L2})/r_{L3}$ in equation (8). We have:

- (i) $r_{M2} - r_{L2} > 0$ ($K > 0$).

When $r_{M2} - r_{L2} > 0$, $d\theta_2$ and $d\theta_3$ are of equal sign. This means that the PIP and DIP will both simultaneously extend, or flex, in a fixed proportion as determined by the proportionality factor K . This is the normal case in the human finger.

- (ii) $r_{M2} - r_{L2} < 0$ ($K < 0$).

When $r_{M2} - r_{L2} < 0$, $d\theta_2$ and $d\theta_3$ are of opposite sign, which means that the PIP and the DIP will move in opposite directions: the DIP extends or flexes, respectively, when the PIP flexes or extends.

In the following we assume that $r_{M2} > r_{L2}$. When $\sigma_L = 0$ (CM active), the mechanism formed by the distal two joints can be replaced by a hypothetical single joint, the 'IP' (interphalangeal joint), which has the same tendon displacements as the PIP–DIP joint mechanism (Spoor and Landsmeer, 1976). The moment arms of this IP joint are:

$$\begin{aligned} \text{extension : } r_{M2}^* &= r_{L2}^* = r_{M2}, \\ \text{flexion : } r_{S2}^* &= r_{S2}, \\ r_{P2}^* &= r_{P2} + \frac{r_{P3}}{r_{L3}} \cdot (r_{M2} - r_{L2}). \end{aligned} \quad (10)$$

The displacement equation (3a) of the FP can then be replaced by

$$d\epsilon_{FP} = r_{P1} \cdot d\theta_1 + r_{P2}^* \cdot d\theta_2 - d\sigma_P. \quad (11)$$

In the *flexing distal finger* ($d\theta_2 > 0$), a close link exists between the activity of the FP and the CM. The FP is the only flexor of the DIP; therefore, the DIP can be flexed ($d\theta_3 > 0$) only if the FP is active ($\sigma_P = 0$). It follows that in the flexing finger an active CM implies an active FP. Conversely, if the DIP is flexed by the FP, the CM will become active at the moment that all slack σ_L has disappeared from the lateral bands. To summarise,

$$d\theta_3 > 0 \Rightarrow \sigma_P = 0,$$

$$d\theta_3 > 0 \text{ and } \sigma_L = 0 \Rightarrow d\theta_2 = \frac{d\theta_3}{K}. \quad (12)$$

If the PIP flexes ($d\theta_2 > 0$) and the FP is inactive ($\sigma_P \neq 0$), the DIP will retain its position ($d\theta_3 = 0$) and the CM will be inactive. The lateral bands will then accumulate the slack σ_L :

$$d\theta_2 > 0 \text{ and } \sigma_P \neq 0 \Rightarrow d\theta_3 = 0;$$

$$\sigma_L = \int (r_{M2} - r_{L2}) \cdot d\theta_2. \quad (13)$$

In the *extending distal finger* ($d\theta_2 < 0$), the DIP can only extend if the lateral band is taut (CM active), since they are its only extensors:

$$d\theta_2 < 0 \quad \text{and} \quad \sigma_L = 0 \Rightarrow d\theta_3 = K \cdot d\theta_2. \quad (14)$$

If initial slack is present in the lateral band, the DIP will remain immobile until all slack is stretched out by the proximal displacement of the ED and the IO, at which point the CM becomes active. This happens when

$$d\varepsilon_{\text{PIP(ED,IO)}} = \int_{\theta_{2,0}}^{\theta_2} (r_{M2} - r_{L2}) \cdot d\theta_2 = \sigma_{L,0}.$$

After substitution of the above results, the final displacement model of the free moving, unloaded finger becomes:

$$d\varepsilon_{\text{FP}} = r_{P1} \cdot d\theta_1 + r_{P2} \cdot d\theta_2 + r_{P3} \cdot d\theta_3 - d\sigma_P, \quad (15a)$$

$$d\varepsilon_{\text{FS}} = r_{S1} \cdot d\theta_1 + r_{S2} \cdot d\theta_2 - d\sigma_S, \quad (15b)$$

$$d\varepsilon_{\text{ED}} = -r_{E1} \cdot d\theta_1 - r_{M2} \cdot d\theta_2, \quad (15c)$$

$$d\varepsilon_{\text{IO}} = r_{I1} \cdot d\theta_1 - r_{M2} \cdot d\theta_2, \quad (15d)$$

$$d\theta_3 = \frac{r_{M2} - r_{L2}}{r_{L3}} \cdot d\theta_2 - \frac{d\sigma_L}{r_{L3}}, \quad (15e)$$

$$\sigma_P \cdot \sigma_S = 0, \quad (15f)$$

$$d\sigma_L = 0 \Rightarrow d\varepsilon_{\text{FP}} = r_{P1} \cdot d\theta_1 + r_{P2}^* \cdot d\theta_2 - d\sigma_P. \quad (15a')$$

In the real finger, the coupling factor K varies from 0.25 to about 0.8 with the PIP going from full extension to full flexion (Landsmeer, 1958; Spoor and Landsmeer, 1976). This relationship is implemented by assuming r_{L2} to be a linear function of θ_2 :

$$r_{L2} = r_{M2} - r_{L3} \left(0.25 + \frac{0.55}{\pi/2} \cdot \theta_2 \right).$$

All other moment arms in the model are taken constant. For normal finger functioning the following additional parameter relationships, which we call the Landsmeer conditions (Landsmeer, 1955; Spoor and Landsmeer, 1976), must be satisfied:

$$\frac{r_{E1}}{r_{S1}} - \frac{r_{M2}}{r_{S2}} > 0 \quad \text{and} \quad \frac{r_{E1}}{r_{P1}} - \frac{r_{M2}}{r_{P2}} > 0. \quad (16)$$

The constraints

Anatomical interconnections usually exist between the tendons of adjacent fingers. In this monodigital model, however, the connections are defined between tendons and a fixed point of reference. The connections are assumed inextensible and of zero length, and do not allow any motion between the tendon and the point of fixation. A physical interpretation is the rigid fixation of the tendon to the metacarpal (tenodesis) proximal to the MCP. A tendon thus constrained can absorb force, because it can be pulled at. However, it cannot produce work, as in the product: $W = \text{force} \cdot \text{displacement}$, the displacement is zero. For further use, the connection will be referred to as a

'zero-excursion constraint'. Mathematically, the constraint implies for the tendon part distal to the connection,

$$d\varepsilon_T = \sum_{j=1}^{n_T} (+/-) r_{Tj} \cdot d\theta_j - d\sigma_T = 0, \quad (17)$$

where n_T is the number of joints the tendon T spans. The interpretation is as follows.

(i) The sum term in equation (17), i.e. the total sum of the displacements of the tendon T over the individual joints, cannot be negative. This would require the tendon T to displace distally, or to elongate. The first is excluded by the constraint, while the second is excluded by definition, as tendons in the model are assumed inextensible.

(ii) The sum of the displacements of the constrained tendon over the individual joints may be positive, indicating the accumulation of slack in the tendon. The constraint is then called *inactive*, since a tendon which is slack cannot limit movement.

The functional problem: the lifting of the finger from the piano key

The functional problem studied here is one of the most simple a pianist can face: the lifting of a finger from the piano key. Initially, the finger is holding down a key in a slightly flexed position, with the metacarpal parallel to the keyboard. From this position the fingertip is to be lifted to a 'sufficient height' with respect to the key. The lifting should be realised without changing the metacarpal position. Mathematically, the problem implies the following condition:

$$\Delta h \geq H,$$

where Δh is the lifting height of the fingertip and H is the minimum height of lifting required. In the initial position all tendons are assumed taut ($\sigma_{T0} = 0$).

The data presented

An exhaustive overview of the application of the zero-excursion constraint to the model is presented. The constraints are applied to the four motors of the model individually, and further to the different motors simultaneously. All the solutions presented are calculated from the same initial joint positions, while the functional end position of the MCP for extension (limit of functional range) is taken to be 10° hyperextension. The parameter values used in the calculations are presented in Table 1. The solutions are presented with stick diagrams, and the tendon displacements with bar diagrams in Fig. 4.

The tendon displacements in Fig. 4, i.e. the height of the bars, are obtained by integration of

$$\sum_{j=1}^{n_T} \int_{\theta_{j,0}}^{\theta_j} (+/-) r_{Tj} \cdot d\theta_j. \quad (18)$$

This integral can have three distinct meanings:

- (i) In the case of a taut, unconstrained motor [$\sigma_T=0$ in equation (15)], it represents the motor displacement.
- (ii) In the case of a constrained motor [$d\epsilon_T=0$ in equation (15)], it represents the slack in the distal tendon.
- (iii) In the case of an unconstrained, inactive (slack) motor, it is meaningless, as by definition the displacements of the inactive motor are undefined.

RESULTS: THE LIFTING OF THE FINGER WITH ZERO-EXCURSION CONSTRAINTS

The lifting of the finger with zero excursion of some of the tendons involves two difficulties. The first is kinematic: the joint displacements must satisfy both the constraints ($d\epsilon_T=0$) and the functional problem ($h_{\text{fingertip}} \geq H$). The second difficulty is dynamic: the constrained tendons cannot generate work since they have zero displacements. A solution in which no motor remains to generate positive work is infeasible. Since muscles can only pull, positive work can only be produced by motors with positive excursions. From this follows the *feasibility condition*: a solution is feasible if at least one motor has a positive excursion.

Lifting the finger with zero excursion of the extensor digitorum (ED)

The kinematic problem. The ED is assumed rigidly fixed to the metacarpal, proximal to the MCP. This implies the following condition for the medial band distal to the fixation [$d\epsilon_{ED}=0$ in equation (15c)]:

$$d\epsilon_{ED} = -r_{E1} \cdot d\theta_1 - r_{M2} \cdot d\theta_2 = 0, \tag{19}$$

from which it follows that

$$d\theta_2 = -\frac{r_{E1}}{r_{M2}} \cdot d\theta_1. \tag{20}$$

This expression shows that finger movement with zero ED excursion is only possible when the MCP and the PIP move in opposite sense. Thereby, the excursion of the ED over the MCP ($d\epsilon_{ED(MCP)} = r_{E1} \cdot d\theta_1$) is annihilated by an equal amount of ED excursion of opposite sign over the PIP ($d\epsilon_{ED(PIP)} = r_{M1} \cdot d\theta_2$) (see Fig. 3). The constraint thus introduces a coupling of the MCP and

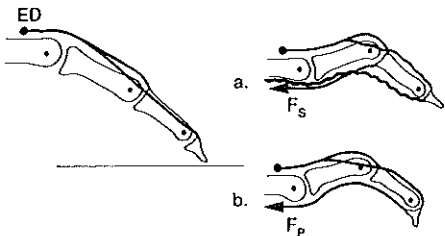


Fig. 3. Lifting the finger with zero excursion of the extensor digitorum: (a) FP inactive; (b) FP active.

the PIP movements, in addition to the already existing coupling mechanism CM, which couples the PIP and the DIP. Therefore, if the CM is active, all joints are coupled, and the whole finger will move as a mechanism as a function of the movement of one joint. If the CM is inactive, only the proximal two joints remain strictly coupled. Condition (20) allows finger movement in two opposite directions, with the MCP either extending ($d\theta_1 < 0$) or flexing ($d\theta_1 > 0$). We discuss both cases.

- (i) $d\theta_1 < 0$.

The movements resulting from the MCP extending from the initial position to the limit of hyperextension are represented in Figs 3 and 4. In Figs 3(a) and 4(a) the CM is inactive, while in Figs 3(b) and 4(b) it is active. Clearly, two contradictory effects exist in these movements: (i) in the MCP, there is a movement of extension which increases the height of the finger tip; (ii) in the PIP, there is a flexion movement that diminishes it. The net result, however, is upward lifting of the fingertip to a sufficient height. The kinematic problem is thus solved.

Both movements present a coordinated zigzag action of the proximal two phalanges, and result in an end position that strongly resembles the collapse or intrinsic minus position. In the following, the term 'collapse movement', or even 'collapse', will be used to indicate any similar zigzag movement.

- (ii) $d\theta_1 > 0$.

The movements resulting from the flexing MCP are the kinematic inverse of the collapse movements resulting from the extending MCP. Since the latter movements increase the lifting height, those with a flexing MCP will reduce it, and no solution can result from them. To summarise, all solutions must be based on the collapse movement of simultaneous MCP extension, and PIP flexion.

Feasibility. A solution is feasible if at least one motor exists with a positive excursion. Since all solutions involve an extension of the MCP, one would expect the ED, the only extensor of the MCP, to be active in powering these solutions. However, the zero-excision constraint excludes this. The IO cannot be a motor either, because it has negative excursions over both the MCP and the PIP. Therefore, only the flexors remain as possible motors. Their excursions are positive if

$$d\epsilon_{FP} = r_{P1} \cdot d\theta_1 + r_{P2}^* \cdot d\theta_2 > 0, \tag{21a}$$

$$d\epsilon_{FS} = r_{S1} \cdot d\theta_1 + r_{S2} \cdot d\theta_2 > 0. \tag{21b}$$

In expression (21a), expression (15a') holds. Indeed, the FP is taut ($\sigma_P=0$) because it is assumed to be an active motor, and the initial slack in the LB is by definition zero ($\sigma_{LO}=0$), so the CM is also active [expression (12)].

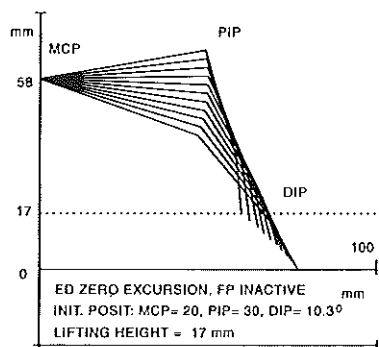
Substituting $d\theta_2$ from equation (20) into expression (21) gives

$$d\epsilon_{FP} > 0 \Leftrightarrow \frac{r_{E1}}{r_{P1}} - \frac{r_{M2}}{r_{P2}^*} > 0,$$

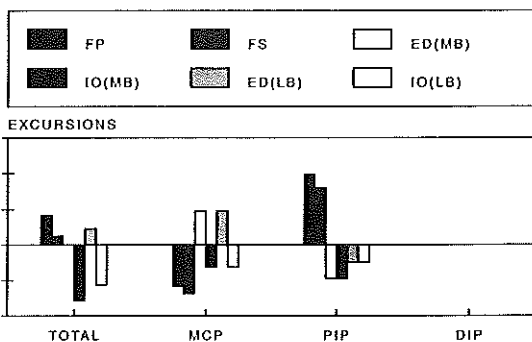
$$d\epsilon_{FS} > 0 \Leftrightarrow \frac{r_{E1}}{r_{S1}} - \frac{r_{M2}}{r_{S2}} > 0. \quad (22)$$

The inequalities on the right-hand side are the Landsmeer conditions (16), which by definition hold.

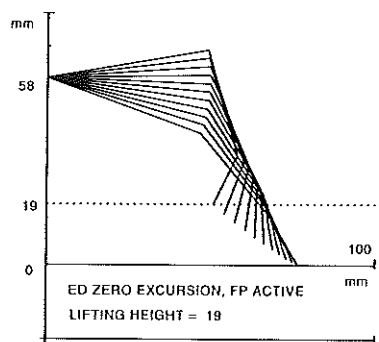
(a)



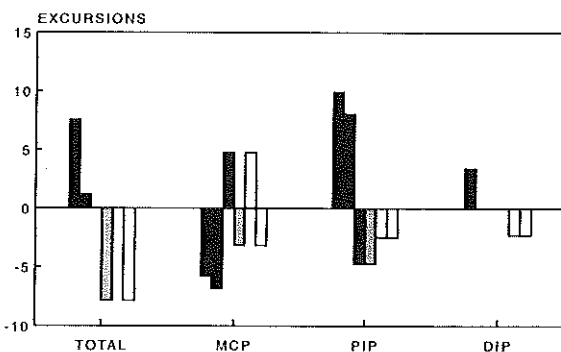
ED ZERO EXC., FS ACTIVE, FP INACTIVE



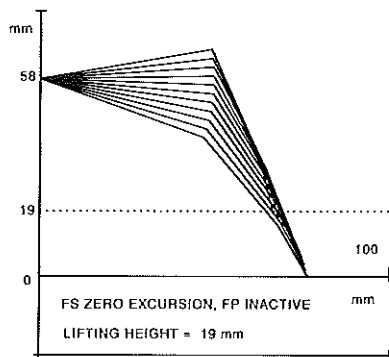
(b)



ED ZERO EXC, FP ACTIVE, FS INACTIVE



(c)



FS ZERO EXCURSION, FP INACTIVE

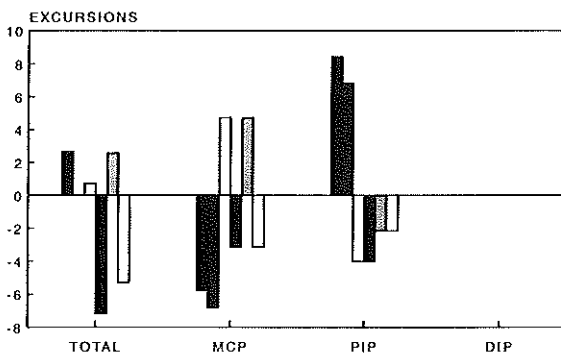


Fig. 4(a-c)

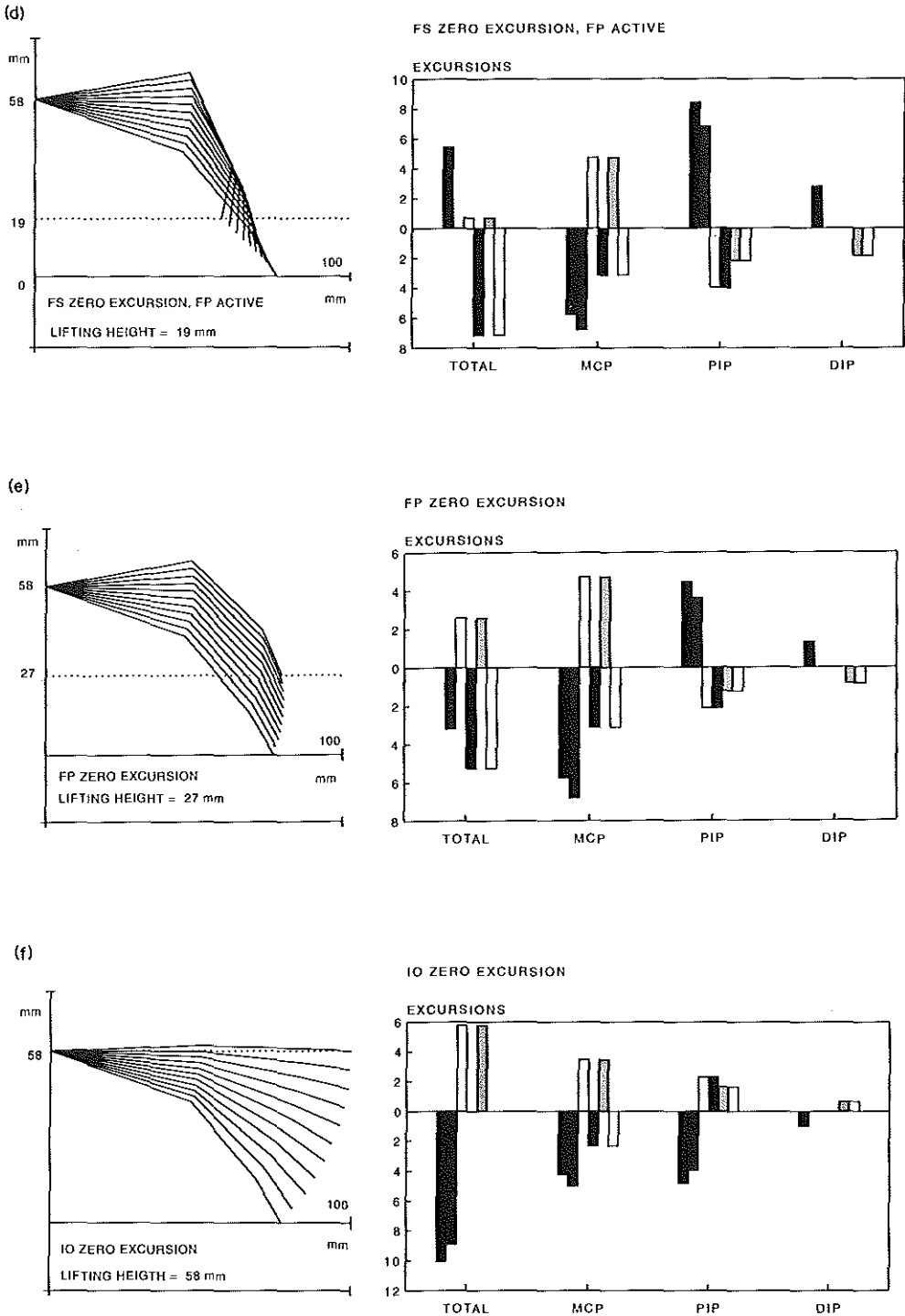


Fig. 4. Lifting the finger with zero excursion of the tendons. Movements: stick diagrams; tendon excursions: bar diagrams. (a) Zero excursion of the extensor digitorum, FP inactive; (b) zero excursion of the extensor digitorum, FP active; (c) zero excursion of the superficial flexor, FP inactive; (d) zero excursion of the superficial flexor, FP active; (e) zero excursion of the deep flexor; (f) zero excursion of the interosseus.

This reveals that the excursions of both flexors are positive. The solutions are, therefore, feasible and will be powered by one or both flexors.

The set of feasible solutions of the zero-ED-exursion problem. The set of solutions consists merely of two elements:

(1) The solution of Fig. 4(a), powered by the FS, with an inactive FP and an immobile distal joint.

(2) The solution of Fig. 4(b), which is powered by the FP, or the FP and the FS together, and has an actively flexed DIP.

Apart from the behaviour of the DIP, these solutions present the same movement, determined by equation (20). Clearly, the constraint on the ED reduces the excursion domain of the constrained system to little more than a plain curve.

Lifting the finger with zero excursion of the superficial flexor (FS)

Now the FS is assumed rigidly fixed to the metacarpal, producing the condition [$d\epsilon_s=0$ in equation (15b)]:

$$d\epsilon_{FS} = r_{S1} \cdot d\theta_1 + r_{S2} \cdot d\theta_2 - d\sigma_s = 0. \quad (23)$$

Similar to the previous case, any lifting movement of the finger implies a collapse as the MCP and the PIP must move in opposite sense:

$$d\theta_2 = -\frac{r_{S1}}{r_{S2}} \cdot d\theta_1 + \frac{d\sigma_s}{r_{S2}}. \quad (24)$$

Slack in the distal tendon of the FS cannot be excluded here, as stated by condition (6c). From equation (24) it follows that the degree of collapse, i.e. the proportion of PIP flexion as a function of MCP extension, increases with the amount of slack σ_s . Two cases, of zero and non-zero slack, are distinguished:

(i) $\sigma_s=0, \sigma_p \neq 0$.

In this case the FS is assumed taut ($\sigma_s=0$), and the FP inactive ($\sigma_p \neq 0$). The latter condition implies that the DIP will not change position during the movement ($d\theta_3=0$) [Fig. 5(a)]. Under these circumstances only one solution is possible, powered by the ED which remains the only motor with a positive, albeit small, excursion [Fig. 4(c)].

(ii) $d\sigma_s \geq 0, \sigma_p = 0$.

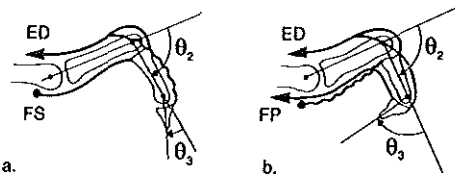


Fig. 5. Lifting the finger with zero excursion of the superficial flexor: (a) FP inactive; (b) FP active.

The FS is now allowed to become slack, which requires the FP to become active [condition (6c)]. When the FS is slack ($\sigma_s \neq 0$), the finger is coordinated by the synergistic actions of the other motors (FP, ED, IO), all of which must be active [conditions (6a)-(6c)]. The synergistic excursion pattern of the ED and the FP as a function of the slack σ_s is given by

$$d\epsilon_E = \begin{bmatrix} r_{E1} & r_{M2} \\ r_{S1} & r_{S2} \end{bmatrix} d\epsilon_p - \frac{r_{P1} r_{P2}^*}{r_{S1} r_{S2}} \begin{bmatrix} r_{E1} & r_{M2} \\ r_{P1} & r_{P2}^* \end{bmatrix} d\sigma_s. \quad (25)$$

Similar relationships exist involving the interosseus [(FP, IO, σ_s) or (ED, IO, σ_s)]. Expression (25) is obtained by substituting $d\theta_2=f(d\theta_1)$ from equation (24) into expressions (15a') (the coupling mechanism is active) and (15c), and subsequent elimination of $d\theta_1$. The coefficient of $d\epsilon_p$ in equation (25) is positive; the numerator is one of the Landsmeer conditions (16), which is positive, while $r_{P2}^* > r_{S2}$ and $r_{P1} < r_{S1}$ hold in the human finger.

Since all variables are continuous, expression (25) defines a continuous domain of tendon excursion patterns. Variations of the slack variable σ_s will produce excursion patterns that imply movements with varying degrees of collapse. These finger movements are not necessarily solutions of the problem. However, it can be easily demonstrated that a non-zero domain of excursion patterns which result in solutions does exist. (i) A first solution of this domain can be obtained by putting the slack to zero ($\sigma_s=0$). This produces the 'lower boundary' of the domain of movements allowed by equation (25), i.e. the movement with the least collapse allowed by the constraint [see Fig. 4(d)]. Figure 4(d) reveals that the solution is feasible, as the excursions of both the ED and the FP are positive. (ii) A second solution is obtained by keeping the ED isometric contracted during the movement ($d\epsilon_E=0$). Here it should be observed that there is no kinematic difference between a movement determined by a zero constraint on a tendon, or by an isometric contracting motor: in both cases the displacement of the motor is zero. From this it follows that the solution with an isometric ED is kinematically identical to the solution of Fig. 4(b), i.e. the solution of the zero-ED-exursion problem with active FP and non-active FS. Note that the positive excursion of the FS in Fig. 4(b) represents in this case the amount of slack σ_s [expression (18)]. (iii) To conclude the argument, because of the continuity, all movements with excursion patterns resulting from varying the slack from zero to that of Fig. 4(b) will also be solutions. It follows that a domain exists from which solutions can be freely selected.

The set of feasible solutions of the zero-FS-exursion problem. In the zero-ED-exursion case the finger action is determined by a constraint which strictly couples the joint displacements of the MCP and the

PIP, and reduces the excursion and movement domains for these joints to plain curves. Such solutions can be interpreted as isolated solutions or 'points' in the set of solutions. The set of solutions of the zero-FS-excision problem also contains such an isolated solution: the solution powered by the ED alone [Fig. 4(c)]. However, in addition to this solution, a 'continuum' of solutions exists, of varying degrees of collapse, as described by equation (25). Note that the intersection of the set of solutions of the zero-ED- and zero-FS-excision problems is not empty: it contains the isolated solution (point) of Fig. 4(b).

Lifting the finger with zero excursion of the deep flexor (FP)

The FP is now rigidly connected to the metacarpal. This implies [$de_{fp}=0$ in equation (15a)] that

$$de_{FP} = r_{P1} \cdot d\theta_1 + r_{P2} \cdot d\theta_2 + r_{P3} \cdot d\theta_3 - d\sigma_P = 0. \quad (26)$$

Substituting $d\theta_3$ from equation (15e) into equation (26) results in

$$d\theta_1 = -\frac{r_{P2}^*}{r_{P1}} \cdot d\theta_2 + \frac{1}{r_{P1}} \left(\frac{r_{P3}}{r_{L3}} \cdot d\sigma_L + d\sigma_P \right). \quad (27)$$

The slack term in equation (27) contains a sum of two slack variables (σ_P and σ_L), which expresses the fact that slack can be shifted between these tendons by changing the position of the DIP. However, since the FP and LB are slack, such a change in position can only be caused by external influences.

In equation (27), two cases are distinguished, depending on the slacks.

$$(i) \quad \sigma_L = \sigma_P = 0.$$

In the case of an active FP, and an active CM, equation (27) becomes

$$d\theta_1 = -\frac{r_{P2}^*}{r_{P3}} \cdot d\theta_2. \quad (28)$$

Here all joint actions are coupled (r_{L2}^* incorporates the coupling of the PIP and the DIP by the active CM). The resulting solution is presented in Figs 4(c) and 6(a). From the first figure it is clear that the resulting lifting height is greater than in former cases, while the collapse is less severe. The solution can be powered solely by the ED alone, or by the ED and the FS together, as both have positive excursions.

$$(ii) \quad \sigma_L, \quad \sigma_P \neq 0.$$

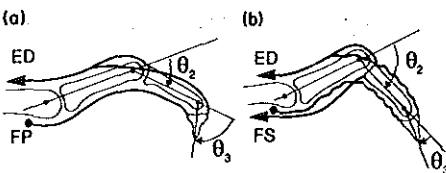


Fig. 6. Lifting the finger with zero excursion of the deep flexor: (a) FS inactive; (b) FS active.

When the FP becomes slack (and the CM inactive, since $d\theta_2 > 0$ in the solutions), the FS must become active to keep the PIP balanced [condition (6c)]. The ED, IO and FS must then act synergistically to produce movement. The synergistic excursion pattern for the ED and the FS as a function of the slack σ_P is (similar expressions can be derived involving the IO):

$$de_E = -\frac{\begin{bmatrix} r_{E1} & r_{M2} \\ r_{P1} & r_{P2}^* \end{bmatrix}}{\begin{bmatrix} r_{S1} & r_{S2} \\ r_{P1} & r_{P2}^* \end{bmatrix}} de_S + \frac{r_{S1} r_{S2}}{\begin{bmatrix} r_{S1} & r_{S2} \\ r_{P1} & r_{P2}^* \end{bmatrix}} \times \left(\frac{r_{P3}}{r_{L3}} d\sigma_L + d\sigma_P \right). \quad (29)$$

The interpretation is analogous to the previous case. Expression (29) defines a continuous domain of solutions, with various degrees of collapse, determined by the slack variables [see Fig. 6(b)]. Zero slack produces the solution with minimal collapse [Fig. 4(e)]. Of interest are the solutions with isometric contracting FS ($de_S=0$) and isometric ED ($de_E=0$) since they are kinematically identical to the solutions of Fig. 4(c) (zero FS excursion and inactive FP) and Fig. 4(a) (zero ED excursion and inactive FP). That both solutions satisfy equation (26) is immediately clear from the positive excursions of the FP, which here equal the slack σ_P [expression (18)].

Similar to the zero-FS-excision case, the set of feasible solutions with zero FP excursion is a continuous domain of solutions with varying degrees of collapse, on one side bordered by the solution with the minimum degree of collapse [Fig. 4(e)].

Lifting the finger with zero excursion of the interosseus

The problems studied until now all involve constraints on the extrinsic finger motors (ED, FS, FP), and fundamental to their solutions is the mechanism of the collapse. This zigzag movement allows for the minimisation of the excursions of the extrinsics in such a way that both the constraints, and the functional problem can be satisfied. A consequence is that the excursion of the intrinsic motor, the IO, becomes large and negative in sign. In the present case, however, the constraint puts the excursion of the IO to zero. The condition is [$de_{IO}=0$ in equation (15d)]:

$$de_{IO} = r_{I1} \cdot d\theta_1 - r_{M2} \cdot d\theta_2, \quad (30)$$

from which it follows that

$$d\theta_2 = \frac{r_{I1}}{r_{M2}} \cdot d\theta_1. \quad (31)$$

Here $d\theta_1$ and $d\theta_2$ have the same sign, meaning that the MCP and the PIP will both move in the same sense. It follows that, in contrast with the previous cases, finger movement with a constrained IO does not imply a collapse. Since in the initial position all tendons are taut (and thus $\sigma_{LO}=0$), extension of the PIP will cause immediate extension of the DIP through the active

CM [expression (14)]. Therefore, under the combined effect of the constraint and the CM, extension of the MCP will result in the simultaneous extension of the PIP and the DIP [see Fig. 4(f)]. Note that the excursions of the extrinsics are now maximal, because all joints move in the same sense. In conclusion, since the whole finger extends as a mechanism with the MCP, the excursion and movement domains are reduced to plain curves, and the feasible set consists of just one single movement.

Lifting the finger with multiple constraints

Generally, the set of solutions corresponding with superimposed constraints will be the intersection of the sets associated with the individual constraints.

For example, in the case of zero-excision constraints simultaneously applied to the ED and the FP, this intersection contains just one element, i.e. the solution of Fig. 4(a) [$de_E = 0$, inactive FP ($\sigma_P \neq 0$), motor: FS]. From the slack in the FP [see Fig. 4(a)] it follows that the constraint on the FP is inactive. This indicates that the collapse resulting from the constraint on the ED is more severe than the collapse implied by the constraint on the FP. The constraint on the FP is, however, not entirely redundant as it keeps the FP from producing work.

Other combinations of two simultaneously applied constraints that still yield solutions are:

—zero FS and zero FP excursion, with the solution of Fig. 4(c): zero FS excursion, FP slack, motor: ED.

—zero FS and zero ED excursion, with the solution of Fig. 4(b): zero ED excursion, FS slack, motor: FP.

Zero-excision constraints on all three extrinsics make any solution infeasible, even if the solution of the kinematic problem remains possible. For example, the movements of Fig. 4(a) and (b) both solve the kinematic problem. However, because of the constraints, all positive excursions in these figures now represent slack, meaning that no motor remains to power these movements.

Truly incompatible are zero-excision constraints involving both intrinsic and extrinsic motors. Indeed, the intrinsic constraint excludes the collapse, while the extrinsic constraint implies it. This combination will block the extension of any joint and result in an empty set of solutions.

DISCUSSION

The significance of the zero-excision constraint for the hand of the musician

Consider two fingers of which the tendons are interdigitally coupled with rigid connections of zero length, and assume both fingers to be in the initial position of the lifting problem. The problem now is to lift one finger, while keeping the other fixed in the initial position. Since the latter finger may not change position, its tendons cannot displace. They can, therefore, be considered a part of the fixed environment.

The connection then is effectively between the tendon of the moving finger and a fixed point of reference, which is the type discussed in the model. In the playing of the piano the finger coordination as here described is frequent (two fingers on the keyboard, of which one subsequently lifts). Therefore, to the extent that the anatomical interconnections between the tendons in the hand of the subject are rigid and strict, the problems studied here represent realistic situations.

The set of feasible solutions and the exercisability of the hand

The set of feasible solutions of a given functional problem is defined as consisting of all movements that kinematically solve the functional problem, and that are realisable by pulling the tendons. This set circumscribes the range of possibilities from which a suitable solution can be selected. As shown in the Results, constraints can drastically restrict the feasible set. For instance, in the cases of zero ED and zero IO excursions, the feasible sets are reduced to a few movements, or even one single movement. In the cases of constraints on flexors, a wider range of variation is possible, albeit still very limited.

Within this framework, the concept of *exercisability* of a hand can be envisaged. Exercise, in broad terms, can be defined as the optimisation of parameters relating to the efficiency of a solution. The smaller the feasible set, the less 'exercisable' the hand will be, as the range within which these parameters can be optimised decreases.

The following may serve as an illustration. The prime parameter that defines a solution is its kinematic 'shape', in other words, the coordinated joint displacements. In the cases of the constrained ED and IO, the actions of at least two joints (MCP and PIP) are completely coupled. Exercise cannot alter this basic pattern of joint coordination, however unsatisfactory it may be, as no other movements are feasible.

From this point of view, the concept of exercisability may be defined in the following way. Consider a functional problem, and a movement which is presumed to be a suitable solution, as for instance proposed by the pedagogue. Then, if this solution is not within the feasible set of the hand of the student, the hand must be considered non-exercisable up to the level of this solution. This defines exercisability with respect to the anticipated result.

Applications

Ideally, the set of feasible solutions could be estimated by hand tests. Knowledge of this set would allow one to determine the best solutions to the given problems feasible in the subjects' hand. The conscious implementation of these solutions would produce the best possible results, while sparing the subject the effort of trying to realise what are for him unachievable movements. One could also determine, even before training, whether these solutions are good

enough with regard to the expectations of the individual.

More generally, the displacement model of the finger as here presented may serve to study the effects on movement of limitations on tendon mobility, e.g. within the clinical context.

CONCLUSION

In this paper, the effect on the motion of a mono-digital system of tendons being rigidly connected to the environment is exhaustively studied. To this end the concept of the set of feasible solutions to a functional problem is introduced, and it is found that constraints on the displacements of the tendons diminish this set. The notion of the set of feasible solutions is used to define the concept of exercisability of the hand of the musician, which may be helpful in understanding how hands handicapped in the mentioned way sometimes cannot fulfil the demands of the music pedagogue or instrumental technique.

Acknowledgements—The authors thank Prof. A. J. Hermans, of the Delft University of Technology, for his support. The authors also thank R. Rammohan and P. Gilbert for their valuable contribution.

REFERENCES

- Austin, G. J., Leslie, B. M. and Ruby, L. K. (1989) Variations of the flexor digitorum superficialis of the small finger. *Am. J. Hand Surg.* 14A, 262–267.
- Baker, D. S., Gaul, J. S. Jr, Williams, V. K. and Graves, M. (1981) The little finger superficialis—clinical investigation of its anatomic and functional shortcomings. *Am. J. Hand Surg.* 6, 374–378.
- Blair, W. F. and Omer, G. E. Jr (1981) Anomalous insertion of the flexor pollicis longus. *Am. J. Hand Surg.* 6, 241–244.
- Culver, J. E. Jr (1980) Extensor pollicis and indicis communis tendon: a rare anatomic variation revisited. *Am. J. Hand Surg.* 5, 548–549.
- Fahrer, M. (1971) Considerations sur l'anatomie fonctionnelle du muscle flechisseur commun profond des doigts. *Ann. Chir.* 25, 945–950.
- Kaplan, E. B. (1965) *Functional and Surgical Anatomy of the Hand* (2nd Edn), pp. 66–86. Pitman, London.
- Landsmeer, J. M. F. (1955) Anatomical and functional investigations on the articulation of the human fingers. *Acta Anat.* (Suppl.) 24, 2511–2569.
- Landsmeer, J. M. F. (1958) A report on the co-ordination of the interphalangeal joints of the human finger and its disturbances. *Acta Morphol. Neerl.-Scand.* 2, 59–84.
- Linburg, R. M. and Comstock, B. E. (1979) Anomalous tendon slips from the flexor pollicis longus to the digitorum profundus. *Am. J. Hand Surg.* 4, 79–83.
- Spoor, C. W. (1983) Balancing a force on the fingertip of a two dimensional finger model without intrinsic muscles. *J. Biomechanics* 16, 497–504.
- Spoor, C. W. and Landsmeer, J. M. F. (1976) Analysis of the zigzag movement of the human finger under influence of the extensor digitorum tendon and the deep flexor tendon. *J. Biomechanics* 9, 561–566.
- van der Meulen, J. C. (1972) Causes of prolapse and collapse of the proximal interphalangeal joint. *The Hand* 4, 147–153.
- Verdan, C. (1960) Syndrome of the quadriga. *Surg. Clin. North Amer.* 40, 425–426.
- von Schroeder, H. P., Botte, M. J. and Gellman, H. (1990) Anatomy of the juncturae tendinum of the hand. *Am. J. Hand Surg.* 15A, 595–602.

THE HAND OF THE MUSICIAN: THE KINEMATICS OF THE BIDIGITAL FINGER SYSTEM WITH ANATOMICAL RESTRICTIONS

J. N. A. L. LEIJNSE,*†‡ C. J. SNIJDERS,* J. E. BONTE,§ J. M. F. LANDSMEER,||
 J. J. KALKER,‡ J. C. VAN DER MEULEN,† G. J. SONNEVELD† and S. E. R. HOVIJUS†

*Department of Biomedical Physics and Technology; †Department of Plastic and Reconstructive Surgery, Erasmus University, Rotterdam, The Netherlands; ‡Department of Mathematics, University of Technology, Delft, The Netherlands; §Emmanuel Hospital, Wetteren, Belgium; and ||Prof. Emer., Department of Anatomy, Leiden, The Netherlands

Abstract—Tendons of the fingers are frequently interconnected by anatomic structures that limit the displacements of these tendons relative to each other. In this paper a bidigital finger system in which such interconnections between tendons are present is kinematically modelled. Using this model, an exhaustive description of the effects on finger movement of connections between the different tendons of the fingers is given. The study provides a context for the interpretation of typical difficulties of finger coordination in musicians, especially in pianists and string players.

NOMENCLATURE

MCP	metacarpophalangeal joint
PIP	proximal interphalangeal joint
DIP	distal interphalangeal joint
FP	flexor digitorum profundus
FS	flexor digitorum superficialis
ED	extensor digitorum
IO	interosseus
MB	medial band of extensor and interosseus
LB	lateral band of extensor and interosseus
M_c	common equivalent motor
$T_c^{(i)}$	connected tendon of finger F_i
r_{ij}	moment arms of the tendons over the respective joints.
	The first index denotes the motor: P=FP, S=FS, E=ED, I=IO, M=MB, L=LB. The second index numbers the joint: MCP=1, PIP=2, DIP=3 (see Table 1)
$\epsilon_T^{(i)}$	displacement of a tendon T_i
$\theta_j^{(i)}$	joint rotations of finger F_i ($j=1, 2, 3$ for MCP, PIP, DIP, respectively)
$\sigma_T^{(i)}$	slack in tendon T of finger F_i
σ_c	slack in the connection between tendons
L_c	length of the connection between tendons
T_p	tendon part proximal to the insertion of the connection
T_d	tendon part distal to the insertion of the connection
L_i	distance between the fixed reference point and the insertion of the connection in tendon T_i

INTRODUCTION

Tendons of the fingers in the human hand are frequently interconnected by tendinous or fascia-like anatomical structures. Well-known examples are the juncturae tendinum between the M. extensor

digitorum (Forbes, 1991; Kaplan, 1965; Von Schroeder *et al.*, 1990), and connections within the M. flexor digitorum profundus (the phenomenon of the quadriga of Verdan) (Verdan, 1960; Fahrner, 1971; Malerich *et al.*, 1987), but many other instances have been described (Austin *et al.*, 1989; Baker *et al.*, 1981; Blair and Omer, 1981; Culver, 1980; Linburg and Comstock, 1979; McGregor and Glover, 1988; Parrot and Harrison, 1980). When sufficiently stiff, these structures limit the mutual displacements of the tendons they connect, and can be modelled as strict kinematic constraints. In this paper the effects of such constraints on the kinematics of finger movement are studied in a two finger model. To this end, the bidigital model with tendons connected with each other is required to execute some simple tasks at the piano keyboard, such as the lifting of fingers, or the striking of keys. The various ways in which the finger model can execute these tasks are calculated, and the effects of the constraints are pointed out. The connections modelled are inextensible, and between tendons of (i) the extensor digitorum (ED), (ii) the flexor digitorum superficialis (FS) and (iii) the flexor digitorum profundus (FP).

In the discussion, mention is made of extensible anatomical constraints, as may exist between muscles. Their effect on movement is compared with the inextensible connections studied in the model, and the findings are discussed with respect to the surgical clearance of the connections. Also discussed is the exerciseability of the hand with anatomic constraints, and the relative applicability of pedagogic models in the instrumental technique.

The present paper is a direct sequel to the paper of Leijnse *et al.* (1992), in which the kinematic functioning of a monodigital system with anatomical constraints was modelled.

METHODS AND MATERIALS

The kinematic two finger model with inextensible connections between tendons (Fig. 1)

The two-finger model studied consists of two equal sized, two-dimensional digits moving in parallel planes perpendicular to the joint axes. The functioning of the individual finger is described by the model of Leijnse *et al.* (1992). This model is based on the simplified representation of the finger as shown in Fig. 1, and specifically describes the controllable movements feasible in the free-moving finger (i.e. the movements that can be realised and controlled by the mere pulling of the tendons). The equations are:

$$d\epsilon_{FP} = r_{P1} d\theta_1 + r_{P2} d\theta_2 + r_{P3} d\theta_3 - d\sigma_P, \tag{1a}$$

$$d\epsilon_{FS} = r_{S1} d\theta_1 + r_{S2} d\theta_2 - d\sigma_S, \tag{1b}$$

$$d\epsilon_{ED} = -r_{E1} d\theta_1 - r_{M2} d\theta_2, \tag{1c}$$

$$d\epsilon_{IO} = r_{I1} d\theta_1 - r_{M2} d\theta_2, \tag{1d}$$

$$d\theta_3 = \frac{r_{M2} - r_{L2}}{r_{L3}} d\theta_2 - \frac{d\sigma_1}{r_{L3}}, \tag{1e}$$

$$\sigma_P * \sigma_S = 0. \tag{1f}$$

The motors are the flexor digitorum profundus (FP), the flexor digitorum superficialis (FS), the extensor digitorum (ED), the interosseus (IO). The Lumbricalis is ignored. The ED and IO insert in both the medial and the lateral bands (MB, LB) of the extensor assembly, which inserts in the basis of the middle (MB) and end phalanx (LB). In this kinematic model, the motors are instances that generate, or take up tendon displacement. The parameters of the model are the lengths of the moment arms of the motors over the respective joints (r_{ij}), and the lengths of the phalanges as measured between successive joint axes. The values used for calculation are given in Table 1. The moment

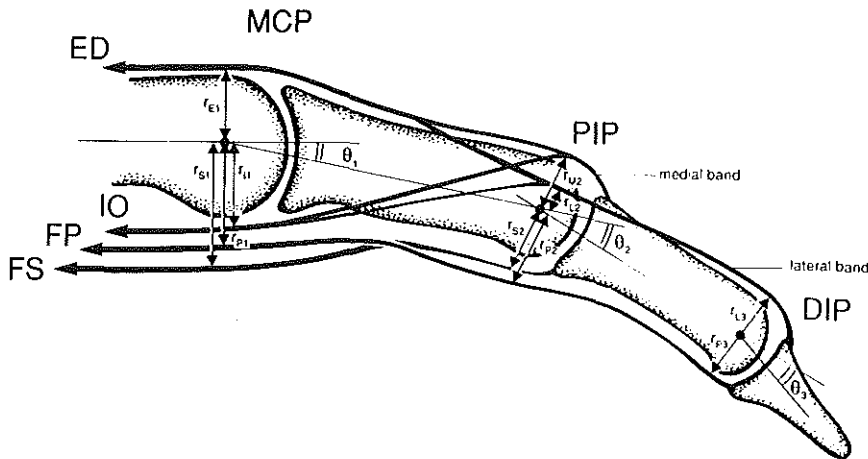


Fig. 1. Model of the finger.

Table 1. Moment arms of the tendons.

Motor joint	Symbol†			Value‡		
	MCP	PIP	DIP	MCP	PIP	DIP
FP	r_{P1}	r_{P2}	r_{P3}	11	10.5	6
FS	r_{S1}	r_{S2}	/	13	8.5	/
ED _{MB}	r_{E1}	r_{M2}	/	9	5	/
IO _{MB}	r_{I1}	r_{M2}	/	6	5	/
ED _{LB}	r_{E1}	r_{L2}	r_{L3}	9	*	4
IO _{LB}	r_{I1}	r_{L2}	r_{L3}	6	*	4

$$* r_{L2} = r_{M2} - r_{L3} \left(0.25 + \frac{0.55}{\pi/2} \theta_2 \right)$$

Proximal, Middle, Distal phalanx: 50, 34, 17

† Notations used in the text.

‡ Real values (in mm) used to calculate the results [From: Spoor (1983)].

/ indicates that the tendon does not cross the joint.

arms for extension have a negative sign. The θ_j are the joint rotations, while the ε_M are the changes of length of the motors as measured between their origin and insertion. Motors are allowed to be active and inactive; in an inactive motor the tendon is slack by definition, and in an unconstrained active motor it is taut. The tendon of an active motor can only be slack when its free course is obstructed, e.g. by an anatomical connection, and the slack can only occur in the part of the tendon distal to the obstruction. The slack in a tendon is quantified by the slack variables σ_T . In the model (1), the slack variables are only indicated for tendons that may be slack without disrupting normal finger function in the unloaded finger: FS, FP and LB. Hereby the condition (1f) (at least one flexor must be taut) must be satisfied.

Anatomical connections are modelled as inextensible ropes of length L_c , connecting two tendons, one in each finger ($T_c^{(1)}$ and $T_c^{(2)}$ in F_1 and F_2 , respectively; c stands for connected), and inserting in the tendons proximal to the MCP (see Fig. 2). Only connections between tendons of the same muscle group will be considered, e.g. ED⁽¹⁾ to ED⁽²⁾ and FS⁽¹⁾ to FS⁽²⁾, etc. The tendons themselves run parallel and at zero distance from each other, so that the connection does not pull them laterally. In the connected tendon, the tendon part proximal to the insertion of the connection is named $T_p^{(j)}$, the part distal to it $T_d^{(j)}$. The tendon lengths between the reference point and the points of insertion of the connection are L_1 and L_2 for $T_c^{(1)}$ and $T_c^{(2)}$, respectively.

Displacement properties of connected tendons

In the following the displacement properties of the system with connected tendons are summarised.

(1) Connected tendons move unconstrained as long as the connection is slack. Let $\Delta\varepsilon_{T_c}$ be defined as

$$\Delta\varepsilon_{T_c} = \varepsilon_{T_c}^{(1)} - \varepsilon_{T_c}^{(2)} \tag{2}$$

and let in the initial position of a movement

$$\begin{aligned} \Delta\varepsilon_{0T_c} &= 0, \\ \Delta L_0 &= L_{01} - L_{02} \quad (\text{with } |\Delta L_0| \leq L_c). \end{aligned} \tag{3}$$

From this initial position the maximal relative displacement possible between the connected tendons is

$$-(L_c - \Delta L_0) \leq \Delta\varepsilon_{T_c} \leq L_c + \Delta L_0. \tag{4}$$

The range of independent tendon displacements in a given finger position is thus determined by two parameters: (i) the length L_c of the connection; and (ii) the relative position ΔL_0 of the insertions of the

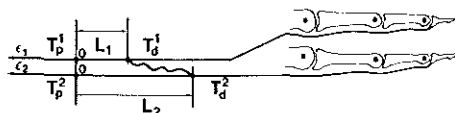


Fig. 2. Model of the bidigital system with connections between tendons.

connection. Expression (4) can be rewritten as

$$\sigma_c = L_c - |\Delta\varepsilon_{T_c} - \Delta L_0| \geq 0 \tag{5}$$

in which σ_c is the slack in the connection, defined as the (positive) displacement needed to taut the connection.

(2) When taut, the connection connects a proximal part of one tendon, with a distal part of another. This will be used to indicate the orientation of the connection, e.g. $T_p^{(1)}T_d^{(2)}$ would mean that the connection is stretched between the proximal part $T_p^{(1)}$ of $T^{(1)}$ and the distal part $T_d^{(2)}$ of $T^{(2)}$. Tautness of the connection implies the tautness of the proximal and distal tendon parts it connects. The other tendon parts may be either taut or slack. In the slack notation

$$\sigma_c = 0 \Rightarrow \begin{cases} \sigma_{T_p}^{(1)} + \sigma_{T_d}^{(2)} = 0 & \text{and } \sigma_{T_d}^{(1)}, \sigma_{T_p}^{(2)} \geq 0, \\ \text{or} \\ \sigma_{T_d}^{(1)} + \sigma_{T_p}^{(2)} = 0 & \text{and } \sigma_{T_p}^{(1)}, \sigma_{T_d}^{(2)} \geq 0. \end{cases} \tag{6}$$

(3) Most generally, movements of fingers with connected tendons are partly constrained [the phases of the movement during which the connection is taut ($\sigma_c = 0$)], and partly unconstrained [the phases in which the connection is slack ($\sigma_c \neq 0$)]. When the connection becomes taut and remains taut during a movement it holds that $\sigma_c = d\sigma_c = 0$. Substitution of equation (5) into the latter equality leads to

$$dL_c = \text{sign} [\Delta\varepsilon_{T_c} - \Delta L_0]_{\sigma_c=0} \cdot d\Delta\varepsilon_{T_c} \tag{7}$$

From this follows that for taut and inextensible connections ($dL_c = 0$), the displacements of the connected tendons must be equal:

$$\left. \begin{aligned} \sigma_c &= 0 \\ d\sigma_c &= 0 \\ dL_c &= 0 \end{aligned} \right\} \Rightarrow d\Delta\varepsilon_{T_c} = 0 \Rightarrow d\varepsilon_{T_c}^{(1)} = d\varepsilon_{T_c}^{(2)}. \tag{8}$$

Inextensible connections of zero length

In this paper, only (phases of) constrained movements, i.e. movements for which $\sigma_c = 0$, will be investigated. Hereby L_c will first be put to zero without loss of generality, since in condition (8) the length L_c is not a parameter. This allows to avoid tedious descriptions of the initial state of the system (definitions of L_{0j} , orientation of the connection, etc.). Physically, tendons connected with connections of zero length ($L_c = 0$) can be imagined as being firmly sewn together proximal to the MCP. In the examples it is assumed that in the tendons thus connected the lengths of the tendon parts distal to the connection are equal, so that when both fingers are in identical positions ($\theta_j^{(1)} = \theta_j^{(2)}$, $j = 1, 2, 3$) these tendon parts are equally taut or slack.

The common equivalent motor

Condition (8) states that when the connection is taut all connected motors have the same displacements.

ment. This means that when a tendon is displaced proximally (by the contraction of its motor), all tendons connected to it must follow this proximal displacement (otherwise this displacement is not possible); conversally, when a tendon is displaced distally (by pulling its distal end), all motors connected to it must elongate to follow this distal displacement, otherwise they would disallow it. Therefore, the motors of the tautly connected tendons can be replaced, without changing the functioning of the system, by a single equivalent motor, which for further use will be called the *common equivalent motor* M_c (Fig. 3). For the common motor it holds that

$$d\epsilon_{M_c} = d\epsilon_{T_c}^{(1)} = d\epsilon_{T_c}^{(2)} \quad (9)$$

with

$$d\epsilon_{T_c}^{(i)} = \sum_{j=1}^{n_{T_c}} \pm r_{T_c}^{(j)} d\theta_j^{(i)} - \sigma_{T_c}^{(i)}, \quad (10)$$

where $T_c^{(i)}$ is the coupled tendon of finger F_i , and n_{T_c} the number of joints this tendon crosses.

In analogy with the unconnected motor, the common motor may be called active when at least one of the connected tendons is taut, and inactive when all connected tendons are slack. In the slack notation:

$$M_c \text{ active} \Leftrightarrow \sigma_{T_c}^{(1)} + \sigma_{T_c}^{(2)} = 0. \quad (11)$$

Elementary bidigital tasks; notations

In this section notations for the bidigital tasks are defined. For further use such tasks are called 'functional problems', and any movement that is able to execute the task (solve the problem) is called a 'solution'. An elementary bidigital problem $p = (p_1, p_2)$ consists of the elementary monodigital problems p_1 and p_2 for the individual fingers F_1 and F_2 . A solution $s = (s_1, s_2)$ to a bidigital problem p consists of the solutions s_i of the individual problems p_i for the respective fingers F_i .

Only two elementary monodigital problems are distinguished here:

- (1) 'strike a key' [notation: 'k' (key-stroke)],
- (2) 'lift the finger tip from the key to a sufficient height ($h_{tip} > H$)' [notation: 'l' (lift)].

Four elementary bidigital problems are thus

possible:

$$\{(l, l), (k, l), (l, k), (k, k)\}.$$

The problem is completely specified when the initial finger positions $i = (i_1, i_2)$ are given. The initial positions i_j of the single digit can be partitioned into two classes C_1 and C_2 , as follows:

C_1 : all positions of holding down a key [notation: D (down)],

C_2 : all positions of keeping the finger lifted at a sufficient height $h_{tip} > H$ [notation: U (up)].

This leads to four classes C_i of bidigital initial positions:

$$\{(D, D), (D, U), (U, D), (U, U)\}.$$

A completely specified functional problem p can now be represented as

$$p = [(i_1, i_2), (p_1, p_2)].$$

In the model, the solving of a problem p is the production of the appropriate end positions $e = (e_1, e_2)$. Thereby the classes of the possible end positions C_e are equal to the classes of the possible initial positions C_i , as any end position may serve as the initial position of a subsequent functional problem.

Monodigital problems p_j in which the required end position e_j is in the same class C_e as the begin position i_j ($C_e = C_i$) will be called *identity problems*. Solving the identity problem is, by definition, the maintaining of the functional position of the finger, i.e. keeping the finger tip at a sufficient height, or holding the key down. As will be further illustrated, this does not mean that the finger must remain immobile, since $C_e = C_i$ does not imply that the specific end position e_j must be equal to the specific begin position i_j .

Example: $p = [(D, D), (l, k)]$

Interpretation:

(i) F_1 initially holds down a key ($i_1 = D$), and has to lift to a sufficient height ($p_1 = l$). F_1 will solve the problem by changing its position from the initial position 'D' to the end position 'U'.

(ii) F_2 holds down a key ($i_2 = D$), and should strike this key ($p_2 = k$). This is an identity problem, since F_2 already holds down the key.

The total solution will be that F_1 lifts to a sufficient height, while F_2 keeps holding its key down. Hereby F_2 may change its position ($e_2 \neq i_2$ or $\theta_{ji}^{(2)} \neq \theta_{je}^{(2)}$, $j = 1 \dots 3$), as long as its fingertip remains on the key ($h_{tip}^{(2)} = h_{key}$).

The presentation of the data

In the following the finger movements are calculated from the parameter values of Table 1. They are presented with stick diagrams, by their begin and end positions. The excursions (excursion is a clinical term indicating 'displacement') of the motors required to bring the finger from the begin position to the end position are presented with bars in the stick diagram of the end position (Fig. 5).

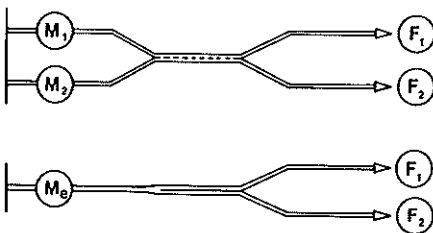


Fig. 3. The common equivalent motor M_c .

RESULTS

The bidigital system with strictly connected extensor tendons (ED) (Fig. 4)

The coupling of the displacements of the finger joints as resulting from a taut and strict ($L_c = 0$) connection is quantified. From equation (9) follows (with $M_c = ED_c$):

$$d\epsilon_{ED_c} \stackrel{(a)}{=} d\epsilon_{ED}^{(1)(b)} = d\epsilon_{ED}^{(2)} \quad (12)$$

This condition (12) expresses that in the strictly connected system only movements are feasible in which the connected tendons have the same displacement (excursion). For further use, such movements will be called *iso-excursion movements*, bearing in mind that the iso-excursion applies to the connected tendons only. Substitution of (1.c) in (12.b) gives the resulting coupling in finger movement:

$$r_{E1} d\theta_1^{(1)} + r_{M2} d\theta_2^{(1)} = r_{E1} d\theta_1^{(2)} + r_{M2} d\theta_2^{(2)} \quad (13)$$

In the following five different problems will be investigated, each illustrating different aspects of the iso-excursion movements.

Problem [(U, U), (k, k)] [Fig. 5(a)]. Both fingers are initially lifted in an identical position ($i_1 = i_2$ or $\theta_{0j}^{(1)} = \theta_{0j}^{(2)}$, $j = 1 \dots 3$), and they have to perform the identical tasks of lifting the finger ($p_1 = p_2 = k$). Such problems, i.e. problems in which the initial positions and the tasks are identical for both fingers, will be further called *unimodal problems*.

Solution. The obvious way to solve an unimodal problem ($p_1 = p_2$) is by an *unimodal solution* ($s_1 = s_2$). Since then holds that $d\theta_j^{(1)} = d\theta_j^{(2)}$ ($j = 1 \dots 3$), condition (13) [or most generally condition (9)] is satisfied whatever the joint rotations $d\theta_j$. The physical interpretation is that when both fingers move in an identical way, no relative displacement of the connected tendons occurs (the fingers being of equal dimension, which we assumed), and the connection merely displaces together with the tendons without causing any restriction of movement.

Problem [(U, U), (k, l)] [Fig. 5(b)]. Initially, both fingers are lifted with all joints extended ($\theta_{0i}^{(i)} = 0$,

$j = 1 \dots 3$, $i = 1, 2$). From this position, F_1 has to strike a key, while F_2 has to solve the identity problem (i.e. maintain its lifting height $h_{tip}^{(2)} \geq H$).

Solution. In order to be able to strike the key, F_1 must flex in at least one joint. To allow this, the common motor ED_c must displace distally, say by a quantity: ϵ_{ED_c} . Hereby the extensor tendon $ED_c^{(2)}$ of the coupled finger F_2 will follow the displacement of the common motor ED_c , while remaining taut as expressed by condition (1c). This poses the problem of how to distribute the distal displacement ϵ_{ED_c} of the common motor over the joints of finger F_2 , while maintaining its lifting height ($h_{tip}^{(2)} \geq H$). Within the model, the problem is formulated as follows: from the initial positions (i_1, i_2), produce the end positions (e_1, e_2), such that:

$$h_{tip}^{(2)} - h_{tip}^{(1)} \geq H \quad (14)$$

(hereby is $h_{tip}^{(1)} = h_{key}$), while satisfying condition (13). The problem is solved in the appendix. It is found that an infinity of feasible solutions exists, one of which is presented in Fig. 5(b). However, characteristic for all solutions is that the lifted finger F_2 shifts into a collapse position (Leijnse *et al.*, 1992), i.e. an intrinsic-minus-like position with a hyperextended MCP and a severely flexed PIP. The reason for this can be physically understood. The distal displacement ϵ_{ED_c} of tendon $ED_c^{(2)}$ due to the distal displacement of the ED_c will cause flexion in either or both the MCP and PIP of F_2 . The loss of height of the finger tip is greater when the MCP flexes, than when the PIP flexes. Therefore, to minimise the loss of height, the displacement ϵ_{ED_c} must be taken up entirely by the PIP. Relative to the position thus obtained, the lifting height can be increased by hyper extending the MCP. This can be realised by flexing the PIP further than strictly required to take up ϵ_{ED_c} , thus creating a shortage of length in the extensor tendon which drives the MCP into hyper extension. Hereby tendon length is transferred from the MCP to the PIP (Leijnse *et al.*, 1992).

For further use, the change of position of F_2 during the key stroke of F_1 will be called a '*conjoined movement*'. Conjoined movements can generally be defined as follows. Take a problem $p = (p_1, p_2, \dots)$ in which some fingers, but not all, have to solve an identity problem. Then conjoined movements in a solution $s = (s_1, s_2, \dots)$ are any changes in the positions ($d\theta_j^{(i)} \neq 0$) of fingers F_i of which the individual problems p_i are identity problems.

As is clear from the example, conjoined movements result from the fact that the connected tendons (i.e. the common motor M_c) have a non-zero displacement. This non-zero displacement requires the simultaneous coordination of all connected fingers even if the problem itself is essentially monodigital (only one finger solves a non-identity problem), as in the present example. Note that in the example the conjoined movement is necessary to obtain a solution. This illustrates that finger problems exist for which the

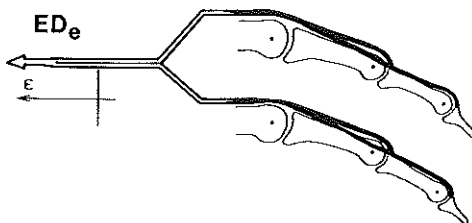


Fig. 4. Model of the bidigital system with connected extensors.

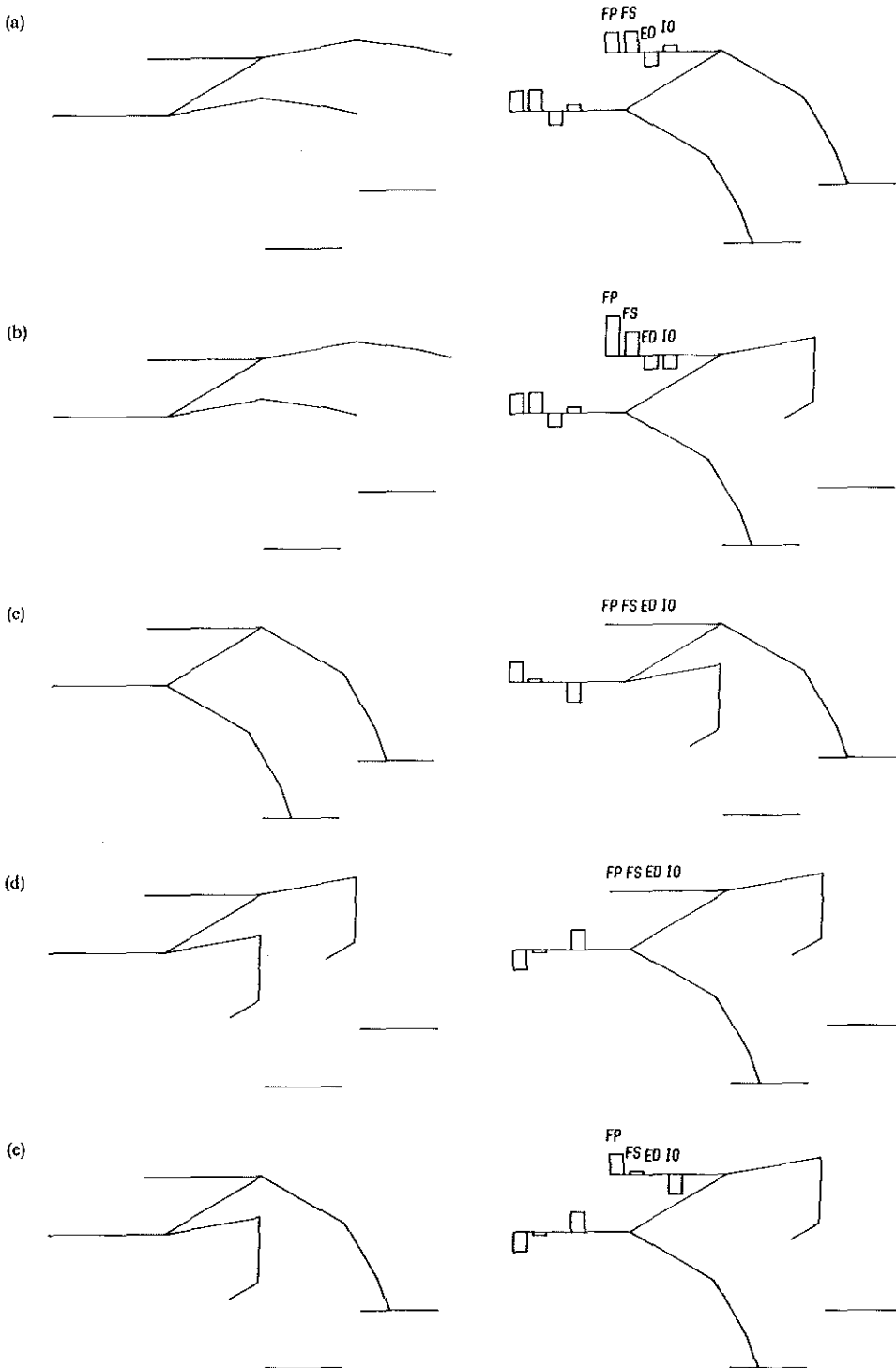


Fig. 5. Movements of the bidigital system with connected extensors: (a) Unimodal solution to the problem $[(U, U), (k, k)]$; (b) Iso-excursion solution to the problem $[(U, U), (k, l)]$; (c) Isometric solution to the problem $[(D, D), (l, k)]$; (d) Isometric solution to the problem $[(U, U), (k, l)]$; (e) Isometric solution to the inverse-symmetric problem $[(U, D), (k, l)]$.

feasible solutions in the connected system are inherently more complex than in the unconnected system, where monodigital problems can always be solved by monodigital solutions, i.e. by moving just one finger.

Problem $[(D, D), (l, k)]$ [Fig. 5(c)]. The initial position of both fingers is the end position of the striking finger in the previous solution. From this position, F_1 has to lift while F_2 must solve the identity problem of keeping its key down.

Solution. As stated above, conjoined movements occur as a result of the non-zero displacement of the connected motors (i.e. the common motor M_c). This implies, however, that the conjoined movements can be avoided by using movements in which the common motor M_c does not displace (i.e. is isometric). In Leijnse *et al.* (1992) it was shown that it is possible to lift the finger from the piano key to a sufficient height while keeping a tendon isometric. The resulting solution for present problem, i.e. the lifting of the finger with an isometric ED_c , is depicted in Fig. 5(c). For further use, such solutions will be called *isometric solutions*, bearing in mind that the isometric displacement is with the common motor.

Problem $[(U, U), (k, l)]$ [Fig. 5(d)]. The second problem of this section [Fig. 5(b)] is now considered again, but with the initial position (i_1, i_2) of both fingers equal to the collapse end position of finger F_1 in Fig. 5(b). From this position, F_1 has to strike a key, while F_2 has to remain lifted.

Solution. Any conjoined movement of F_2 can be avoided when F_1 strikes the key with an isometric ED_c . This key stroke movement exists as the kinematic inverse of the lifting movement in the previous solution [Fig. 5(c)]. The result is presented in Fig. 5(d).

Problem $[(U, D), (k, l)]$ [Fig. 5(e)]. This problem is presented to demonstrate the special nature of the isometric solution in the multidigital finger system with connected tendons. The initial positions are the end positions of the previous solution [Fig. 5(d)]. From these positions finger F_1 , initially lifted, strikes a key, while F_2 , initially on the keyboard, must lift. In other words, the individual problem of each finger is the inverse of the problem of the other finger. To indicate this basic symmetry, this problem will be further called the *inverse-symmetric problem*.

Solution. From the given initial positions, solutions are possible with a (limited) non-zero displacement ϵ_{ED_c} , positive or negative, of the common motor ED_c . Hereby the end position of the finger which lifts will always be a collapse position (see Appendix). However, of all the possible solutions, only the isometric solution (with $\epsilon_{ED_c} = 0$) reflects the basic symmetry of the problem in the sense that the fingers solve their individual problems, which are each others inverse, with solutions that are also each others exact inverse (as $e_1 = i_2$ and $e_2 = i_1$).

Application: the 'thrill' on the piano as a sequence of inverse-symmetric problems. Consider a 'thrill' on the piano. This is a sequence (or 'chain') of inverse-symmetric problems in which each problem is the inverse of the predecessor. This problem chain can be completely solved by the isometric solution for the starting problem and its exact inverse [interchange the digits in Fig. 5(e)]. Hereby the symmetry of the problem chain is reflected in the solution chain. Non-isometric solutions cannot generate solution chains with the same degree of symmetry. This is because the non-zero displacement (ϵ_{M_c}) of the common motor M_c in the solution of the starting problem will have to be inverted ($-\epsilon_{M_c}$) in the solution of the next (inverse) problem, otherwise the displacement of the M_c would keep increasing as the problem chain is executed. These symmetry/asymmetry properties have implications on the level of control. When the problem chain is executed very fast, as in a thrill on the piano, a solution chain that has the same symmetry as the problem chain should be simpler to execute than a less symmetric chain. Therefore it can be speculated that in the real hand with strictly connected tendons ($L_c = 0$), chains of inverse-symmetric problems will tend to be solved by isometric solutions.

The bidigital system with strictly connected flexor tendons

In this section, the bidigital system with strictly ($L_c = 0$) connected flexor tendons (FS, FP) is considered. Substitution of equation (1a) or (1b) into equation (9) with $M_c = F_c$ (F stands for either the FS or the FP) produces the condition imposed by the connection on the movements of the connected fingers:

$$\sum_{j=1}^{n_{F_1}} r_{F_1} d\theta_j^{(1)} - d\sigma_{F_1}^{(1)} = \sum_{j=1}^{n_{F_2}} r_{F_2} d\theta_j^{(2)} - d\sigma_{F_2}^{(2)} \quad (15)$$

The case of connected flexors is fundamentally different from the case of connected extensors, because the finger can still function properly when one of the flexors is slack, while it cannot do so with a slack extensor. When the ED is slack, the free-moving finger is uncontrollable at the MCP, for which the ED is the only extensor. However, the flexors can partly substitute each other, as expressed by condition (1f). For instance, when the FP is slack, the proximal two joints of the finger can be properly coordinated by the FS, ED and IO —be it that the position of the \hat{DIP} cannot be controlled. Conversely, when the FS is slack, the finger can be properly coordinated by the FP, ED and IO . Therefore, when a flexor tendon of one finger is connected with a flexor tendon of the other, three kinds of finger movements must be considered, i.e. the movements in which (i) both connected tendons are taut, (ii) both connected tendons are slack (meaning that the common motor is inactive) and (iii) one connected tendon is taut, and one is slack.

(i) *Movements with both connected flexor tendons taut* ($\sigma_F^{(1)} \equiv \sigma_F^{(2)} = 0$). When both connected flexor ten-

dons are taut, the case is similar to the ED-connected case. Only iso-excursion solutions are feasible, with the mentioned important applications for the *unimodal*, and *isometric* solutions (no conjoined movements).

(ii) *Movements with both connected flexor tendons slack* ($\sigma_F^{(1)}, \sigma_F^{(2)} \neq 0$). When all connected flexor tendons are slack (in other words, when the common motor is inactive), the connection also will be slack and therefore inactive as a constraint. The fingers will then move unconstrained as if the connections were not present at all. In other words, when the connected flexors are not used at all, the coupling between the finger actions, as resulting from the connection, does not become manifest. Consequently, movements with inactive (slack) connected flexors will be further called *decoupling solutions*. In these solutions, however, the fingers will function with the disadvantages resulting from the non-use of the connected motors. For instance, in the case of FP tendons connected with each other, the DIP remains uncontrollable when the FP is inactive. In the FS connected case, when the FS is inactive, the PIP will lack flexion force.

(iii) *Movements with one connected flexor tendon taut and one slack*. When one flexor tendon is taut (say in F_1), the other finger (F_2) may execute unconstrained any movement as long as its connected flexor is slack ($\sigma_{F_2}^{(2)} \geq 0$). However, this finger (F_2) will hereby function with the disadvantages resulting from the non-use of this tendon $T_c^{(2)}$.

The initial positions of the fingers as determining factors of a solution

The initial positions of the fingers determine to a large extent the kind of solutions that can be used. For example, in the problem of Fig. 5(b) an isometric solution is not feasible because from the initial positions (extended fingers) the striking finger cannot reach the key except if the common motor, the ED_c, is allowed a non-zero distal displacement.

The movements of fingers with tendons connected with connections of non-zero length ($L_c > 0$)

In this section, connections of non-zero length ($L_c > 0$) are investigated, with the focus on the effect on finger function of the initial position of the constraint [parameter ΔL_0 in equations (4) and (5)]. Hereby ΔL_0 is defined with respect to a "neutral position" of the fingers, being that in which both fingers are in identical positions ($\theta_j^{(1)} = \theta_j^{(2)}$, $j = 1 \dots 3$, with all tendon parts taut. Two cases are compared. In the first case the connection is taut ($\sigma_c = 0$) in the neutral position, meaning that $\Delta L_0 = L_c$ [from equation (5) with $\sigma_c = \Delta \epsilon_{T_c} = 0$] and in the other the connection is maximally slack ($\sigma_c = L_c$) in the neutral position, meaning that $\Delta L_0 = 0$ [from equation (5) with $\sigma_c = L_c$ and $\Delta \epsilon_{T_c} = 0$].

(i) *Movements with the connection taut in the neutral position* ($\sigma_{c_0} = 0$). When the connection is taut with the fingers in the neutral position, the functioning of

the bidigital system is asymmetric. This may be formally demonstrated as follows. When in a bidigital problem $p = (p_1, p_2)$ the digits are interchanged (to produce the mirror problem p' with $p'_1 = p_2$ and $p'_2 = p_1$), the interchanging of the digits in a random solution $s = (s_1, s_2)$ of p will not result in a feasible solution s' (with $s'_1 = s_2, s'_2 = s_1$) of p' , except when this solution is an iso-excursion solution ($\Delta \epsilon_{T_c} = 0$). In other words, the mirror image of any solution in which the connection becomes slack cannot be applied to solve the mirror problem p' . This asymmetry is illustrated by the fact that two superimposed taut connections of opposite orientation (see paragraph 3 of "displacement properties of connected tendons" in methods and materials) allow only movements in which [from equation (4)]:

$$\left. \begin{aligned} T_{c_p}^{(1)} T_{c_d}^{(2)} &\rightarrow -2L_c \leq \Delta \epsilon_{T_c} \leq 0 \\ T_{c_p}^{(2)} T_{c_d}^{(1)} &\rightarrow 0 \leq \Delta \epsilon_{T_c} \leq 2L_c \end{aligned} \right\} \Rightarrow \Delta \epsilon_{T_c} = 0 \tag{16}$$

which is the isoexcursion condition as resulting from a connection of zero length [$L_c = 0$ in equation (5)].

(ii) *Movements with the connection maximally slack in the neutral position* ($\sigma_{c_0} = L_c$). In contrast, when the connection is initially maximally slack ($\Delta L_0 = 0$) with the fingers in the neutral position, a symmetrical functioning system results. Formally, when in the problem $p = (p_1, p_2)$ the digits are interchanged (problem p' with $p'_1 = p_2$ and $p'_2 = p_1$), the interchanging of the digits in any solution $s = (s_1, s_2)$ of p will result in a feasible solution s' (with $s'_1 = s_2, s'_2 = s_1$) of p' . Moreover, the corresponding phases of s and s' will be constrained in exactly the same way.

Application: the pianistic 'thrill' with $L_c \neq 0$. In the above example of the pianistic thrill the symmetry relationships between chains of inverse-symmetric problems and their solutions were investigated for connections of zero length between tendons ($L_c = 0$). In this paragraph these relationships are investigated for connections of non-zero length ($L_c \neq 0$).

(i) In the asymmetric system ($\sigma_c = 0$ in the neutral position) holds the systemic condition for symmetric functioning: $\Delta \epsilon_{T_c} = 0$, which means that only iso-excursion solutions can be "mirrored" to solve a problem p and its mirror problem p' ($p'_1 = p_1, p'_2 = p_2$). However, under this condition the system functions identically to the system with connections of zero length [see equation (8)]. The requirement of having a symmetric solution chain for the inverse-symmetric problem chain of the pianistic thrill puts an additional condition of symmetry on these iso-excursion movements, i.e. that the end position of one finger should equal the begin position of the other and *vice versa* ($e_1 = i_2$ and $e_2 = i_1$). Within the class of the iso-excursion solutions, this condition can only be satisfied by the isometric solutions ($\epsilon_{M_c} = 0$). It follows that under the given demands for symmetry, the bidigital system with taut connections of non-zero length in the neutral position behaves identically to the system with connections of zero length.

(ii) On the other hand, in the symmetric system with the connection maximally slack ($\sigma_c = L_c$) in the neutral position, any solution of an inverse-symmetric problem can be inverted to solve the inverse problem, because the slack range (5) of the connection is symmetric.

It follows that, in addition to its length L_c , the orientation of a connection is an important parameter in the functioning of the multifinger system with connected tendons.

Extensible connections between tendons ($dL_c \neq 0$)

When the connection is taut and extensible [$dL_c \neq 0$ in equation (7)], the relative displacements $\Delta \varepsilon_{T_c}$ of the connected tendons can be increased by the use of force:

$$dF_c = k dL_c = k \cdot \text{sign} [\Delta \varepsilon_{T_c} - \Delta L_0]_{\sigma_c=0} \cdot d\Delta \varepsilon_{T_c} \quad (17)$$

with $\sigma_c = 0$, k the stiffness of the connection, and F_c the force by which it is stretched. In that case, movements that would be inhibited if the connection were inextensible, may be executable with effort. Clearly, the stiffer the connections are (by build, or by the fact that they become stretched to their limits), the more their functioning will be similar to the inextensible connections.

DISCUSSION

Anatomical connections within the muscles of the fingers

The results obtained in this study show that interconnections between tendons of different fingers cause limitations in the movements of these fingers. These limitations in movement are of the same nature as the limitations caused by restrictions on the displacements of the tendons of the individual finger, as studied in Leijnse *et al.* (1992). Although the present paper only models connections between tendons, other anatomical causes of restricted multidigital finger movement have been pointed out, e.g. by Kaplan (1965), whose views are discussed in this section.

Kaplan notes that the (extrinsic) motors of the fingers originate from muscle groups in which the muscle parts running to the individual tendons do not always form independent muscle bellies. Often, these muscle parts are anatomically strongly interconnected, so that the displacements of these parts relative to each other are limited. Kaplan describes an experiment in which he electrically activates a muscle part, and observes that the connected muscle parts are pulled with it. Although Kaplan does not state so explicitly, from this description two main causes of functional dependency between muscle parts to individual fingers may be outlined. The first is anatomical interconnections, as muscle parts are interconnected by connective tissues. The second may be called 'co-innervation': in the poorly individualised muscle group it cannot be excluded that muscle fibres insert-

ing in one tendon are motorically conjointly innervated with the muscle part of another tendon. As Kaplan observed, dependencies within the muscle will produce similar effects as the (inextensible) connections between tendons studied in this paper. When one muscle part contracts, or is pulled distally by its tendon, the connected parts must follow this displacement; if they do not, this displacement is inhibited. However, since dependencies within the muscle are to be considered extensible (muscles or connective tissues can be stretched), their effects may be to a degree amendable by the use of force, as indicated in the results [equation (17)].

Clearance of anatomical connections

The idea of surgically removing connections between tendons, in order to obtain greater finger independence, is not new (Kaplan, 1965; Forbes, 1991; McGregor and Glover 1988). The results of this paper indicate that such a procedure is in principle viable, as it would facilitate or allow the execution of finger movements otherwise difficult or inexecutable. Clinically, the clearance of well-defined connections between tendons may be feasible. However, the clearance of connections within the muscle may not be feasible. The problem then is, as Kaplan (1965) stated, that the isolated clearance of the connections between the tendons will merely leave the fingers independent up to the level of the muscle.

It is therefore important to know the exact connective structure within the muscle-tendon groups. This may be investigated by the testing of finger function. However, it hereby holds that when constraints of varying extensibility are simultaneously present, the lesser constraints will be masked by the stiffer and stricter, and can only be detected within the slack range of the latter. Therefore, it is difficult or impossible [as e.g. in the case of inextensible connections of zero length between tendons ($L_c \rightarrow 0$)] to obtain by mere function tests complete information about the connections within the musculotendinous apparatus.

Finger independence and exercise

The limited ability to execute finger movements is frequent in musicians and is known as lack of finger independence. Because it is disturbing in the playing of the instrument, exercises have been devised to overcome it. Many of these exercises have the specific purpose of increasing the net range of finger independence (i.e. the maximal amplitude of relative motion between the fingers), and attempt this by forcing the fingers, in one way or another, to exceed their normal range of independent movement. However, since finger independence is ultimately determined by the relative displacements possible between the motors, the real purpose of such exercises is to increase the relative motor displacements. Hereby it is questionable whether stiff tendinous connections or connections within the muscle can be significantly and permanently stretched by such procedures. If this is not the case, exercises of this kind are useless, the more so since

they may in their excess damage the musculotendinous apparatus.

A pedagogy tailored to the musicians hand

The above discussion suggests that anatomical variations in the hand are systemic parameters, more or less invariant to exercise. In this view, each hand has unique functional characteristics, determined by its unique anatomical built. This perception cautions against too strict a concept of the 'ideal' instrumental technique. Especially in piano playing, many attempts have been made to formulate such a codex (of the 'ideal' key stroke, the 'ideal' hand position, etc.). However, from the discussion follows that the results of these investigations cannot properly be applied without taking into account the anatomic parameters of the individual hand. Within the view of the hand as a constrained and invariant system, the purpose of exercise can only be the selection and assimilation of the most functional movements compatible with the (anatomic) constraints, and paedagogic models should be flexible enough to be of guidance at the level of the individuals' possibilities.

CONCLUSION

In this paper, the effect on the motion of a bidigital system of tendons connected with each other is exhaustively studied. It is found that connections between tendons restrict the movements of the connected fingers in typical ways, e.g. by causing conjoined movements of the fingers, as tendons of one finger pull with them tendons of the other. These characteristic phenomena may be observed in the real hand, and are known by the musician as lack of finger independence. It can therefore be concluded that anatomical connections between tendons decrease finger independence. As an important result, it is shown that the conjoined movements may be avoided in finger movements in which the connected tendons are isometric. Further, it is indicated that the clearance of stiff anatomical constraints between tendons does not guarantee that in the real hand finger independence or control will improve, because similar handicaps may be caused by other anatomical constraints, as may be present within the muscle itself. Lastly, the study questions

$$\begin{aligned}
 h_{F1p}^{(2)} - h_{F1p}^{(1)} &= -l_1 [\sin(\theta_1^{(2)}) \\
 &= -l_2 [\sin(\theta_1^{(2)} + \theta_2^{(2)}) \\
 &= -l_3 [\sin(\theta_1^{(2)} + \theta_2^{(2)} + \theta_3^{(2)}) \\
 &\geq H
 \end{aligned}$$

whether net finger independence can be substantially increased by exercises, and motivates that pedagogic models of the instrumental technique should take into account the anatomical possibilities of the individual hand.

Acknowledgements—The authors wish to thank R. Ram-mohan for her valuable contribution.

REFERENCES

Austin, G. J., Leslie, B. M. and Ruby, L. K. (1989) Variations of the flexor digitorum superficialis of the small finger. *J. Hand Surg. (Amer.)* 14A, 262–267.
 Baker, D. S., Gaul, J. S., Jr., Williams, V. K. and Graves M. (1981) The little finger superficialis—clinical investigation of its anatomic and functional shortcomings. *Am. J. Hand Surg.* 374–378.
 Blair, W. F. and Omer, G. E. Jr. (1981) Anomalous insertion of the flexor pollicis longus. *Am. J. Hand Surg.* 6, 241–244.
 Culver, J. E. Jr. (1980) Extensor pollicis and indicis communis tendon: a rare anatomic variation revisited. *Am. J. Hand Surg.* 5, 548–549.
 Fahrer, M. (1971) Considérations sur l'anatomie fonctionnelle du muscle fléchisseur commun profond des doigts. *Ann. Chir.* 25, 945–950.
 Forbes, W. S. (1991) Liberating the ring finger (1885: Annual Report of the Music Teachers' National Association), *Medical Problems of Performing Artists* 6(1), 28–30.
 Kaplan, E. B. (1965) *Functional and Surgical Anatomy of the Hand* (2nd Edn), pp. 66–86. Pitman Medical Publishing, London.
 Leijnse, J. N. A. L., Bonte, J. E., Landsmeer, J. M. F., Kalker, J. J., van der Meulen, J. C. and Snijders, C. J. (1992) Biomechanics of the finger with anatomical restrictions: the significance for the exercising hand of the musician. *J. Biomechanics* 25, 1253–1264.
 Linburg, R. M. and Comstock, B. E. (1979) Anomalous tendon slips from the flexor pollicis longus to the digitorum profundus. *Am. J. Hand Surg.* 4, 79–83.
 Materich, M. M., Baird, R. A., McMaster, W. and Erickson, J. M. (1987) Permissible limits of flexor digitorum profundus tendon advancement: an anatomic study. *Am. J. Hand Surg.* 12A, 30–33.
 McGregor, I. A. and Glover, L. (1988) The E-flat hand. *Am. J. Hand Surg.* 13A, 692–692.
 Parrot, J. R. and Harrison, D. B. (1980) Surgically dividing pianists' hands (Letter to the editor). *Am. J. Hand Surg.* 5, 619.
 Spoor, C. W. (1983) Balancing a force on the fingertip of a two dimensional finger model without intrinsic muscles. *J. Biomechanics* 16, 497–504.
 Verdan, C. (1960) Syndrome of the quadriga. *Surg. Clin. North Amer.* 40, 425–426.
 Von Schroeder, H. P., Botte, M. J., Gellman, H. (1990) Anatomy of the juncturae tendinum of the hand. *Am. J. Hand Surg.* 15A, 595–602.

APPENDIX

The solutions to the problem [(U, U), (k, l)]; connected extensors (ED), fingers initially fully extended [Fig. 5(b)]

The problem is (see Fig. A1)

$$\begin{aligned}
 &-\sin(\theta_1^{(1)}) \\
 &-\sin(\theta_1^{(1)} + \theta_2^{(1)}) \\
 &-\sin(\theta_1^{(1)} + \theta_2^{(1)} + \theta_3^{(1)})
 \end{aligned} \tag{A1}$$

with the condition that

$$r_{E1} d\theta_1^{(1)} + r_{M2} d\theta_2^{(1)} = r_{E1} d\theta_1^{(2)} + r_{M2} d\theta_2^{(2)} \tag{A2}$$

with

$$\theta_4^{(i)} = \theta_{k0}^{(i)} + \Delta\theta_4^{(i)} \tag{A3}$$

We assume all tendon parts taut [$\sigma_p = \sigma_L = 0$ in equation (1)]. Then holds that the rotation of the DIP is coupled to the rotation of the PIP. For this coupling, a linear approximation (Leijnse *et al.*, 1992) is used:

$$d\theta_3^{(i)} = (a\theta_2^{(i)} + b) d\theta_2^{(i)} \tag{A4}$$

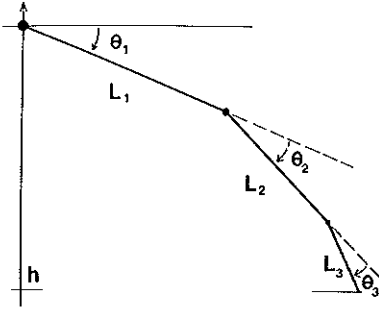


Fig. A1. Parameters of the finger model.

Integration gives

$$\Delta\theta_3^{(2)} = \frac{a}{2} [(\theta_{20}^{(1)} + \Delta\theta_2^{(1)})^2 - (\theta_{20}^{(1)})^2] + b \Delta\theta_2^{(1)}, \quad (A5)$$

while integration of equation (A2) produces (all moment arms are constant):

$$\Delta\theta_2^{(2)} = \frac{r_{E1}}{r_{M2}} [\Delta\theta_1^{(1)} - \Delta\theta_1^{(2)}] + \Delta\theta_2^{(1)}. \quad (A6)$$

The expressions (A5) and (A6) allow the elimination of $\Delta\theta_3^{(1)}$, $\Delta\theta_3^{(2)}$ and $\Delta\theta_2^{(2)}$ from (A1). Further holds that $\theta_{k0}^{(1)} = 0$ ($k = 1 \dots 3$), since initially all joints are fully extended. Under these conditions (A1) becomes

$$\begin{aligned} h_{F_{ip}}^{(2)} - h_{F_{ip}}^{(1)} &= -l_1 [\sin(\Delta\theta_1^{(2)}) - \sin(\Delta\theta_1^{(1)})] \\ &= -l_2 \left[\sin(\Delta\theta_1^{(2)} + \frac{r_{E1}}{r_{M2}} (\Delta\theta_1^{(1)} - \Delta\theta_1^{(2)} + \Delta\theta_2^{(1)}) - \sin(\Delta\theta_1^{(1)} + \Delta\theta_2^{(1)}) \right] \\ &= -l_3 \left[\sin \left\{ \Delta\theta_1^{(2)} + \frac{r_{E1}}{r_{M2}} (\Delta\theta_1^{(1)} - \Delta\theta_1^{(2)} + \Delta\theta_2^{(1)}) + \frac{a}{2} \left(\frac{r_{E1}}{r_{M2}} (\Delta\theta_1^{(1)} - \Delta\theta_1^{(2)} + \Delta\theta_2^{(1)}) \right)^2 \right. \right. \\ &\quad \left. \left. + b \left(\frac{r_{E1}}{r_{M2}} (\Delta\theta_1^{(1)} - \Delta\theta_1^{(2)} + \Delta\theta_2^{(1)}) \right) \right\} - \sin \left\{ \Delta\theta_1^{(1)} + \Delta\theta_2^{(1)} + \frac{a}{2} (\Delta\theta_2^{(1)})^2 + b \Delta\theta_2^{(1)} \right\} \right]. \quad (A7) \end{aligned}$$

Three independent variables remain: $\theta_1^{(1)}$, $\theta_2^{(1)}$ and $\theta_1^{(2)}$. From these $\theta_1^{(2)}$ is physically determined since the lifting height of F_2 increases with the extension of the MCP⁽²⁾. This means that to achieve maximum lifting height the MCP⁽²⁾ must extend up to its functional end position, here taken to be 10° hyper extension. This puts

$$\Delta\theta_1^{(2)} = -10^\circ \quad (A8)$$

and leaves two independent variables: $\theta_1^{(1)}$ and $\theta_2^{(1)}$. From the iso-height curves in Fig. A2, follow the MCP⁽¹⁾ and PIP⁽¹⁾ end positions of the candidate solutions in function of the criterium H. The domain of the feasible solutions is determined by the limit of flexion of the PIP⁽²⁾, which is taken to be 100°:

$$\Delta\theta_2^{(2)} \leq 100^\circ. \quad (A9)$$

Substituting equations (A8) and (A9) into (A6) produces the dashed boundary line of the domain of feasible solutions in Fig. A2.

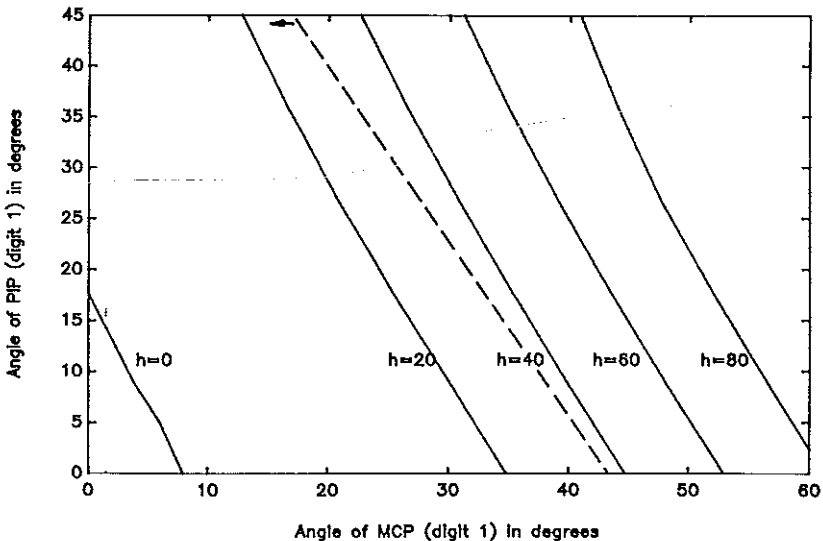


Fig. A2. Solutions to the problem: [(U, U), (k, l)], in the bidigital system with connected extensors. (—) iso-height curves of the finger tip of digit 2. (---) 100° limit of flexion of the PIP of digit 2 [the domain of feasible solutions is indicated by the little arrow (←)].



0021-9290(94)00070-0

A TWO-DIMENSIONAL KINEMATIC MODEL OF THE LUMBRICAL IN THE HUMAN FINGER

J. N. A. L. Leijnse*† and J. J. Kalker‡

*Department of Plastic and Reconstructive Surgery; †Department of Biomedical Physics and Technology, Erasmus University, Rotterdam, The Netherlands; and ‡Department of Mathematics, University of Technology, Delft, The Netherlands

Abstract—The functioning of the lumbrical muscle in the human finger is difficult to visualise. This is mainly due to the fact that the origin and insertion of the lumbrical is on tendons of other motors (the deep flexor and the extensor assembly, respectively), instead of on bone. In this paper the functioning of the lumbrical in the human finger is kinematically investigated by explicitly considering the slackness or tautness of tendon parts which are in parallel or in series with the lumbrical, and by deriving from a standard finger model equivalent representations from which the functioning of the lumbrical is visually more clear. These models are used to review and interpret the results of previous studies. Further, it is indicated that the lumbrical is in an ideal position to contribute to the control of certain fast movements, as may be of importance for the musician, and that its role in other fast movements may be limited because of its large displacements (contraction speed).

NOTATION

MCP	metacarpophalangeal joint
PIP	proximal interphalangeal joint
DIP	distal interphalangeal joint
P	flexor digitorum profundus
S	flexor digitorum superficialis
E	extensor digitorum
I	interosseus
L	lumbrical
M	medial band of extensor, interosseus and lumbrical
T	lateral band of extensor, interosseus and lumbrical
P _p	deep flexor tendon proximal to the insertion of the lumbrical
P _d	deep flexor tendon distal to the insertion of the lumbrical
r _{ij}	anatomic moment arms of the tendons at the resp. joints. The first index denotes the motor. The second index indicates the joint: MCP=1, PIP=2, DIP=3 (see Table 1).
r _{ij} [*]	systemic moment arm of motor <i>i</i> at joint <i>j</i>
ε _M	displacement of motor <i>M</i> (taken positive when contracting)
θ _j	angle of rotation of joint <i>j</i>
σ _T	slack in tendon T

INTRODUCTION

In Leijnse *et al.* (1992), a kinematic four-tendon finger model in which the explicit quantification of the slackness of tendons allowed a concise description of the kinematically feasible and controllable free finger movements was presented. In present paper the lumbrical is implemented in this model. Anatomically, the lumbrical differs from other finger motors through its origin, which is on the tendon of another motor (the

deep flexor) instead of on bone. As such, the lumbrical forms with the deep flexor tendon distal to its origin two parallel systemic parts which are in series with the deep flexor motor. The functioning of this system (the lumbrical–deep-flexor complex) is before all determined by the slackness or tautness of these systemic parts. In the following, these functions are kinematically investigated. Hereby the case with all tendon parts taut, which assumably represents the prime mode of lumbrical functioning, is studied in detail. While the results provide a formal mathematical analysis, the discussion presents a qualitative view based on equivalent finger model representations from which the function of the lumbrical is visually clear. Apart from the analysis of the kinematic properties of the model, central questions investigated are (i) the equivalence of the interosseus and lumbrical in the control of the finger (Thomas *et al.*, 1968; Long, 1968), (ii) the differences in their displacements in a number of well-defined finger movements, (iii) the effect of the lumbrical at the MCP joint, as illustrative to the experiments of Backhouse and Catton (1954), Ranney *et al.* (1987) and Ranney and Wells (1988), (iv) the fast execution of movements with isometric lumbrical or isometric MCP.

The present study provides a quantitative kinematic synthesis of past research on lumbrical function, and presents a simple but comprehensive model for the analysis of the kinematics, or the kinematic impairments of the finger in the sagittal plane.

MATERIALS AND METHODS

The kinematic finger model with lumbrical

In this paper, the two-dimensional kinematic finger model of Leijnse *et al.* (1992):

$$d\epsilon_P = r_{P1}d\theta_1 + r_{P2}d\theta_2 + r_{P3}d\theta_3 - d\sigma_P, \quad (1a)$$

Received in final form 26 May 1994.
 Address correspondence to: J. N. A. L. Leijnse, Department of Biomedical Physics and Technology, Erasmus University, Rotterdam. The Netherlands.

$$d\epsilon_S = r_{S1} d\theta_1 + r_{S2} d\theta_2 - d\sigma_S, \quad (1b)$$

$$d\epsilon_E = -r_{E1} d\theta_1 - r_{M2} d\theta_2 - d\sigma_E, \quad (1c)$$

$$d\epsilon_I = r_{I1} d\theta_1 - r_{M2} d\theta_2 - d\sigma_I, \quad (1d)$$

$$d\theta_3 = \frac{r_{M2} - r_{T2}}{r_{T3}} d\theta_2 - \frac{d\sigma_T}{r_{T3}}, \quad (1e)$$

$$\sigma_E + \sigma_I + (\sigma_P + \sigma_T)\sigma_S = 0, \quad (1f)$$

is expanded with the lumbrical muscle (Fig. 1). The model (1) provides a kinematic description of the movements feasible in the free moving finger in the sagittal plane. The equations describe the changes of length ($d\epsilon_i$) of the motors M_i with the joint rotations ($d\theta_j$). The joint rotations and moment arms are taken positive for flexion. Motor contraction (shortening) is taken positive. The extensor (E), interosseus (I) and lumbrical (L) all join two common end tendons, called the medial (M) and lateral (T) band, which insert in the middle and end phalanx, respectively. Tendons can be slack; this is quantified by the non-negative slack variables σ_i ($\sigma_i \geq 0$). The control equation (1f) states which slacks must be zero for controllable free movement. The parts of the deep flexor (P) proximal and distal to the origin of the lumbrical are further called P_p and P_d , respectively. In the following, distinction is made between 'anatomic' and 'systemic' moment arms. Both moment arms are formally defined by the expression:

$$r_{Xj} = \frac{\partial \epsilon_X}{\partial \theta_j}. \quad (2)$$

With the anatomic moment arms, in expression (2) the displacements ϵ_X are of the tendons X when the joints are considered disjunct parts of the system, and correspond to the anatomic distance between the tendon and the joint axis of rotation. With the systemic moment arms, the displacements are the changes of motor length in well-defined conditions of systemic functioning (e.g. tautness of tendons). When the systemic moment arm differs from the anatomic moment arm, it is written with an asterisk (r_{Xj}^*).

The system equations of the lumbrical are derived as follows. The proximal part of the deep flexor (P) and the lumbrical (L) are two motors in series. The proximal and distal part of the deep flexor (P_p , P_d) are a motor and a fixed tendon length in series. The

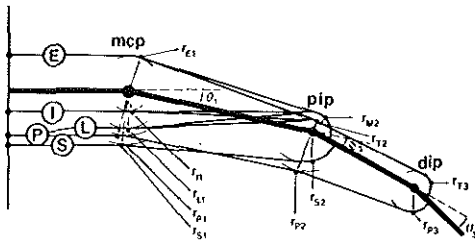


Fig. 1. Model of the finger.

displacement relationships of both system parts are

$$d\epsilon_P + d\epsilon_L = r_{L1} d\theta_1 - r_{M2} d\theta_2 - d\sigma_P - d\sigma_L, \quad (3a)$$

$$d\epsilon_P = r_{P1} d\theta_1 + r_{P2} d\theta_2 + r_{P3} d\theta_3 - d\sigma_P - d\sigma_P. \quad (3b)$$

[Note that in equation (3a) the displacement of the lumbrical at the PIP is equal to the displacements of extensor and interosseus in the model (1) (same insertions), and that this displacement is determined only by the medial band (Leijnse *et al.*, 1992).] The subtraction of expression (3b) from expression (3a), and the substitution the coupling mechanism of the PIP and DIP joint [equation (1e)] in the result and also in the expression (3b), results in the equations (4a) and (4e) of the displacement model of the finger with lumbrical:

$$d\epsilon_P = r_{P1} d\theta_1 + r_{P2}^* d\theta_2 - d\sigma_P^*, \quad (4a)$$

$$d\epsilon_S = r_{S1} d\theta_1 + r_{S2} d\theta_2 - d\sigma_S, \quad (4b)$$

$$d\epsilon_E = -r_{E1} d\theta_1 - r_{M2} d\theta_2 - d\sigma_E, \quad (4c)$$

$$d\epsilon_I = r_{I1} d\theta_1 - r_{M2} d\theta_2 - d\sigma_I, \quad (4d)$$

$$d\epsilon_L = -r_{L1}^* d\theta_1 - r_{L2}^* d\theta_2 - d\sigma_L^* + d\sigma_P^*, \quad (4e)$$

$$d\theta_3 = \frac{r_{M2} - r_{T2}}{r_{T3}} d\theta_2 - \frac{d\sigma_T}{r_{T3}}, \quad (4f)$$

$$\sigma_E + \sigma_P^* \sigma_S + \sigma_L^* \sigma_I = 0, \quad (4g)$$

$$\sigma_i = \sigma_{i0} + \int d\sigma_i \geq 0 \quad \forall i,$$

in which the systemic moment arms r_{L1}^* , r_{L2}^* , r_{P2}^* are given by

$$r_{P2}^* = r_{P2} + \frac{r_{P3}}{r_{T3}} (r_{M2} - r_{T2}), \quad (5a)$$

$$r_{L1}^* = r_{P1} - r_{L1}, \quad (5b)$$

$$r_{L2}^* = r_{M2} + r_{P2}^*, \quad (5c)$$

and the generalised slack variables $\sigma_{P,T}^*$, σ_P^* and σ_L^* by

$$\sigma_{P,T}^* = \sigma_{P,T} + [r_{P3}/r_{T3}] \sigma_T, \quad (6a)$$

$$\sigma_P^* = \sigma_P + \sigma_{P,T}^*, \quad (6b)$$

$$\sigma_L^* = \sigma_P + \sigma_L. \quad (6c)$$

The meaning of these slacks is explained further.

Anatomic data

—In the normal finger, the moment arm of the lumbrical at the MCP is generally smaller, but almost equal to the moment arm of the deep flexor (Brand, 1985). From this it follows that

$$r_{L1}^* = r_{P1} - r_{L1} \geq 0. \quad (7)$$

—During PIP flexion, the lateral band (T) at the PIP shifts palmarly and may even pass to the flexion side of the PIP joint axis (Garcia-Elias *et al.*, 1991). This change in the moment arm r_{T2} determines the relative rate of DIP and PIP rotation in the coupling mechanism of expression (4f). In the stick diagrams of Fig. 4, an acceptable visual result was obtained by

Table 1. Moment arms of the tendons

MCP	r_{P1} 11	r_{S1} 13	r_{E1} 9	r_{I1} 6	r_{L1} 9
PIP	r_{P2} 10.5	r_{S2} 8.5	r_{M2} 5	r_{T2} *	
DIP	r_{P3} 6	r_{T3} 4			

Note. Real values (in mm) used to calculate the results. From: Spoor (1983).

* Function of PIP position, see expression (9).

approximating the moment arm r_{T2} as a second order polynomial of the PIP rotation θ_2 , with the following properties:

$$\begin{aligned} r_{T2} &= r_{M2}; & \theta_2 &= 0, \\ r_{T2} &= 0; & \theta_2 &= \frac{\pi}{2}, \\ \frac{dr_{T2}}{d\theta_2} &= 0; & \theta_2 &= \frac{\pi}{2}. \end{aligned} \tag{8}$$

This leads to

$$r_{T2} = r_{M2} \left[1 - \frac{2\theta_2}{(\pi/2)} + \frac{\theta_2^2}{(\pi/2)^2} \right]. \tag{9}$$

All other moment arms are taken constant; the values used for calculation are given in Table 1.

RESULTS

Motor function as expressed by the slack variables

In this section the functioning of the model as resulting from slackness or tautness of tendon parts is analysed. First the physical meaning of the generalised slack variables is investigated.

The generalised slack variables [expression (6)]. (i) $\sigma_{P,T}^*$: expresses that slack in the P_d and the lateral band T can be exchanged by rotating the DIP (by external action) without altering the position of the PIP. The P_d is therefore only truly taut, in the sense that its tautness fixes the DIP joint, when the lateral band is also taut. Only then the P_d is a functional system element in series with the P_p .

(ii) $\sigma_P^* = \sigma_{Pp} + \sigma_{P,T}^*$: expresses the slackness of the deep flexor, as consisting of P_p and P_d in series.

(iii) $\sigma_L^* = \sigma_{Pp} + \sigma_L$: expresses the slackness of the lumbrical and P_p in series.

The functioning of the lumbrical-deep-flexor complex as determined by the slack variables. Expression (4c) describes the change of length of the loop formed by the lumbrical L and the distal part of the deep flexor P_d in parallel. It contains a sum of slacks of opposite sign, which means that together these slacks can increase indefinitely without any effect on joint position or lumbrical motor length. Physically this corresponds to a displacement of the common origin

of lumbrical and P_d , which changes the slack in both parallel parts with equal quantity. The slacks themselves are the sum of a common series and an individual parallel term (expression (6)). This expresses that equal amounts of slack in both parallel parts ($\sigma_L, \sigma_{P,T}^*$) can be exchanged for an equal amount of slack in the common tendon (σ_{Pp}). The slacks distinguish following systemic functions of the lumbrical-deep-flexor complex:

(i) $\sigma_L^*, \sigma_P^* \neq 0$: deep flexor inactive (e.g. when P_p is cut); no function at all.

(ii) $\sigma_L^* \neq 0, \sigma_P^* = 0$: lumbrical inactive and deep flexor in series with its end tendon: model (1) holds.

(iii) $\sigma_L^* = 0, \sigma_P^* \neq 0$: lumbrical in series with the deep flexor as a digastric motor (further called P_L). Equation (4c) is inactive (the parallel loop of lumbrical and P_d is slack), and the equation (3a) holds (with zero slacks). P_L effectively functions as an interosseus, with a somewhat greater moment arm for the MCP (Long, 1968). For a clinical application, see Parkes (1970).

(iv) $\sigma_L^*, \sigma_P^* = 0$: lumbrical and P_d taut in parallel, and together in series with the taut P_p tendon. This is assumed to be the main mode of functioning of the L-P complex, and is further investigated.

The different motor combinations which allow controlled finger movement. Equations (4) show that the displacements of the finger motors with zero slacks are only function of the proximal two joints (MCP, PIP), which means that the free moving model effectively functions as a bi-articular chain. In this chain, five motors are present, while for full control mathematically three suffice (Spoor and Landsmeer, 1976). Therefore, two motors will be mathematically redundant. In the normal finger the redundancies are with the flexors (P and S), and the intrinsics (L and I). The conditions for flexor redundancy were investigated in Spoor and Landsmeer (1976). The redundancy of the intrinsics is investigated further. These redundancies are expressed in the control equation (4g), which defines the motor combinations which in the normal finger allow controlled finger movement. With the normal redundancy conditions satisfied, these motor combinations are:

(i) $\sigma_P^* = 0$: the {P, E, I or L} control system. When $\sigma_P^* = 0$, the finger can be completely controlled by the motors E, P, I and/or L, i.e. the equations (4a) and (4c)-(4e). These equations are basically identical to the bi-articular model with lumbrical of Thomas *et al.*, (1968).

(ii) $\sigma_P^* \neq 0, \sigma_S = 0$: the {S, E, I or P_L } control system. (a) $\sigma_L^* \neq 0$: With the deep flexor and lumbrical slack, the proximal bi-articular chain of the finger can be controlled by the motors S, E, I, while the DIP remains uncontrolled [equations (4a) and (4c) are inactive].

(b) $\sigma_L^* = 0$: the P_L , i.e. the lumbrical in series with the deep flexor with the P_d slack, may in principle also provide the interosseus function required for the control of the proximal bi-articular chain, resulting in the control system: E, S, P_L (Long, 1968).

The lumbrical-deep-flexor complex with zero slacks

The bi-articular equivalent model of the finger with taut tendons. In equation (4), with zero slacks, the lumbrical is mathematically indistinguishable from a motor with fixed origin. This indicates that it must be possible to represent the model (4) as a bi-articular chain in which the lumbrical originates from the fixed environment, and not from the tendon of the deep flexor. This representation is given in the Fig. 2(a), and is further called the *bi-articular equivalent model*. Fig. 2(a) represents the lumbrical displacements as seen by an observer who sits on the tendon of the deep flexor tendon at the lumbrical origin, and moves with it. This observer notices only displacements at the distal end of the lumbrical, and can explain these displacements as a function of the MCP and the coupled PIP-DIP rotations only by assuming the systemic moment arms as present in the Fig. 2(a).

The systemic moment arms of the lumbrical-deep-flexor complex with taut tendons ($\sigma_L^* = \sigma_P^* = 0$). With respect to the systemic moment arms of the L-P complex, the following statements hold (Fig. 2) :

(1) r_{L1}^* : the lumbrical systemic moment arm at the MCP is of extension, and it is very small [expression

(7)]. When it is zero ($r_{L1}^* = 0$), the lumbrical length is independent of the MCP position (Stack, 1962; Thomas *et al.*, 1968). This means that the lumbrical is effectively a quasi mono-articular finger motor of which the length is almost completely determined by the PIP position. This in contrast with the other finger motors E,P,S,I which are basically bi-articular.

(2) r_{L2}^*, r_{P2}^* : the lumbrical (Thomas *et al.*, 1968) and (to a lesser extent) also the deep flexor (Spoor and Landsmeer, 1976) have huge systemic moment arms (r_{L2}^*, r_{P2}^*) at the PIP joint. These moment arms increase with PIP flexion [fig. 3(a)], because they depend on the variable moment arm r_{T2} [from equations (5a), (5c) and (9)]. This means that displacements of the lumbrical and deep flexor vary non-linearly with PIP rotation [Fig. 3(b)]. In Fig. 2(b) and 2(c) these systemic moment arms are visualised for the extended and the flexed finger, as calculated from expression (9). For the sake of completeness, it may be noted that with finger extension ($\theta_2 \rightarrow 0$), the ratio r_{L2}^*/r_{P2}^* increases [Fig. 3(c)], meaning that when $\theta_2 \rightarrow 0$ the lumbrical extension action at the PIP becomes slightly more efficient relative to the P_4 flexion action.

The mutual redundancy of lumbrical and interosseus in the control of the finger in the sagittal plane. In this section, the conditions for mutual redundancy of the interosseus and the lumbrical in the L-P complex with all tendon parts taut ($\sigma_L^* = \sigma_P^* = 0$) are derived. Assume the finger in a non-specified position with all tendon parts taut, and replace the lumbrical by a taut and inextensible rope. In this position, keep the motors of either the motor triplet E,P,I or the motor triplet E, P, L isometric. It then holds that the finger is controllable by such a motor triplet when, while keeping the motors isometric, it is not possible to rotate (by external action) any joint. Under the above conditions only joint rotations are feasible which cause slack in tendons, as the tendons are inextensible and initially taut. The feasibility of such rotations would indicate that the slackened motors can contract without causing elongation of any other motor. This means that the resulting movement has no antagonists and that it is irreversible, and therefore that the finger cannot be properly controlled. To check this, the set of equations

$$\begin{aligned} r_{P1} d\theta_1 + r_{P2}^* d\theta_2 - d\sigma_P &= 0, \\ -r_{E1} d\theta_1 - r_{M2} d\theta_2 - d\sigma_E &= 0, \\ r_{X1}^* d\theta_1 + r_{X2}^* d\theta_2 - d\sigma_X &= 0, \end{aligned} \tag{10}$$

is solved for $d\theta_j$, with the condition that the slacks must be positive: $d\sigma_P, d\sigma_E, d\sigma_X \geq 0$ (X stands for either L or I). This set has a non-trivial solution when the determinant is zero, i.e. when

$$\begin{aligned} (r_{P1} r_{X2}^* - r_{P2}^* r_{X1}^*) d\sigma_E + (r_{X1}^* r_{M2} - r_{X2}^* r_{E1}) d\sigma_P \\ + (r_{E1} r_{P2}^* - r_{M2} r_{P1}) d\sigma_X = 0. \end{aligned} \tag{11}$$

When in the expression (11) the coefficients of the slacks are strictly positive, the slacks must be zero ($d\sigma_i = 0$), and the rank of the moment arm matrix in

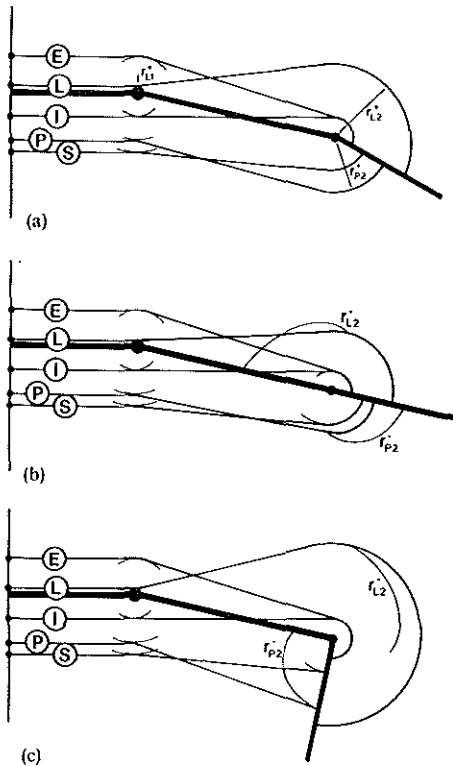


Fig. 2. (a) Bi-articular equivalent finger model; (b) systemic moment arms of lumbrical and deep flexor in extension; (c) systemic moment arms of lumbrical and deep flexor in flexion.

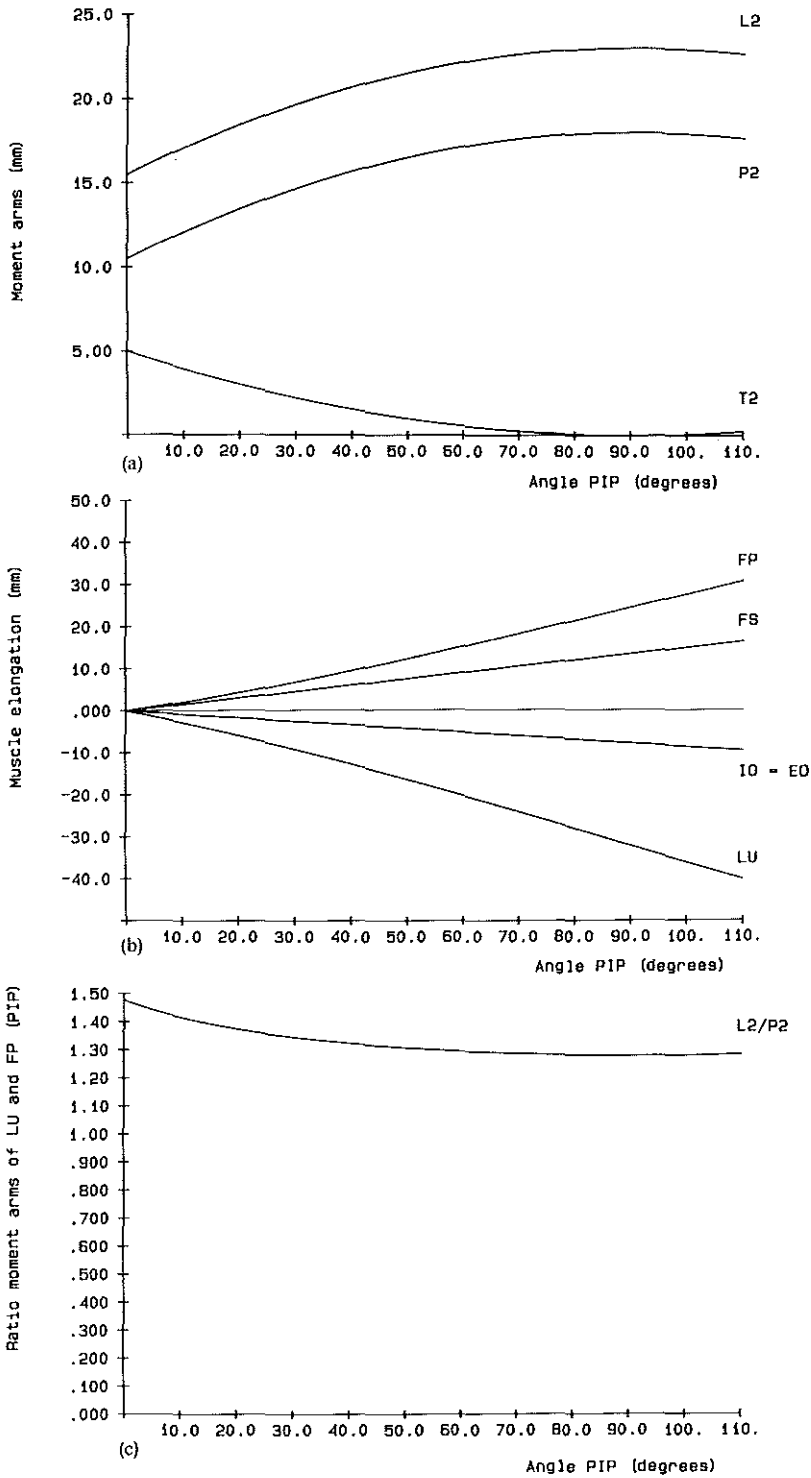


Fig. 3. Systemic moment arms as calculated from Table 1 and expression (9): (a) systemic moment arms as a function of the PIP position. T: lateral band, P: deep flexor, L: lumbrical; (b) muscle displacements as a function of the PIP position; (c) ratio of the systemic moment arms r_{L2}^*/r_{P2}^* as a function of the PIP position.

expression (10) is equal to two. Expression (10) then only allows the zero solution ($d\theta_i = 0$), meaning that no joint can be moved without elongation of tendons, and that the chain is controllable. The positivity of the slack coefficients leads to the following conditions:

$$\frac{r_{E1}}{r_{P1}} - \frac{r_{M2}}{r_{P2}^*} > 0 \quad (12a)$$

$$\frac{r_{I1}}{r_{E1}} + \frac{r_{M2}}{r_{M2}} > 0 \quad (12b)$$

$$\frac{r_{I1}}{r_{P1}} + \frac{r_{M2}}{r_{P2}^*} > 0 \quad (12c)$$

$$\frac{r_{L2}^*}{r_{M2}} - \frac{r_{L1}^*}{r_{E1}} > 0 \quad (12d)$$

$$\frac{r_{L2}^*}{r_{P2}^*} - \frac{r_{L1}^*}{r_{P1}} > 0 \quad (12e)$$

The expressions (12b) and (12c) correspond to $X = I$ and the expressions (12d) and (12e) to $X = L$ while the expression (12a) holds for both the lumbrical and the

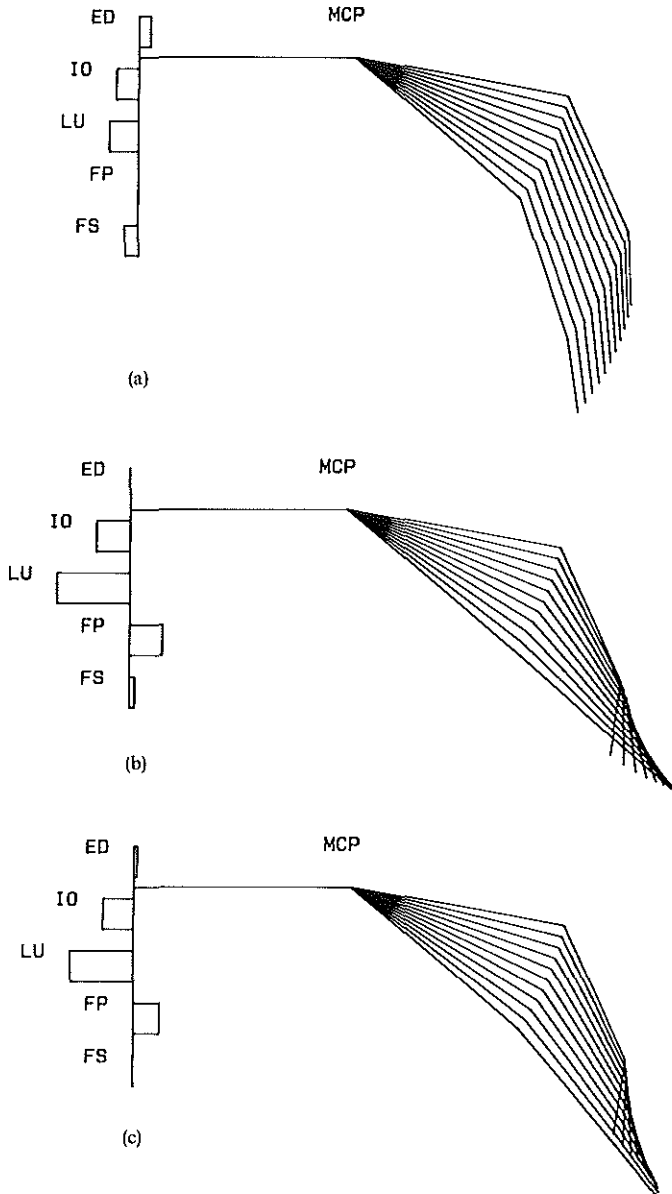


Fig. 4(a-c).

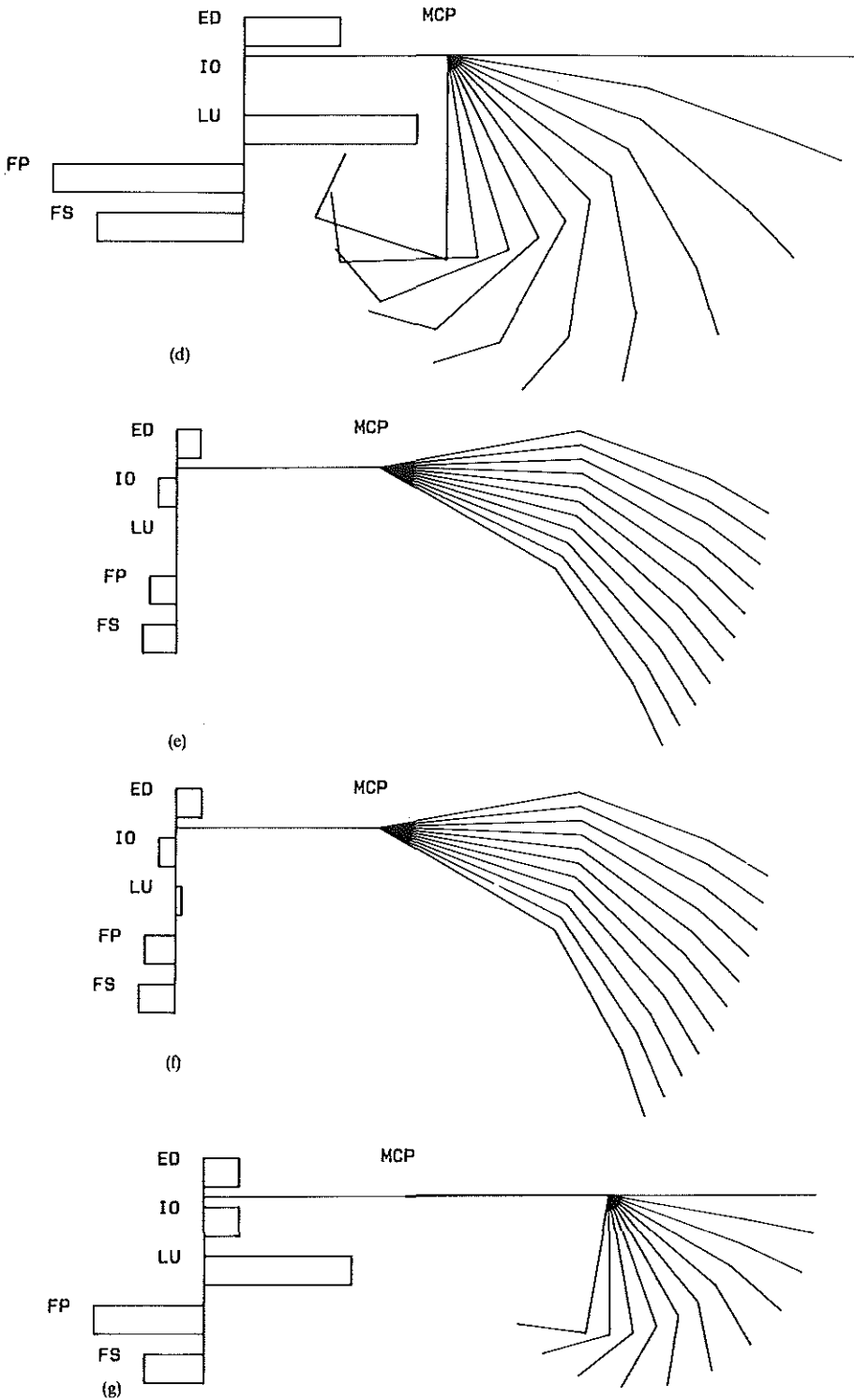


Fig. 4. Finger movements and displacements, calculated from Table. 1 and expression (9): (a) isometric deep flexor; (b) isometric extensor; (c) isometric superficial flexor; (d) isometric interosseus; (e) isometric lumbrical; (f) isometric PIP; (g) isometric MCP.

interosseus as it contains only the moment arms of extensor and deep flexor (the extrinsics). This condition (12a) is satisfied in the normal finger, as $r_{E1} > r_{M2}$, and $r_{P1} < r_{L2}^*$. Conditions (12b) and (12c) for the interosseus are satisfied because all terms are positive. Conditions (12d) and (12e) for the lumbrical hold because $r_{L2}^* \gg |r_{L1}^*|$, and $r_{E1} > r_{M2}$. It thus follows that, when $\sigma_L^*, \sigma_P^* = 0$, the interosseus and lumbrical in the normal finger are mathematically mutually redundant. This was also concluded by Thomas *et al.* (1968) from a force model.

The displacements of lumbrical and interosseus in some basic finger movements. Even though in the two-dimensional finger model with all tendons taut ($\sigma_L^*, \sigma_P^* = 0$) the interosseus and lumbrical are mutually redundant, their systemic moment arms greatly differ:

$$\begin{aligned} |r_{L1}^*| &\ll r_{L1}, \\ r_{L2}^* &\gg r_{M2}, \end{aligned} \quad (13)$$

which implies that the way in which they effectuate their mathematically equivalent functions may also be quite different. This is investigated by calculating the motor displacements in the finger movements generated by keeping alternately one motor or joint isometric [as in Leijnse *et al.* (1992)].

Finger movement with isometric deep flexor ($d\varepsilon_P = 0$). With the deep flexor taut and isometric [$d\varepsilon_P = 0$, $\sigma_P^* = 0$ in expression (4a)], the feasible joint rotations and the relative displacements of lumbrical and interosseus are (with r_{L1} the anatomic moment arm) [Fig. 4(a)]:

$$\begin{aligned} d\theta_1 &= -\frac{r_{P2}^*}{r_{P1}} d\theta_2, \\ d\varepsilon_I &= \frac{r_{L1}r_{P2}^* + r_{M2}r_{P1}}{r_{L1}r_{P2}^* + r_{M2}r_{P1}} d\varepsilon_L. \end{aligned} \quad (14)$$

Figure 4(a) shows that with isometric deep flexor the MCP flexes and the PIP extends when the interosseus or lumbrical contract. From equation (14) it follows that their displacements differ only to the degree that $r_{L1} > r_{L1}$. Physically this is easily understood. With isometric deep flexor, the lumbrical origin is fixed, and can be imagined on the metacarpals, just as the interosseus. As the tendons of the interosseus and lumbrical are almost identical (the only difference being: $r_{L1} > r_{L1}$), their displacements are also almost equal.

Isometric extensor ($d\varepsilon_E = 0$); *isometric superficial flexor* ($d\varepsilon_S = 0$). With the extensor or the superficial flexor isometric, with all tendon parts taut, the joint rotations [see Fig. 4(b) and 4(c)] are, respectively, given by

$$d\theta_1 = -\frac{r_{E2}}{r_{E1}} d\theta_2, \quad d\theta_1 = -\frac{r_{S2}}{r_{S1}} d\theta_2. \quad (15)$$

Isometric interosseus ($d\varepsilon_I = 0$). With an isometric interosseus, the joint rotations and motor displacements [Fig. 4(d)] are given by

$$d\theta_1 = \frac{r_{M2}}{r_{I1}} d\theta_2, \quad (16a)$$

$$d\varepsilon_L = -\frac{r_{L1}^*r_{M2} + r_{L2}^*r_{I1}}{r_{I1}} d\theta_2, \quad (16b)$$

$$d\varepsilon_P = \frac{r_{P1}r_{M2} + r_{P2}^*r_{I1}}{r_{I1}} d\theta_2, \quad (16c)$$

$$d\varepsilon_E = -\frac{r_{E1}r_{M2} + r_{E2}r_{I1}}{r_{I1}} d\theta_2. \quad (16d)$$

From equations (16a) and (4f), it follows that in this movement all joints extend or flex together, as in the opening and closing of the hand (fist). While the displacement of the interosseus is zero, the displacements of all other motors, including the lumbrical, are maximal. Clearly, in this movement the functioning of interosseus and lumbrical is completely different. The interosseus acts as a tenodesis, while the lumbrical maximally contracts or extends.

Isometric lumbrical ($d\varepsilon_L = 0$). With the lumbrical isometric and all tendon parts taut, the joint rotations and motor displacements are [Fig. 4(e)]:

$$\begin{aligned} d\theta_2 &= -\frac{r_{L1}^*}{r_{L2}^*} d\theta_1, \\ d\varepsilon_P &= \frac{r_{P1}r_{L2}^* - r_{P2}r_{L1}^*}{r_{L2}^*} d\theta_1, \\ d\varepsilon_E &= \frac{-r_{E1}r_{L2}^* + r_{M2}r_{L1}^*}{r_{L2}^*} d\theta_1, \\ d\varepsilon_I &= \frac{r_{I1}r_{L2}^* + r_{M2}r_{L1}^*}{r_{L2}^*} d\theta_1. \end{aligned} \quad (17)$$

Figure 4(e) shows that in this movement the PIP is quasi isometric.

Isometric PIP ($d\theta_2 = 0$). The quasi isometry of the PIP in movements with isometric lumbrical is illustrated by the fact that the small approximation of putting the systemic moment arm $r_{L1}^* = r_{P1} - r_{L1}$ equal to zero ($r_{L1}^* = 0$) in expression (17) results in a finger movement with a strictly isometric PIP [Fig. 4(f)]:

$$\begin{aligned} d\theta_2 &= 0, \\ d\varepsilon_P &= r_{P1} d\theta_1, \\ d\varepsilon_E &= -r_{E1} d\theta_1, \\ d\varepsilon_I &= r_{I1} d\theta_1. \end{aligned} \quad (18)$$

In other words, with $r_{L1}^* = 0$ and the lumbrical isometric, the distal joints (PIP and DIP) are fixed ($d\theta_2 = d\theta_3 = 0$), while the displacements of the other motors move only the MCP. In the Fig. 4(f) the displacement of the lumbrical is as in a finger with isometric PIP and normal r_{L1}^* value.

Isometric MCP ($d\Theta_1 = 0$). The movement of PIP rotation with immobile MCP is presented in Fig. 4(g). Notice that in this movement the displacement of the lumbrical is the largest of all motors.

DISCUSSION

The lumbrical loop

The systemic moment arm r_{L1}^* of the lumbrical at the MCP is small. Therefore, the functioning of the lumbrical will not be substantially altered when this moment arm is assumed zero ($r_{L1}^* = 0$), as in the Fig. 5(a) and 5(b). The lumbrical origin may then be shifted distal to the MCP without any effect on function, as in the Fig. 5(c) and 5(d) [in Fig. 5(c) a pulley is introduced to keep the tendons on a longitudinal course]. The equivalent representations of these figures in Fig. 5(e) and 5(f) clearly illustrate that the lumbrical-deep flexor complex consists of three systemic parts: (i) the lumbrical, (ii) the part P_p of the deep flexor proximal to the lumbrical origin, and (iii) the part P_d of the deep flexor distal to the lumbrical origin. Hereby the lumbrical and the P_d form a closed loop around the distal two joints, which is kept taut by the P_p . This construct may be explored as follows.

First, assume the lumbrical to be a rope of fixed length; the MCP immobile (arthrodised); and the L- P_d loop slack. When the deep flexor (P_p) then shortens, the attachment of the lumbrical loop displaces proximally, thus removing equal slackness in both sides of the loop until either the lumbrical rope or the P_d tautens. As the P_p further shortens, the PIP-DIP joints will extend or flex, depending on which part of the loop is taut, until the other part of the loop also tautens. At that point, the PIP-DIP joints become locked, since further shortening of the P_p would require them to flex and extend at the same time. This phenomenon can be appreciated from the equivalent model of Fig. 5(d): when the lumbrical and the deep flexor are taut, the equivalent PIP joint is blocked.

When the MCP is now rotated up and down (say, by manually moving the proximal phalanx) while the P_p is kept taut, the lumbrical loop will remain taut and the distal joints will remain stably fixed, even if the P_p elongates or shortens because of its displacement at the MCP. No changes of length within the lumbrical loop occur because this loop does not cross the MCP, which means that the PIP-DIP positions are independent of the MCP movement.

When the MCP is let free, with the P_p taut, the extensor E must tauten to control the MCP at the extension side. When the conditions (12) hold, the extensor will not disturb the position of the distal joints, and the lumbrical loop will remain taut.

EPL-MCP rotation

From the above, it follows that when the lumbrical loop is taut and of constant length, the distal finger is a rigid entity, and the finger is only mobile at the

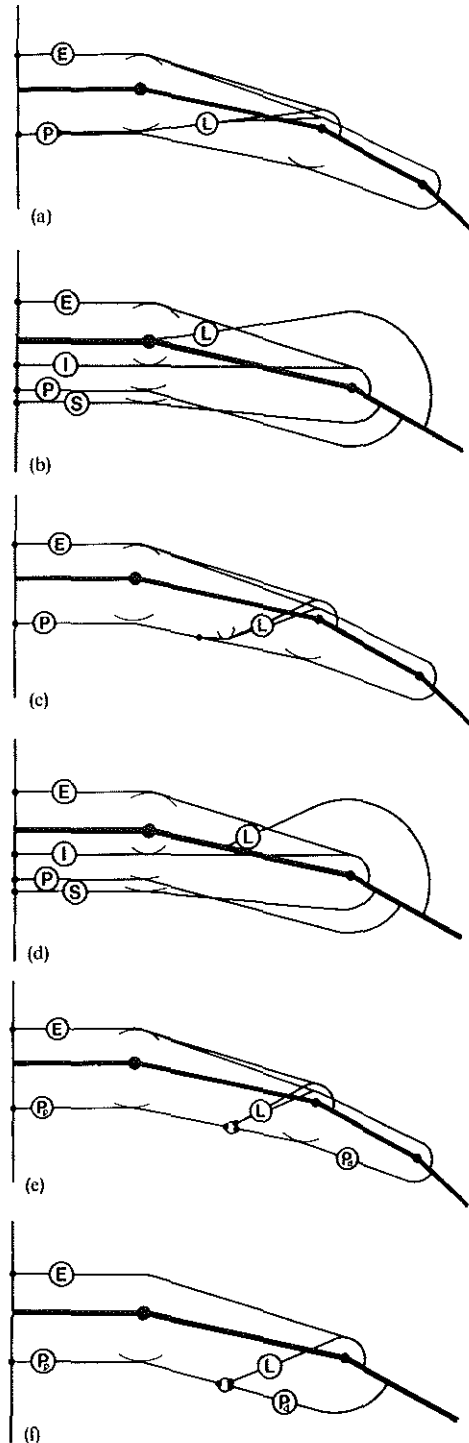


Fig. 5. (a) Finger model with $r_{L1}^* = 0$; (b) bi-articular equivalent model of Fig. 5(a); (c) finger model with lumbrical origine distal to the MCP; (d) bi-articular equivalent model of Fig. 5(c); (e) the lumbrical loop; (f) bi-articular equivalent of Fig. 5(e) (with r_{E2}^* and r_{L2}^* constant).

MCP. At this joint, the deep flexor and extensor form an antagonistic motor pair which can rotate (oscillate) the entire rigid finger as a simple one-joint-two-tendon unit. Hereby the condition of tautness of the lumbrical loop required to lock the distal joints equals the condition of tautness of the P_p required for flexion control of the MCP. The EPL-MCP rotation movement corresponds to the expression (18), and Fig. 4(f).

Lumbrical control of the position of the distal joints

The position of the PIP-DIP joints is determined by the relative lengths of the flexion (P_d) and extension (L) part of the lumbrical loop. To change the PIP-DIP position, it suffices to change the length of one part of the loop relative to the other part. A lengthening of the lumbrical slackens the extension side of the loop, and when the P_p shortens to keep the loop taut, the PIP-DIP joints flex until the lumbrical is taut again. Conversely, the shortening of the lumbrical pulls the P_p distally and slackens the P_d , causing the distal joints to extend until the P_d is taut again.

The effects of changes in lumbrical length on the MCP position

The lengths of the other bi-articular motors are not independent of the length of the lumbrical. Changes in lumbrical length cause changes in the position of the distal joints, which result in shortages or excesses of length in the motors which cross these joints. Since for proper finger control these motors must remain taut, these excesses or shortages of length must be corrected, and the way in which this is done determines the total finger movement. The first two movements of Fig. 4 may serve as an illustration, when interpreted as resulting from lumbrical shortening. In the first example [Fig. 4(a)], the P_p remains isometric, while the extensor lengthens despite excess length produced by the extending distal joints, since its distal displacement at the MCP is greater. In the second movement [Fig. 4(b)], the extensor is isometric, while the P_p lengthens to accommodate the shortage of length created by the extending distal joints.

The experiments of Backhouse and Catton, and Ranney et al.

In the experiments of Backhouse and Catton (1954), and Ranney *et al.* (1987), the lumbrical is made to contract against the real (Backhouse) or simulated (Ranney) elastic forces of the other finger motors. Hereby it was invariably noted that simultaneous MCP flexion, and PIP-DIP extension occurred. These results were explained in Ranney *et al.* (1987) and Ranney and Wells (1988) as due to the interaction of the lumbrical with the elastic forces of the bi-articular extrinsic motors (E, P, S) of the finger. To illustrate their argument further, especially the effect of isolated lumbrical contraction on the MCP, the experiments of Ranney *et al.* (1987) are imaginarily repeated with the model of Fig. 5(d). Notice that in this model the lumbrical has no direct effect on the MCP, as it does not cross this joint.

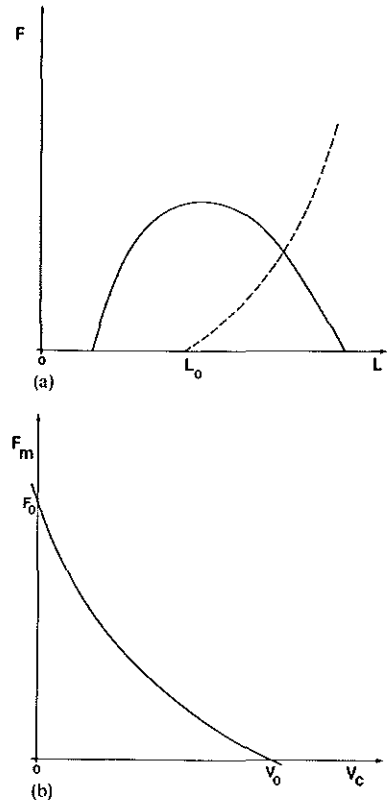


Fig. 6. (a) Elastic force (---) and maximal active force (—) length relationship of a muscle; (b) maximal force-contraction speed (F_m - v_c) relationship of a muscle.

Assume the finger motors with their normal physiological elastic properties [Fig. 6(a)], and the finger in the resting position. While keeping the MCP externally fixed, let the lumbrical in Fig. 5(d) contract. As described above, this contraction will extend the PIP joint, thus creating an excess of length in the extensor, which leads to a shortening of the extensor and a decrease in its elastic pull. Meanwhile, the deep flexor is stretched by the extending PIP joints, and its elastic pull is increased. The lumbrical contraction thus results in a net flexion moment at the MCP. Therefore, when let free this joint will flex, thereby increasing and decreasing the length (and the elastic pull) of the extensor and the flexor, respectively, until it is balanced again. The resulting movement will be quasi identical to the movements in the experiments of Ranney *et al.*, the only difference resulting from the approximation $r_{L1}^* = 0$. This shows that even if the lumbrical in Fig. 5(d) has no direct effect on the MCP, its action will flex this joint through the coupling of the MCP-PIP joint rotations by the bi-articular motors. The resulting movement will be some average of the movement with isometric P and isometric E (Fig. 4(a) and 4(b), respectively), i.e. with flexing MCP and extending PIP, and with both the extensor and deep flexor a bit elongated.

The mutual redundancy of the lumbrical and interosseus in the Landsmeer model

An illustration to the above discussion is the interpretation of the mutual redundancy of the lumbrical and interosseus within the three-tendon bi-articular model of Spoor and Landsmeer (1976), which focusses on the coupling of the MCP-PIP rotations by the extrinsics (flexor and extensor). The flexor and extensor span both joints as antagonists, and their simultaneous actions result in a collapse (zigzag movement) of the chain. This movement cannot be reversed by these two motors (since they cause it), meaning that for complete control of the chain a third motor is required, which is capable of reversing this zigzag. The conditions (12) may be interpreted from this point of view. Condition (12a) only contains the moment arms of the flexor and extensor, and asserts that the zigzag movement is with extending MCP and flexing PIP. The other expressions (12b) and (12c), or (12d) and (12e) provide the ranges of the moment arms of the lumbrical and interosseus which allow these motors to reverse the zigzag. These expressions allow for a wide variability in the moment arms of the lumbrical and interosseus which still allow effective finger control:

$r_{M2} = 0$: mono-articular interosseus,
 $r_{I1} = 0$: bi-articular interosseus with zero MCP moment arm,
 $r_{L1}^* = 0$: mono-articular lumbrical, as in Fig. 5(d),
 $r_{I1} < 0$, with $|r_{I1}| < (r_{P1}/r_{P2}^*) r_{M2}$: interosseus shifted to the extension side of the MCP, etc.

Whatever their appearance, all these variations produce an equal effect: the reversal of the joint rotations as resulting from extrinsic action. A mono-articular interosseus will achieve this by antagonising the extension of the MCP in the zigzag, while a mono-articular lumbrical will do so by opposing the flexion of the PIP. The collapse antagonist may even be a zigzag agonist at one joint, as long as it antagonises the movement of the other joint to a greater extent, as is the case with an interosseus with $r_{I1} < 0$ (i.e. with a moment arm of extension at the MCP) and $|r_{I1}| < (r_{P1}/r_{P2}^*) r_{M2}$. With respect to the experiments of Ranney *et al.* (1987), it follows that in the free moving finger all motors satisfying expression (12) will produce a movement of simultaneous MCP flexion and PIP extension (albeit of different degree) as the inverse of the simultaneous MCP extension and PIP flexion of the extrinsic zigzag, even if e.g. their (systemic) moment arms at the MCP are of extension, as is the case with the lumbrical in the human finger.

The lumbrical as PIP-DIP position proprioceptor

The role of the lumbrical as a proprioceptor of the position of the distal joints has been pointed out, on the basis of its anatomic position and the extent of its proprioceptive innervation (Rabichong, 1962; Ranney and Wells 1988; Stack, 1962). The above discussion conforms with this view, as (i) the lumbrical length is quasi independent of the MCP position, while (ii) the very large systemic moment arm r_{L2}^* allows for good

conditioned measurement, as small rotations of the PIP-DIP joint mechanism correspond to large lumbrical displacements. The latter point also holds to a somewhat lesser extent for the deep flexor.

Fast movements with isometric lumbrical ($d\epsilon_{L1} = 0$) and isometric MCP ($d\theta_1 = 0$)

In fast movements, physiological constraints which limit execution speed become active, such as the 'maximal muscle force-contraction speed' ($F-v$) relationship [Fig. 6(b)]. The lumbrical displacements in movements with large PIP-DIP rotations are considerable, because of the large systemic moment arm r_{L2}^* . Since the lumbrical is also a weak motor, the physiological ($F-v$) constraint may limit effective lumbrical function when such movements are executed fastly. In the following two movements are compared from this point of view: (i) the movement with isometric lumbrical, and (ii) the movement with isometric MCP.

Isometric lumbrical [Fig. 4(e)]. In the movement with isometric lumbrical (EPL-MCP rotation) the lumbrical contraction speed is zero, and the physiologically applicable lumbrical force is maximal. The displacements of the other motors serve only to control the MCP trajectory, as the isometric lumbrical loop blocks the distal joints, and the finger functions basically as a mono-articular joint. Such a movement has the aspect of being easily controllable in the fast execution: only one joint trajectory must be effectively controlled, and as none of the motor displacements is large, no motor in particular will be subjected to the ($F-v$) constraint. With respect to application, such a control strategy seems well apt as a basis for e.g. a fast key stroke in playing of piano.

Isometric MCP [Fig. 4(g)]. In the flexion/extension movement of the distal finger (PIP-DIP joints) with isometric MCP ($d\theta_1 = 0$), the lumbrical displacement approaches the physiological maximum, and exceeds that of any other motor [Fig. 4(g)]. Therefore, in the fast execution, the ($F-v$) constraint should be most active in the lumbrical. This implies that the amplitude of the PIP oscillation, when lumbrical controlled, should decrease with speed, and/or that the interosseus must provide support. It can also be noticed that the isometry of the MCP ($d\theta_1 = 0$) is the result of a strict relationship between the simultaneous non-zero displacements of minimally three motors (E, P, I or L). This may indicate that this movement requires a greater coordinative effort than the EPL-MCP rotation, in which the (quasi-) isometry condition $d\theta_2 = 0$ corresponds to the isometry condition of a single motor: $d\epsilon_{L1} = 0$.

Movements with isometric MCP or PIP in the real finger: some intuitive experimental evidence

Some direct experimental evidence about the existence of the EPL-MCP rotation strategy in the human finger may be obtained by executing a fast pianistic 'thrill', or a fast tapping with a single finger on the table. The reader may notice that such movement is

well executable with (quasi) isometric PIP-DIP joints. Hereby the relative 'stiffness' of the immobile distal finger does not appreciably influence the mobility of the MCP [the independence of MCP mobility and lumbrical activity was noted in the EMG studies of Backhouse and Catton (1954) and Long and Brown 1964]. This movement may be compared with the movement of PIP-DIP flexion/extension with isometric MCP [during this movement, the MCP joint should not be in a position of hyper-extension, as in such position the volar ligaments are taut (functional end-position), and the model (4) does not apply anymore]. When slowly executed, the PIP-DIP flexion/extension movement is unproblematic and well controllable. However, with increasing execution speed, it is generally more difficult to keep the MCP immobile, and/or to maintain a large amplitude of PIP-DIP flexion/extension. On the whole, most subjects tested at our department found that keeping the MCP immobile with fast PIP-DIP flexion/extension movements required greater effort than keeping the distal joints immobile during MCP rotations with isometric PIP-DIP joints.

The coupled action of lumbrical and interosseus in the finger with bi-axial MCP joint

In the real finger, the MCP is bi-axial (flexion/extension, abduction/adduction), and the moment arm of the lumbrical for the abduction/adduction axis of the MCP is non-zero. This means that the actions of the lumbrical (radial abduction) and the contralateral interosseus (ulnar abduction) are coupled by the abduction-adduction equilibrium condition of the MCP. Therefore, in the real finger the lumbrical and the interossei are not entirely mutually redundant; as any lumbrical action necessarily implies (some) ulnar interosseus activity.

General constraints on fast movements in the hand of the musician

The above discussion suggests that not all feasible finger movements can be executed fast, because of physiological and coordinative constraints which become active when movements are speeded up. In the real hand, other constraints on movement are possible, such as the limitations on tendon displacements as resulting from anatomic connections between tendons (Leijnse *et al.*, 1992, 1993). These anatomic constraints may further limit the feasible fast movements in the individual hand, the more so since they may cause slack in tendon parts on which systemic lumbrical function depends.

CONCLUSION

In this paper the functioning of the lumbrical is studied in a kinematic model which describes the feasible movements of the freely moving finger in the

sagittal plane. To this end, a standard finger model is represented in equivalent forms from which lumbrical function is visually more clear. From the kinematic equations and the equivalent models, the following statements about lumbrical function can be verified.

The lumbrical-deep-flexor complex consists of the deep flexor proximal to the lumbrical origin in series with two parallel elements: the lumbrical and the deep flexor tendon distal to the lumbrical origin. The functioning of the lumbrical depends critically on the slackness or tautness of these three tendon parts. Hereby the distal deep flexor tendon is systemically taut only when the lateral band of the extensor assembly is also taut. On the basis of tendon slacks, the following functions can be distinguished:

(a) When the part of the deep flexor proximal to the lumbrical origin is slack, the lumbrical loses its fixation, and any effective function.

(b) When the tendon of the deep flexor distal to the lumbrical origin is slack, the lumbrical and the deep flexor motor form a single (digastric) motor, which is systemically equivalent to an interosseus with a slightly greater moment arm at the MCP joint.

(c) With all mentioned tendon parts taut, the following statements hold:

—the lumbrical forms with the distal deep flexor tendon a loop enclosing and able to control the PIP and DIP joints, which coordinate as a mechanism. The length of this loop is quasi independent of the MCP position, and the lumbrical effectively functions as a dedicated controller of the position of the distal two joints. Hereby it has a very large systemic moment arm of extension for the PIP-DIP mechanism.

—in the two-dimensional model, the lumbrical and the interosseus provide mathematically the same function, and are therefore mutually redundant. However, their displacements in movements may be quite different, as e.g. when making a fist: in that case the interosseus is quasi isometric, while the lumbrical elongates maximally.

—the systemic moment arms of the deep flexor and lumbrical for the PIP-DIP-mechanism increase with PIP flexion, because they are function of the variable moment arm of the lateral band at the PIP joint.

—the lumbrical is in an optimal position for proprioceptive feedback on the position of the PIP-DIP joint mechanism because of its large systemic moment arm for this mechanism, and its very small systemic moment arm at the MCP.

—the effect of the lumbrical on the MCP results basically from the coupling of the MCP-PIP joint rotations by the bi-articular finger motors (extrinsics).

—with the PIP/DIP position controlled by the lumbrical loop, the MCP joint (in the sagittal plane) can be controlled by only the extensor and deep flexor.

—with isometric lumbrical, the distal joints are fixed and the finger can be controlled at the MCP by the extensor and deep flexor as a simple one-joint-two-tendon structure. This movement may be of

importance as a basis of fast movements in e.g. the musicians' hand.

Acknowledgements—The authors cordially thank J. M. F. Landsmeer, C. J. Snijders, J. C. Van der Meulen, S. E. R. Hovius and G. J. Sonneveld for their valuable contributions.

REFERENCES

- Backhouse, K. M. and Catton, W. T. (1954) An experimental study of the functions of the lumbrical muscle in the human hand. *J. Anat.* **88**, 133–141.
- Brand, P. W. (1985) *Clinical Mechanics of the Hand*, C. V. Mosby, St. Louis, p. 285.
- García-Elias, M., An, K. N., Berglund, L., Linscheid, R. L., Cooney W. P. and Chao E. Y. S. (1991) Extensor mechanism of the fingers. I. A quantitative study. *J. Hand Surg.* **16A**, 1130–1136.
- Leijnse, J. N. A. L., Bonte, J. E., Landsmeer, J. M. F., Kalker, J. J. and Van Der Meulen, J. C., Snijders, C. J. (1992) Biomechanics of the finger with anatomical restrictions: the significance for the exercising hand of the musician. *J. Biomechanics* **25**, 1253–1264.
- Leijnse, J. N. A. L., Snijders, C. J., Bonte, J. E., Landsmeer, J. M. F., Kalker, J. J., Van Der Meulen, J. C., Sonneveld, G. J. and Hovius, S. E. R. (1993) The hand of the musician: the kinematics of the bidigital finger system with anatomical restrictions. *J. Biomechanics* **26**, 1169–1179.
- Long, C. (1968) Intrinsic-extrinsic muscle control of the fingers. *J. Bone Jt Surg.* **50A**, 973–984.
- Long, C. and Brown, M. E. (1964) Electromyographic kinematics of the hand: muscles moving the long finger. *J. Bone Jt Surg.* **46A**, 1683–1706.
- Parkes, A. (1970) The "lumbrical plus" finger. *Hand*, **2** (2) 164–165.
- Rabischong, P. (1962) L'innervation Proprioceptive des muscles lombricaux de la main chez l'homme. *Revue Chir. Orthopedique* **48**, 234–245.
- Ranney, D. A., Richard, P. W. and Dowling, J. (1987) Lumbrical function: interaction of lumbrical contraction with the elasticity of the extrinsic finger muscles and its effect on metacarpophalangeal equilibrium. *J. Hand Surg.* **12A**, 566–575.
- Ranney, D. and Wells, R. (1988) Lumbrical muscle function as revealed by a new and physiological approach. *Anat. Rec.* **222**, 110–114.
- Spoor, C. W. (1983) Balancing a force on the fingertip of a two dimensional finger model without intrinsic muscles. *J. Biomechanics* **16**, 497–504.
- Spoor, C. W. and Landsmeer, J. M. F. (1976) Analysis of the zigzag movement of the human finger under influence of the extensor digitorum tendon and the deep flexor tendon. *J. Biomechanics* **9**, 561–566.
- Stack, G. H. (1962) Muscle function in the fingers. *J. Bone Jt Surg.* **44 B**, 899–909.
- Thomas, D. H., Long II, C. and Landsmeer, J. M. F. (1968) Biomechanical considerations of lumbricalis behaviour in the human finger. *J. Biomechanics* **1**, 107–115.

CHAPTER II

FORCE MODELS AND INDETERMINATE PROBLEMS

A graphic analysis of the biomechanics of the massless bi-articular chain

J.N.A.L. Leijnse

To be published in J. Biomechanics, 1995

The controllability of the unloaded finger with superficial or deep flexor

J.N.A.L. Leijnse

Resubmitted to J. Biomechanics, 1995

Why the lumbrical muscle should not be bigger - a force model of the lumbrical muscle in the unloaded human finger

J.N.A.L. Leijnse

Being revised for J. Biomechanics

A GRAPHIC ANALYSIS OF THE BIOMECHANICS OF THE MASSLESS BI-ARTICULAR CHAIN - APPLICATION TO THE PROXIMAL BI-ARTICULAR CHAIN OF THE HUMAN FINGER

J.N.A.L. Leijnse ^{F§}

^(F)Department of Plastic and Reconstructive Surgery, ^(§)Department of Biomedical Physics and Technology, Erasmus University, Rotterdam, The Netherlands.

ABSTRACT

In this paper a model is presented which visualises the biomechanical functioning of the loaded and unloaded three-tendon bi-articular chain. This model allows to graphically determine in any position of the chain (i) the exact ranges of loads which can be sustained by the different motors; (ii) the motor forces; (iii) the feasibility of the (unloaded) equilibrium; and (iv) the conditions for the good controllability of the bi-articular chain. These results are applied to the proximal three-motor bi-articular chain of the human finger, when controlled by the superficial flexor, interosseus, and extensor only. It is shown that (i) the anatomic position of the superficial flexor and extensor is a prime determinant in the good functioning of this chain; (ii) the proximal bi-articular chain of the human finger can well sustain certain (flexion) loads but is structurally weak for extension loads; and (iii) the chain is not optimally controllable.

NOMENCLATURE

- MCP, PIP: : metacarpophalangeal joint, proximal interphalangeal joint of the finger.
- F : (force in the) flexor
- E : (force in the) extensor
- I : (force in the) interosseus
- Θ_j : angle of joint j (j=1,2 for MCP and PIP, resp.)
- r_{Mj} : moment arm of motor M at joint j.
- v_{Kj} : moment arm of load vector **K** at joint j.
- \mathbf{R}_M : moment arm vector of motor M, with cartesian coordinates (r_{M1}, r_{M2}) .
- \mathbf{V}_K : moment arm vector of load **K**, with cartesian coordinates (v_{K1}, v_{K2}) .
- $\mathbf{K} \cdot \mathbf{u}_K$: modulus and unit vector of load $\mathbf{K} = \mathbf{K} \cdot \mathbf{u}_K$.
- $\mathbf{u}_F, \mathbf{u}_E, \mathbf{u}_I$: unit load vectors of the flexor, extensor and interosseus, resp.
- L_1, L_2 : length of first and second phalanx.
- ϕ : angle of the distal phalanx and the load vector \mathbf{u}_K .

Vector notations and expressions

- The scalar value representing the magnitude and direction (positive or negative) of the vector product $\mathbf{R}_i \times \mathbf{R}_j$ is indicated between brackets:

$$[\mathbf{R}_i \times \mathbf{R}_j] = r_{i1} \cdot r_{j2} - r_{i2} \cdot r_{j1} \quad (1)$$

- A "non-negative sum" of two vectors $a_1 \cdot \mathbf{R}_1 + a_2 \cdot \mathbf{R}_2$ is with $a_1, a_2 \geq 0$. "positive sum" is with $a_1, a_2 > 0$.

INTRODUCTION

The functioning of motors in a bi- or multi-articular chain is difficult to analyse because the motors simultaneously affect each joint they span. In 1955, Landsmeer provided a massless and frictionless bi-articular model to explain the control of the unloaded proximal bi-articular three-tendon chain of the human finger - later mathematically reformulated by Spoor and Landsmeer (1976), and further discussed in Leijnse and Kalker (1995). The Landsmeer model considers as the basis of control of the bi-articular chain the combined actions of two motors (the extensor and the flexor, clinically called "extrinsic" motors), which cause the chain to collapse irreversibly. A third motor able to reverse this collapse is sufficient for complete control of the chain. The Landsmeer model provides a useful theoretical explanation of clinical phenomena, such as the claw-hand and the swan-neck deformity. However, it also presents some conceptual and practical limitations. Conceptually, it describes bi-articular control as the balance of the actions of a motor pair (the extrinsics) with respect to a single third motor (the interosseus, clinically called an "intrinsic" motor), i.e. the "extrinsic-intrinsic balance". However, a comprehensive control model should be symmetric, in the sense that where it is possible to distinguish an "intrinsic-extrinsic" balance, for the same reasons an extensor/interosseus-flexor balance, or a flexor/interosseus-extensor balance, or a mere three-tendon balance may also be distinguished. Moreover, controllable bi-articular chains without "Landsmeer extrinsics" exist, i.e. in which no two tendons cross two joints at opposite sides. In that case the model cannot be applied. Another limitation is that the model only describes the functioning of the unloaded chain. More practically, the Landsmeer model is a kinematic (displacement) model, which implies that while its functioning is well demonstrable in physically moving models, it cannot be well visualised in a textbook, where the formulation of the results in mathematical expressions makes their appreciation by the clinician difficult. The present paper attempts to remedy the limitations outlined above, and presents a model which (i) covers both the loaded and unloaded bi-articular chain, (ii) is completely graphically representable, and (iii) describes motor functioning in a symmetric way, i.e. without any assumption about the position of tendons. The model is based on the static torque equilibrium equations of the two joints. For the unloaded chain, the torque equations and the Landsmeer displacement model contain the same parameters (the moment arms of the motors at the different joints) and are therefore equivalent, as discussed in Spoor and Landsmeer (1976). The force model, however, also includes loaded situations. Moreover, it can be graphically analysed from two two-dimensional vector diagrams. These diagrams are obtained by associating with each motor or load two two-dimensional vectors (the *moment arm vector*, and the *load vector*) which together completely describe the effects of the motor or load. Since vectors are abstract entities, this representation effectively reveals the symmetry in the functioning of the motors. The diagrams are: (i) the "*moment arm vector diagram*", which allows to determine the motor forces and the feasibility of equilibrium, and (ii) the "*load vector diagram*", from which the loads which can be balanced by any two motors can be obtained as a function of the finger position. The diagrams are further used to define the general conditions on the loadability and the controllability of bi-articular chains. As an illustration, these conditions are investigated in the proximal bi-articular chain of the finger, when controlled by three motors: the interosseus, the extensor, and the

superficial flexor. For the reader with a theoretical interest the present model is discussed with respect to the results of Landsmeer (1955) and Spoor and Landsmeer (1976) in the Appendix 3.

THE MODEL

The torque equilibrium equations of the bi-articular three-tendon chain of fig. 1.a are:

$$E. \begin{bmatrix} r_{EI} \\ r_{E2} \end{bmatrix} + I. \begin{bmatrix} r_{II} \\ r_{I2} \end{bmatrix} + F. \begin{bmatrix} r_{FI} \\ r_{F2} \end{bmatrix} = -K. \begin{bmatrix} v_{KI} \\ v_{K2} \end{bmatrix} \quad (a) \quad (2)$$

$$\infty > F, E, I, K \geq 0 \quad (b)$$

The motors are: the Extensor (E), the Flexor (F), and the Interosseus (I). The motors and their forces are noted by the same letter, the meaning follows from the context. The moment arms of a motor M are denoted as r_{Mi} , these of the load K as v_{Ki} . They are positive when the motor or the load induces an extension torque in a joint, otherwise (flexion torque) they are negative.

The moment arm vector diagram

The moment arms of a motor or load can be considered as the cartesian coordinates of a vector, further called the *moment arm vector* $R_M(r_{M1}, r_{M2})$ or $V_K(v_{K1}, v_{K2})$ of this motor or load. As such, the expression (2) can be written as a vector equation:

$$E.R_E + I.R_I + F.R_F = -K.V_K \quad (3)$$

The forces E, I, F, K are now non-negative scalars of vector multiplication. The moment arm vectors can be represented in a vector diagram, further called the *moment arm vector diagram*. This diagram allows to graphically determine the motor forces from a force parallelogram. For the *unloaded* chain (K=0), this parallelogram is obtained by expressing the negative of the moment arm vector of one motor (e.g. the flexor F) as a non-negative sum of the moment arm vectors of the other motors (fig.2.a):

$$E.R_E + I.R_I = -F.R_F \quad (4)$$

The forces E and I are then graphically obtained from the decomposition of the vector $-R_F$ on the vectors R_E and R_I :

A graphic analysis of the bi-articular chain

$$\frac{E}{F} = \frac{\|p_{R_I}^{R_E}(-R_F)\|}{\|R_E\|} \qquad \frac{I}{F} = \frac{\|p_{R_E}^{R_I}(-R_F)\|}{\|R_I\|} \quad (5)$$

(in which e.g. $p_{R_I}^{R_E}(-R_F)$ is the projection of $-R_F$ on R_E along the direction of R_I). For the loaded chain, the moment arm vector $-V_K$ of the load is decomposed as a non-negative sum of the moment arm vectors of the motors (from expression (3)) (fig.2.b). Since the vector diagram is two-dimensional, any load moment arm vector $-V_K$ can be written as the sum of maximally two moment arm vectors, which means that any load in the bi-articular chain can be sustained by maximally two motors. When no motor moment arm vectors are collinear, the motor forces in the unloaded (a) and loaded (b) case can be written as (see Appendix 1):

$$\begin{aligned} \frac{E}{F} &= \frac{[R_I \times R_F]}{[R_E \times R_I]} & \frac{M_i}{K} &= \frac{[R_j \times V_K]}{[R_i \times R_j]} \\ \frac{I}{F} &= \frac{[R_F \times R_E]}{[R_E \times R_I]} & \frac{M_j}{K} &= \frac{[V_K \times R_i]}{[R_i \times R_j]} \end{aligned} \quad (a) \qquad (b) \quad (6)$$

with M_i and M_j the motor pair balancing the load K . These expressions illustrate that in this model mathematically no difference exists between a motor and a load with the same moment arms.

The load vector diagram

Presently explained is a diagram (fig.1.b), which allows to graphically determine, in any position of the bi-articular chain, which motors balance a given load. For any motor M in the bi-articular chain, a load vector $K_M = K_M \cdot u_M$ (with u_M a unit vector) exists which can be balanced by this motor alone, without the help of any other motor. The moment arms of this load vector can be determined from the generic expression (3) (set all motor forces except the generic motor M to zero):

$$V_M = -\alpha_{MK} \cdot R_M ; \qquad \alpha_{MK} = \frac{M}{K_M} > 0 \quad (7)$$

The expression (7) states that the moment arms v_{Mi} of the load vector u_M must be proportional to the moment arms r_{Mi} of the motor M , and of opposite sign. The load vector u_M can be graphically constructed from a schematic drawing of the chain (fig.1.b). In this figure, the intersections of the lines tangent to the circles centered at the joint axes, with radii equal to the moment arms of the motors, and the line connecting both joint axes provide the points P_I, P_E, P_F . The load lines of the load vectors u_I, u_E, u_F , of the motors I, E, F , respectively, are the lines connecting these points and the point of application of the load. This follows from the fact that (e.g. for the flexor F):

$$|r_{Fj}| = \overline{A_j P_F} \cdot \sin\theta \quad (j=1,2) \quad (8)$$

$$|v_{Fj}| = \overline{A_j P_F} \cdot \sin\theta^*$$

From which follows that:

$$\frac{|v_{F1}|}{|r_{F1}|} = \frac{|v_{F2}|}{|r_{F2}|} = \frac{\sin\theta^*}{\sin\theta} = \alpha_{FK} \quad (9)$$

which defines the factor α_{MK} in expression (7) in geometric terms. The fig.1.b shows that the direction of the load vector changes with the point of application and the joint positions. With extended second joint ($\Theta_2=0$), all load vectors are collinear with the line through the joint axes. This phenomenon is discussed further.

In the following, all loads which can be balanced by two motors alone are called the "load range" of this motor pair. This load range consists of all loads which can be decomposed as a positive sum of the load vectors of the motor pair, according to the generic expression (in which for each motor pair the third motor is put to zero):

$$K_E \cdot u_E + K_I \cdot u_I + K_F \cdot u_F = K \cdot u_K \quad (10)$$

with $K_E, K_I, K_F \geq 0$. The load vector diagram straightforwardly provides the load ranges of the different motor pairs (fig.3.a). However, it does not allow to determine the exact motor forces. This is because the factors K_i in the expression (10) are only proportional (by the factors α_{MK}) to the motor forces (expression (7)). Moreover, the factors α_{MK} generally differ for each motor, as they depend on unrelated quantities (the moment arms of motors and load). However, these factors α_{MK} are positive, from which follows that mathematically the motor forces M and the decomposition factors K_M in fig.3.a have the same sign. This means that the load vector diagram and moment arm vector diagram are *consistent*. When in the moment arm vector diagram the negative moment arm vector $-V_K$ of a load K is a positive sum of two motor moment arm vectors R_i, R_j , then in the load vector diagram the load K will also be a positive sum of the load vectors u_i and u_j of these motors M_i and M_j , and vice versa.

Summary: the moment arm versus the load vector diagram

Together, the moment arm vector and load vector diagrams visualise all information enclosed in the force model (2).

(i) The moment arm vector diagram (expression (3)) allows to graphically determine the motor forces in the loaded and in the unloaded chain. It is independent of the position of the chain to the degree that the moment arms of the motors are independent of the joint position. The position of the chain is only reflected in the moment arm vector of the load.

(ii) The load vector diagram (expression (10)) shows in any position of the chain which motors balance a given load, but it does not allow to graphically derive the motor forces themselves.

THE CONDITIONS FOR UNLOADED EQUILIBRIUM, LOADABILITY, AND CONTROLLABILITY OF THE BI-ARTICULAR CHAIN

The conditions for unloaded equilibrium

The equilibrium of the unloaded chain is feasible only when the motor forces in expression (2) (with $K=0$) are non-negative and finite. From the expressions (6.a) follows that the motor forces are strictly positive and finite when:

$$\begin{aligned} [R_I \times R_F] \cdot [R_E \times R_I] &> 0 \\ [R_F \times R_E] \cdot [R_E \times R_I] &> 0 \end{aligned} \quad (11)$$

(in appendix 2, equivalent conditions are derived in the load vector diagram). The conditions (11) can be interpreted in different ways from the vector diagram of fig.2.a.

(i) The left hand members of the expressions (6.a) are the coefficients of the projections of the vector $-R_F$ on the vectors R_E and R_I , as defined by the expression (5). The conditions (11) state that these coefficients must be positive, i.e., that the vector $-R_F$ must be a positive sum of R_E and R_I . The conditions are symmetric: when the negative of one moment arm vector is expressible as a positive sum of the two other moment arm vectors, any of the three moment arm vectors is expressible as a positive sum of the other two moment arm vectors.

(ii) Each vector product term $[R_i \times R_j]$ is proportional to the sinus of the angle β_{ij} , measured anti-clockwise between the vectors $\langle R_i, R_j \rangle$. As such, the conditions (11) express that the equilibrium of the three-tendon chain is feasible when the sinus functions of the cyclic angles β_{FI} , β_{IE} , β_{EF} between resp. $\langle R_F, R_I \rangle$, $\langle R_I, R_E \rangle$ and $\langle R_E, R_F \rangle$ are all of the same sign, meaning that either $0 < \beta_{FI}, \beta_{IE}, \beta_{EF} < \pi$ or $\pi < \beta_{FI}, \beta_{IE}, \beta_{EF} < 2\pi$.

(iii) An interpretation in Landsmeer's model is given in Appendix 3.

Mathematically, equilibrium may also be feasible with one or both conditions (11) equal to zero. This is explored in the next section. Note that a condition (11) is zero only when two moment arm vectors are collinear, i.e. $R_i \times R_j = 0$ if and only if:

$$R_i = \alpha \cdot R_j \quad (12)$$

Exact antagonism, well-loadable and well-controllable bi-articular chains

Presently, the mono-articular concept of muscular "antagonism" is generalised for multi-articular motors, and the concepts of loadability and controllability of the multi-articular chain are defined.

D1) Two motors M_i, M_j with collinear moment arm vectors of opposite directions ($\alpha < 0$ in expression (12)) are further called *exact antagonists*. Conversely, two motors with collinear

moment arms of the same direction ($\alpha > 0$) are called *exact agonists*. When the moment arm vectors $\mathbf{R}_i, \mathbf{R}_j$ of two motors are collinear and opposite, their load vectors $\mathbf{u}_i, \mathbf{u}_j$ are also collinear and opposite. Contrary to the mono-articular antagonism, the concept of bi-articular exact antagonism is purely mathematic. In reality moment arms change, however slightly, with joint position and motor force, which means that in the real bi-articular chain the condition (12) cannot be consistently satisfied.

D2) A chain is *loadable* when it can withstand any unit load \mathbf{u}_K with finite motor forces ($M_i < \infty$). When the chain is loadable, it is also *controllable*, since it can withstand any perturbations of its equilibrium with finite motor forces.

D3) The bi-articular chain is *well-loadable* when it can withstand any unit load \mathbf{u}_K with "reasonable" motor forces ($M_i < \infty$). When the chain is well-loadable, it is also *well-controllable*.

The conditions for loadability and controllability of the three-tendon bi-articular chain

The concept of exact antagonism allows to formulate the conditions for equilibrium, loadability and controllability in physical terms.

(i) Two not exact antagonistic motors cannot balance the unloaded bi-articular chain. They cannot sustain any load outside their load range, which is less than 180° . The first statement follows from the fact that their moment arm vectors cannot balance out (in the generic expression (3)). The second can be immediately verified from a load vector diagram (fig.3.a).

(ii) Two exact antagonists can mathematically balance the unloaded bi-articular chain. However, they cannot sustain any load not collinear with their load vectors, and therefore cannot control the chain. Two exact antagonists M_i, M_j can keep the unloaded (massless) bi-articular chain in equilibrium (substitute (12) in the generic expression (3) with $K=0$). The force in a third motor must then be zero, except when its moment arm vector is also collinear with these of the exact antagonists. In the loaded two-tendon chain, the forces in the exact antagonists with load vectors not collinear with their load vectors are infinite ($M_i, M_j = \infty$): the vector product of the collinear moment arm vectors of the exact antagonists is zero ($[\mathbf{R}_i \times \mathbf{R}_j] = [-\alpha \cdot \mathbf{R}_j \times \mathbf{R}_i] = 0$) in expression (6.b), while the product of these vectors with the moment arm vector of the load is not ($[\mathbf{R}_i \times \mathbf{V}_K] = [-\alpha \cdot \mathbf{R}_j \times \mathbf{V}_K] \neq 0$).

(iii) Three motors satisfying expression (11) suffice for complete control of the bi-articular chain, in both the loaded and unloaded situation. When the expressions (11) are satisfied, no motor pair is exact antagonistic, and the three moment arm vectors can balance out with positive forces. The moment arm vector of any load can then be written as a unique finite non-negative sum of two of the three moment arm vectors (fig.2.b)), meaning that the chain is fully loadable and controllable.

(iv) The bi-articular chain is well-loadable, and well-controllable, when the conditions (11) are satisfied, and no motor pair is too antagonistic. When two motors approach exact antagonism, the conditions (11) remaining satisfied, their forces required to balance loads in their common load range become very large, as $[\mathbf{R}_i \times \mathbf{R}_j] \rightarrow 0$ in the expression (6). Therefore, by definition, the loadability and the controllability of the chain decreases. A similar argument is as follows. In the unloaded chain, with two quasi-exact antagonists, the equilibrium force in the third

motor is quasi-zero, meaning that the ratio of the forces in the quasi-exact antagonists and the force in the third motor is quasi-infinite. Since motors are physiologically limited in their (control of) force, such disbalances in the motor forces do not allow good control. Note that according to the above definitions, the controllability and loadability are optimal when the moment arm vectors of the motors are at 120° - i.e. with all motors of equal degree of antagonism.

PROPERTIES AND APPLICATIONS

Parameter analysis: the effects of changes in the moment arm vectors on motor force, loadability and controllability

The vector diagrams allow the easy validation of the effects of changes in the motor moment arms on the motor forces, the feasibility of equilibrium, and the controllability and loadability of the bi-articular chain. Changes in moment arm vectors can be: (i) in the *size* of the moment arm vector, and (ii) in the *direction* of the moment arm vector. It holds that:

(i) A change in the size of the moment arm vector of a motor merely changes the effectiveness of this motor to the same proportion, and does not change the equilibrium forces in the other motors. This follows from:

$$\sum_i F_i R_i + F_j R_j = -K V_K \Rightarrow \sum_i F_i R_i + \left(\frac{F_j}{\alpha}\right) (\alpha R_j) = -K V_K \quad (13)$$

which shows that changing a moment arm vector R_j by a factor $\alpha > 0$ changes the corresponding motor force by a factor $1/\alpha$, while leaving all other forces unchanged. In the unloaded case ($K=0$), the change of effectivity is with respect to the other motor forces:

$$\sum_i F_i R_i + F_j R_j = 0 \Rightarrow \sum_i (\alpha F_i) R_i + F_j (\alpha R_j) = 0 \quad (14)$$

which means that the increase of the moment arm vector R_j of a motor is equivalent with a decrease in the relative effectivity of all other motors.

(ii) A change in the direction of a moment arm vector changes the relative forces in other motors, the load ranges, the loadability and the controllability. A change in the direction of the moment arm vector of a motor also changes the direction of its load vector in the load vector diagram, which means that the load ranges which this motor together with the other motors can sustain also change. Consequently, loads in the original load range of this motor will be balanced by different motors, or by the same motors with different forces, or cannot be balanced at all. Similarly, in the unloaded chain the variation of a moment arm vector direction changes the equilibrium forces of the motors relative to each other, and, most critically, may cause the violation of the positivity conditions (11) on the motor forces, resulting in an unbalanceable chain.

To summarise, the feasibility of unloaded equilibrium, the loadability, and the controllability of the chain depend essentially on the relative directions of the moment arm vectors

of the motors, while the effectiveness of the force-torque relationship of the individual motor depends on the moment arm vector size.

The moment arm vector and load vector diagrams of the bi-articular chain with extended second joint ($\Theta_2=0$)

(i) The moment arm vector diagram

In the chain with an extended second joint ($\Theta_2=0$) (fig.3.c), any load vector \mathbf{K} can be decomposed in a tangential component \mathbf{K}_t (collinear with the phalanges), and a normal component \mathbf{K}_n (perpendicular to the phalanges):

$$\mathbf{K} = \mathbf{K}_t + \mathbf{K}_n = K \cdot |\cos\phi| \cdot \mathbf{u}_t + K \cdot |\sin\phi| \cdot \mathbf{u}_n \quad (15)$$

The moment arm vectors of \mathbf{u}_t and \mathbf{u}_n are \mathbf{V}_t and \mathbf{V}_n , respectively. The torque resulting from the tangential component \mathbf{u}_t is zero in both joints, since $\mathbf{V}_t=0$. For all loads applied at the same point, the moment arms of the normal component \mathbf{u}_n are of equal length, while their sign depends only on whether the load is applied on the flexion (f) or the extension (e) side of the chain. In other words:

$$\mathbf{V}_n^e = -\mathbf{V}_n^f; \quad \|\mathbf{V}_n\| = \text{Constant} \quad (16)$$

From this follows that in the extended chain all loads can be balanced by only two motor pairs, with one pair balancing all flexion-, the other balancing all extension loads. The forces in these motor pairs are of a constant ratio, independent of the load direction, as from expression (6.b) follows that:

$$\left[\begin{array}{c} M_i \\ M_j \end{array} \right]^{(e \text{ or } f)} = \frac{[\mathbf{V}_K^{(e \text{ or } f)} \times \mathbf{R}_j]}{[\mathbf{R}_i \times \mathbf{V}_K^{(e \text{ or } f)}]} = \frac{[\mathbf{V}_n^{(e \text{ or } f)} \times \mathbf{R}_j]}{[\mathbf{R}_i \times \mathbf{V}_n^{(e \text{ or } f)}]} = \text{Constant} \quad (17)$$

since all vectors $\mathbf{V}_n^e, \mathbf{V}_n^f, \mathbf{R}_i, \mathbf{R}_j$ are independent of the load direction. In other words, where in the flexed chain different load directions applied at the same point are balanced by different motor pairs or by the same motor pair with different forces, in the extended chain the relative loading of the motors is constant for all flexion, or extension loads.

(ii) The load vector diagram

With extended second joint ($\Theta_2=0$), the load vector diagram is undefined. When $\Theta_2 \rightarrow 0$, the load vectors \mathbf{u}_M of all motors M become collinear with the joint axes (fig.4.a). Since their moment arms are then zero ($\mathbf{V}_M=0$, and $\alpha_{MK}=0$ in expression (7)), they cannot balance any motor force anymore. Therefore, in the extended chain the load ranges of the motors cannot be straightforwardly determined in the load vector diagram. Graphically, however, this problem can

A graphic analysis of the bi-articular chain

be circumvented by taking the limit of the load ranges for $\Theta_2 \rightarrow 0$. For instance, in the fig.4.a it is clear that when the second joint extends, the (F,E)-load range converges to the 180° range of all extension loads; the (F,I)-load range converges to the 180° range of all flexion loads; and the (E,I)-load range converges to zero. From the corresponding moment arm vector diagram of fig.2.d it can be verified that the motor pair (F,E) indeed balances the unique moment arm vector V_n^e of all extension loads, and the motor pair (F,I) balances the unique moment arm vector V_n^f of all flexion loads.

The controllability and loadability of the proximal three-tendon bi-articular chain of the human finger

The proximal bi-articular chain of the human finger with the superficial flexor (F), extensor (E), and interosseus (I), is given in fig.3.a, and the moment arm vector diagram in fig.2.a (from the values of table.1). From the above it follows that the feasibility of equilibrium, the loadability, and the controllability are determined by the two most antagonistic motors. These are the extensor and flexor, which are almost exact antagonists. From this fact the following conclusions can be formulated:

(i) The proximal three tendon bi-articular chain of the human finger is weak for loads in the load range of the extensor and flexor. In other words, the forces in extensor and flexor required to sustain unit loads in their common load range will be high.

(ii) The controllability of the chain is not very good. This follows by definition from (i).

(iii) The functioning of the chain is not "safe" with respect to small changes in the moment arms of extensor and flexor.

From the expression (a.7) in appendix.3 or the fig.2.c it can be verified that the changes in the moment arms which result in unfeasible equilibrium (corresponding to the dashed vectors R_E^* or R_F^* in fig.2.c) are relatively small. For instance, for changes in the moment arms at the MCP joint, equilibrium is unfeasible when:

$$|r_{EI}| < \frac{|r_{FI}|}{|r_{F2}|} \cdot |r_{E2}| \approx 7.2mm \quad \text{or} \quad |r_{FI}| > \frac{|r_{EI}|}{|r_{E2}|} \cdot |r_{F2}| \approx 16.2mm \quad (18)$$

which is a change of less than 2 mm and little more than 3 mm for the extensor or flexor, respectively. Clinically, such changes would correspond to extensor subluxation ($r_{EI} \downarrow$), or rupture of the flexor pulleys ($r_{FI} \uparrow$) at the MCP. The fig.2.c also shows that simultaneous changes of about 1mm in the extensor or flexor moment arms, e.g. along the vectors ΔR_E or ΔR_F , may result in an unbalanceable chain. Notice that such changes, especially in the extensor (subluxation of the tendon at the MCP in combination with (dorsal) swelling of the PIP joint), may well be caused by rheumatoid arthritis.

(iv) Loads as may occur when carrying a bag, i.e. with $\phi=90^\circ$, and $\Theta_2=90^\circ$ (fig.3.b), are within the flexor-extensor load range, and therefore cannot be well sustained. The reader may notice that this is well against intuition.

(v) The most efficient load range is of the flexor and interosseus (fig.3.a). This follows

immediately from the fact that the angle between \mathbf{R}_I and \mathbf{R}_F is smallest of all angles of the moment arm vectors. Note that this load range comprises the pinch grip loads.

To summarise, the proximal three-tendon bi-articular chain of the finger in itself cannot be considered as an optimal design: it cannot well sustain all physiologically occurring load situations, and is not especially adapted for good control. This indicates that in the real three-articular finger the other motors (deep flexor, lumbrical) will have to substantially improve upon the general load bearing capacity and the controllability.

The forces in the extended proximal three tendon bi-articular chain of the human finger

In the above it is shown that with extended second joint ($\Theta_2=0$), all loads of flexion and extension, respectively, can be balanced by motor pairs with forces in a constant ratio. The question presently investigated is which motors and with what forces sustain these loads in the proximal bi-articular chain of the human finger. The parametric exploration of this question will illustrate the close relationship between geometry and function in the bi-articular chain, and the peculiar weakness for extension loads in the proximal bi-articular chain of the human finger.

The moment arm vector diagram of fig.2.d, or the load vector diagram of fig.4.a show that a load applied at the flexion side to the tip of the extended chain is balanced by the flexor and the interosseus, while a load applied at the extension side is balanced by the extensor and the flexor (!). The latter fact is somewhat against intuition. Indeed, the extensors of the two joints are the extensor (MCP,PIP) and the interosseus (PIP). Therefore it could be expected that the extensor and the *interosseus* would balance extension loads. This may be compared with the fig.4.b, where a bi-articular chain with a longer distal phalanx is considered. In this chain extension loads with $\Theta_2=0$ are indeed balanced by the extensor and the interosseus (the (E,I)-load range converges to the hemisphere of the extension loads). The only difference between the fig.4.a and 4.b is the length of the distal phalanx, which determines the direction $v_{K2}/v_{K1}=L_2/(L_1+L_2)$ of the moment arm vector $-\mathbf{V}_n^e$ in the moment arm vector diagram of fig.2.d. From this diagram it is clear that:

- (i) when $[-\mathbf{V}_n^e \chi \mathbf{R}_E] > 0$, extension load is balanced by the extensor and flexor,
- (ii) when $[-\mathbf{V}_n^e \chi \mathbf{R}_E] < 0$, extension load is balanced by the extensor and interosseus,
- (iii) when $[-\mathbf{V}_n^e \chi \mathbf{R}_E] = 0$, extension load is balanced by the extensor alone,
- (iv) when $[\mathbf{R}_F \chi -\mathbf{V}_n^f] > 0$, flexion load is balanced by the flexor and the extensor.

With extension loads at the end of the second phalanx of the proximal bi-articular chain of the human finger (case (i) of the above) (fig.4.a), the extensor force is quite large, while the flexor force is about a third of the extensor force (fig.2.d), even if $-\mathbf{V}_n^e$ is almost collinear with the extensor moment arm vector \mathbf{R}_E . When the load is applied closer to the second joint (i.e. when L_2 decreases), the vector $-\mathbf{V}_n^e$ is shifted towards the middle of the (F,E)-load range (fig.2.d), and the extensor and flexor forces still increase considerably. This weakness for extension loads in the proximal finger can be self-verified by applying an extension load close and distal to the PIP joint of ones own fingers (hereby the PIP joint must be kept slightly flexed, so that the palmar joint ligaments, i.e. the volar plate, remain slack). One will experience that even small loads are difficult to balance, and that the PIP will tend to extend completely. Also it can be observed that when the PIP is fully extended and the volar plate is taut, much greater extension loads can be

A graphic analysis of the bi-articular chain

sustained. The taut volar plate effectively functions as a mono-articular flexor of the PIP, with a moment arm vector \mathbf{R}_{vp} as in fig.4.d. This "flexor" force of the volar plate may completely substitute the superficial flexor, and creates a more efficient load range in which the extensor requires less than half of the force with a slack volar plate.

DISCUSSION

In present paper a model is introduced which visualises the relationship between morphology and function in the bi-articular chain, and which allows to graphically analyse the motor forces in the unloaded and loaded chain, the load ranges of the motors, the ranges of preferential loading (i.e. the loads which can be sustained with minimal force), the feasibility of equilibrium and the condition of control. The present model generalises the results of Landsmeer (1955) and Spoor and Landsmeer (1976), who investigated the control of the unloaded bi-articular chain in morphological terms. The graphic representation of the present model is possible because the kinematics and statics of the massless frictionless bi-articular chain depend entirely upon its geometry, i.e. the lengths of the moment arms of motors and loads.

The present model may be valuably applied to investigate the functioning of bi-articular chains in which the motor forces and loads are large as compared to the masses of the phalanges, as is the case in fingers or toes, or to investigate the statics of chains in the horizontal plane, i.e. with the gravity forces parallel to the joint axes. Hereby the moment arms may well be functions of the joint position, since at any given position of the chain they have a fixed value, and the model is valid. In the text the model is applied to investigate the properties of the proximal three-tendon bi-articular chain of the human finger. It clearly emerges that this chain is especially designed to sustain (certain) "flexion" loads, that it is structurally weak for extension loads, and that its controllability is not optimal. This indicates that the third joint, and the other finger motors (deep flexor, and lumbrical) play an important role in improving finger control.

The two dimensional vector diagrams here presented cannot be extended to the n-articular chain, with $n > 2$. In the vector diagrams the moment arms of each independent joint axis are represented at an independent cartesian axis, which means that a n-articular chain requires a n-dimensional vector representation. Moreover, for the n-articular chain (with $n > 2$), the load vectors of the motors generally do not exist, since their load line must be tangential to all circles, centered at the joint axes, and of which the radii are in a fixed proportion (by the constant α_{MK} in expression (7)) to the moment arms of their motors at these joints. Generally, this condition is not satisfied for $n > 2$.

CONCLUSION

A model is presented which allows to graphically investigate the equilibrium conditions, the loadability and the controllability of the bi-articular chain. To allow a concise formulation of the results, the concept of exact antagonism of bi- (or multi) articular motors is introduced. It is shown that:

(i) Two not exact antagonistic motors cannot keep the chain in equilibrium, and cannot sustain all

Chapter II.i

loads.

(ii) Two exact antagonists can mathematically balance the chain, but cannot control it.

(iii) The bi-articular chain with three motors is fully controllable and loadable when no two motors are exact antagonists, and no moment arm vector can be written as a positive sum of the others. The bi-articular chain with n motors is fully loadable and controllable when a motor triplet exists which satisfies this criterion.

(iv) All loads can be sustained by maximally two motors.

(v) When two motors approach exact antagonism, the three-motor chain cannot be well controlled. Moreover, the common load range of these quasi exact antagonists is structurally weak.

(vi) With extended second joint, all loads of extension can be balanced by the same motor pair with forces in a fixed ratio. Similarly, a (different) motor pair with fixed force ratio will balance all flexion loads.

In the proximal three-tendon bi-articular chain of the human finger, the loadability and controllability is critically determined by the pronounced antagonism of the extensor and superficial flexor. The other motor pairs are not at all antagonistic. The chain is structurally weak in the extensor-flexor load range, and is not well conditioned for good control. Moreover, relatively small changes in the moment arms of extensor and/or flexor may result in an uncontrollable chain.

ACKNOWLEDGEMENTS

The author cordially thanks Prof. Emer. J.M.F. Landsmeer, Prof. J.J. Kalker, Dr. C.W. Spoor, Prof. C.J. Snijders, Prof. J.C. Van der Meulen, and Dr. S.E.R. Hovius for their valuable contributions.

REFERENCES

Landsmeer, J.M.F. (1955) Anatomical and functional investigations on the articulation of the human fingers. *Acta Anat.* 25, 1-69.

Leijnse, J.N.A.L., and Kalker, J.J. (1995) A two dimensional kinematic model of the lumbrical in the human finger. *J. Biomechanics* 28, 237-249.

Spoor, C.W., Landsmeer, J.M.F. (1976) Analysis of the zigzag movement of the human finger under influence of the extensor digitorum tendon and the deep flexor tendon. *J. Biomechanics* 9, 561-566.

Spoor, C.W. (1983) Balancing a force on the fingertip of a two dimensional finger model without intrinsic muscles. *J. Biomechanics* 16, 497-504.

APPENDIX.1. The motor forces in the terms of the moment arm vectors

Assume no moment arm vectors collinear. The expressions (6) are obtained by taking the vector product of the motor moment arms and the vector equation (3). For instance, the vector product of the extensor moment arm vector R_E with expression (3) is:

$$E.[R_E \times R_E] + I.[R_E \times R_I] + F.[R_E \times R_F] = -K.[R_E \times V_K] \quad (a.1)$$

It holds that $R_E \times R_E = 0$. Therefore, for the unloaded case ($K=0$), the relationship I/F of expression (6) is obtained:

$$\frac{I}{F} = \frac{-[R_E \times R_F]}{[R_E \times R_I]} = \frac{[R_F \times R_E]}{[R_E \times R_I]} \quad (a.2)$$

The other forces can be derived similarly.

APPENDIX.2: The conditions for equilibrium in the load vector diagram

The massless chain is in equilibrium with a motor and its load vector. Therefore, the superposition of all motors and their load vectors also results in a chain in equilibrium. This equilibrium is not disturbed when for any motor the motor force and its load vector are multiplied by the same positive number K_M . The vector sum of all load vectors is the effective load with which the chain with the given motor forces is in equilibrium. When this sum is zero (the load vectors, themselves not zero, balance out), an unloaded chain is obtained. From this follows that the motors can keep the chain in equilibrium, when the vector sum of their load vectors can be put to zero:

$$K_F \cdot u_F + K_I \cdot u_I + K_E \cdot u_E = 0 \quad (a.3)$$

with $K_F, K_I, K_E \geq 0$, and not all of them zero. This expression is similar to expression (3) and leads, similarly to expression (11), to the conditions that $\infty > K_F, K_E, K_I > 0$ when:

$$\begin{aligned} [u_I \times u_F][u_E \times u_I] &> 0 \\ [u_F \times u_E][u_E \times u_I] &> 0 \end{aligned} \quad (a.4)$$

The conditions (a.4) and the conditions (11) are consistent: the expressions (a.4) hold if and only if the expressions (11) hold (except in the extended chain ($\Theta_2=0$) where the vectors u_i are undefined), while also the graphic interpretation is similar to the expression (11).

APPENDIX.3. The Landsmeer conditions for equilibrium of the proximal bi-articular chain of the human finger

With expression (1), the conditions (11) can be written as:

Chapter II.i

$$\begin{aligned} [r_{E1} \cdot r_{I2} - r_{E2} \cdot r_{H1}] \cdot [r_{H1} \cdot r_{F2} - r_{I2} \cdot r_{F1}] &> 0 \\ [r_{E1} \cdot r_{I2} - r_{E2} \cdot r_{H1}] \cdot [r_{F1} \cdot r_{E2} - r_{F2} \cdot r_{E1}] &> 0 \end{aligned} \quad (a.5)$$

For the proximal bi-articular chain of the human finger it holds that: $r_{E1}, r_{E2}, r_{I2} > 0$, and $r_{H1}, r_{F1}, r_{F2} < 0$ (see the table.1 or the fig.1.a). With these values, the inequalities (a.5) become:

$$\begin{aligned} \left[\frac{|r_{I2}|}{(-|r_{H1}|)} - \frac{|r_{E2}|}{|r_{E1}|} \right] \cdot \left[\frac{(-|r_{F2}|)}{(-|r_{F1}|)} - \frac{|r_{I2}|}{(-|r_{H1}|)} \right] &< 0 \\ \left[\frac{|r_{I2}|}{(-|r_{H1}|)} - \frac{|r_{E2}|}{|r_{E1}|} \right] \cdot \left[\frac{|r_{E2}|}{|r_{E1}|} - \frac{(-|r_{F2}|)}{(-|r_{F1}|)} \right] &> 0 \end{aligned} \quad (a.6)$$

Each term between square brackets is the difference of the directions r_{M2}/r_{M1} of the moment arm vectors \mathbf{R}_M of two motors, and therefore provides a measure for their degree of antagonism. For exact antagonists (or agonists), the term is zero. In the expression (a.6) two terms are "safe", that is, not likely to change in sign with small variations in the ratios r_{M2}/r_{M1} . These are the (E,I)-term, which is the sum of two negative ratios, and the (F,I)-term, which is the sum of two positive ratios. These terms express that the (F,I) and (E,I) motor pairs are not at all antagonistic. However, the (F,E)-term is the sum of two ratios of *different* sign, and its sign may well change with small variations in the moment arm ratios. Therefore, this term (which expresses the antagonism of the F and E) critically determines the feasibility of equilibrium of the chain. When the term is negative, the chain is controllable; when it is positive, the chain cannot be balanced. In Landsmeer (1955), and Spoor and Landsmeer (1976), the terms of (F,I) and (E,I) were not considered (they are not critical) and the controllability condition of the chain was derived in the form:

$$\frac{|r_{E1}|}{|r_{F1}|} - \frac{|r_{E2}|}{|r_{F2}|} > 0 \quad (a.7)$$

FIGURES

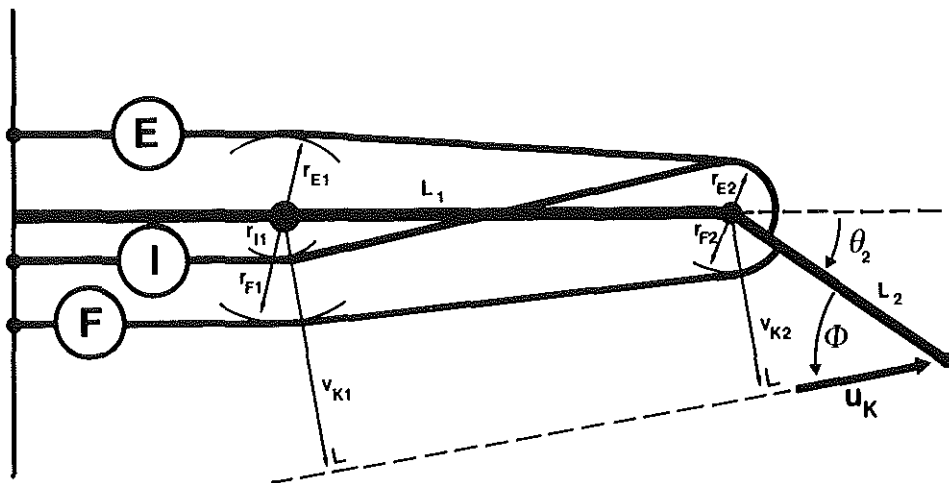


Figure 1 a a. Bi-articular chain with three motors and unit load vector u_K .

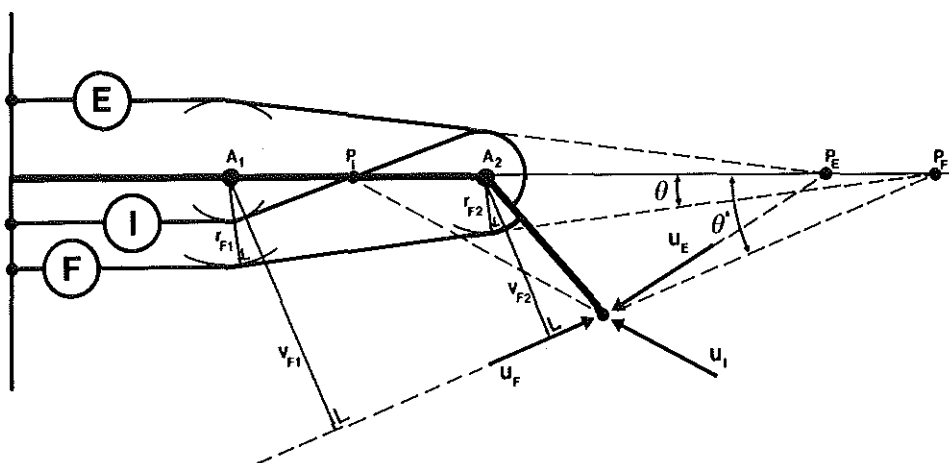


Figure 1 b Graphic construction of the load vector diagram. Three lines intersect at the points P : (i) the line tangential to the circles centered at the joint axes, and with radii equal to the moment arms of considered motor at these joints, (ii) the line A_1-A_2 connecting both joint axes, and (iii) the load line of the load vector u_K .

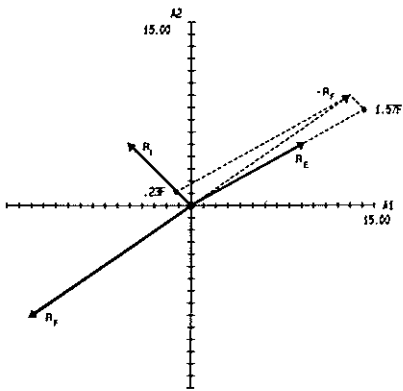


Figure 2 a

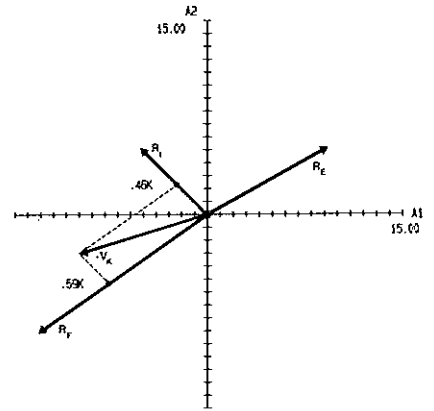


Figure 2 b

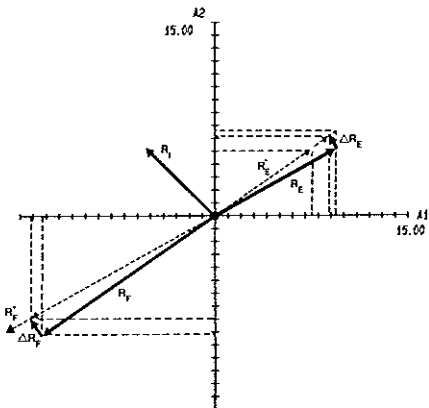


Figure 2 c

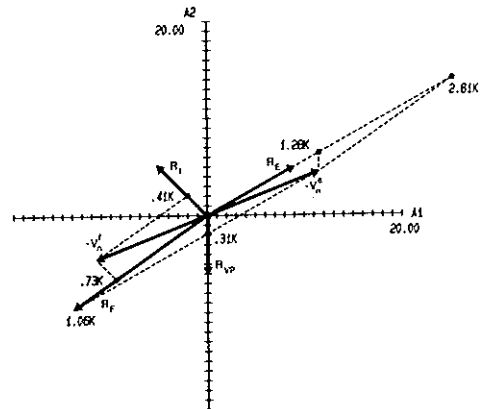


Figure 2 d

Figure 2

a) Moment arm vector diagram of the unloaded proximal bi-articular chain of the human finger. Moment arm values from table 1. A_1, A_2 : axes for the moment arms of first and second joint. The motor forces follow from the force parallelogram: $F=F$; $E/F=1.57$; $I/F=0.23$.

b) The motor forces with load K as in fig.3.a. The moment arm vector V_K of the load is scaled down by a factor 10 to fit in the picture. The motor forces are: $I/K=4.6$; $F/K=5.9$; $E/K=0$.

c) Sensitivity analysis of the equilibrium of the proximal bi-articular chain of the human finger. When R_F or R_E are rotated so that they become collinear with R_E or R_F , resp., (dashed vectors ΔR_F^* or ΔR_E^*), the chain becomes uncontrollable. The dashed projection lines indicate the changes required. Changes of minimally 1.5mm are required in one single moment arm to obtain an unstable chain, while these changes are somewhat greater in the moment arms of the first joint (A_1 axis) than with the second joint (A_2 axis). However, with simultaneous changes in the moment arms of the first and second joint, e.g. along the vectors ΔR_F or ΔR_E , changes of less than 1mm will unbalance the chain.

d) Motor forces in the extended proximal chain of the human finger loaded at the tip. R_{VP} : moment arm vector of the volar plate of the PIP joint. The moment arms of the extension and flexion load (V_n^*, V_n^f) at the finger tip are scaled down by a factor 10 to fit in the picture. With slack volar plate the extension load (moment arm vector $-V_n^*$) is balanced by the flexor and extensor. Note the extremely large forces: $E/K=28.1$; $F/K=10.6$. With taut volar plate and relaxed flexor, the extensor force is more than halved: $E/K=12.8$; $VP/K=3.1$. A flexion load (moment arm vector $-V_n^f$) is balanced by the flexor and the interosseus with the forces: $F/K=7.3$; $I/K=4.1$.

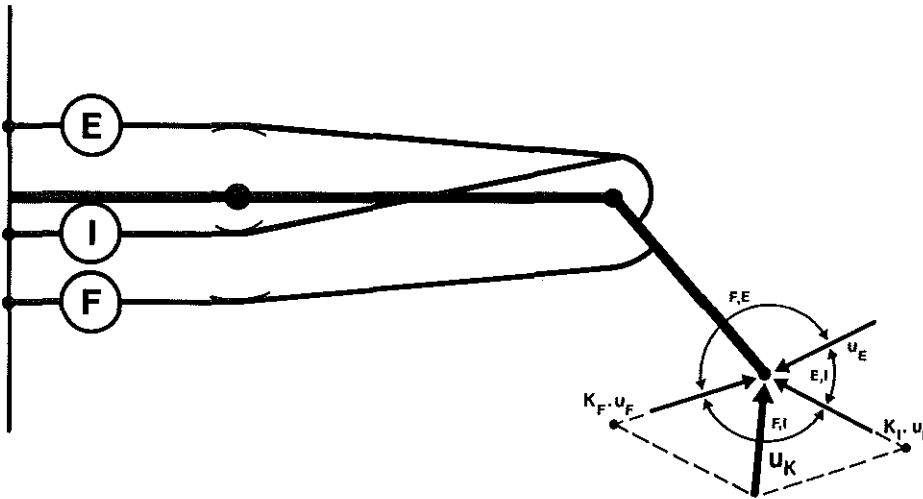


Figure 3 a Load vector diagram of the proximal bi-articular chain of the human finger. K_F, K_I : moduli of the decomposition of the load on the unit load vectors u_F, u_I of the motors F and I. (F,E); (E,I); (F,E): the load directions which can be balanced by these two motors alone.

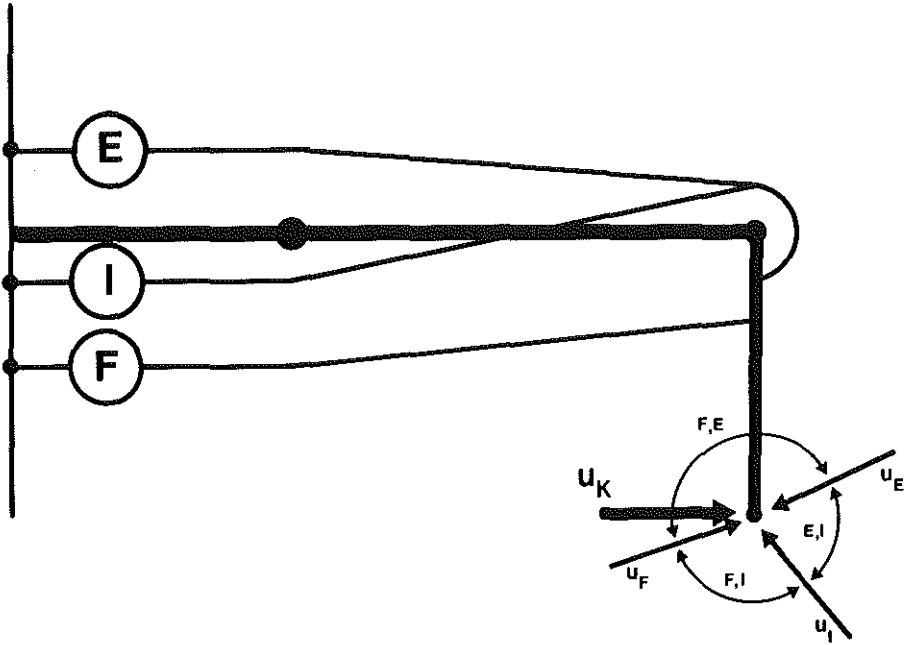


Figure 3 b Load u_K as with carrying a bag with a bi-articular finger ($\Theta_2=90^\circ$, $\phi=90^\circ$). This load is within the F,E load range.

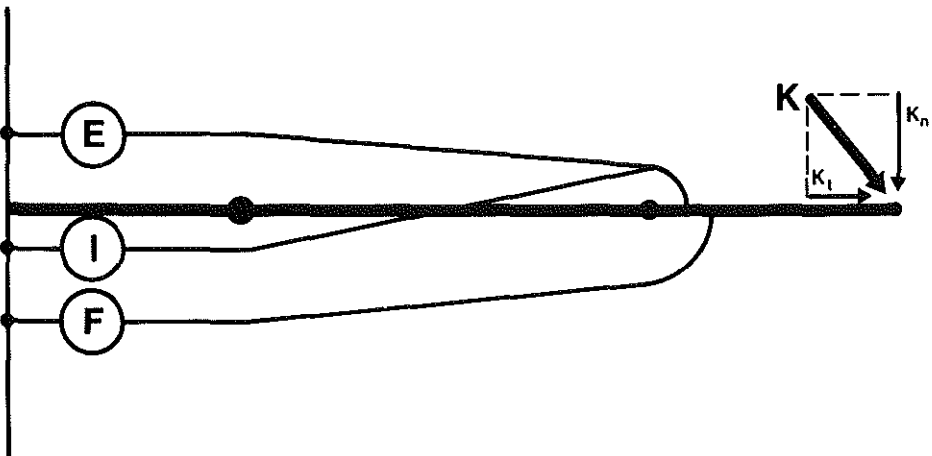
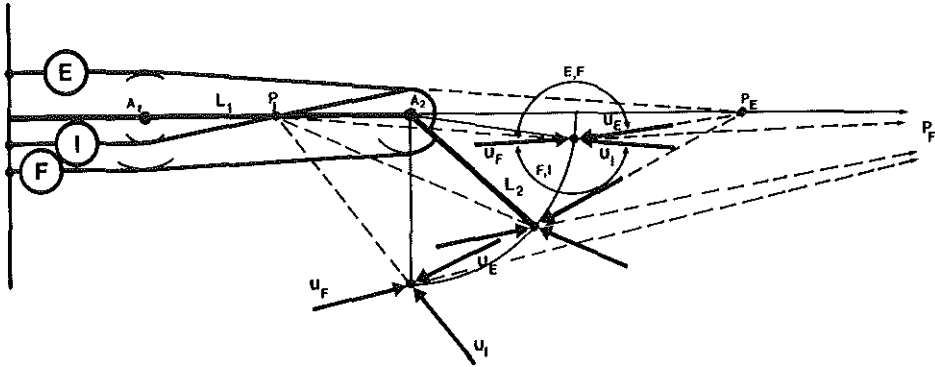
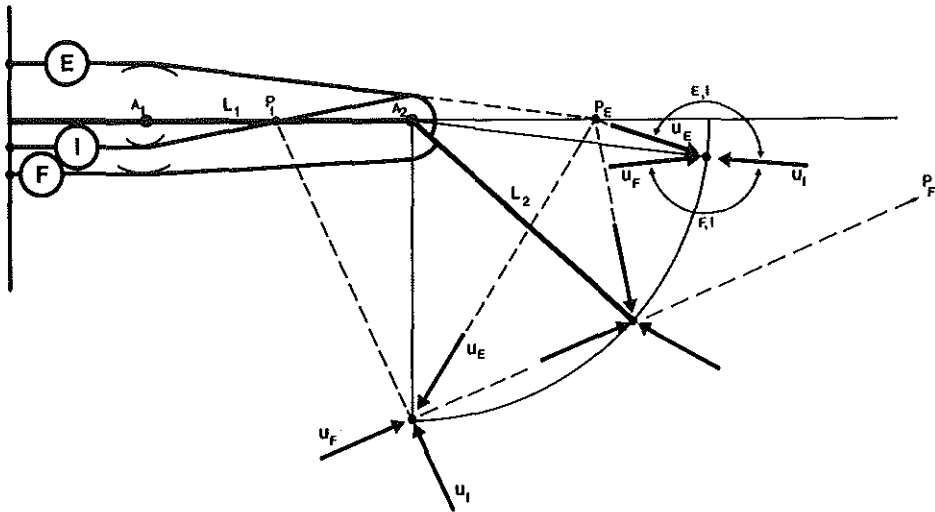


Figure 3 c The extension load at the finger tip of the extended finger can be decomposed into a tangential load K_t with zero moment arms ($V_t=0$), and a normal load K_n with moment arms $V_n=(L_1+L_2, L_2)$.

A graphic analysis of the bi-articular chain



(a)



(b)

Figure 4 a) Load vector diagram of the extending proximal bi-articular chain of the human finger. Three PIP positions ($\Theta_2=90^\circ, 45^\circ, 10^\circ$) are drawn to demonstrate the changes in the load vector directions with PIP position. With extending PIP joint ($\Theta_2 \rightarrow 0$), the F,E load range increases to the 180° range comprising all extension loads, the F,I load range converges to the 180° load range comprising all flexion loads, and the E,I load range converges to zero. b) Same figure as fig.4.a, but with an elongated second phalanx. With extending PIP joint ($\Theta_2 \rightarrow 0$), the E,I load range converges to all extension loads; the F,I load range converges to all flexion loads, and the F,E load range converges to zero.

THE CONTROLLABILITY OF THE UNLOADED HUMAN FINGER WITH SUPERFICIAL OR DEEP FLEXOR

J.N.A.L. Leijnse^{F3}

^(F)Department of Plastic and Reconstructive Surgery, ⁽⁹⁾Department of Biomedical Physics and Technology, Erasmus University Rotterdam, The Netherlands. Resubmitted J. Biomechanics, 1995.

ABSTRACT

The unloaded human finger functions as a bi-articular structure, because the angulations of the distal two joints are mechanically coupled. In this bi-articular chain two flexors exist: the superficial and deep flexor. The present paper discusses the functional differences between these flexors in the control of the unloaded finger. It is concluded that the deep flexor is anatomically better positioned for the control of unloaded finger movement, and that the chiasma tendinum, and the coupled actions of the distal two finger joints are fundamental to the good controllability of the finger.

NOMENCLATURE

MCP, PIP, DIP	: metacarpophalangeal, proximal interphalangeal, and distal interphalangeal joint
MCP, IP	: fist and second joint in the bi-articular model
P	: (force in the) flexor digitorum profundus
S	: (force in the) flexor digitorum superficialis
E	: (force in the) extensor digitorum
I	: (force in the) interosseus
M	: medial band of extensor and interosseus
T	: lateral band of extensor and interosseus
Θ_j	: angle of joint j ($j=1,2,3$ for MCP, PIP, DIP respectively)
r_{ij}	: moment arms of the tendons over the resp. joints. The first index denotes the motor: P,S,E,I,M,T. The second index indicates the joint.
r_{ij}^*	: equivalent moment arm
R_M	: moment arm vector of motor M , defined by the cartesian coordinates: (r_{M1}, r_{M2})

INTRODUCTION

The human finger (as modelled in the fig.1.a) presents some striking morphological properties, of which the significance is not immediately obvious. One is the bifurcation of the extensor tendon distal to the MCP into two end tendons, anatomically called the medial and lateral bands, which insert in the base of the middle and distal phalanx, respectively. Another is the crossing of the flexor tendons in between the first and second joint. This crossing is anatomically realised by the chiasma tendinum in the superficial flexor (S), through which the deep flexor perforates the superficial flexor tendon from a deep course at the MCP joint to a superficial course at the PIP

joint. The effect of the bifurcation of the extensor tendon is that when both the medial and lateral insertions are taut the distal two joints function as a mechanism with one degree of freedom, i.e. with their angulations mechanically coupled (Landsmeer, 1958, Spoor and Landsmeer, 1976, Leijnse et al, 1992). This mechanism can be formally replaced by a single equivalent joint, called the IP (Inter-Phalangeal) joint in Spoor and Landsmeer (1976), which means that the finger with taut medial and lateral bands functions as a bi-articular chain. This system-equivalent bi-articular model is presented in fig.1.b. In this bi-articular model four motors are present. However, for the complete control of a bi-articular chain three motors suffice (more precisely: when the bi-articular chain can be controlled by four (or more) motors, three of these motors can control the chain by themselves) (Landsmeer, 1955, Leijnse, 1995). Assuming that the model of fig.1.b is controllable, then one of the four motors must be redundant. When certain conditions on the moment arms of the motors are satisfied, as is the case in the normal finger, either one of both flexors P or S is redundant (Landsmeer, 1955, Spoor, 1983, Leijnse, 1995). This leads to the question investigated in present paper: assuming their mutual redundancy, which of the two flexors is most adapted for control of the unloaded finger model? It is further shown that the deep flexor is structurally superior to the superficial flexor in unloaded control, and that this difference increases with the crossing angle of their tendons in the bi-articular model. This crossing angle finds its cause in the both the chiasma tendinum and the PIP-DIP coupling mechanism, which means that these anatomic constructs obtain a further biomechanical significance. The arguments are based on the concepts about the controllability of bi-articular chains introduced in Leijnse (1995). Some clinical applications are briefly discussed, such as the controllability of fingers prone to swan-neck deformities, the relative contribution of the flexors to the claw-hand deformity in the case of intrinsic paralysis, and the functioning of the finger with impaired coupling mechanism in fast finger movements, as in the playing of a musical instrument.

MATERIAL AND METHODS

The bi-articular force model of the human finger

Studied in this paper are the torque equilibrium equations of the massless unloaded finger model of the fig.1.a (from Spoor, 1983):

$$\begin{aligned}
 r_{EI} \cdot E + r_{II} \cdot I + r_{SI} \cdot S + r_{PI} \cdot P &= 0 \quad (1) \\
 r_{M2} \cdot M + r_{T2} \cdot T + r_{S2} \cdot S + r_{P2} \cdot P &= 0 \quad (2) \\
 r_{T3} \cdot T + r_{P3} \cdot P &= 0 \quad (3) \\
 T + M - E - I &= 0 \quad (4) \\
 E, I, S, P, T, M &\geq 0
 \end{aligned}
 \tag{1}$$

(in which the forces are: E: extensor, S: superficial flexor, P: deep flexor, I: interosseus, M: medial band, T: lateral band). Moment arms of motors which extend a joint are positive, moment arms of flexion are negative. The elimination of M and T by use of the equations (1.3) and (1.4) results in the equilibrium equations of a bi-articular chain, further called the bi-articular equivalent model (fig.1.b):

$$E. \begin{bmatrix} r_{E1} \\ r_{E2} \end{bmatrix} + I. \begin{bmatrix} r_{I1} \\ r_{I2} \end{bmatrix} + S. \begin{bmatrix} r_{S1} \\ r_{S2} \end{bmatrix} + P. \begin{bmatrix} r_{P1} \\ r_{P2}^* \end{bmatrix} = 0 \quad (2)$$

with $r_{E2}=r_{I2}=r_{M2}$, and with the "equivalent moment arm" r_{P2}^* given by:

$$r_{P2}^* = r_{P2} + \frac{r_{P3}}{r_{T3}}.(r_{M2}-r_{T2}) \quad (3)$$

In the equivalent model the PIP and DIP joint of the three-articular model (1) are condensed to one single equivalent joint, further called the IP joint (Spoor and Landsmeer, 1976). In the human finger the moment arm r_{T2} of the lateral band at the PIP decreases with PIP flexion, which means that the equivalent moment arm r_{P2}^* increases with IP flexion (expression (3)). In the following $r_{T2}(\Theta_2)$ is approximated as (Leijnse and Kalker, 1994):

$$r_{T2} = r_{M2} \cdot \left[1 - \frac{2 \cdot \theta_2}{(\pi/2)} + \frac{\theta_2^2}{(\pi/2)^2} \right] \quad (4)$$

This function is represented, with $r_{P2}^*(\Theta_2)$, in the fig.2.a. The change in the equivalent moment arm r_{P2}^* with IP position is visualised in the figs.1.b and 1.c for the extended and flexed IP joint, respectively.

The moment arm vector diagram of the unloaded finger

In Leijnse (1995) it was shown that the static equilibrium of the bi-articular chain can be represented in the form of a vector diagram, further called the *moment arm vector diagram*. This diagram is obtained by assuming that the column matrices of the expression (2) are the cartesian coordinates (r_{M1}, r_{M2}) of two-dimensional vectors, the *moment arm vectors* R_M of the motors M. The equation (2) can thus be written as:

$$E.R_E + I.R_I + S.R_S + P.R_P^* = 0 \quad (5)$$

with the forces $E, I, S, P \geq 0$ scalars of vector multiplication. The chain is in equilibrium when the vectors R_M , multiplied by the appropriate non-negative motor forces, balance out. The moment arm vector diagram of the equivalent bi-articular chains of the figs.1.b and 1.c is given in the fig.3.a (from the moment arm values given in table.1).

Exact antagonism; (good) controllability of the bi-articular chain

From the paper of Leijnse (1995), some definitions and conclusions are repeated without further comment.

D1. Exact antagonism:

Two motors M_i and M_j are called *exact antagonists* when their moment arm vectors are exactly opposite: $\mathbf{R}_i = \alpha \cdot \mathbf{R}_j$, $\alpha < 0$. When $\alpha > 0$ (moment arms of the same direction and sense), the motors are called *exact agonists*.

D2. Controllability of the three-tendon bi-articular chain

The three-tendon bi-articular chain is *fully controllable* when no two motors are exact antagonists/agonists ($\mathbf{R}_i \neq \alpha \cdot \mathbf{R}_j$), i.e. when their moment arm vectors are not collinear, and when they can balance each other out when multiplied by appropriate positive scalars.

D3. Good controllability of the three-tendon bi-articular chain

The three-tendon bi-articular chain is *well controllable* when it is controllable (D2 holds), and when no two motors are too antagonistic/agonistic.

The deviation of exact antagonism/agonism corresponds to the deviation of the collinearity of the moment arm vectors in the moment arm vector diagram. For further use, the degree of antagonism is quantified as:

$$A(M_i, M_j) = \frac{[\mathbf{R}_i \times \mathbf{R}_j]_z}{\|\mathbf{R}_i\| \|\mathbf{R}_j\|} = \sin \beta_{ij} \quad (6)$$

i.e. the value of the vector product of the normalised moment arm vectors $\mathbf{R}_i, \mathbf{R}_j$, which is equal to the sinus of the counter-clockwise angle β_{ij} between the vectors \mathbf{R}_i and \mathbf{R}_j . This function is not uniquely defined since vectors at angles of $\pi/2 \pm \beta_{ij}$ have the same value. When $\pi/2 < |\beta_{ij}| < \pi$, the motors are defined as antagonists. When $0 < |\beta_{ij}| < \pi/2$, the motors are defined as agonists. $\beta_{ij} = 0$ is exact agonism, $\beta_{ij} = \pi$ is exact antagonism. When $\beta_{ij} = \pi/2$, the moment arm vectors are orthogonal, and the motors are neither antagonists, nor agonists. When $0 < \beta_{ij} < \pi$, $A(M_i, M_j) > 0$; conversely, when $0 < -\beta_{ij} < \pi$, $A(M_i, M_j) < 0$. It further holds that $A(M_i, M_j) = -A(M_j, M_i)$.

The problem

In Leijnse (1995) it was shown that the three-tendon bi-articular chain is fully controllable when the following conditions on the motor moment arms are satisfied:

$$\begin{aligned} A(E, I) \cdot A(I, F) &> 0 \\ A(I, F) \cdot A(F, E) &> 0 \end{aligned} \quad (7)$$

In the bi-articular equivalent model of the human finger, as represented by the moment arm vector diagram of fig.3.a, four tendons are present. When the conditions (7) are satisfied for both flexors

(with $F=S$ or $F=P$), the bi-articular model can be controlled by either motor triplet (S,E,I) or (P,E,I), which means that the flexors are mutually redundant. The question then is which motor triplet is best suited for unloaded finger control. In the following this question will be discussed in the moment arm vector diagram of the bi-articular model. Since the unloaded bi-articular model and the three-articular model of fig.1.a are mathematically equivalent, the conclusions also hold for the unloaded three-articular finger model. Hereby it must be noted that in the three-articular model the redundancy of the (S,E,I) and (P,E,I) triplet is not complete, since the motor triplet (S,E,I) can control only the proximal bi-articular chain of the finger (i.e. MCP,PIP), while the (P,E,I) triplet controls the whole finger (including the DIP) with the PIP and DIP articulating as a mechanism. However, these differences do not affect the analysis at the level of abstraction here presented. From the fig.3.a (based on the normal moment arm values of table 1) it can be verified that the interosseus is quasi-orthogonal to both the extensor and the flexors:

$$A(I,P) \approx 1; \quad A(I,S) \approx 1; \quad A(E,I) \approx 1 \quad (8)$$

Both flexors, however, are quite antagonistic to the extensor. This means that the controllability of the chain is basically determined by the flexor-extensor antagonism. When the expressions (8) hold, the condition (7) is satisfied (i.e. the chain is controllable by the (S,E,I) or (P,E,I) motor triplet) when:

$$A(P,E) > 0; \quad A(S,E) > 0 \quad (9)$$

RESULTS

The differences in the antagonism of the flexors P and S with respect to the extensor E in the equivalent bi-articular model

In the following it is assumed that all moment arms are constant, except for the moment arm $r_{P_2}(\Theta_2)$. For the normal values of the moment arms of the finger, as given in the table.1, it then holds that:

(i) The flexor S and the extensor E are almost exact antagonists (see fig.3.a).

(ii) The flexor P becomes less antagonistic to the extensor E with PIP flexion. The moment arm vector of the flexor P varies as a function of the PIP position (through $r_{P_2}^*(\Theta_2)$ in expression (3)). In fig.3.a the moment arm vectors of the flexor P are drawn for the extended PIP ($\Theta_2=0$, moment arm vector $\mathbf{R}_{P_e}^*$), and the completely flexed PIP ($\Theta_2=90^\circ$, moment arm vector $\mathbf{R}_{P_f}^*$). The antagonisms $A(P,E)$ and $A(S,E)$, as defined by expression (6), are presented in the fig.2.b as a function of the PIP position.

(iii) In the human finger the lateral bands are not fixed by pulleys, and they may bowstring with PIP hyperextension (fig.1.d). Hereby it holds that for all PIP positions with the PIP not too hyperextended ($\Theta_2 > \Theta_{2PS}$, with Θ_{2PS} the PIP angle for which $A(P,E)=A(S,E)$), the deep flexor is less antagonistic to the extensor than the superficial flexor:

$$A(P,E) > A(S,E) \quad (\theta_2 \geq \theta_{2r'}) \quad (10)$$

(iv) With increasing hyperextension of the PIP and bow-stringing of the lateral bands, the deep flexor may become more antagonistic to the extensor than the superficial flexor. The function $A(P,E)$ may even become negative ($A(P,E) < 0$), thus violating the conditions (7) (fig.2.b). In that case the finger with the (P,E,I) motor triplet is unbalanced and uncontrollable.

(v) With PIP flexion (and the increase of r_{P2}), the equilibrium forces in the extensor and interosseus also increase. This increase is most pronounced in the interosseus: the interosseus force with the deep flexor and flexed PIP is almost six times that with the superficial flexor, and about three times that with the deep flexor with extended PIP (fig.3.b). The moment arm vector diagram of fig.3.b shows that this increase is due to two causes: first, an increase in the size of the moment arm vector R_p^* due to the increase of r_{P2} ; second, a change in the direction of the moment arm vector R_p^* .

DISCUSSION

From the results (i) through (v), and the definitions D1-D3, the following can be concluded.

(i) The three-tendon (S,E,I) bi-articular chain is not well controllable, as S and E are too antagonistic (Leijnse, 1955).

(ii) For all PIP positions with $\Theta_2 > \Theta_{2PS}$, the finger is better controllable by the (P,E,I) motor triplet than by the (S,E,I) motor triplet.

(iii) The controllability of the finger by the (P,E,I) motor triplet improves with PIP flexion.

(iv) In the finger with hyper-extended PIP, the controllability with the motor triplet (P,E,I) may become worse than with the (S,E,I) motor triplet, or even impossible.

In the following, these conclusions will be commented.

The dominance of the deep flexor over the superficial flexor in the control of the unloaded finger

For all PIP positions with $\Theta_2 > \Theta_{2PS}$, the deep flexor is better positioned for good control of the unloaded finger than the superficial flexor. From this it can be conjectured that in the real finger the (P,E,I) motor triplet will dominate the (S,E,I) motor triplet in unloaded finger control. This is clinically confirmed by the fact that the superficial flexor can be removed (in fact, it is a motor of choice for many tendon transpositions) without causing apparent disfunction in the unloaded finger. This means that after the loss of the superficial flexor the control of the unloaded finger must not be relearned, which indicates that the functioning of the finger motors in the unloaded finger with and without the superficial flexor is basically not different. It also holds that the flexor P guarantees good functioning of the finger, even when the flexor S becomes exactly antagonistic to the extensor, or when $A(S,E)$ changes sign ($A(S,E) < 0$) and the bi-articular chain with the motors (S,E,I) is unbalanceable. However, as indicated in the above, this may not be the case in the finger with a hyperextended PIP (see further).

Two anatomic constructs which minimise the antagonism of the deep flexor and the extensor
In the above it was shown that for good controllability and robustness of the finger it is essential that the antagonism of the deep flexor and the extensor is minimised (i.e. expression (6) is maximised). From the fig.3.a it can be verified that this antagonism is minimised with the ratio r_{P1}/r_{P2}^* : the greater r_{P2}^* , and the smaller r_{P1} , the less antagonistic the deep flexor and the extensor will be. In the real finger, two anatomic constructs exist which minimise this ratio.

Maximisation of r_{P2}^*

A first anatomic construct is the "coupling mechanism" of the PIP and DIP joints. The coupling mechanism depends essentially on the extensor tendon, which bifurcates into a medial and two lateral slips which insert into the second and third phalanx respectively. As a result, the DIP and PIP in the (unloaded) finger move as a mechanism (Landsmeer (1958), Spoor and Landsmeer, 1976, Leijnse et al, 1992, Leijnse and Kalker, 1994). The major consequence of this mechanism is that the finger (in the sagittal plane) can be completely controlled by only three motors: the (P,E,I) triplet. Indeed, if such mechanism would not exist, the finger would have three independent joints, which cannot be controlled by three motors (this follows e.g. from the fact that without a coupling mechanism the equilibrium equations of the three-motor unloaded finger are a homogeneous set of three independent equations in three variables (the equation (1.4) is than void), which, except when the determinant is zero (a physical singularity which does not result in any viable solution), has only the trivial solution with all equilibrium forces zero). The coupling mechanism provides the large equivalent moment arm r_{P2}^* of the flexor P, which is greater than the anatomic moment arm r_{P2} of the flexor P when $r_{M2} - r_{T2} > 0$ (i.e. when $\Theta_2 > 0$) (expressions (3),(4)).

Minimisation of r_{P1}

A second anatomic construct is the "chiasma tendinum" which allows that $r_{P1} < r_{S1}$ at the MCP, and $r_{P2} > r_{S2}$ at the PIP. Anatomically, the deep flexor approaches the MCP deep to the superficial flexor, and between the MCP and PIP joints it perforates the superficial flexor tendon to a tract superficial to the superficial flexor at the PIP. Without the chiasma, the deep flexor would have to run superficial to the superficial flexor at both joints, meaning that less functional differentiation between the deep and superficial flexor would be possible. It thus can be concluded that from the point of view of the good controllability of the (unloaded) finger, both the chiasma tendinum and the coupling mechanism have a fundamental significance.

Simply assessing the differences in the unloaded finger control with active and inactive coupling mechanism of the PIP and DIP joints

(i) The difference in finger control with and without the active coupling mechanism of the PIP and DIP can be intuitively appreciated (i.e. "sensed") by mechanically blocking the coupling mechanism in ones own finger, e.g. by fixing the DIP position in extension with a mallet finger splint, or even a simple taping (applied at the dorsum of the distal extended finger so as to prevent DIP flexion). Especially in quick movements, the blocking of the coupling mechanism leads to a

The controllability of the unloaded human finger

markedly diminished "feeling of control".

(ii) The difference in the controllability of the unloaded finger with extended and flexed PIP can also be self-tested. This by performing quick and small PIP-DIP flexion-extension movements with free moving finger with the PIP in almost complete extension (i.e. a movement with the PIP oscillating in the range with $\Theta_2 = 10^\circ \pm 10^\circ$), and (intermediate) flexion (i.e. with the PIP oscillating in the range with $\Theta_2 = 45^\circ \pm 10^\circ$). One will "feel" that with an extended PIP greater forces are required, and that these movements are more "difficult" to execute than with a flexed PIP.

CLINICAL APPLICATIONS

The dominance of the flexor P over the flexor S in the control of the unloaded finger

In the above it is indicated that in the model the deep flexor is better positioned for unloaded finger control than the superficial flexor. From this it was conjectured that in the control of the unloaded real human finger the flexor P will dominate the superficial flexor. This would ensure the best control possible in the normal finger. However, in the abnormal finger the predominance of the flexor P may aggravate pathologic behaviour. In the following two examples are given.

The "driving force" of the "claw hand" deformity

When the interossei are paralysed, the unloaded finger cannot be balanced anymore. Under the (tonus) forces of the intact motors (extensor and flexors) it will "collapse" into a "clawing" position, i.e. a position with a hyperextended MCP and a flexed PIP and DIP, in which the interosseus function is taken over by passive stretching of joint ligaments and soft tissues (Landsmeer, 1955, Spoor and Landsmeer, 1976). The fig.3.b shows that in the unloaded finger with $\Theta_2 > \Theta_{2FS}$ the ratio of the interosseus force to the deep flexor force is much greater than the ratio of the interosseus force to the superficial flexor force. It follows that when the interosseus is paralysed, it will primordially be the forces of the P,E motor pair which are unopposed. From this can be concluded that: (i) the claw hand deformity results primordially from the actions of the motor pair (P,E); (ii) the clawing tendency increases with increasing PIP-DIP flexion (i.e. increasing moment arm r_{P2}); (iii) with only the flexor S the clawing will not be so pronounced. In other words, the constant strain on the soft tissues in the clawing end position (which may result in an extreme degree of hyper-extension of the MCP) will be far less with the flexor S than with the flexor P (note that with the flexor S the clawing is only with the MCP and PIP, and does not involve the DIP).

The controllability of the finger with hyper-extended PIP joint ($\Theta_2 < 0$) by the motor triplet (P,E,I)

The relative antagonism A(P,E) of the flexor P and extensor E is a function of the PIP position, through the shift of the lateral band $r_{T2}(\Theta_2)$. In the real finger the extensor tendon at the PIP has no pulleys, and with hyper-extension of the PIP the lateral bands may bow-string, i.e. luxate dorsally, away from the PIP joint axis (fig.1.d). Since the medial band is fixed by its insertion in

the second phalanx, the situation in which $r_{T2} > r_{M2}$ (i.e. with $r_{P2}^* < r_{P2}$) may well occur. As the bowstringing increases, eventually the sign of $A(P,E)$ will become negative:

$$A(P,E) = \frac{\left[|r_{P2}| + \frac{|r_{P3}|}{|r_{T3}|} \cdot (|r_{M2}| - |r_{T2}|) \right] \cdot |r_{E1}| - |r_{P1}| \cdot |r_{E2}|}{\|R_P\| \cdot \|R_E\|} < 0 \quad (11)$$

(for simplicity the moduli of the moment arms are used. For further use, the PIP angle with $A(P,E)=0$ is noted as Θ_{20}). When (11) holds, the conditions (7) are violated, and the finger becomes unbalanceable by the (P,E,I) motor triplet (it can be shown that the model will collapse into a swan-neck position (Landsmeer, 1958)). For this singularity in controllability, the amount of bow-stringing of the lateral bands need not be large. For instance, for the values r_{P1} , r_{E1} and r_{M2} of table.1, and the moment arm values $|r_{P2}| = 8, 9$, or 10 , the finger is unstable when $|r_{M2}| - |r_{T2}| < -1.25; -1.9; -2.6$ mm respectively (from the expression (11)) (fig.2.b). Depending on the degree of bow-stringing of the lateral bands, and the relative antagonism of the flexor S and the extensor E, the following situations are possible:

$$0 < A(S,E) < A(P,E) \quad (1)$$

$$0 < A(P,E) < A(S,E) \quad (2)$$

$$A(S,E) < 0 < A(P,E) \quad (3) \quad (12)$$

$$A(P,E) < 0 < A(S,E) \quad (4)$$

$$A(P,E) < 0; \quad A(S,E) < 0 \quad (5)$$

The expression (12.1) corresponds to the normal situation, in which the controllability of the finger with the flexor P is better than with the flexor S. In the case (12.2) the controllability with the flexor S is better than with the flexor P. In (12.3) the finger can only be controlled by the triplet (P,E,I). In (12.4), only the proximal bi-articular chain of the finger can be controlled (by the motor triplet (S,E,I)), while the (P,E,I) motor triplet will provoke a swan-neck. In the case (12.5) the finger cannot be controlled at all: it will collapse into a swan-neck like position with either of the triplets (P,E,I) and (S,E,I).

The case (12.4) is of interest. Here the proximal bi-articular chain of the finger is controllable by the triplet (S,E,I), while the finger with hyperextended PIP ($\Theta_2 < \Theta_{20}$, with Θ_{20} the PIP angle for which $A(P,E)=0$) is uncontrollable by the triplet (P,E,I). However, for the PIP positions with $\Theta_2 > \Theta_{20}$, the lateral bands are sufficiently close to the PIP axis of rotation to allow normal control by the (P,E,I) motor triplet. Therefore, theoretically, non-pathological finger function could be obtained by controlling the finger by the (P,E,I) motor triplet when $\Theta_2 > \Theta_{20}$, and by the (S,E,I) motor triplet when $\Theta_2 \leq \Theta_{20}$, i.e. the positions of PIP hyper-extension (Landsmeer, 1958). However, in reality such strategy of finger control may be difficult to execute. When the flexor P dominates in the normal control of the finger, it will also tend to

dominate in the control of the finger with hyper-extended PIP, thus provoking a swan-neck with PIP hyperextension even if the proximal bi-articular chain of the finger is controllable by the (S,E,I) motor triplet.

The finger of the musician with impaired PIP-DIP coupling mechanism

From the above it follows that the good controllability of the finger is the result of two very particular anatomic constructs: the coupling mechanism, as implemented by the extensor assembly, and the chiasma tendinum. Even minor disturbances of the integrity of these constructs may affect the controllability of the finger, which may become manifest when fast and accurate finger movements are required, as in the playing of an instrument. Examples are increased friction, or limitation of the differential gliding of the flexor tendons in the chiasma tendinum, or soft tissue connections in the extensor assembly which prevent the lateral bands from shifting properly and smoothly with PIP rotation. Such complications may well occur after e.g. fractures of the proximal phalanx or crush injuries which may result in slight adhesions between the flexor tendons or between the fibres of the extensor assembly. The affected finger may then be experienced as "slow", or "falling out with the other fingers" during playing. Mechanically, the effect of an impaired shift of the lateral band at the PIP due to reduced differential gliding of the fibres in the dorsal aponeurosis is twofold. Firstly, a loss of muscle power due to friction. Secondly, the fact that the coupling mechanism disfunctions (the DIP lags behind the PIP in finger flexion). This means that the equivalent moment arm $r_{P_2}^*$ remains small with finger flexion, and that the deep flexor remains quite antagonistic to the extensor. The controllability of the finger is then decreased. In such cases therapy consists of the maximal mobilisation of dorsal aponeurosis, and the differential gliding of the deep and superficial flexors.

CONCLUSIONS

In the present paper the controllability of the unloaded finger (without lumbrical) with the motor triplets formed by the deep flexor, extensor, interosseus, and the superficial flexor, extensor, interosseus is theoretically investigated. It is shown that the controllability of the finger is determined by the "degree of antagonism" (a concept defined in the text) of the flexors and extensor. For the deep flexor and the extensor this antagonism is a function of the PIP position. The following conclusions can be made:

- (i) The three-tendon (S,E,I) bi-articular chain is not well controllable, as S and E are too antagonistic.
- (ii) For all PIP positions with the PIP not too (hyper) extended, the finger is better controllable by the (P,E,I) motor triplet than by the (S,E,I) motor triplet.
- (iii) The controllability of the finger by the (P,E,I) motor triplet improves with PIP flexion.
- (iv) In the finger with hyper-extended PIP, the controllability with the motor triplet (P,E,I) may become worse than with (S,E,I) motor triplet, or even impossible.

Mention is made of two anatomic constructs which fundamentally improve the controllability of the finger with the (P,E,I) motor triplet: the chiasma tendinum, and the coupling mechanism of

the PIP and DIP joints. Clinically, it is indicated that the claw-hand as resulting from interosseus paralysis is primarily caused by the (tonus) forces of the deep flexor and extensor, and not of the superficial flexor and extensor, and further that small trauma affecting the proper functioning of the mechanism which couples the PIP and DIP actions may fundamentally worsen the controllability of the unloaded finger, e.g. in fast finger movements of the musician.

ACKNOWLEDGEMENTS

The author thanks Prof. Emer. J.M.F. Landsmeer, Prof. J.J. Kalker, Dr. C.W. Spoor, Prof.Dr.Ir. C.J. Snijders, Prof. J.C. Van der Meulen, Dr. G.J. Sonneveld and Dr. S.E.R. Hovius cordially for their valuable contributions.

REFERENCES

Landsmeer, J.M.F. (1955) Anatomical and functional investigations on the articulation of the human fingers. Acta anat. 25, 1-69.

Landsmeer, J.M.F. (1958) A report on the co-ordination of the interphalangeal joints of the human finger and its disturbances. Acta Morph. Neerl.-Scand. 2, 59-84.

Leijnse, J.N.A.L., Bonte, J.E., Landsmeer, J.M.F., Kalker, J.J., van der Meulen, J.C., Snijders, C.J. (1992) Biomechanics of the finger with anatomical restrictions:- the significance for the exercising hand of the musician, J.Biomechanics 25, 1253-1264.

Leijnse, J.N.A.L, Kalker, J.J. (1994) A two dimensional kinematic model of the lumbrical in the human finger, J. Biomechanics 28, 237-249.

Leijnse, J.N.A.L. (1995) A graphic analysis of the biomechanics of the massless proximal bi-articular chain of the human finger. To be published J. Biomechanics.

Spoor, C.W., Landsmeer, J.M.F. (1976) Analysis of the zigzag movement of the human finger under influence of the extensor digitorum tendon and the deep flexor tendon. J.Biomechanics, 9,561-566.

Spoor, C.W. (1983) Balancing a force on the fingertip of a two dimensional finger model without intrinsic muscles. J. Biomechanics 16, 497-504.

<i>MOTOR</i>	<i>Moment arm</i>			<i>Value</i>		
	<i>MCP</i>	<i>PIP</i>	<i>DIP</i>	<i>MCP</i>	<i>PIP</i>	<i>DIP</i>
<i>P</i>	r_{P1}	r_{P2}	r_{P3}	-11	-8/-9/-10	-6
<i>S</i>	r_{S1}	r_{S2}	/	-13	-9	/
<i>E</i>	r_{E1}	r_{M2}	r_{T3}	9	5	4
<i>I</i>	r_{I1}	r_{M2}	/	-6	5	/

r_{T2} : function of PIP position

Tabel I Moment arms of the motors (in mm). From: Spoor (1983)

FIGURES

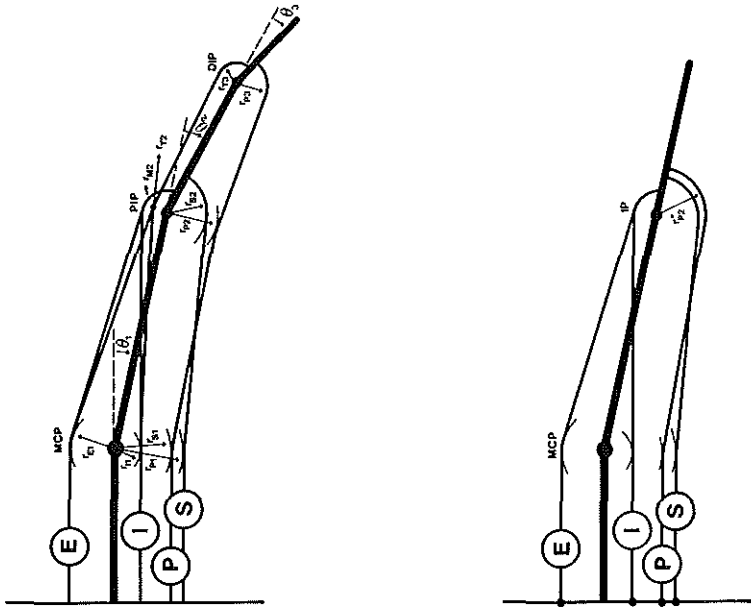


Figure 1 a) Finger model. b) Bi-articular equivalent finger model with extended IP joint.

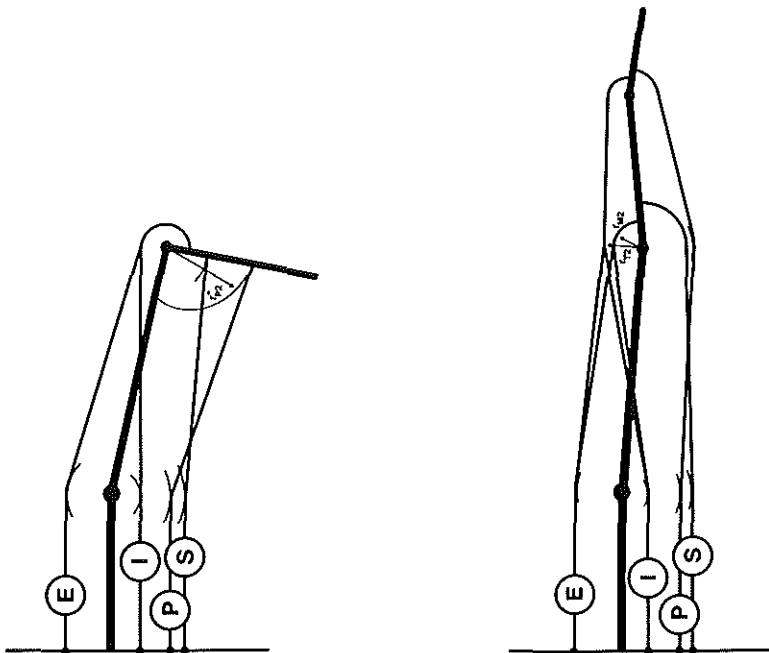


Figure 1 c) Bi-articular equivalent finger model with flexed IP joint. d) Three-articular finger model with hyperextended PIP and bow-stringing lateral band ($r_{M2} < r_{T2}$).

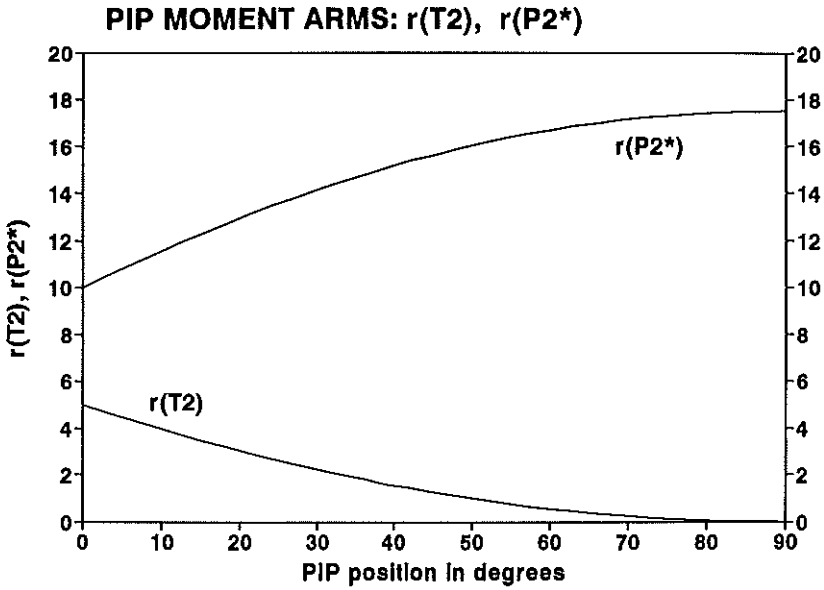


Figure 2 a Moment arm of lateral band ($r(T_2)$) at the PIP and equivalent IP moment arm of deep flexor ($r(P_2^*)$) as a function of the PIP angle.

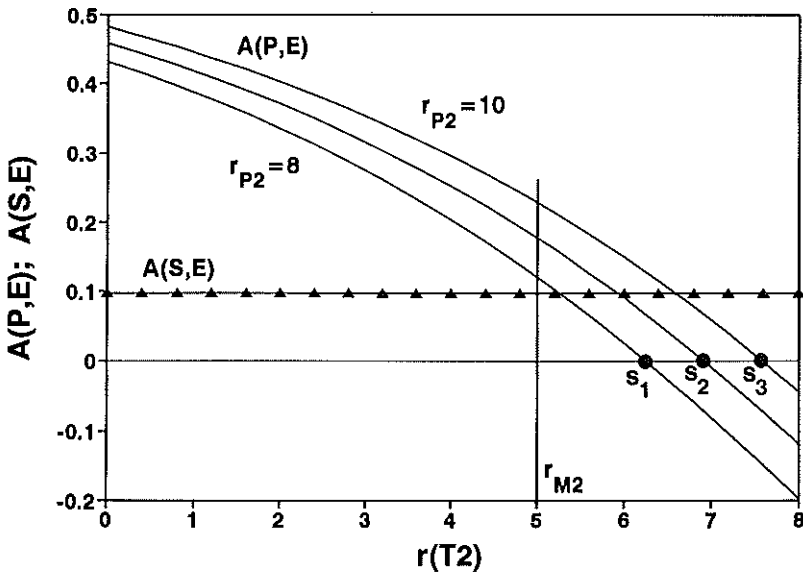


Figure 2 b Antagonism of extensor and deep ($A(P,E)$) and superficial ($A(S,E)$) flexor as a function of the moment arm r_{T_2} of the lateral band. $A(S,E)$ is constant. $A(P,E)$ decreases with increasing r_{T_2} . The three $A(P,E)$ curves correspond with the anatomic moment arms $|r_{P_2}| = 8, 9, 10$ respectively. s_1, s_2, s_3 : moment arms r_{T_2} at which the finger with the (P,E,I) motor triplet becomes unbalanced (with $|r_{P_2}| = 8, 9, 10$ respectively).

The controllability of the unloaded human finger

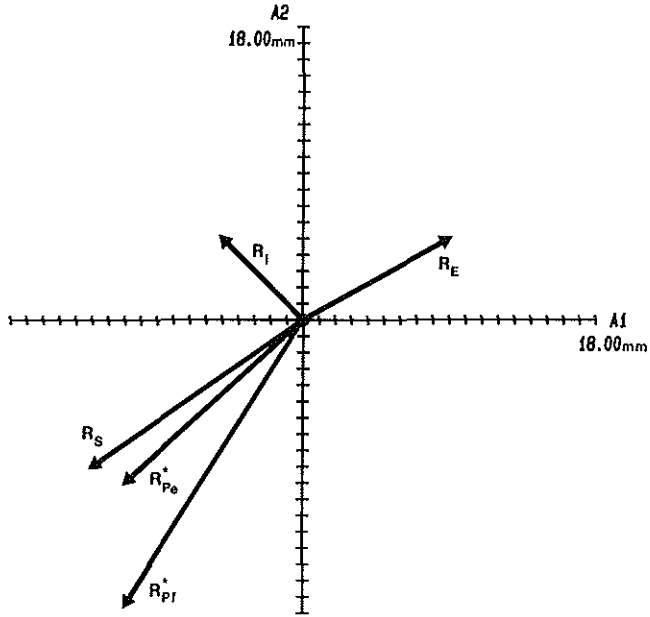


Figure 3 a Moment arm vector diagram of the equivalent bi-articular model. $R_{P_e}^*$, $R_{P_f}^*$: moment arm vector of the deep flexor with extended and flexed IP joint.

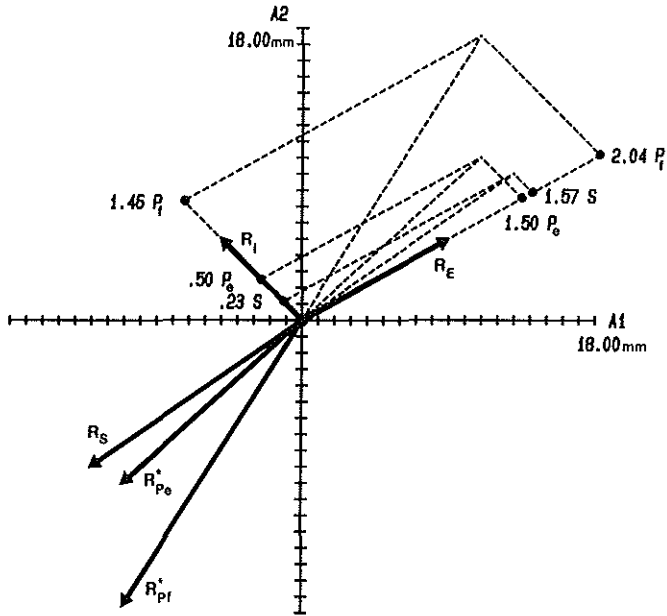


Figure 3 b Forces in extensor and interosseus as a function of the flexor forces, as determined by a force parallelogram. Three situations are presented. (i) $S=S$, $P=0$, which results in: $E=1.57 S$, $I=0.23 S$; (ii) $S=0$, $P=P_e$ (extended IP joint): $E=1.5 P_e$, $I=0.5 P_e$; (iii) $S=0$, $P=P_f$ (flexed IP joint): $E=2.04 P_f$, $I=1.46 P_f$.

WHY THE LUMBRICAL MUSCLE SHOULD NOT BE BIGGER; A FORCE MODEL OF THE LUMBRICAL IN THE UNLOADED HUMAN FINGER

J.N.A.L. Leijnse ^{†§}

^(†)Department of Plastic and Reconstructive Surgery, ^(§)Department of Biomedical Physics and Technology, Erasmus University, Rotterdam, the Netherlands.

ABSTRACT

The present paper investigates the forces in the lumbrical and the other finger motors in a two and a three dimensional unloaded human finger model (without and with the ab-adduction degree of freedom of the MCP joint, resp.). It is concluded that in the three dimensional model the lumbrical, as it is present in the human finger, is sufficiently strong to realise its maximal mechanical potential in the control of the unloaded finger. Also is pointed out the natural synergism of the lumbrical and the ulnar interosseus in the control of the finger in the sagittal plane.

NOMENCLATURE

MCP	: Metacarpophalangeal joint
PIP	: Proximal Interphalangeal joint
DIP	: Distal Interphalangeal joint
P	: (force in) Flexor Digitorum Profundus
S	: (force in) Flexor Digitorum Superficialis
E	: (force in) Extensor Digitorum
I	: (force in) Interosseus
L	: (force in) Lumbrical
R	: (force in) Radial interosseus
U	: (force in) Ulnar interosseus
M	: (force in) Medial Band of the extensor assembly
T	: (force in) Lateral Band of the extensor assembly
P_d	: (force in) deep flexor tendon distal to the insertion of the lumbrical
X_L	: force in lumbrical relative to deep flexor force ($X_L=L/P$)
r_{ij}	: anatomic moment arm of motor i at joint j
r_{ij}^*	: systematic moment arm of motor i at joint j; MCP,PIP,DIP=1,2,3
r_{AR}, r_{AU}, r_{AL}	: abduction moment arms at MCP of R,U,L
R_X	: moment arm vector of the motor X, defined by the moment arms (r_{X1}, r_{X2})
c_{XY}	: $[R_X \times R_Y]_z = r_{X1} \cdot r_{Y2} - r_{X2} \cdot r_{Y1}$, with the sign of the moment arms r_{X1}, r_{Y1} as in the model (1) or (6)
θ_j	: angle of joint j
PCA_i	: physiological cross-sectional area of motor i

INTRODUCTION

The lumbrical is a finger motor with two striking properties. One is that its origin and insertion are on the tendons of other motors (the deep flexor, and the extensor assembly) instead of on bone. The other is its small size, as its cross-section is less than a third of the next smallest finger motor, the palmar interosseus (Brand, 1985). The implications of the mobile origin, and the general kinematic properties of the finger with lumbrical have been recently investigated by Leijnse and Kalker (1994) in a two dimensional kinematic model. In this study it was indicated that the lumbrical could play an important role in the control of unloaded finger movements in the sagittal plane, and in the two dimensional model could even entirely substitute the interosseus. However, such analysis is incomplete as long as it doesn't account for the lumbrical's small size. Also, in the real finger the MCP functions as a bi-axial joint (flexion-extension, ab-/adduction), and the lumbrical has a non-zero moment arm at the MCP for radial abduction. As a result, the ulnar interosseus (i.e. the ulnar abductor of the MCP) must be active with the lumbrical to maintain the MCP in ab-adduction equilibrium. This implies that in the real finger the lumbrical and (ulnar) interosseus are active synergists in the control of the finger in the sagittal plane.

The present study investigates these two questions:

(i) are the lumbrical forces required for the lumbrical's mechanically maximal possible role in unloaded finger control within its physiological capacity;

(ii) what is the effect of the co-activation of the ulnar interosseus with the lumbrical on the lumbrical forces in the control of the finger in the sagittal plane.

These questions are investigated by comparing the motor forces in a two and a three dimensional finger model (the three dimensional model is the two dimensional model with the ab-adduction degree of freedom at the MCP). To obtain unique solutions these forces are optimised for minimal maximal motor stress. In the discussion these results are physically interpreted, and discussed with respect to literature. The present paper is a direct sequel to the paper of Leijnse and Kalker (1994), and follows their notations and terminology.

MATERIALS AND METHODS

The model

Two models will be studied in this paper: a two dimensional force model (2D model) of the unloaded finger in the sagittal plane (fig.1.a), and a three dimensional model (3D model), which is the two dimensional model with a bi-axial MCP joint (flexion/extension, abduction/adduction). These models consist of the torque equilibrium equations of the joints (MCP,PIP,DIP), and are valid only when the passive joint structures (volar plates, etc.) are slack. The motors are: the extensor (E); the radial (R) and ulnar (U) interosseus (I), the superficial flexor (S), the deep flexor (P), and the lumbrical (L). The force in the deep flexor tendon distal to the lumbrical origin is noted as P_d . The extensor assembly is modelled as a medial (M) and a lateral (T) band, in which the extensor, lumbrical and interossei insert. The extensor and the flexors are further called "extrinsic" finger motors, while the lumbrical and interosseus are called "intrinsic" motors.

Moment arms of flexion are taken negative, and written with explicit sign. The abduction moment arms of extensor and flexors at the MCP are taken zero. The 3D model is:

$$r_{EI} \cdot E - r_{II} \cdot I - r_{LI} \cdot L - r_{SI} \cdot S - r_{PI} \cdot P_d = 0 \quad (1)$$

$$r_{M2} \cdot M + r_{T2} \cdot T - r_{S2} \cdot S - r_{P2} \cdot P_d = 0 \quad (2)$$

$$r_{T3} \cdot T - r_{P3} \cdot P_d = 0 \quad (3)$$

$$T + M - E - I - L = 0 \quad (4)$$

$$P - P_d - L = 0 \quad (5)$$

$$I - R - U = 0 \quad (6)$$

$$r_{AR} \cdot R - r_{AU} \cdot U + r_{AL} \cdot L = 0 \quad (7)$$

$$E, I, L, U, R, T, M, S, P, P_d \geq 0 \quad (8)$$

(1)

The 2D model is given by the equations (1.1) through (1.5). The equations (1.1) through (1.3) are the torque equilibrium equations in the sagittal plane of MCP, PIP and DIP; the equation (1.4) expresses the continuity of E,I,L with the extensor assembly (Spoor, 1983); (1.5) expresses the continuity of the deep flexor P with P_d and L. For simplicity, the flexion moment arms r_{RI} and r_{UI} of radial and ulnar interosseus at the MCP are taken equal (r_{RI}=r_{UI}=r_{II}). It then holds that:

$$r_{RI} \cdot R + r_{UI} \cdot U = r_{II} \cdot (R+U) = r_{II} \cdot I \quad (2)$$

which explains the equation (1.6) and the interosseus term in the equation (1.1). The equation (1.7) is the abduction-adduction (A-A)-equilibrium of the MCP. The non-negativity conditions of the forces (1.8) express that muscles can only pull, not push. The lumbrical force L and the force P_d in the tendon of the deep flexor P distal to the lumbrical origin can also be expressed as:

$$\begin{aligned} L &= X_L \cdot P \\ P_d &= (1-X_L) \cdot P \end{aligned} \quad (3)$$

with: $0 \leq X_L \leq 1$, and P the force in the deep flexor motor itself. In the real finger the moment arm r_{T2} decreases with PIP flexion (Garcia-Elias et al, 1991). In the calculations, this function r_{T2}(θ₂) is approximated by (Leijnse and Kalker, 1994) (fig.2.a):

$$r_{T2} = r_{M2} \cdot \left[1 - \frac{2 \cdot \theta_2}{(\pi/2)} + \frac{\theta_2^2}{(\pi/2)^2} \right] \quad (4)$$

All other moment arms are taken constant; the values used for calculation are given in table.1.

Optimization criterion

The models are undetermined and a unique solution must be obtained by optimization. The optimization criterion is the minimisation of the maximal muscle stress as described by An et al. (1984):

$$\text{Min } \sigma ; \quad \frac{F_i}{PCA_i} \leq \sigma \quad (5)$$

with F_i the muscle force, and PCA_i the physiological cross-sectional area of the motors M_i , given in the table 2 (from Chao et al, 1989). In the following the model will be minimized by variation of the forces F_i , and also by varying both the forces F_i and the lumbrical cross-sectional area PCA_L . Hereby a penalty on lumbrical cross-section (spare capacity) is introduced by the condition that the lumbrical stress should equal the minimax stress ($\sigma_L = \sigma_m$), as explained further.

RESULTS

Equivalent representations and analytical solutions of the 2D model

The bi-articular equivalent 2D model

The elimination of the variables M , T , and P_d from the 2D model (1.1) through (1.5) leaves two equations:

$$E. \begin{bmatrix} r_{E1} \\ r_{M2} \end{bmatrix} + I. \begin{bmatrix} -r_{I1} \\ r_{M2} \end{bmatrix} + L. \begin{bmatrix} r_{L1}^* \\ r_{L2}^* \end{bmatrix} + S. \begin{bmatrix} -r_{S1} \\ -r_{S2} \end{bmatrix} + P. \begin{bmatrix} -r_{P1} \\ -r_{P2} \end{bmatrix} = \begin{bmatrix} 0 \\ 0 \end{bmatrix} \quad (6)$$

in which the systematic moment arms r_{P2}^* , r_{L1}^* and r_{L2}^* are given by (Spoor and Landsmeer, 1976; Leijnse and Kalker, 1994):

$$\begin{aligned} r_{P2}^* &= r_{P2} + \frac{r_{P3}}{r_{T3}} \cdot (r_{M2} - r_{T2}) \\ r_{L1}^* &= r_{P1} - r_{L1} \\ r_{L2}^* &= r_{P2}^* + r_{M2} \end{aligned} \quad (7)$$

The equations (6) describe the equilibrium of the bi-articular chain of fig.1.b, in which the lumbrical is present with a fixed origin (Leijnse and Kalker, 1994), with the condition that $L \leq P$.

The analytical solutions of the 2D model

In the terms of the equivalent 2D model (expression (6)) of fig.1.b, and the expression (3), the analytical solutions are:

$$I = \left[\frac{c_{PE}^*}{c_{EI}} - \frac{c_{EL}^*}{c_{EI}} X_L \right] \cdot P + \frac{c_{SE}}{c_{EI}} \cdot S \quad (a)$$

(8)

$$E = \left[\frac{c_{IP}^*}{c_{EI}} - \frac{c_{LI}^*}{c_{EI}} X_L \right] \cdot P + \frac{c_{IS}}{c_{EI}} \cdot S \quad (b)$$

which can also be written as:

$$I = \frac{c_{PE}^*}{c_{EI}} \cdot (1 - X_L) \cdot P - \frac{c_{EL}^*}{c_{EI}} \cdot X_L \cdot P + \frac{c_{SE}}{c_{EI}} \cdot S \quad (a)$$

(9)

$$E = \frac{c_{IP}^*}{c_{EI}} \cdot (1 - X_L) \cdot P + \frac{c_{LI}^*}{c_{EI}} \cdot X_L \cdot P + \frac{c_{IS}}{c_{EI}} \cdot S \quad (b)$$

Hereby the coefficients c_{XY} are calculated as:

$$c_{XY} = r_{X1} r_{Y2} - r_{X2} r_{Y1} \quad (10)$$

with the moment arms with the sign as in the model equations (1). The c_{XY}^* and c_{XY} are calculated with the systematic and anatomic moment arms respectively. The expressions (8) and (9) are derived from each other by taking into account that: $c_{EL}^* = c_{PE}^* + c_{EL}$; and $c_{LI}^* = c_{IP}^* - c_{IL}$. In the normal finger it holds that in the expressions (8) and (9) all factors $c_{XY} > 0$.

The moment arm vector diagram of the bi-articular equivalent 2D model

The column matrices in expression (6) can be interpreted as the cartesian coordinates of the "moment arm vectors" $\mathbf{R}_E, \dots, \mathbf{R}_P^*$. As such, the equations (6) can be represented by the vector equilibrium of these moment arm vectors (fig.3.a) (Leijnse^a, 1995). Hereby the motor forces are the scalars of vector multiplication to obtain a zero vector sum.

Muscle forces in the 2D model

The redundancies in the finger model

In the 2D model five motors are present, while three suffice for control of the bi-articular chain (for a general approach, see Leijnse, 1995^(b)). The vector diagram of fig.3.a shows that redundancies exist with the intrinsics (I,L), and the flexors (P,S) (not with the extensor, as this motor alone controls the extension side of the MCP in the model (1)). This redundancy follows from the fact that in the fig.3.a any non-negative combination of the moment arm vectors $\mathbf{R}_P^*, \mathbf{R}_S$ of the flexors can be balanced by any non-negative combination of the moment arm vectors $\mathbf{R}_I, \mathbf{R}_L^*$ of the intrinsics, and the extensor \mathbf{R}_E :

Why the lumbrical should not be bigger

$$K_1 \cdot [\lambda_1 \cdot R_p^* + (1-\lambda_1) \cdot R_S] + K_2 \cdot [\lambda_2 \cdot R_I + (1-\lambda_2) \cdot R_L^*] + E \cdot R_E = 0 \quad (11)$$

$$0 \leq \lambda_i < 1 ; K_p, E \geq 0$$

From the expression (11) it can be derived that the mutual redundancy of the flexors, and of the intrinsics requires that:

$$\frac{c_{FE}}{c_{EX}} > 0; \quad \frac{c_{XF}}{c_{EX}} > 0 \quad (12)$$

(with F=P or S, and X=I or L). These conditions are satisfied in the normal finger (fig.3.a), since: $c_{EX} > 0, c_{XF} > 0$ and $c_{FE} > 0$. When the conditions (12) are not satisfied the redundancies change: e.g. a flexor for which $c_{FE} < 0$ while $c_{EX} > 0$ and $c_{FX} > 0$, would be redundant with the intrinsics (Spoor, 1983). The effect of the mutual substitution of interosseus force and lumbrical force is given by the equations (8), and is presented in the fig.4.a (with S=0, and P=1), and more generally in the figs.5.a,c (with S \geq 0, and P=1), as calculated with the moment arm values of table 1.

The effect of the PIP position on the equilibrium forces of the motors

The systematic moment arms r_{L2}^* , and r_{P2}^* increase considerably with PIP flexion (fig.2.a), as they depend on the moment arm r_{T2} (expression (7)), which decreases with PIP flexion (expression (4)). The fig.3.a provides the systematic moment arm vectors R_p^*, R_L^* for the completely extended (e) and 90°-flexed (f) PIP, as calculated from the expression (4). These changes in moment arms imply that with PIP flexion the motors E and I become mechanically less effective with respect to the deep flexor and lumbrical, as can be appreciated from the fig.4.a where the extensor and interosseus forces are given for the flexed and extended finger. These diagrams show that the effect of PIP position changes is most pronounced with L=0 in the interosseus ($I^e \approx 0.33 I^f$, with L=0), and is much less in the extensor ($E^e \approx 0.7 E^f$). In the combined vector diagram of fig.3.b these forces are given for the extended and flexed finger for the cases in which I=0 or L=0.

Maximum lumbrical force in the 2D model

The lumbrical force is maximal when the interosseus force is zero (I=0 in expression (8.a)), and is given in fig.4.a as a function of the PIP position (with S=0). The fig.2.b shows that the lumbrical force (with S=0) as a fraction X_L of the deep flexor force, is maximally $X_{2Dmax} \approx 0.3$ with extended, to $X_{2Dmax} \approx 0.55$ with flexed PIP. When the lumbrical force exceeds these values the 2D model (with S=0) is unbalanced. From expression (8.a) follows that excess lumbrical forces can only be balanced by the superficial flexor, when the flexor redundancy conditions (12) hold, i.e. when $c_{SE}/c_{EI} > 0$.

The lumbrical-interosseus substitution rate in the 2D model

The slope of the line of the interosseus force as a function of the lumbrical force in the fig.4.a is:

$$-\frac{c_{EL}^*}{c_{IE}} = -\frac{r_{L2}^* r_{EI} - r_{LI}^* r_{M2}}{r_{II} r_{M2} + r_{M2} r_{EI}} \quad (13)$$

and is given as a function of the PIP position in the fig.2.c. The greater this ratio, the less lumbrical force is required to obtain equal intrinsic effect as with the interosseus. The L-I substitution rate is well in favour of the lumbrical ($1.8 \leq c_{EL}^*/c_{IE} \leq 2.7$), because of the large systematic moment arm r_{L2}^* which increases with PIP flexion. The rate also increases with a decreasing systematic moment arm $r_{LI}^* = r_{PI} - r_{LI}$, meaning that for maximal lumbrical effectivity the anatomic moment arm r_{LI} of the lumbrical at the MCP should be as large as possible.

The effect of the lumbrical on the loading of the extensor in the unloaded 2D model

The substitution of interosseus force by lumbrical force somewhat decreases the extensor force (fig.4.a, fig.3.b). This effect is greater with flexed than with extended PIP ($E_{Lf} = 0.6 * E_{Ie}$; $E_{Le} = 0.8 * E_{Ie}$, fig.3.b). It may be analysed from the MCP equilibrium equation of expression (6):

$$r_{EI} \cdot E = -r_{LI}^* \cdot L + r_{II} \cdot I + r_{SI} \cdot S + r_{PI} \cdot P \quad (14)$$

At complete I/L substitution ($I=0$), the interosseus term $r_{II} \cdot I$ in expression (1.1) is zero. To the degree that $r_{LI}^* > 0$, the lumbrical force further decreases the extensor load, by reducing the deep flexor torque at the MCP (this (small) effect is clear from the equivalent model (fig.1.b)). When $r_{LI}^* = 0$, $I=0$ and $S=0$, the extensor force is only function of the deep flexor torque at the MCP: $E/P = r_{PI}/r_{EI}$. This ratio is independent of the PIP position, as can be verified from the fig.3.b, or the line (e,f) in the fig.4.a, which interpolates the extensor forces with $I=0$ for all PIP positions from the force with flexed and extended PIP. This is the force-equivalent view of the extensor-deep flexor-lumbrical MCP control system discussed in Leijnse and Kalker (1994). Hereby the lumbrical controls the PIP-DIP positions, while the extensor and deep flexor control the MCP position, with a force ratio unaffected by the PIP-DIP positions.

Muscle forces in the 3D model

In the 3D model, the lumbrical moment arm r_{AL} of MCP abduction is non-zero. Therefore, the substitution of the interossei by the lumbrical cannot be complete, as lumbrical forces at the MCP must be balanced by the ulnar interosseus. This is quantified by the analytical solutions of the 3D model (1):

Why the lumbrical should not be bigger

$$\begin{aligned}
 \left(\frac{r_{AU} + c_{EU}}{r_{AR} + c_{ER}} \right) \cdot U &= \frac{c_{SE}}{c_{ER}} \cdot S + \left[\frac{c_{PE}^*}{c_{ER}} - \left(\frac{c_{EL}^*}{c_{ER}} - \frac{r_{AL}}{r_{AR}} \right) \cdot X_L \right] \cdot P \\
 \left(\frac{r_{AR} + c_{ER}}{r_{AU} + c_{EU}} \right) \cdot R &= \frac{c_{SE}}{c_{EU}} \cdot S + \left[\frac{c_{PE}^*}{c_{EU}} - \left(\frac{c_{EL}^*}{c_{EU}} + \frac{r_{AL}}{r_{AU}} \right) \cdot X_L \right] \cdot P \\
 (r_{AU}c_{ER} + r_{AR}c_{EU}) \cdot E &= r_{AU} \cdot \left((c_{RP}^* - c_{LR}^* \cdot X_L) \cdot P + c_{RS} \cdot S \right) + r_{AR} \cdot \left((c_{UP}^* - c_{LU}^* \cdot X_L) \cdot P + c_{US} \cdot S \right) \\
 &\quad - r_{AL} r_{M2} (r_{RI} - r_{UI}) \cdot X_L \cdot P
 \end{aligned} \tag{15}$$

When $r_{RI} = r_{UI} = r_{II}$, as is assumed in the calculations, then $c_{EU} = c_{ER} = c_{EI}$, $r_{RS} = r_{US} = r_{IS}$, and $r_{RP}^* = r_{UP}^* = r_{IP}^*$, from which follows that the extensor forces as a function of the lumbrical force in the 2D model and 3D model are equal ($E_{3D}(X_L) = E_{2D}(X_L)$) for $X_L \leq X_{3D,max}$. The calculated forces are shown in the fig.6.a,c for the extended and flexed PIP. The maximal lumbrical force ($X_{3D,max}$) with $S=0$ is when the radial interosseus force is zero ($R=0$), and is presented in fig.2.b as a function of the PIP position. With $R=0$, the ulnar interosseus force is minimal, and determined by the MCP abduction equilibrium equation: $U = r_{AL}/r_{AU} \cdot L \approx 5/6 \cdot L$, or about 83% of the lumbrical force. However, the effective contribution of the ulnar interosseus to the finger equilibrium in the sagittal plane (i.e its effective "intrinsic capacity") is less than this percentage, because in the sagittal plane the interosseus is mechanically less effective than the lumbrical. This can be shown as follows (fig.2.b). In the 2D model, the lumbrical may provide the total intrinsic function ($X_{2D,max}$, with $I=0$). Hereby its force depends only on the extrinsic forces (P,S,E). With $r_{RI} = r_{UI} = r_{II}$, the extrinsic forces in the 2D- and 3D-model are the same (see expression (15), where $E_{3D}(X_L) = E_{2D}(X_L)$), which means that the total intrinsic force required in the 3D-model for equilibrium of the finger in the sagittal plane is equal to the 2D-model. From this follows that the maximal contribution of the lumbrical to the total intrinsic function in the 3D model is given by the ratio $X_{3D,max}/X_{2D,max}$. This ratio is presented in the fig.2.b (MAX % IF). The figure shows that in the 3D model the lumbrical can maximally (i.e. when $R=0$) provide 68-76% of the intrinsic function (for the extended and flexed finger, resp.). The remainder of the intrinsic function is then provided by the ulnar interosseus. To conclude, while the ulnar interosseus force is about 83% of the maximal lumbrical force (when $R=0$), i.e. about 45% of the total intrinsic force ($U+L$), its effective contribution to intrinsic function in the finger equilibrium in the sagittal plane is about 30%.

Sensitivity analysis of lumbrical cross section in the 2D and 3D models of the unloaded finger

In this section, the 2D and 3D models are optimized for minimal maximal muscle stress (expression (5)). The sensitivity of these optima with respect to the lumbrical cross section (as a measure of lumbrical strength) is investigated. To this end, the optimization problem (5) is solved with the lumbrical cross section as a variable. To avoid spare capacity in the lumbrical, the condition is put that the lumbrical stress must be equal to the minimax stress ($\sigma_L = \sigma_m$). The minimized forces and stresses as corresponding to the fixed physiological lumbrical cross section

PCA_{Lp} are indicated as X_m and σ_m . The minimized forces and stresses with the optimized variable lumbrical cross section PCA_{Lo} are denoted by X_o and σ_o . The motor forces and stresses in the 2D and 3D models are given in the figs.5 and 6, both for the extended and flexed finger. These diagrams are calculated with respect to the (unit) force in the deep flexor ($P=1$). The optimal stresses and lumbrical cross sections are summarised in the table.3 (the optimal lumbrical cross sections are given relative to the physiological cross section: PCA_{Lo}/PCA_{Lp}).

Minimax stress with zero superficial flexor force ($S=0$)

- The figs.5.a,d and 6.a,d show that in the unloaded 2D and 3D models (with $S=0$), the extensor determines the maximal stress, which is minimised by the lumbrical to the optimal solution with $\sigma_L=\sigma_E$. The stress in all other motors (P,S,I) is considerably less than the minimax stress, which means that in unloaded equilibrium these motors have "spare capacity" with respect to the extensor and lumbrical.

- In all cases it holds that $\sigma_m > \sigma_o$, i.e. the physiological minimax stress is greater than the minimax stress with PCA_{Lo} . This means that in these static equilibrium models the physiological lumbrical size is smaller than the optimal lumbrical size ($PCA_{Lp} < PCA_{Lo}$) (see table 3). The table 3 also shows that the physiological and optimal lumbrical cross sections (PCA_{Lp}, PCA_{Lo}) differ less in the 3D- model than in the 2D model, and that this difference increases with PIP-flexion. In the extended 3D model the difference is smallest, and it is also rather small in relative terms ($PCA_{Lo}=1.3*PCA_{Lp}$).

Minimax stress with non-zero superficial flexor force ($S > 0$)

From the MCP equilibrium equation (14) it follows that the extensor force increases at a rate $r_{SI}/r_{EI}=1.5$ as a function of the superficial flexor force (figs.4.b and 4.c). With increasing superficial flexor force, the difference in extensor and lumbrical stress decreases in relative terms in both the 2D-and 3D- models (figs.5 and 6). From this follows that the ratio of optimal (PCA_{Lo}) over physiological (PCA_{Lp}) lumbrical cross section also decreases (see table 3). In the extended 3D model (fig.6.b), this leads to a second physiological optimum (with $\sigma_m=\sigma_o=\sigma_L=\sigma_E$) at $S \approx 0.6*P$. For superficial flexor forces above this optimum ($S > 0.6*P$), the physiological lumbrical stress is even less than the minimax extensor stress. In the flexed 3D model, and in the 2D models, the differences between the optimal lumbrical cross section and the physiological cross section remain large (ratio 1.4 (3D) and 2 (2D)).

DISCUSSION

A physical interpretation of the minimax stress criterium, and the lumbrical-extensor synergism

In order to physically interpret the results, especially the figs.5 and 6, the synergistic model (5) is more strictly formulated. In the model (5), muscle stress can be minimized by variation of the forces and the muscle cross sections. The minimax stress with fixed cross sections is further called σ_m . With variable cross sections, a non-trivial solution (i.e. with finite cross sections) can be

obtained only by introducing a penalty on "spare motor capacity". Spare motor capacity must be defined relative to a "physiologically optimal" muscle stress, further called σ_o . This is a physiological muscle property which causes muscles with stresses less than σ_o to decrease in cross section (atrophy), and muscles with stresses greater than σ_o to increase in cross section (hypertrophy). When this generalised model with variable cross-sections is optimized ("exercised") for a single task, the solution is with all muscle stresses equal to the physiologically optimal muscle stress: $\sigma_i = \sigma_o$. Indeed, cross sections which are initially too small ($\sigma_i > \sigma_o$) will increase (minimizing the stress), and those which are too great ($\sigma_i < \sigma_o$) will decrease in cross section (minimizing the penalty). However, when the model is optimized for multiple tasks, the cross sections will be such that for each individual task some motors, possibly all of them, will have spare capacity ($\sigma_i < \sigma_o$), while for each motor a (number of) tasks will exist in which it reaches the physiologically optimal muscle stress ($\sigma_i = \sigma_o$). Clearly, the cross section of these motors is then determined by these task(s). With respect to this introduction, from the results the following can be remarked.

(i) In the unloaded finger, the minimax stress is set by the extensor, which, being the only extensor of the MCP, cannot escape load. This extensor stress $\sigma_E \leq \sigma_o$ is minimized by the variation of the other motor forces, within the redundancy ranges expressed by expression (11).

(ii) Relative to the extensor stress σ_E , the motors P,S,I have considerable spare capacity, as $\sigma_P, \sigma_S, \sigma_I < \sigma_E$. This means that the cross sections of these motors are determined by other tasks than unloaded finger control, i.e. by loaded situations.

(iii) The extensor stress is minimized by the lumbrical force (for given flexor forces). In the 3D model of the extended finger, the minimax stresses resulting from the optimization with the physiological cross sections, and the optimization with the variable lumbrical cross section is almost equal, for $S \geq 0$. From this it can be concluded that the lumbrical cross section in the normal finger is "tuned" to the extensor cross section for the task of the control of the unloaded extended finger. In the finger model with a flexed PIP joint this does not hold, since $PCA_{Lo} = 2.5 * PCA_{Lp}$ ($\Theta_2 = 90^\circ$; $S = 0$). This is discussed in the next section.

The minimax stress as a function of the PIP position

The results (figs.4) show that with PIP flexion, E and I and to a lesser degree also L, become less efficient than the flexors, as the ratio of their forces increases. This is not incompatible with the physiological functioning of the finger. In reality, muscle forces consist of active and elastic components. Therefore, the stresses σ_i in E, I and L can be written as a sum of the stress resulting from the active (a) and the elastic (k) flexor forces: $\sigma_F = \sigma_{Fa} + \sigma_{Fk}$ (F stands for P or S). The elastic flexor forces increase unavoidably with the stretching of the flexors in finger extension; therefore σ_{Fk} is large in the extended finger. With flexed PIP, the elastic flexor forces are small, and the term σ_{Fa} dominates, while for unloaded finger control these active flexor forces need not be large in absolute terms. Therefore, in absolute terms the stress in E and I is likely to be smaller with flexed (f) than with extended (e) PIP joint. The relative mechanical extensor/flexor efficiency, and the role of the lumbrical in the extensor apparatus, can thus be seen as optimized for the position with greatest absolute stress, which is in the extended finger.

The flexor redundancy and lumbrical function in the unloaded finger model

For control of the entire finger the deep flexor force must be non-zero, as it alone flexes the DIP joint. Minimizing motor forces for a given deep flexor force results in a zero superficial flexor force ($S=0$), which means that the active use of the superficial flexor in the unloaded finger model is non-optimal. Physically, the reason is clear. The superficial flexor force increases the overall loading, especially of the extensor, but it does not provide any function which the deep flexor cannot provide (on the redundancy of the flexors in the unloaded finger, see Leijnse^b (1995)). However, in the extended finger the elastic force of the superficial flexor is unavoidable. The fig.6.b shows that the lumbrical may maximally balance the elastic superficial flexor force in the extended finger without incurring stresses much in excess of the extensor stress (with $X \geq X_0$), which means that such lumbrical action is physiologically realistic. Hereby the lumbrical force may not equal or exceed the deep flexor force as this would impair the control of the DIP (the deep flexor tendon distal to the lumbrical origin would become slack). This condition is well satisfied in both the 2D and 3D models in all positions, as the figs.5 and 6 show (for $S \leq P$). The lumbrical and interosseus forces as a function of the superficial flexor force are also given in the moment arm vector diagram of fig.3.c.

Should the lumbrical be bigger?- the synergism of the lumbrical and ulnar interosseus in the 3D model

The fig.6.b gives the minimax stresses in the extended finger, which according to the above correspond to the maximal stresses in the finger motors in absolute terms. The figure shows that in the unloaded extended 3D model a stronger-than-physiological lumbrical is not useful, as this would merely result in surplus lumbrical capacity. The fig.5.b shows that in the extended 2D model with maximal lumbrical force the lumbrical stress with the physiological lumbrical cross section PCA_{Lp} is $\sigma_L/\sigma_E=2-1.4$ ($0 \leq S \leq P$). In the 3D model these ratio's are $\sigma_L/\sigma_E=1.3-0.93$ ($0 \leq S \leq P$) (fig.6.b). The difference in the lumbrical stress in the 2D-and 3D- models results from the action of the ulnar interosseus in the 3D model, which is a lumbrical antagonist for MCP abduction, but an agonist in the finger equilibrium in the sagittal plane. This indicates that the lumbrical size is physiologically optimized with respect to the extensor stress, taking into account the synergistic action of the ulnar interosseus. With respect to the redundancy of lumbrical and interossei, it holds that the finger without lumbrical remains fully controllable. However, the controllability of the finger without interossei is impaired in the abduction plane of the MCP, and equilibrium of the finger in the sagittal plane requires greater than physiological lumbrical strength, as shown by the 2D model. This indicates why in the real finger with paralysed interossei but intact lumbrical, the "clawing" of the finger eventually still occurs: the lumbrical on its own is physiologically not strong enough to withstand in the long run the collapse inducing extrinsic motor forces.

The influence of lumbrical force on interosseus and extensor force and stress

The stress diagrams of the 3D model (fig.6.b,d) show that the interosseus has considerable spare capacity (indicating its importance in the loaded situation), while the lumbrical functions at

Why the lumbrical should not be bigger

minimax stress level. It follows that the prime function of the lumbrical in the unloaded finger cannot be the static unloading of the interossei, as $\sigma_I < \sigma_L$. Moreover, in the 3D model the unloading effect in the ulnar interosseus, especially in the extended finger, is very small (fig.6.b). Neither is it obvious that the prime function of the lumbrical is the reduction of the extensor stress. In the extended finger the maximal extensor stress reduction is relatively small (fig.4.b), while with flexed PIP the extensor stress reduction is potentially greater (fig.4.c) but requires a physiological lumbrical stress much in excess to the extensor stress ($\sigma_L > \sigma_E$) (fig.6.d). Mechanically, the extensor stress reduction is increased when the lumbrical moment arm r_{Li} at the MCP decreases (this can be verified from the expression (14), where r_{Li}^* is of negative sign). However, anatomical provisions exist to keep this moment arm r_{Li} about equal to the deep flexor moment arm ($r_{Li} \approx r_{Pi}$). A shift towards the MCP axis is prevented by the volar plate, while a shift away from it, i.e. the "bowstringing" of the lumbrical with flexing MCP, is prevented by the fibrous channel through which the lumbrical runs, and which acts as a pulley (Kaplan, 1965).

U-E-P-L control of the unloaded finger.

In the above it is shown that the lumbrical in the unloaded 3D model may mechanically provide about 70% of the intrinsic function, and that it is physiologically strong enough to do so. It is also indicated that in the static unloaded finger its prime role cannot be the unloading of the interosseus or extensor. The question then arises of what the "real function" of the lumbrical is. In the 2D model the lumbrical can completely determine the PIP-DIP positions (with $I=0$). The finger can then be moved at the MCP by the deep flexor and extensor alone (Leijnse and Kalker, 1995). When at the MCP the lumbrical moment arm r_{Li} equals the deep flexor moment arm ($r_{Li} \approx r_{Pi}$), the ratio of extensor over deep flexor force is independent of both the PIP and MCP positions. As indicated in the above, this condition $r_{Li} \approx r_{Pi}$ is satisfied in the real finger by appropriate pulley mechanisms. The extensor-deep flexor-lumbrical control mechanism is especially adapted for executing finger movements with isometric PIP-DIP joints, a condition corresponding to an isometric lumbrical. A similar concept of finger control can also be envisaged in the 3D model in the sagittal plane, when the MCP moment arm of flexion of the ulnar interosseus is zero. In that case both the ulnar interosseus and lumbrical change length only with PIP-DIP joints, while the ratio of extensor over deep flexor force remains independent of the MCP and PIP-DIP positions (equation (14) with $I=U$, $r_{II}=0$, $r_{Li}^*=0$). Keeping both the PIP-DIP joints isometric, and the finger in the same position of abduction then corresponds to keeping the ulnar interosseus and the lumbrical at fixed length, while the MCP is then controlled by the deep flexor and the extensor as a simple antagonistic motor pair. In Chao et al. (1989), it is reported that the moment arm of the ulnar interosseus in the real finger with an MCP in near extension is indeed close to zero. Also is reported that the insertions of the ulnar interosseus are predominantly in the extensor assembly, and therefore affect the PIP position, while the radial interossei have more substantial insertions at the base of the proximal phalanx. Such anatomic findings correlate to this concept of finger control. To conclude, in the unloaded 3D model moving in the sagittal plane, a basic control concept can be envisaged formed by the extensor, deep flexor, lumbrical and ulnar interosseus.

Physical interpretations of lumbrical function

The expressions (8) and (9) provide different views of lumbrical function. The expression (8) describes the unloaded finger model in the terms of the systematic lumbrical moment arms, i.e. with a lumbrical with a fixed origin as in the fig.1.b (Leijnse and Kalker, 1994). The expression (9), however, contains the anatomic moment arms and allows for physical interpretations of the lumbrical-deep flexor construct as anatomically present in the real finger. In the following it is assumed that $S=0$.

(i) Putting $X_L=0$ in (9.a) gives the interosseus force with inactive lumbrical. The equation may be rewritten as:

$$c_{EI} \cdot I = c_{PE}^* \cdot P \quad (16)$$

which mathematically reflects the Landsmeer view of the control of the bi-articular chain as a balance of intrinsic and extrinsic muscle forces (Spoor and Landsmeer (1976), Leijnse and Kalker (1994)). It gives the interosseus and deep flexor forces with respect to a given extensor force. The right hand side of expression (16) expresses the extrinsic "collapse-inducing" force, as a product of the extrinsic "collapse-inducing efficiency c_{PE}^* " (the factor c_{PE}^* contains only extrinsic parameters) and the extrinsic force P. The left hand side represents the total amount of intrinsic "collapse-reducing" force required for finger equilibrium, as a product of the "intrinsic interosseus efficiency c_{EI} " and the interosseus force I.

(ii) With $X_L > 0$ in equation (9.a), the lumbrical substitutes (part of) the interosseus force. This substitution is effectuated by two distinct terms, each of which has a physical meaning.

a) the term $c_{PE}^*/c_{EI} \cdot (1-X_L) \cdot P$:

The lumbrical force X_L reduces the term $c_{PE}^* \cdot P$, i.e. the total extrinsic "collapse-inducing" force, by the factor $(1-X_L)$. This reduction may be called the "extrinsic effect" of the lumbrical. The total product term $c_{PE}^* \cdot (1-X_L) \cdot P$ allows for two interpretations, which mathematically can be written as:

$$\begin{aligned} [c_{PE}^* \cdot (1-X_L)] \cdot P &= c_{PEX}^* \cdot P & (a) \\ c_{PE}^* \cdot [(1-X_L) \cdot P] &= c_{PE}^* \cdot P_d & (b) \end{aligned} \quad (17)$$

The first interpretation, given by (17.a), is in the terms of the intrinsic/extrinsic balance, and states that the lumbrical reduces the efficiency c_{PEX}^* of the collapse-inducing action of the extrinsics. The second interpretation (17.b) corresponds to what has been named the "reduction of the elastic pull" of the deep flexor (Long, 1968): the lumbrical force reduces the force $P_d=(1-X_L) \cdot P$ in the deep flexor tendon distal to the lumbrical origin.

b) the term $c_{EL}/c_{EI} \cdot X \cdot P$

This term expresses the purely "intrinsic effect" of the lumbrical. In the above, the factor c_{EI} is interpreted as the "intrinsic efficiency" of the interosseus as the antagonist of the extrinsic collapse-inducing forces. In analogy, c_{LE} can be interpreted as the "intrinsic efficiency" of the lumbrical, when it is considered as an interosseus, i.e. with a fixed origin on the metacarpals, and with its normal anatomic moment arms. The factor c_{EL}/c_{IE} then expresses the relative intrinsic efficiency of lumbrical and interosseus. This ratio is somewhat to the advantage of the lumbrical, as $r_{L1} > r_{I1}$, and therefore $c_{LE}/c_{IE} > 1$.

Why the lumbrical should not be bigger

(iii) The equation (9.b) can be similarly interpreted.

- extrinsic effect: the reduction in extensor force due to the extrinsic effect (1-X) of the lumbrical is clear.

- intrinsic effect: when the interosseus is replaced by an interosseus with lumbrical moment arms, the extensor force increases to the degree that $r_{L,I} > r_{II}$, which corresponds to: $c_{IL} > 0$. In the normal finger the extrinsic effect (1-X) dominates the intrinsic effect (X) since $c_{PI}^* >> c_{IL}$, meaning that lumbrical/interosseus substitution reduces the extensor force, as was shown in the section on extensor loading.

To summarise, the lumbrical action can be interpreted as consisting of two superimposed effects: (i) the decrease of the extrinsic collapse tendency of the chain by diminishing the tension in the P_d and extensor, and (ii) the balancing of the remaining collapse tendency by a true intrinsic (interosseus) action. This view is illustrated in the fig.1.c, and in the fig.3.d, where these two effects are represented by two separate motors. One motor deviates deep flexor force to the environment proximal to the MCP (in the fig.3.d this effect is represented by the exact antagonist $R_{PL} = -R_P^*$ (Leijnse, 1995^(b)) of the deep flexor moment arm vector). The other motor is an interosseus with lumbrical moment arms. The fig.1.c is kinematically consistent with the fig.1.a or fig.1.b when the displacements of both motors are mathematically added.

Some remarks about the validity of the model

(i) *The finger with flexed PIP.* In Chao et al (1989) it is stated that in the real finger with completely flexed PIP, the lateral bands are relaxed. This is in contradiction with the model (expression 1.3), which states that in all PIP positions the force in the lateral band must be: $T = r_{P3}/r_{T3} \cdot P_d$. This indicates that the above results for the severely flexed PIP should be interpreted with caution.

(ii) *The finger with flexed MCP.* In the above the influence of the MCP position on motor forces was not discussed. In the real finger, with MCP flexion the prime pull of the intrinsics shifts from the longitudinal structures of the extensor assembly towards the proximal structures, i.e. the sling-like fibres around the proximal phalanx. This phenomenon is not incorporated in the present models.

To summarise, it follows that the present results should be considered only for MCP and PIP positions ranging from extension to intermediate flexion.

CONCLUSION

The present paper provides a parameter study of a force model of the unloaded human finger with lumbrical muscle. Two models are compared: (i) of the finger in the sagittal plane, and (ii) of the finger with the ab-adduction degree of freedom of the MCP joint. The models are optimized for minimal maximal muscle stress, and optimal lumbrical cross section. From the results, the following conclusions can be drawn.

(i) In the human finger, the mechanical advantage of the PIP extensors decreases with respect to the PIP flexors with PIP flexion. It is greatest in the extended finger, when the passive

flexor forces are maximal.

(ii) In the unloaded finger models, the active use of the superficial flexor is not necessary for equilibrium and leads to non-optimal muscle forces.

(iii) In the 2D model, the lumbrical may substitute the interosseus entirely. In the 3D model the lumbrical action of radial abduction must be balanced by the ulnar interosseus. This ulnar interosseus force, however, is synergistic with the lumbrical force in the control of the finger in the sagittal plane.

(iv) In the unloaded 3D model, the lumbrical can maximally provide about 70% of all intrinsic function. The remaining intrinsic function is then provided by the ulnar interosseus, while the radial interosseus is zero.

(v) The most simple concept for unloaded 3D-finger model control in the sagittal plane is with the deep flexor, extensor, ulnar interosseus, and lumbrical.

(vi) In the extended unloaded 3D model, the lumbrical may maximally exert about a third of the force in the deep flexor (when $P=S$), and in the flexed finger about half (when $P=S$), otherwise the finger becomes unbalanced.

(vii) In the extended 3D model, the physiological extensor stress, and the lumbrical stress with maximal lumbrical force are almost equal for all flexor forces. This indicates that the lumbrical strength is synergistically tuned to the extensor strength for the control of the extended finger.

(viii) When assuming that the extensor stress in the extended finger is a reference for the physiologically allowable muscle stress, in the unloaded 3D model a stronger lumbrical would not be useful.

ACKNOWLEDGEMENTS

The author cordially thanks Dr. C.W. Spoor, Prof. Emer. J.M.F. Landsmeer, Prof. C.J. Snijders, Prof. J.J. Van Der Meulen, Dr. G.J. Sonneveld and Dr. S.E.R. Hovius for their valuable contributions.

REFERENCES

- An, K.N., Kwak, B.J., Chao, E.Y. and Morrey, B.F. (1984) Determination of muscle and joint forces: a new technique to solve the indeterminate problem. *J. Biomed. Engng* 106, 364-367.
- Chao Y.S., An, K.N., Cooney, III W.P., Linscheid, R.L., (1989) Biomechanics of the hand; a basic research study, pp. 43-44, World Scientific Publishing Co., Singapore
- Garcia-Elias, M., An, K.N., Berglund, L., Linscheid, R.L., Cooney, W.P., Chao, E.Y.S. (1991) Extensor mechanism of the fingers. I. A quantitative study, *J. Hand Surg.* 16A, 1130-1136.
- Kaplan, E.B. (1965) Functional and surgical anatomy of the hand (2nd edn), 84-85, Pitman, London.
- Leijnse, J.N.A.L., Bonte, J.E., Landsmeer, J.M.F., Kalker, J.J., van der Meulen, J.C., Snijders, C.J. (1992) Biomechanics of the finger with anatomical restrictions:- the significance for the exercising hand of the musician, *J. Biomechanics* 25, 1253-1264.
- Leijnse, J.N.A.L., and Kalker, J.J. (1995) A two dimensional kinematic model of the lumbrical in the human finger, *J. Biomechanics* 28, 237-249.
- Leijnse^a, J.N.A.L. (1995) A graphic analysis of the biomechanics of the bi-articular chain - application to the proximal bi-articular chain of the human finger, *J. Biomechanics*, to be published 1995.

Why the lumbrical should not be bigger

Leijnse^b, J.N.A.L. (1996) The controllability of the finger with the superficial or deep flexor, J. Biomechanics, resubmitted 1995.

Long, C. (1968) Intrinsic-extrinsic muscle control of the fingers, J. Bone Joint Surg. 50A, 973-984.

Spoor, C.W. and Landsmeer, J.M.F. (1976) Analysis of the zigzag movement of the human finger under influence of the extensor digitorum tendon and the deep flexor tendon. J.Biomechanics 9, 561-566.

Spoor C.W. (1983) Balancing a force on the fingertip of a two dimensional finger model without intrinsic muscles. J.Biomechanics 16, 497-504.

<i>MCP</i>	r_{PI}	r_{SI}	r_{EI}	r_{UI}	r_{RI}	r_{LI}
	11	13	9	6	6	9
<i>PIP</i>	r_{P2}	r_{S2}	r_{M2}	r_{T2}		
	10.5	9	5	*		
<i>DIP</i>	r_{P3}	r_{T3}				
	6	4				

Tabel 1 Moment arms of the tendons.
 Real values (in mm) used to calculate the results. From: Spoor (1983).
 (*): function of PIP position, see expression (9).

<i>Motor</i>	<i>P</i>	<i>S</i>	<i>E</i>	<i>U</i>	<i>R</i>	<i>L</i>
<i>PCA</i>	4.1	4.2	1.7	2.8	2.2	0.2

Table 2 Physiological Cross-sectional Area of the finger motors, in cm² (from Chao et al, 1989).

	2D _{Ext}	2D _{Flx}	3D _{Ext}	3D _{Flx}
S=0	2.1	3.7	1.3	2.5
S=P	1.5	2	0.9	1.4

Table 3 Ratio of the optimal and the physiological lumbrical cross sections (PCA_{Lo}/PCA_{Lp}) in the 2D and 3D model, for the flexed and extended finger, with S=0 and S=P.

FIGURES

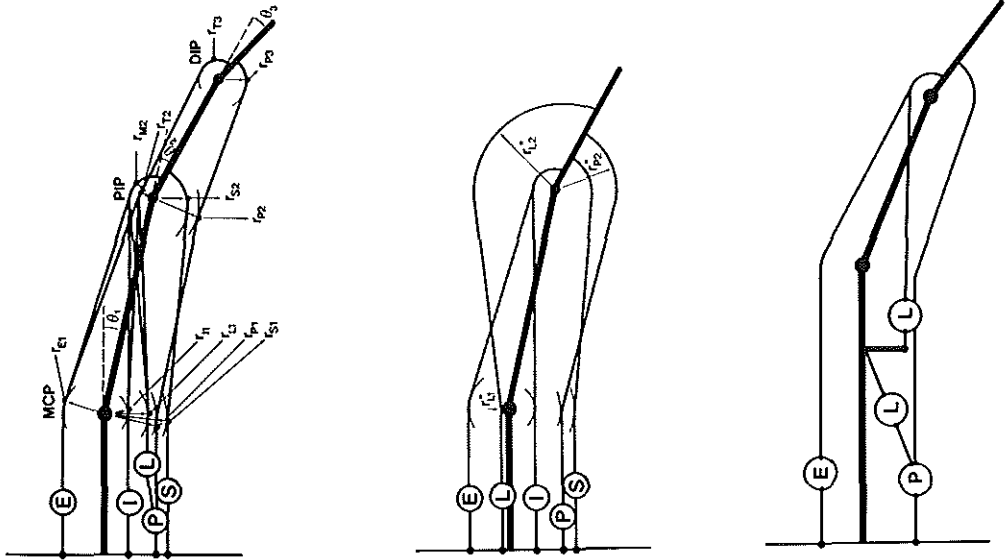


Figure 1 a,b,c a) Two dimensional model of the human finger. b) Bi-articular equivalent model. c) Lumbrical function as represented by two separate motors.

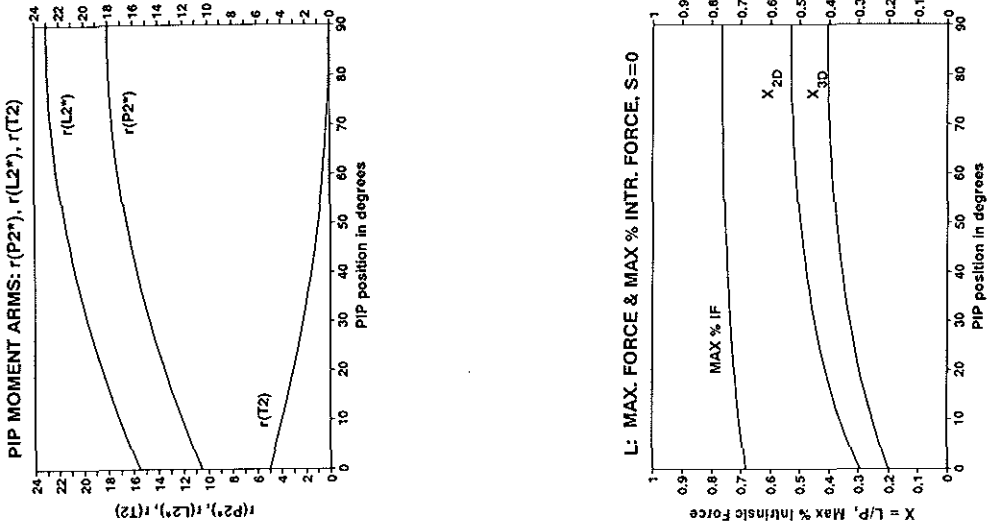


Figure 2 a,b a) Moment arm of lateral band (T), r_{L2^*} , and r_{P2^*} , as a function of the PIP position b) Maximum fraction of deep flexor force in the lumbrical as a function of the PIP position. X_{2D} : 2D model, X_{3D} : 3D model, Max %IF= X_{3D}/X_{2D} fraction of maximal lumbrical contribution to intrinsic function.

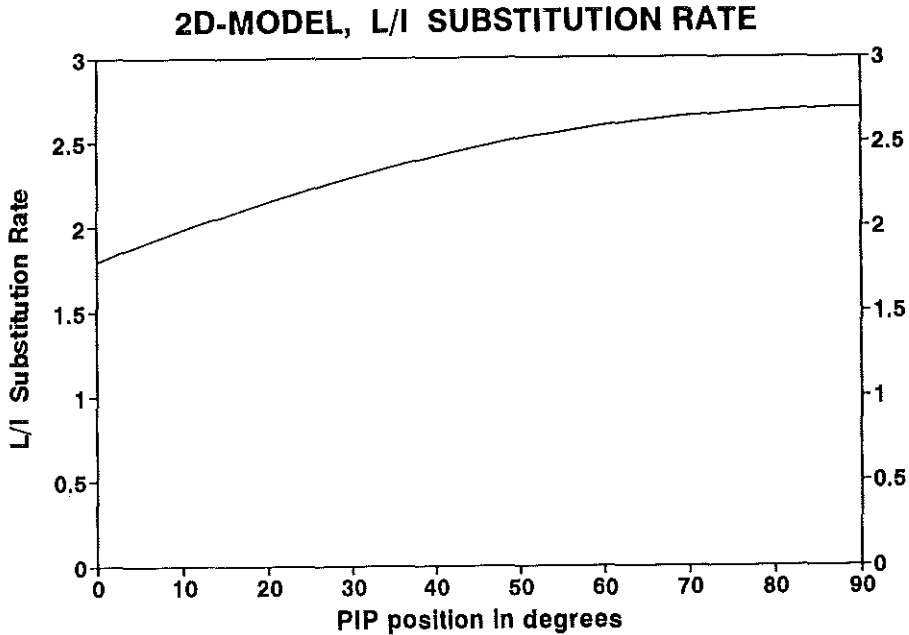


Figure 2 c Lumbrical/interosseus substitution rate in the 2D-model, as a function of the PIP position

Figure 3 (see next page)

a) Moment arm vectors of the finger motors, with extended (e) and flexed (f) PIP. Only the moment arm vectors R_p^* and R_L^* change with PIP flexion.

b) Combined moment arm vector diagram presenting the motor forces as a function of the deep flexor force P , in the flexed (f) and extended (e) finger. The motor forces are equal to the positive projections of the moment arm vector of $-R_p^*$ on the moment arm vectors of two other motors, relative to their moment arm length. The lumbrical force

with $I=0$ is the projection of the moment arm vector $-R_p^*$ on R_L ; the interosseus force with $L=0$ is the projection of $-R_p^*$ on R_I . The fact that the deep flexor moment arm vector can be balanced by both R_E, R_I and R_E, R_L demonstrates the intrinsic redundancy; the extensor is needed in all cases.

c) Combined moment arm vector diagram of the motor forces as a function of the superficial flexor force S . The comments are similar to (b).

d) Moment arm vector diagram of the lumbrical R_L as decomposed into the actions of two separate motors $R_{L,P}$ and $R_{L,I}$. $R_{L,P}$ directly opposes R_p^* , and reduces its effectivity by about half. $R_{L,I}$ and R_E balance the remaining deep flexor forces. The forces in $R_{L,I}$ and $R_{L,P}$ are equal.

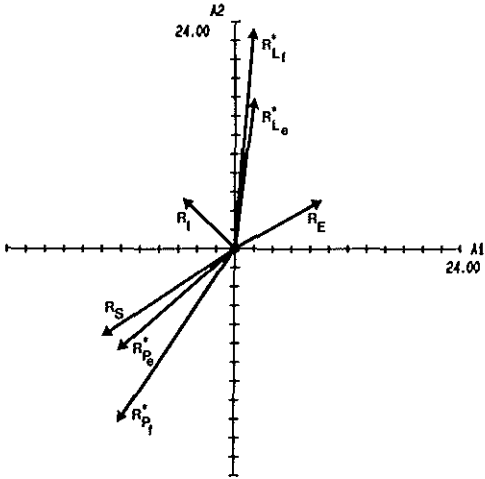


Figure 3 a

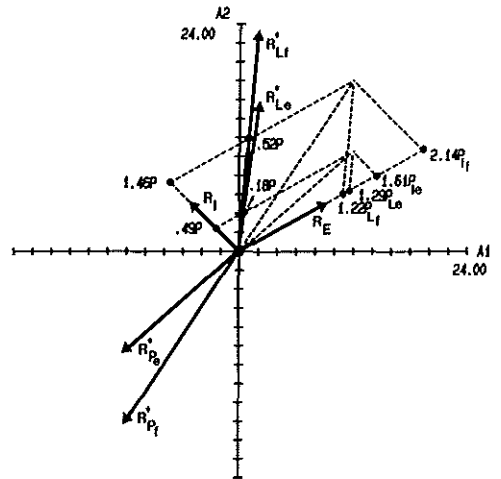


Figure 3 b

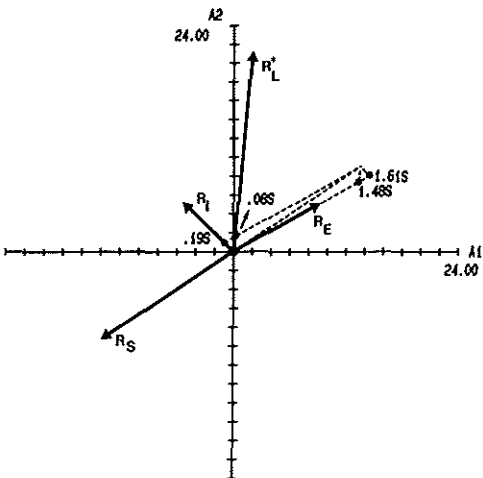


Figure 3 c

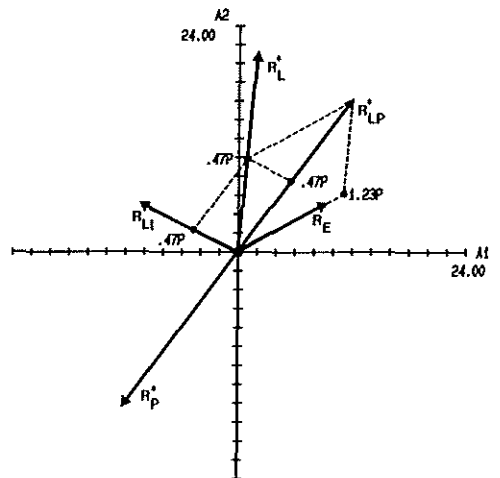


Figure 3 d

Why the lumbrical should not be bigger
2D-MODEL, FORCE, S=0

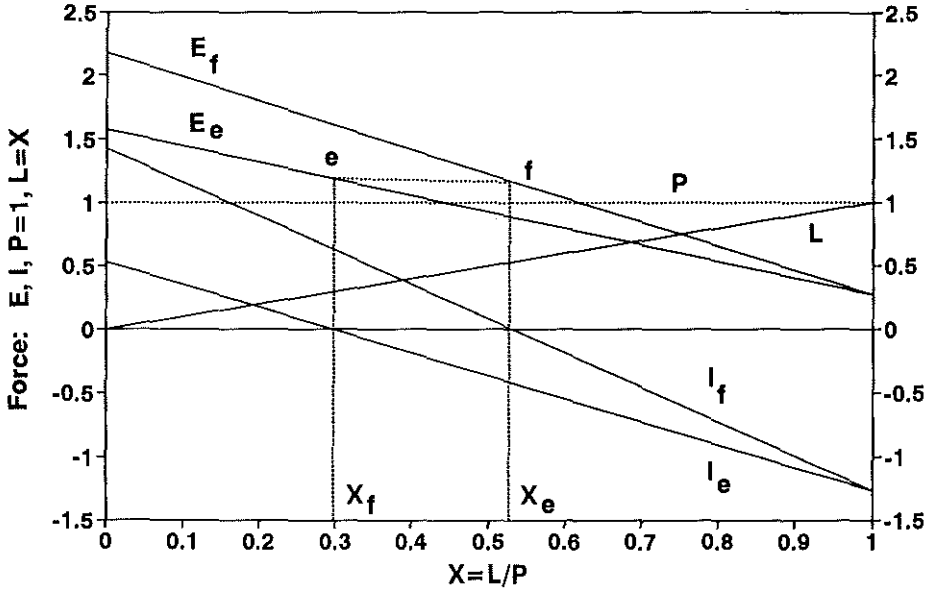


Figure 4 a Forces in extensor and interosseus in the extended and flexed 2D-model as a function of the lumbrical force $X=L/P$, with $S=0$ and $P=1$. (e): extended PIP, (f): flexed PIP (90°). The line (e,f) interpolates the extensor forces as the PIP flexes, with maximal lumbrical force (i.e. with $I=0$).

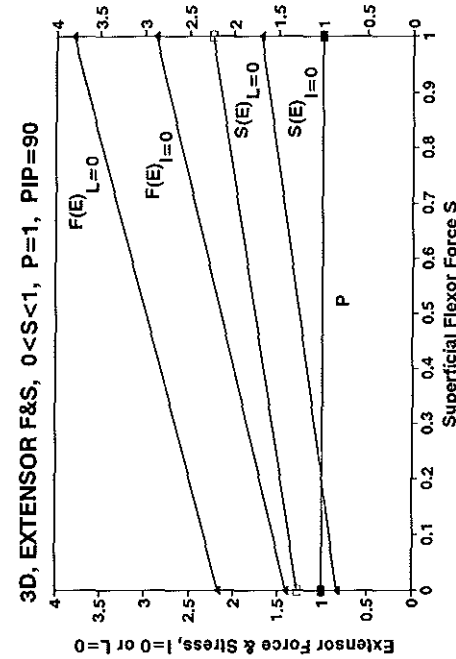
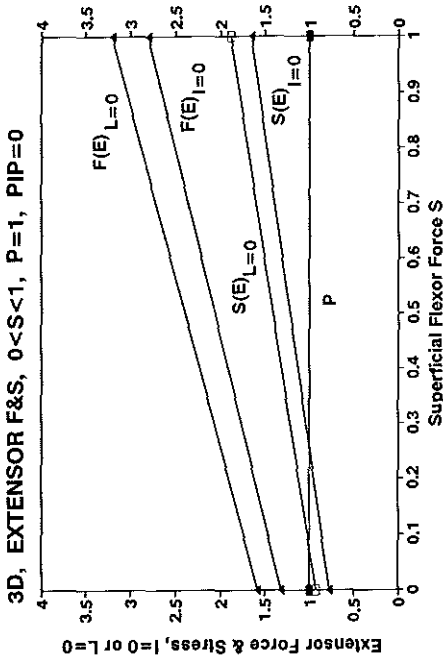


Figure 4 b,c Force $F(E)$ and stress $S(E)$ in the extensor as a function of the superficial flexor force S , with $L=0$ or $I=0$, and $P=1$.

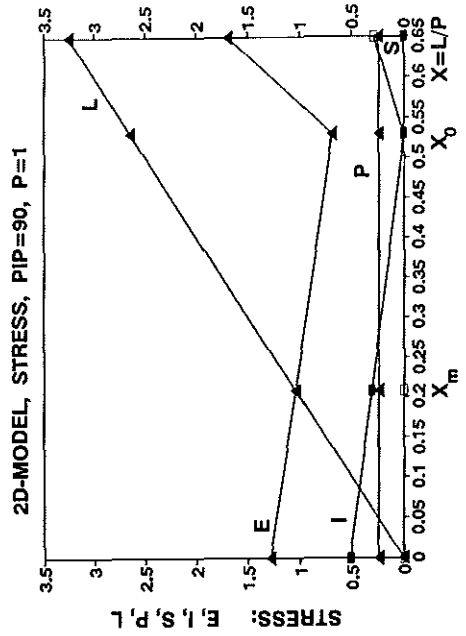
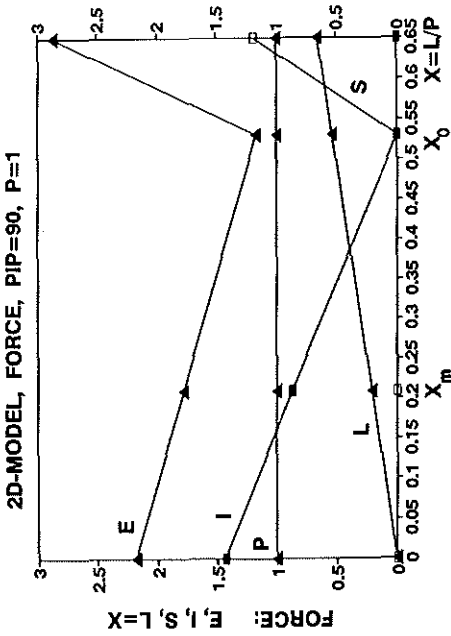
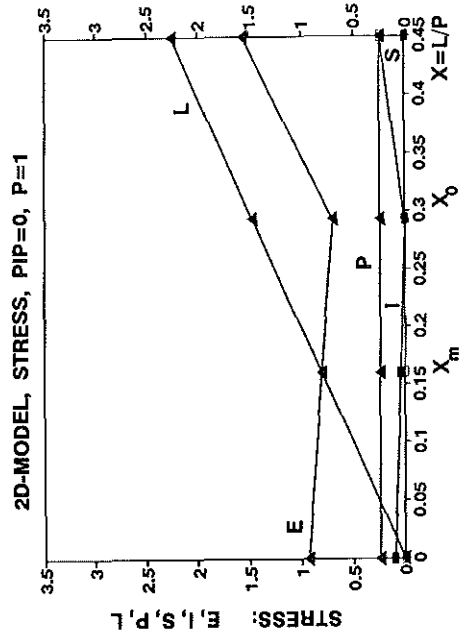
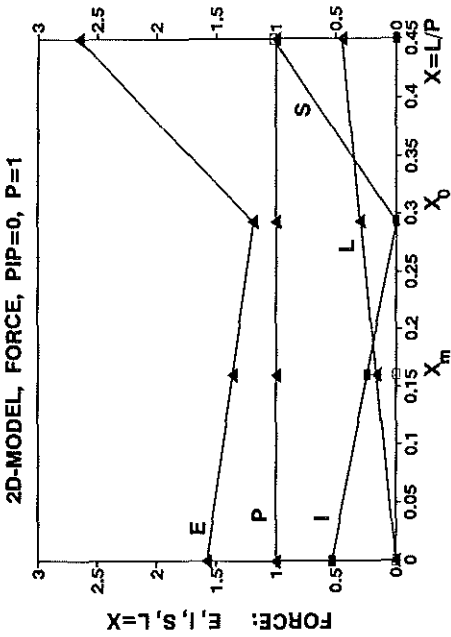


Figure 5 Forces and stresses (N/cm²) in the 2D-model as a function of the lumbrical force fraction $X=L/P$ of the deep flexor force. a) Forces, extended finger. b) Stresses, extended finger. c) Forces, flexed finger. d) Stresses, flexed finger.

Why the lumbrical should not be bigger

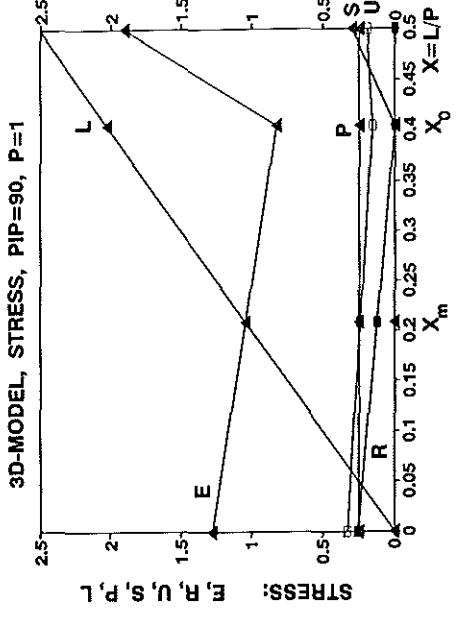
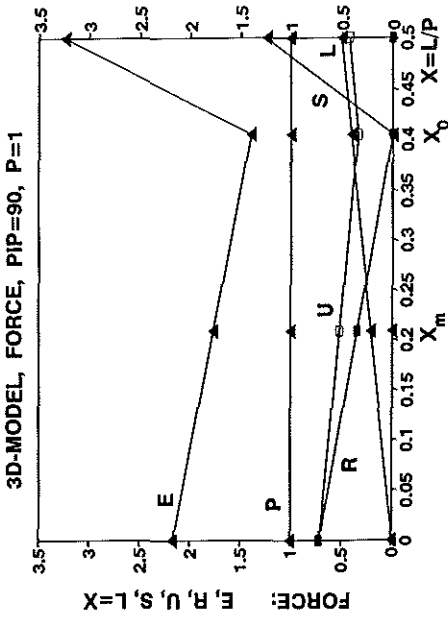
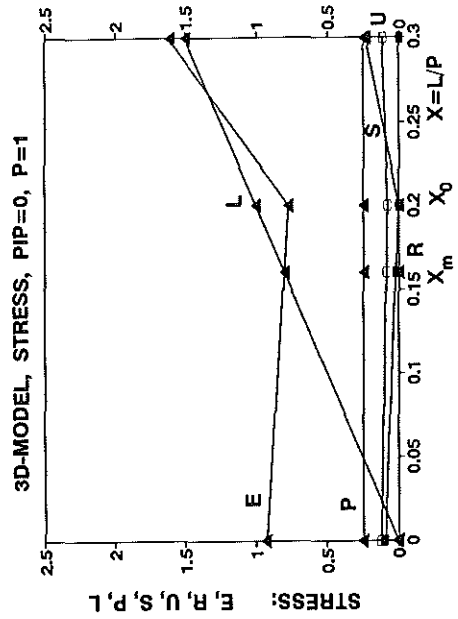
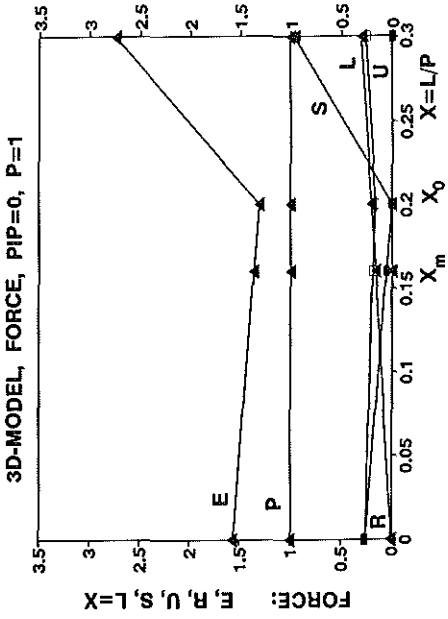


Figure 6 a,b,c,d Forces and stresses (N/cm^2) in the 3D-model as a function of the lumbrical force fraction $X=L/P$ of the deep flexor force. a) Forces extended finger. b) Stresses extended finger. d) Forces flexed PIP. e) Stresses flexed PIP.



CHAPTER III

MEASURING FORCE TRANSFERS IN THE M. FLEXOR DIGITORUM PROFUNDUS

**Measuring force transfers in the deep flexors of the musician's hand -
theoretical analysis, clinical examples**

J.N.A.L. Leijnse

Submitted to J. Biomechanics, 1995

**Measuring force transfers in the deep flexors of the musician's hand - device
and systematic measuring errors**

J.N.A.L. Leijnse

Accepted by J. Biomechanics, 1995

MEASURING FORCE TRANSFERS IN THE DEEP FLEXORS OF THE MUSICIAN'S HAND: THEORETICAL ANALYSIS, CLINICAL EXAMPLES

J.N.A.L. Leijne

Department of Plastic and Reconstructive Surgery & Department of Biomedical Physics and Technology, Erasmus University, Rotterdam, The Netherlands.

ABSTRACT

In the present paper the anatomical and functional interdependencies which regularly exist between the deep flexor tendons of the different fingers are modelled. The model results are validated by measurements on real hands. The results show that intertendinous force transfers may be caused by (i) co-activation of muscle fibres inserting in different tendons, and (ii) passive connections between tendons or muscle bellies. The co-activation is validated by the measuring results of a hand in which all intertendinous connections were surgically removed. The present models and measurements are currently used for diagnosis of hand problems in musicians at our hand clinic.

NOTATIONS

- D^i : digit i
- FP^i, FP^j : deep flexors of digits D^i and D^j
- T_p^i, T_p^j : end tendon of flexor FP^i, FP^j
- L_p^i, L_p^j : length of FP^i and FP^j between origin and insertion
- ΔL_p^{ij} : $L_p^j - L_p^i$; all length differences are calculated similarly
- L_c, L_{c0} : length and resting length of a connection.
- L_{pp} : length from the motor origin to the attachment of the connection
- L_T, L_{T0} : length and resting length of the tendon part distal to the attachment of the connection
- ϵ_T, λ_T : strain and slack of tendon part T distal to the attachment of the connection
- F_p^i, F_p^j : forces in deep flexor muscles FP^i, FP^j
- F_T^i, F_T^j : forces in deep flexor tendons at their insertion
- F_K^i, F_K^j : forces in the sensors at the tip of fingers D^i, D^j
- k_c, k_T, α : stiffness of the connection and tendon T, resp, with $\alpha = k_c/k_T$.
- r_P, r_{Kt} : moment arms of motor P and load K, resp., at joint t.
- c^{ij} : co-activation. Fraction of F_p^i transferred to F_T^j when the connections are slack
- Θ_t^i : angle of joint t of finger i.
- $\delta_{e_i}^{e_j}$: Kronecker delta function. When expression $e_i = e_j$, then $\delta = 1$, otherwise $\delta = 0$.
- CT^{ij} : co-activation term
- ST^{ij} : stiffness term
- T_{LB}, T_{vb} : torque of lateral bands and volar plate, resp., at the DIP joint

INTRODUCTION

In recent studies hand problems in musicians have been related, amongst others, to interdigital anatomical interconnections between tendons or muscles (Markison, 1990; Stern, 1990; Leijnse et al., 1992, 1993; Leijnse^a, 1996). Such intertendinous connections are regularly found between the finger extensor tendons (von Schroeder et al., 1990), between the superficial flexors FS4 and FS5 (Baker et al., 1981; Austin et al., 1989), between the long thumb flexor and the deep flexor of the index (Linburg and Comstock, 1979; Blair and Omer, 1981; Aguado and del Pino Paredes, 1988; Stern, 1990), and also between the deep flexors themselves (Verdan, 1960; Fahrner, 1971; Malerich, 1987; Leijnse^{a,b} et al., 1996). From the latter studies follows that intertendinous or intermuscular connections appear systematically in between the deep flexors of the ulnar three fingers, and may well be present in between the deep flexors of index and medius. In the following it is demonstrated that these interdependencies result from two distinct causes, schematically presented in fig.1. (i) A first cause can be described as *co-activation of muscle bellies to different fingers*. Physically, co-activation would be caused by muscle fibres which are activated with the deep flexor of one finger but which insert into the deep flexor tendon of another finger. The activation of the deep flexor of one finger will then result in a force transfer proportional to the number of co-activated muscle fibres inserting into the other tendon. Schematic examples of possible causes of co-activation are presented in fig.2. (ii) A second cause is *passive connections between muscles or tendons*. These can be connective tissue between muscle fibres of different muscle bellies, tendinous cross-overs between different tendons, synovial sheaths adhering to the tendons (Leijnse^b et al., 1996), or the tightly connected origins of bipennate lumbricals. In the following these interdependencies are modelled for a two motor system. The results are experimentally validated by measurements in real hands. The measuring device and measuring procedures are presented in Leijnse^b (1996), which also discusses the systematic errors possible in the measurements. The present models and measurements are currently used in diagnosis and for the prognosis of surgical treatment of focal dystonia complaints in musicians at our hand clinic.

MODEL ANALYSIS

Force transfers between two FDP tendons with co-activation and a single connection

Consider the model of fig.1, with a passive connection with stiffness k_c and resting length L_{c0} , and with the deep flexor FP^i active ($F_p^i > 0$) and the deep flexor FP^j inactive ($F_p^j = 0$). A constant fraction $c^{ij} \cdot F_p^i$, $0 \leq c^{ij} \leq 1$, called the *coactivation force* of F_p^i , is at all times transferred to the tendon T_p^j . Let L_p be the shortest anatomic distance between the origin and insertion of a deep flexor FP. It holds that:

$$\begin{aligned}
 L_p &= L_{p_i} + L_{T0} + \epsilon_T - \lambda_T \\
 \epsilon_T &= (L_T - L_{T0}) \cdot \delta_{sign}^1 [L_T - L_{T0}] \\
 \lambda_T &= (L_{p_j} + L_{T0} - L_p) \cdot \delta_{sign}^1 [L_{p_j} + L_{T0} - L_p]
 \end{aligned} \tag{1}$$

Chapter III.i

L_{T0} , λ_T , ϵ_T are the resting length, slack and strain, resp., of the tendon part T distal to the attachment of the connection; L_{Pp} is the length from muscle origin to the attachment of the connection. Let:

$$\begin{aligned}
 \Delta L_P^y &= L_P^j - L_P^i & \Delta \epsilon_T^y &= \epsilon_T^j - \epsilon_T^i \\
 \Delta L_T^y &= L_T^j - L_T^i & \Delta \lambda_T^y &= \lambda_T^j - \lambda_T^i \\
 \Delta L_{P_p}^y &= L_{P_p}^j - L_{P_p}^i & \Delta L_P^{*y} &= \Delta L_P^y - \Delta L_{T0}^y
 \end{aligned} \tag{2}$$

ΔL_P^{*ij} is further used to denote the relative displacement of the tendons. It holds that:

$$\Delta L_P^{*y} = \Delta L_P^y + \Delta \epsilon_T^y - \Delta \lambda_T^y \tag{3}$$

ΔL_{Pp}^{ij} is the distance between the attachments of the connection. ΔL_P^{*ij} is zero in the middle of the slack range of the connection, except for the relative slack or strain of the end tendons Tⁱ,T^j. The effective stiffness k_c^* of the connection is zero when the connection is slack:

$$k_c^* = \delta_{\lambda_c}^0 \cdot k_c \tag{4}$$

The system equations of the model of fig.1 with $F_P^j=0$ are (see appendix A):

$$\begin{bmatrix} F_T^i \\ F_T^j \end{bmatrix} = \begin{bmatrix} \frac{1+\alpha^* - c^y}{1+2\alpha^*} \\ \frac{\alpha^* + c^y}{1+2\alpha^*} \end{bmatrix} \cdot F_P^i + \int_0^{\Delta L_P^{*y}} \begin{bmatrix} \frac{-k_c^*}{1+2\alpha^*} \\ \frac{k_c^*}{1+2\alpha^*} \end{bmatrix} \cdot d\Delta L_P^{*y} \tag{5}$$

with $F_T^i, F_T^j, F_P^i \geq 0$, $\alpha^* = k_c^*/k_T$, $k_T = k^i = k^j$, $0 \leq \alpha^* < \infty$. When the connection is slack ($k_c^* = \alpha^* = 0$) equation (5) becomes:

$$\begin{bmatrix} F_T^i \\ F_T^j \end{bmatrix} = \begin{bmatrix} 1 - c^y \\ c^y \end{bmatrix} \cdot F_P^i \tag{6}$$

Slack ranges of connection and tendons

When a tendon force F_{T^k} equals the motor force F_P^i , the other tendon must be slack, and vice versa. When one tendon T^k is slack as a result of a taut connection, an increase of $|\Delta L_P^{*ij}|$ without an increase of F_P^i does not further stretch the connection but merely displaces its attachments by equal amounts:

$$d\Delta L_p^{*ij} = d\Delta \lambda_T^j \quad (7)$$

thereby increasing the slack in the slack end tendon ($d\Delta L_p^{ij} = d\Delta \epsilon_T^j = 0$ in the differential of expression (3), for which it holds that $\lambda_T^i \lambda_T^j = 0$ since at least one tendon must be taut). The following cases must be distinguished.

i) The co-activation inserts in Tⁱ proximal to the connection (fig.1)

When the co-activation inserts proximal to the connection, the connection is slack when:

$$|\Delta L_p^{ij}| - L_{c0} < 0 \quad (8)$$

With a slack connection the relative strain $\Delta \epsilon_{T0}^{ij}$ of the tendons is:

$$\Delta \epsilon_{T0}^{ij} = \frac{2c^{ij}-1}{k_T} \cdot F_p^i \quad (9)$$

The end tendons Tⁱ or T^j become slack when their force is zero: $F_T^i = 0$ or $F_T^j = 0$. Substituting the latter conditions in expression (5), and the conditions (8) and (9) in expression (3) gives the ranges in which the connection and both tendons are taut:

$$\begin{aligned} \{\lambda_T^j > 0\} \quad \left[-\frac{\alpha^* + c^{ij}}{k_c} \right] &\leq \left[\frac{\Delta L_p^{*ij} + L_{c0}}{F_p^i} \right] \leq \left[\frac{2c^{ij}-1}{k_T} \right] \quad \{\lambda_c > 0\} \quad (1) \\ \{\lambda_c > 0\} \quad \left[\frac{2c^{ij}-1}{k_T} \right] &\leq \left[\frac{\Delta L_p^{*ij} - L_{c0}}{F_p^i} \right] \leq \left[\frac{1+\alpha^* - c^{ij}}{k_c} \right] \quad \{\lambda_T^i > 0\} \quad (2) \end{aligned} \quad (10)$$

(the slack tendon parts at the end of the ranges are indicated between braces). An example of this system output is given in fig.3.a. ΔL_p^{*ij} in expression (10.2) is with the connection stretched as in fig.1. ΔL_p^{*ij} in expression (10.1) is with the connection directed as in fig.5.b. This connection redirects the co-activation force $F_T^j = c^{ij} \cdot F_p^i$ from T^j back to Tⁱ; this is further called "auto-coactivation".

ii) The co-activation inserts distal to the connection (fig.2.b, fig.5.c)

When the co-activation inserts proximal to the connection, the slack range of the connection is unilaterally unbounded, because in one direction the connection is slack in series with the slack (inactive) motor F_p^j . No auto-coactivation occurs. Expression (11.1) is void, and the slack range is:

$$\Delta L_P^{*ij} < L_{c0} + \left[\frac{2c^{ij}-1}{k_T} \cdot F_P^i \right] \quad (11)$$

This system output is exemplified in fig.3.b.

Force transfers between two FDP tendons with multiple connections simultaneously present

Consider the general case of n connections with stiffnesses k_{cm} , lengths L_{c0m} , and tendon lengths distal to the attachments $L_{Tdm}^i, L_{Tdm}^j, m=1..n$. The common slack range of these connections is the cross-section of the individual slack ranges $\lambda_{cm} > 0$ defined by expressions (10) or (11). When the tendon parts in between the attachments of the connections are assumed inextensible, connections can be modelled as springs in parallel, which, however, are not all necessarily taut at the same time. Let ΔL_{P0}^{ij} be defined so that the variable ΔL_P^{*ij} :

$$\Delta L_P^{*ij} = \Delta L_P^{ij} - \Delta L_{P0}^{ij} \quad (12)$$

is zero in the middle of the common slack range with unstrained tendons (in the case of one connection, $\Delta L_{P0}^{ij} = \Delta L_{T0}^{ij}$). The position with $\Delta L_P^{*ij} = 0$ is further called the *neutral tendon position*. Define k_c^* and k_c^{*+} as the stiffness of the connections which are tautened within the range of expression (10.1) and (10.2), resp. Then k_c^{*+} is the equivalent stiffness of all connections. However, k_c^* , which determines the auto-coactivation, is the equivalent stiffness of only these connections which insert in T^j distal to the insertion of the co-activation $c^{ij} \cdot F_P^i$.

Measuring stiffness and coactivation in the model

The co-activation fraction c^{ij} , the stiffnesses k_c^{*+} and k_c^* , and the slack range of the connections can be derived from the following expressions (with $F_P^i = F_T^i + F_T^j$):

$$CT^{ij} = \frac{dF_T^j}{d(F_T^i + F_T^j)} = \frac{\alpha^* + c^{ij}}{1 + 2\alpha^*} + \frac{k_c^*}{1 + 2\alpha^*} \cdot \frac{d\Delta L_P^{*ij}}{dF_P^i} \quad (13)$$

$$ST^{ij} = \frac{dF_T^j}{d\Delta L_P^{*ij}} = \left[\frac{\alpha^* + c^{ij}}{1 + 2\alpha^*} \right] \frac{dF_P^i}{d\Delta L_P^{*ij}} + \frac{k_c^*}{1 + 2\alpha^*} \quad (2)$$

Stiffness test

ST^{ij} is called the *stiffness term*. With isotonic force ($dF_P^i = 0$) it yields the stiffness characteristics of the coupled tendon system. The ST^{ij} test with ΔL_P^{*ij} as in expression (10.2) is with $k_c = k_c^{*+}$ and is called the ST^{ij+} test; ST^{ij} with ΔL_P^{*ij} as in expression (10.1), is with $k_c = k_c^*$ and is called the ST^{ij-} test or *auto-coactivation test*. When F_T^i and F_T^j are independent of ΔL_P^{*ij} , the connections are slack. In the real hand, the insertion of the co-activation distal to the connection will result in an unbounded slack range (expression (11)). The inverse is not necessarily true: an unbounded slack

range may also result from the insertion of the co-activation proximal to the connection, when the connection is directed from proximal FP^i to distal FP^j in the resting position of the fingers, and when it is too long to be tautened within the physiological displacement with $d\Delta L_p^{*ij} < 0$. The ST^{ij+} test ($F_p^i, F_p^j = (0, F)$) can be used to cross-reference the ST^{ij-} results, since they both measure the same connections except for those bypassed by the insertion of the co-activation. It holds that:

$$\frac{\partial F_T^i}{\partial \Delta L_p^{*ij+}} \Big|_{\{F_i^i=0\}} = ST^{ij+} \geq \frac{\partial F_T^j}{\partial \Delta L_p^{*ij-}} \Big|_{\{F_i^j=0\}} = ST^{ij-} \quad (14)$$

The equality holds when the co-activation inserts proximal to all connections which are tautened in the ST^{ij+} test.

The effect of non-constant activation force F_p^i on the ST^{ij} measurement results (figs.3,c,d,e,f)

Isotonic force ($dF_p^i=0$) in the ST^{ij} tests may be difficult to realise in the real subject. $dF_p^i \neq 0$ in expression (13.2) introduces a "virtual" stiffness term which may increase or decrease the measured stiffness with respect to the real characteristics. With $\alpha=1$ (very stiff connections), the changes are primordialy due to the stiffness effects (fig.3,c,d); with low stiffness connections ($\alpha < 0.2$), the changes are basically proportional to the co-activation force $c^{ij} \cdot F_p^i$, and quasi independent of the stiffness characteristics (fig.3.e.f).

Co-activation test

CT^{ij} is called the *co-activation term*. Two cases can be distinguished.

(i) **Non-zero slack range.** When the connection is slack ($k_c^* = \alpha^* = 0$), c^{ij} follows directly from expression (13.1). In reality, the fraction c^{ij} will be a function of the length differences of the motors due to the physiological muscle force/fibre length relationship. In the results, the tendon displacements are quantified by the PIP rotations only (Leijnse^b, 1996), and within this limited displacement range the effect of the force-length relationship on c^{ij} may be assumed small. Any effect can be excluded by putting the motors in positions of equal fibre length when these are within the slack range.

(ii) **Zero slack range.** A zero slack range can result from connections of zero length, but also from two taut connections of non-zero length of opposite directions (fig.5.d). With unstretched connections the CT^{ij} test directly yields $CT^{ij} = c^{ij}$. The connections are unstretched when $\Delta L_{FP}^{ij} = 0$. This condition requires an adjustment $\Delta L_p^{*ij} = \Delta \epsilon_{T0}^{ij}$ of the motor lengths as a function of the force F_p^i during the test (from expression (3)), since $\Delta \epsilon_T^{ij}$ is a function of F_p^i (expression (9)). However, $\Delta \epsilon_{T0}^{ij}$ is also function of c^{ij} and k_r (expression (9)), both of which are unknown, so that the required motor length adjustment ΔL_p^{*ij} cannot be determined. This problem can be avoided by keeping the motors isometric during the test: $d\Delta L_p^{*ij} = 0$ (in practice: by keeping the fingers in fixed positions). Moreover, when in the measurements the motors are positioned so that the

connections are initially unstretched ($\Delta L_p^{*ij}=0$), a constant passive force transfer term is also avoided (the corresponding finger position, further called the *neutral finger position*, is discussed further). With the condition $d\Delta L_p^{*ij}=0$, CT^{ij} is a function of the relative stiffness of connection and tendons (expression (13.1)). The stiffness contribution decreases with decreasing α^* . This is investigated in fig.4.a for the following cases: (1) fused end tendons ($\alpha > 1$); (2) high stiffness connections ($\alpha=1$); (3),(4): medium stiffness connections ($\alpha=0.2;0.1$); (5) low stiffness connections ($\alpha < 1$). The fig.4.a shows that:

- A co-activation $c^{ij}=0.5$ always yields a co-activation term $CT^{ij}=0.5$, independently of α .
- With fused tendons ($\alpha > 1$) the co-activation term is independent of c^{ij} and equal to $CT^{ij}=0.5$. Therefore, it is not possible to distinguish between real co-activation (neurologically fused muscles with fused tendons) and stiffness effects (independent muscles with fused tendons).
- With very stiff connections ($\alpha \approx 1$) the co-activation cannot be well quantified. This because the slope of the $CT^{ij}-c^{ij}$ line (fig.4.a, line 2) is too small.
- With $\alpha \leq 0.2$, the real co-activation c^{ij} can be realistically estimated. c^{ij} is the X-axis value corresponding to the measured CT^{ij} value (Y-axis), the accuracy follows from the fact that the slope of the $CT^{ij}-c^{ij}$ line approaches 45° (lines 3,4,5).
- With $\alpha < 1$, $CT^{ij} \approx c^{ij}$.

From this follows that very stiff connections with a zero slack range will mask any co-activation, whereas with moderately stiff or lax connections ($\alpha < 1$) the co-activation c^{ij} can be well estimated. The value of α can be estimated from the ST^{ij} test (see results).

Measuring intertendinous force transfers in real hands

The measured variables

In the measuring device of Leijnse^b (1996), by which the results are obtained, the tendon displacements ΔL_p are derived from the PIP rotations $\Delta\theta_2$, positive for flexion, and the tendon forces F_T follow from force sensors at the finger tips, as follows:

$$F_T = \frac{r_{K3}}{r_{P3}} \cdot F_K + \frac{1}{r_{P3}} [T_{LB3} - T_{VP3}] \quad (1) \tag{15}$$

$$\Delta L_p = -r_{P2} \cdot \Delta\theta_2 = -r_{P2} \cdot (\theta_2 - \theta_{20}) \quad (2)$$

Expression (15.1) is the DIP equilibrium equation, with T_{LB3} and T_{VP3} the torques of the lateral bands and the volar plate of the DIP. The possible errors introduced by these variable transformations, and further systematic measuring errors are discussed in Leijnse^b (1996).

Finger positions in which connections with zero slack range are minimally stretched

In the CT^{ij} test with a zero slack range the fingers should be positioned so that the connections between the tendons are minimally stretched, i.e. with $\Delta L_p^{*ij}=0$. How can this position be determined? It cannot be obtained by the ST^{ij} test, since with a zero slack range the switching point between active and co-active force transfers cannot be traced, except when k_c^{*+} and k_c^{*-} differ substantially. It is presently argued that normally the connections are minimally stretched

when the fingers are in equal positions of extension:

$$\theta_2^i = \theta_2^j = 0 \quad \Rightarrow \quad \Delta L_p^{*ij} = 0 \quad (16)$$

Assume that the deep flexor tendons of two fingers with normal joints are fused at the level of the carpus. When these fingers are put in equal positions of near extension, i.e. with slack volar plates ($\Theta_i^i = \Theta_i^j > \approx 0$), then either both flexor tendons distal to the connection are taut, or one of them is slack. The finger with the slack tendon has no (flexion) control over the DIP joint, and will therefore tend to extend further until its deep flexor tendon becomes taut and DIP balance is restored. Therefore, when the deep flexors are not both taut with equally extended fingers, the natural position of extension (with slack volar plates) of both fingers is likely to be different. When such differences in the extended positions is present, the fingers should be checked. Conversely, when the subject can effortlessly keep his extended fingers in equal positions of (near) extension with slack volar plates, no connection can be forcefully stretched. Assuming that the neutral tendon position is obtained with extended fingers, then with flexed PIP positions it is given by (from expression (15.2), with $\Theta_{20}^i = \Theta_{20}^j = 0$):

$$\Delta L_p^{*ij} = -r_{P2}^j \left[\Delta \theta_2^i - \Delta \theta_2^j \right] - \left[r_{P2}^j - r_{P2}^i \right] \cdot \Delta \theta_2^j = 0 \quad (17)$$

This expression states that with PIP flexion the finger with the smaller PIP moment arm should be flexed a little further than the finger with the larger PIP moment arm.

The slack ranges in terms of differential PIP rotations

The slack ranges of different connections are presently expressed in terms of the relative PIP joint rotations $\Delta \Theta_2^{ij}$ (figs.5).

i) $\Delta L_{pp}^{ij} > 0$ (fig.5.a). The slack range is $0 < \Delta \Theta_2^{ij} \leq \Delta \Theta_2^{ij+}$, with $\Delta \Theta_2^{ij+}$ the differential PIP rotation at which the connection becomes taut with $\Delta L_{pp}^{ij} < 0$, as in fig.5.b.

ii) $\Delta L_{pp}^{ij} < 0$ (fig.5.b). The slack range is $\Delta \Theta_2^{ij-} \leq \Delta \Theta_2^{ij} < 0$, with $\Delta \Theta_2^{ij-}$ the differential PIP rotation at which the connection becomes taut with $\Delta L_{pp}^{ij} > 0$, as in fig.5.a.

(iii) Co-activation which bypasses the passive connection (fig.5.c). As discussed above, the co-activation c^{ij} can be detected independently of the passive forces in the unbounded slack range of expression (11).

iv) Zero slack range (fig.5.d). No co-activation can be detected independently of the stiffness characteristics, except when the co-activation bypasses the connections (dotted lines in fig.5.d). Then it can be measured similarly to fig.5.a, i.e. with $0 \leq \Delta \Theta_2^{ij} \leq \Delta \Theta_2^{ij+}$, with $\Delta \Theta_2^{ij+}$ depending on which connection is bypassed.

RESULTS: CLINICAL MEASUREMENTS AND INTERPRETATION

In fig.6, samples of measuring results of different subjects are presented. Fingers are numbered 2 (index) through 5 (little finger). Results are coded by, in consecutive order, the active and passive finger, and the hand side (L/R). Different measurements are indicated at the X-axis by small case letters. The range of the sensor force was limited to 15N, so as not to dwarf the smaller force transfers in the graph. The sample rate is 25/s, the X-axis gives the number of samples. The upper half of the graphs presents the sensor forces (ranging from 0..15N), the lower half presents the PIP joint rotations (0..110°).

Clinical evidence of co-activation

Fig.6, Subj.1 presents a hand in which all passive connections between all deep flexor tendons were surgically removed. The muscle bellies were left untouched. The follow-up is nine years, the tendon mobilisation is complete. Therefore, force transfers between the deep flexors can only result from co-activation or from passive connections between the muscle bellies. This allows the unambiguous experimental validation of co-activation (expression (6)). The case-study is presented in Leijnse and Bonte (1996).

- 34L(a): CT³⁴ test. The variation of the force with isometric joints shows that the forces in passive and active finger are strictly proportional, satisfying expression (6). c^{34} is about 0.2..0.25. 34L(b,c): these ST³⁴ tests show that with increasing relative joint rotations minor passive connections become active, as the ratio F_K^3/F_K^4 somewhat decreases, meaning that a greater proportion of F_p^3 is transferred to F_T^4 . This force transfer should be due to the connective tissue between the proper muscle part m_p^3 which inserts in tendon T_p^3 and shortens, and the co-activated muscle part c_p^{34} which moves with the tendon T_p^4 and therefore lengthens.

- 43L(a): ST⁴³ test with Θ_2^4 moving from extension to flexion and back, with $\Theta_2^3 \approx 0$. Some passive connections become stretched with $\Delta\Theta_2^{34} > 80^\circ$, as F_K^3 peaks over F_K^4 . 34L(b): Θ_2^3 moving from extension to flexion and back, with $\Theta_2^4 \approx 0$. No sign of auto-coactivation. The co-activation varies over the graph. However, this variation seems to be systematic: in the entire graph (a) the coactivation force F_K^3 is less than in (b), except for the effect of the passive connections. This may correspond to the fact that in (a) the passive finger D³ is extended ($\Theta_2^3 = 0$), which allows for its lateral bands to be taut ($T_{LB3} \neq 0$ in expression (15.1)). The active finger D⁴ is flexed, and its lateral bands should be slack (Leijnse^b, 1996). In (b) the inverse situation exists: the active finger D⁴ is extended and its lateral bands may be taut, while D³ is flexed. The effect of the tautness of the lateral bands in one or the other finger is to offset the balance between the two sensor forces (expression (15.1)). This would underestimate the co-activation in (a), and possibly overestimate it in (b). If this holds, the average value would be about $c^{43} \approx 0.45..0.5$.

Co-activation and passive connections

Subj.2 presents the results of a guitar player with a focal dystonia problem in the medius.

- 34R: (a) CT³⁴ test with $\Theta_2^3 \approx \Theta_2^4$. (b): auto-coactivation test ST³⁴; active finger extending and passive finger isometric and flexed. No auto-coactivation occurs; therefore, the co-activation should insert into T_p^4 distal to the strong passive connections shown in 43R(c) (see further). The

coactivation is: $c^{34} \approx 0.15$. 34R(c): ST^{34+} test with isometrically flexed active finger D^3 and extending passive finger D^4 ; 34R(d): ST^{34+} test with isometrically extended passive finger, and flexing active finger. These tests show strong passive connections. However, the stiffness (slope of F_K^4) in (c) is much greater than in (d), but the total force $F_K^3 + F_K^4$ increases in (c) and decreases in (d) ($dF_p^3 \neq 0$ in expression (13.2)). The question is whether the variation in the F_K^4 slopes in (c) and (d) can be explained by the variation in F_p^3 , or whether it is a systematic measuring error, as discussed in Leijnse^b (1996). If the measurement results were correct, it would hold that (see appendix B):

$$\alpha = \frac{(\Delta F_{T_i}^4 - \Delta F_{T_i}^3) - c^{34} \cdot (\Delta F_{P_i}^3 - \Delta F_{P_i}^4)}{(\Delta F_{P_i}^3 - \Delta F_{P_i}^4) - 2 \cdot (\Delta F_{T_i}^4 - \Delta F_{T_i}^3)} \quad (18)$$

With $\Delta F_p^3 = 16 \cdot r_{K3}/r_{P3} (=17/6) \approx 45N$ and $\Delta F_T^4 = 9 \cdot r_{K3}/r_{P3} \approx 25N$, as obtained from fig.7, the expression (18) is negative ($\alpha < 0$), which is physically excluded. Therefore, the results of (c) and (d) are inconsistent. This can also be verified from the figs.3.e,f. First, the constant $\alpha = k_c/k_T$ must be estimated. Ignoring the contribution of the co-activation due to the non-constant force F_p^3 , the ST^{34} terms in (c) and (d) are : $ST_{(c)}^{34} \approx 3800N/m$, $ST_{(d)}^{34} \approx 1700N/m$ (from: $ST^{34} = \Delta F_T^4 / \Delta L_p^{34}$, $\Delta F_{K(c)}^4 \approx 20N$, $\Delta F_{K(d)}^4 \approx 9N$, $r_{K3}/r_{P3} = 17/6$, and $\Delta L_p^{34} \approx \pi/2 \cdot r_{P2} \approx 15mm$). From the fig.4.b it then follows that: $\alpha_{(c)} \approx 0.33$, $\alpha_{(d)} \approx 0.12$. The value $\alpha_{(c)}$ is an over-estimation since the contribution $c^{34} \cdot \Delta F_{P(c)}^3 > 0$, while $\alpha_{(d)}$ is an under-estimation since $c^{34} \cdot \Delta F_{P(d)}^3 < 0$. Assume therefore that $\alpha \approx 0.2$. This allows the results of 34R(c) and (d) to be compared with the theoretical results of fig.3.e,f, which present a similar force difference ΔF_p^1 with $\alpha = 0.2$. Fig.3.f overestimates the difference in the slope of F_T^4 in 34R(c,d) by more than half, as the co-activation is $c^{34} = 0.5$ instead of 0.15. However, even with $c^{34} = 0.5$ the fig.3.f does not show a difference in the slopes of F_T^4 as exists between 34R(c) and (d), which demonstrates the inconsistency. It may be hypothesised that in (d) in the extended passive finger D^4 the lateral bands are taut ($T_{LB3} > 0$, expression (15.1)).

- 43R (a): CT^{43} test with slow and fast oscillations at maximal force F_p^4 , (b): CT^{43} test with fast oscillations of small forces. Both show a consistent CT^{43} value of about 0.5. (c): ST^{43+} test (D^3 extending and D^4 isometric and flexed) shows stiff and short passive connections of about the same stiffness as in 34R(c). 43R(d) is the auto-coactivation test (ST^{43-}), with D^4 extending and $\Theta_2^3 \approx 90^\circ$. This test is positive: the co-activation force $c_{43} \cdot F_p^4$ is added to F_K^4 and subtracted from F_K^3 as D^4 extends, while $F_K^3 + F_K^4$ remains approximately constant ($dF_p^4 = 0$). The slope of F_K^4 in the ST^{43-} test is about equal to the slope of F_K^4 in the ST^{34+} test of 34R(c) (the equality holds in expression (14)), which shows that c^{43} inserts proximal to the stiffest passive connections shown in 34R(c). The tests (c) and (d) show that the slack range of the connections is quasi zero. However, with the estimated value of $\alpha \approx 0.2$, the real co-activation is distinguishable from stiffness effects (fig.4.a), and it holds that: $c^{43} \approx CT^{43} \approx 0.5$.

Example of a connection between the deep flexors of index and medius

Subj.3 is a female violin player with D²-D³ coordination problems. 23L(a): the CT^{ij} test shows moderate co-activation, but the ST²³ test (b) shows strong passive connections, which transfer all F_p² force to F_T³ with ΔL_p^{*23} as corresponding to barely $\Theta_2^2 - \Theta_2^3 = 70^\circ$.

DISCUSSION

Properties of anatomical interconnections in the deep flexor

(i) *Co-activation.* The figs.6, subj.1 experimentally validate the existence of co-activation (expression (6)): force transfers which are proportional to the force and independent of the displacements, within the slack range of the passive connections.

(ii) *Extensibility of passive connections.* The figs.6 show that the stiffness of passive connections is greatly variable. The extensibility of the connections means that the relative mobility of the connected tendons can be increased by the use of force, as assumed in Leijnse^a (1996). The stiffer connections may transfer all muscle force to the connected tendons, leaving no force available in the end-tendon of the active flexor (e.g. subj.3, 23L).

(iii) *Interdigital variability.* The results show a great variety in the connectivity of the deep flexors. Generally, the strongest connections are between the FP³-FP⁴-FP⁵. However, subj.3 shows that also the deep flexors of index and medius may be strongly interconnected.

(iv) *Asymmetry.* The co-activation and the passive connections are generally asymmetric with respect to the neutral finger position (extended fingers). In other words, flexing either finger with an active deep flexor will pull the other finger by different forces.

Diagnosis of hand problems in musicians.

The theoretical studies of Leijnse et al (1992, 1993) and Leijnse^a (1996), and the clinical evidence as reported by e.g. Stern (1990) and Markison (1990), and Leijnse and Bonte (1996), indicate that in hand complaints in musicians intertendinous connections should be considered as possible causes. For this diagnosis, the quantification of the connections is of prime importance. Present results show that it is possible to distinguish between the neurological muscle structure (co-activation), and the effects of mechanical connections. This allows for an effective prognosis of the result of the surgical clearance of the connections.

Surgical clearance of passive connections

Surgical clearance of passive connections is likely to improve relative tendon mobility, as was the case with subj.1 (Leijnse and Bonte, 1996). However, by the same measure it will reduce the auto-coactivation. The auto-coactivation implies that even for the strongly connected fingers "resting" positions exist in which the end tendon of the passive deep flexor can be (almost) slack, and the passive finger can be relaxed, while the deep flexor in the connected finger is active. These positions correspond to the range with $\lambda_T^j > 0$ in expression (10.1). Complete removal of all passive connections removes this possibility, and implies that the active flexor will always pull the flexor tendon of the other finger by the co-activation force, whatever the finger position.

Measuring model and validation of interdependencies in the FDP

Therefore, with a large co-activation c^j the clearance of passive connections will not necessarily prevent excess loading of finger motors due to intermotor force transfers. The effects of such force transfers on muscle loading in the musician's hand are investigated in Leijnse^a (1996).

CONCLUSION

A model is presented of the functional interdependencies between the deep flexors in the human hand. These interdependencies can result from two causes. (i) Anatomical connections between muscles or tendons. These connections transfer force between the tendons in proportion to their stiffness and strain. (ii) Force transfers caused by co-activation of muscle parts inserting in different end tendons. The model results are validated by measurements of connections in real hands. Co-activation is unambiguously demonstrated in a hand from which all passive connections between the deep flexor tendons were surgically removed. The measurements further illustrate the variation in the coactivation, and the stiffness, slack range and orientation of the passive connections. It is concluded that the effects of co-activation and passive connections can be well differentiated, except when the connections have no slack range, and are very stiff (fused tendons). The quantification of these interdependencies should be of prime importance for diagnosis and treatment of finger coordination problems in musicians.

ACKNOWLEDGEMENTS

The author cordially thanks Dr.C.W. Spoor for the close reading of the manuscript, and Dr.G.J. Sonneveld, head of the special clinic for musicians at the Erasmus University Rotterdam, Prof.Dr.Ir. C.J. Snijders, Prof.Emer.Dr.J.M.F. Landsmeer, Dr. S.E.R. Hovius, and Prof.Dr. J.C. Van der Meulen, and Dr. J.E. Bonte for their valuable contributions.

REFERENCES

- Austin, G.J., Leslie B.M., and Ruby, L.K. (1989) Variations of the flexor digitorum superficialis of the small finger. *J. Hand Surg.* 14A, 262-267.
- Baker, D.S., Gaul, J.S., Jr, Williams, V.K. and Graves M. (1981) The little finger superficialis - clinical investigations and functional shortcomings. *J. Hand Surg.* 4A, 374-378.
- Blair, W.F., and Omer, G.E. Jr. (1981) Anomalous insertion of the flexor pollicis longus. *J. Hand Surg.* 5A, 548-549.
- Fahrer, M. (1971) Considérations sur l'anatomie fonctionnelle du muscle fléchisseur commun profond des doigts. *Ann. Chir.* 25, 945-950.
- Leijnse, J.N.A.L., Bonte, J.E., Landsmeer, J.M.F., Kalker, J.J., van der Meulen, J.C., Snijders, C.J. (1992) Biomechanics of the finger with anatomical restrictions - the significance for the exercising hand of the musician, *J. Biomechanics* 25, 1253-1264.
- Leijnse, J.N.A.L., Snijders, C.J., Landsmeer, J.M.F., Bonte, J.E., van der Meulen, J.C., Sonneveld, G.J., Hovius, S.E.R. (1993) The hand of the musician:- The biomechanics of the bidigital finger system with anatomical restrictions. *J. Biomechanics* 26, 1169-1179.
- Leijnse, J.N.A.L., and Bonte J.E. (1996) Surgical clearance of anatomic connections between the deep

Chapter III.i

- flexors in a musician - a case study. To be submitted sept. 1995.
- Leijnse^a, J.N.A.L. (1996) Anatomical factors predisposing to focal dystonia in the musician's hand - principles; theoretical examples of clinical significance, accepted J. Biomechanics, Jan. 1995.
- Leijnse^b, J.N.A.L. (1996) Measuring anatomic interconnections between the deep flexors: device and systematic measuring errors. Accepted J. Biomechanics, 1995.
- Leijnse, J.N.A.L., Walbeehm, E.T., Sonneveld, G.J., Hovius S.E.R. (1996) Anatomical interconnections within the M. flexor digitorum profundus - the significance for the hand of the musician. Submitted to the Anatomical Record, 1995.
- Leijnse^b, J.N.A.L., Walbeehm, E.T., Sonneveld, G.J., Hovius, S.E.R., Kauer, J.M.G. (1996) Interconnections between the tendons of the M. flexor digitorum profundus formed by the synovial sheaths in the carpal tunnel (1996^b), Submitted to Anatomical record, 1995.
- Linburg, R.M., and Comstock, B.E. (1979) Anomalous tendon slips from the flexor pollicis longus to the digitorum profundus. J. Hand Surg. 4A, 79-83.
- Malerich, M.M., Baird, R.A., McMaster, W., and Erickson, J.M. (1987) Permissible limits of flexor digitorum profundus tendon advancement - an anatomic study. Am. J. Hand Surg. 12A, 30-33.
- Markison, R.E. (1990) Treatment of musical hands: redesign of the interface. Hand Clinics 6, 525-544.
- Rico Aguado, A., and del Pino Paredes, V. (1988) Flexor digitorum profundus common to thumb and index finger, associated with a post-traumatic distal adherence of both tendons. J. Hand Surg. 13-B, 72-74
- Stern, P.J. (1990) Tendinitis, overuse syndromes, and tendon injuries, Hand Clinics 6, 467-476.
- Verdan, C. (1960) Syndrome of the quadriga. Surg. Clin. North Amer. 40, 425-426.
- von Schroeder, H.P., Botte, M.J., Gellman, H. (1990) Anatomy of the juncturae tendinum in the hand. J. Hand Surg. 15A, 595-602.

APPENDIX A: the system equations

Assume in fig.1 a connection of zero resting length ($L_{c0}=0$). The system equations are:

$$\begin{aligned}
 (1-c^j).F_p^i &= F_T^i + F_c & k^i.\epsilon_T^i &= F_T^i \\
 c^j .F_p^i &= F_T^i - F_c & k^j.\epsilon_T^j &= F_T^j \\
 \epsilon_c &= \Delta L_p^{*ij} + \epsilon_T^i - \epsilon_T^j & k_c.\epsilon_c &= F_c
 \end{aligned} \tag{A.1}$$

with $\epsilon_c, \epsilon_T^i, \epsilon_T^j$ the elongation of connection or tendons distal to the attachment of the connection. The tendon forces are:

$$\begin{aligned}
 F_T^i &= \left[\frac{k^i.(k^j+k_c) - k^i k^j c^j}{K} \right] .F_p^i - \frac{k^i k^j k_c}{K} .\Delta L_p^{*ij} \\
 F_T^j &= \left[\frac{k^j k_c + k^i k^j c^j}{K} \right] .F_p^i + \frac{k^i k^j k_c}{K} .\Delta L_p^{*ij}
 \end{aligned} \tag{A.2}$$

with $K=k^i.k^j+k^i.k_c+k^j.k_c$. These equations hold for $k^i, k^j, k_c > 0$. Connections of non-zero length can become slack, at which point their stiffness is zero (expression (4)), which leads to the integral form of expression (5), which is zero in the slack range. Expression (5) follows when both end tendons are assumed of equal stiffness ($k_T^i=k^i=k^j$). k_T can be modelled by considering all

length changes in the muscle/tendon complex:

$$\sum_{i=1}^3 r_{P_i} \cdot d\theta_i + dL_{P_f} = \left[\frac{\partial L_{T_t}}{\partial F_P} - \sum_{i=1}^3 \frac{\partial L_P}{\partial r_{P_i}} \cdot \frac{\partial r_{P_i}}{\partial F_P} \right] \cdot dF_P \quad (\text{A.3})$$

t denotes the finger joints, L_{P_f} is muscle fibre length, and:

$$r_{P_i} = \frac{\partial L_P}{\partial \theta_i} \quad (\text{A.4})$$

The left-hand side of expression (A.3) presents the kinematic changes. At the right-hand side are the dynamic changes: the strain of the end tendon itself and the changes in the moment arms of the tendons as a function of the force F_P (pulley strain with flexion; compression of the volar plates with hyper-extension). Changes due to joint compression are disregarded. The term between brackets equals $k_T^{-1} = k_{T_e}^{-1} + k_{P_u}^{-1}$, i.e., the end tendon stiffness (k_{T_e}) and the pulley stiffness (k_{P_u}) in series. In fig.3, k_T is estimated by arbitrarily assuming a 3mm strain with a sensor force of $F_K = 20\text{N}$. This results in (with $r_{K3}/r_{P2} = 17\text{mm}/6\text{mm}$):

$$k_T = \frac{F_T}{\Delta L_P} = \frac{F_K}{\Delta L_P} \frac{r_{K3}}{r_{P3}} = 19,000\text{N/m} \quad (\text{A.5})$$

APPENDIX B: expression (18)

For the measurements (c) and (d) in subj.2, 34R, it holds that:

$$\begin{aligned} \Delta F_{T_c}^j &= CT^{ij} \cdot \Delta F_{P_c}^i + ST^{ij} \cdot \Delta L_{P_c}^j \\ \Delta F_{T_d}^j &= CT^{ij} \cdot \Delta F_{P_d}^i + ST^{ij} \cdot \Delta L_{P_d}^j \end{aligned} \quad (\text{A.6})$$

in which $\Delta L_{P_c}^{ij} \approx \Delta L_{P_d}^{ij}$. With this condition, the subtraction of the second from the first equation results in:

$$\Delta F_{T_c}^j - \Delta F_{T_d}^j = CT^{ij} \cdot (\Delta F_{P_c}^i - \Delta F_{P_d}^i) \quad (\text{A.7})$$

Substitution of $CT^{ij} = (\alpha + c^{ij}) / (1 + 2\alpha)$ gives the expression (18). The values of $\Delta F_{T_c}^j$, $\Delta F_{T_d}^j$, $\Delta F_{P_c}^i$, $\Delta F_{P_d}^i$ are estimated from fig.7.

FIGURES

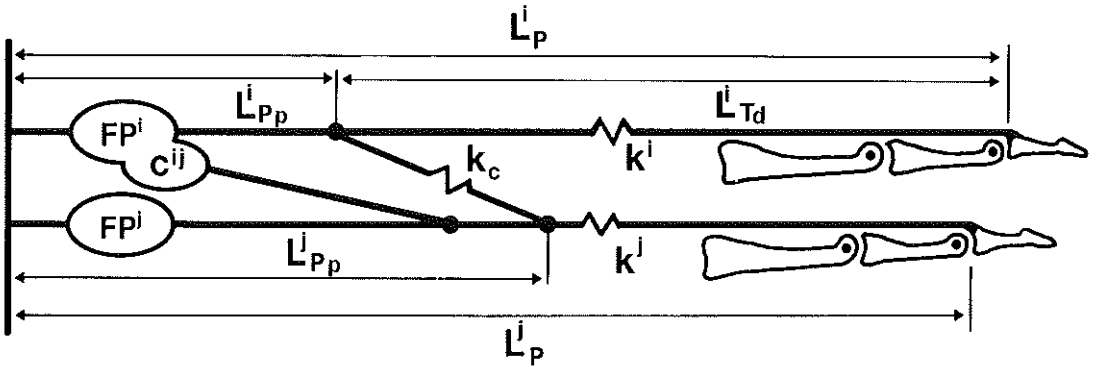


Figure 1 Model of two deep flexors with co-activation c^{ij} of FP^j with FP^i , and interconnected by a connection with stiffness k_c .

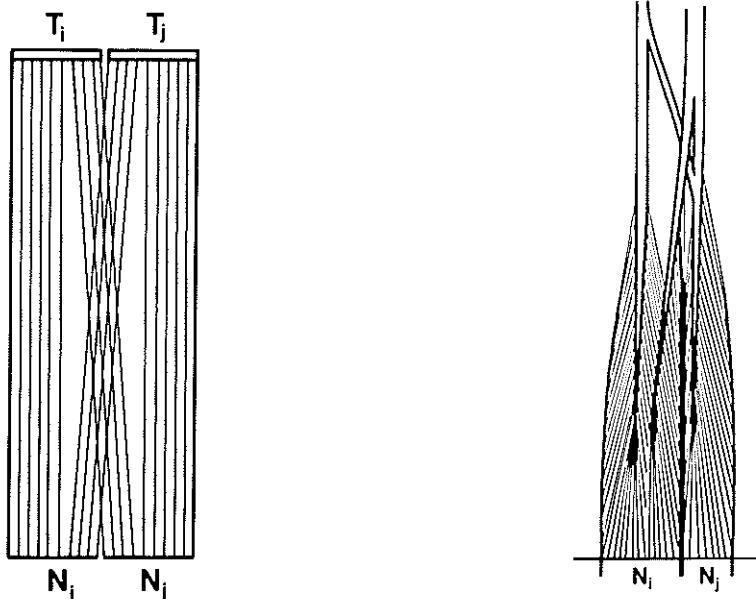


Figure 2 a,b Models of co-activation. a) N_i and N_j are the muscle fibres activated with muscle M_i and M_j , resp. Some of these fibres cross-insert into the wrong tendon. b) Muscle fibres activated with N_i insert into the other end tendon distal to a strong passive connection.

Measuring model and validation of interdependencies in the FDP

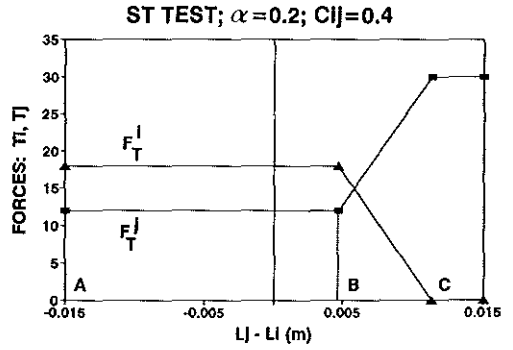
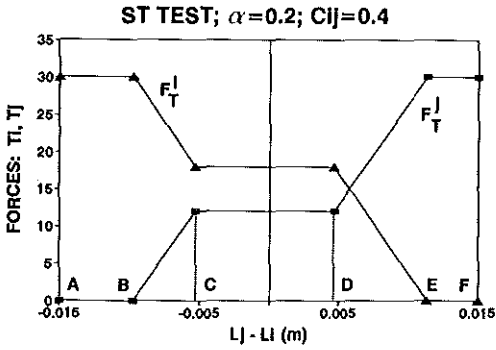


Figure 3 a,b

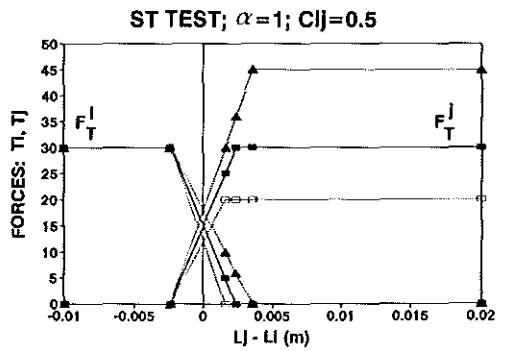
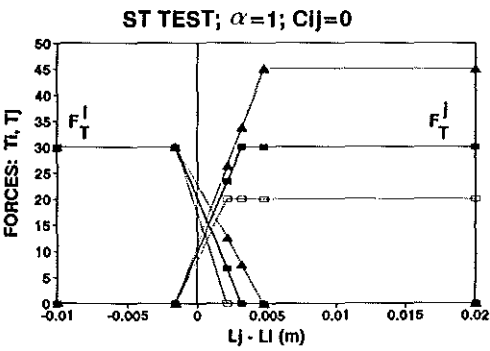


Figure 3 c,d

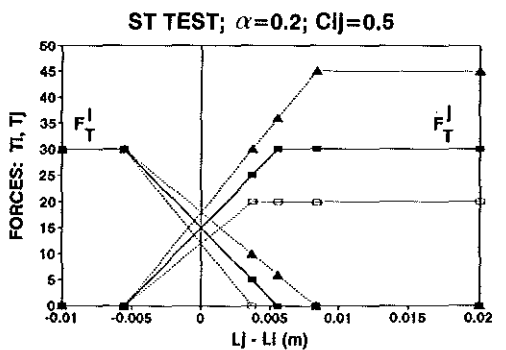
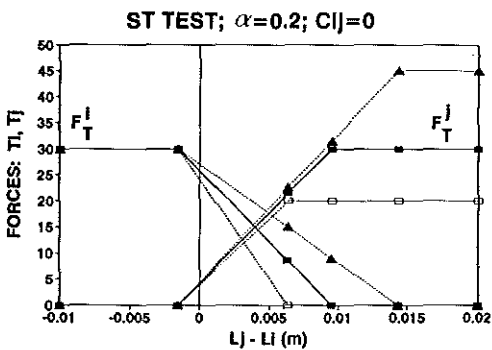


Figure 3 e,f

Figure 3 (comments with figs. of previous page) System output with different connections, and co-activations. End tendon forces F_T^i, F_T^j as a function of ΔL_p^{*ij} (indicated as L_j-L_i at the X-axis).

a) Connection of resting length $L_{c0}=5\text{mm}$, with $F_p^i=30\text{N}$ and constant, $k_T=19,000\text{N/m}$ (see appendix). Filled triangle: F_T^i , filled square: F_T^j . [A,B]: $F_T^i=F_p^i$ and T^j slack (expression (7) holds); [B,C]: auto-coactivation range ST^{ij} (expression (10.1) holds); [C,D]: slack range with co-activation $c^{ij}=0.4$; (expression (6)) holds; [D,E]: ST^{ij+} test (expression (10.2) holds); [E,F]: $F_T^j=F_p^j$ and T^i slack (expression (7) holds).

b) ST^{ij} test with the same connection as fig.3.a, and co-activation $c^{ij}=0.4$ inserting distal to the connection. [A,B]: unbounded slack range (expression (11)).

c,d,e,f) ST^{ij} tests of connections with zero slack range. Per graph three cases are presented: (i) constant force $F_p^i=30\text{N}$ during test (solid squares), (ii) F_p^i linearly increasing with ΔL_p^{*ij} from 30N to 45N (solid triangles), (iii) F_p^i linearly decreasing from 30N to 20N (empty squares). The parameter values are: $\alpha=k_j/k_T$: 1; 0.2; 0.5; c^{ij} : 0; 0.5. $k_T \approx 19,000\text{N/m}$. At the left of all graphs: $F_T^i=F_p^i, F_T^j=0$. At the right $F_T^j=F_p^j, F_T^i=0$.

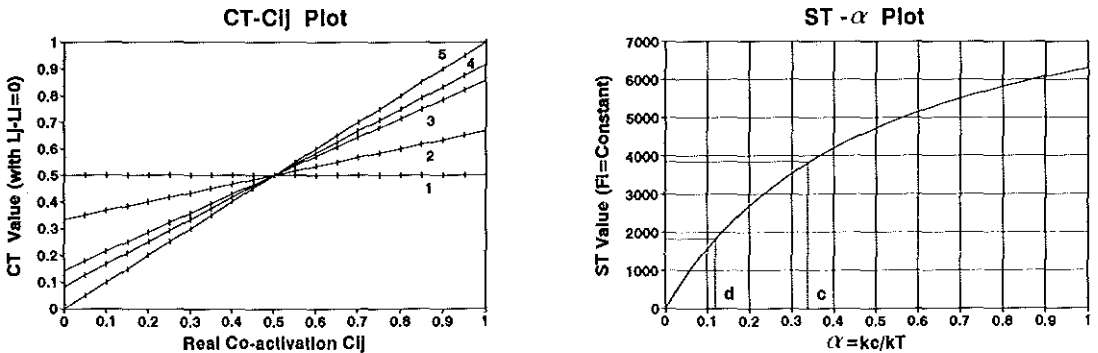


Figure 4 a,b

a) CT^{ij} term with a connection with zero slack range as a function of the real co-activation c^{ij} for different ratios $\alpha=k_j/k_T$. Line (1): $\alpha > 1$; (2): $\alpha=1$; (3): $\alpha=0.2$; (4): $\alpha=0.1$; (5): $\alpha < 1$.

b) ST^{ij} term as a function of $\alpha=k_j/k_T$, with $k_T \approx 19,000\text{N/m}$. (c) and (d) are the stiffness values corresponding to the fig. 7, subj.2:34R,(c,d) (see text).

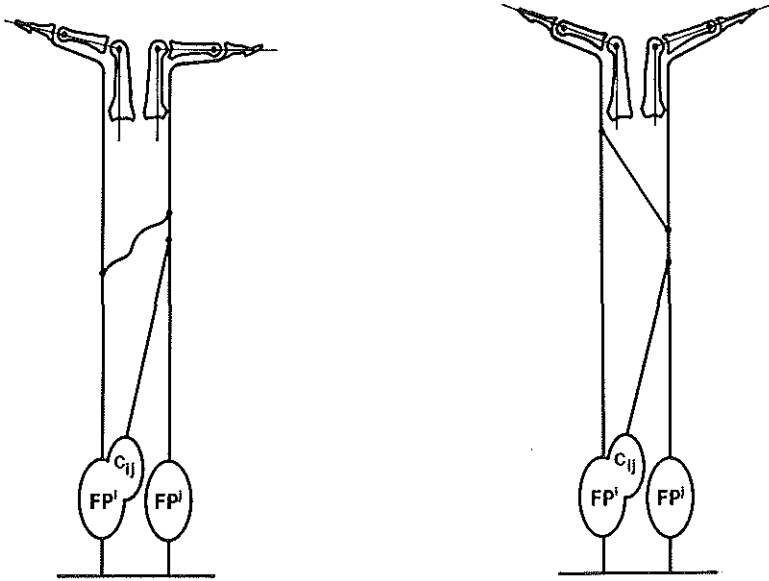


Figure 5 a,b

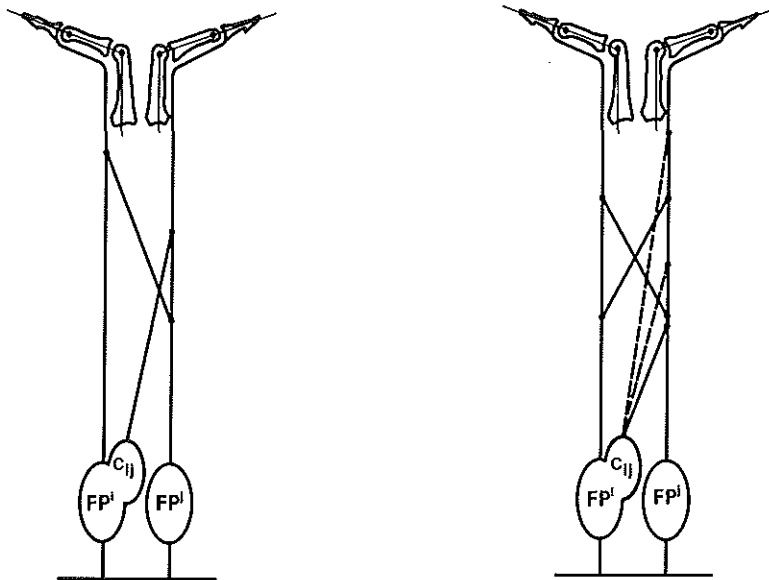


Figure 5 c,d

Figure 5 Connections of different directions become slack with different relative joint displacements. a) Connection with $\Delta L_{pp}^{ij} > 0$; b) Auto-coactivation. When $\Delta L_{pp}^{ij} < 0$, the connection retransfers the co-activation force $c_{ij} \cdot F_p^i$ back to T^i ; c) The co-activation inserts in T^j distal to the attachment of the connection: no auto-coactivation; d) Connection of zero length, composed of two taut connections of non-zero length of opposite directions.

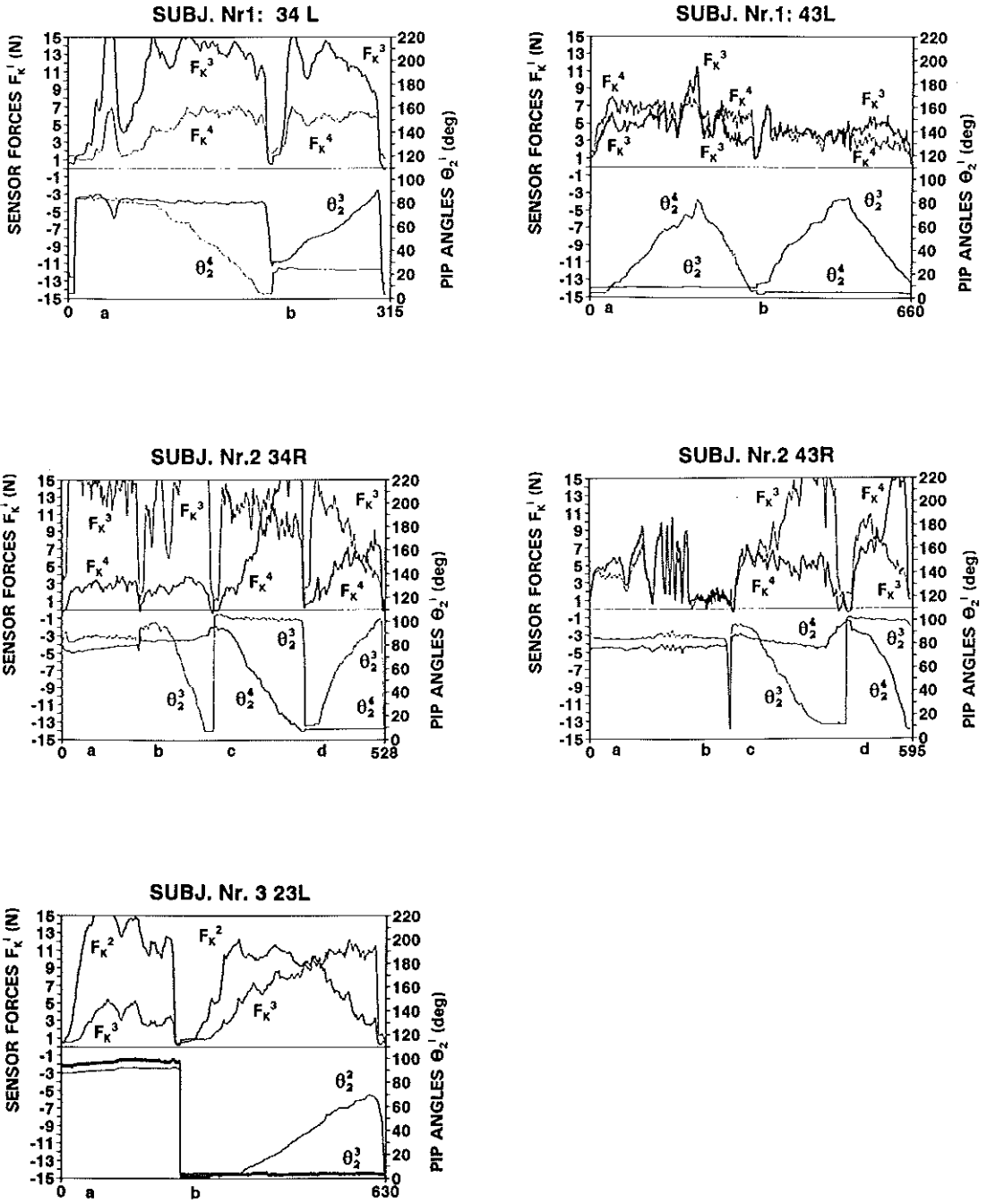


Figure 6 Subj. 1, 34L, 43L; Subj. 2, 34R, 43R; Subj. 3, 23L

Measuring model and validation of interdependencies in the FDP

Figure 6 (comments with figs. of previous page) CT^j and ST^j measurement results, subj.1 and subj.2. The upper half of each graph corresponds to the left Y axis, and presents the fingertip sensor forces F_K^i, F_K^j (Newton); only the positive range is considered. The lower half of each graph corresponds to the right Y-axis, and presents the PIP rotations Θ_2^i, Θ_2^j in degrees; only the range $0..110^\circ$ is considered. Dotted or full lines in upper and lower half of the graph correspond to the same finger. Subj.1. 34L,43L: F_K^3, Θ_2^3 : full line; F_K^4, Θ_2^4 : dotted line. Subj.2. 34R,43R: F_K^3, Θ_2^3 : dotted; F_K^4, Θ_2^4 : full. Subj.3. Connection between the deep flexor of index and medius. 23R: F_K^2, Θ_2^2 : dotted; F_K^3, Θ_2^3 : full line.

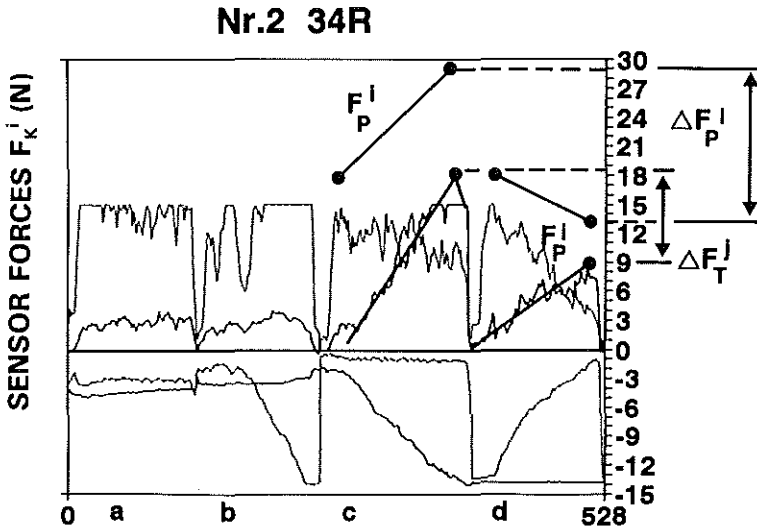


Figure 7 The forces $\Delta F_{Tc}^j, \Delta F_{Td}^j, \Delta F_{Pc}^i, \Delta F_{Pd}^i$ obtained from fig.6, subj. 2, 34R (c,d)), as input of the expression (18). The lines in the graph indicated with " F_p^i " are a linear approximation of the sum of the sensor forces $F_K^i + F_K^j$.

MEASURING FORCE TRANSFERS IN THE DEEP FLEXOR OF THE MUSICIAN'S HAND: DEVICE AND SYSTEMATIC MEASURING ERRORS

J.N.A.L. Leijnse

Department of Plastic and Reconstructive Surgery, Erasmus University, Rotterdam, The Netherlands.

ABSTRACT

The deep flexor tendons of different fingers are anatomically often highly interconnected by tendinous bands or fibrous tissue. Also, muscle fibres activated with the deep flexor of one finger may insert in the tendons of other fingers, directly or through intermediate tendons. When such muscle is activated, the other tendons are pulled in proportion to the number of co-activated fibres inserting in them. These phenomena limit independent finger movement and may cause problems in the hand of the musician. In this paper a device to accurately measure the dynamic and kinematic effects of these connections is presented. In these measurements important systematic errors are possible. These are modelled, illustrated by measurement results, and ways to avoid them are discussed. The measuring device is currently used at our clinic to obtain functional anatomic information in musicians with hand problems.

NOTATIONS

- MCP(Θ_1), PIP(Θ_2), DIP(Θ_3) : metacarpo-phalangeal, proximal interphalangeal, and distal interphalangeal joint, with their respective flexion angles.
- FP, FS : flexor digitorum profundus, flexor digitorum superficialis
- ED : extensor digitorum
- MB : medial band (part of the extensor assembly inserting in the middle phalanx)
- LB : lateral band (part of the extensor assembly inserting in the distal phalanx)
- VP : volar plate
- E : external extension force at joint
- i : as right upper index, denotes finger i
- F_P^i, F_T^i, F_K^i : forces of the deep flexor FP^i itself, in its tendon T^i at the insertion, and as measured by the load cell K^i , resp.
- T_{VP3}, T_{LB3} : torque from the taut volar plate and lateral bands, resp., at the DIP joint
- T_{E2} : external extension torque at the PIP joint
- L_P^i, L_{P0}^i : length and reference length of FP^i from origin to insertion.
- $\Theta_2^i, \Theta_{20}^i$: angle and reference angle of the PIPⁱ
- $F_P, F_T, F_K, T_{VP3}, T_{LB3}, \Delta L_P, L_{P0}, \Delta \Theta_2, \Theta_{20}, \Delta L_P^*, \Delta \Theta_2^*, \Theta_2^*, R_{P2}^*, R_{P3}, R_{K3}, \Delta R_{P2}^*$: see appendix
- r_{ij} : moment arms; i: motor or external force (P,S,K,LP,MB); j: number of joint
- c^{ij} : co-activation. Fraction of the force in FP^i going to the tendon of FP^j
- k_i^{ij} : stiffness of the connections between FP^i and FP^j when $F_p^* = \delta_0^i \cdot F$, $i=1..3$
- C, K_c : see expression (3)
- δ_i^j : Kronecker delta. When $i=j$, then $\delta=1$; when $i \neq j$, then $\delta=0$.

INTRODUCTION

In this paper a device to measure the effects of anatomic connections between deep flexor muscles in the hand is presented. These anatomic interconnections were theoretically modelled and experimentally validated in Leijnse^b (1996), of which the concepts, terminology and methods will presently be used. Mentioned paper also contains the anatomical and clinical references. In the device here presented, the deep flexor forces are quantified by load cells at the fingertips, and the tendon displacements by PIP rotations, all other joints being fixed. The measuring procedures are as follows. Two (or more) adjacent fingers are positioned in the device, each fingertip at a force sensor. The subject is asked to press one sensor (the "active" sensor) at a time. Simultaneously the forces in the other (passive) fingertip sensors are measured, together with the PIP positions. The stiffnesses of the intertendinous connections are measured by the variation of the PIP positions with constant motor force; the co-activation of deep flexors with other deep flexors is measured by variation of the motor forces with fixed finger position. Important systematic errors are possible. These find their cause in the indeterminates in the system equations. In the following the errors are investigated in a model of three fingers with connected deep flexors, and ways are presented to prevent them: by the design of the instrument itself, by appropriate finger fixation, or by appropriate testing procedures. The errors are further illustrated by real measurement results. In the discussion, it is pointed out that the couplings between motors resulting from intertendinous connections increase the number of indeterminates in muscle function in the hand, and may be actively used in instrumental playing.

MATERIALS AND METHODS

The measuring device

The hand is placed with the dorsum on a flat support, and fixed with the wrist in the neutral position ($\Theta_0=0^\circ$) by straps at the forearm and palm. The proximal phalanx of each finger is fixed by a strap to an individual finger support, with the MCP extended ($\Theta_1=0^\circ$) (fig.3.a). To this finger support a proximally/distally movable part, further called the "base", is attached. The base contains the axis about which the support of the force sensor at the fingertip rotates. To measure the PIP rotation, this axis is positioned collinear to the PIP axis. This is achieved by proximal-distal adjustments for finger length of the base relative to the finger support, and palmar-dorsal adjustments for finger thickness of the axis relative to the base. With collinear PIP and sensor support axes, no relative displacement occurs between the fingertip and the force sensor with PIP rotation. With this criterion, the axis is positioned by trial and error. The middle phalanx is then firmly strapped to the sensor support; this fixation is explained further. The force sensor is adjusted to the fingertip by proximal-distal displacements relative to the sensor support.

MODELS OF MEASURING DEVICE AND MEASUREMENTS

Model of three fingers with interconnected deep flexors in the measuring device

The input/output relationship of the measuring device in fig.1 is:

$$F_K = R_{K3}^{-1} \left[R_{P3} \cdot \left(C \cdot F_P - K_c \cdot \left(R_{P2}^* \cdot \Delta\theta_2^* + \Delta R_{P2}^* \cdot \theta_2^* \right) \right) - T_{LB3} + T_{VP3} \right] \quad (1)$$

(for proper variable definitions, see Appendix). This equation (1) can be decomposed as:

$$F_T = C \cdot F_P + K_c \cdot \Delta L_P^* \quad (1)$$

$$F_K = R_{K3}^{-1} \left[R_{P3} \cdot F_T - T_{LB3} + T_{VP3} \right] \quad (2)$$

$$\Delta L_P^* = -R_{P2}^* \cdot \Delta\theta_2^* - \Delta R_{P2}^* \cdot \theta_2^* \quad (3)$$

Expression (2.1) gives the system equations of the interconnected three-motor system. The expressions (2.2) and (2.3) relate the system outputs F_T , ΔL_P^* to the measured variables F_K , θ_2 . F_P , F_T , F_K are the motor, end tendon and sensor forces; T_{LB3} , T_{VP3} are the magnitudes of the torques of the lateral bands (DIP extensors) and the plamar ligaments (volar plates) at the DIP. C is the *co-activation matrix*. Its columns are the fractions of F_P^i which are at all times and uncontrollably transferred to each of the three end tendons. Effects on the c^{ij} values of tendon elasticity with taut connections are modelled in Leijnse^b (1996). K_c is the *stiffness matrix*, and contains the stiffnesses of the intertendinous connections which become stretched in proportion to the tendon displacement differences ΔL_P^* . With positive or negative tendon displacement differences different connections may be stretched. In fig.1, these are denoted as k^{ij} and k^{ji} ; in the text both are noted as k_i^{ij} . The insertions of the co-activations may bypass intertendinous connections, so that with different motors being active different connections are stretched between the same tendons. k_i^{ij} is the stiffness of the connections stretched between the tendons T^i and T^j with only FP^i active (notation: $F_P^k = \delta_k^i \cdot F$, $k=1..3$). With unconnected motors $K_c=0$; with independent motors $K_c=0$ and $C=I$, the unit matrix. Expression (2.2) consists of the DIP torque equilibrium equations (fig.2). The expression (2.3) is the kinematic motor length-PIP rotation relationship with inextensible end-tendons. The system equations (2.1) are independent of the absolute motor lengths L_P , except for the c^{ij} which depend on the physiological muscle force/fibre length relationship. Only in fingers with equal PIP moment arms ($\Delta R_{P2}^*=0$), expression (2.3) is independent of the absolute joint positions. In the appendix some system properties are given.

Measuring c^j , k_t^j

The coactivations c^j and stiffnesses k_t^j can be obtained from the expressions (from equations (2)):

$$\frac{F_K^j}{\sum_i F_K^i} \stackrel{(4)}{=} \frac{F_T^j}{\sum_i F_T^i} = c^j + \frac{[K_c \cdot \Delta L_P^*]^j}{F_P^i} \quad F_P^s = \delta_s^i \cdot F; \quad s=1..3 \quad (1)$$

$$-\frac{r_{K3}^j}{r_{P3}^j} \cdot \frac{\partial F_K^j}{\partial [r_{P2}^j \cdot \Delta \theta_2^j + (r_{P2}^j - r_{K3}^j) \cdot \theta_2^j]} \stackrel{(4.1)}{=} \frac{\partial F_T^j}{\partial \Delta L_P^{*j}} = k_t^j \quad F_P^s = \delta_s^i \cdot F; \quad s=1..3 \quad (2)$$

F_P^i is equal to the sum of the tendon forces when $F_P^s = \delta_s^i \cdot F$ (Appendix (A.4.1)). The left hand equation of expression (3.1) holds only with the conditions:

$$T_{LB3} = T_{VP3} = 0 \quad (1)$$

$$r_{P3}^j / r_{K3}^j = r_{P3}^i / r_{K3}^i \quad (2)$$

The left hand equation of expression (3.2) holds when (4.1) is satisfied.

Co-activation test (notation: CT^j test) (expression (3.1)). The co-activation can be straightforwardly calculated from the sensor forces when all connections are slack ($K_c=0$) or unstretched ($\Delta L_P^*=0$), and when the conditions (4) hold. In the real hand, the connections are likely to be minimally stretched when the fingers are in equal positions of extension (Leijnse^b, 1996):

$$\theta_2 = \theta_{20} = 0 \quad \Rightarrow \quad \Delta L_P^* = 0 \quad (5)$$

With $\theta_{20}=0$ taken as the reference PIP position, the condition $\Delta L_P^*=0$ in expression (2.3) gives all the PIP positions with slack or minimally strained connections:

$$R_{P2}^* \cdot \Delta \theta_2^* = -\Delta R_{P2}^* \cdot \theta_2^* \quad (6)$$

The expression (3.1) and condition (4.2) show that when the ratio r_{P3}/r_{K3} is equal for all fingers, neither the individual moment arms r_{P3} , r_{K3} , nor the ratio r_{K3}/r_{P3} must be known to calculate the c^j from the sensor forces. The condition (4.2) is approximately true in the human hand, where fingers which are thinner ($r_{P3} \downarrow$) are also shorter ($r_{K3} \downarrow$).

Stiffness test (notation: ST_t^j test) (expression (3.2)). The stiffness is the slope of the tendon force/displacement difference curve.

Example

The present example will illustrate the measuring errors. Assume that c^{21}, c^{22}, c^{23} and $k_2^{12}, k_2^{13}, k_2^{23}$ must be measured. The correct relationship is:

$$F_T = \begin{bmatrix} c^{21} \\ c^{22} \\ c^{23} \end{bmatrix} \cdot F_P^2 + \begin{bmatrix} -k_2^{12} & -k_2^{13} & -k_2^{13} \\ k_2^{12} & & -k_2^{23} \\ k_2^{13} & & k_2^{13} + k_2^{23} \end{bmatrix} \cdot \begin{bmatrix} \Delta L_P^{*12} \\ \Delta L_P^{*23} \end{bmatrix} \quad (7)$$

The variation of ΔL_P^{*12} with $\Delta L_P^{*23}=0$ provides the stiffnesses $k_2^{12}+k_2^{13}$, k_2^{12} , and k_2^{13} as the slopes of F_T^1 , F_T^2 , and F_T^3 , resp. Generally, these stiffnesses will differ for $\Delta L_P^* < 0$ and $\Delta L_P^* > 0$, as different connections become taut (indicated by k^{ij} and k^{ij} in fig.1). With $\Delta L_P^{*12} > 0$ and $\Delta L_P^{*23} < 0$, the co-activation forces in T^1 and T^3 will be redirected to T^2 by the passive connections k_2^{12} and k_2^{23} ; this was called *auto-coactivation* in Leijnse^b (1996). The stiffness k_2^{23} follows from the variation of ΔL_P^{*23} with $\Delta L_P^{*12}=0$. Note that k_2^{13} can only be measured when $c^{23}, c^{21} > 0$, as only co-active forces can tauten these connections.

SYSTEMATIC MEASURING ERRORS

Errors due to the violation of the conditions $F_P^i = \delta_i^1 \cdot F$ in expression (3)

e.1) Unconscious avoidable activation of the deep flexor of the passive finger

Unconscious co-activation is muscle activity in a passive flexor in excess to the co-activation force, and which the subject can avoid with better concentration. This results in measured values in *excess* to the real values c^{ij} and k^{ij} , in contrast to the further errors.

Avoidance of the error. A voluntary force error does not result from a strict coupling of motor force $c^{ij} \cdot F_P^i$, and will not be exactly reproducible. To investigate this, the subject can vary the force in the active motor F_P^i during measurement (slow and fast oscillations of F_P^i). When the force F_K^j does not follow the force F_K^i exactly, a voluntary error must be concluded. Further, the subject should be continuously encouraged to minimize the sensor force F_K^j of the passive fingertip by keeping this finger as relaxed as possible. Feedback from a real time force signal display may be helpful.

e.2) The deep flexor force of a non-tested finger substitutes deep flexor force in the active finger

The error is explained from the example of expression (7). Assume that c^{21} and k_2^{12} must be measured. The error occurs when F_P^3 substitutes F_P^2 in the measurement. The measuring result then is:

$$F_T = \begin{bmatrix} c^{31} \\ c^{32} \\ c^{33} \end{bmatrix} \cdot F_P^3 + \begin{bmatrix} -k_3^{12} - k_3^{13} & -k_3^{13} \\ k_3^{12} & -k_3^{23} \\ k_3^{13} & k_3^{13} + k_3^{23} \end{bmatrix} \cdot \begin{bmatrix} \Delta L_P^{*12} \\ \Delta L_P^{*23} \end{bmatrix} \quad (8)$$

When the co-activation c^{32} is large and/or the passive connections k_3^{23} are stiff enough, the FP^3 may transfer up to its entire force to the T^2 end tendon. When (i) the coactivation c^{31} is small; (ii) the passive connections k_3^{32} bypass the stiffest connections between FP^2 and FP^1 , and (iii) the connections k_3^{13} are lax, the substitution of F_P^2 by F_P^3 will yield measured values substantially smaller than the real values c^{21} and k_2^{12} . Unlike error (e.1), this artefact is reproducible since it corresponds to real co-activation and stiffness values. In fig.4 an example is given with $c_{ij}=k_3^{12}=k_3^{13}=0$. To formalise, the substitution of F_P^2 by F_P^3 will diminish the force transfer from FP^2 to FP^1 when:

$$c^{32} \cdot F_P^3 - k_3^{23} \cdot \Delta L_P^{*23} \approx c^{22} \cdot F_P^2 \quad (1)$$

$$c^{33} \cdot F_P^3 + (k_3^{23} + k_3^{13}) \cdot \Delta L_P^{*23} + k_3^{13} \cdot \Delta L_P^{*13} \approx 0 \quad (2)$$

$$c^{31} \cdot F_P^3 < c^{21} \cdot F_P^2 \quad (3)$$

$$(k_3^{12} + k_3^{13}) \cdot \Delta L_P^{12} + k_3^{13} \cdot \Delta L_P^{23} < k_2^{12} \cdot \Delta L_P^{12} \quad (4)$$

The "substitution equation" (9.1) states that the fraction of F_P^3 transferred to F_T^2 by co-activation or connections must be of the order of magnitude of F_P^2 . When expression (9.2) holds, all force F_T^3 is transferred to T^2 and $F_K^3=0$, which means that the activation of FP^3 goes undetected by the force sensors. Expressions (9.3) and (9.4) guarantee that the erroneously measured c_{12} and k_2^{12} values are smaller than the real ones. k_3^{12} in expression (9.4) is the stiffness of the FP^2 - FP^1 connections of which the attachments to FP^2 are distal to the attachments of the k_3^{23} connections. The conditions (9) are well satisfied when:

$$k_3^{12}, k_3^{13} \ll k_2^{12}, k_3^{23} \quad (1)$$

$$c^{31} \ll c^{21} \quad (2)$$

$$\Delta L_P^{*23} \approx -\frac{c^{22} \cdot F_P^2 - c^{32} \cdot F_P^3}{k_3^{23}} \approx -\frac{c^{33} \cdot F_P^3 + k_3^{13} \cdot \Delta L_P^{*12}}{k_3^{23} + k_3^{13}} \quad (3)$$

$$F_P^3 \approx \frac{c^{22}}{c^{33} + c^{32}} \cdot F_P^2 \approx \frac{c^{22} \cdot F_P^2 - k_3^{23} \Delta L_P^{*23}}{c^{32}} \quad (4)$$

Expression (10.1) states that substitution is effective when the stiffness k_3^{13} of the direct FP^3 - FP^1 connections is small, and the stiffest FP^2 - FP^1 connections are bypassed by the FP^3 - FP^2 connections. Expression (10.2) is obvious. Expression (10.3) provides the displacement

$\Delta L_p^{*23} < 0$ required for complete substitution of F_p^2 by F_p^3 with $F_T^3 = 0$. Clearly, the greater the co-activation c^{32} and the stiffer the connections k_3^{23} , the smaller this displacement must be. The negative sign means that for substitution D^3 must be flexed in advance to D^2 ($\Delta\Theta_2^{23} > 0$). With stiff connections this flexion difference need not be large, and may go unnoticed during the measurement. Expression (10.4) states that with conditions (10.1) and (10.2), F_p^3 must be of the same magnitude as F_p^2 .

Avoidance of the substitution. Our experience is that when the conditions (10.1,2) are satisfied, the substitution occurs reflexmatic. Avoidance consists of suppressing both co-active and passive substitution forces. (i) co-activation $c^{32} \cdot F_p^3$ must be minimized by requesting the subject to relax D^3 as much as possible. However, even when $F_p^3 = 0$, the sensor force F_K^3 may be large due to a large co-active force $c^{23} \cdot F_p^2$. Such large co-activation cannot be distinguished from the case with $F_p^3 > 0$ and $F_p^2 = 0$. In fact, when the co-activations are $c^{23} = c^{32} = 0.5$, both motors are perfectly interchangeable as they pull each others tendons with the same force as their own. (ii) Non-measured fingers should be kept in the same position as adjacent fingers ($\Delta L_p^{*i,i+1} = 0$) to exclude passive force transfers ($\Delta L_p^{*23} = 0$ in the example). With small c^{32} the F_p^3 force for effective substitution will then be forbiddingly great (expression (10.4, right hand equality), which will suppress the reflex.

The error (e.2) cannot occur in the CT_3^j or ST_3^j tests (little finger deep flexor active), as there is no sixth flexor to pull the FP^5 . However, it can occur in the CT_2^j and ST_2^j tests (index flexor active) when a connection from the flexor pollicis longus (FPL) to the index is present; the FPL may then pull the FP^2 . The hand should be standard tested for such connections, which are usually tautened when the thumb flexes in advance of the index, and relaxed when the index flexes in advance of the thumb (Linburg and Comstock, 1979). With such a connection, the error is excluded when the thumb is kept in extension during the CT_2^j or ST_2^j tests.

Errors in the estimation of the tendon forces

e.3) The force in the lateral bands is not zero ($T_{LB3} \neq 0$ in expression (2.2))

This occurs especially in the passive finger. The subject tries to minimize the sensor force F_K^j by activating the finger extensors which tauten the lateral bands (fig.3.b). In the active finger, $T_{LB3} > 0$ would decrease the sensor force F_K^1 , which is contrary to the demand for maximal force; this makes activation of the extensors less likely. In the passive finger, $T_{LB3} > 0$ leads to an underestimation of c^{ij} and k_i^{ij} ; in the active finger to an overestimation. The error can be avoided by using a property of the extensor assembly. When the PIP flexes ($\Theta_2 > 0$) while the DIP remains extended ($\Theta_3 \approx 0$), the lateral bands become slack and all extensor force runs through the medial band (Landsmeer, 1958; Leijnse et al., 1992) (fig.3.c). Therefore, when the PIP is kept in $\Theta_2 > 30^\circ$ while the DIP remains extended, the lateral bands can be tautened only when the medial band is sufficiently stretched. The large extensor forces required for this will be noted during measurement (see further).

e.4) The force in the volar plate is not zero ($T_{VP3} \neq 0$ in expression (2.2))

This error occurs especially in the active finger. With DIP hyperextension, the volar plate becomes taut to prevent further extension (fig.3.c). Through the taut volar plate the superficial flexor can provide a flexion torque T_{VP3} at the DIP, and substitute the deep flexor force in the sensor. When the superficial flexor is not connected to the deep flexors of the passive fingers, $T_{VP3} > 0$ increases the active sensor force without increasing the passive sensor forces, which will underestimate c^j and k_i^j . The substitution happens reflexmatic when the connections become too stretched, and easily goes unnoticed because the active sensor force F_K^i remains at level. The error can be eliminated by keeping the DIP of the active finger slightly flexed ($\Theta_3 \geq 0$), so that the volar plate remains slack.

Errors in the measuring of the motor length differences

e.5) Non-measured joints are not isometric

In the measuring device only the PIP position is measured. However, the deep flexor crosses the wrist, MCP, PIP, DIP, so that (with constant moment arms):

$$d\Delta L_p^* = -\sum_{i=0}^3 (R_{Pi}^* \cdot d\Delta\theta_i^* - \Delta R_{Pi}^* \cdot d\theta_i^*) \quad (11)$$

Without fixation, non-measured joints may exchange tendon length with the PIP joint without the muscle itself changing length ($d\Delta L_p^* = 0$ in expression (11)). However, the proper fixation of the proximal phalanx in small fingers with large webs is problematic, and sometimes infeasible.

FINGER FIXATION AND POSITION CONTROL IN THE MEASURING DEVICE

The fixation of the second phalanx (fig.3.a)

To avoid errors (e.3) ($T_{LB3} > 0$) and (e.4) ($T_{VP3} > 0$), the PIP must not extend completely, while the DIP is kept in near extension ($\Theta_3 \geq 0$). The latter is realised by a threshold just distal to the DIP joint axis, so that the DIP must slightly flex to push the sensor; this flexion increases somewhat with the sensor force as the finger pad is compressed. The moment arm of the threshold at the DIP must be small to not affect the DIP equilibrium equation (2.2). To prevent overflexing ("clawing") of the DIP and the tautening of the lateral bands (e.3), the middle phalanx must be firmly fixed to the sensor support.

The control of the PIP rotations and sensor load

In fig.3.a, the fingertip load is transfered to the middle phalanx by the DIP joint ligaments, and by the fixation (F_2) back to the sensor holder. The torque of fixation and load is balanced by the reaction force at the axis (fig.3.a (A)). Therefore, the sensor can be loaded without external force. However, any deep flexor or superficial flexor force will flex the PIP joint which is free, and must be balanced by the extensors or by an external torque T_{E2} :

$$r_{P2} \cdot F_P + r_{S2} \cdot F_S - r_{LB2} \cdot F_{LB} - r_{MB2} \cdot F_{MB} = T_{E2} \quad (12)$$

With an appropriate torque T_{E2} , no extensor force is mechanically required to execute the tests. In the present device, T_{E2} is manually provided by the examiner, which by this force also controls the PIP rotations. Manual PIP control allows to feel when the extensors in the passive fingers are active (error (e.3)), i.e., when the PIP flexion torque is less than expected from the sensor force F_K . The subject can then be reminded to relax the extensors.

The maximal displacements of the deep flexors in the device

During the measurement the DIP at all times remains in near extension, while the PIP moves within the approximate range: $0^\circ \leq \Theta_2 \leq 100^\circ$. With this PIP range, the connections can only be tested within: $|\Delta L_p^{*ij}| < 17\text{mm}$ (with an average $r_{p2} = 10\text{mm}$). The maximal displacement of the deep flexor in a finger of this size is more than 50mm. Therefore, the deep flexor muscles will not become insufficient in the tests, and the coefficients c^{ij} will change little due to the physiological muscle force-fibre length relationship.

MEASURING PROCEDURES

Stiffness test

For manipulative ease, only one set of fingers is moved at a time by rotating their sensor holders, while the others are kept in fixed position. The same connections can be tested in two ways: (i) with the passive finger fixed and the active finger rotated from extension to flexion or inversely, and (ii) with the active finger fixed and the passive finger being moved about. These two possibilities allow to double check the results. Adjacent non-tested fingers must be rotated with their tested neighbours according to expression (6), to exclude error (e.2). Presently, the test is described with the passive finger fixed. Put both fingers with $\Theta_2^i = \Theta_2^j = 30^\circ$ to exclude error (e.3), and let the subject press the active sensor with a constant force F_p^i . F_p^i is constant when the sum of the sensor forces F_K^j is constant at the display, except when the errors (e.1), (e.2), or (e.4) hold. The examiner then rotates the active finger D^i to $\Theta_2^i > 90^\circ$, while D^j remains in fixed position; this covers the range $-60^\circ \leq \Delta \Theta_2^{ij} \leq 0^\circ$. To test the $0^\circ \leq \Delta \Theta_2^{ij} \leq 60^\circ$ range, the PIP joints are put in $\Theta_2^i = \Theta_2^j = 90^\circ$, and the active finger is extended to about $\Theta_2^i = 30^\circ$. Allowing the fingers to extend to 0° increases the displacement difference of the motors by $r_{p2} \cdot \pi/6$, but error (e.3) cannot be excluded anymore.

Co-activation test

In the co-activation test (expression (7.1)) the PIP joints are put with $\Theta_2 > 30^\circ$ to avoid artefact (e.3), and with $\Delta \Theta_2^*$ as in expression (6), to put $\Delta L_p^* = 0$ (expression (5)). With the fingers fixed, the subject pushes one sensor, while maximally relaxing the other fingers. The force in the active finger can be slowly or quickly varied to exclude error (e.1).

RESULTS

In fig.5 measuring results are presented to illustrate the artefacts (e.2..e.4). The graphs are coded by, in consecutive order, the subject number, active and passive digit and the hand side (L/R). E.g. subj. 1, 23R reads as: subject 1, FP² (index) active, FP³ (medius) inactive, right hand. The present device only measures two fingers at a time. The position of non-measured fingers when causing errors is specified in the text.

Error (e.2): deep flexor force substitution by an adjacent deep flexor

Fig.5, Subj. 1 illustrates the substitution of F_p^3 by F_p^4 in the measurement of the ST_3^{32} test.

23R: The graph 23R (FP² active) shows little co-activation, but very stiff passive connections which only allow the displacement difference of the tendons up to 80° PIP rotation difference.

32R(A): in contrast, the ST_3^{32} test (b) (FP³ active and FP² passive) shows almost no passive connections, not even with a PIP rotation difference of 100°. However, the ST_3^{32} test is clearly erroneous, as the co-activation demonstrated in (a) does not show up in (b). Since in (b) the passive finger was completely extended ($\Theta_2^2=0$), it was concluded that the lateral bands had been tautened during the test (b) (error (e.3)). The subject was measured again in a second session, with all mentioned errors carefully checked. A totally different result was obtained, given in subj 1, 32R(B).

32R(B), (a,b): ST_3^{32} tests with Θ_2^3 flexing and Θ_2^2 extended and isometric. (c): the ST_3^{32} test with Θ_2^3 flexed and isometric and Θ_2^2 extending. In contrast to subj 1, 32R(A)(b), the results of 32R(B) show strong passive connections. The difference between 32R(A) and 32R(B) cannot be accounted for by taut lateral bands only. The strong passive connections shown in 32R(B) would still to some degree stretch the lateral bands and flex the passive fingertip unto the sensor. This would diminish F_K^2 as a function of $\Delta\Theta_2^{32}$, but not to zero. Therefore, the main error must have been the pull of FP³ by FP⁴ through the FP⁴³ connections. These connections are measured in subj. 1, 43R(B), for $\Theta_2^4 > \Theta_2^3$. This figure shows:

43R(B), (a) is the auto-coactivation test, which reveals a co-activation force of about 50%. This force is rerouted to F_K^4 when Θ_2^4 goes to zero while Θ_2^3 remains at 90°, and the connections get stretched from proximally FP³ to distally FP⁴. (b) is the ST_4^{43} test with the active finger isometric in flexion, and the passive finger extending. The largest force (full line) is the force F_K^3 , i.e. the force transferred from FP⁴ to F_K^3 . (b) shows that the FP⁴³ connections are very stiff, and capable of transferring the entire force F_p^4 to F_K^3 , which happens when $\Theta_2^4 - \Theta_2^3 \approx 85^\circ$.

In the ST_3^{32} tests of 32R(B) digit D⁴ was carefully kept in the same position as D³ ($\Delta\Theta_2^{34}=0$), so that $\Delta L_p^{43} \approx 0$. This reduces a possible force transfer of F_p^4 to F_K^3 to the co-activation force $c^{43} \cdot F_p^4 \approx 0.5 \cdot F_p^4$, while with substitution the force F_K^4 would be: $(1 - c^{43}) \cdot F_p^4 \approx 0.5 \cdot F_p^4$ (the c^{ij} are here estimated without counting the transfers to the little finger). On the other hand, the co-activation $c^{34} \approx 0.25$ (from the CT³⁴ test in 34R(B)(b)). Therefore, with F_p^3/F_p^4 substitution ($F_p^4 > 0$, $F_p^3 = 0$) and with $\Delta\Theta_2^{34}=0$ the sensor force F_K^4 would be twice as large as with correct testing ($F_p^3 > 0$, $F_p^4 = 0$). Such a difference can be manually checked, and

can also be appreciated by the subject, which is asked to minimize the force F_K^4 . The erroneous results of subj. 1, 32R(A) were reproducible: it sufficed to allow D^4 to flex freely in advance to D^3 during the ST_3^{32} test. The results clearly validate the conditions (10.1,2): no substantial FP^{32} connections exist distal to the FP^{43} connections; any direct FP^{42} connections are lax, and $c^{42} \approx 0$. Note that with $F_p^4 = 0$, the deep flexor FP^3 in 32R(B) could barely realise the 15N sensor force so easily achieved in 32R(A).

Error (e.3): tautening of the lateral bands

Consider fig.5, subj. 2, 34R. In the ST_3^{34} tests (c,d) the slopes of F_K^4 are quite different. In Leijnse⁵ (1996) it is concluded on theoretical grounds that this difference is due to a systematic error. No passive connections were present between D^2 and D^3 , so error (e.2) ($F_p^2 > 0$) can be excluded. Error (e.4) is excluded by the DIP threshold. So either (e.1) ($F_p^3 > 0$) holds in (c), or (e.2) ($T_{L.B3} > 0$) holds in (d).

Error (e.4): substitution of deep flexor force by superficial flexor force

Subj. 3, 34R presents examples of error (e.4), measured after removing the threshold T in fig.3.a from the device. Four measurements are taken, the first without, the others with FP/FS substitution. In 34R(a) the subject has managed, by extreme effort, to load the sensor F_K^3 by the FP^3 force in the range $0 < \Delta\Theta_2^{34} < 90^\circ$. The graphs 34R(b,c,d) show what happens normally. Initially, the sensor is loaded by the deep flexor FP^3 alone. The substitution happens at b', c', d' , and was clearly noticeable by the collapse of the DIP^3 joint into hyperextension. The switch points b', c', d' can be obtained from the comparison with 34R(a). F_K^4 in (a) is the sensor force corresponding to the motor force F_p^3 which is required to stretch the connections so that it remains that $F_T^3 = F_p^3 - k_3^{34} \cdot \Delta L_p^{*34} > 0$. Therefore, any F_K^4 force less than in (a) for an equal $\Delta\Theta_2^{34}$ value results in a slack FP^3 end tendon ($F_T^3 = 0$). It follows that from b', c', d' onwards, the sensor force F_K^3 necessarily results from the FS^3 ($F_{K3}, r_{K3} = T_{VP3}$). Error (e.2) (FP^3/FP^2 substitution) was excluded as no FP^{23} connections were present. Note that even when $F_T^3 = 0$, the force F_K^4 does not become zero. This means that either $F_p^4 > 0$ (error e.1), or that FP^3 remains active ($F_p^3 > 0$) during the test in a vain attempt to load the sensor of D^3 . The consistency of the results is remarkable. E.g. in (a) and (b) the forces F_K^4 are almost equal as a function of the joint rotations up to the point when FS^3 takes over in (b) (compare $a'-b'$ and $a''-b''$). The switch from the FP^3 to FS^3 in the loading of F_K^3 occurs in b,c,d for about the same F_K^4 force. This illustrates the reflex to switch from deep flexor to superficial flexor force when the force transfers in the deep flexors become too great.

DISCUSSION

Some general remarks

The above examples illustrate that the measuring of the functional interdependencies in the deep flexor group is not a straightforward matter. The avoidance of mentioned errors requires considerable attention of examiner and subject. Further difficulties are the adjustments for the individual finger size and shape. The fixation of the middle phalanx must be firm and inextensible, yet must not hurt the finger. A practical problem may be the physical fatigue in the subject's hand, especially when affected by a focal dystonia complaint. As a general observation, it remains amazing that musicians, who assumably have a high conciousness in hand use, can have strongly connected tendons without being aware of it.

System indeterminates and motor function analysis in instrumental playing

Three basic indeterminates in the system equations (2) allow to diminish the effect of the connections: the co-activation of the extensors (error (e.3)), the FP/FS substitution (error (e.4)), and the FP/FP substitution (error (e.2)) (expression (10)). The reflexmatic occurrence of these errors in measurement suggests that they also occur in actual functioning, as in the playing of the instrument. In the FP/FS substitution, connections are avoided by mobilising unconnected muscles. However, in the FP/FP substitution, connections are themselves used to avoid the effects of other connections. Adverse effects of connections are, amongst others, conjoined movements in which the motors of "active" fingers pull other fingers (Leijnse et al, 1993; Leijnse^a, 1996). In the FP/FP substitution, the inverse happens: motors of "passive" fingers become "agonists" of "active" fingers. Such "agonistic" passive fingers also move conjointly with the active fingers, as their positions depend on the lengths of their motors which serve the active finger. However, in the "passive" conjoined movement the passive finger is pulled by the active finger, and therefore moves "after" it, while in the "active" conjoined movement the passive finger pulls the active finger, and moves "ahead" of it (expression (10.3)). The stiffer and shorter the connections, the smaller this difference will be, and with inextensible connections of zero length these conjoined movements are identical. A necessary condition for agonistic finger movements is that the agonistic finger must not perform a proper task at the moment of substitution. A typical example thereof is in the right hand of the classical guitar player, of which the little finger is not used in playing. Therefore, with strong FP⁵ connections, the FP⁵ may freely assist the FP⁴ in the flexing of D⁴. Such possibilities of finger control caution against too simple a view of motor function in instrumental playing.

CONCLUSION

A device is presented to measure the force transfers resulting from anatomical interconnections between the deep flexors. In these measurements systematic errors may occur, which find their cause in the indeterminates in the muscle forces. Intertendinous connections increase the number of indeterminates, as they allow the interchange of force between connected motors. The errors are studied in a three finger system with connected deep flexors, and are illustrated by measuring results. It is shown that some of these errors can be avoided by appropriate finger fixation and

positioning during measurement. It is argued that the mentioned indeterminates in motor function, also those created by the intertendinous connections, are actively used in instrumental playing, which complicates analysis of motor function in hands with interconnected motors.

ACKNOWLEDGEMENTS

The author thanks Dr. C.W. Spoor for the close reading of the manuscript, and Dr. G.J. Sonneveld, head of the special clinic for musicians at the Erasmus University Rotterdam, Prof.Dr. C.J. Snijders, Prof.Dr. J.M.F. Landsmeer, Dr. S.E.R. Hovius, and Prof.Dr. J.C. Van der Meulen and Dr. J.E. Bonte for their valuable contributions.

REFERENCES

- Landsmeer J.M.F. (1958) A report on the co-ordination of the interphalangeal joints of the human finger and its disturbances. Acta Morph. Neerl.-Scand. 2, 59-84.
- Linburg, R.M., and Comstock, B.E. (1979) Anomalous tendon slips from the flexor pollicis longus to the digitorum profundus. Am. J. Hand Surg. 4, 79-83.
- Leijnse, J.N.A.L., Bonte, J.E., Landsmeer, J.M.F., Kalker, J.J., van der Meulen, J.C., Snijders, C.J. (1992) Biomechanics of the finger with anatomical restrictions:- the significance for the exercising hand of the musician, J.Biomechanics 25, 1253-1264.
- Leijnse J.N.A.L., Snijders C.J., Landsmeer J.M.F., Bonte J.E., van der Meulen J.C., Sonneveld, G.J., Hovius, S.E.R. (1993) The hand of the musician - the biomechanics of the bidigital finger system with anatomical restrictions. J. Biomechanics 26, 1169-1179.
- Leijnse^a, J.N.A.L., (1996) Anatomical factors predisposing to focal dystonia in the musician's hand, Accepted J. Biomechanics, juli 1995.
- Leijnse^b J.N.A.L., (1996) Measuring anatomic connections in the deep flexor of the musician's hand: theoretical analysis, clinical examples, Submitted J. Biomechanics, 1995.

APPENDIX

Variables and parameters

The kinematic variables are (L_p is the distance between origin and insertion of a deep flexor):

$$\begin{aligned}
 L_p &= [L_p^1, \dots, L_p^3]^T & \theta_2 &= [\theta_2^1, \dots, \theta_2^3]^T \\
 L_{p0} &= [L_{p0}^1, \dots, L_{p0}^3]^T & \theta_{20} &= [\theta_{20}^1, \dots, \theta_{20}^3]^T \\
 \Delta L_p &= L_p - L_{p0} & \Delta \theta_2 &= \theta_2 - \theta_{20} \\
 \Delta L_p^* &= [\Delta L_p^2 - \Delta L_p^1, \Delta L_p^3 - \Delta L_p^2]^T & \theta_2^* &= [\Delta \theta_2^1, \Delta \theta_2^2]^T \\
 & & \Delta \theta_2^* &= [\Delta \theta_2^2 - \Delta \theta_2^1, \Delta \theta_2^3 - \Delta \theta_2^2]^T
 \end{aligned} \tag{A.1}$$

The reference lengths L_{p0} are chosen so that when $\Delta L_p^* = 0$ the intertendinous connections are slack or minimally strained. In the normal hand this is with extended fingers ($\Theta_2 = \Theta_{20} = 0$). The

force variables are:

$$\begin{aligned}
 \mathbf{F}_P &= [F_P^1, \dots, F_P^3]^T & \mathbf{T}_{VP3} &= [T_{VP3}^1, \dots, T_{VP3}^3]^T \\
 \mathbf{F}_T &= [F_T^1, \dots, F_T^3]^T & \mathbf{T}_{LB3} &= [T_{LB3}^1, \dots, T_{LB3}^3]^T \\
 \mathbf{F}_K &= [F_K^1, \dots, F_K^3]^T & F_P^i, F_T^i, F_K^i, T_{VP3}^i, T_{LB3}^i &\geq 0
 \end{aligned} \tag{A.2}$$

The system parameters are the moment arms, co-activation fractions c_{ij} , and the stiffnesses k_i^{ij} of the connections:

$$\begin{aligned}
 \mathbf{R}_{K3} &= \text{Diag} [r_{K3}^1, \dots, r_{K3}^3] & \mathbf{R}_{P2}^* &= \text{Diag} [r_{P2}^2, r_{P2}^3] \\
 \mathbf{R}_{P3} &= \text{Diag} [r_{P3}^1, \dots, r_{P3}^3] & \Delta \mathbf{R}_{P2}^* &= \text{Diag} [r_{P2}^2 - r_{P2}^1, r_{P2}^3 - r_{P2}^2] \\
 \mathbf{C} &= \begin{bmatrix} c^{11} & c^{21} & c^{31} \\ c^{12} & c^{22} & c^{32} \\ c^{13} & c^{23} & c^{33} \end{bmatrix} & \mathbf{K}_c &= \begin{bmatrix} -k_i^{12} & -k_i^{13} & -k_i^{13} \\ k_i^{12} & -k_i^{23} & \\ k_i^{13} & k_i^{13} + k_i^{23} & \end{bmatrix}
 \end{aligned} \tag{A.3}$$

(all $r_{ij}, c^{ij}, k_i^{ij} \geq 0$). \mathbf{R}_{P2}^* , $\Delta \mathbf{R}_{P2}^*$, \mathbf{R}_{P3} , \mathbf{R}_{K3} are diagonal matrices with the diagonal elements composed of the moment arms of the deep flexor for the PIP (Θ_2) and DIP (Θ_3) joints, and of the load \mathbf{F}_K at the DIP, resp.

Properties of the system equations

The following properties hold:

$$\begin{aligned}
 \sum_j F_T^j &= \sum_j F_P^j & (1) \\
 \sum_j c^{ij} &= 1 & (2) \\
 \sum_i [K_c]_{ij} &= 0 & j=1,2 \quad (3) \\
 \sum_i c^{ij} \cdot F_P^i + [K_c, \Delta L_P^*] &\geq 0 & j=1,2,3 \quad (4)
 \end{aligned} \tag{A.4}$$

Expression (A.4.1) is the total equilibrium condition of tendon and motor forces. Expression (A.4.2) holds by definition. Expression (A.4.3) follows from the summation of expressions (2.1), with expression (A.4.1). Expression (A.4.4) is the explicit condition $\mathbf{F}_T \geq 0$. It states that the sum of the forces in the connections leaving a tendon cannot exceed the sum of the co-activations and the connective forces entering the tendon.

FIGURES

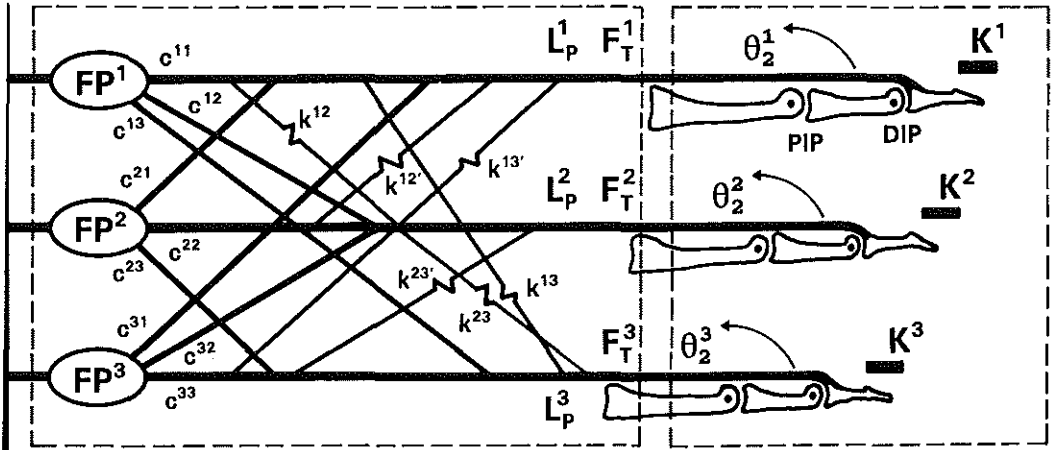


Figure 1 Model of three interconnected deep flexors. The box at the left contains the connected flexor system itself. The system variables are: the motor forces FP^i , the motor lengths L_p^i , and the tendon forces F_T^i distal to the connections. The system parameters are: the co-activations c^{ij} and the stiffnesses k^{ij} of the anatomical connections. The stiffnesses of connections between the same tendons, but of opposite direction are indicated by k^{ij} , k^{ji} . The box at the right of the picture contains the variables measured by the device: the PIP angles θ_2^i and the forces F_K^i in the sensors K^i .

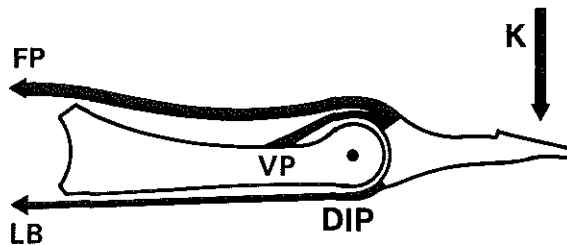


Figure 2 Forces at the DIP joint with load K at the finger tip.

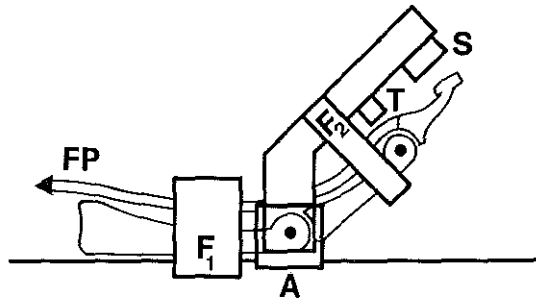


Figure 3 a

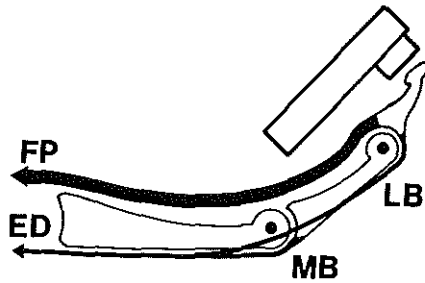


Figure 3 b

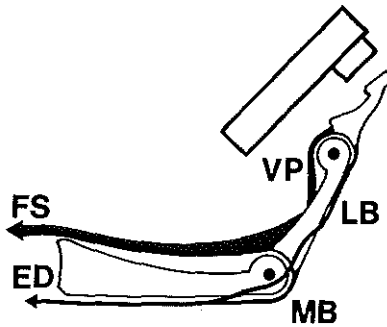


Figure 3 c

a) Schematic drawing of the fixation of a finger in the measuring device. F_1 , F_2 : fixation of the proximal and middle phalanges. A: base with axis of the sensor support, collinear to the PIP joint axis. T: threshold to eliminate flexion torque from a taut volar plate. S: force sensor.

b) Finger with taut lateral and medial insertions of the extensor assembly (lateral and medial bands (LB,MB)). c) The superficial flexor (FS) can load the load cell when the volar plate (VP) of the DIP joint is taut. In the picture, the DIP joint is extended while the PIP joint is flexed, therefore the lateral band (LB) is slack.

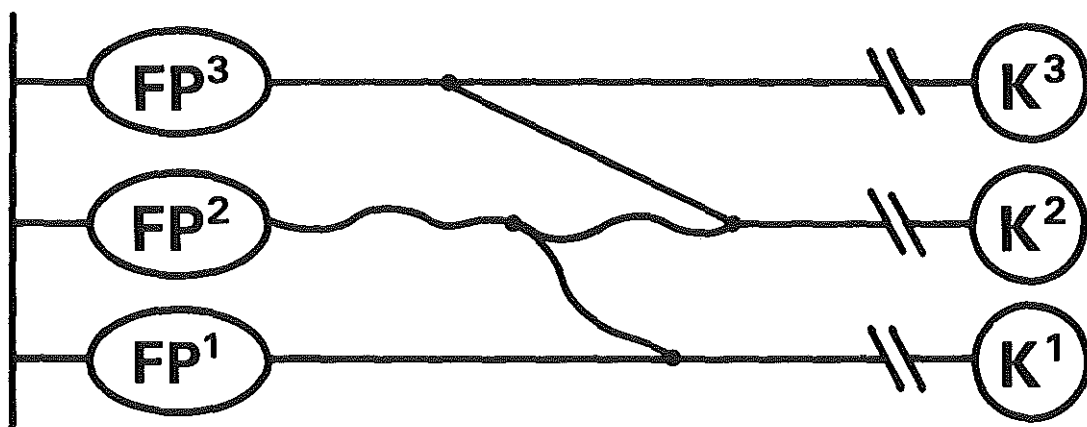


Figure 4 Substitution of the FP^2 by FP^3 in the ST_2^{21} test. The load cell K^2 is loaded by FP^3 while FP^2 is inactive. The force F_p^3 bypasses the connections between FP^2 and FP^1 . Therefore, no connections between FP^1 and FP^2 will be measured in the ST^{21} test.

Figure 5 (comments with figs. of next page) Examples of systematic measuring errors. Subj. 1: substitution of FP^3 by FP^4 in the ST_3^{32} test (error e.2). Subj. 2: taut lateral bands (error e.3). Subj. 3: substitution of FP^3 by FS^3 in the ST_3^{34} test (error e.4). Only two fingers are measured at one time. The upper half of the graphs presents the forces F_K^1 , F_K^2 in the fingertips, indicated at the left-hand Y-axis. The lower half of the graphs presents the angles Θ_2^1 of the PIP joints, indicated at the right-hand Y-axis. X-axis: number of samples, 25 samples/s. For further comments, see results.

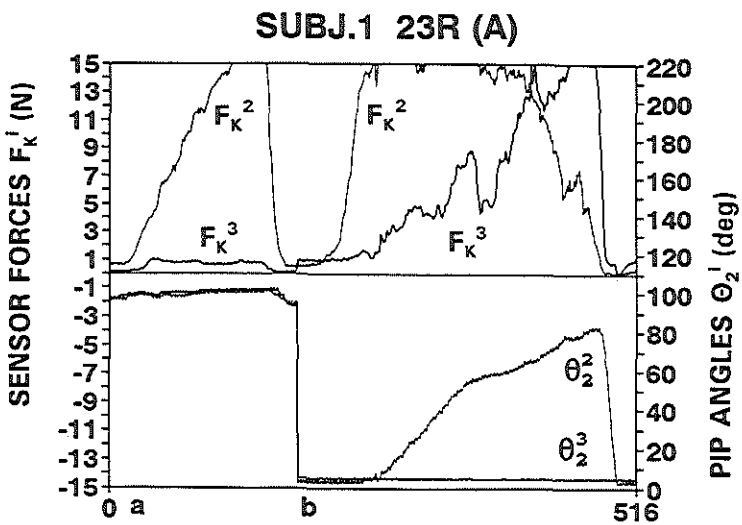
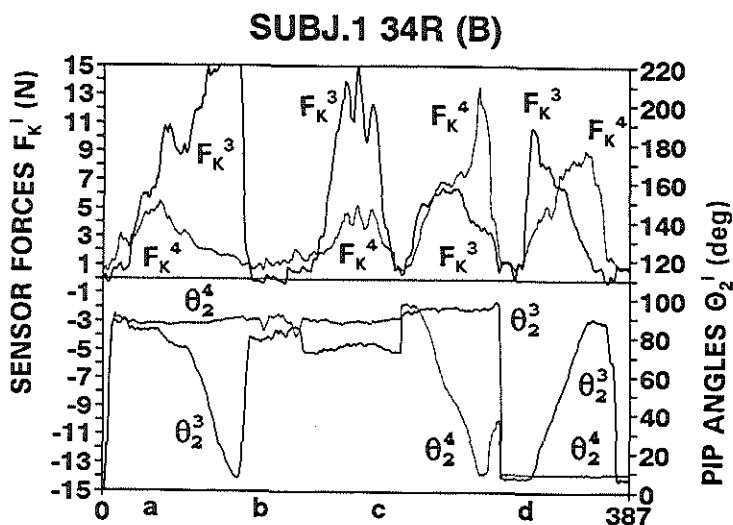
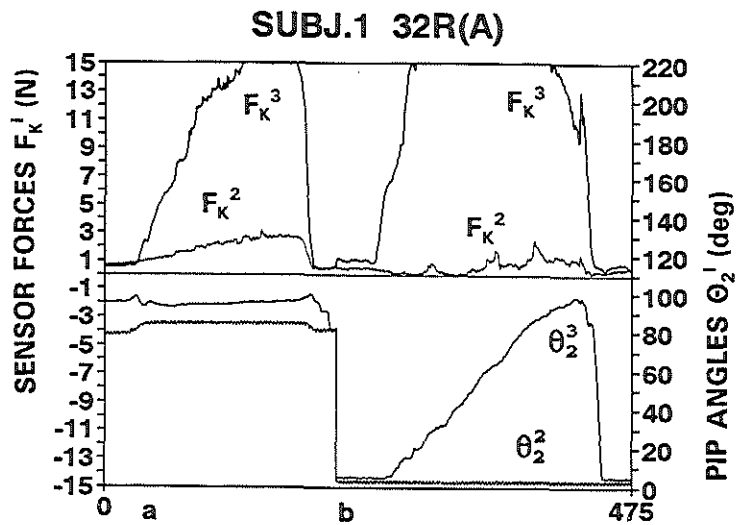


Figure 5 a,b

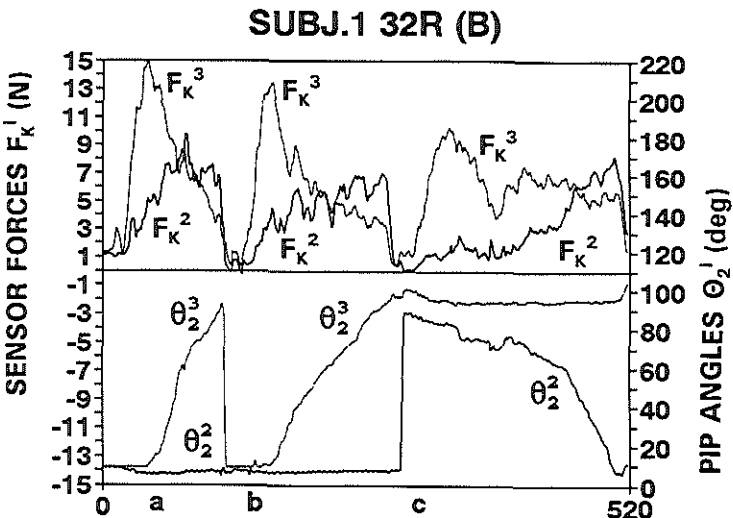
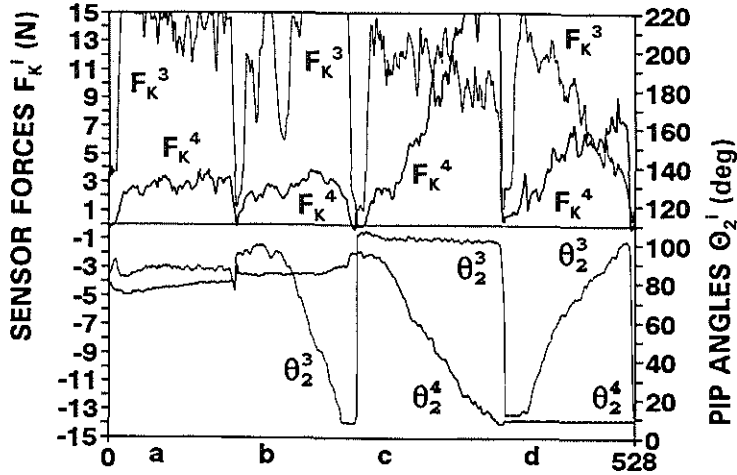
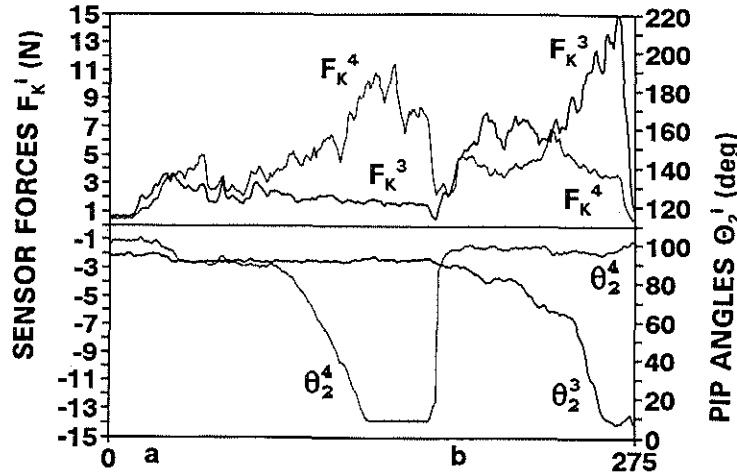


Figure 5 c,d

SUBJ.2 34R



SUBJ.1 43R (B)



SUBJ.3 34R

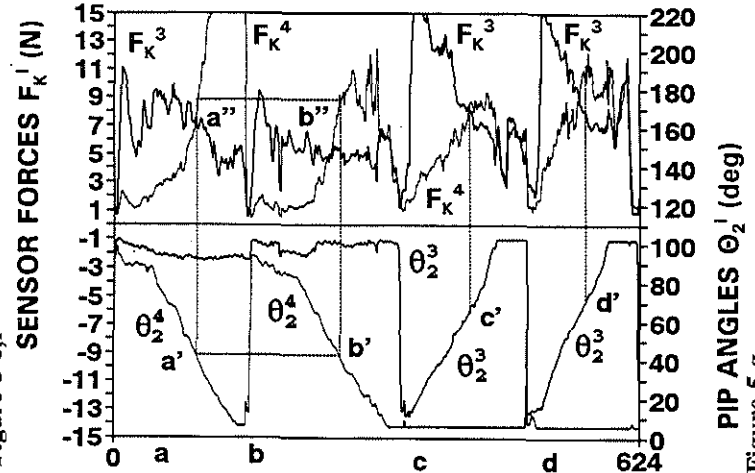


Figure 5 e,f

Figure 5 g

CHAPTER IV

ANATOMIC FACTORS PREDISPOSING TO FOCAL DYSTONIA IN THE MUSICIAN'S HAND

Anatomic factors predisposing to focal dystonia in the musician's hand

J.N.A.L. Leijnse

Accepted by J. Biomechanics, 1995

ANATOMICAL FACTORS PREDISPOSING TO FOCAL DYSTONIA IN THE MUSICIAN'S HAND - PRINCIPLES, THEORETICAL EXAMPLES, CLINICAL SIGNIFICANCE

J.N.A.L. Leijnse

Department of Plastic and Reconstructive Surgery, Erasmus University, Rotterdam, the Netherlands. Resubmitted J. Biomechanics, 1995.

ABSTRACT

In this paper, anatomical interconnections between tendons, between tendons and their environment, and anatomical constraints on joint mobility are considered as possible causes of focal dystonia in the hand of the musician. By hypothesis, focal dystonias arise when the constraints on movement resulting from these anatomic limitations impede playing movements with sufficiently low energy expenditure. This hypothesis is modelled for connections between the deep finger flexors. The displacements, forces, stresses, and work per volume in the finger motors in some common piano playing movements are calculated. The results indicate that with mentioned connections, in certain movements the extensor and lumbrical, and in others the lumbrical and interossei are most strained, while the interossei may become the main power source in loaded instrumental movements. Also discussed are compensatory movements. The biomechanical principles of surgical and conservative treatment are summarised.

NOMENCLATURE

- D^i : Digit number i
MCP,PIP,DIP : proximal, middle and end joint of the finger
CMC,MCP,IP : carpal, middle and end joint of the thumb
FPL(PL),FP(P),
FS(S),ED(E),
IO(I),LU(L) : flexor pollicis longus, deep flexor, superficial flexor, extensor, interosseus, lumbrical (notations in text,; and in figures and moment arms, resp.)
U,R : ulnar and radial interosseus (notation in figures)
MB : medial band of the extensor assembly
LB : lateral band of the extensor assembly
 r_{ik} : moment arms; i =motor: P,S,I,U,R,LU,E,PL; k =1,2,3 for MCP,PIP,DIP, resp. (see table I)
 r_{AR}, r_{AU}, r_{AL} : abduction moment arms at MCP of ulnar and radial interosseus and lumbrical
 L_M : length of motor M measured between origin and insertion
 Θ_k : angle of joint k , positive for flexion
 λ_{TM} : slack in tendon of motor M distal to attachments of connections
 L_{Mp} : distance between the origin of motor M and the attachment of the connection
 L_{RM} : resting fibre length of motor M
 L_{c0} : resting length of the connection
 V_M : contraction speed of muscle M

Anatomical factors predisposing to focal dystonia

σ_M	: stress in motor M ($\sigma_M = F_M / PCA_M$)
PCA_M	: physiological cross-sectional area of motor M.
V_M	: volume of muscle M ($V_M = PCA_M \cdot L_{RM}$)
ν_M	: physiological contraction speed of motor M (speed over resting fibre length)
R_M, R_K	: moment arm matrices of motors and external load
F_M, F_{TM}, F_c	: vectors of motor forces, end tendon forces, and forces in the connections, resp.
F_K	: vector of external loads
C	: co-activation coupling matrix
c_t^{ij}	: fraction of the force in motor M_i^i of D^i transferred to motor M_t^j in D^j ; t indicates the muscle group
F_{Mp}, F_{Md}	: force in tendon proximal and distal to the attachment of the connection.

INTRODUCTION

Focal dystonia or "overuse" has become a well recognised problem in musicians (Cohen et al, 1989; Fry^(a), 1986; Fry^(b), 1986; Lockwood, 1989; Hochberg et al, 1990; Tubiana, 1993). The symptoms are dysfunction of specific muscle groups in playing, most often the extensors or intrinsic. The causes are still a matter of debate, but it is generally regarded as a repetitive strain injury (RSI) (Amadio and Rusotti, 1990). Yet, with many subjects playing the same instrument for comparable periods of time, a fundamental question is why some develop the complaint and others don't. Joint mobility and hand size have been considered as predisposing factors (Wagner, 1988). Presently, anatomic interconnections of tendons or muscles are discussed. Intertendinous connections have been described between the extensors (von Schroeder et al., 1990), the deep flexor of the index and the long flexor of the thumb (Linburg and Comstock, 1979; Blair and Omer, 1981), the superficial flexors of the ulnar two fingers (Baker et al., 1981; Austin et al., 1989), and they are systematically present in the deep flexors (Verdan, 1960; Fahrer, 1971; Malerich et al., 1987; Leijnse et al., 1996). Previous authors have discussed their association with hand difficulties in musicians (Markison, 1990, Stern, 1990; Leijnse et al., 1992, 1993). In Leijnse^{a,b} (1996) the force transfers between the deep flexors were quantified. They result either from passive connections between muscles or tendons, or from co-activation of muscle bellies to different fingers. In the following, four instances in which intertendinous connections increase muscle load are discussed. (i) *Muscle load as a result of the stretching of intertendinous connections*. In movements with stretched connections two superimposed sets of muscle forces can be distinguished: (a) forces required to execute the same movement with unconnected tendons, and (b) forces required to stretch the connections. The stretching forces are from antagonistic muscles of which the actions balance out within the hand, and cannot be traced from external work. Therefore, muscles in hands with different intertendinous connections may be quite differently loaded in identical tasks without this being apparent. As a cause of focal dystonia, this satisfies two clinical facts: focality, as the loading is with the muscles antagonistically stretching the connections, and individuality, as the loading relates to the individual anatomy. (ii) *Muscle load in*

movements in the slack range of the connections. Movements in which the connections are not stretched may also cause focal muscle loading when they imply inefficient muscle use. It is shown that the power expenditure in the intrinsics (interosseus, lumbrical) may increase considerably as a result of limitations on deep flexor displacements. (iii) *Co-activation.* Co-activation is the transfer of a constant force fraction from an activated deep flexor motor to another deep flexor end tendon. The excess loading is with the antagonists of the co-activated motor, which for proper finger control must at all times counterbalance the co-activation forces. (iv) *Muscle loading due to compensatory movements.* Limitations in the hand may require compensatory joint actions of wrist, elbow, and shoulder, which increase the loading of muscles generally associated with posture. These instances of increased motor load are investigated for a connection between the long thumb flexor, and the deep flexor of the index. The example is chosen for easy visualisation, and most results apply to interconnected deep flexors as well. An additional constraint is introduced, on the flexion range of the MCP of the thumb, to illustrate the effect of superimposed constraints. The model results are discussed with respect to conservative therapy and surgery. The present paper is a close sequel to the kinematic studies of finger movements with connected tendons (Leijnse et al., 1992; Leijnse et al, 1993), and the model studies of the kinematics (Leijnse and Kalker, 1995) and the motor forces and stresses (Leijnse^a, 1996) of the finger with lumbrical.

MATERIALS AND METHODS: THE MODELS

Static forces in coupled fingers, a general expression

The static equilibrium equations of a two finger system with some muscles anatomically interconnected are written in a general form. The equations of the independent fingers D^i and D^j with external load F_K^i , F_K^j can be generally expressed as (for symbols, see notations):

$$\begin{aligned} R_M^i \cdot F_{MT}^i &= R_K^i \cdot F_K^i \\ R_M^j \cdot F_{MT}^j &= R_K^j \cdot F_K^j \end{aligned} \quad (1)$$

Motors M_t^i , M_t^j can be anatomically interconnected by co-activations c_t^{ij} and c_t^{ji} , or by passive connections with a stiffness k_t (Leijnse, 1996). For a connected motor pair M_t^i , M_t^j it holds that (fig.1):

$$\begin{bmatrix} F_{TM}^i \\ F_{TM}^j \end{bmatrix} = \begin{bmatrix} 1-c_t^{ij} & c_t^{ji} \\ c_t^{ij} & 1-c_t^{ji} \end{bmatrix} \cdot \begin{bmatrix} F_{M_t}^i \\ F_{M_t}^j \end{bmatrix} + \begin{bmatrix} -F_{ct} \\ F_{ct} \end{bmatrix} \quad (2)$$

These equations give the end tendon forces F_{TM} as a function of the motor forces F_{M_t} , co-activations c_t^{ij} and c_t^{ji} , and the total force F_{ct} in the connections. F_{ct} is given by:

Anatomical factors predisposing to focal dystonia

$$F_{cl} = \int k_i \cdot \delta_{sign\{\Delta L_{M_P}^j - L_o\}} \cdot d\Delta L_{M_P}^j \quad (3)$$

in which the stretching of the connections is a function of the relative finger positions:

$$\Delta L_{M_P}^j = \int \sum_k r_{M_k}^i \cdot d\theta_k^i - \int \sum_k r_{M_k}^j \cdot d\theta_k^j - (\Delta \lambda_{TM}^j, -\Delta \lambda_{TM}^i) \quad (4)$$

Substitution of expression (2) in expression (1) gives the coupled finger system:

$$\begin{bmatrix} R_M^i & 0 \\ 0 & R_M^j \end{bmatrix} \cdot C \cdot \begin{bmatrix} F_M^i \\ F_M^j \end{bmatrix} = \begin{bmatrix} R_K^i & 0 \\ 0 & R_K^j \end{bmatrix} \cdot \begin{bmatrix} F_K^i \\ F_K^j \end{bmatrix} - \begin{bmatrix} R_M^i & 0 \\ 0 & R_M^j \end{bmatrix} \cdot \begin{bmatrix} -F_c \\ F_c \end{bmatrix} \quad (5)$$

with C an appropriately dimensioned co-activation coupling matrix.

Definition: agonists and antagonists of a motor M

The motor forces in an unloaded finger D^i can be expressed as a function of n independent motor forces, with n the number of indeterminates. For each independent motor M, motors exist of which the forces *increase* with the independent motor force, the other independent motor forces being constant. These are called the *antagonists* of M. Motors which decrease are called agonists of M.

The connected FPL-FP² finger system with an additional constraint on MCP¹ mobility

The text example is a connection between the FPL and the FP² (fig.2). The connection is taut when index and thumb are extended, and runs from proximally the FPL to distal the FP² (fig.2 and fig.3). To investigate how superimposed constraints can reinforce each other, a second constraint is further added. This is a limitation of the flexion range of the MCP¹ joint of the thumb to $0 \leq \theta_{MCP^1} \leq 10^\circ$.

Quantification of physiological muscle load

Physiological muscle load is commonly quantified by muscle stress σ_M , which is the ratio of force over physiological cross-sectional area (PCA). Similarly, a kinematic quantity can be envisaged, further called the *physiological contraction speed* ν_M , as the ratio of contraction speed over resting fibre length (ν_M/L_{RM}). The product $\sigma_M \cdot \nu_M$ gives the *power per muscle volume*, which will further quantify "dynamic physiological muscle load". To summarise:

$$\sigma_M = \frac{F_M}{PCA_M} \quad (1)$$

$$\nu_M = -\frac{1}{L_{RM}} \cdot \frac{dL_M}{dt} \quad (2) \quad (6)$$

$$\frac{P_M}{V_M} = \sigma_M \cdot \nu_M \quad (3)$$

The physiological properties of a muscle are commonly described by: (i) the maximal force/fibre length relationship, and (ii) the maximal force/contraction speed relationship. From the latter follows that maximal muscle power $P_{Mmax} = F_{Mmax} \cdot \nu_M$ increases with $0 \leq \nu_M \leq \nu_{M0}$ from zero to a maximum ν_{M0} , and for $\nu_M > \nu_{M0}$ it decreases to zero. Substitution of ν_M by ν_M and F_M by σ_M should make this relationship identical for all muscles (barring effects of fast or slow twitch fibre types, muscle architecture, etc.). It follows that in slowly contracting (isometric) muscles physiological muscle load can be quantified by muscle stress (σ_M), while in fastly contracting muscles ($\nu_M > \nu_{M0}$) it can be quantified by power expenditure per volume. Of muscles with equal power per volume and $\nu_M > \nu_{M0}$, those with greater speeds are physiologically more stressed, because the ratio of their power expenditure over their physiological maximal power (P_M/P_{Mmax}) is greater, since P_{Mmax} declines with increasing speed.

MODEL RESULTS

Results generally holding for interconnected finger systems (interpretation of expression (5))

i) $F_K = F_c = 0$: unloaded fingers within the slack range of the connections

With unloaded fingers and slack connections, the motor forces are interdigitally coupled only by co-activation. Since no external conditions must be satisfied, the motor forces can be arbitrarily small, and the fingers can assume all positions in a relaxed way. In fast unloaded movements, however, the inertia and friction forces function as an external load, and will increase the magnitude of forces and co-activation forces. This leads to the next case.

ii) $F_K^i = F_c = 0$; $F_K^j > 0$: D^i loaded; D^j unloaded; connection slack

The load F_K^j requires a minimum force in the muscles of D^j . The equilibrium forces in D^i depend by the co-activation forces $c_i^j \cdot F_{N_i}^j$ on the external load of D^j . The force increases in D^i are with the *antagonists* of the co-actively pulled tendons of D^j . Therefore, *with large co-activations, the unloaded finger D^i will be tensed by the co-actively pulled tendons and their antagonists*. The finger D^i cannot be relaxed, which may hamper controlled movement. With all $c_i^j = 0$, the tension in D^i does not affect D^j . However, with $c_i^j > 0$, the forces $c_i^j \cdot F_{N_i}^j$ are retransferred from D^i to D^j , where they may cause motor forces in excess to those required to balance the load. In that case both fingers "stiffen" with the load F_K^j . Clearly, with large co-activations, motor forces can be much greater than in the unconnected system.

iii) $F_K^l = F_K^d = 0$; $F_c > 0$: unloaded fingers with stretched connections

A connection is stretched between its proximal and distal attachments. Proximally, the pull is from the proximally connected muscle. Distally, the pull derives from the antagonists of the distally connected tendon. Therefore, F_c increases the load in the proximal motor in one finger, and in the antagonists of the connected tendon in the other finger. The latter finger is then tensed by the end tendon force F_c and the forces in its antagonists. With $c_i^j, c_i^k > 0$, the motor forces causing F_c may cause additional reciprocal "stiffening" of the digits. These effects can be considerable, since F_c can be as large as the strength of the motors stretching the connections allows.

The motor forces in loaded fingers with stretched connections follow from the above cases.

Some pianistic movements in the FPL-FP² connected system

In fig.2, the connection is stretched between proximally the FPL and distally the FP² tendon, which is tautened by its antagonists: ED², IO², and LU². When with extended index and thumb the FP² contracts in advance of the FPL, the connection is slack and inactive as a constraint until tautened in the opposite direction. With sufficiently long connection, most normal hand movements are within this slack range: making a fist, pinch grips, and also many piano playing movements. When the FPL contracts in advance of FP², i.e when the thumb flexes *with an active FPL* in advance to the index, the connection is tautened and will pull the index in conjoint flexion. Such thumb flexion is basic to the playing of scales and harpeggios, in which the thumb must play keys ulnar to the index, medius or fourth finger. In fig.4.a the end positions of conjoined index flexion (1* and 2*) are calculated for an inextensible connection, with the thumb flexing from extension to: $(\Delta\theta_1^1, \Delta\theta_2^1, \Delta\theta_3^1) = (10, 55, 35)$ and $(10, 10, 70)$ degrees. The first case simulates thumb flexion with an unconstrained MCP¹ joint, the second with a 10° MCP¹ flexion limitation. The index positions follow from: (i) equal FP² and FPL displacements ($\Delta L_{FP} = \Delta L_{FPL}$), and (ii) maximization of the lifting height of the index tip, with MCP² extension limited to -10° (Leijnse et al., 1993). Fig.4.b presents the joint rotations and motor displacements when from position 1* in fig.4.a the index strikes a key with isometric FP² (Leijnse et al., 1993).

Muscle force and stress in the finger with a deep flexor proximally pulled by a connection

Assume that the FPL pulls the FP² of the unloaded index by a force F_c . F_c then causes a proportional increase of the unloaded equilibrium forces in the antagonists of FP². These forces are functions of the PIP position; in fig.5 they are given for the extended (a) and the completely flexed PIP (b), while for intermediate PIP positions they can be estimated by interpolation. Independent forces are FS, FP and LU; assumed is that $F_{FPd} = F_c = F_{FPL} = 1$, while the FS force is taken zero where possible. X is the lumbrical force over the deep flexor force distal to the attachment of the connection ($X = F_{LU} / F_{FPd}$). The PCA are given in table.2. The solution with minimal maximal muscle stress is indicated by X_m (Leijnse^a, 1996). At X_0 the radial interosseus force would become zero; with $X > X_0$, the superficial flexor must be non-zero ($F_s > 0$), or the radial interosseus force becomes negative ($F_r < 0$). Pianistically, fig.5 gives the forces and stresses when (i) the extended index opposes the flexion pull $F_{FPd} = F_c$ (5.a,c), and (ii) when the index

extends from the positions 1^* or 2^* in fig.4.a against the flexor force F_c (5.b,d). The figs.5 show following. (i) At the minimax force X_m , the extensor and lumbrical stress is at least three times that of the other motors, including the interossei, both with extended and flexed PIP. This holds even if the cross sections of the interossei in the model would be overestimated. The interossei have different insertions, with different moment arms and cross-sectional areas (Chao et al., 1989). In the simplified model of Leijnse^a (1996) all insertions are in the extensor assembly. (ii) With a flexed PIP the ED, LU, and interossei are more stressed than with extended PIP.

Physiological displacements and work per volume in typical movements

In fig.6 the work per volume (W/V) in some unloaded finger movements is estimated as the product of the static stresses of fig.5 and the physiological displacements $\Delta L_M/L_{RM}$ of table.2, calculated from the model of Leijnse and Kalker (1995). Fig.6.a gives the W/V with fixed MCP and the PIP approaching full extension ($d\Theta_1=0$, $d\Theta_2<0$, $\Theta_2\approx 0^\circ$), and fig.6.b with extension of the flexed PIP ($d\Theta_1=0$, $d\Theta_2<0$, $\Theta_2=90^\circ$). When the PIP extends to $\Theta_2=0^\circ$, the W/V in the ulnar interosseus is half that of the extensor; when the PIP extends from $\Theta_2=90^\circ$, it is about equal. The W/V in the lumbrical, which mathematically may freely choose its force, can be much larger than in any of the other motors. Fig.6.c applies to MCP flexion with extended PIP ($d\Theta_1>0$, $d\Theta_2=0$, $\Theta_2=0$). The (positive) W/V in the ulnar interosseus is a third of the extensor (negative), and in the lumbrical it is far less than in the extensor, because of its small displacement (Leijnse and Kalker, 1995). With simultaneous MCP and PIP/DIP rotations, for each muscle its work at each joint can be mathematically added. With $\text{sign}(d\Theta_1)=\text{sign}(d\Theta_2)$, it holds for the extrinsics (FP, FS, ED) that: $\text{sign}(W_1)=\text{sign}(W_2)$, and for the interossei: $\text{sign}(W_1)=-\text{sign}(W_2)$. Therefore, for equal directions of MCP and PIP-DIP rotations, the work per unit force $((W_1+W_2)/F)$ can be large for the extrinsics and small for the interossei, and vice versa for MCP rotations opposite to the PIP/DIP rotations. The following examples illustrate this. Fig.6.d gives the W/V in the key stroke of fig.4.b. The positive W/V in the ulnar interosseus is about 1.5 times the negative W/V of the extensor. In fig.6.e the W/V is given with equal and opposite MCP-PIP rotations ($d\Theta_1=-d\Theta_2>0$) with a flexed PIP joint ($\Theta_2\approx 90^\circ$). The positive W/V in the ulnar interosseus is more than twice the negative W/V of the extensor. However, in both movements the W/V in the lumbrical may be far greater.

DISCUSSION

A summary of the general effects of anatomical interconnections on muscle load

- i) Anatomical interdependencies couple two independent fingers into a single system (expression (5)). This increases the complexity of control. E.g., even in single finger movements the motor forces in both fingers must be simultaneously controlled.
- ii) In the connected finger system the relationship between external and muscle force is fundamentally disturbed. Even in unloaded fingers muscles can be greatly stressed. These excess forces result from muscles mutually loading each other, and cannot be deduced from external work or load. Therefore, with different connections hand muscles can be very differently loaded

Anatomical factors predisposing to focal dystonia

in equal tasks, while this is not apparent from superficial observation.

iii) When intertendinous connections are slack, the fingers function unconstrained. However, co-activations are independent of the finger position (Leijnse^b, 1996).

iv) Interdigital force transfers may increase the motor forces beyond the forces required in "relaxed" playing. This "tension" may disturb proper finger control in high dexterity tasks.

Critical muscle loading with interconnected deep flexors

Static muscle stress with stretched connections

With the static stretching of a deep flexor connection the greatest stress occurs in the extensor and lumbrical of the extending finger, while these stresses are greatest with a flexed PIP (fig.5).

Dynamic physiological muscle load with slack connections

Forces in connections can be avoided by limiting the relative displacements of the connected tendons to their slack range. In many playing movements, in particular with oppositely moving fingers, small *relative* tendon displacements also result in small *absolute* displacements (Leijnse et al., 1993). Movements with small absolute displacements of the extrinsics, such as the deep flexors, are characterised by opposite MCP and PIP rotations: $d\theta_1 = -\phi \cdot d\theta_2$, with ϕ a function of the length of the connections and the moment arms of the connected tendon (Leijnse et al., 1992). In these movements the interossei have large physiological displacements, and therefore a large W/V even with small muscle stress.

The driving force of the key stroke with isometric deep flexor - example 1

The fig.4.b gives a key stroke from the initial position of fig.4.a.1*. The connection is assumed inextensible and the FPL isometric, leading to the condition $dL_{FP} = dL_{FPL} = 0$. This condition also determines the kinematics of the *loaded phase* of the key stroke, when the finger pushes down the key. This loaded phase is powered by the FS and the interossei, i.e. the only motors with (i) a positive displacement, and (ii) sufficient strength (PCA, table 2). However, the physiological displacement of the interossei is about five times or more than that of the FS (table 2), while in the loaded phase the force in each interosseus is about half that in the FS (fig.8). Therefore, the W/V in the interossei is more than 2.5 times that of the FS. The effective physiological load difference is even greater because of the force/contraction speed relationship, as the interossei with their greater contraction speed will reach the physiological power limit well before the FS. Therefore, the key stroke of fig.4.b will be weak in the fast execution and limited in maximal speed, because the interossei become insufficient. This shows that avoiding the stretching connections (i) does not necessarily reduce overall muscle load, but may merely shift it to other motors, and (ii) may result in playing movements "of lesser quality".

Dynamic muscle stress with stretched connections - example 2

Assume that the index must strike a "black" key just out of reach by the movement of fig.4.b, without moving the hand. The FPL is isometric, the connection extensible. Then the PIP must extend a bit further than in fig.4.b, so that the movement approaches the movement with $d\theta_1 = -$

$d\Theta_2$ of fig.6.e. In this movement the middle phalanx remains parallel to itself, which allows its easy extrapolation from fig.4.b. The FS displacement is then very small, and the deep flexor elongates because the connection is stretched (table 2). The lumbrical and interossei then are the only power sources in the free phase with displacements even larger than in fig.4.b, while the interosseus is the only real power source in the loaded phase. The W/V in LU, R, U in the free phase is more than twice that in the extensor (negative); in the interossei because of large physiological displacements; in the lumbrical because of high stress. High stress also exists in the extensor, but its physiological displacement is small. To conclude, in this movement the intrinsics are particularly heavily loaded.

Disconnecting movements: movements in which the connected flexors are not used at all

The constraints caused by anatomical interconnections can be completely avoided by *not using* the proximally connected motors (Leijnse et al., 1993). This is feasible only when other motors can substitute their function. Deep flexor substitutes are the superficial flexors; FPL substitutes are the short thumb flexors (fig.3.b). A realistic example is the non-use of strongly connected deep flexors in the piano-playing, which can most frequently be observed in the fourth finger. The relaxed DIP joint is then stabilised by its volar plate, while the superficial flexor controls the PIP. This possibility of finger use at the piano has been reported, although not in relation with deep flexor connections (Tubiana, 1993).

Complicating factors in the use of disconnecting movements - example 3

Consider the thumb-index system with both an inextensible connection and a flexion limitation to $0 \leq \Theta_{MCP^1} \leq 10^\circ$. This is not entirely unrealistic, as the mobility of the MCP¹ is highly variable. Wagner (1988) measured in 450 pianists' hands ranges varying from 26° to 89°, but smaller ranges are occasionally found (e.g. 15°, own observation). The keyboard outlined in fig.4.a shows the ulnar reach of a normally sized thumb with and without constraints. An unconstrained thumb reaches the width of three keys (position 2). With inactive FPL (disconnecting thumb flexion, fig.3.b) and MCP¹ flexion of 55°, the reach is about the same (dotted line 3). Positions 1 and 4 are with 10° MCP¹ flexion range and active and inactive FPL, resp. Clearly, thumb flexion with inactive FPL and MCP flexion constraint is not functional, as only one ulnar key is reached. Therefore, *the MCP¹ flexion limitation necessitates the active use of the FPL in playing ulnar keys with the thumb*, and excludes the disconnecting solution of fig.3.b. However, an active FPL unavoidably results in conjoined flexions of the index. Fig.4.a shows that less severe MCP¹ flexion limitations (20..25°) may still produce similar effect.

Compensatory movements - postural stress

Compensatory movements are of large body segments in tasks which without constraints could be realised by smaller segments, e.g. the fingers themselves. The large-segmental movements must be executed as fast as the small-segmental ones, which may prove impossible with high playing speeds. They increase muscle load twofold: (i) greater inertia forces, (ii) by increased demand for body frame stability. While inertia forces increase energy expenditure in muscles of larger

Anatomical factors predisposing to focal dystonia

segments, the stability requires increased "stiffness" of arm, shoulder, and trunk muscles. Intertendinous connections or other constraints in the hand are possible causes of compensatory movements, and in this way may even affect posture. Four examples are given.

Example 4. Assume that the index, with taut, inextensible connection and isometric FPL ($dL_{FP}^2 = dL_{FPL} = 0$), must strike a "black" key out of reach by the movement of fig.4.b. Without relaxing the FPL, the only way is to shift the entire hand towards the key, and then strike it by the movement of fig.4.b. Clearly, a shoulder-elbow rotation must compensate for an impeded finger movement.

Example 5. Consider the *unconnected* thumb-index system with a 10° MCP^I flexion range, and the following task (fig.7.a): (i) strike with the thumb a key two keys ulnar to the index, and (ii) subsequently strike with the index the key ulnar to the thumb. At all time one of the fingertips must remain at the keyboard, as in the "legato playing". With *unconstrained* MCP^I (fig.7.a), this sequence can be played by simply translating the hand ulnarwards over the distance of three keys, which merely requires a small shoulder rotation. In contrast, with *constrained* MCP^I two large compensatory hand rotations in the plane of the keyboard are required. Firstly, a radial hand abduction about the index tip to bring the thumb tip to the ulnar key (fig.7.b.B); secondly, an opposite rotation about the tip of the thumb to bring the index tip to the key ulnar to the thumb, while simultaneous rotations in the thumb joints and wrist reposition the hand. These hand rotations also require two opposite shoulder rotations, far greater than in fig.7.a, and some elbow extension/flexion. As an aside remark, in both cases the hand displaces proximally by the distance "h" (figs.7), so that with sequential execution of the task it will drop off the key board. This can be avoided by keeping the hand at all time somewhat radially abducted, so that the thumb strikes the key at the same level.

Example 6 Consider example (ii), with both 10° MCP^I flexion range and *inextensible FPL-FP² connection*. With the MCP^I flexion constraint, thumb flexion with inactive FPL cannot perform the task, since the thumb cannot reach any key ulnar to the index (example 3). However, with active FPL, the unavoidable conjoined index flexion decreases the distance "d" between the thumb and index tips (fig.7.c). This in its turn increases the compensatory hand rotations of fig.7.b. This illustrates how superimposed constraints can reinforce each other's effect.

Example 7. In the above it is shown that the key-stroke movement of fig.4.b will be slow and weak. Therefore, in real playing such a key-stroke may have to be reinforced by e.g. small simultaneous wrist flexion. This is dynamic compensation, in contrast to the previous examples where compensatory movements were required for kinematic reasons.

Viscosity constraints

For theoretical interest, an intradigital connection is mentioned, called a "viscosity constraint". It is modelled as a tendon with a dot of adhesions which impair frictionless gliding, but which are

too loose to limit displacements. Clinically, this may result from post-operative adhesions, tenosynovitis, etc. The excess load is with the muscle of the afflicted tendon in proximal displacements, and with its antagonists in distal displacements. The power loss is:

$$P_{\mu} = F_{\mu} \cdot v_{TM} = \mu \cdot v_{TM}^2 \quad (7)$$

with F_{μ} the viscous force. P_{μ} increases with speed, while maximal muscle power decreases. The effect of the connection therefore is to limit the speed of the tendon, which implies either slowing down the movement, or reducing the displacement. In fast playing, movement speed cannot be tampered with, meaning that eventually the displacement itself of the tendon will be minimized by fatigue. Therefore, while in slow movements viscosity constraints may not be restrictive, in fast movements they may function effectively as a tenodesis.

Clinical applications of the model results

The nature of the "flexion cramping" in focal dystonias

Focal dystonia is an affliction in which with certain playing movements (unloaded) fingers unavoidably flex or become uncontrollable. The flexion is predominantly in the PIP-DIP joints, but may also involve the MCP, and has been referred to as a "cramping" of the flexors (Hochberg et al., 1990). By present hypothesis, interconnective forces may be a causal factor. It is shown above that connections may cause muscle stress in multiple ways. However, with deep flexor connections the major stress invariably is in the connected flexors' antagonists: lumbrical, extensor, and interossei. Therefore, when connective stress causes dysfunction, it will be in these motors. The "flexion cramp" is then explained by their acquired inability to oppose the flexor forces. Other factors must also be considered. (i) Flexion of fingers may relax stretched connections between flexors, and may even reduce the effective co-activation forces (auto-coactivation, Leijnse, 1996). (ii) Joints in flexion end-positions are stable under the flexor forces without extensor forces. Therefore, the flexion tendency may involve a subconscious attempt to obtain a finger position which minimizes the activity of the failing extensors. Full flexing of the PIP-DIP joints would relieve the lumbrical and interossei of their PIP-DIP extension task, while additional flexing of the MCP would also relieve the extensor. Our personal experience is that with a focal dystonia a compulsory flexing unloaded finger can usually be balanced by a "normal" external extension force at the fingertip, indicating that the "cramp" does not result from a flexor "spasm" in the real sense. (iii) Intertendinous connections between other motors (FS, ED, LU) or other constraints may also cause excess muscle loading, and may therefore provoke similar symptoms. This leads to the following general concept.

A general view of overuse in musicians: incompatible constraints

Hands at instruments operate in highly constrained environments. Finger positions and even trajectories may be kinematically predescribed by hand size and key outline (flute, oboe, clarinet, saxophone...). Some instruments require the active use of muscles prone to intertendinous connections. E.g. active DIP control and therefore deep flexor use is required with the violin (left

Anatomical factors predisposing to focal dystonia

hand), the classical guitar (left and right hand), the harp. Limitations on tendon displacements or joint mobility, as studied above, constitute additional constraints. By hypothesis, an overuse situation arises when these combined constraints exclude movements which satisfy the playing requirements with sufficiently low energy expenditure. This situation results from an unsuccessful *process*, in which the hand seeks to minimize energy expenditure by making full use of the indeterminates in motor forces and the kinematic freedom allowed by the constraints. Physiological properties clearly play a role, as stress leads to problems only when limits of endurance are exceeded. Therefore, trigger events such as a few extra hours of practice, or a new piano with heavier key action should not be seen as absolute causes, but as the final blow to a compromised system. By this hypothesis, one clear strategy of treatment is the elimination of sufficient constraints to allow less stressful movements. This may be done by instrumental redesign, changes in hand use, but also by clearance of intertendinous connections.

Treatment of focal dystonia in view of the model results

The use of movements in which the connections are less stretched.

These are movements in the slack range of connections, and disconnecting movements. Example 2 shows that also in movements within the slack range high physiological muscle load can occur and that they may be inefficient, while example 4 shows that disconnecting movements may be compromised by additional constraints. Disconnecting movements in instruments requiring the explicit use of the connected muscles are by definition excluded. By present hypothesis, success crucially depends on the possibility to adjust the kinematic playing demands to the slack range of the connections. This may be achieved by a different technique, or changes to the instrument (Markison, 1990). However, intertendinous connections may simultaneously exist in different motors (e.g. FS, FP, ED), while the trajectories allowed by their respective slack ranges may not overlap. Then no safe playing movements exist at all, indiscriminate of instrumental geometry.

Surgical removal of the connections

Ideally, surgical clearance of passive connections results in $F_c=0$ in expression (5), which may effectively reduce excess muscle stress. Moreover, the increased relative tendon displacements may allow a better instrumental technique. However, with large co-activations the benefit remains unclear; aspects are discussed in Leijnse^b (1996), and Leijnse and Bonte (1996).

Basic problems with posture correction in musicians

Therapy with focal dystonia often focusses on posture, involving slow motion playing movements with or without biofeedback (Tubiana, 1993). Some basic comments can be formulated.

(i) Bad posture may well induce muscle stress or affect performance. However, postural aberrations may result from compensatory movements to which constraints in the hand are causal. Then posture correction will not be successful on long term, as the cause for compensation remains. Moreover, suppression of compensatory movements may push the functional conflict back to the hand (where it originated), and aggravate focal complaints instead of cure them. This is corroborated by the fact that musicians more than once develop complaints after changing

Chapter IV

teachers and learning a new technique (Tubiana, 1993).

(ii) Slow motion exercise at the instrument does not guarantee a better fast execution. In the fast execution compensatory muscle forces due to inertia and stability requirements may unavoidably reach the level they had before therapy.

CONCLUSION

In this paper, it is shown that anatomical interconnections between tendons or muscles, or anatomical constraints on joint mobility may increase the load of specific muscles, and that therefore they may be causal to problems such as focal dystonia in the musician's hand. With connections between the deep flexors, as is the text example, increased muscle load occurs directly in extensor, lumbrical and interossei with stretched connections. However, even with unstretched connections physiological muscle load can be large, e.g. in the interossei which in certain key stroke movements become the main power source. Intertendinous connections, or constraints on joint mobility may necessitate compensatory movements, which increase the load of muscles of larger body segments. The general view presented is that overuse situations arise when the combination of instrumental playing demands and individual anatomic constraints mutually exclude functional movements with sustainable energy expenditure. Diagnosis then is the evaluation of these constraints, while treatment consists of the elimination of sufficient constraints to allow less stressful playing movements.

ACKNOWLEDGEMENTS

The author cordially thanks Dr.C.W. Spoor for the close reading of the manuscript, and Dr. G.J. Sonneveld, head of the special clinic for musicians, Prof. Dr.Ir. C.J. Snijders, Prof. Dr. J.C. van der Meulen, Prof. Emer. Dr. J.M.F. Landsmeer, Dr. S.E.R. Hovius, and Dr. J.E. Bonte for their valuable contributions.

REFERENCES

- Amadio, P.C., Rusotti, G.M. (1990) Evaluation and treatment of hand and wrist disorders in musicians. *Hand Clinics* 6, 405-416.
- Austin, G.J., Leslie, B.M., Ruby, L.K. (1989) Variations of the flexor digitorum superficialis of the small finger. *Am. J. Hand Surg.* 14, 262-267.
- Baker, D.S., Gaul, J.S., Jr, Williams, V.K. and Graves M. (1981) The little finger superficialis - clinical investigations and functional shortcomings. *Am. J. Hand Surg.* 6, 374-378.
- Blair, W.F., and Omer, G.E.Jr. (1981) Anomalous insertion of the flexor pollicis longus. *Am. J. Hand Surg.* 5, 548-549.
- Chao, E.Y.S., An, K.N., Cooney, W.P.(III), Linscheid, R.L. (1989) Biomechanics of the hand;- a basic research study. 42-44. World Scientific Publishing Co., Singapore.
- Cohen, L.G., Halett, M., Geller, B., Hochberg, F. (1989) Treatment of focal dystonias of the hand with botulinum injections. *J. Neurology, Neurosurgery, and Psychiatry* 52, 355-363.
- Fahrer, M. (1975) Considérations sur l'anatomie fonctionnelle du muscle fléchisseur commun profond des doigts. *Ann. Chir.* 25, 945-950.
- Fry^{*}, H.J.H. (1986) Overuse syndrome in musicians: prevention and management. *The Lancet*, sept 27, 728-731.

Anatomical factors predisposing to focal dystonia

- Fry^b, H.J.H. (1986) Overuse syndrome in musicians - 100 years ago;- an historical review. *The Medical J. of Australia* 145, 620-624.
- Hochberg, F.H., Harris, S.U., Blattert, T.R. (1990) Occupational hand cramps: professional disorders of motor control. *Hand Clinics* 6, 417-428.
- Kaplan, E.B. (1965) *Functional and surgical anatomy of the hand* (2nd Edn). 99-100 Pitman Medical Publishing, London.
- Leijnse, J.N.A.L., Bonte, J.E., Landsmeer, J.M.F., Kalker, J.J., van der Meulen, J.C., Snijders, C.J. (1992) Biomechanics of the finger with anatomical restrictions - the significance for the exercising hand of the musician. *J. Biomechanics* 25, 1253-1264.
- Leijnse, J.N.A.L., Snijders, C.J., Landsmeer, J.M.F., Bonte, J.E., van der Meulen, J.C., Sonneveld, G.J., Hovius, S.E.R. (1993), The hand of the musician - the biomechanics of the bidigital finger system with anatomical restrictions. *J. Biomechanics* 26, 1169-1179.
- Leijnse, J.N.A.L., and Kalker, J.J. (1995) A two dimensional model of the lumbrical in the human finger. *J. Biomechanics* 28, 237-239.
- Leijnse^a, J.N.A.L. (1996) Why the lumbrical should not be bigger - a force model of the lumbrical in the human finger. Accepted *J. Biomechanics*.
- Leijnse^b, J.N.A.L. (1996) Measuring anatomical interconnections in the deep flexors of the musician's hand: theoretical analysis, clinical examples. Submitted *J. Biomechanics*, aug, 1995.
- Leijnse^c, J.N.A.L. (1996) Measuring anatomical interconnections in the deep flexor of the musicians' hand - device and systematic measuring errors. Submitted *J. Biomechanics*, aug. 1995.
- Leijnse, J.N.A.L., and Bonte, J.E. (1996) Total clearance of intertendinous connections and surgical cleavage of the lumbrical origins in a musician's hand - a case study. To be submitted, 1995.
- Leijnse, J.N.A.L., Walbeehm, E.T., Sonneveld, G.J., Hovius S.E.R., (1995) Anatomical interconnections within the flexor digitorum profundus - the significance for the hand of the musician. Submitted to the *Anatomical Record*
- Linburg, R.M., and Comstock, B.E. (1979) Anomalous tendon slips from the flexor pollicis longus to the digitorum profundus. *Am. J. Hand Surg.* 4, 79-83.
- Lockwood A.H. (1989) Medical problems in musicians. *The New England J. Medicine* 320, 221-227.
- Malerich, M.M., Baird, R.A., McMaster, W., and Erickson, J.M. (1987) Permissible limits of flexor digitorum profundus tendon advancement - an anatomic study. *Am. J. Hand Surg.* 12, 30-33.
- Markison R.E. (1990) Treatment of musical hands: redesign of the interface. *Hand Clinics*, 6, 525-544.
- Rico Aguado, A., and del Pino Paredes, V. (1988) Flexor digitorum profundus common to thumb and index finger, associated with a post-traumatic distal adherence of both tendons. *J. Hand Surg.* 13-B, 72-74
- Spoor, C.W. (1983) Balancing a force on the fingertip of a two dimensional finger model without intrinsic muscles. *J. Biomechanics*, 16. 497-504.
- Stern, P.J. (1990) Tendinitis, overuse syndromes, and tendon injuries. *Hand Clinics* 6, 467-476.
- Tubiana, R. (1993) *The Hand*. 873-885, W.B. Saunders Company.
- Verdan, C. (1960) Syndrome of the quadriga. *Surg. Clin. North Amer.* 40, 425-426.
- von Schroeder, H.P., Botte, M.J., Gellman, H. (1990) Anatomy of the juncturae tendinum in the hand. *Am. J. Hand Surg* 15, 595-602.
- Wagner, CH. (1988) The pianist's hand: anthropometry and biomechanics. *Ergonomics* 31, 97-131.

Chapter IV

INDEX	MCP	r_{PI}	r_{SI}	r_{EI}	r_{UI}	r_{RI}	r_{LUI}	r_{AR}	r_{AU}	r_{AL}
		11	13	9	6	6	9	6	6	5
	PIP	r_{P2}	r_{S2}	r_{MB2}	r_{LB2}					
		10	9	5	*					
	DIP	r_{P3}	r_{LB3}							
		6	4							
THUMB		r_{PL1}	r_{PL2}	r_{PL3}						
		12	15	8						

Table 1. Moment arms of the finger motors. Notations and values in mm used to calculate the results. From: Spoor (1983). (*): function of PIP position (Leijnse and Kalker, 1995).

	E	LU	U	R	S	P	PL
PCA	1.7	0.2	2.8	2.2	4.2	4	5
L_R	6	6	1.3	1.7	7	6.7	4.6
Volume	10.2	1.2	3.64	3.74	29.4	26.8	23
$\Delta L_{MCP}(d\theta_1 > 0, d\theta_2 = 0)$	0.9	0.2	-0.6	-0.6	-1.3	-1.1	/
$\Delta L_{MCP}/L_R$	0.15	0.03	-0.46	-0.35	-0.19	-0.16	/
$\Delta L_{PIP}(d\theta_2 > 0, d\theta_1 = 0)$	0.5	1.5\2.25	0.5	0.5	-0.9	-1.0\1.75	/
$\Delta L_{PIP}/L_R$	0.08	0.25\0.37	0.39	0.29	-0.13	-0.15\0.26	/
$\Delta L(dL_P = 0, d\theta_1 > 0)$	0.49	-1.1	-0.82	-0.82	-0.63	0.0	/
$\Delta L/L_R(dL_P = 0)$	0.08	-0.16	-0.63	-0.48	-0.09	0.0	
$\Delta L/L_R(d\theta_1 = -d\theta_2 > 0)$	0.07	-0.22\0.34	-0.85	-0.64	-0.06	-0.015\0.1	/

Tabel 2. From top row to bottom: 1) Physiological Cross-sectional Area (PCA) (cm²). 2) Fibre resting length L_R (cm). 3) Muscle Volume (cm³) (PCA· L_R). 4) Motor displacements per radian MCP flexion in cm. These displacements are equal to the moment arms of table 1, except for the LU. 5) Physiological displacements ($\Delta L/L_R$) per radian MCP flexion. 6) Motor displacements per radian PIP flexion. For the lumbrical and deep flexor the systemic moment arms (r_{L2}^* , r_{P2}^*) increase with PIP flexion (Leijnse and Kalker, 1995). The two values represent the displacement per radian with the moment arm of the extended ($\theta_2 = 0$) and flexed PIP ($\theta_2 \approx 90^\circ$), resp. 7) Physiological displacements per radian PIP flexion. 8) Motor displacements in the key stroke with isometric deep flexor of fig.4.b. 9) Physiological displacements in the key stroke of fig.4.b. 10) Physiological displacements with MCP and PIP moving with equal and opposite rotations, per radian MCP flexion (row 5 minus row 7).

FIGURES

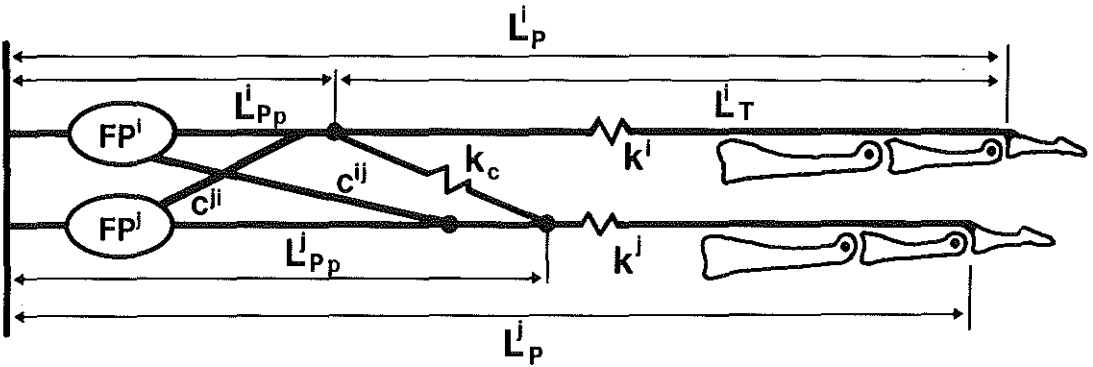


Figure 1 Model of interconnected motors. c^{ij} , c^{ji} : co-activations; k_c : stiffness of connection.

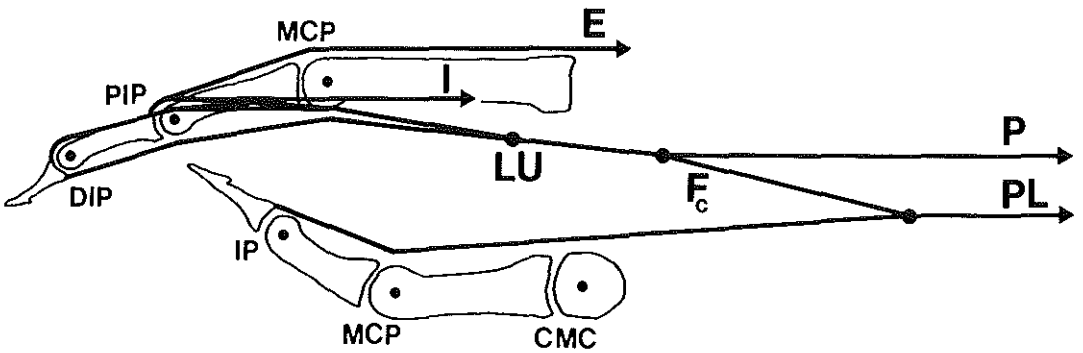


Figure 2 Thumb-index system with connected flexor pollicis longus (PL) and deep flexor (P) of the index. The superficial flexor has been omitted. F_c : force in connection.

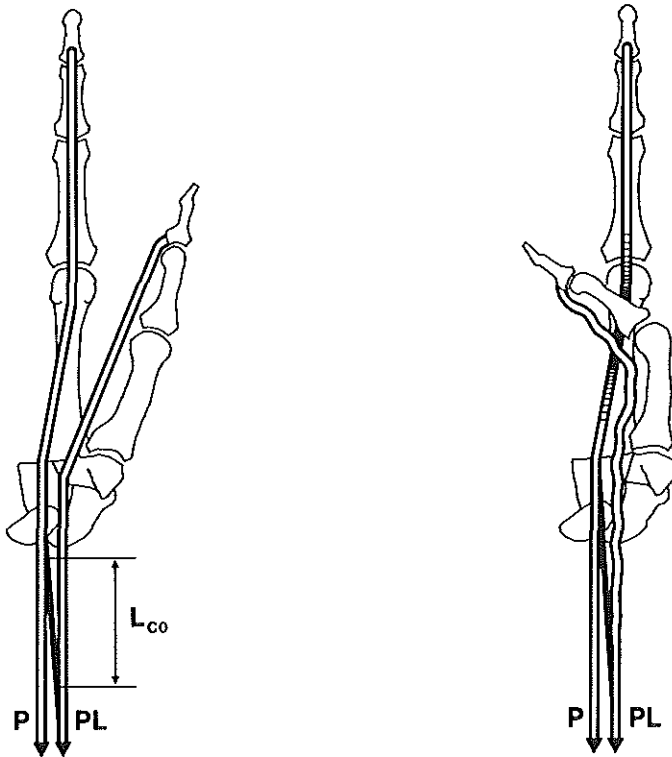


Figure 3 a,b Anatomic representation of the connection of fig. 2. a) The connection is taut with extended thumb and index. b) Disconnecting thumb flexion: inactive PL. The PL tendon distal to the attachment of the connection is slack, therefore the IP joint remains extended. The connection is only pulled by the tonus force of the PL.

Figure 4 a,b (comments with figs. of next page)

a) Conjoined movements of index with thumb, and inextensible connection. Index: upper finger, viewed sideways; positions numbered with asterisk (1*,2*). Thumb: lower finger, viewed from dorsal and positioned at a keyboard of three keys; positions numbered without asterisk (1 through 5). (1): Thumb with 10° flexion range of MCP^I and active PL. (1*): Conjoined flexion of index with thumb position 1. (2): Thumb with 55° flexion range of MCP^I. (2*): Conjoined flexion of index with thumb position 2. (3): Inactive PL and 55° MCP^I flexion (disconnecting movement). (4): Inactive PL and 10° MCP^I flexion (disconnecting movement). (5): Thumb in extension, the position in which the connection is taut with fully extended index. P,PL: Displacements 1' and 2' of the FPL and the FP² in proportion to finger size, with thumb flexion from position 5 to position 1 and 2, resp.

b) Index finger striking a piano key from the position of fig.4.a.1*, with isometric deep flexor. The bars are the motor displacements, in proportion to finger size. Motors at the left of the vertical contract: I,LU,S. The extensor (E) elongates. The deep flexor P is assumed proximally fixed by the inextensible connection to an isometric PL (see figs.2. and 3); its displacement is therefore zero. B: "black" key.

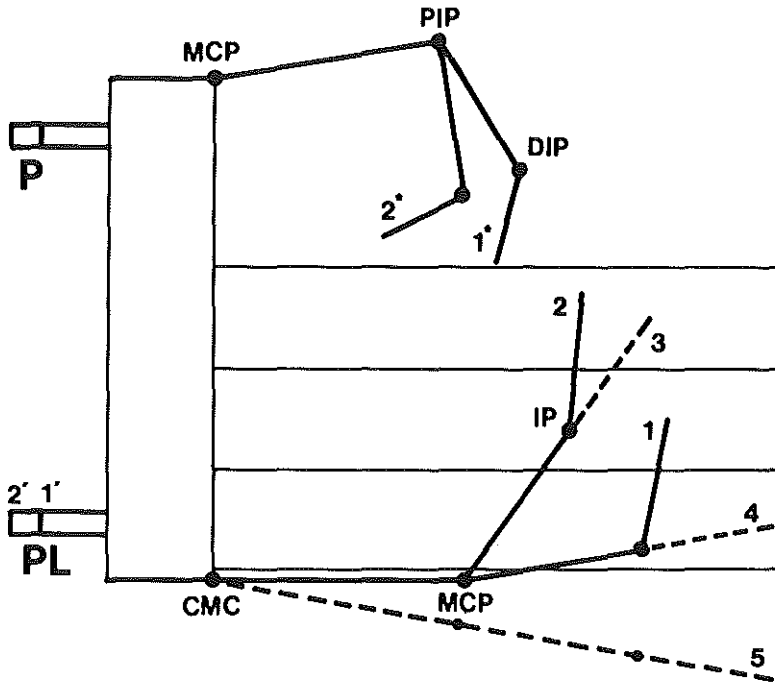


Figure 4 a

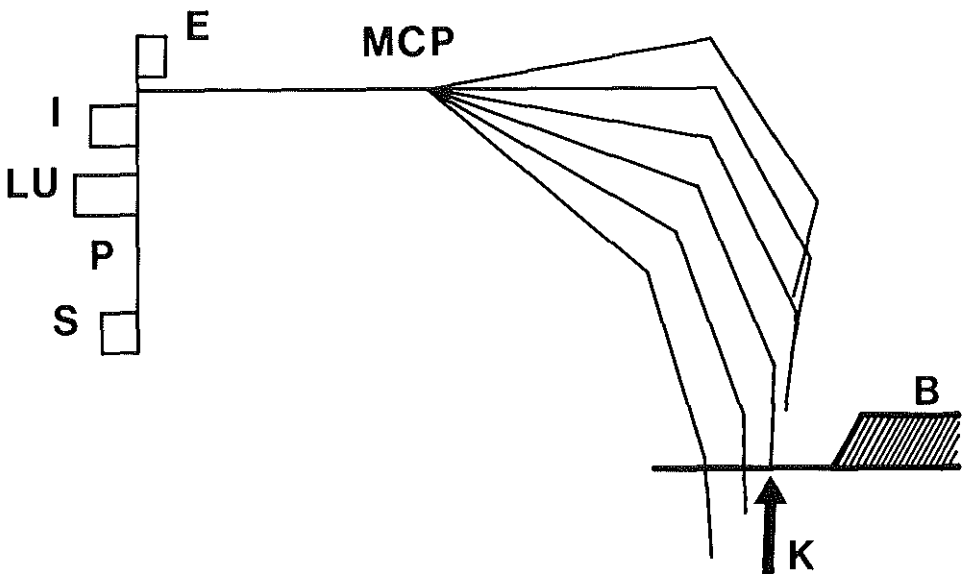


Figure 4 b

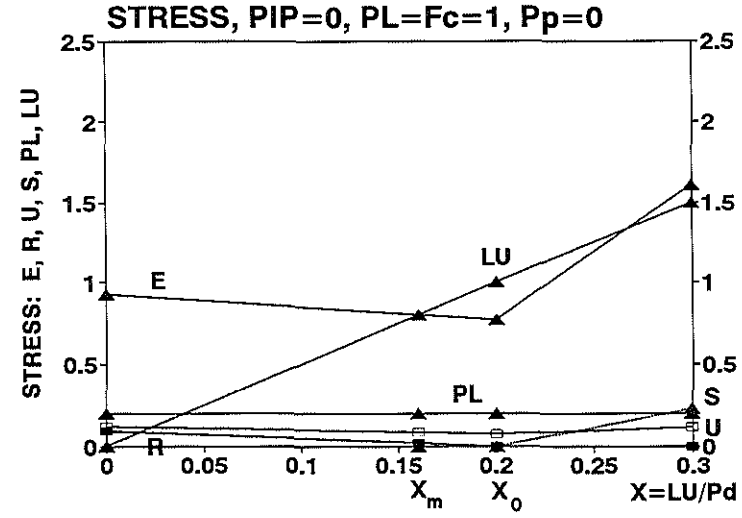
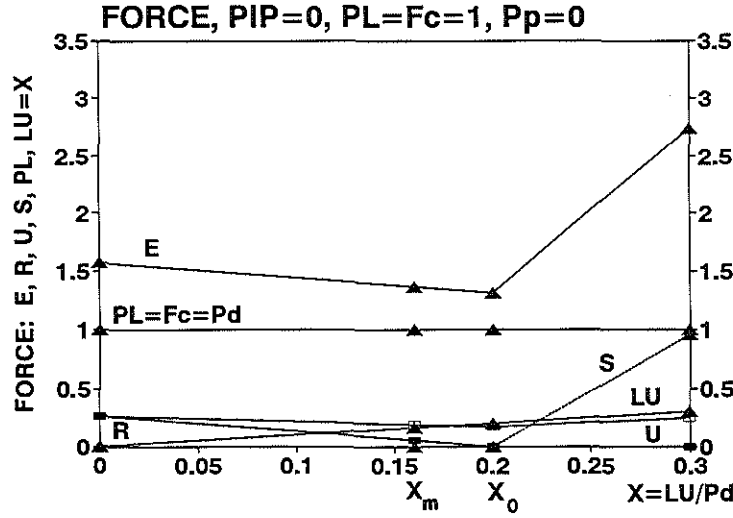
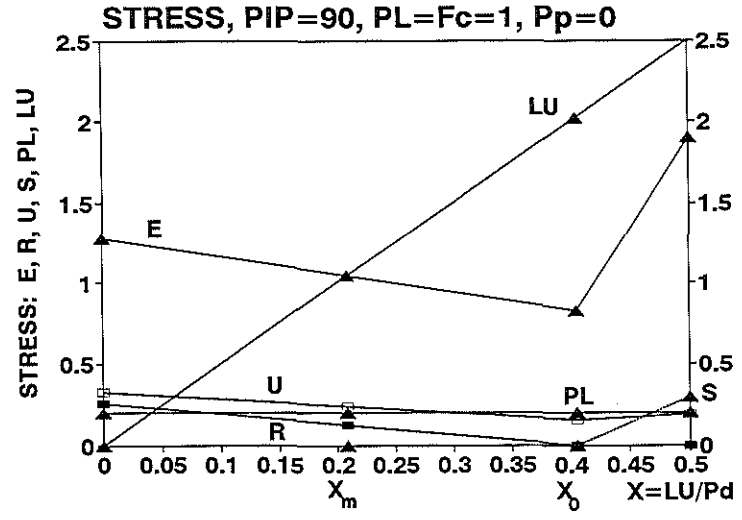
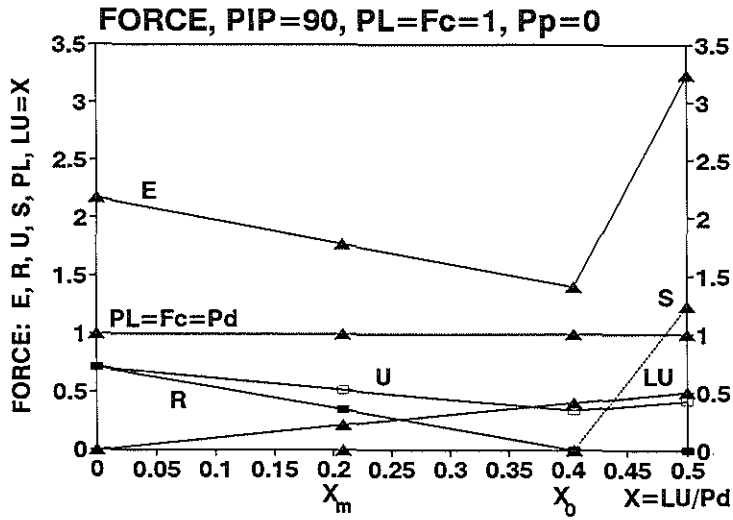


Figure 5 a,b

Figure 5 c,d

Anatomical factors predisposing to focal dystonia

Figure 5 (comments with figs. of previous page) Forces (N) and stresses (N/cm²) in the index motors and the FPL when the connection is stretched with force $F_c = F_{PL} = 1N$. F_c is the force in the deep flexor tendon of the index distal to the attachment of the connection, F_p itself is zero. X_M : lumbrical force with minimal maximal muscle stress. X_0 : the point at which the both F_s and the radial interosseus force F_R are zero. (a,c) and (b,d): Forces and stresses in extended finger, and with flexed PIP ($\Theta_2 = 90^\circ$), resp.

Figure 6 Work per volume (N.cm/cm³) in some movements of the frictionless and massless finger model. A force of 1N is assumed in the deep flexor tendon. a) W/V per radian PIP flexion; forces as with extended PIP. b) Same as (a); forces as with flexed PIP. c) W/V per radian MCP flexion; forces as with extended PIP. d) W/V in the unloaded key stroke of fig.4,b; forces as with flexed PIP. e) W/V per radian MCP flexion with equal and opposite rotations of MCP and PIP.

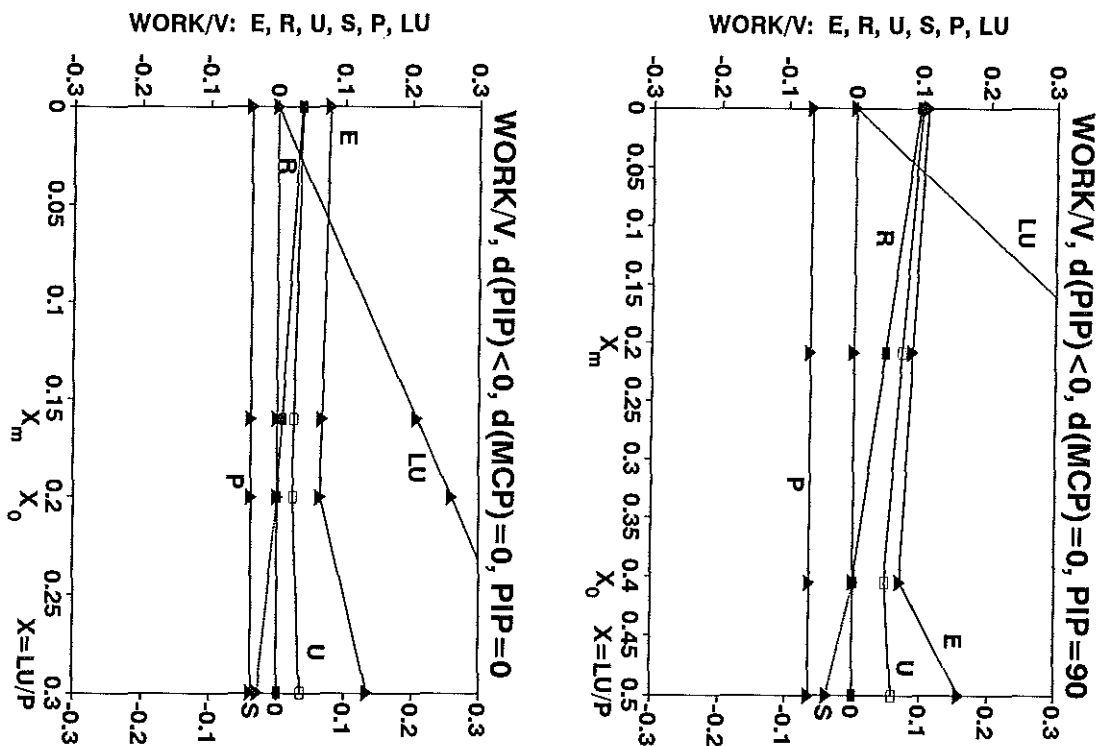


Figure 6 a,b

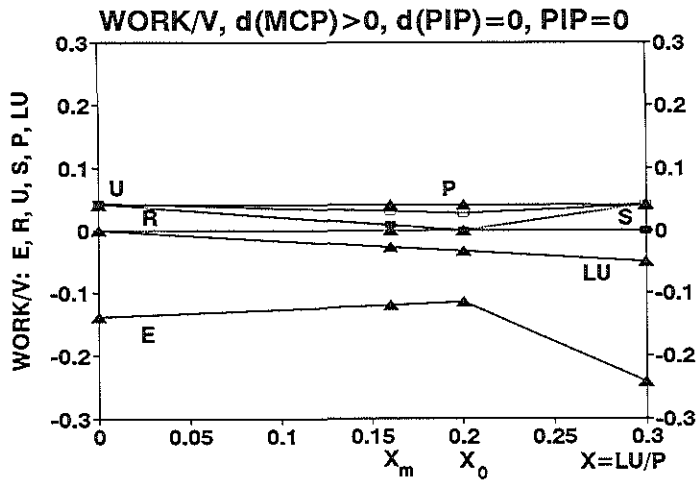
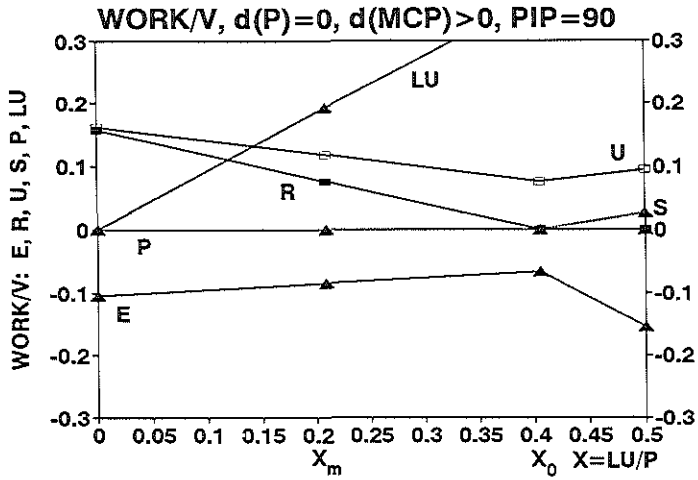


Figure 6 c,d

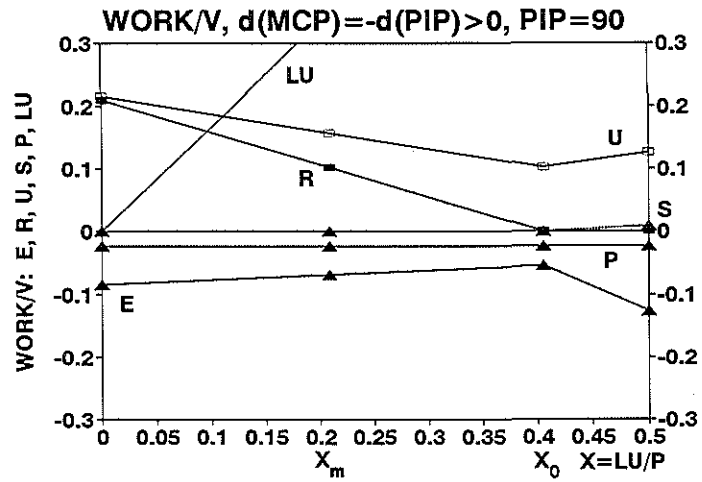


Figure 6 e

Anatomical factors predisposing to focal dystonia

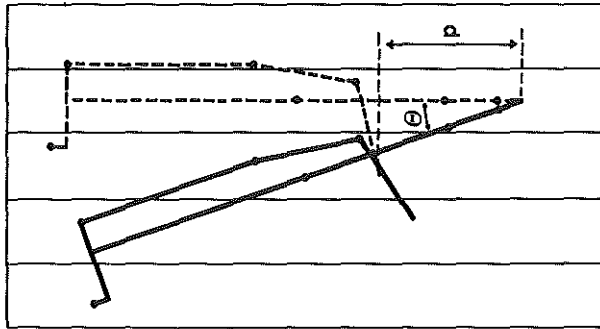


Figure 7 c

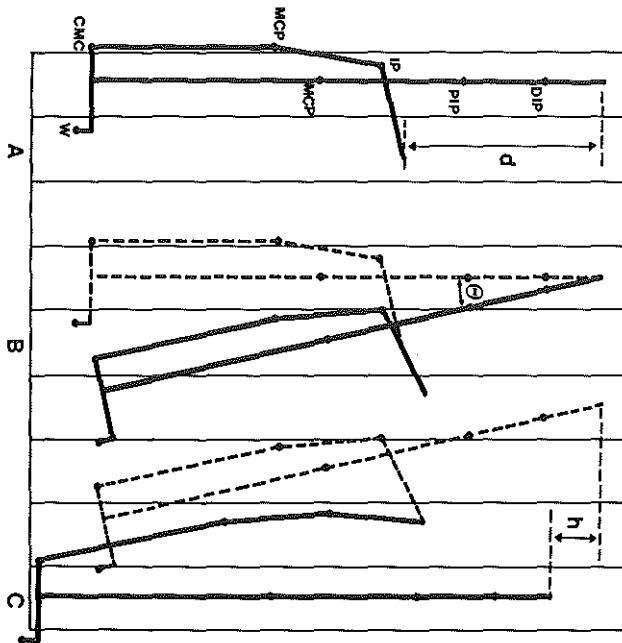


Figure 7 b

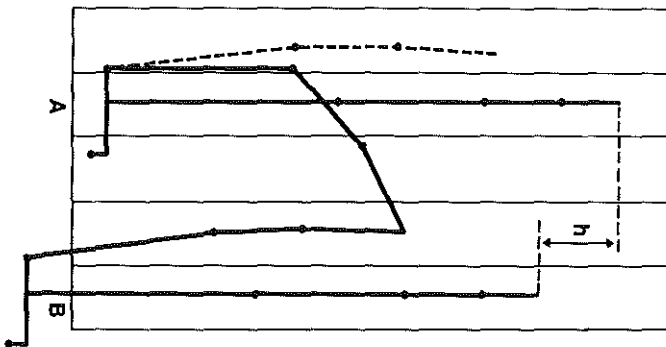


Figure 7 a

Chapter IV

Figure 7 (comments with figs. of previous page) Top view of thumb-index system at the keyboard. The following tasks are performed: (i) thumb strikes key two keys ulnar to index, while index tip remains on keyboard; (ii) index strikes key ulnar to thumb key, while thumb tip remains on keyboard.

a) Unconnected thumb-index system.

b) Compensatory rotations required with a 10° MCP¹ flexion range. A: Initial position. B: Thumb key stroke, hand rotates about index tip to full line position. C: index strikes key ulnar to thumb; hand returns to normal position.

c) Increased hand abduction Θ with decreased distance "d" between index tip and thumb tip. "h": proximal shift of hand in execution of the task.

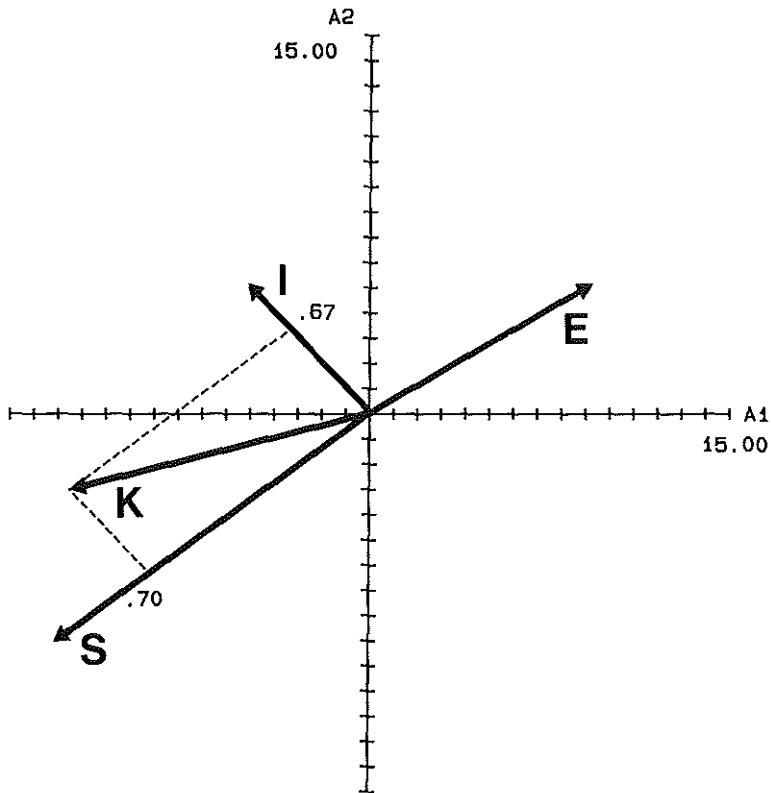


Figure 8 Forces in interosseus and superficial flexor in the loaded phase of the key stroke of fig. 4.b, as estimated from the moment arm vector diagram (Leijnse, 1995). Assumed is: $F_I = F_U + F_R$, $F_{LU} = 0$. The DIP moment arm of the load K in fig.4.b is zero, therefore F_P can be assumed zero. This reduces the finger to a bi-articular chain, to which the moment arm vector diagram applies. The motor forces are: $F_I = 0.67 \cdot \alpha \cdot K$; $F_S = 0.7 \cdot \alpha \cdot K$. α is the scalings factor required to fit the moment arm vector of the load K in the picture. These forces are the ratios of the length of the projection of the moment arm vector of the load K on the moment arm vectors I and S, over the length of the moment arm vectors I and S themselves. It follows that: $F_U \approx F_R \approx F_S/2$.

CHAPTER V

MODELS OF MUSCLES AND APONEUROSES

A generic model of a muscle group - application to the muscles of the forearm

J.N.A.L. Leijnse

Resubmitted to *Anatomical Record*, 1995

The morphology of holes in aponeuroses caused by perforating nerves or vessels at the medial epicondyle of the elbow

J.N.A.L. Leijnse

Resubmitted to *Anatomical Record*, 1995

A GENERIC MODEL OF A MUSCLE GROUP - APPLICATION TO THE MUSCLES OF THE FOREARM

J.N.A.L. Leijnse

Department of Plastic and Reconstructive Surgery, Erasmus University Rotterdam, The Netherlands. Resubmitted to Anatomical Record

ABSTRACT

A muscle model is presented to explain the morphology of muscles in muscle groups within the body. The model is constructed from the observation that the skeletal surfaces are insufficient to accommodate the origin of all muscles, and that therefore the skeletal surfaces must necessarily be enlarged by aponeuroses of muscular origin. These aponeuroses are flexible origins which can be folded into the various spaces available in the body. The folding of these origin areas determines the shape of the muscles and their end tendons; this relationship is closely investigated. Hereby it is, amongst others, shown that bipennateness of muscles results primordially from the degree of folding of the origin aponeuroses, and not because of functional reasons. The models are verified by dissection examples of the muscle groups at the elbow. An overview of the construction principles of these muscle groups is given, and specific end tendon shapes are interpreted with respect to the shape of the muscle compartments. The dissection results correlate strongly with the model results, which should find their application in a more conceptual way of anatomy teaching.

NOTATIONS

- BR : M. Brachioradialis
ED : M. Extensor Digitorum
ECRB : M. Extensor Carpi Radialis Brevis
ECRL : M. Extensor Carpi Radialis Longus
FCR : M. Flexor Carpi Radialis
FCU : M. Flexor Carpi Ulnaris
FDP : M. Flexor Digitorum Profundus
FDS : M. Flexor Digitorum Superficialis
FPL : M. Flexor Pollicis Longus
PL : M. Palmaris Longus
PT : M. Pronator Teres
 d_m, d_t : diameter of a muscle fibre and a tendon fibre
 s_m, s_t : cross-sectional area of a muscle fibre and tendon fibre
 l_f : muscle fibre length
 l_o, b_o : length, and width of the muscle origin
 O_T, S_T : circumference and cross-section of tendon T

INTRODUCTION

The study of the musculo-skeletal system allows for many approaches. Classic anatomy often identifies muscles as individual entities, which at the dissection table will conveniently be separated up to the point where muscle fibres originate from bone, which is called the origin. The view of muscles thus gained is of elongated structures suspended between a bony origin and insertion. Anatomical variations are merely described, and statistically enumerated. Another view is presented by the system modellers (e.g. Ettema and Huijing, 1990; van Leeuwen and Spoor, 1992, 1993). For them, muscles are highly structured units consisting of more or less parallel muscle fibres of more or less equal length, connecting an origin area or tendon plate of origin, with an end tendon plate. Generally, also a rather strict distinction is made between unipennate, bipennate, and fusiform muscle types. While the theoretical models demonstrate that the custom of identifying muscles in the dissection class as originating from bony origins is a gross reduction of reality, at the dissection table these ideal models are equally difficult to imagine. The aim of the present paper is to provide a synthesis of both approaches. This synthesis is obtained by considering the morphology as determined by elementary means and inescapable constraints. The means are: the muscle fibre as a basic contractile element; the skeleton as a supporting articular chain; and tendon fibres as ways to attach the two. The constraints are (i) that muscle fibres within a muscle must be at a minimum distance from each other, otherwise they will strangle each other; (ii) that the skeletal surface area is too small to provide the origin area for all muscle fibres of the body; and (iii) that muscles must be fittable within the confined volumes of the body parts. Further hold the geometric properties of muscle build as determined by optimal efficiency, which, in our simple approach, are summarised in the ideal unipennate model, in which all muscle fibres are strictly parallel and of equal length.

The fundamental observation from which the model is developed is the following. For proper locomotion, the body requires many strong muscles. Muscle strength is proportional to the number of muscle fibres in parallel, and since each fibre has a non-zero cross-section, strong muscles require large areas of origin. The total required area of origin for all muscles in the body utterly exceeds the available area on bone. The question then is how to attach all these muscles to the skeleton. To pinpoint the problem, consider the limit case in which the skeleton has no surface area at all, as a stick diagram. To this one-dimensional structure, no muscle whatsoever can be directly attached. Therefore, to accommodate a muscular system this stick diagram must be changed into a two-dimensional structure. This can be done by tendinous sheets of origin. These sheets can be attached to points or lines on bone, i.e. zero surface areas, while they themselves provide the required two-dimensional surfaces of muscular origin (fig.1). This holds generally. Fundamental to the construction of any body locomoted by parallel contractile elements of non-zero thickness and supported by a slim skeleton is the transformation of the limited skeletal surface areas into large surface areas by two-dimensional sheets of origin strong enough to support the three-dimensional muscle bulk, which again transforms into two-dimensional structures, the end tendon sheets, which insert into lines or points on bone. This implies that the construction of the body in its actual shape is rendered possible by the singular fact that a tendon fibre is much thinner for equal strength than a muscle fibre. While fig.1 shows that a great bulk of ideal muscle

models can be stacked to little skeletal surface, it shows as clearly that major geometric adaptations of these models are required to make them functional and "body-like". These geometric transformations are the object of this study. In a first part, these transformations are discussed, and a realistic geometric model of a muscle group is constructed. In the results, the muscle geometries theoretically derived are illustrated by dissection examples derived from the human forearm. In the discussion, some morphological and practical applications of the model are considered.

MATERIAL AND METHODS: THE MODEL OF A MUSCLE GROUP

Definitions

The contractile unit

An elementary contractile unit is modelled as a tendon fibre (diameter d_t), a much thicker muscle fibre (diameter d_m), and a tendon fibre in series. A multi-gastric contractile unit is a number of these units in series. In the body, contractile units are suspended between the insertions of their end tendon fibres.

The ideal unipennate muscle model

The ideal unipennate muscle model consists of a number of contractile units in parallel. The muscle fibres are of equal length, and are equidistal to each other (fig.2.a). The tendon fibres at both ends form two-dimensional sheets, further called *aponeuroses*, of strictly parallel tendon fibres which are attached to a continuous line on bone. Arbitrarily, one tendon sheet is called the origin, the other is called the end tendon.

Aponeuroses

By the above definitions, an aponeurosis contains one tendon fibre for each inserting, or originating muscle fibre. This aponeurotic tendon fibre originates from or ends in this muscle fibre. Therefore, an aponeurosis becomes thinner/thicker to the degree that muscle fibres arise from it or insert in it, and it ends or starts with the last or first muscle fibre. More strictly, let S_o and S_r be the cross-sectional area of the aponeuroses of origin and insertion, s_t the cross-section of the individual tendon fibre, and N the total number of muscle fibres in the muscle. Then it holds that: $S_o = s_t \cdot (N - n)$ and $S_r = s_t \cdot n$, with n the n^{th} muscle fibre leaving the origin aponeurosis, or inserting into the end tendon aponeurosis.

The minimal distance between muscle fibres, geometric transformations

In the following the ideal muscle model of fig.2.a will be transformed into the various muscle geometries (bipennate, short and thick, broad and flat, etc.) found in the body. In these transformations a fundamental constraint must be satisfied, which is that the distance (d) between the midlines of two muscle fibres at any point cannot be less than their diameter d_m ($d \geq d_m$), otherwise the fibres will strangle each other. Furthermore, muscle fibre parallelism in the projected cross-section of the muscle is used as an intuitive criterion for acceptability of muscle

Generic model of a muscle group

shape. Assumed is that muscle fibres in the ideal unipennate model insert in the origin and end tendon plate at maximal density. Geometric transformations of the unipennate model then necessarily consist of the *stretching* of one of the aponeuroses relative to the other. Indeed, any shrinking of their surface area would violate the minimum distance constraint. The stretching of an aponeurosis increases the average distance between the muscle fibres, which disturbs the ideal muscle fibre parallelism. These changes should be acceptable as long as they are smooth. Examples of transformations with minimal disturbance of parallelism are the bending and torsion of the unipennate model to allow it to follow the curved surfaces of bone or deeper muscles. This bending is achieved by the local stretching of one aponeurosis relative to the other, producing either a convex or concave shape of the model.

Exchanging muscle width for muscle thickness with equal muscle length: the bipennate muscle

The problem

For a given length of origin (l_0), a muscle with a given number (N) of fibres (minimal origin area = $N \cdot d_m^2$, assuming square fibres) must have a certain width (b) ($b \leq N \cdot d_m^2 / l_0$). Assume that a strong muscle is required somewhere in a body part where the length of the origin area is limited to l_0 , and assume further that the unipennate manifestation of the muscle with the given length of origin is too broad to fit within the diameter b_p of the body part ($b > b_p$). How then can such a muscle be accommodated in the body?

The folding of the unipennate muscle model

This fundamental construction problem can be solved by the *wrapping up of the unipennate model*, which is basically *the exchange of muscle width (b) for muscle thickness (h)*. Ideally, this transformation maintains volume: $b \cdot h \cdot l_0 = \text{constant}$. The geometric shape with the smallest diameter per cross-sectional area is the cylinder; therefore, for a given l_0 the minimal muscle diameter (D_m) which can be achieved is: $D_m = 2 \cdot (b_0 \cdot h_0 / \pi)^{1/2}$, with b_0, h_0 the width and thickness of the unipennate model. However, the constraint on minimum muscle fibre distance must also be satisfied. This is investigated in fig.2. The rolling up of the ideal model of fig.2.a produces the cylindrical model of fig.2.b. This model is obtained by stretching the outer aponeurosis with respect to the inner one, in which the muscle fibres insert at maximal density and of which the surface remains constant. The rolled up model is entirely wrapped up in its outer aponeurosis: a closed muscle compartment has been created. However, the aponeurosis at the inside, further called the end tendon, has become a hollow cylinder, while the proximal end of the model is a hollow cone. Clearly, this hollowness is anatomically impossible, and must be removed. However, the end tendon cannot be solidified by merely reducing the inner diameter R in fig.2.c to zero, thus creating a slim cylindrical tendon. This would reduce the surface area of the end tendon and violate the minimum fibre distance constraint, since the muscle fibres already insert at maximal density. Therefore, the straightforward cylindrification of the unipennate model is infeasible. However, when the model is merely flattened (fig.3.a), the tendon becomes solid while its surface remains constant. The inner surfaces of this end tendon may grow together without any

change in the model's functioning. In this way a bipennate muscle model is created, of about half the width of the unipennate model. The tendon of a bipennate muscle is further called a bipennate tendon. Fig.3.a shows that in the projected cross-section the muscle fibre parallelism is well maintained, except at the edges. However, at the edges the local density of the muscle fibres is low due to the extreme stretching of the outer aponeurosis, and the aponeurosis will be thin. The excess volume at the edges can be reduced by flattening the lateral parts of the aponeurosis against the sides of the bipennate muscle, or the stretched part of the aponeurosis may even simply degenerate. The hollowness at the origin (left hand side) of fig.2.b can be reduced by shrinking the outer aponeurosis onto a cone, as in fig.2.c. However, this will violate the maximal density constraint of the muscle fibres at the outer aponeurosis. Therefore, when a conic aponeurosis of origin must be obtained, the surface area of the proximal end tendon must also be reduced, and muscle bulk shifted to the distal end. When no conic origin shape is required, the model can be merely flattened proximally; the origin is then a line on bone as long as the width of the bipennate model.

The end tendon shape within a bipennate muscle

Let a muscle be constructed of n layers of muscle fibres. Each layer has the thickness of one muscle fibre and contains m muscle fibres, which insert into the end tendon at the same levels. To accommodate the insertion of a layer of m fibres, the circumference of the tendon must be: $O_T = m \cdot d_m$, with d_m the minimum distance between the muscle fibres. The cross-section of the tendon after the insertion of k layers of m muscle fibres is: $S_T = k \cdot m \cdot s_t$ with s_t the cross-sectional area of a tendon fibre. The ratio of the minimally required circumference over the local cross-section of the tendon is: $O_T/S_T = d_m/(k \cdot s_t)$. This ratio is independent of m , and decreases with the number k of inserting muscle fibre layers. As this ratio decreases, the end tendon can become more elliptical without reduction of circumference. Even, when the cross-sectional area of the tendon is large enough, it may become cylindrical. This happens when the required circumference can be obtained from the radius of the cross-section, which requires the insertion of k_c muscle fibre layers, with: $k_c/m = d_m^2/(4\pi s_t)$ [from: $S_T = k_c \cdot m \cdot s_t = \pi R^2$; $O_T = m \cdot d_m = 2\pi R$]. The right-hand-side of this expression is, by model definition, constant. It follows that end tendons at their origin in the muscle will always be thin and broad (width = $m \cdot d_m$ in unipennate, and $m \cdot d_m/2$ in bipennate muscles), but that they may become cylindrical within the muscle after a length proportional to the number of muscle fibre layers (k) inserting per length, and in inversely proportional to the number of muscle fibres (m) inserting per layer. In long muscle bellies (many muscle fibre layers) with a small number of fibres per layer (m small), the end tendons may become cylindrical within the muscle. Even, when $k > k_c$, the circumference of the tendon becomes greater than required. The tendon may then develop a surface line without insertions. This simple model does not take into account the angle of insertion of the muscle fibres. More comprehensive models are presented in van Leeuwen and Spoor (1992 and 1993).

Partially bipennate and very compact muscles

The above principles allow to derive from an unipennate model any existing muscle shape. A few examples are given.

(i) The partial folding of the unipennate model into the cross-sectional shape of fig.3.b, and the subsequent folding of the end tendon at 120° produces the partly bipennate, partly unipennate muscle model of fig.3.c. In this model two deviations of the muscle fibre parallelism in the projected cross-section are found. One is of muscle fibres *converging towards the end tendon* because of the local concavity of the outer aponeurosis, which results from stretching the outer aponeurosis relative to the tendon. The other is of muscle fibres *converging towards the outer aponeurosis* because of the local concavity of the end tendon, which results from stretching the end tendon relative to the aponeurosis. These deviations balance each other out, so that the overall parallelism of muscle fibres is well maintained. However, this reversal of the convergence of the muscle fibres implies differences in muscle fibre length, as can be noted from the projected cross-section of fig.3.c. This results in deviations of parallelism in the longitudinal section. However, these deviations are locally small and the changes are smooth. The result is a morphologically acceptable muscle shape, which is very compact. An example is the ECRB, shown in figs. 12 (ventral view) and 13 (lateral view) (see results).

(ii) More compact still is the muscle cross-section of fig.3.e. This cross-section is derived from the folding of the bipennate model of fig.3.a to an angle of 60° , which results in the intermediate stage of fig.3.d. Fig.3.e follows by removing the slack from the outer aponeurosis. In fig.3.e the overall parallelism of the fibres in the projected cross-section is well preserved, but the projected length of the muscle fibres differs considerably at the convex and concave parts of the end tendon. This indicates a greater variation in muscle fibre length and in longitudinal parallelism than in the previous example, while, however, these variations are locally small and smooth. An example is the FCR in figs.10 and 11.

(iii) Another very compact cross-section is given in fig.3.f. In this figure the surface of the bipennate end tendon is increased by an extra fold. Also here muscle parts with fibres converging towards the end tendon alternate with muscle fibres converging towards the aponeurosis. An example is the PT in fig.14.

Bipennateness of muscles due to the origin area crossing a joint (intra-originous joint)

In the above it is shown that bipennate muscles necessarily arise when muscle width is exchanged for muscle thickness, the muscle volume remaining basically constant. Presently, another cause of bipennateness is modelled, which is the origin area of a muscle spanning a joint. Consider fig.5.a, which represents the elbow, with the brachioradialis and the extensor carpi radialis longus (see fig.13). These muscles have no pulleys at the elbow, meaning that their fibres may freely bowstring. Consider first the BR, of which the origin area does not span the elbow joint. Its origin is spread longitudinally along the humerus, which means that fibres arising more proximally have a greater moment arm at the elbow than fibres arising more distally. Therefore, the proximal fibres will elongate more with elbow extension, and must be longer. This difference in fibre length can be accommodated by letting the fibres which originate more proximally at the

humerus insert more distally into the end tendon. In this way a unipennate muscle is naturally formed (fig.13). Consider now the ECRL. Its origin area starts at the humerus, but continues distal to the elbow joint by means of an aponeurosis which attaches to the lateral epicondyle at about the level of the joint axis, i.e. with a zero moment arm at the elbow joint. The humeral part is similar to the BR, and therefore inserts unipennately into the upper side of the end tendon. However, in the part distal to the elbow all muscle fibres are of the same length, which is determined only by the displacement of the end tendon, and not by the elbow joint. These fibres are therefore shorter than the humeral fibres, but their origin itself expands distally. As a result, the humeral fibres, and the distal muscle fibres must insert at the same level into the end tendon. This problem is solved by inserting them at opposite sides of the tendon, which results in a bipennate end tendon. It follows that a muscle with an intra-originous joint is necessarily bipennate, with the proximal and distal fibres inserting at opposite sides of the end tendon.

Bipennateness due to the reduction of muscle width, and bipennateness due to an intra-originous joint can be clearly distinguished. In the first case, bipennateness results from an origin area folded around the end tendon, and corresponds to a partially or totally closed muscle compartment. With the intra-originous joint, the origin area shape may be flat, and even very narrow. Of course, mixed forms may occur, in which a muscle arises from a largely closed muscle compartment which also extends over a joint. An example is the PT in fig. 14.

The model of a muscle group

From the above models, a muscle group with a minimal bony surface of origin can be easily assembled. A stepwise formation is given in fig.4. Fig.4.a presents three muscles arising from three different lines of bony aponeurotic origin. These lines can be reduced to three points of origin by bipennification and coneshaping of the models (fig.4.b). These distinct origins can be further compacted into a single compact origin, as in fig.4.c. Where the aponeuroses of the individual muscle models are in contact they can grow together without any change in muscle function. In this way intermuscular septa are formed from which bilaterally muscle fibres of two different muscles arise. Intermuscular septa can therefore be interpreted as two unipennate aponeuroses of origin grown together. This is the reciprocal of the bipennate end tendon (fig.3.a), which was modelled as a double folded unipennate end tendon plate. The reciprocity of the intermuscular septum and the bipennate end tendon, i.e. of the aponeuroses of origin and insertion, is complete when viewed within the box of fig.4.c: there is no way to tell which is end tendon and which is origin aponeurosis.

When all the muscles in the muscle group of fig.4.c contract at the same time, large proximal bulging occurs, which results in power losses as the muscles strangle each other. This can be remedied by rearranging the muscles into the cascade structure of fig.4.d, which provides a more homogeneous longitudinal distribution of muscle bulk (see fig.16). Muscles within the group need not be completely folded. The unfolded parts of these aponeuroses will then continue from lines on bone.

Muscle groups in the real body

In the real body, the origins of muscles are as follows. First, the deeper layers of muscles will occupy the available surfaces on bone. Between between the origins of these muscles, lines on bone remain from which aponeuroses can expand; these form the fibrous skeleton for the superficial muscle groups. At certain limited areas of bone the aponeurotic origins of many muscles may accumulate for biomechanical or other reasons (e.g. at the elbow epicondyles). The muscles of such groups are likely to be bipennate muscles in more or less coneshaped compartments formed by their aponeuroses of origin, in cascade arrangements as in fig.4.d.

RESULTS

In the following the above models are validated by dissection results of forearm muscles. The focus is twofold. First, to validate the shape of the end tendons within the muscles, and the correlation between the shape (uni- or bipennateness, degree of folding) of the end tendon and the shape of the aponeurosis of origin. Second, to demonstrate the structure of the aponeurotic compartments of the muscle groups of the forearm. The main examples of these aponeuroses are from the medial epicondyle. These aponeuroses are first exposed from the outside, and their structure within the arm is revealed by opening the arm between the compartments they outline.

Cross-sections of tendons at different levels in the muscle belly

The figs.6,a,b show cross-sections of the wrist area taken proximal to, and at the radio-ulnar joint, resp. These cross-sections show the end tendon cross-sections at different levels in muscle bellies. In the most proximal cross-section (fig.6.a) two kinds of tendons with inserting muscle fibres can be distinguished. (i) tendons with a more or less cylindrical cross-section (FDS_3 (7), FPL (1), FDP_2 (2)); and (ii) tendons with a flattened cross-section (FDS_2 (6), FDS_5 (9)). With the cylindrical tendons the muscle belly is at its end. These tendons contain already so much tendon fibre volume that they have sufficient circumference to accommodate the further inserting muscles fibres even when (almost) cylindrical. However, in the flattened tendons (FDS_2 (6), FDS_5 (9)) the number of muscle fibres which must insert distal to the cross-section is still large, and the number of muscle fibres already inserted is relatively small. Therefore, these tendons still have a large ratio of circumference to cross-sectional area.

In Fig.6.b the FDS_2 (6) muscle belly has almost ended; the situation is similar to the FPL (1) and FDS_3 (7) in fig.6.a. Much of the FDS_2 muscle mass has inserted in the tendon, which however still remains flat at the side at which the remainder of the muscle fibres will insert. The FDS_5 has become almost cylindrical.

Aponeuroses of origin and end tendons of the forearm muscles

Fig.7 presents an overview of the medial-volar forearm. The picture illustrates the superficial aponeuroses of origin at the proximal medial surface of the arm, and their positions relative to the end tendons. The superficial aponeuroses of origin form the deeper layer of the fascia antebrachii, which is a two layered structure. The superficial layer of this fascia consists of

transverse fibres which, amongst others, derive from the lacertus fibrosus of the *M. biceps*. This superficial layer has been largely removed by careful dissection to expose the deep layer, which consists of longitudinally running aponeurotic tendon fibres of muscle origin. These fibres form an apparently continuous sheet, which in fact consist of the superficial aponeurotic fibres of the compartments of the PT (7), FCR (8), PL (9), FDS (10), and FCU (11). The borders of these muscle compartments are outlined by black-dotted lines. At these borders the aponeuroses of adjacent compartments continue deep into the arm, where they merge into intermuscular septa. These borders can be recognised by local concentrations of aponeurotic fibres, to which the superficial layers of the fascia antebrachii tend to adhere more strongly. This is illustrated by the remaining part of the lacertus fibrosus (8), which in this specimen continues into the PT-FCR intermuscular septum, instead of running superficially and transversely. Distally, the muscle fibres have been removed from the surface of the end tendons up to either proximally the beginning of the end tendon, or up to the distal end of the aponeurosis of origin in the case that the end tendon and the aponeurosis overlap. Traces of muscle fibres were left on the tendons to indicate the areas of insertion. The picture clearly illustrates the very large surface areas of the tendons within the muscles, and the tendency of tendons to become cylindrical in their distal course. In the picture, this is most clear in the *M. Palmaris Longus* (3), of which the tendon at the beginning is at least three times as broad as at its end.

Fig.8 illustrates the looseness with which muscle compartments are sometimes stacked upon each other. (1) is the PL, of which the entire compartment could be lifted out of the arm without cutting even a single muscle fibre from the deeper aponeurosis on which it lay. This deeper aponeurosis consists partly of the aponeurosis of origin of the FCR, and partly of the aponeurosis of the FDS; their junction is indicated by the dotted line. Small arrows indicate the innervation and blood supply of the PL, which enter the PL compartment by perforating the FDS aponeurosis. (5) is the FCU compartment, which by blunt dissection was easily separated from the FDS compartment up to the medial epicondyle. Clearly visible are the separate FDS and FCU aponeuroses of origin at the adjacent sides of their compartments. In situ, these aponeuroses are in contact with each other. However, they did not blend into an inseparable intermuscular septum, as may be the case in other specimens, except very proximally and deep, i.e. at the level where the ulnar nerve leaves the FCU compartment and enters the FDS compartment (large arrow in fig.8).

Fig.9 presents the end tendon of the FCU, and shows how long and broad end tendons may be within the muscle. The length of the tendon is explained by the small muscle fibre length, and the fact that the most proximal muscle fibres arise at the medial epicondyle itself. Therefore, the tendon must start no further distal to the medial epicondyle than the muscle fibre length. The muscle derives virtually no muscle fibres from bone itself: its entire mass originates from aponeurotic fibres which arise from the medial epicondyle and the proximal ulna (see also fig.8). The tendon is proximally bipennate and about half as wide as the compartment itself, and becomes unipennate distally. Only the fibres on the exposed side of the tendon have been removed. In its distal course, the tendon grows thicker and a bit narrower, but in this specimen also develops some small longitudinal folds (1-2mm high) at its surface, which further increase its surface area. These folds present as lines at the midline of the tendon (small arrows); they are somewhat clearer

Generic model of a muscle group

in fig.7 (1). Distally, the compartment grows broader with respect to the tendon, as can be verified by the dotted line which marks its dorsal border. Therefore, to reach the end tendon the muscle fibres arising distally at the dotted line should either increase their fibre length, and/or approach the tendon more transversely. However, in this specimen another solution is effectuated, in the form of an extra tendinous flap at the distal tendon (large arrow). This flap (i) increases the distal tendon surface area. This is required because distally the muscle fibres insert unipennately. Therefore, the distal tendon must be twice as broad per number of inserting muscle fibres than the bipennate proximal part. (ii) It also expands the tendon into the direction of the dotted line, which reduces the necessity for changes in length or orientation of the fibres arising at the distal dotted line. This illustrates the strict relationship between end tendon shape, and origin shape.

Fig.10 presents two inseparable compartments, of the FCR and FDS, with their exposed end tendons. The compartment borders are marked by dotted lines. The FDS₃ tendon (2) evolves similar to the FDS₂ tendon in the cross-sections of fig.6. It starts as a thin, and remarkably broad unipennate tendon plate, almost four times as broad as the tendon in the carpal tunnel. Distalwards, as more muscle fibres insert, the tendon grows more cylindrical. The FCR tendon (1) is presented as a clear validation of the relationship between the uni- or bipennateness of a tendon, and the shape of its compartment. Two phenomena must be explained. First, proximal to the dotted line (1), the tendon is half as wide as distal to the line. Second, proximal to the dotted line the tendon is bipennate, while distal to the line it is unipennate (with muscle fibres inserting only at the back). The cause is modelled in fig.5.b: the superficial side of the FCR compartment (fig.8 (2)) is a great deal shorter than the deep side (fig.14 (4)). Therefore, the most distal fibres originating from the superficial aponeurosis insert into the end tendon no further than the dotted line. Further, the compartment is cone-shaped, meaning that even as the superficial aponeurosis ends, the deeper aponeuroses increase in surface area, so that the total muscle cross-section remains more or less constant. Consequently, about an equal number of muscle fibres (m) must insert per length in the bipennate and the unipennate parts of the tendon. As a result, the width of the unipennate part must be twice that of the bipennate part, as the bipennate part can accommodate the same number of muscle fibres with half the tendon width. The FCR also illustrates the muscle cross-section shape derived in fig.3.e., in which the end tendon blade is folded at about 60°. In fig.10 the tendon is unfolded to show its true width. In fig.11 it is shown in its anatomical shape, which is clearly folded. In situ, the inside of the fold faces the PT-FCR intermuscular septum, which is the longest side of the compartment. The outside of the fold can be seen in fig.8 (2) and in fig.9 (2).

Fig.12 and fig.13 will validate (i) the proximal end tendon width in unipennate muscles, (ii) the intra-originous joint as a cause of bi-pennateness of end tendons, and (iii) the muscle cross-section shape of fig.3.c. (i) The BR (1) is a truly unipennate muscle, as modelled in fig.5.a. Its end tendon is as broad as the muscle itself (fig.12). The structure of the muscle belly is somewhat more complex than suggested in fig.5.a, amongst others because the muscle fibres not only originate from the brachialis-triceps intermuscular septum at the humerus (fig.13), but also from aponeurotic expansions (fig.12 (12)) within the arm. These expansions cause deviations in the muscle architecture relative to fig.5.a, which will not further be discussed. (ii) Also very

broad and flat is the largely unipennate tendon of the ECRL (fig.12 (2)). Proximally this tendon is bi-pennate (fig.13,(2)), which modelwise corresponds to the intra-originous elbow joint (fig.5.a). The humeral fibres at the upper side of the tendon, the fibres originating distal to the joint axis insert at the under side of the tendon; their separation is indicated by the dotted line. (iii) The tendon of the ECRB is also partly bipennate and partly unipennate, but in the transverse section. Moreover, in the transverse section the tendon is folded at about 100° , along the dotted line (3) in fig (12). This cross-sectional shape is modelled in the fig.3.c. In fig.12 the tendon of the ECRB is unfolded to show its width. In fig.13 the tendon is shown in lateral view in situ. This shows that the tendon is bipennate at the lateral part, and unipennate at the upper part. The aponeurosis of origin of the ECRB is triangular (fig.12 (10)). Laterally, it forms the intermuscular septum of the ECRB-ED (dotted line (3) in fig.13). Notice also the parallelism between the line of the distal insertion of the lateral muscle fibres into the lateral part of the tendon, and the dotted line (3) which is the aponeurotic origin of the laterally inserting muscle fibres. Inside the tendon fold, the muscle belly continues further than the dotted border of the lateral insertions in the end tendon.

Fig.14 shows the PT tendon, and will illustrate the cross-section shape of fig.3.f, which presents an end tendon with an extra fold. The PT muscle is bipennate for two different reasons. First, its origin crosses the elbow joint, which leads to a bipennateness as in fig.5.a; second, its aponeurosis of origin forms a half-enclosed compartment, which must necessarily result into a largely bipennate tendon. However, the plane of the bipennate end tendon sheet corresponding to intra-originous elbow joint, and the plane of the bipennate end tendon sheet corresponding to the folding of the origin aponeurosis are almost perpendicular. As a result, the PT tendon commonly develops an extra fold (large arrow), perpendicular to the main plain of the tendon. The main plane of the tendon (fig.14 (1)) corresponds to the folding of the origin aponeurosis (2). This aponeurosis (2), which is the PT-FCR intermuscular septum, is folded backwards by about 150° , with a thick carpet of trimmed PT muscle fibres left in situ. The fold resulting from the intra-originous elbow joint is about perpendicular to this plane. In the present specimen even a second, smaller fold is present (small arrow) which further enlarges the tendon surface area. The folded character of the end tendon blade can be verified from top view of the PT in fig.12 (5), which shows that the tendon inserts as a zig-zag folded flat end tendon blade. The dotted line indicates the rim of the FCR-PT intermuscular septum in which the remainder of the lacertus fibrosus inserts.

Fig.14 may also illustrate the concept of an intermuscular septum being two unipennate aponeuroses blended together. Fig.14 (3) is the distal part of the origin aponeurosis of the FDS. This aponeurosis clearly consists of two types of fibres: proximal-distal fibres which continue from the FCR-FDS intermuscular septum (see also fig.15), and more transverse fibres which arise from a line on the radius between the FPL, and the insertions of the supinator and the PT. The FCR-FDS intermuscular septum divides at the end of the FCR compartment into a proper unipennate FDS aponeurosis (fig.14.(3)), and some tendon fibres which continue as a short unipennate FCR aponeurosis (fig.14.(4)). This splitting up of the FCR-FDS intermuscular septum shows that it contains the tendon fibres of origin of both muscles, and that these fibres may separate into independent aponeuroses in their distal course.

Generic model of a muscle group

Fig.15 shows a coneshaped compartment arising from a tiny spot on bone (medial epicondyle), as an illustration of the figs.4. It is the FCR compartment after removal of the muscle, opened at the rim of the PT-FCR aponeurosis (upper dotted line, above (1)). In situ, the upper dotted line and the lower dotted line proximal to the large black dots coincide. The bottom (2) is the FDS-FCR intermuscular septum. The radial wall (1) of the compartment is the FCR-PT intermuscular septum. The ulnar wall (3), which is folded backwards, is the FCR-PL intermuscular septum. The dotted line 2-3 corresponds to the dotted line 1-2 in fig.10. No muscle fibre of the FCR arises from bone. (4) is the FDS aponeurosis, which continues from the FDS-FCR intermuscular septum (see comments of above section).

Fig.16 shows the medial epicondylar flexor group, and illustrates the cascade arrangement of muscles in a muscle group as modelled in fig.4.d. The muscle compartments are exposed by removing a part of their superficial aponeuroses (the "roofs") together with the muscle fibres, while leaving a greater part of their deep aponeuroses (the "floors" of the compartments) in situ. (1) is the "roof" of the PL, formed by the longitudinal fibres of the fascia antebrachii. (2), (3) and (4) together form the "floor" of the PL compartment. (2) and (3) are the PL-FCR intermuscular septum. In this specimen, the most proximal muscle fibres of the FCR originate distal from the white dotted line (2-3), i.e. only about 4 cm distal to the epicondyle (in the specimen of fig.15 they originate much more proximal). Proximal to the white dotted line the FCR compartment contains no muscle fibres, and is merely a flat folded double intermuscular septum separating the PL and the PT. (4) is the PL-FDS intermuscular septum. The nerve (small arrow) and vessels of the PL enter the PL compartment from the FDS compartment through the hole in their intermuscular septum. (5) is the FCR-PT intermuscular septum, i.e. the floor of the FCR compartment, and the roof of the PT compartment. (6) is the FCR-FDS intermuscular septum. The dotted line between 5-6 is the border between the PT and FDS compartments. (7) are the aponeurotic tendon fibres of origin of the FDS from the fascia antebrachii. (8) is the aponeurotic origin of the FCU from the fascia antebrachii. These aponeurotic fibres originate from the medial epicondyle (10), as well as from the proximal ulna (11). (9) is the deep flexor.

Fig.17. illustrates the fact that anatomical variations also must use the available lines of bony origin. This extra "wrist flexor" (1) developed from an extra fold in the radial aponeurosis of origin of the FDS, which arises from a constant line on bone between the FPL, and the supinator and PT end tendon.

DISCUSSION

Morphological considerations

Muscle types: a morphological continuum

In anatomic literature distinction is made between unipennate, bipennate, and fusiform muscles. The above models allow to produce these shapes from the elementary unipennate model. Muscle shape thus appears as a morphological continuum, which allows to flexibly determine the shape of the individual muscle as a function of the available space, the required displacements (fibre length), the required strength (number of fibres), and other biomechanical demands (see further). Basic to this flexibility are the aponeuroses of origin, which expand the bony origins and can be freely folded into an appropriate origin shape.

The relationship between bipenniformity and muscle strength

Bipennate muscles are usually strong muscles. This sometimes leads to the notion that bipennate muscles have a "special quality" of strength. However, in the above model bipenniformity arises as either a necessity to accommodate large muscles within spaces of limited width, or the result of an intra-originous joint. Therefore, uni- or bipennateness of muscles should be regarded as the result of geometric constraints, rather than a functional quality. The interchangeability of unipennate and bipennate muscles is well illustrated by the fact that mixed forms with partly bipennate and partly unipennate tendons are readily found, e.g. the ECRB (fig.12) or the FCR (fig.10).

Evolutionary adaptability and anatomic variations

The transformation model illustrates an inherent capacity in muscles to adapt their size, shape and position (area of attachment to bone) and consequently their functions in evolutionary terms. The aponeurotic muscle origins allow the expansion and migration of muscles on narrow lines on bone, which avoids straight-on competition with other muscles for limited origin space on bone itself. "New" muscles may develop even without any sizeable bony area available, from muscle parts of an established muscle group which develop extra folds in the aponeuroses to become autonomous entities. E.g. it can be imagined in evolutionary terms that the insertion of an end tendon spreads out a little bit, and finally splits up into different parts which develop their own muscle belly within a proper aponeurotic fold. Such separate tendon insertions may migrate, changing their moment arms in the process to create new functions. Such events are easily recognised in anatomic anomalies, as in fig.17. Here an anomalous "radial wrist flexor" has developed, using the only available origin on the radius, which is the narrow bony line between the FPL muscle belly and the end tendon of the PT. Along this line the FDS origin expands radially from an aponeurosis (fig.14 (3)). The anomalous muscle arises from an extra expansion of the FDS aponeurosis along this origin line on bone.

Biomechanical considerations

The above models do not clarify why muscles of a certain strength are needed in a certain position in the body. They merely state that when such muscles are needed, they can be implemented with

Generic model of a muscle group

sufficient flexibility to satisfy a diversity of criteria. One criterion may be a reasonable distribution of muscle bulk. More biomechanical criteria can be imagined. For instance, the end tendons of muscles generally have localised insertions, and in the limbs they also have a well-defined course often secured by pulleys. However, aponeurotic origins, even of large muscles, can also be compact areas on bone. This allows for a precise local positioning of these origins, which then function similar to end tendon insertions. Such localised insertions are clearly found at the epicondyles of the elbow. When the wrist extensors or flexors are active in loading the wrist, they also compress the elbow joint and increase its lateral stability. Moreover, their moment arms at the elbow are quasi zero (FCR, FCU, ECRB, ED) so that their force does not affect elbow torque.

Surgical orientation and approach

Surgical approaches are pathways to the inside of the body along which the anatomic structures are separable with minimal collateral damage. The knowledge of the structure of the muscular compartments and their innervations and blood supply are essential to the quick location and safe use of these pathways in surgery. Obviously, good approaches in a muscle group consisting of muscles with totally closed compartments do not exist: to reach deep sites, the surgeon must necessarily pass through more superficial compartments and cause damage to muscle fibres. However, generally not all compartments are closed, nor of equal length. Natural approaches are through the open sides of partially closed compartments, between the bellies of muscles of which the aponeuroses of origin have already ended, or between compartments of which the aponeuroses have not blended in intermuscular septa. The latter approaches may differ individually. For instance, in the specimen of fig. 8. the compartments of the FCU and FDS were separated by two independent unipennate aponeuroses. Therefore, the ulnar nerve could easily be approached over its entire length by blunt dissection. In other cases, however, these aponeuroses are blended into a proper intermuscular septum, and muscle fibres must be cut to reach the nerve up to the epicondyle.

ACKNOWLEDGEMENTS

The author cordially thanks Dr. J. Zguricas and Dr. E.T. Walbeehm for their assistance in dissections; Dr. C.W. Spoor for the close reading of the manuscript; and Prof. Emer. J.M.F. Landsmeer, Dr. S.E.R. Hovius, Dr. G.J. Sonneveld, Prof. J.M.G. Kauer, Prof. C.J. Snijders, Prof. Emer. J.C. Van der Meulen, and Prof. J. Voogd for the discussion of the material; and C. Entius and J. Velkers, the custodians of the dissection theatre, for their kind support.

REFERENCES

- Ettema, G.J.C. and Huijing P.A. (1990) Architecture and elastic properties of the series elastic element of muscle-tendon complex. Multiple muscle systems: biomechanics and movement organisation, Edited by Winters, F.M. and Woo, S.L.-Y. pp. 57-68. Springer, New York.
- Van Leeuwen, J.L., and Spoor, C.W. (1992) Modelling mechanically stable muscle architectures. Phil. Trans. R. Soc. Lond. B 336, 275-292.
- Van Leeuwen, J.L., and Spoor, C.W. (1993) Modelling the pressure and force equilibrium in unipennate muscles with in-line tendons. Phil. Trans. R. Soc. Lond. B 342, 321-333.

FIGURES

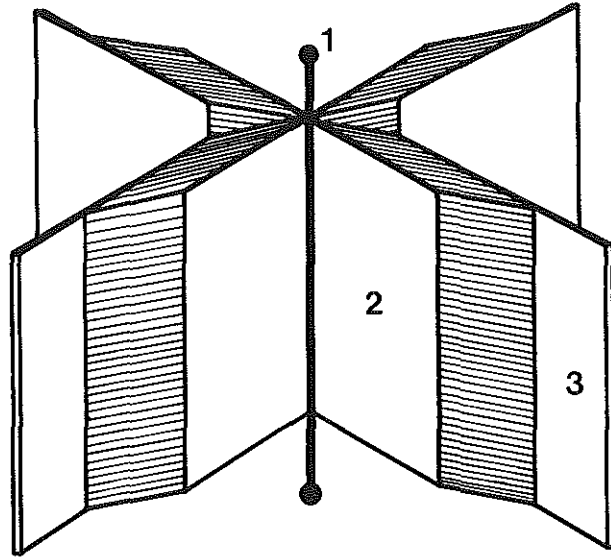


Figure 1 Unipennate muscle models attached to a one-dimensional skeletal segment (1) by means of aponeuroses of origin (2). 3: end tendon aponeurosis.

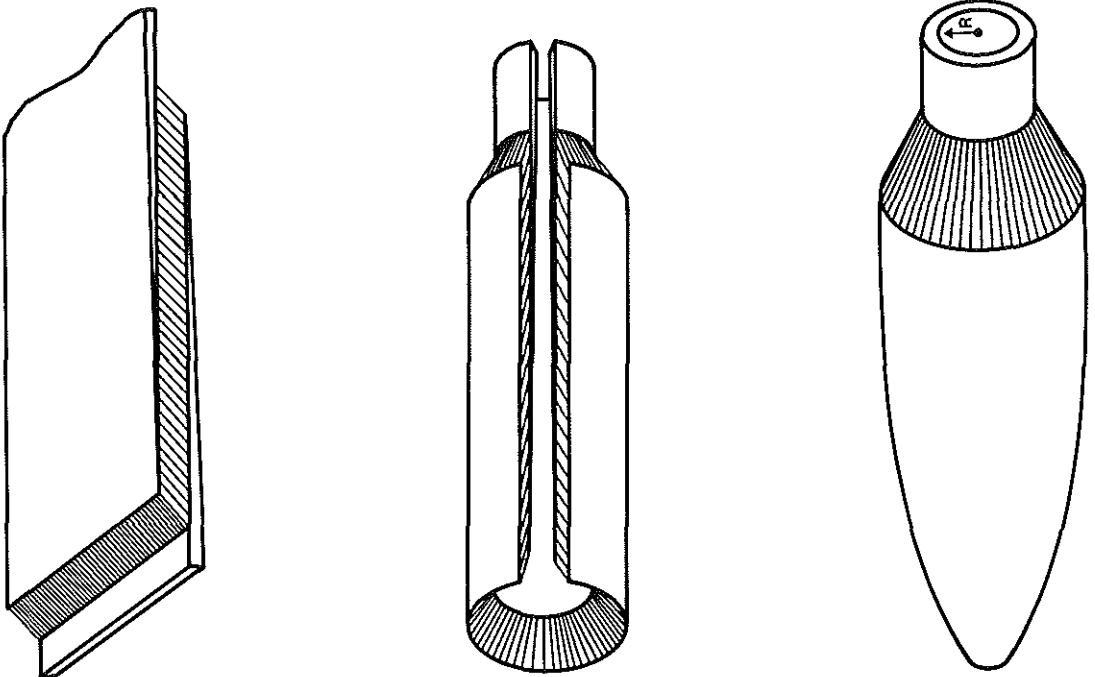


Figure 2 a,b,c a) Ideal Unipennate muscle model. b) Model of fig.1.a rolled up as a cilinder. c) Model of fig.1.b with the proximal end compressed into a cone.

Generic model of a muscle group

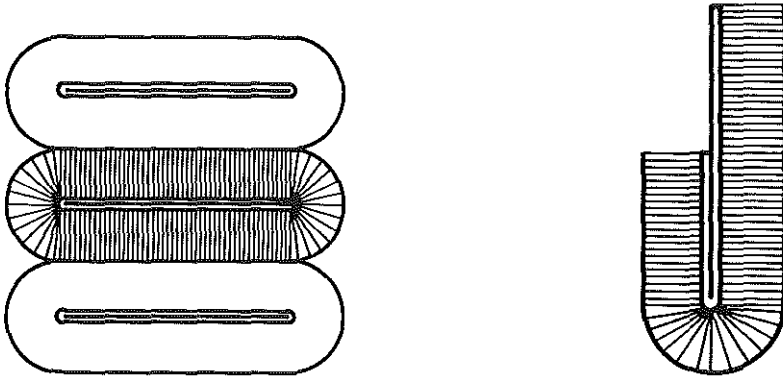


Figure 3 a,b



Figure 3 c,d



Figure 3 e,f Cross-sections of different muscle types. a) cross-section of bipennate muscle models stacked upon each other. The end tendons are double folded unipennate tendons. The aponeuroses of origin are grown together in bipennate intermuscular septa. b) Partly folded unipennate model. c) Model (b) with end tendon folded to an angle of 120° . The end tendon is partly unipennate, and partly bipennate. d) Bipennate model (a) folded to an angle of 60° . e) Model (d) with slack removed from the outer aponeurosis. f) Cross-section of a very compact muscle, with end tendon with an extra fold.

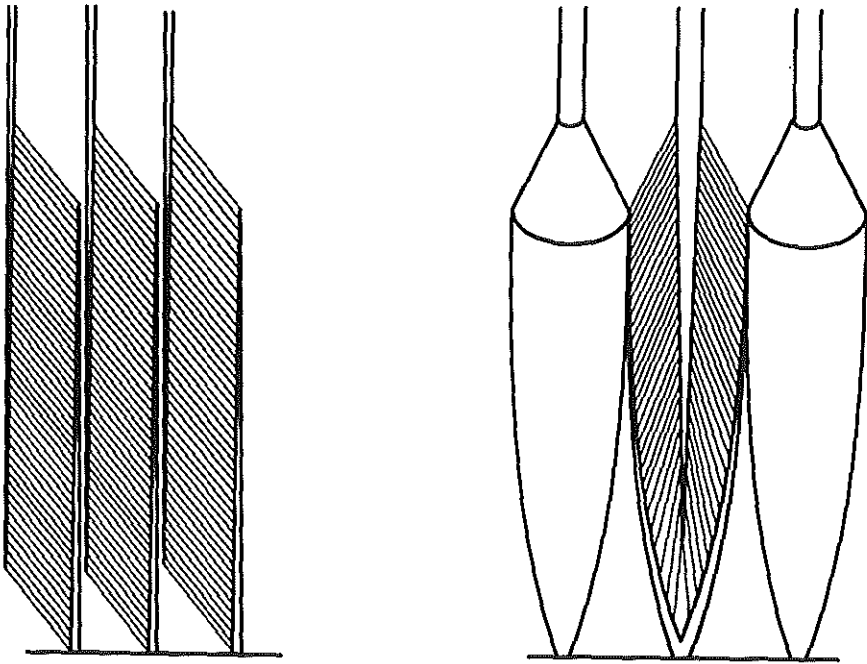


Figure 4 a,b

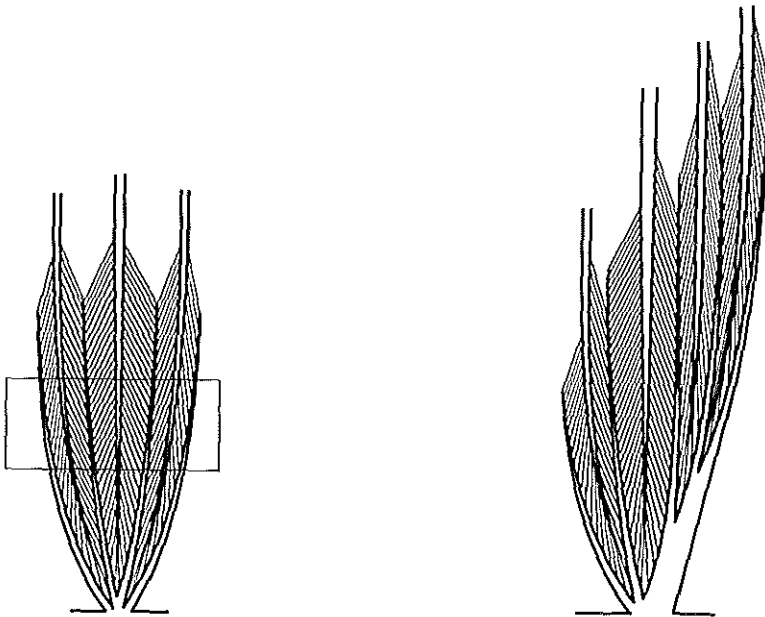


Figure 4 c,d Construction of a muscle group. a) Three unipennate models stacked upon each other. b) Models (a) transformed into cones with a point origin on bone. c) Cross-section of models (b) compacted into a muscle group. d) Model (c) with muscles in a cascade arrangement to obtain a homogeneous distribution of muscle bulk.

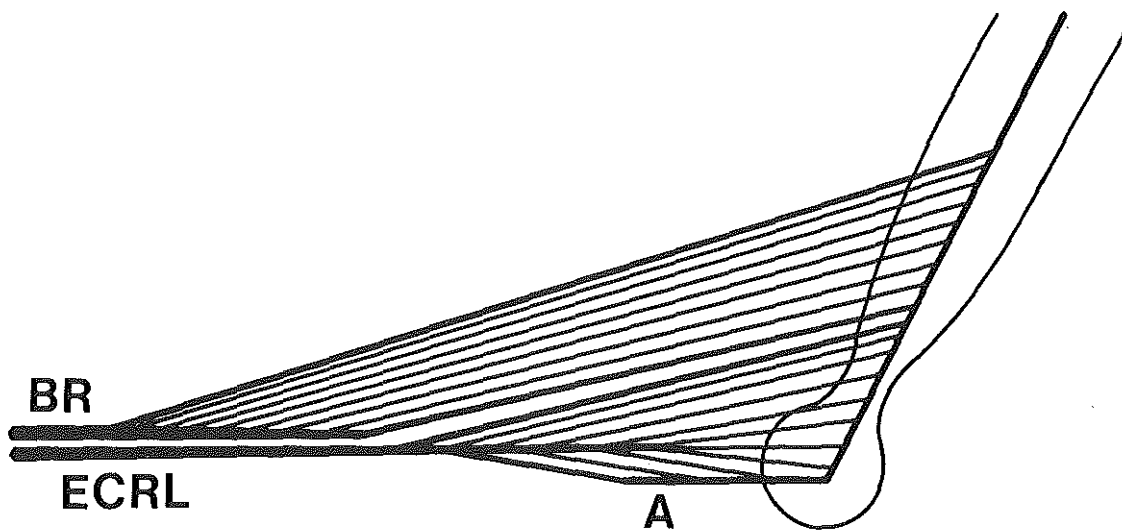


Figure 5 a Model of the M. Brachioradialis (BR) and M. Extensor Carpi Radialis Longus (ECRL) at the elbow. The BR is unipennate. The ECRL is bipennate; the muscle fibres originating from the humerus insert at the top (volar side) of the tendon; the fibres originating distal to the joint axis insert at the dorsal side of the tendon.

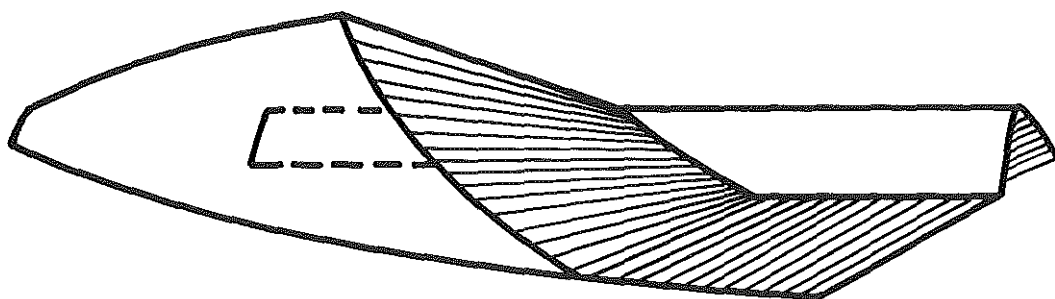


Figure 5 b Model of the FCR compartment. The "floor" of the compartment is much longer than the "roof", so that the tendon must become unipennate in its distal course. To allow the insertion of all muscle fibres at its unipennate part, the end tendon must become broader.

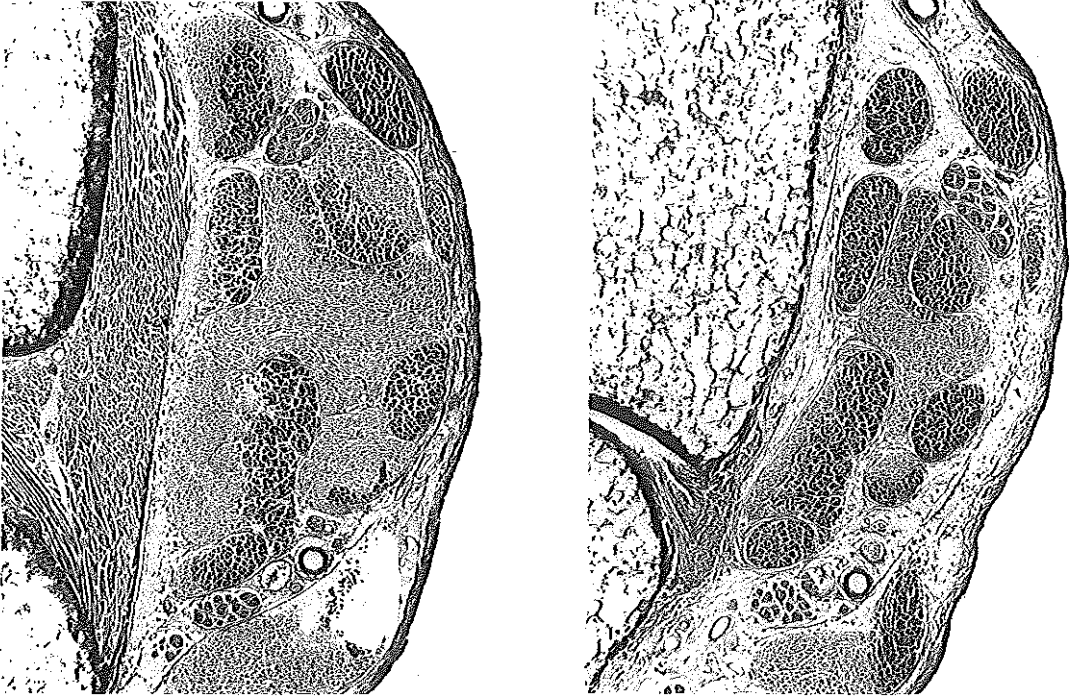


Figure 6 a,b Cross-sections of the forearm at the wrist area. a) proximal to the radio-ulnar joint. b) through the radio-ulnar joint.

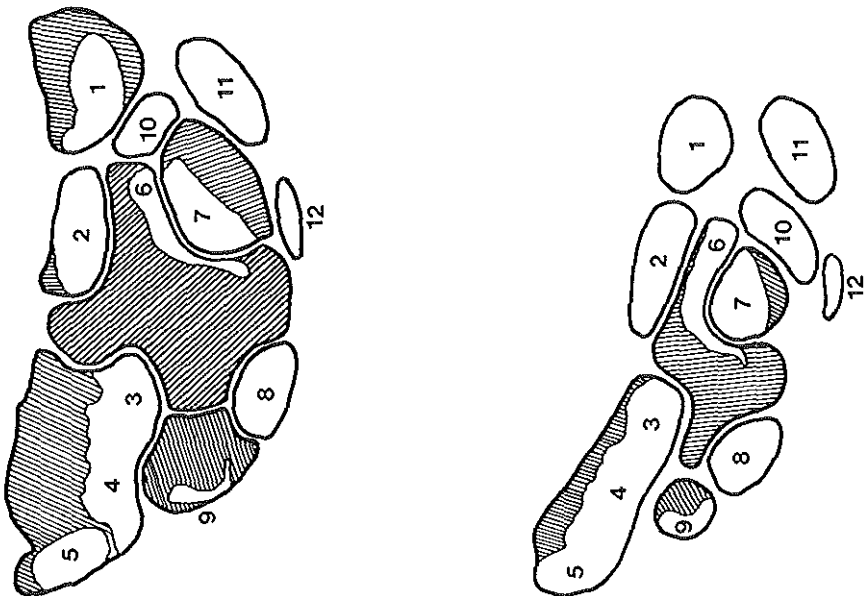


Figure 6 c,d Legend figures with (a) and (b), resp. 1: FPL. 2..5: FDP₂..FDP₃. 6..9: FDS₂..FDS₃. 10: Median Nerve. 11: FCR. 12: PL. Shaded areas: muscle fibres.

Generic model of a muscle group

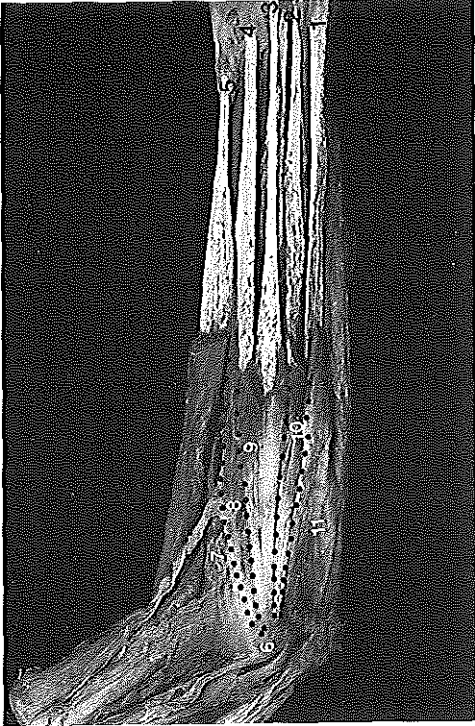


Figure 7



Figure 8

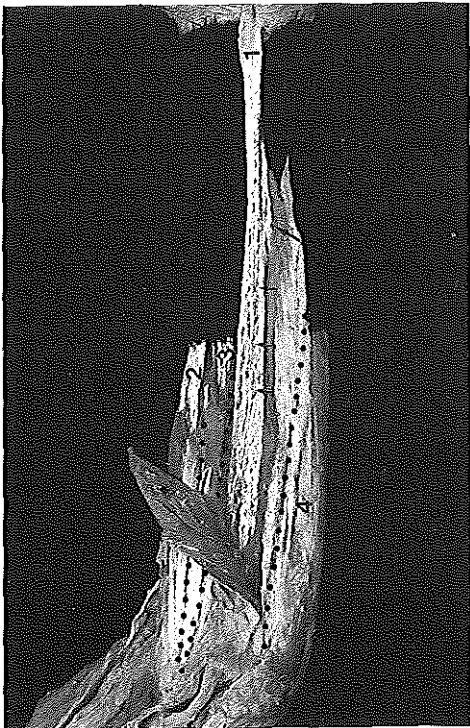


Figure 9

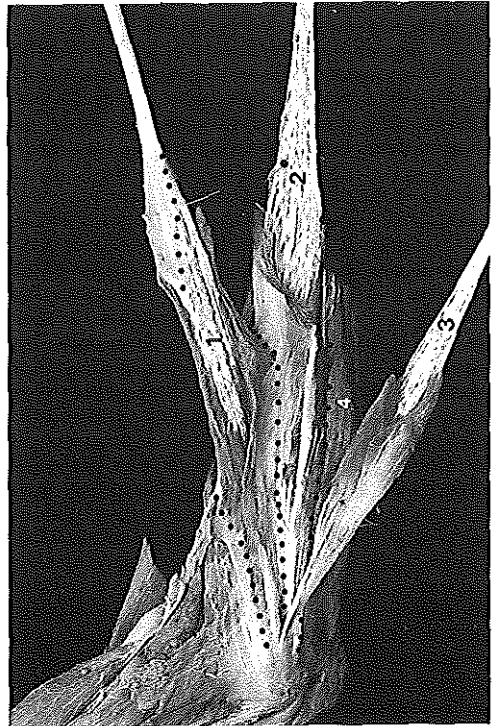


Figure 10

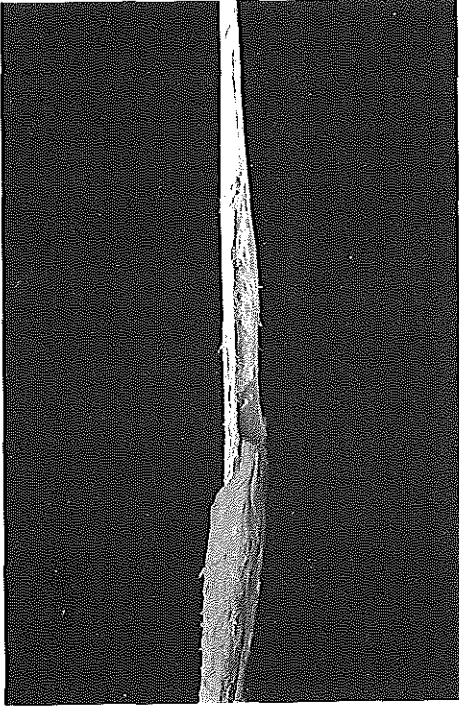


Figure 11



Figure 12

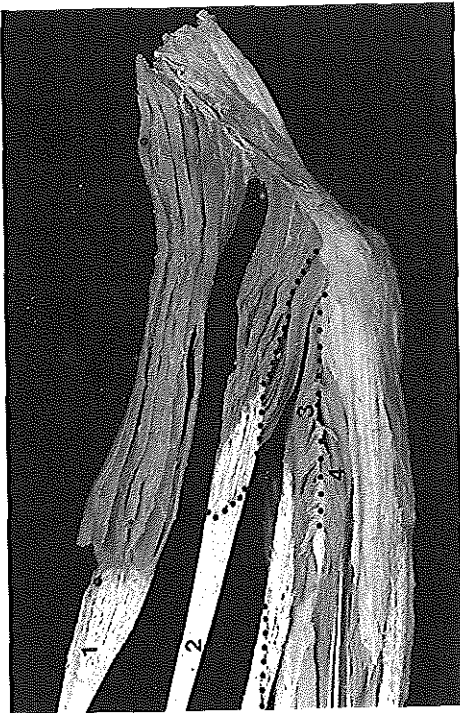


Figure 13

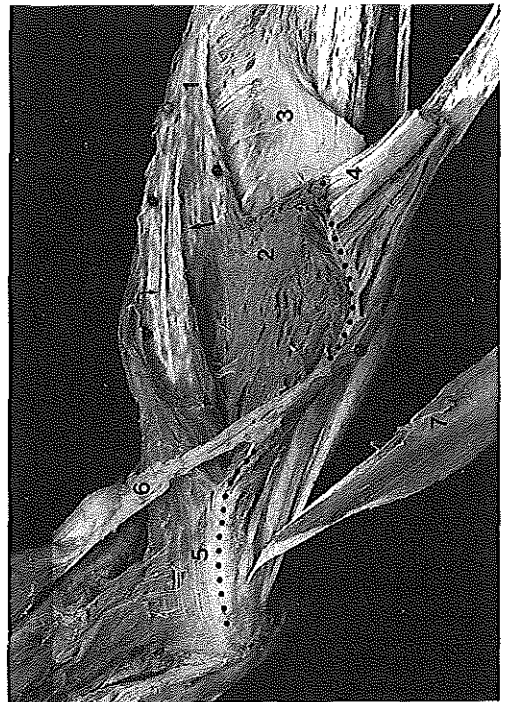


Figure 14

Generic model of a muscle group



Figure 15

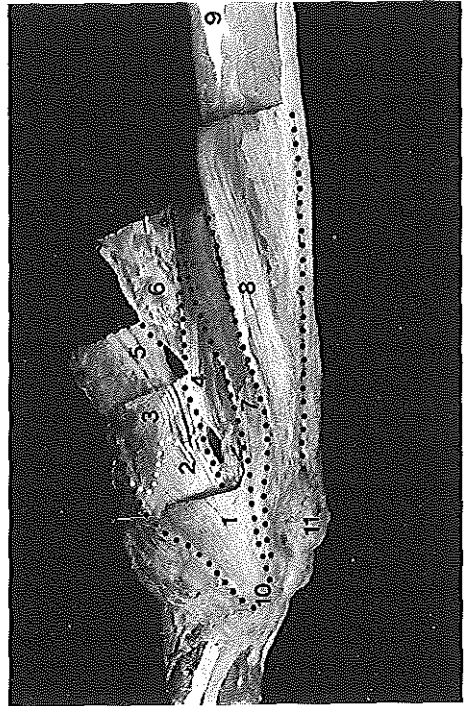


Figure 16

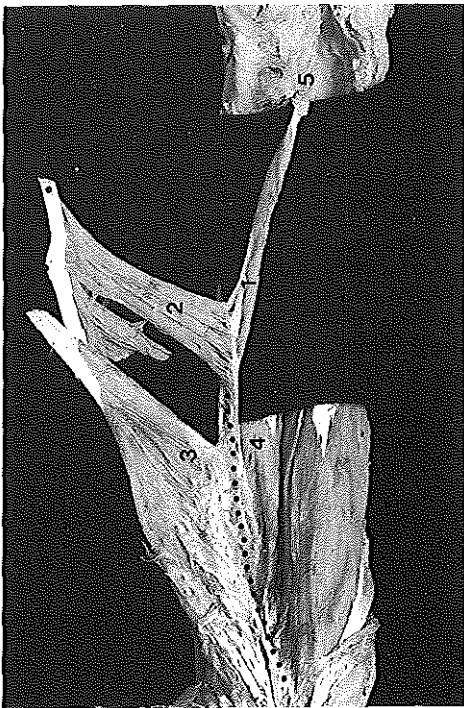


Figure 17

Captions with figs. 7 - 17

Figure 7 Medial-volar aspect of the forearm. The superficial transverse fibres of the fascia antebrachii have been removed. Muscle fibres are removed from the tendons from distally to proximally the beginning of the tendon, or the distal end of the aponeuroses of origin when this overlaps with the tendon. 1: FCU. 2: FDS₃ and FDS₂, 3: PL. 4: FCR. 5: BR. 6: medial epicondyle with ulnar nerve exposed. 7: PT aponeurosis. 8: FCR aponeurosis. 9: PL aponeurosis. 10: FDS aponeurosis. 11: FCU aponeurosis.

Figure 8 Medial epicondyle with retracted compartments of PL and FCU. 1: PL. 2: FCR. 3: FDS₃ and FDS₄. 4: FDP muscle belly. 5: FCU muscle. Small arrows: innervation (proximal) and blood supply (distal) of PL. large arrow: ulnar nerve leaving the FCU compartment through a perforation of the FCU-FDS intermuscular septum.

Figure 9 FCU tendon exposed up to its origin. The aponeurosis of origin with a remainder of trimmed muscle fibres has been folded back. 1: FCU. 2: FCR. 3: FDS. 4: dorsal border of the compartment. Dorsal to this line is the FDP.

Figure 10 FCR (1), FDS₃ (2) and PL (3) in detail. 4: FCU compartment. The proximal dotted lines outline the borders of the compartments. The dotted line at the FCR tendon indicates the distal border of the insertions of the muscle fibres at the exposed side of the tendon.

Figure 11 Detail of the tendon of the FCR, which shows the folded end tendon from the inside.

Figure 12 Ventral view of the forearm with exposed tendons. 1: BR. 2: ECRL. 3: ECRB. 4: Supinator. 5: PT end tendon. The exposed part of the PT is marked with white dotted lines. 6: FDS. 7: FCR. 8: tendon of biceps. 9: radial nerve entering the supinator. 10: exposed rim of the aponeurosis of origin of the ECRB. 11 and 12: aponeurotic origins of the ECRL and BR. resp. 13: Brachialis.

Figure 13 Lateral view of the lateral epicondyle. 1: BR. 2: ECRL. 3: ECRB. 4: ED. Dotted line 3-4: ED-ECRB intermuscular septum. Dotted lines 2: outline of the insertions and muscle fibres of the humeral part of the ECRL.

Figure 14 Exposed end tendon of the PT (1). 2: trimmed remainder of muscle fibres of the PT, originating from the PT-FCR intermuscular septum, of which the border is marked by the black dotted line. 3: FDS aponeurosis. 4: distal part of the FCR aponeurosis. 5: aponeurosis of origin of the PT from the humerus. 6: lacertus fibrosus. 7. PL.

Figure 15 Compartment of the FCR after complete removal of the muscle belly. (1) PT-FCR intermuscular septum. (2) FCR-FDS intermuscular septum. (3) FCR-PL intermuscular septum. (4) FDS aponeurosis.

Generic model of a muscle group

Figure 16 Overview of the muscle compartments of the medial epicondyle. 1: roof of PL compartment. 2, 3: PL-FCR intermuscular septum. 4: PL-FDS intermuscular septum. 5: FCR-PT intermuscular septum. 6: FCR-FDS intermuscular septum. 7: FDS origin from the deep longitudinal tendon fibres of the fascia antebrachii. 8: FCU origin from the fascia antebrachii. 9: FDP. 10: Medial epicondyle. 11: olecranon.

Figure 17 Anomalous muscle (1), which inserts into the retinaculum flexorum, and which arises from the line of origin of the FDS aponeurosis on the radius (dotted line). 2: FDS. 3: FCR, arising from the backside of the FDS-FCR aponeurosis which originates at the dotted line. (4) FPL. 5: retinaculum flexorum.

THE MORPHOLOGY OF HOLES IN APONEUROSES CAUSED BY PERFORATING NERVES OR VESSELS AT THE MEDIAL EPICONDYLE OF THE ELBOW

J.N.A.L. Leijnse

Department of Plastic and Reconstructive Surgery, Erasmus University Rotterdam, The Netherlands. Resubmitted to Anatomical Record.

ABSTRACT

In the present paper the morphology of holes in aponeuroses of origin of muscles is modelled. These holes result from perforations of the aponeuroses by nerves or vessels, but also from joints which the line of origin of an aponeurosis crosses. The concept of aponeurotic holes explains many small-scale anatomic variations of muscles, such as muscles with multiple separate origins in parallel. It may also contribute to better understanding of complex anatomical areas, such as the medial epicondyle of the elbow, and of clinical phenomena such as nerve compressions and their surgical treatment.

NOTATIONS

BR: M. Brachioradialis

FCR: M. Flexor Carpi Radialis

FCU: M. Flexor Carpi Ulnaris

FDP: M. Flexor Digitorum Profundus

FDS: M. Flexor Digitorum Superficialis

FPL: M. Flexor Pollicis Longus

PT: M. Pronator Teres

INTRODUCTION

The attachment of a muscle group to a small area on bone requires the expansion of this origin area by tendinous aponeuroses of origin (Leijnse, 1996). These aponeuroses provide the muscles' main areas of origin, while they themselves originate from narrow spots or lines on bone. The aponeuroses form extended intermuscular tendinous sheets which the nerves and vessels may have to perforate in their distal course. The aim of this paper is to study the architecture of these perforations or "aponeurotic holes", the morphological principles which determine their formation, and their effect on the anatomic aspect of the muscles which arise from the perforated aponeuroses. It is shown that the concept of aponeurotic holes as morphological entities is fundamental to the explanation of many small-scale anatomic variations, which in their diversity defy comprehensive description. Moreover, it may help in understanding the nature of compressions, e.g. as resulting when nerves or vessels pass through holes which are not well formed. The text examples will be the intermuscular septum of the M. flexor digitorum superficialis and M. pronator teres at the elbow, which is perforated by the median nerve and brachial artery, and the intermuscular septum of the M. flexor superficialis and the M. flexor carpi ulnaris at the medial epicondyle, which is perforated by the N. ulnaris.

MATERIALS & METHODS: THE MODELS

Model of an aponeurosis

An aponeurosis of origin of a muscle is modelled as a sheet of tendon fibres, which originate from a continuous line on bone. This origin may also be a "point" on bone, in which case the aponeurosis develops as a cone-shaped compartment, with the apex at the bony origin. Each tendon fibre is the origin of a single muscle fibre in which it ends. The muscle fibres arise from the aponeurosis in a regular density from the bony origin onwards. The aponeurosis becomes thinner as more tendon fibres end in muscle fibres, and it ends with the most distal muscle fibre. By definition, for the aponeurotic tendon fibres a principle of parallelism holds. This is that tendon fibres which originate next to each other will run next to each other in their entire course, unless separated by a physical cause, and will not crisscross within the plane of the aponeurotic sheet. This principle allows for coordinated changes in the course of the aponeurotic fibres. E.g. they may fan out a bit or run somewhat closer together in their distal course, as long as this does not result in fibres crossing over.

Passages of nerves and vessels through a single aponeurosis: the problem

Consider a nerve or vessel which approaches an aponeurosis at an angle Φ (fig.1). The safe passage, without compression of the perforating structure, requires a hole in the aponeurosis with a minimal diameter equal to the diameter of the nerve or vessel. When the approach is perpendicular to the aponeurosis ($\Phi=90^\circ$), the minimal hole is a circle of the diameter of the perforating structure. When $\Phi < 90^\circ$, the minimal hole is an ellipsis, with the shortest axis equal to the diameter, and the longest axis in the direction of the axis of the nerve or vessel. The more oblique the approach, the more oblong the hole will be. A hole can only be created by the *rearrangement* of aponeurotic tendon fibres, since these fibres can only originate from bone and can only end in a muscle fibre, and cannot end into or start at the border of the hole.

The general morphology of a hole in an aponeurosis (fig.2)

In the present model, a hole in an aponeurosis can be imagined as created by inserting a sharp pencil of the diameter of the perforating structure into the aponeurosis (fig.2.a). In doing so, the tendon fibres at the surface of the hole at either side of the pencil point are compacted into the boundaries of the hole. Hereby the fibres next to each other remain next to each other, except when they are separated by the hole. Since no physical cause exists for abrupt changes of direction, the tendon fibres will split up somewhat proximally to the hole. Moreover, at the distal border of the hole the tendon fibres will tend to recombine in a crisscross pattern, which is caused by fibres overshooting the original line of direction from which they deviated to create the hole (fig.2.b). Only fibres from the opposite borders of the hole may crisscross, for the principle of parallelism excludes crisscrossing of fibres running within the same border of the hole. The larger the hole, the greater the amount of crisscrossing at its distal border, as the fibres deviate more from their original course (fig.2.b). As such an aponeurosis with a hole mimics a "flow pattern", which starts as a regular (laminar) flow of parallel fibres, the course of which is disturbed by the perforating structure, and which recombine at the distal border of the hole in some pattern of

controlled "turbulence". With increasing diameter, the borders of the hole will become increasingly thick, as the number of fibres compressed into them increases.

Aponeurotic holes as causes of anatomic variability in the origins of muscles: model assumptions, the muscle archetype

The presence and variability in the shapes of holes in aponeuroses can explain frequent small-scale anatomic variations in the gross aspect of muscle build. In this explanation the following assumptions must be accepted.

(i) Any muscle can be imagined as having a single continuous area of origin. This continuous manifestation of the muscle is further called the "archetype". When the origin of the muscle is an aponeurosis, the origin of the archetype is a continuous line or spot on bone, and the archetype aponeurosis is a continuous sheet without holes.

(ii) In the real body, the continuous aspect of the archetype can only be disturbed by a well defined physical cause. Such physical cause may be: the perforation of the muscle by a nerve or vessel or the tendon of another muscle; or it can be an intra-originous joint (i.e. a joint which is overlapped by the muscle origin, see further).

Large holes in aponeuroses which result in bi-originous muscles

When a hole in an aponeurosis becomes so large that it overlaps with the bony line of origin, the line of origin of the aponeurosis may appear discontinuous (fig.2.b), and the aponeurosis may appear to have two separate origins. As a result, also the muscle arising from this aponeurosis will seem to have two origins. Such a muscle is further called bi-originous (two muscle origins in parallel), in contrast to di-gastric (two muscle bellies in series). Two variants of bi-originous muscles may be distinguished, depending on the size of the hole relative to the length of the longest aponeurotic tendon fibres.

(i) *Bi-originous muscles with a single main muscle belly.* When the longest aponeurotic tendon fibres are sufficiently long to recombine distal to the hole, the distal part of the aponeurosis is still a single continuous sheet. Consequently, the muscle arising from this aponeurosis will have a single continuous main body, with two separate origins in between which a nerve, vessel, tendon or joint runs.

(ii) *Bi-originous muscles with separate muscle bellies.* When the longest fibres of the aponeurosis are too short to recombine distal to the hole (as in fig.2.e), and when this hole also overlaps with the bony origin, it will completely split up the aponeurosis into two separate parts. As a result, the muscle originating from this aponeurosis is also likely to split up into two separated muscle bellies up to the end tendon, especially so when the separated parts of the aponeurosis are forced to take a different course. This happens when one or both parts of the aponeurosis are pushed out of the plane of the archetype by the perforating nerve or vessel, or when they are pulled in somewhat different directions by the muscle fibres which arise from them, and which insert into the end tendon at a different angle of incidence.

The morphology of perforations of aponeuroses

Two or more juxtaposed holes which result in tri- or multi-originous muscles

When two holes in an aponeurosis are sufficiently large and close, all tendon fibres in their intermediate borders will be compressed into a single tendinous cord, with the aspect of a tendon in the classic sense (as a finger tendon) (fig. 2.c). When these holes also overlap with the line of origin of the aponeurosis, the tendinous cord will appear to originate as a separate structure, not related to the aponeurosis (fig. 2.d). The muscle arising from this aponeurosis will then look as having three separate origins (tri-originous), separated by nerves, vessels or other instances: two aponeurotic origins at the outer sides of both holes, and a central tendon of origin. Similarly, n-1 large holes may create a n-originous muscle.

The morphology of anomalous muscle flaps

A related anatomical variant is the anomalous muscle flap, which can be modelled as follows. Consider an aponeurosis with a hole, and its archetype. Two kinds of aponeurotic fibres can be distinguished in the archetype at the projected surface of the hole: (i) short tendon fibres which run over the surface of the hole and which end in muscle fibres before they reach the distal border of the hole, and (ii) tendon fibres long enough to recombine at the distal border. When the hole is large, the number of short fibres is substantial. Assume now that when the hole is created these short fibres fall "through the hole", i.e. out of the main aponeurosis. Then these short fibres may combine into a separate aponeurotic "flap", which has about the shape and size of the hole. With its muscle fibres, this aponeurotic flap may take an altogether different course than the main aponeurosis, with the restriction that its muscle fibres must insert into the main tendon, or at least into an end tendon which inserts into the main tendon. This aponeurotic muscle flap then has the aspect of a (small) accessory (anomalous) muscle belly. In figure 3, such an aponeurotic flap is depicted, without the muscle fibres.

An intra-originous joint as the cause of an aponeurotic hole

Consider a joint which is crossed by the line of origin of an aponeurosis; with the side of the joint at which the aponeurosis runs defined as the flexion side. The length L of this origin line, as measured over bone, changes with the position Θ of this joint, according to: $\Delta L = r_A \cdot \Delta \Theta$, with r_A the moment arm of the line of origin with respect to the joint axis. When $r_A \neq 0$, the part of the aponeurosis originating across the joint will become slack with joint flexion (i.e. with $\Delta \Theta > 0$), and will become taut with joint extension ($\Delta \Theta < 0$) and prevent further extension. This means that aponeurotic lines of origin crossing a joint may in principle limit joint movements. However, the stretching of the aponeurosis along its line of origin with joint extension ($\Delta \Theta < 0$) only stretches the connective tissue in between the aponeurotic fibres. Indeed, the aponeurotic fibres themselves merely originate at this line, but end in muscle fibres, and therefore cannot be stretched in between the two bones of the joint. Since this connective tissue is weak, the aponeurosis will be torn apart from its origin upwards, as one part of the origin moves with one bone, and the other part moves with the other bone (fig.4). In this way a hole is created which allows the free movement of the joint. The fibres at both sides of the hole will recombine into a single aponeurosis just as with a hole of a perforating vessel. When $r_A = 0$, the line of origin may cross a

joint without the aponeurosis being torn apart, because no changes in its length of origin occur with joint movement, and the aponeurosis is not transversely stretched. The condition $r_A=0$ corresponds to the tract of the collateral joint ligaments, which maintain their length with joint rotation. It follows that when the line of origin of an aponeurosis crosses a joint, either (i) a hole is created, with the fibres at the opposite sides of the hole originating from the opposite bones of the joint, or (ii) the aponeurosis is continuous, and its origin follows the tract of the collateral ligaments. Examples of the latter are the aponeuroses of the medial and lateral epicondyles of the elbow; they follow and strengthen the collateral ligaments of the elbow. An example of the first possibility is the hole caused by the radio-ulnar joint in the radial FDS aponeurosis, of which the line of origin runs from the medial epicondyle over the ulna to the radius (see further).

RESULTS

In the following the models are validated by dissection results.

Fig.5 shows the median nerve (2) perforating the aponeurosis of origin of the M. Pronator Teres (PT) (3,4,5) distal to the insertion of the M. Brachialis (1). The angle of approach of the nerve to the aponeurosis is very small. As a result, the nerve creates an elongated, almost perfectly elliptical hole (fig.6). The distal border of the hole is formed by fibres from the two parts separated by the hole which recombine in a crisscross pattern. Fibres of each part do not crisscross between themselves. An aponeurotic muscle flap (fig.5.3) has been pushed out of the surface of the hole by the nerve, which illustrates fig.3. This flap consists of short aponeurotic fibres which end in muscle fibres before they reach the distal border of the hole. One side of the flap is still attached to the main aponeurosis. The long fibres of the flap recombine with the main aponeurosis. By the traction of its muscle fibres and the push of the nerve, the aponeurotic muscle flap has been folded at an angle of more than 120° to the main aponeurosis. The muscle fibres arise from the back of the flap, while the muscle fibres of the main aponeurosis, which were removed except for the part distal to the hole, arise from the exposed side. In fig.7 the flap is folded back onto the surface of the hole, which it covers accurately. The muscle fibres of the flap are now at the superficial side, as in the main aponeurosis, which indicates that this was indeed the position of the flap in the "archetype" of the aponeurosis. The dotted line in fig.7 shows that the line of origin of the flap is continuous with the line of origin of the main aponeurosis. This line runs from the medial epicondyle along the insertion of the M. Brachialis in the ulna. From this line both the short fibres of the flap and the long fibres which recombine with the main aponeurosis originate, indistinguishable from each other at their origin.

Figs. 8 and 9 present a similar case, the difference being that the hole created by the median nerve is here so large that it completely splits up the aponeurosis to create a bi-originous pronator teres muscle. Fig.8 shows the tract of the N. Medianus and the A. Brachialis. The nerve runs more superficial and medial than in Fig.5, and completely splits up the aponeurosis. This is because the longest fibres of the aponeurosis at the point of the entry of the nerve are too short to recombine at the distal border of the hole. In fig.9 the part separated from the aponeurosis is folded back onto the main aponeurosis, demonstrating that it arises from a line of origin

The morphology of perforations of aponeuroses

continuous with the line of origin of the main aponeurosis. This shows that separate aponeuroses belong to the same archetype.

Fig. 10 shows the FDS aponeurosis exposed from the ulnar side. The FCU compartment has been retracted, with the FDS-FCU intermuscular septum (1) facing upwards. The muscle fibres of the FDS originating from bone (2) have been removed. The aponeurosis with the holes is the radial wall of the FDS compartment. The upper hole is for the median nerve, the lower hole is for the artery. These holes clearly illustrate the model principles of fig.2.c. The fibres originally running on the surface of the holes have been compacted in the borders, which are thick and tendinous. In between and proximal to the thickened borders, a narrow stretch of the original archetype aponeurosis can be identified, showing a homogeneous distribution of tendon fibres in parallel. Distal to both holes, the fibres recombine into the main aponeurosis in a smooth, controlled crisscross pattern.

Figs. 11 and 12 show what happens when the holes as in fig.10 increase in size: a "multi-originous" muscle is created. Fig.11 shows the radial aponeurosis (1) of the FDS compartment. The FDS muscle fibres originating from bone have been removed (5), while the FDS fibres originating from the FDS-FCU intermuscular septum (4) (the ulnar wall of the FDS compartment) have been trimmed. The origins of the radial aponeurosis (1) are from: the medial epicondyle, a strong tendinous chord from the ulna (modelled in fig.2.d), and a line of bone on the radius, where the aponeurosis presents some minor holes. The most proximal hole is from the median nerve, the large middle hole is from the radial artery. The removal of all muscle fibres from the radial aponeurosis (fig.12) reveals that the fibres of the different "origins" recombine into one single aponeurotic sheet. This sheet is proximally the FDS-PT intermuscular septum, and becomes more distally the FDS-FCR intermuscular septum.

Figs. 13 and 14 present an aponeurosis, viewed from proximal and distal, with two medium sized holes for the nerve (upper hole) and the brachial artery. Fig.13 is the PT aponeurosis; fig.14 is the FDS aponeurosis. The median nerve has pushed a small aponeurotic muscle flap out of the main aponeurosis (white number (1) in fig.12). A third large hole with a small intermediate origin is spanned above the M. Supinator (4). This hole is created by the radio-ulnar joint; its proximal border arises from the ulna, while its distal border arises from the radius. If the aponeurosis would pass from ulna to radius as a continuous structure, supination would be restricted. In the fig. 11, the hole created by the radio-ulnar joint and the hole created by the artery coincide. In fig.8 the rudimentary remains of the aponeurosis spanning the radio-ulnar joint are indicated by arrows (above (4)). Fig.14 also shows the perforation (arrow at (4)) of the FDS-FCU intermuscular septum by the ulnar nerve. The ulnar nerve approaches the aponeurosis at a very small angle (see fig.16) and in this specimen splits it up completely, as modelled in fig.2.e.

Figs. 15 and 16 show the PT aponeurosis and the FDS aponeurosis with nerves and arteria in situ. Fig.15 is the PT aponeurosis (6), which continues as the radial aponeurosis of the FDS compartment (5). The holes are rather small; also the hole spanning the radio-ulnar joint arrows between (4) and (5). Fig.16 shows the FDS compartment with the FDS muscle removed, except for the part of the aponeurosis originating from the radius. Clearly visible are the median nerve (1) and the ulnar artery (2) perforating the aponeurosis. The radial artery did not perforate the

aponeurosis, but took a superficial course; its branching can be seen in fig.15. The ulnar nerve (3) leaves the FCU compartment to join the ulnar artery. The medial recurrent artery is also visible, as it enters the FDS compartment through a hole in the FDS-PT aponeurosis, and runs towards the medial epicondyle which it approaches through a hole in the FDS-FDP intermuscular septum.

DISCUSSION

Geometric parameters of anatomic variability

In the medial epicondylar flexor group a great variability exists, especially in the passages of nerves and vessels through the aponeuroses. This makes it difficult to obtain, by mere description as in the classical anatomy, a realistic but concise outline of this anatomic area and its variations. The present model may be helpful as it provides a qualitative model of these anatomic variations. First, it identifies the main variables which contribute to anatomic variability. These are (i) the variations in the bony lines of origin and the direction and length of the tendon fibres of the aponeurosis, and (ii) the diameters, angles of approach, and sites of perforation of the perforating structures: nerves, vessels, biceps tendon, radio-ulnar joint. Second, it establishes the morphological principles by which these structures interfere. This allows to estimate, or rather, generate the "ranges" of anatomic variability by considering the range of variation of the perforated and perforating structures. The model also allows for educated guesses about the anatomical structure of an area only partly exposed, as during surgery. For instance, when a nerve or vessel is encountered in a certain position, a general idea about the shape and position of its passage through muscles and aponeuroses out of view can be conceived. As such, the model may help the surgeon or trainee to structure his surgical-anatomical experience in an orderly way.

Surgical applications

Nerve compressions. Compressions of nerves within muscles have been well substantiated (Hill et al., 1985; Amadio and Beckenbaugh, 1986; Dellon, 1986; Dellon and Mackinnon, 1987). Two causes of compression have been distinguished. (i) The mechanical compression of the nerve within the muscle belly itself, or in between a muscle belly and e.g. bone. An example is the compression of the median nerve between the humeral expansion of the PT or the lacertus fibrosus of the M. biceps and the end tendon (and underlying bone) of the M. Brachialis (Dellon, 1986). (ii) The irritation or compression of the nerve in its passage through aponeuroses, due to repeated friction at the borders, and/or because the hole is too small or narrow. The present model clearly outlines the possibilities for surgical treatment. In case (i) the decompression of the nerve may be obtained by changing the course or shape of the muscle. This can be done without harm to the muscle itself by transposing or releasing its aponeurotic origins. In case (ii) the hole in the aponeurosis must be enlarged. In principle, this merely requires the longitudinal incision of the distal border, whereby the edges can be folded back and sutured on themselves, so that they will adhere to the main aponeurosis, and do not form adhesions (Hill et al., 1985).

ACKNOWLEDGEMENTS

The author cordially thanks Dr. J. Zguricas and Dr. E.T. Walbeehm for their assistance in dissections; Dr. S.E.R. Hovius, Dr. G.J. Sonneveld, Dr. C.W. Spoor, Prof. C.J. Snijders, Prof. Emer. J.C. Van der Meulen, Prof. Emer. J.M.F. Landsmeer, Prof. J.M.G. Kauer and Prof. J. Voogd for the discussion of the material, and C. Entius and J. Velkers, the custodians of the dissection theatre, for their kind support.

REFERENCES

- Amadio, P.C., and Beckenbaugh, R.D. (1986) Entrapment of the ulnar nerve by the deep flexor-pronator aponeurosis. *J. Hand Surg.* 11A, 83-87.
- Dellon, A.L. (1986) Musculotendinous variations about the medial humeral epicondyle. *J. Hand Surg.*, 11B, 175-181.
- Dellon, A.L., and Mackinnon, S.E. (1987) Musculoaponeurotic variations along the course of the median nerve in the proximal forearm. *J. Hand Surg.* 12B, 359-363.
- Hill, N.A., Howard, F.M., Huffer, B.R. (1985) The incomplete anterior interosseus nerve syndrome. *J. Hand Surg.* 10A, 4-16.
- Leijnse, J.N.A.L. (1996) A generic model of a muscle group - application to the muscles of the forearm. Resubmitted *Anatomical Record*, sept. 1995

FIGURES

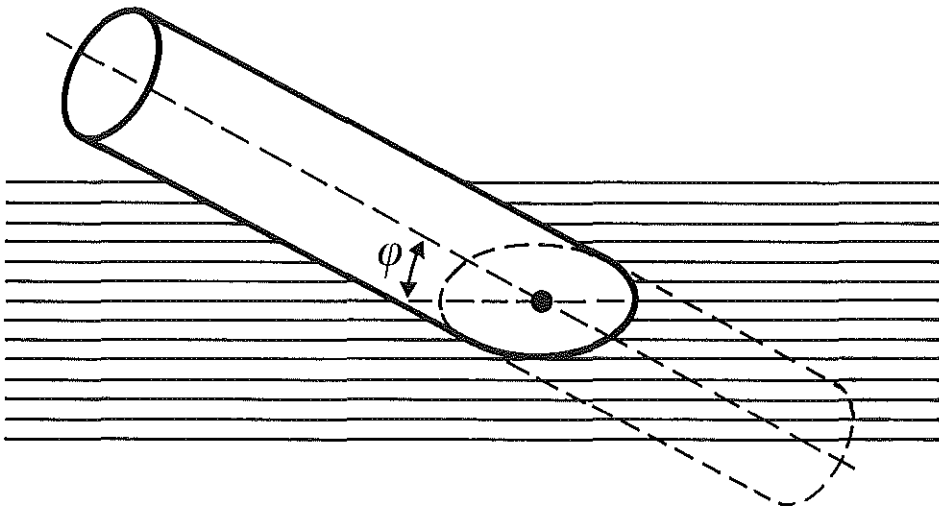


Figure 1 Nerve or vessel approaching an aponeurosis, outlining the surface of the hole minimally required for safe passage.

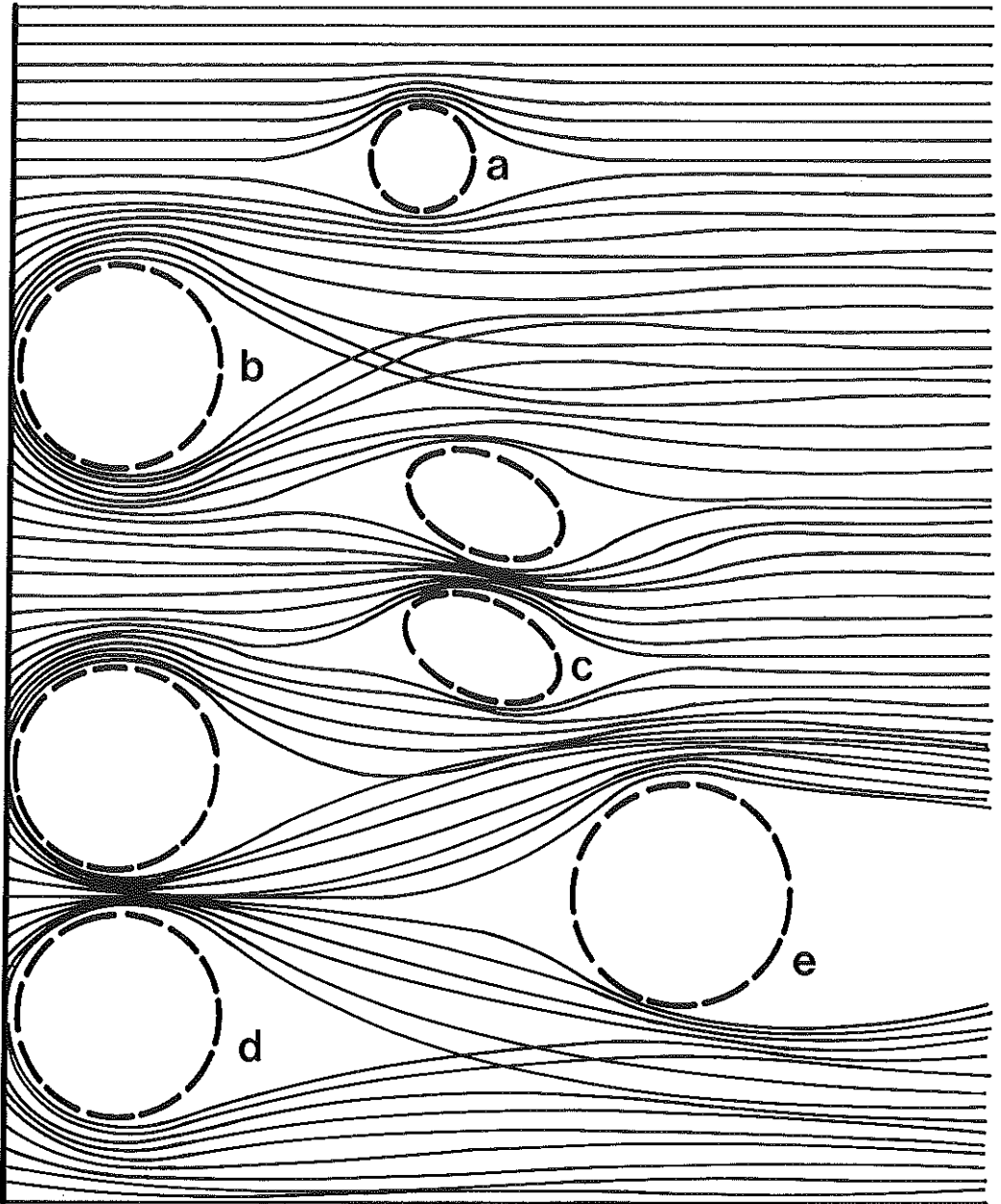


Figure 2 Models of small and large holes. a) Small hole. b) Large hole overlapping with the area of origin. Fibres distal to the hole recombine in a crisscross pattern into a single aponeurosis. c) Two small juxtaposed holes. The tendon fibres in between them are compressed into a tendinous cord. d) Two large juxtaposed holes overlapping with the line of origin. The aponeurosis is split into three parts: two normal aponeuroses with thickened tendinous borders, and an intermediate tendon, all of which recombine into a single aponeurosis. e) Large hole which completely splits up the aponeurosis: the fibres are too short to recombine distal to the hole.

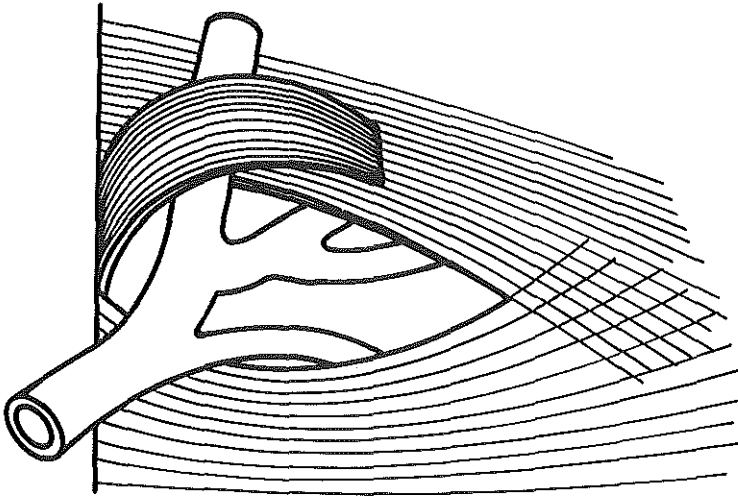


Figure 3 Generic model of an anomalous muscle flap. The artery creates a large hole. Long fibres at the surface of this hole recombine into the distal border. Fibres too short to reach the distal border fall out of the hole and form an aponeurotic flap by themselves. An arterial branch pushes this flap into a course different from the main aponeurosis. When the muscle fibres which arise from the aponeurotic flap contract, the arterial branch may be compressed.

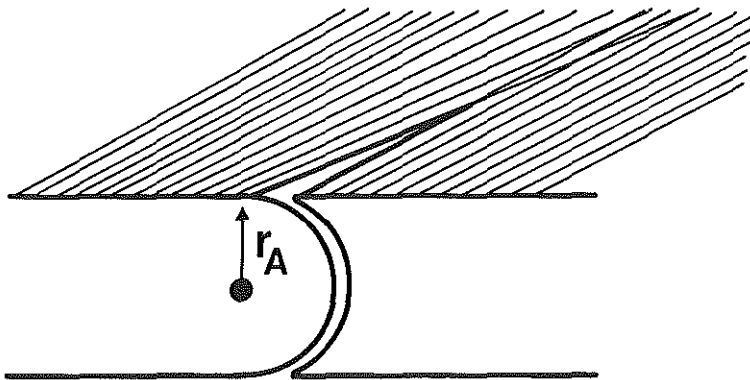


Figure 4 Hole in an aponeurosis created by an intra-originous joint.

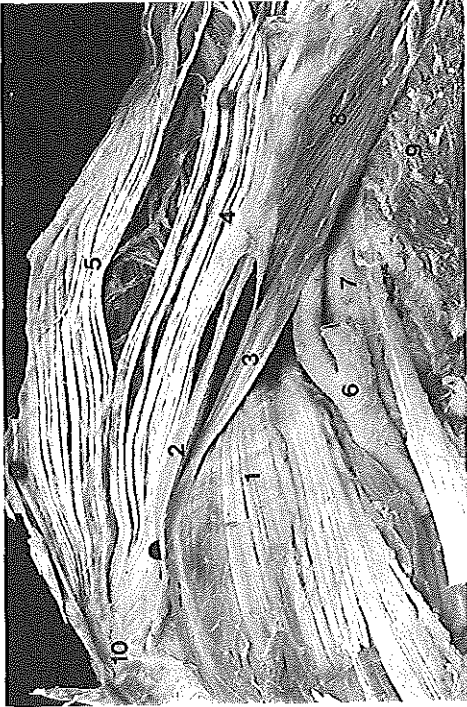


Figure 5

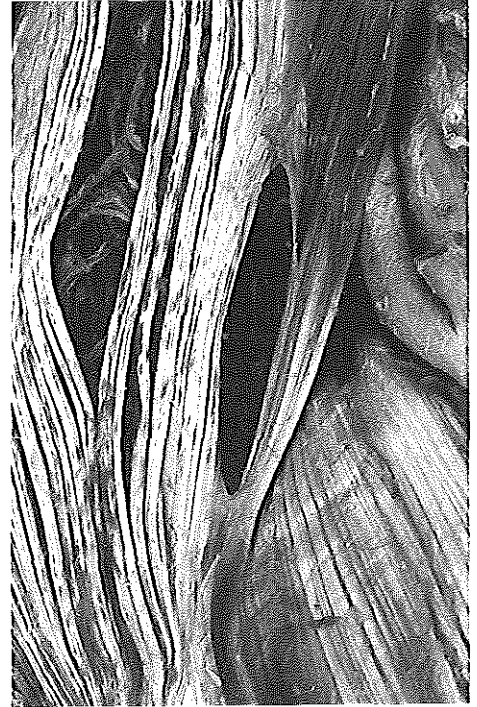


Figure 6



Figure 7



Figure 8

The morphology of perforations of aponeuroses



Figure 9

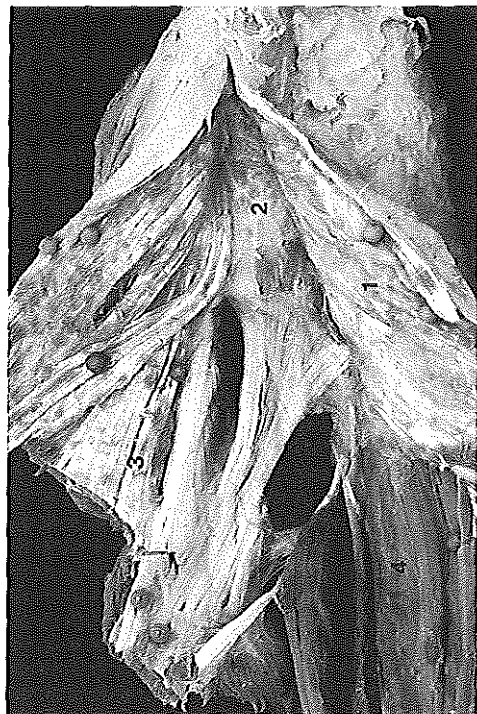


Figure 10

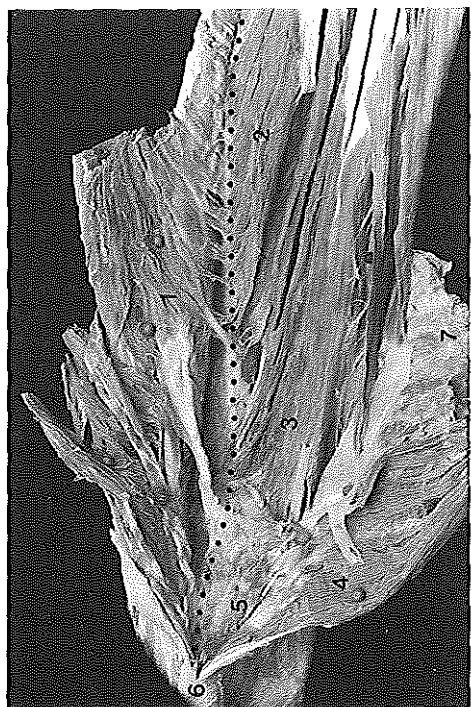


Figure 11

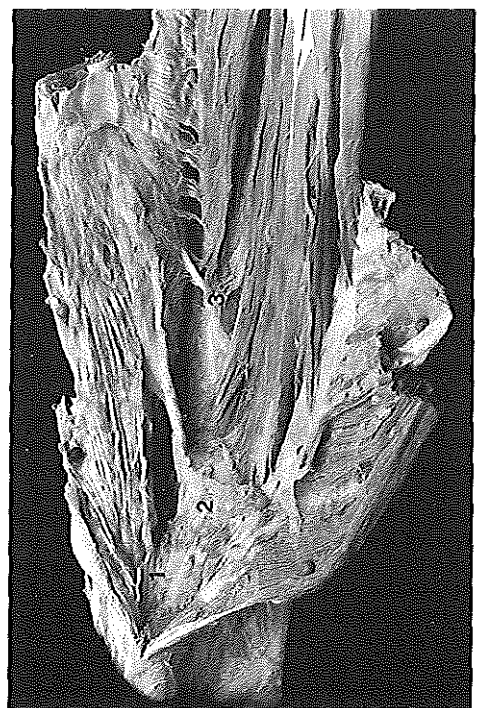


Figure 12

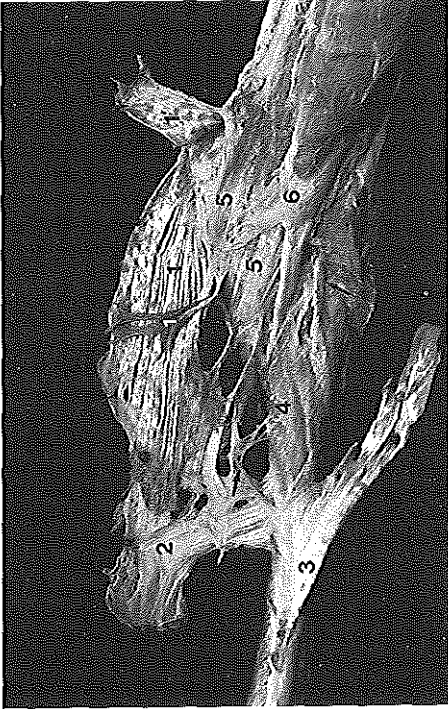


Figure 13

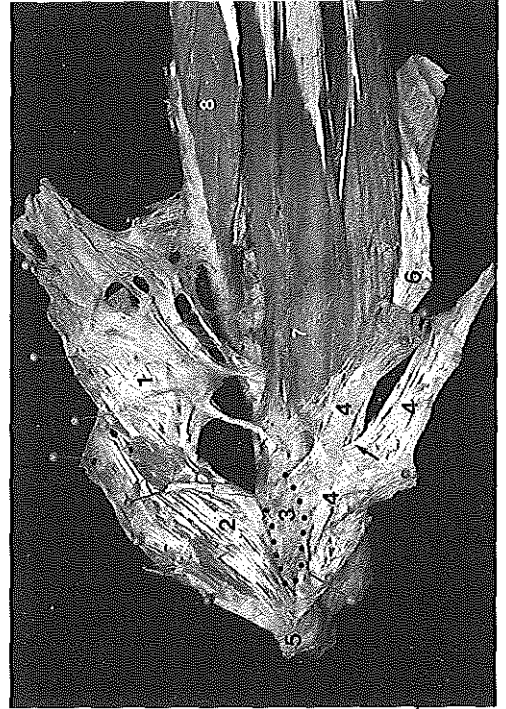


Figure 14



Figure 15

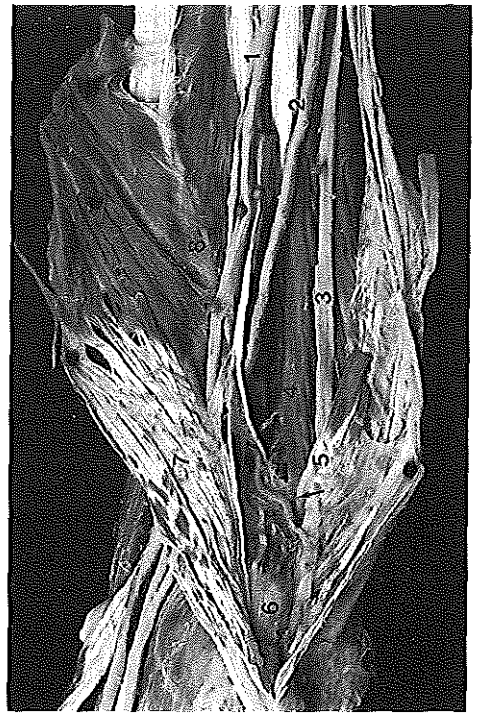


Figure 16

Captions with the figures 5 - 16

Figure 5 Median nerve (2) creating a long elliptical hole in the aponeurosis of origin of the pronator teres (4,5), with an aponeurotic muscle flap. (1): Brachialis, (2): median nerve, (3): aponeurotic muscle flap, (4,5): aponeurosis of the PT with muscle fibres removed, folded open and flattened out. The hole at (5) is a dissection artefact, and shows the FCR muscle which arises from the backside of the aponeurosis, (6): brachial artery, (7): supinating tendon of biceps, (8): muscle fibres from the PT left in situ. (9): supinator, (10): medial epicondyle.

Figure 6 Hole of fig.5 with median nerve removed.

Figure 7 Aponeurotic flap folded back upon the main PT aponeurosis. The flap fits the hole perfectly. The dotted line indicates the line of origin of the aponeurotic flap, which is continuous with the origin of the main PT aponeurosis.

Figure 8 Median nerve creating a bi-originous PT muscle belly by splitting up the PT aponeurosis. (1): PT aponeurosis, main part. (2): separated part of the PT aponeurosis with muscle fibres left intact. (3): end tendon of the PT, folded back by 180°. (4): Supinator. (5): FDS aponeurosis, with fibres originating from the medial epicondyle, and fibres originating from the radius. Arrows: hole created in the FDS aponeurosis by the intra-originous radio-ulnar joint. (6): Brachialis. (7): Median nerve. (8): Brachial artery. (9): Biceps. (10): Medial epicondyle.

Figure 9 Specimen of fig.8 with aponeurotic flap (2) folded back into the plane of the main aponeurosis (1), showing the continuous line of origin. The fibres of the aponeurosis crisscross with the end tendon fibres of the brachialis, which shows that the origin of the aponeurosis on the ulna is along and a little proximal to the insertion of the end tendon of the brachialis. (3): End tendon of the PT viewed from opposite side of fig.8.

Figure 10 Radial aponeurosis of the FDS compartment, showing two holes close to each other. (1): FDS-FCU intermuscular septum. (2): bony origin of the FDS. (3): radial aponeurosis of origin of the FDS, with perforations by median nerve (upper hole) and radial artery. (4): deep flexor.

Figure 11 Multi-originous muscle: radial aponeurosis of the FDS compartment. (1): FDS originating from the radial aponeurosis. Dotted line: continuous origin of the archetype of the radial FDS aponeurosis (compare with fig.10), which runs from the medial epicondyle towards and along the radius. (2): FPL. (3): FDP, originating from the ulna, and from the aponeuroses separating it from the FDS and FCU. (4): Part of FDS originating from the FDS-FCU intermuscular septum, and the fascia antebrachii. (5): Origin of the FDS directly from bone. (6): Medial epicondyle. (7): FCU.

Figure 12 Specimen of fig.11 with the FDS muscle fibres removed from the radial aponeurosis, showing its continuity distal to the holes. The holes separate the aponeurosis in multiple parts. (1): origin from medial epicondyle and medial collateral bands of the elbow joint. (2): Origin from the ulna. (3): Origin from the radius, with successively smaller holes. Hole (1-2): median nerve; hole (2-3): radial artery and radio-ulnar joint.

Figure 13 PT-FDS aponeurosis with medium sized successive holes for, from ulnar to radial, the median nerve, the radial artery, and the radio-ulnar joint (arrow left to (4)). (1): PT aponeurosis, distal-medial part; (1'): PT aponeurosis, humeral part proximal to the medial epicondyle. White number (1): small aponeurotic muscle flap pushed out of the PT aponeurosis by the median nerve. (2): FDS aponeurosis, which fibres from radius and ulna crisscrossing. (3): PT end tendon. (4): Supinator. (5): Brachialis. (6): Biceps. Arrow below (6): radial nerve entering the supinator.

Figure 14 Specimen of fig.13 viewed from the ulnar side. (1,2): FDS aponeurosis. (3): FDS origin from bone. (4): FDS-FCU intermuscular septum. Arrow: hole created by the ulnar nerve. (5): medial epicondyle. (6): fascia antebrachii. (7): FDP. (8): FPL.

Figure 15 PT aponeurosis with median nerve and brachial artery in situ. (1): median nerve, the smaller branch is the innervation of the FCR. (2): brachial artery with radial artery cut. This branch ran superficial to the PT, along the brachioradialis. (3): biceps tendon. (4): supinator. (5): FDS aponeurosis (the FDS originates from the back). Arrow: hole for the radio-ulnar joint (arm is pronated, hole is closed). (6): PT aponeurosis, (7): medial epicondyle, (8): Brachialis.

Figure 16 Same specimen as fig.15, viewed from within the FDS compartment. (1): median nerve. (2): ulnar artery. (3): ulnar nerve. (4): FDP. (5): FDS-FCU intermuscular septum. (6): Bony origin of FDS. Arrow: recurrent artery. (7): radial FDS aponeurosis. (8): FDS muscle fibres arising from the part of the radial FDS aponeurosis which originates from the radius.

CHAPTER VI

MODELLING THE MORPHOLOGY OF ANATOMICAL INTERCONNECTIONS IN THE M. FLEXOR DIGITORUM PROFUNDUS

**Anatomical interconnections within the M. flexor digitorum profundus - the
significance for the hand of the musician**

J.N.A.L. Leijnse, E.T. Walbeehm, G.J. Sonneveld, S.E.R. Hovius

Submitted to Anatomical Record, 1995

**Connections between the tendons of the M. flexor digitorum profundus
formed by the synovial sheaths in the carpal tunnel**

J.N.A.L. Leijnse, E.T. Walbeehm, G.J. Sonneveld, S.E.R. Hovius, J.M.G. Kauer

Submitted to Anatomical Record, 1995

**A generic model of the anatomic variability in the M. flexor digitorum
profundus, M. flexor pollicis longus, and Mm. lumbricales complex - the
significance for the musician**

J.N.A.L. Leijnse

Submitted to Anatomical Record, 1995

ANATOMICAL INTERCONNECTIONS WITHIN THE M. FLEXOR DIGITORUM PROFUNDUS - THE SIGNIFICANCE FOR THE HAND OF THE MUSICIAN

J.N.A.L. Leijnse, E.T. Walbeehm, G.J. Sonneveld, S.E.R. Hovius

Department of Plastic and Reconstructive Surgery, Erasmus University Rotterdam, The Netherlands.

ABSTRACT

The flexor digitorum profundus is the only flexor of the distal interphalangeal joints. Therefore, its good functioning is of prime importance in the musician's hand. However, often the tendons to the different fingers are anatomically strongly interconnected. This limits their independent displacements, and with it the independence of the fingers in playing. In the present paper an overview is presented of the main causes of anatomical interdependence between the deep flexors. From proximal to distal, interconnections (i) exist within the muscle bellies themselves, (ii) are caused by the cross linking of tendon fibres in the distal forearm and in the carpal tunnel, (iii) are caused by the synovial sheaths interconnecting the tendons in the carpal tunnel, and (iv) result from the tight origins of lumbricals originating from two adjacent tendons. Moreover, lumbricals which insert into two different fingers may further cause functional interdependencies. These findings are illustrated by dissection results, and the biomechanical and clinical significance is discussed.

NOTATIONS

BR : M. Brachioradialis
FCR : M. Flexor Carpi Radialis
FCU : M. Flexor Carpi Ulnaris
FDP : M. Flexor Digitorum Profundus
FDS : M. Flexor Digitorum Superficialis
FPL : M. Flexor Pollicis Longus
PT : M. Pronator Teres

INTRODUCTION

The flexor digitorum profundus is the only flexor of the distal interphalangeal (DIP) joints. In the playing of instruments such as the violin (left hand), the classical guitar (left and right hand), and the harp its use cannot be discarded, as good performance with slack DIP joints is impossible. Anatomically, however, the deep flexor tendons of the different fingers are often interconnected to the extent that the independent displacements of these tendons is limited, or even impossible. Such anatomical interconnections or their functional effects have been described by, amongst others, Fahrer (1971, 1975), Malerich et al. (1987). These limitations in independent tendon displacements can seriously affect the instrumental technique, as was shown in the models of Leijnse et al. (1992, 1993), while also a possible relationship between intertendinous connections and hand complaints such as focal dystonia in musicians have been pointed out (Markison, 1990;

Anatomical interconnections within the FDP

Stern, 1990; Leijnse^c, 1996). The force transfers resulting from anatomic interdependencies between muscles and tendons were modelled and measured in Leijnse^{a,b} (1996), where it was hypothesised that these force transfers resulted from two causes: (i) co-activation of muscle bellies to different fingers, and (ii) the stretching of passive interconnections between adjacent muscle bellies and tendons. In the present study, the main sites of the anatomical interconnections between the deep flexors, and between the deep flexors and the long flexor of the thumb are identified at the dissection table. The aim is to present a systematic overview of these connections, some indication of their variability, and to establish possible anatomical causes for the co-activations measured by Leijnse^a (1996), and Leijnse and Bonte (1996). The results show that interdependencies in the normal hand can be present at following levels: (i) within the muscle bellies; (ii) between the tendons in the forearm, (iii) in the carpal tunnel, where they are caused by crisscrossing tendon fibres and adhesive synovial sheaths, and (iv) in the proximal midhand as caused by tightly interconnected bi-tendinous origins of lumbrical muscles, while also malinserting lumbrical muscles are frequent. Each of these sites is documented by photographs of typical dissection results. The present paper is complemented by two further studies by the same authors, one of which proposes an explanation for frequent adherence of the synovial sheaths to the flexor tendons in the carpal tunnel (Leijnse et al., 1996), while the second provides a comprehensive model of the morphology of the anatomic variability in the FDP-FPL-LU complex (Leijnse^d, 1996).

MATERIAL AND METHODS

The photographs of which the further data consist are representative samples of the dissections of some 20 embalmed arms.

RESULTS

Gross description of the skeletal and aponeurotic origins of the FDP and FPL

The *M. flexor digitorum profundus* (FDP) and the *M. flexor pollicis longus* (FPL) form a continuous muscle layer which occupies, proximal to the *M. pronator quadratus*, the entire ventral surface of the radius, the *membrana interossea*, and the volar and ulnar side of the ulna, except for the most proximal area which is occupied by the *M. flexor digitorum superficialis* (FDS) (figs.1 and 2). Ulnarly and proximally, the origin of the deep flexor continues on the fascia *antebrachii*, where it is volarly delimited by the *M. flexor carpi ulnaris* (FCU) (fig.3). The FCU derives its entire origin from aponeuroses, which proximally form a closed compartment. The outer wall of the FCU compartment is the fascia *antebrachii*; the radial wall is the intermuscular septum separating it from the FDS (line 2-3, fig.2), while proximally and deeply it is separated from the FDP by a variable intermuscular septum (line 1-3, fig.2), from which the FDP may draw some additional fibres. At the fascia *antebrachii*, the aponeurotic origins of FDP and FCU are composed of clearly distinguishable longitudinal tendon fibres, which lie deep to the transverse fibres of the fascia *antebrachii*, and which originate from a bony line on the medial-dorsal border of the proximal half of the ulna (lines 1-4, 3-4, and 3-9 in fig.2). The deep flexor can be palpated

between FCU and the ulna (fig.4). Only in the proximal part of the palpable origin between the ulna and the FCU the muscle fibres actually arise from the fascia antebrachii (fig.4). By the proximal expansion of the muscle body along the medial surface of the ulna and the fascia antebrachii, the greater part of the FDP is positioned ulnarly in the forearm, with the index tendon arising from the membrana interossea, i.e. approximately at the midline of the distal forearm. Anatomically, the FDP and FPL are named separately. However, they form a clear morphological unit, similar in aspect and course up to the end of the carpal tunnel. Their usual physical separation is the deep A. and N. interosseus antebrachii anterior, but it is not uncommon to find the nerve and artery running through the base of the FDP₂ muscle belly, or through the base of the FPL muscle belly, so that the FDP₂ and FPL muscles are truly adjacent. As shown further, the morphological similarity between the FDP and FPL is reflected in their intertendinous connections, which are of a similar nature as the connections between the FDP tendons themselves.

Gross description of the muscle bellies and end tendons

The gross aspect of the deep flexor muscle is simple and constant. From the extensive origins, muscle fibres of about 6-7 cm in the normal adult (Brand, 1985) run more or less parallel distalwards to their end-tendons (fig.3). These end tendons pass through the carpal tunnel, distal to which they give rise to the lumbrical muscles, and spread out to the different fingers. Anatomically, the deep flexor tendons are constant; missing, malformed or malinserting tendons are rare, this in contrast to e.g. the superficial flexor of digit V (Austin et al, 1989). The striking constructive similarity of the FDP of all fingers, including the thumb, contrasts strongly with the complex structure of the superficial flexor, which is partly digastric (Brand, 1985) (fig.3). In contrast to the constant gross structure of the deep flexor, the lumbrical muscles are highly variable. Lumbricals inserting in different fingers, or in the wrong finger, or absent lumbrical muscles are not rare (Perkins and Hast, 1993). Also highly variable is the anatomic independence of the muscle bellies and end tendons to the individual fingers. Anatomically independent are further called deep flexors of which the muscle bellies can be easily and completely separated by blunt dissection, and of which the tendons run independently in their entire course.

Anatomic interdependence of the FDP muscle bellies and the end tendons in the forearm

The origin area of the FDP is rather long and narrow. Of this origin area the muscle belly to each finger occupies a long and narrow stretch. In the muscle belly, the end tendons arise as proximally as the fibre length distance from the most proximal origin of muscle fibres. The following anatomical variants are regularly found.

Completely independent muscle bellies (fig.5). Completely independent muscle bellies consist of regularly arranged parallel muscle fibres. These muscle fibres arise from a well delineated origin area, from which no muscle fibres to other end tendons arise, and insert into a single, well formed end tendon plate, which becomes more or less cylindrical in its distal course. Such independent muscle bellies have an interface of well mobilised connective tissue, and can easily be separated by blunt dissection, except for the nerves and vessels running between them.

Fig.6 shows that even between fully independent muscle bellies nerves and vessels, also remarkably thin ones, may frequently cross over. When these muscle bellies are pulled upwards by lifting the end tendons parallel to the ulna, they stretch into parallelogram shaped homogeneously thin muscle blades consisting of parallel fibres (Brand, 1985) (fig.6). In the rare case (one personal undocumented observation), all muscle bellies and end tendons are completely independent. The case of two fully independent muscle bellies, of the thumb and index, is most common, although also these muscle bellies are regularly interdependent.

Interdependent muscle bellies. The FDP to the ulnar three fingers regularly present as a unit, in which the muscle bellies to the different fingers are highly interconnected with connective tissue, and cannot be clearly outlined. This has the following causes.

(i) The tendons do not arise as independent, thin, homogeneous tendon blades, but as collections of many thin tendon fibre strands more or less loosely interconnected by connective tissue into tendon blades (figs.7,8). Such tendon strands may crisscross between end tendons, or may split up to insert into different end tendons (fig.10, white 3). An example of extensively crisscrossing tendon fibres is shown in fig.7. In this specimen, a substantial part of the strands to the third finger cross over to insert into the FDP₄ at the level of the lumbrical origins. Different tendons may even present as a tendon plate in which the strands running to the same finger can be barely identified as individual units. In a few undocumented specimens, the ulnar three tendons formed a single, inseparable tendon blade.

(ii) Muscle fibres inserting crisscross into different end tendons. The dissection of such muscle bellies reveals isolated packs of muscle fibres which are themselves highly interconnected by connective tissue, but which are as a whole somewhat less connected to adjacent muscle fibre packs. Muscle fibres from such packs may insert into different end tendon strands running to end tendons of different fingers. The highly interconnected muscle fibres in such a pack may be assumed to be activated together, even if inserting into strands to different fingers. An example is presented in fig.10 (which is a detail of fig.9), and fig.11.

Interconnections between the FDP tendons caused by the synovial membranes in the carpal tunnel

In the carpal tunnel, the deep flexor tendons run deep and somewhat ulnarly to the superficial flexor tendons. At the entry of the carpal tunnel the deep flexor tendons are often distinctly fibrous, or even present as mere collections of fibrous strands (figs.12-16). In contrast, the superficial flexor tendons generally are smooth and cylindrical, like the flexor tendons in the finger itself (Leijnse et al., 1996). Within the short length of the carpal tunnel, the deep flexor tendons, however disassembled and crisscrossing they may be at the entry, transform into round, compact and smooth finger tendons. The figs.12-16, especially fig.13, show that the required structural reorganisation can be quite spectacular. Within the carpal tunnel all flexor tendons are enveloped by thick masses of synovial sheaths. These consist of multiple layers of thin synovial membranes, which present in their totality as a thick opaque mass. The synovial membranes frequently adhere to the deep flexor tendons themselves. They may then form strong and tight connective membranes, which can interconnect the deep flexor tendons to the different fingers

over distances of centimeters, sometimes from the proximal end of the carpal tunnel up to and including the lumbrical origins (fig. 18). Even if these membranes are thin, the combined strength of their continuous insertion in the tendons is well able to resist large forces, especially since the opposite displacement of the connected tendons will generally tauten all connecting membrane fibres at the same time. This is illustrated by the FDP₄-FDP₃ connections in fig.18, which shows within these synovial membranes regular parallel transversely running tendinous fibres. The strong adhesion of the synovial sheaths to the tendons is paradoxal, as in principle these sheaths serve to improve independent tendon gliding. In Leijnse et al. (1996) it is argued that the synovial sheaths are trapped between the individual tendon strands which make up the tendons. The synovial interconnections are infrequent between tendons which are cylindrical and smooth, such as the superficial flexor tendons, the long thumb flexor, or even well-shaped smooth deep flexor tendons, such as regularly the index tendon.

Individual tendon strands dissolving into the synovial membranes

Another frequent morphological phenomenon in the carpal tunnel is that tendon strands which run isolated from the main tendons seem to dissolve in the synovial sheaths (Fahrer, 1975). A typical example is presented in fig.18, which shows a thick tendon strand gradually disintegrating in its distal course into large numbers of minute tendon fibres, which are too small to be macroscopically detected within the synovial sheaths. The majority of these fibres join the FDP₄, a lesser part inserts into the FDP₃, and the remainder continues as tendon fibres of origin for lumbrical muscle fibres. The dissolution of such tendon strands corresponds to the reorganisation of the tendon strands of the main FDP tendons into well-defined finger tendons. The tendon fibres leaving the individual strands may run quite parallel to the main tendons, and further strengthen the interconnecting synovial membranes.

The origins of the lumbrical muscles

Distal to the carpal tunnel the lumbrical muscles arise from the deep flexor tendon mass, or from the tendon strands from which these tendons consist. Close observation reveals that the lumbrical muscle fibres arise from tendon fibres of origin which split off from the main tendons, and which can sometimes be traced proximally up to the FDP muscle bellies, especially in very loosely assembled tendon strands. The fact that tendon fibres of the deep flexor tendons give rise to, and therefore end into lumbrical muscle fibres implies that the FDP tendons are thicker proximally to the lumbrical origins than distally. The existence of proper tendon fibres of lumbrical origin is shown in figs.15 and 16. In fig.16 tendon fibres of origin are dissected out of the main tendon; in fig.15 the tendon strands of origin were naturally preformed. In compact, round and smooth tendons, such as usually the FDP₂, the lumbrical muscle fibres arise directly from an apparently smooth tendon surface. However, close dissection of such a tendon revealed tendon fibre strands dissolving beneath the surface of lumbrical origin into minute tendon fibres, which then break through the tendon surface to give rise to lumbrical muscle fibres of microscopic thickness. These combine into muscle fibre strands which can be macroscopically observed. Occasionally, an isolated tendon strand almost exclusively gives rise to part of a lumbrical muscle, which then

forms a true digastric muscle part (fig.17). In Leijnse^d (1996) it is hypothesised on theoretical grounds that even from such isolated tendon strands of lumbrical origin, quantities of tendon fibres, however minute, are likely to separate to join the FDP tendons. In fig. 17 such small strands are present. The origins of the lumbricals may be mono-tendinous, or bi-tendinous. The origins may also span continuously from one FDP tendon to another, bridging the intertendinous space. Within the intertendinous spaces, the lumbrical muscle fibres then arise from independent tendon strands (LU₃ and LU₄ in fig.13), or from what may appear to be the synovial sheaths themselves (LU₄ in fig.12). However, in the latter case the lumbrical muscle fibres to all probability arise from dissolved FDP tendon fibres within the synovial sheaths (Leijnse^d, 1996). The lumbrical origins, and their proximal muscle bodies are enveloped by the synovial sheaths, together with the tendons from which they arise. Frequently, the ulnar three FDP tendons are so interconnected by synovial sheaths and crisscrossing tendon fibres that the radial, ulnar, and intermediate lumbrical origins are an inseparable entity (figs. 15 and 16). However, sometimes the radial and ulnar heads of origin are independent and continue into the lumbrical body with a distinct V-shape (fig.12). Such a V-shape would allow a relative displacement of the FDP tendons of origin equal to $2*(L_{VR}+L_{VU})$, with L_{VR} and L_{VU} the contraction lengths of the free running radial or ulnar heads. In Leijnse and Bonte (1996), a case study is presented of a musician whose FDP tendon independence was increased by severing the connective synovial membranes and deepening the free V insertion of the radial and ulnar lumbrical heads without loss of function.

Tendon strands crisscrossing between the FDP tendons in the carpal tunnel

Tendon strands frequently crisscross between the FDP tendons proximal to the lumbrical insertions. Such crisscrossing tendon strands interconnect donor and receptor tendons, and limit their relative displacement in one way or the other. Figs. 7 and 8 show tendon strands crossing mainly from the FDP₃ and FDP₅ to the FDP₄. This was found the predominant direction of cross-insertions by Fahrer (1971). Fig. 12 shows strands crossing in the opposite direction, from FDP₄ to FDP₅ and FDP₃, and from FDP₃ to FDP₂. Fig. 15 shows strands crisscrossing between the FDP₃ and FDP₄ tendons.

Connections between the FPL and FDP

Tendinous connections between the FPL and the FDP of the index have been amply reported (e.g. Lindburg and Comstock, 1979; Blair and Omer, 1981; Rico Aguado and del Pino Paredes, 1988). These connections usually run from proximally the thumb flexor to distally the deep flexor of the index. The sheaths may also interconnect the FPL and FDP by adhering to both these tendons, forming connections similar to those between the FDP tendons themselves. Figs. 8 and 14 present examples of tendinous and synovial connections simultaneously present between the FPL and the FDP₂. Fig. 12 presents a connection formed by an independent muscle body which derives from the area of origin of the FPL, and which is strongly connected to the FPL by synovial membranes, before inserting into the FDP₂ tendon. With such connections, the index and/or other fingers will flex conjoinedly when the thumb is flexed with active FPL. Both the connections between the FPL and FDP, and between the FDP themselves consist of tendinous cross-overs as

well as synovial membranes, and have a morphological similar aspect. This indicates that anatomically the FPL and the FDP form a unity, i.e. the five muscles of a general deep flexor group. This is further emphasized by the fact that the first lumbrical occasionally arises bi-tendinously from both the FPL and FDP₂ (Goldberg, 1970), as if the FPL tendon were just another deep flexor tendon.

Bi-insertional and malinserting lumbricals

Perkins and Hast (1993) report in a sample of 80 hands that about half of the lumbricals were abnormal, with 34% of the third lumbricals inserting into both the third and fourth finger. These conclusions agree with our own dissection results, in which the incidence of abnormalities was even higher, but in a small sample (20). Examples of bi-insertional lumbricals are LU₃ in figs. 3, 13, 14 and 16. In fig. 15 LU₃ inserts exclusively in the third finger, instead of in the fourth. No correlation was apparent between the relative size of the radial and ulnar heads of origin, and the relative size of the insertions in the bi-insertional lumbricals.

DISCUSSION

Anatomical variability in the FDP-FPL-LU complex

Fahrer (1971), and others, distinguish in the deep flexor complex three independent units: the FPL, the FDP₂, and a "common muscle" comprising the FDP₃-FDP₅. Such a distinction, however, makes abstraction of the overall homogeneity of this muscle complex. First, the FDP₂ and even the FPL are not always completely independent, and the causes of their lack of independence are morphologically identical to those of the FDP₃-FDP₅ tendons: crossing tendon strands, tendinous-synovial interconnections, crisscross insertions of muscle fibres in tendons of different fingers. Also, in our measurements *in vivo*, with the measuring device of Leijnse^b (1996), sometimes the FDP₃-FDP₄ are found more independent than the FDP₂-FDP₃. Therefore, a more realistic view seems that of a muscle group giving rise to five tendons, and in which the causes of interdependence of tendons and muscle bellies are incorporated as a fundamental property, the manifestation of which can be expressed in statistical terms. Such a view is presented in the model of the FDP-FPL-LU complex of Leijnse^d (1996), to which the present paper is intended as a factual introduction. In mentioned model the interdependence of the individual motors in the group is considered the result of a "degree of disorder" in the arrangement of their muscle-tendon fibre material. This degree of disorder consists of the deviation of the strict parallelism of the muscle-tendon fibres in the muscle group, which results in a crisscrossing of muscle and tendon fibres. The generally decreasing independence of the motors from radially to ulnarly then correlates with the increasing degree of disorder in the parallel arrangement of individual muscle-tendon fibres in the muscle group. Morphological phenomena of tendons dissociating and re-arranging in the carpal tunnel are in this model described in similar simple terms. Within such a generalised view, anatomical variations limiting motor independence in the deep flexor group, even when rare, cannot be seen as anomalies, but merely as the chance occurrence of a predictable pattern of "ordering" of the muscle fibre material of the muscle group.

ACKNOWLEDGEMENTS

The author cordially thanks Dr. J. Zguricas for assistance in dissections; Prof. Emer. Dr. J.M.F. Landsmeer, Prof. Emer. Dr. J.C. van der Meulen, Prof. Dr. Ir. C.J. Sniijders, and Prof. Dr. J. Voogd, for the discussion of the material, and C. Entius and J. Velkers, custodians of the dissection theatre, and E. Dalm and P. Smaal, photographers, for their kind support.

REFERENCES

- Austin, G.J., Leslie, B.M., Ruby, L.K. (1989) Variations of the flexor digitorum superficialis of the small finger. *Am. J. Hand Surg.* 14, 262-267.
- Blair, W.F., and Omer, G.E. Jr. (1981) Anomalous insertion of the flexor pollicis longus. *Am. J. Hand Surg.* 5, 548-549.
- Brand, P.W. (1985) *Clinical mechanics of the hand.* pp. 257-268. The C.V. Mosby Company, St. Louis, USA.
- Fahrer, M. (1971) Considérations sur l'anatomie fonctionnelle du muscle fléchisseur commun profond des doigts. *Ann. Chir.* 25, 945-950.
- Fahrer, M. (1975) Considérations sur les insertions d'origines des muscles lombricaux: les systèmes digastriques de la main. *Ann. Chir.* 29, 979-982.
- Goldberg S., (1970) The origin of the lumbrical muscles in the hand of the south african native. *The hand* 2, 168-171.
- Leijnse, J.N.A.L., Bonte, J.E., Landsmeer, J.M.F., Kalker, J.J., van der Meulen, J.C., Sniijders, C.J. (1992) Biomechanics of the finger with anatomical restrictions - the significance for the exercising hand of the musician. *J. Biomechanics* 25, 1253-1264.
- Leijnse, J.N.A.L., Sniijders, C.J., Landsmeer, J.M.F., Bonte, J.E., van der Meulen, J.C., Sonneveld, G.J., Hovius, S.E.R. (1993), The hand of the musician - the biomechanics of the bidigital finger system with anatomical restrictions. *J. Biomechanics* 26, 1169-1179.
- Leijnse^a, J.N.A.L. (1996) Measuring anatomical interconnections in the deep flexors of the musician's hand: theoretical analysis, clinical examples. Submitted *J. Biomechanics*, 1995.
- Leijnse^b, J.N.A.L. (1996) Measuring anatomical interconnections in the deep flexor of the musicians' hand - device and systematic measuring errors. Accepted *J. Biomechanics*, 1995.
- Leijnse^c, J.N.A.L. (1996) Anatomical factors predisposing to focal dystonia in the musician's hand - principles, theoretical examples, clinical significance. Resubmitted to *J. Biomechanics*, 1995.
- Leijnse^d, J.N.A.L. (1996) A generic model of the anatomic variability in the M. flexor digitorum profundus, M. flexor pollicis longus and MM. lumbricales complex - the significance for the hand of the musician. Submitted to *Anatomical Record*, 1995.
- Leijnse, J.N.A.L., and Bonte, J.E. (1996) Total clearance of intertendinous connections and surgical cleavage of the lumbrical origins in a musician's hand - a case study. To be submitted, 1995.
- Leijnse, J.N.A.L., Walbeehm, E.T., Sonneveld, G.J., Hovius S.E.R. (1996) Anatomical interconnections between the tendons of the M. flexor digitorum profundus formed by the synovial sheaths in the carpal tunnel. Submitted to the *Anatomical Record*.
- Linburg, R.M., and Comstock, B.E. (1979) Anomalous tendon slips from the flexor pollicis longus to the digitorum profundus. *Am. J. Hand Surg.* 4, 79-83.
- Malerich, M.M., Baird, R.A., McMaster, W., and Erickson, J.M. (1987) Permissible limits of flexor digitorum profundus tendon advancement - an anatomic study. *Am. J. Hand Surg.* 12, 30-33.
- Markison R.E. (1990) Treatment of musical hands: redesign of the interface. *Hand Clinics* 6, 525-544.

Chapter VI.i

- Perkins, R.E., and Hast, M.H. (1993) Common variations in muscles and tendons of the human hand. *Clinical Anatomy* 6, 226-231.
- Rico Aguado, A., and del Pino Paredes, V. (1988) Flexor digitorum profundus common to thumb and index finger, associated with a post-traumatic distal adherence of both tendons. *J. Hand Surg.* 13B, 72-74.
- Stern, P.J. (1990) Tendinitis, overuse syndromes, and tendon injuries. *Hand Clinics* 6, 467-476.

FIGURES

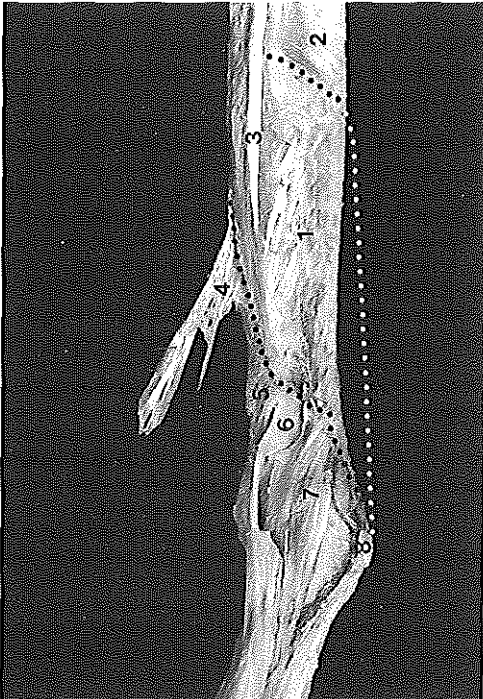


Figure 1

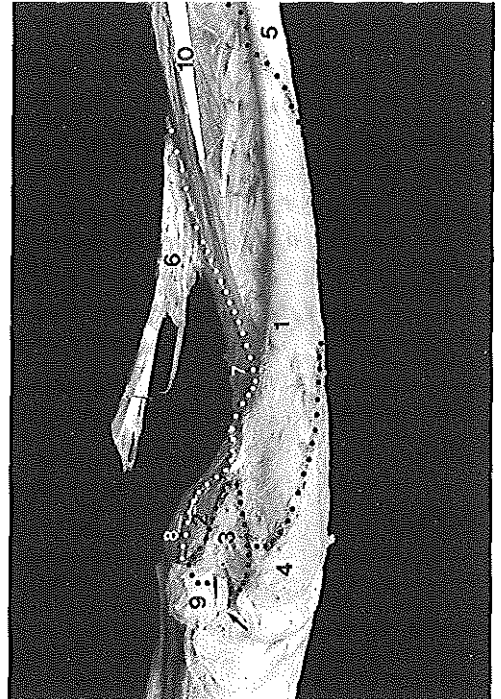


Figure 2

Anatomical interconnections within the FDP

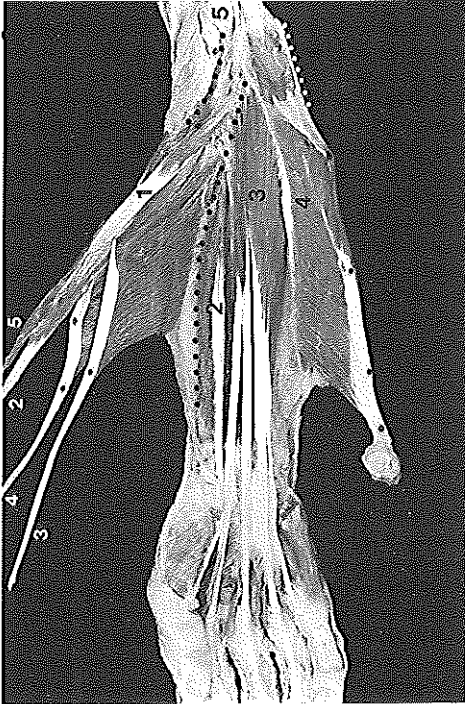


Figure 3

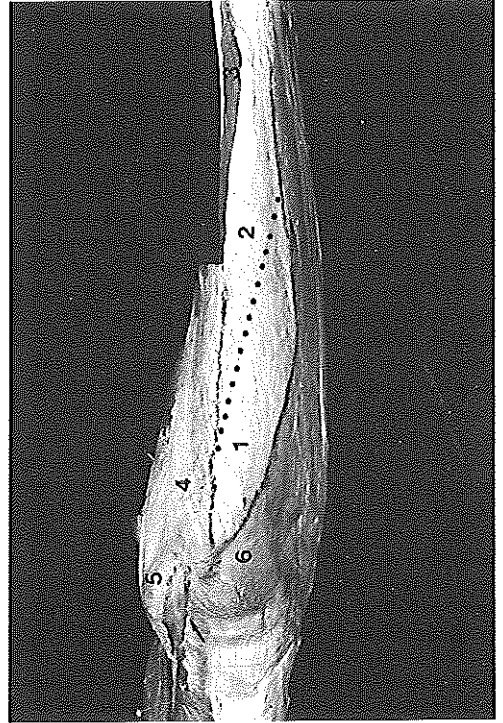


Figure 4



Figure 5

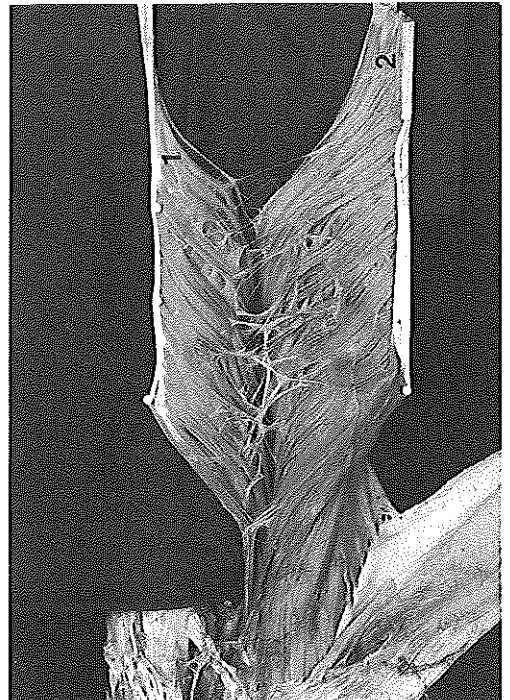


Figure 6



Figure 7



Figure 8



Figure 9

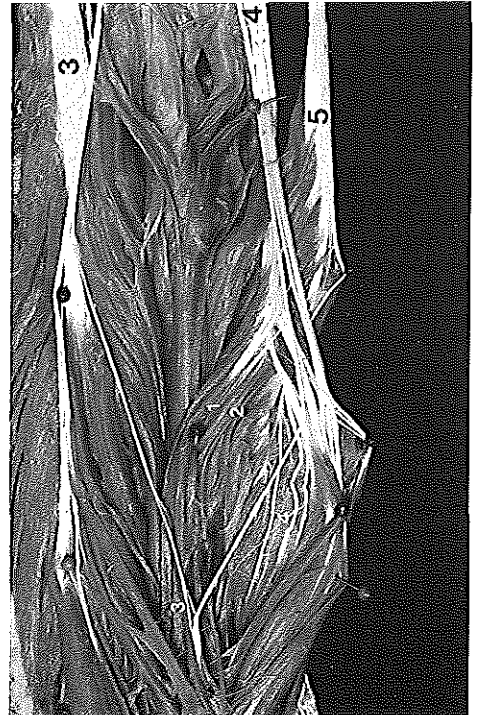


Figure 10

Anatomical interconnections within the FDP

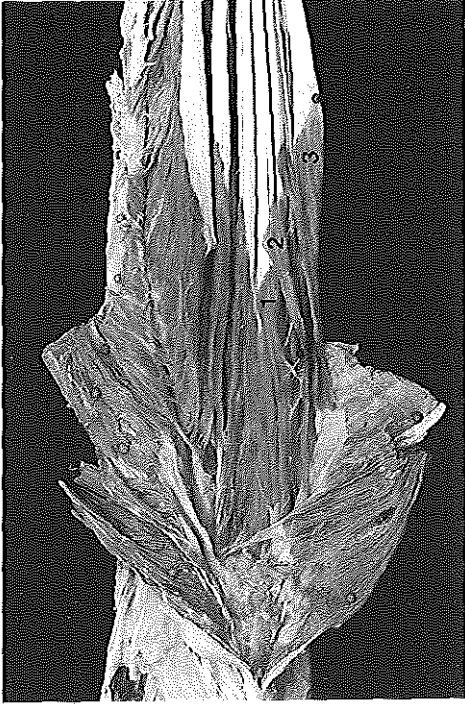


Figure 11

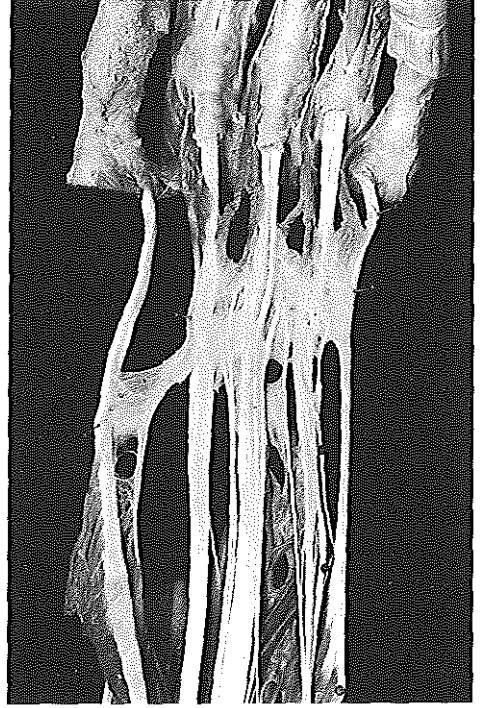


Figure 12



Figure 13

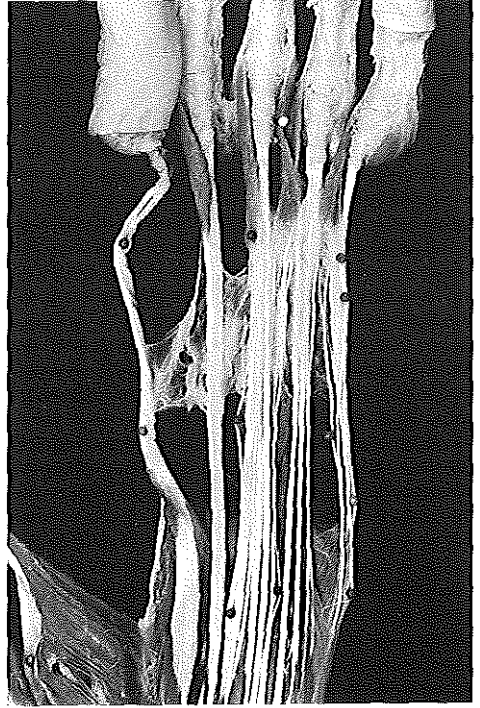


Figure 14

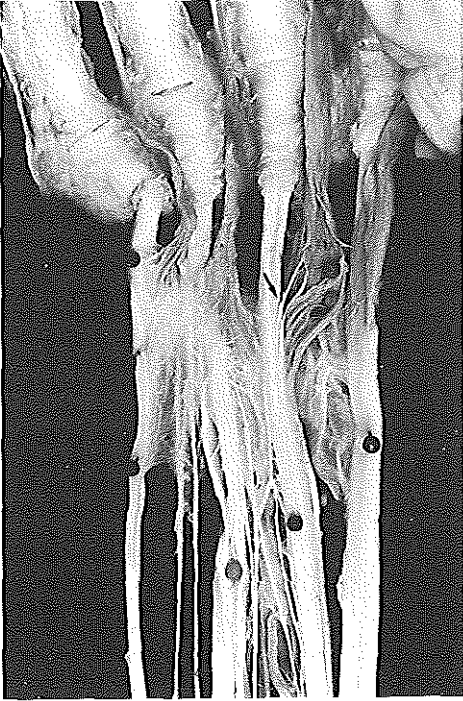


Figure 15

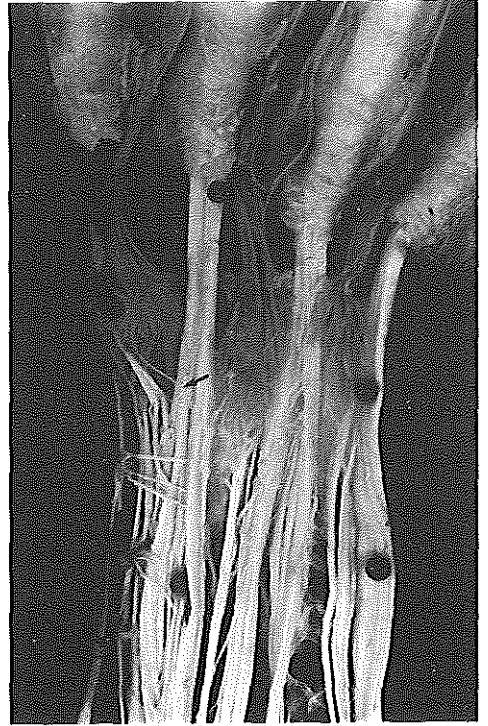


Figure 16



Figure 17



Figure 18

Captions with the figures

Figure 1 Origins of the FDP and FPL, volar view. Black dotted line: delimitation of origin area on bone. White dotted line: profile outline of the FDP. Proximally, a part of the bulging mass of the FDP arises from the fascia antebrachii. 1: FDP origin. 2: Pronator quadratus. 3: FPL. 4: PT end tendon. 5: Supinator. 6: Supinating tendon of biceps. 7: Brachialis. 8: medial epicondyle.

Figure 2 Origins on bone, and lines of origin of the aponeuroses of origin of the FDP, FPL, FDS, and FCU. The dotted lines are further referenced by the numbers of the bony areas they separate. 1: bony origin of the FDP. 2: bony origin of the FDS. 3: bony origin of the FCU. 4: subcutaneous medial-proximal ulna. 5: subcutaneous distal ulna. 6: end tendon of the PT inserting in radius. 7: Supinator, radial insertion. 8: end tendon of the brachialis. 9: medial facet of the medial epicondyle. 10: flexor pollicis longus with muscle fibres left intact. Dotted lines 1-4, 3-4, 3-9: origins of the aponeurotic tendon fibres of origin of the FDP and FCU within the fascia antebrachii. Line 1-3: origin of the FDP-FCU intermuscular septum. Line 2-3: line of origin of the FDS-FCU intermuscular septum. Line 2-8: origin of the FDS-PT intermuscular septum. Line 1-6, 1-7: origin of the radial FDS aponeurosis. Line 1-5: line marking the distal border of the FDP origin on the ulna. Arrow (beneath 9): ulnar nerve leaving the cubital tunnel and entering the compartment of the FCU.

Figure 3 Specimen 1. Overview of the deep flexor group of the forearm. The central black dotted line delineates the radial origin of the FPL. The black dotted line at the medial epicondyle (5) (with the cut end of the ulnar nerve proximally exposed) and the white dotted line at the bottom are corresponding sides of the incision to open up the fascia antebrachii, which is folded back by 180°, showing that the FCU (4), with pisiform bone at end tendon, arises completely from the fascia antebrachii. The black numbers are: 1: FDS, central tendon of digastric part. 2: FPL. 3: FDP; a substantial part of the proximal-ular muscle belly originates from the fascia antebrachii. White numbers: 2: FDS₂, distal head. 3: FDS₃. 4: FDS₄. 5: FDS₅, distal head. The third lumbrical inserts bipennately; the fourth lumbrical inserts into the fourth finger, instead of the fifth.

Figure 4 Specimen 2. Palpable parts of the FDP. 1: origin of the FDP from the fascia antebrachii. Dotted line 1-2: distal border of the origin of the FDP muscle fibres; this line is variable. The FDP origin may continue proximally deep to the FCU compartment on the variable FDP-FCU intermuscular septum. 2: palpable FDP muscle fibres distal to the aponeurotic origin. The distal longitudinal fibres of the fascia antebrachii, removed in the picture to expose the FDP muscle, continue in situ to give serve as origin for the distal muscle fibres of the FCU. 3: FDP muscle exposed. 4: FCU, distally cut to expose the FDP muscle belly. 5: medial epicondyle. 6: subcutaneous ulna. Arrow: ulnar nerve in open cubital tunnel, entering the FCU compartment. Lines 1-4 and 2-4: separation of FCU and FDP. Line 1-6: ulnar origin of the longitudinal fibres of the fascia antebrachii.

Figure 5 Specimen 3. Independent muscle bellies of FPL (1) and FDP₂ (2). 3: FDP₃, FDP₅ tendons. 4: FCU. 5: FDS.

Chapter VI.i

Figure 6 Specimen 4. Independent FDP₂ (1) and FDP₃..FDP₅ (2) muscle bellies with nerves and vessels intact. Nerves and vessels enter the muscle fibres halfway; very small nerves cross between the separated muscle bellies. These muscle bellies were more strongly connected by connective tissue than those in the specimen of fig.5.

Figure 7 Specimen 5. Deep flexor group with spread-out tendons. Extensive origins from the fascia antebrachii. Tendons of the FDP₃..FDP₅ consist of tendon strands which in situ form a loosely interconnected tendon strand plate. The FDP₂ tendon is well shaped. A fibrous-synovial membrane interconnects the FPL and FDP₂.

Figure 8 Specimen 6. Similar view as fig.7. The FCU is left in situ. FPL-FDP₂ connection, stronger than in fig.7. The muscle bellies of the FDP₄ and FDP₅ have been separated by blunt dissection up to the ulna. Although the muscle bellies were strongly interconnected by connective tissue, such separation was well feasible.

Figure 9 Specimen 7. Dissected and separated muscle bellies of FDP₃..FDP₅, total view. Details in fig. 10 and fig.12.

Figure 10 Specimen 7, detail. White 1,2: muscle fibres from the same muscle pack inserting in tendon strands running to fourth (1) and fifth (2) fingers. White 3: tendon strand splitting up and inserting into both the FDP₃ and FDP₄ tendons. White 4: muscle fibres from the same pack inserting in FDP₄ and FDP₅ tendons. Black 3,4,5: FDP₃..FDP₅ tendons.

Figure 11 Specimen 8. Muscle fibres from the same pack inserting into different end tendons. The three FDP₃..FDP₅ tendons consist of four identifiable tendons, and some tendon strands. The three muscle packs (1,2,3) all insert in two adjacent tendons at the same time, which shows that at least one of these packs inserts into tendons to different fingers.

Figure 12 Specimen 7, detail of end tendons. An independent muscle belly arises from the FPL origin and inserts in the FDP₂ tendon, while its end tendon is proximally strongly connected to the FPL tendon by synovial membranes.

Figure 13 Specimen 6, detail of end tendons. Within a distance of less than 2 cm, the chaotic collection of tendon strands entering the carpal tunnel changes into three well formed end tendons. The third lumbrical is bi-insertional, the fourth lumbrical inserts in fourth finger. The synovial membranes interconnecting the FDP₂ and FDP₃ have been removed.

Figure 14 Specimen 5, detail of end tendons. Fibre strands cross over from the FDP₃ and FDP₅ to the FDP₄. The third lumbrical is bi-insertional.

Figure 15 Specimen 4, detail of end tendons (top: little finger). Tendon fibre strands crisscross between the FDP₃ and FDP₄. The arrow indicates a tendon strand of origin of the lumbrical. The third lumbrical inserts in the fourth finger.

Anatomical interconnections within the FDP

Figure 16 Specimen 9, FDP₃..FDP₅. Crisscrossing tendon fibres and strands interconnect the tendons into a plate. In the FDP₃, the tendons of origin of the second lumbrical have been dissected (arrow). The third lumbrical is bi-insertional.

Figure 17 Specimen 10, FDP-LU complex (FDP₂; lower tendon). White 1: independent tendon of lumbrical origin. A small strand splits off just before the lumbrical fibres arise, and joins the FDP₂ tendon.

Figure 18 Specimen 11, FDP-LU complex. Well formed FDP tendons, but strongly interconnected by synovial membranes. The synovial membranes between FDP₄ and FDP₅ (bottom) are reinforced by thin transverse tendon fibres. The tendon strand between FDP₃ and FDP₄ represents the opposite phenomenon of fig.17: it ends abruptly *before* the lumbrical muscle arises. Clearly visible is that the strand dissolves into minute tendon fibres which join the FDP₄ tendon, while a small remainder continues to give rise to lumbrical muscle fibres.

CONNECTIONS BETWEEN THE TENDONS OF THE M. FLEXOR DIGITORUM PROFUNDUS FORMED BY THE SYNOVIAL SHEATHS IN THE CARPAL TUNNEL

J.N.A.L. Leijnse[‡], E.T. Walbeehm[‡], G.J. Sonneveld[‡], S.E.R. Hovius[‡], J.M.G. Kauer^{*}

[‡]Department of Plastic and Reconstructive Surgery, Erasmus University Rotterdam, The Netherlands; ^{*}Dept. of Anatomy and Embryology, University of Nijmegen, The Netherlands.

Submitted to Anatomical Record

ABSTRACT

In the carpal tunnel anatomical interconnections between the tendons of the M. flexor digitorum profundus are systematically present. In present paper it is shown that these interconnections are formed by the synovial sheaths. A model is put forward to explain this anatomic phenomenon, and why such interconnections generally do not exist between the tendons of the M. flexor digitorum superficialis. The model is validated by dissection results, and cross-sections of the flexor tendons in the carpal tunnel.

NOTATIONS

FPL : Flexor pollicis longus

FDP₂..FDP₅ : Flexor digitorum profundus of index (2) to little finger (5), resp.

FDS₂..FDS₅ : Flexor digitorum superficialis of index to little finger

FCR : flexor carpi radialis

PL : Palmaris longus

INTRODUCTION

In this paper the synovial sheaths in the carpal region are investigated as anatomical causes of systematic and strong interconnections between the deep flexor tendons, including the FPL (Fahrer, 1975; Leijnse et al., 1996; Stern, 1990). The classical notion of synovial sheaths is of a two-layered concentric structure surrounding the tendon. The inner layer adheres to the tendon, and is connected by areolar tissue to the outer layer which adheres to the environment. These layers glide relative to each other, and the loose connective tissue between them is stretched only with larger than physiological tendon displacements. The function of the sheaths is the reduction of friction of the tendons relative to the fixed environment or other tendons, and they are constructed such that nerves and vessels can safely reach the tendons. Within the carpal tunnel, however, this simple picture is hard to recognise, because the synovial sheaths present as a substantial mass consisting of many layers of thin membranes. These layers are well attached to the environment, proximal and distal to the carpal tunnel. These attachments keep the sheaths stretched and prevent them from wrapping up as a dot around the tendons. In order to distinguish them from the "classic" two-layered tendon sheaths, the synovial sheaths in the carpal region will be further referred to as "synovial membranes". The membranes envelop the tendons in the carpal

FDP interconnections formed by the synovial sheaths

tunnel at different levels: (i) all flexor tendons together; (ii) each flexor group separately (FDP, FDS, FPL); (iii) the individual tendons. A curious fact, but of grave importance to the musician, is that the synovial membranes in the carpal tunnel frequently and massively adhere to the deep flexor tendons. In doing so, they may form strong connections between adjacent deep flexor tendons, consisting of multiple layers of membranes which adhere to both tendons over distances of centimetres. The combined strength of these membranes is large, and they can be extremely tight, so as to limit the opposite displacements of the connected tendons to little more than millimetres. This is a paradoxical situation: synovial sheaths should facilitate independent movement of the tendons, while in this case the opposite results. The present paper provides a model to explain this paradox, by taking into account the morphology of the tendons themselves.

MATERIAL AND METHODS: MODEL OF SYNOVIAL INTERCONNECTIONS

The morphology of the flexor tendons in the carpal tunnel

At the entry of the carpal tunnel, the deep flexors tendons frequently present as a collection of many more or less loosely interconnected tendon strands, rather than as the smooth round tendons encountered in the finger (Leijnse et al., 1996). This is especially the case with the ulnar three tendons FDP₃, FDP₄, FDP₅. In contrast, the tendons of the superficial flexors normally develop from the muscle belly onwards as compact tendons with a smooth surface. This is also regularly the case with the deep flexor of index, and the long flexor of the thumb (Leijnse et al., 1996).

What to a synovial membrane is a tendon?

Synovial sheaths isolate the tendons from their environment to reduce friction. As such, the synovial membranes in the carpal tunnel can be thought of as "programmed" to enwrap any tendinous structures they encounter - be it true finger tendons, anomalous tendons, or the median nerve. So it can be seen that the synovial membranes in the carpal tunnel systematically envelop the individual tendons, all tendons of each muscle group together, and all moving parts within the tunnel together, including the median nerve. The synovial membranes do not originate as isolated structures around the tendons, but extend from origins at the fixed environment, folding themselves around and in between the tendons. The enwrapment of a compact, smooth tendon should pose no problem to the membranes: they grow around them just as the synovial sheaths grow around the finger tendons. However, what if a tendon consists of loosely interconnected tendon strands - do the synovial membranes recognise such a tendon as a single entity, or do they "see" every individual strand as an individual tendon?

Model hypothesis

By model hypothesis it is assumed that the synovial membranes will enwrap any individually identifiable tendinous structure, however minute, as if it were a proper tendon. According to this principle, tendons with a smooth surface will be recognised as a single entity, and enveloped as a whole. However, tendons consisting of fibrous strands will be invaded by the synovial membranes in their attempt to envelop each strand individually. In such a tendon in the carpal

tunnel, two conflicting mechanisms are then active. (i) *The synovial mechanism*, which will try to work open the fibrous tendon into individually isolated tendon strands; and (ii) the *finger tendon formation mechanism*, which tries to bind the fibrous strands together by collagenous tissue into a proper smooth finger tendon. The result is that the ingrowing synovial membranes become trapped in between the individual strands by the collagenous tissue which binds them together in the tendon formation process. In this way the synovial blades may become solidly anchored into the tendons.

Interconnections formed by the synovial membranes

The synovial membranes span towards the tendons from fixed origins. Consequently, when they invade a fibrous tendon, they may also pass through adjacent fibrous tendons. When the synovial membranes by the above described mechanism become trapped within two adjacent tendons, they form a continuous interconnecting membrane which may span for several centimeters along the tendons. Many such membranes in parallel then form a thick and tight connective structure which is well able to resist permanent stretching by any flexor force. Some morphological properties of these interconnecting membranes can be mentioned. (i) The main direction of the synovial membrane fibres is transverse to the tendons. Therefore, when they grow in between two adjacent tendons, they will interconnect these tendons with predominantly transversely running fibres. This means that with opposite displacements of the connected tendons the membranes are stretched in their strongest direction. (ii) A substantial amount of connective membranous fibres will become taut at the same time. This follows geometrically from the fact that the membranes grow transversely through the tendons, which lay in parallel, so that the interconnecting fibres will be of the same length. However, this morphology can also be mechanically argued. Assume that all fibres are of different lengths. Then with increasing opposite displacements of the tendons, the shortest fibres will be much more strained than the longer fibres. When they are too few to resist the stretching forces of the oppositely moving interconnected tendons, they will permanently elongate or rupture until a sufficient amount of fibres is stretched in parallel to safely absorb the stretching force.

RESULTS

The above hypothesis is validated by two kinds of data. First are presented some representative samples of gross dissection results on embalmed specimens. Second, cross-sections of the flexors in the carpal tunnel are analysed.

Gross dissection results

Fig.1 shows a deep flexor tendon complex at the level of the carpal tunnel. The FDS tendons have been removed, together with their synovial membranes. The picture shows that the ulnar three tendons (lower tendons) consist of a multitude of fibrous strands which are massively enwrapped by the synovial membranes. The FDP₅ and the FDP₄ are also visibly interconnected by tendinous cross-overs. However, the FDP₄ and the FDP₃ are primarily interconnected by synovial

FDP interconnections formed by the synovial sheaths

membranes, although a small tendon strand (arrow) dissolves into the membranes into minute tendon fibres which insert in both the FDP₃, FDP₄, and the third lumbrical.

In fig.2 a deep flexor complex, harvested from the carpal tunnel, has been stretched out. To demonstrate that the membranes adhere by ingrowth into to the tendons, the tendons have been repeatedly, deeply and continuously incised in the longitudinal direction at both the back and the front. The incision marks are clearly visible. If all synovial membranes would merely pass around the tendons, they would be completely cut dorsally and volarly, and should be easily removable from the tendons. However, the membranes still firmly adhere to the tendons and resist the lateral stretching forces. It may be argued that the embalment is causal to the adherence of the membranes. Therefore, the superficial flexors were similarly investigated. In all (30) specimens investigated, a single incision at only one side of the superficial flexor tendons allowed to remove these tendons almost effortless from their surrounding membranes, showing no adherence except from the very thin inner membranes. In these same specimens, the synovial membranes could not be pulled from the deep flexor tendons, except by tearing them apart. The arrow points to a non-adhesive part of the synovial membranes folded back from the FDP₂ tendon. Deep at the FDP₂ tendon the membranes strongly adhere.

Fig.3. presents all tendons harvested from the carpal tunnel of a single specimen. From left to right: FDS₅ through FDS₂, FPL, FDP₂, through FDP₅. In this specimen the deep flexor tendons were very smooth as compared to many other specimens. This correlates to the fact that the interconnecting synovial membranes were not extremely strong. Nevertheless, interconnecting membranes were present, especially between the FDP₃, FDP₄, and FDP₅ tendons. The difference in the smoothness of surface of the FDS and FPL tendons as compared with the FDP tendons is quite clear. Although large parts of the FDP tendons have smooth surfaces, in all tendons some fibrous strands are clearly distinguishable, most pronounced in the FDP₄. Also in the FDS and FPL tendons fibrous strands can be distinguished, but these strands are strongly interconnected with each other into a solid tendon.

Fig.4 shows another specimen with strong interconnective synovial membranes, in which isolated tendon strands run parallel to the main tendons. These tendon strands gradually decrease in thickness, because they give off fibres to the main tendons all through their course (see further), while what remains of them continues straight on distalwards to give rise to lumbrical muscles. The tendon fibres which leave these tendon strands reinforce the connective synovial membranes, and form further causes for adhesion of the membranes.

Fig.5 shows synovial membranes which adhere to the FPL tendon. When the FPL tendon is pulled, the force in the proximal FPL tendon is transferred to the mass of the synovial membranes, and not to the distal FPL tendon, which remains slack. Clearly, the proximal displacement of the FPL will progressively pull the FDP₂, FDP₃, FDP₄ and even the FDP₅ tendons through the tautening of the synovial membranes adhering to these tendons. Fig.6, of the same specimen, shows that the adhesion of the synovial membranes to the otherwise smooth FPL tendon is provoked by a small tendon strand crossing over from the FPL to the FDP₂ tendon. Fig.1 shows a similar synovial connection adhering to a much stronger tendinous cross-over from the FPL to the FDP₂.

Cross-sections of the flexor tendons in the carpal area

The figs. 7 through 13 present cross-sections of the same wrist, from proximal to the radio-ulnar joint to distally the mid-metacarpal area. The figs. 14 through 16 are midcarpal cross-sections of different specimens.

Fig.7. Cross-section proximal to radio-ulnar joint, specimen 1

In this cross-section, the muscle bellies of the FDP₃, FDP₄, FDP₅, FDS₂, FDS₅ and FPL are still visible (shaded areas in legend drawing). No synovial membranes are yet present. The FDP₃, FDP₄ and FDP₅ form a complex in which the individual muscle bellies or tendons are not clearly outlined; the numbering in the legend drawing only indicates the approximate position of the individual tendons. Moreover, the muscle fibres are clustered in small packs separated by more or less clearly outlined areolar tissue. These packets do not correspond to three clearly outlined muscle bellies, and show that within the FDP muscle mass many muscle parts have (slightly) different displacements. This structural fragmentation of the muscle belly is not present to the same degree in the other muscle bellies, as e.g. the FDP₂. Also, the individual tendon strands which make up the FDP₂..FDP₅ complex are much clearer outlined than in the FDP₂, FPL and FDS₂..FDS₅ tendons. The end tendon of the FDS₂ is broad and flat. This extended shape is necessary to accommodate the large amount of muscle fibres which must still insert into the tendon (Leijnse^a, 1996).

Fig.8. Cross-section through radio-ulnar joint, specimen 1

In this cross-section, the muscle bellies of the FDP₃..FDP₅ have almost ended. A larger part remains of the muscle belly of FDS₂, of which the thinnest part of the end tendon has been damaged in the cutting of the slice. The synovial membranes are already identifiable as continuous lines which envelop the entire carpal content, the individual flexor groups, and within these groups also the individual tendons. Already it is visible that the synovial membranes tend to grow between the individual strands of the FDP₃..FDP₅ tendon complex.

Fig.9. Cross-section through proximal carpal row and the styloid of radius, specimen 1

The muscle bellies have all but disappeared. The FDP₂ tendon is still very flat, but will become cylindrical within the next few centimeters within the tunnel, as is shown in the next cross-sections. The FDP₃..FDP₅ tendons are a chaotic collection of tendon strands in which no three independent tendons are recognisable at all, and into which the synovial membranes branch out. Also in other tendons some ingrowing of the membranes is present, e.g. in FDS₃ (7).

Fig.10. Cross-section at the level of the os pisiform-trapezium, specimen 1

In this cross-section the synovial membranes have become massive in their numbers, and have thoroughly enveloped all tendons, including the median nerve. The FDP₃..FDP₅ complex has disintegrated into a collection of tendon strands in which the three end tendons are by no means recognisable. Into this fibrous complex, the synovial membranes grow in from all sides but especially palmarly, encapsulating the individual tendon strands. The membranes surrounding the

FDP interconnections formed by the synovial sheaths

other tendons clearly form proper concentric layers, conform to the classic notion of a synovial sheath. The innermost of these concentric membranes also grow into the tendons, e.g. in FDS₃. In contrast, the FDP₃..FDP₅ complex is invaded by all surrounding layers. The way in which the synovial membranes will isolate even small tendon strands becomes clear from the tendon strand (2'), which has become dissociated from the main FDP₂ tendon (2). In fig.3 this strand is still an unsuspected part of the FDP₂ tendon. However, in present cross-section the synovial membranes have grown in between the strand and the main tendon, and have encapsulated this small tendon strand as if it were a proper tendon.

Fig.11. Cross-section at the level of the hamulus of the hamate bone, specimen 1

The tendon strand (2') from the FDP₂ has been further isolated from the main FDP₂ tendon. The FDP₃..FDP₅ complex is starting to break up into three tendons, while the synovial membranes massively invade it from the volar and dorsal side. Some tendon strands are indicated by arrows. These tendon strands are followed up in the next cross-sections.

Fig.12. Cross-section through the base of the metacarpals, specimen 1

The FDP₃..FDP₅ complex is here in full process of dissociation. This dissociation occurs partly by the fragmentation of tendon strands (arrows) in between the main tendon parts into even smaller, almost microscopic tendon fibre entities. In Leijnse^b (1996) it is established that some of these tendon fragments will further give rise to lumbrical muscle fibres, while the remainder will join the deep flexor tendons. However, as these tendon strands dissociate they invite the entry of even more synovial membranes, of which the total invasive mass has reached the thickness of the tendons themselves. The tendon strand (2') which was dissociated from the FDP₂ remains an individual unit, encapsulated by synovial membranes as a real tendon.

Fig.13. Cross-section through the mid-metacarpals, specimen 1

The FDP₃..FDP₅ complex is now separated into three distinct parts, still quite fibrous and disorganised as compared to the FDS tendons. The tendon strands originally indicated by an arrow have now broken up into fibrous units too thin to identify within the synovial membranes, and which present as a "grey-speckled mass" in between the three ulnar tendons (arrows). Clearly, the resolution of encapsulation of tendon strands by the synovial membranes has reached microscopic level. The interconnecting quality of the synovial membranes is here indisputable. The part marked with "X" in the legend drawing assumably belongs to the FDP₄ tendon. However, it is also very tightly and extensively connected to the FDP₅ tendon. The tendon strand (2') has rejoined the main FDP₂ tendon, but is also being fragmented, as well as the part of the FDP₂ tendon indicated by the arrow. Radial to the FDP₃ tendon the second lumbrical muscle is already visible (shaded area in the legend figure).

Fig.14. Midcarpal cross-section, specimen 2

The cross-section of this specimen shows well formed FDS, FDP₂ and FPL tendons with proper synovial sheaths, and well identifiable FDP₃, FDP₄, FDP₅ tendons with some synovial

interconnections, and some stray tendon strands.

Fig.15. Midcarpal cross-section, specimen 3

This cross-section shows well formed FDP₂, FPL and FDS tendons. However, the FDP₃..FDP₅ tendons present as a tendinous unit. In this unit the FDP₅ can be more or less identified, but it is impossible to differentiate between the FDP₃-FDP₄ tendons.

Fig.16. Midcarpal cross-section, specimen 4

Cross-section showing well formed FDP₂, FDP₃, FPL and FDS₂..FDS₄ tendons. The FDS tendon of the little finger is not with certainty identifiable. It may be congenitally absent, which occasionally occurs (Austin et al., 1989); it may be the tendon strand radial to the FDS₄ (8), which would be the remainder of a degenerated FDS₅ muscle; or it may be the tendon part at the ulnar/palmar corner of the FDS₃ (7). The FDP₄ and FDP₅ are unidentifiable within a common group of tendon strands which is well interconnected by synovial membranes. The cylindrical shape of the tunnel cross-section disturbs the "normal" outline of the tendons in the tunnel, which makes their identification speculative. The numbering of the tendons FPL and FDS₂ in the legend figure is therefore somewhat arbitrary; it may well be that what is labeled as FDS₂ (6) is the FPL. However, from the figs. 10, 14 and 15 it seems that the FPL is inclined to occupy the most palmar-radial corner of the tunnel, while the FDS₂ would rather shift between the FDP₂ and the FPL, instead of between the FPL and the FDS₃.

DISCUSSION

Connections due to synovial membranes are systematic and non-pathological

The dissection results correlate well to the hypothesis that synovial membranes form interconnections especially between tendons of a distinct fibrous build. It should be stressed that the intertendinous connections formed by the synovial membranes in the carpal tunnel are systematically present, and do not result from a pathological process such as tenosynovitis. This was also observed by Fahrer (1975). In our dissected specimens (20), no obvious tenosynovitis was present.

Connections between the FDP and FPL

The FDP and FPL form a morphological unit. They arise from adjacent, and sometimes common origins, have a similar muscle structure and end tendon tract up to the end of the carpal tunnel. In the carpal tunnel the FDP₂ and FPL tendons are adjacent, and the FPL is enveloped similarly to the other tendons by synovial membranes. Tendinous interconnections between the FPL tendon and FDP₂ tendon are not infrequent. They generally run from proximally the FPL to distally the FDP (Linburg and Comstock, 1979; Rico Aguado and del Pino Paredes, 1988; Blair and Omer, 1981). In vivo, the presence of such connections is revealed by the impossibility to extend the index when the thumb is flexed with an active FPL. However, occasionally not only the index,

FDP interconnections formed by the synovial sheaths

but also the medius and even the ring finger flex conjointly with the thumb with active FPL. This cannot be explained by mere tendon strands running from the FPL to the FDP tendons, as these strands as a rule insert only in the FDP₂ tendon, which is adjacent to the FPL tendon. Therefore, synovial membranes interconnecting the FPL tendon to FDP tendon complex must be the cause. Since these membranes may span multiple tendons, they may interconnect more than one FDP tendon to the FPL. The figs.1, 5 and 6 illustrate this. Fig.1 shows a clear tendon strand running from proximally the FPL to distally the FDP₂. Moreover, this tendon strand is encapsulated by the synovial membranes, which are partly removed but which can easily be imagined as continuous with the mass of the FDP synovial membranes. Fig.5 shows an interconnection consisting primordially of synovial membranes. However, these membranes also contain a number of thin longitudinally running tendon fibres, which cross over from the FPL to combine into a thin tendon strand which inserts at the base of the first lumbrical, while the synovial membranes themselves adhere strongly to the FDP₂ tendon. Clearly, such tendinous crossovers, even when in substance minute, will invite the adhesion of the synovial membranes to the FPL and FDP₂ tendons. When the membranes adhesive to the FPL continue into the synovial mass of the FDP₃..FDP₅ complex, flexion of the thumb with an active FPL would flex, in order of decreasing severity, the index, medius, ring finger, even up to the little finger (fig.5). This is the order of the usual conjoint finger flexion with the thumb. Tendinous crossovers from the FPL are further investigated in Leijnse^b (1996).

The lumbrical origins

In the figs.1 and 4 parts of the lumbrical muscles seem to originate from the synovial membranes (Farher, 1975). The cross-sections of fig.11, 12, and 13 clearly show that deep flexor tendon strands may fragment up to the point that they become macroscopically untraceable in the mass of the synovial membranes. This can also be seen in fig.1 (tendon strand indicated with arrow, and others) and fig.4. Therefore, it can be assumed that the lumbrical muscle fibres arising from such mass of synovial and dissolved tendon fibres actually arise from these microscopically fragmented tendon fibres, and not from the membranes themselves. In Leijnse^b (1996) it is shown that masses of dissolved minute tendon fibres often run quite transversely between the tendons, and as such further reinforce the connective synovial membranes. In mentioned paper a comprehensive model of the deep flexor group is presented to describe these phenomena.

ACKNOWLEDGEMENTS

The author cordially thanks Dr. J. Zguricas and Dr. D. Nio for their assistance in dissections; and Dr. C.W. Spoor, Prof. Emer. J.M.F. Landsmeer, Prof. C.J. Snijders, Prof. Emer. J.C. van der Meulen, and Prof. J. Voogd for the discussion of the material; and the custodians of the dissection theatre, C. Entius and J. Velkers, for their support.

Chapter VI.ii

REFERENCES

- Austin, G.J., Leslie B.M., and Ruby, L.K. (1989) Variations of the flexor digitorum superficialis of the small finger. *J. Hand Surg (Amer.)* 14A, 262-267.
- Blair, W.F., and Omer, G.E., Jr (1981) Anomalous insertion of the flexor pollicis longus. *Am. J. Hand Surg.* 5, 548-549.
- Fahrer, M. (1975) Considérations sur les insertions d'origines des muscles lombricaux: les systèmes digastriques de la main. *Ann. Chir.* 29, 979-982.
- Leijnse, J.N.A.L., Walbeehm, E.T., Sonneveld, G.J., Hovius, S.E.R. (1996) Anatomical interconnections within the flexor digitorum profundus. Submitted Anatomical Record, 1995.
- Leijnse^a, J.N.A.L. (1996) A generic model of a muscle group - application to the muscles of the forearm. Resubmitted Anatomical Record, sept. 1995.
- Leijnse^b, J.N.A.L. (1996) A generic model of the anatomical variability in M. flexor digitorum profundus, M. flexor pollicis longus and the Mm. lumbricales of the human hand - the significance for the musician. Submitted Anatomical Record, 1995.
- Linburg, R.M. and Comstock, B.E. (1979) Anomalous tendon slips from the flexor pollicis longus to the digitorum profundus. *Am. J. Hand Surg.* 4, 79-83.
- Malerich, M.M., Baird, R.A., McMaster, W., and Erickson, J.M. (1987) Permissible limits of flexor digitorum profundus tendon advancement - an anatomic study. *Am. J. Hand Surg.* 12A, 30-33.
- Rico Aguado, A. and del Pino Paredes, V. (1988) Flexor digitorum profundus common to thumb and index finger, associated with a post-traumatic distal adherence of both tendons. *J. Hand Surg.* 13-B, 72-74.
- Stern P.J. (1990) Tendinitis, overuse syndromes, and tendon injuries, *Hand Clinics*, 6, 467-476.

FDP interconnections formed by the synovial sheaths



Figure 1

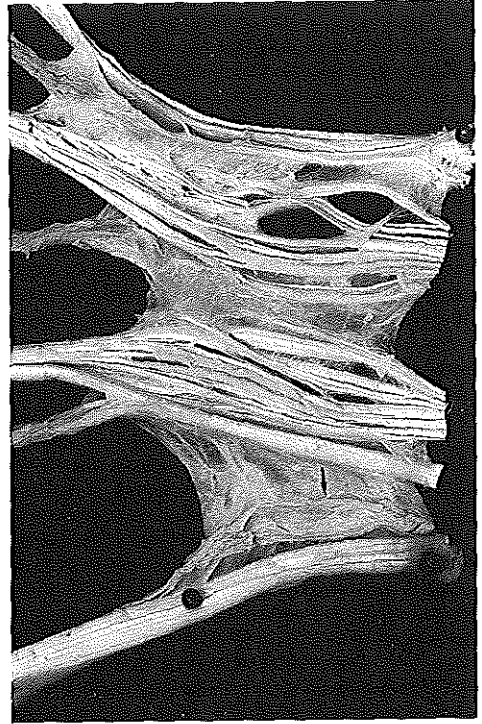


Figure 2



Figure 3



Figure 4



Figure 5



Figure 6

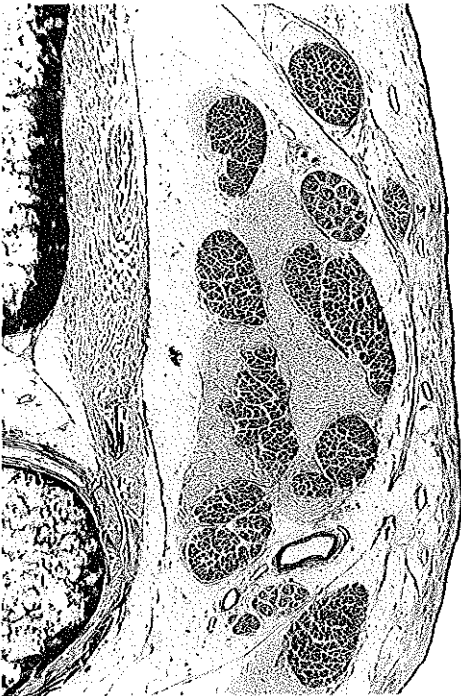


Figure 7

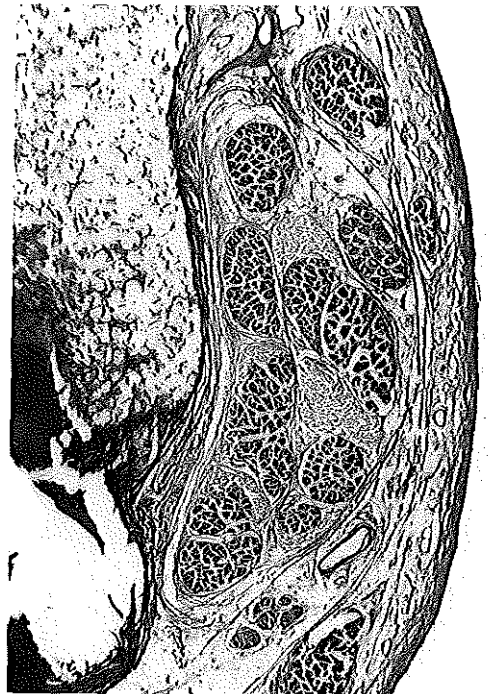


Figure 8

FDP interconnections formed by the synovial sheaths

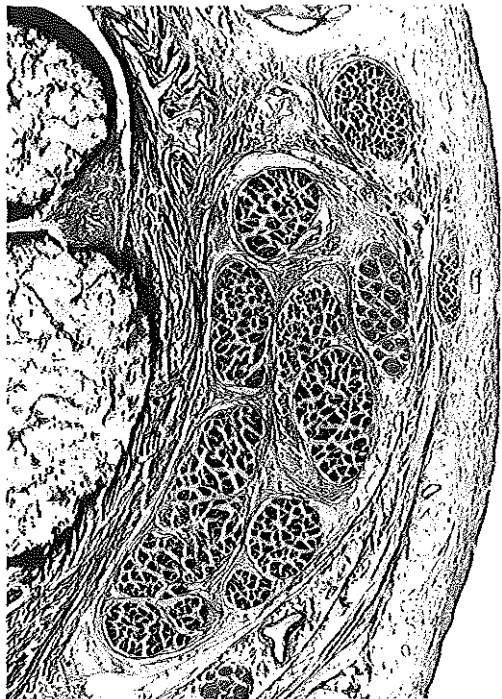


Figure 9

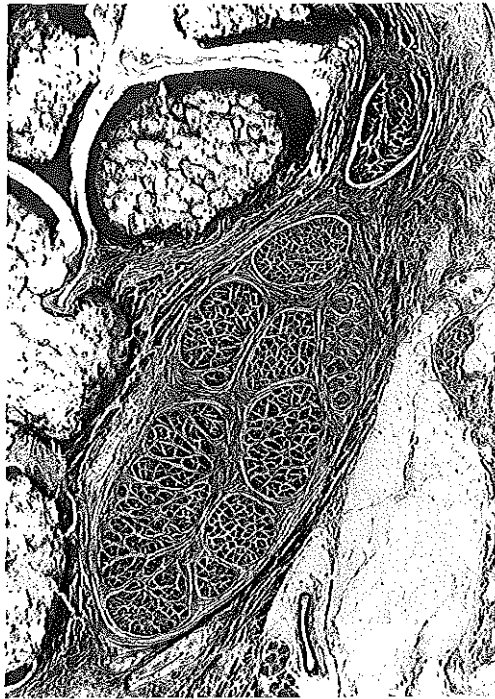


Figure 10

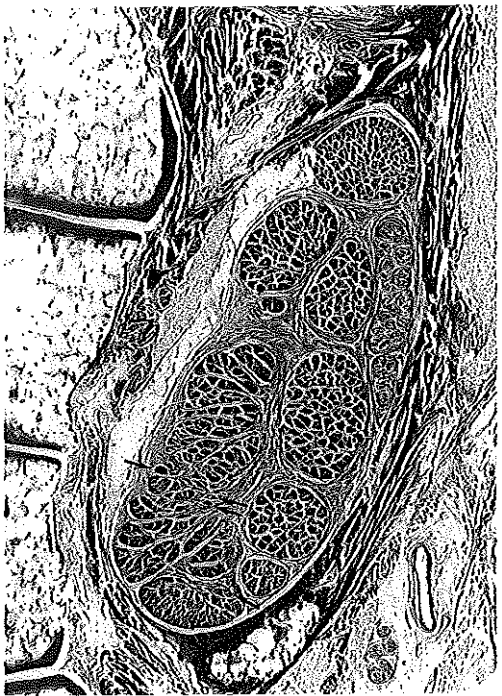


Figure 11



Figure 12



Figure 13

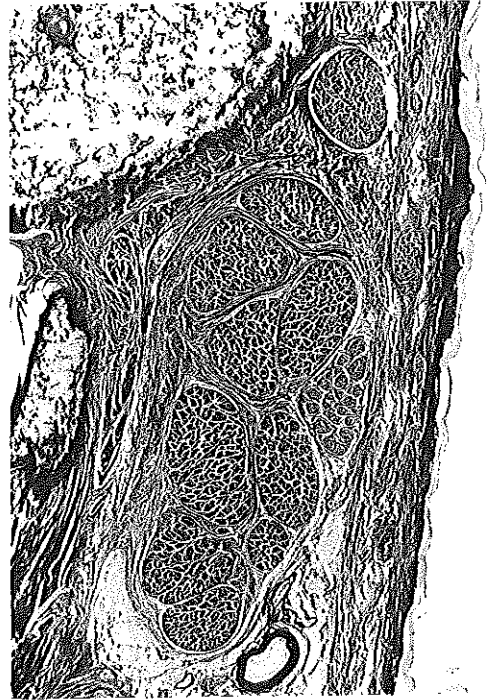


Figure 14



Figure 15

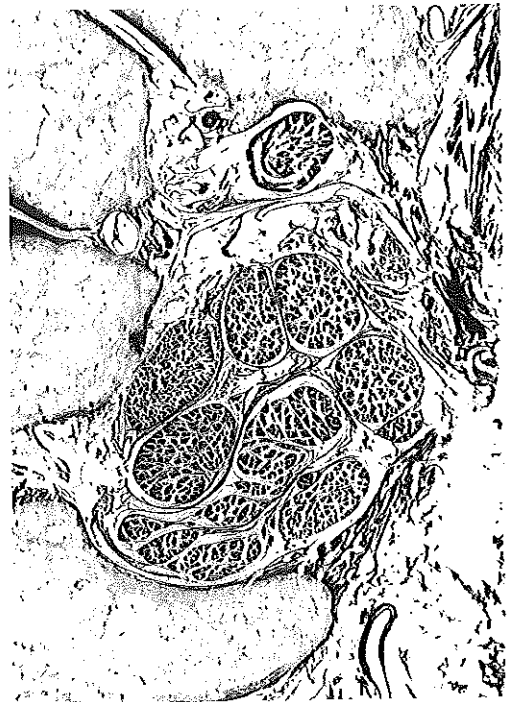
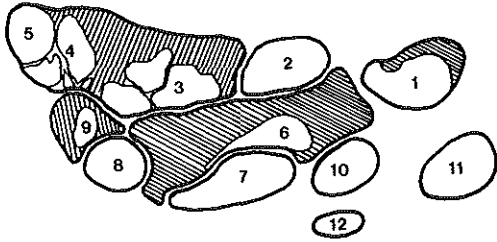


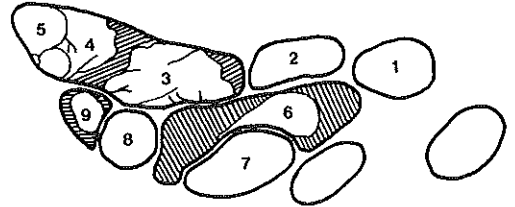
Figure 16

FDP interconnections formed by the synovial sheaths

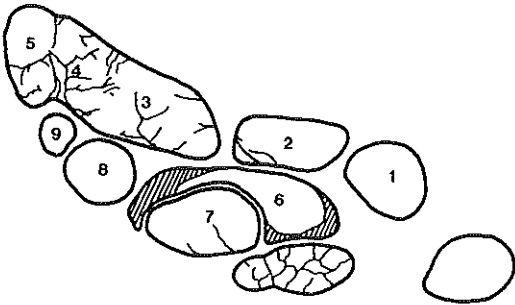
Legends of the figures 7 - 16



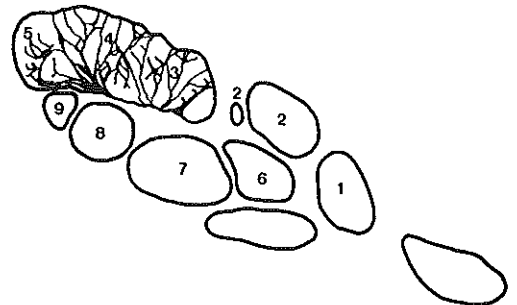
7



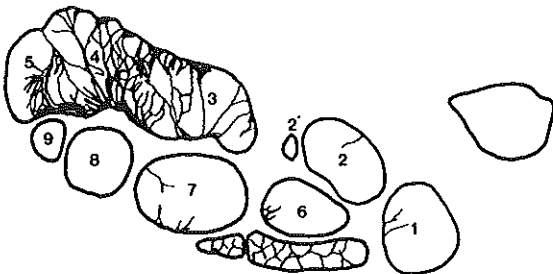
8



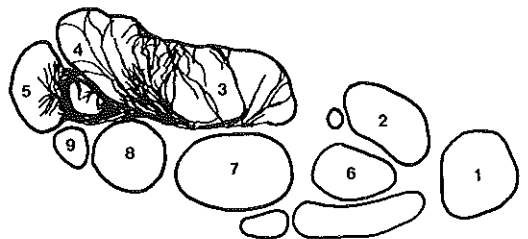
9



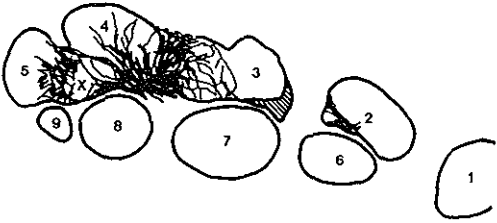
10



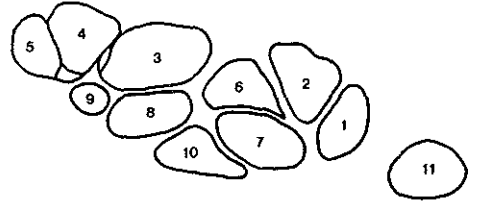
11



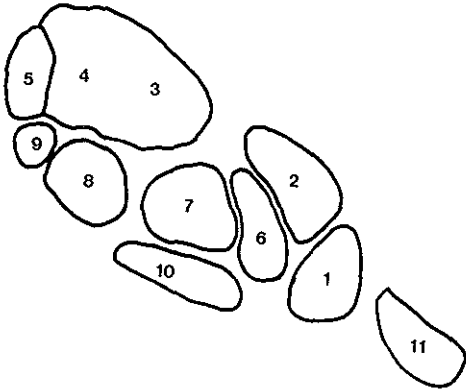
12



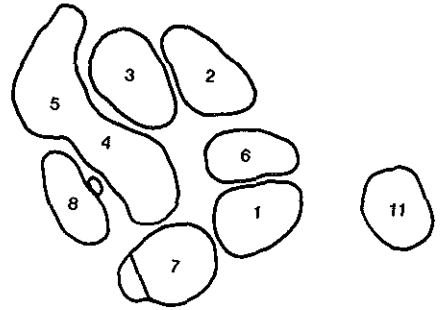
13



14



15



16

FDP interconnections formed by the synovial sheaths

Captions with figures and legends

Figure 1 FDP and FPL tendons at the level of the carpal tunnel. Top: FPL tendon. A tendinous-synovial connection runs from the FPL to the FDP₂ tendon. The ulnar three tendons are highly interconnected by synovial membranes, tendinous crossovers, and minute tendon fibres dissolved in the synovial membranes.

Figure 2 FDP tendons harvested from the carpal tunnel. Left: FDP₂ tendon, right: FDP₃ tendon.

Figure 3 From left to right: FDS₅ through FDS₂, FPL, FDP₂ through FDP₃ tendons of the same specimen. The FDS and FPL tendons are smooth of surface, the FDP tendons are distinctly fibrous.

Figure 4 FDP-lumbrical complex. Top: FDP₂ tendon.

Figure 5 Tendinous synovial connection between the FPL (top tendon) and the FDP tendons. Proximal displacement of the FPL tendon also pulls the FDP tendon complex.

Figure 6 Same specimen of fig.5, with the synovial FPL-FDP₂ connection carefully dissected, and wetted to make it transparent, to demonstrate the diffuse mass of tendon fibres crossing over from the FPL to the FDP₂ tendon.

In the legend figures of the cross sections, all tendons are numbered as follows: 1: FPL; 2 through 5: FDP₂ through FDP₃; 6 through 9: FDS₂ through FDS₅; 10: Median nerve; 11: FCR; 12: PL.

Figure 7 Specimen 1, section proximal to radio-ulnar joint.

Figure 8 Specimen 1, section through radio-ulnar joint.

Figure 9 Specimen 1, section through proximal carpal row and styloid of radius.

Figure 10 Specimen 1, section through os pisiform-trapezium.

Figure 11 Specimen 1, section through hamulus of hamate bone.

Figure 12 Specimen 1, section through base of metacarpals.

Figure 13 Specimen 1, section through mid-metacarpals.

Figure 14 Specimen 2, midcarpal section.

Figure 15 Specimen 3, midcarpal section.

Figure 16 Specimen 4, midcarpal section.

A GENERIC MODEL OF THE ANATOMIC VARIABILITY IN THE M. FLEXOR DIGITORUM PROFUNDUS, M. FLEXOR POLLICIS LONGUS AND MM. LUMBRICALES COMPLEX - THE SIGNIFICANCE FOR THE MUSICIAN

J.N.A.L. Leijnse

Department of Plastic and Reconstructive Surgery; Dept. of Anatomy, Erasmus University Rotterdam, The Netherlands. Submitted to Anatomical Record.

ABSTRACT

In present paper a generic model is presented of the anatomic variability in the muscle group formed by the M. flexor digitorum profundus, M. flexor pollicis longus and Mm. lumbricales. This model clearly outlines the structural causes of interdependence of tendons and muscle bellies in this muscle group. The model considers the muscle group as composed of two simple elementary building blocks: the monogastric elementary contractile units of the FDP-FPL, and the digastric elementary contractile elements of the lumbrical, and shows that by the application of simple principles these units can be assembled into complex entities, to which a third structural element, the synovial membranes, adds a further complexity. The model results well describe the known anatomical variants, and predict future ones. The problem of surgically increasing functional independence in this muscle group is discussed in view of the model results.

NOTATIONS

FDP ₂ ..FDP ₅	: M. flexor digitorum profundus (2: index, 5: little finger)
FPL	: M. flexor pollicis longus
LU ₁ ..LU ₄	: M. lumbricalis (1: index, 4: little finger)
ECU _p	: elementary contractile unit of the FDP and FPL
ECU _l	: elementary digastric contractile unit of the lumbrical

INTRODUCTION

Anatomic variations which limit the relative independence of the deep flexor tendons have been well documented (Fahrer, 1975; Materich et al., 1987; Leijnse^{a,b} et al., 1996). Interdependencies systematically arise from the close crisscrossing of muscles fibres inserting in different tendons, the crisscrossing of tendon strands between the end tendons themselves, the adhesion of the synovial membranes to adjacent tendons (Leijnse^b et al., 1996) and tightly connected bitendinous lumbrical origins (i.e. origins from two adjacent deep flexor tendons). Moreover, while the deep flexor tendons are anatomically constant, a great variability exists in the origins and insertions of the lumbrical muscles (Goldberg, 1970; Fahrer, 1975; Perkins and Hast, 1993). Lumbricals may arise from one deep flexor tendon; bipennately from two tendons (which is further called "bitendinous"); from two tendons and their interconnecting synovial membranes; or even from three tendons. Usually the first lumbrical has monotendinous origins, but it may be bitendinous, arising from both the FDP₂ and the FPL. The ulnar two lumbricals are usually bitendinous of origin, but occasionally are monotendinous. All lumbricals may be bitendinous. All lumbricals

may be monotendinous. Lumbricals may split up into two muscle bellies and insert into two different fingers (which is further called "bi-insertional"). A similar variability is encountered in the morphological aspect of the deep flexor tendons in the forearm and carpal tunnel. In the rare case, all tendons may be completely independent, or, in contrast, fused into a single tendon plate. Some tendons may be highly connected by crisscrossing tendon fibres. Tendons may be well defined and smooth of surface, or merely loose collections of tendon fibre strands. Some of such end tendon strands may run independently of the main tendon mass and may seem to disappear into the synovial sheaths, or give rise to lumbrical muscles. Also, there is the relatively high incidence of tendinous connections running from the FPL to the FDP of the index, and a low incidence of the inverse. In all, the anatomic variability in the deep flexor group is so great that it defies exhaustive description. The present paper attempts to solve the descriptive problem by providing a model which allows to *generate*, i.e. to predict these variations from a simple set of idealised anatomic structures and principles. This may help to understand the muscle group in the individual, e.g. in the problematic hand of the musician (Leijnse^{b,c,d}, 1996), and also to envisage its entire structure from a limited exposed site, as in surgery. The present study supplements other recent studies of the lumbrical-deep flexor complex. Its kinematics were modelled in Leijnse and Kalker (1995), the forces in the unloaded finger were analysed in Leijnse^e (1996), and the anatomical interconnections between the deep flexor tendons formed by the synovial sheaths were studied in Leijnse^b et al. (1996).

MATERIAL AND METHODS

The model of the FDP-FPL-LU muscle complex

Monogastric and digastric contractile elements

By definition, the "deep flexor group" consists of the four FDP muscle bellies to the different fingers, plus the M. flexor pollicis longus (FPL), which is considered as the first deep flexor. The FDP tendons are numbered FDP₂ (index) to FDP₅ (little finger). The FDP-FPL-lumbrical complex is modelwise constructed from two kinds of elementary contractile units (ECU), a monogastric element for the FDP or FPL, and a digastric element for the LU. The contractile unit of the FDP and FPL (ECU_p) consists of an elementary muscle fibre in series with an end tendon fibre. The digastric contractile unit of a lumbrical (ECU_L) consists of a proximal muscle fibre, an intermediate tendon fibre, a lumbrical muscle fibre, and a lumbrical end tendon fibre in series. These units are mixed in a proportion as in the human hand, and distributed over the origins of the FDP and FPL. The local relative density of ECU_p and ECU_L fibres along the origin area is a model parameter.

Construction of the deep flexor and lumbrical end tendons

The FDP-FPL-LU muscle complex is modelwise created as follows. The ECU_p and ECU_L are distributed over the FDP-FPL origins, and their end tendon fibres are distally arranged into two end tendon fibre plates. One tendon plate consists of all ECU_p end tendon fibres, the other contains all ECU_L end tendon fibres. At the *distal end* the tendon plate of the ECU_p end tendon

fibres is split up into five parts, which will form the FDP and FPL end tendons. Similarly, the distal end of the lumbrical end tendon fibre plate is divided into seven parts, which form all possible normal or anomalous lumbrical end tendons of the fingers 2 through 5. For each finger there is a radially as well as an ulnarly inserting lumbrical end tendon, except for the little finger, which only has a radial lumbrical insertion, and the thumb, which has none.

The generic hypothesis of the anatomic variability in the deep flexor lumbrical complex

The fundamental model hypothesis further developed is that *the anatomic variations in the FDP-FPL-LU complex correspond to the possible distributions of the ECU_p and the ECU_L over the end tendons, i.e. to the choice which elementary end tendon fibres are included in which end tendon*. Physically, the model can be interpreted as describing a crucial stage in the embryological development. In the embryo the hand develops from a hand plate, in which fingers are not yet expressed, and the deep flexor develops from a single structure, with a single end tendon blade. When the fingers develop, this end tendon blade splits up into the finger tendons. Basically, this splitting up consists of the selection of which tendon fibres (ECU_p , ECU_L) will insert into which finger, and according to our model hypothesis, this selection determines the structure of the individual muscle bellies. Within the model, it is essential that the splitting up of the end tendon plate starts distally at the digits, and not proximally at the origin. In other words, the decision to include a contractile element into a certain finger tendon is made on the basis of the distal position of its end tendon fibre in the end tendon plate, and not on the basis of the position of its origin (fig.1).

Anatomic variability in the FDP without lumbricals

Overlapping areas of origin of the muscle fibres to the different tendons

The model is first considered without lumbricals. By model assumption, the end tendon fibres of the deep flexor initially run distally to the fingers as a flat, loose, broad sheet of tendon fibres; moreover, it is assumed that in this sheet *the individual end tendon fibres may crisscross slightly, according to a statistical distribution with zero average* (fig.1). When then the end tendon fibre sheet is split up at the distal end into the five FDP and FPL end tendons, five areas of origin are defined, each containing all muscle fibres inserting into one tendon. When the ECU_p crisscross in their distal course, these origin areas will overlap, as muscle fibres arising from the same area of origin may crisscross differently and end up in different tendons. Clearly, the overlapping of origin areas will increase with increasing crisscrossing of the ECU_p (fig.1).

An anatomic cause of co-activation of muscle bellies in the FDP

In the overlapping origin areas, muscle fibres which originate next to each other may yet insert into different end tendons. If it holds that the resolution of the activation of these cross-inserting muscle fibres is less than the fineness of their mixture, the activation of the muscle fibres to one tendon will unavoidably co-activate muscle fibres inserting in the other tendon. In this way co-active force transfers, as measured in Leijnse^b (1996), can be explained.

Muscle fibre parallelism: a geometric criterion for independence of muscle bellies in the FDP

When no ECU_p crisscross, i.e., when all ECU_p are strictly parallel, the distal partitioning of the end tendon plate will create five muscle fibre blocks of which the areas of origin will not overlap and will be delimited by straight lines (see T_1 in fig.1, and fig.4). Within such an individual muscle block, all muscle fibres will contract or lengthen by equal amounts, since they are connected to the same tendon. Therefore, any connective tissue separating these individual blocks will be continuously mobilised by the independent displacements of these blocks, while all nerve endings within the individual blocks can act consistently in synchrony. Such a situation must necessarily result in independent muscle bellies. This model correlates the functional independence of muscle bellies to a geometric property, i.e. the ECU_p parallelism in individual muscle build. By variation of the deviation of ECU_p parallelism an interindividual variation of muscle belly independence ranging from nil to complete can be constructed.

The formation of end tendons consisting of fibrous strands

In Leijnse^a et al. (1996), it was observed that deep flexor tendons in the forearm often are mere assemblages of tendon fibre strands (fig.7), rather than homogeneous end tendons as in the superficial flexor. On the other hand, the FPL and FDP_2 regularly arise with homogeneous, smooth end tendons, especially when their muscle bellies are independent. These phenomena are explainable by the above model assumptions, as visualised in fig.1. In tendon T_1 all ECU_p are strictly parallel. This results in a homogeneous tendon fibre blade, which, when compacted into a tendon, is likely to produce a homogeneous, smooth end tendon. Clearly, ECU_p parallelism implies an independent muscle belly, as well as a smooth end tendon (fig.4). In contrast, the slight crisscrossing of the ECU_p in the other tendons (T_2 and T_3) disturbs the homogeneity of the tendon plate, and creates local concentrations of end tendon fibres, separated by empty spaces. Clearly, such a situation predisposes to the formation of tendons which present as collections of tendon fibre strands, rather than smooth compact tendons. When the degree of crisscrossing is too high, the individual tendon fibre strands will further interconnect to form an interwoven tendon fibre "fabric" which will encompass tendons to different fingers. In such a way the fusion of deep flexor tendons to different fingers into a single end tendon plate can be modelwise explained.

Anatomic variability in the FDP-FPL-LU muscle complex

Consider the above FDP model to which the ECU_L are added, distributed in a proper mix over the FDP and FPL origins. This distribution may be homogeneous, or it may e.g. reflect the layout of the insertions of the lumbrical end tendons. In the latter case, four concentrations of ECU_L can be imagined alternating with five concentrations of ECU_p fibres. By assumption, the ECU_L run distally in a statistical crisscross pattern similar to the ECU_p .

Variability due to the partitioning of the lumbrical end tendon fibre plate

A first level of anatomical variability results from the distribution of the ECU_L over the seven lumbrical end tendons. By model assumption, the relative size of the insertions of the second, third and fourth lumbricals in radial or ulnar tendons varies as a continuum in the population: with

N_{LU} the total number of lumbrical fibres in the lumbrical, the amount of fibres in the radial (N_{LUR}) or in the ulnar (N_{LUU}) insertion is: $N_{LUR} = X \cdot N_{LU}$, $N_{LUU} = (1-X) \cdot N_{LU}$, $0 \leq X \leq 1$, with X a stochastic variable. Bi-insertional lumbricals or ulnar insertions are shown in figs.6,7,8,9.

Variability due to the position and degree of fusion of the intermediate lumbrical tendon fibres

Fundamental to proper lumbrical function is that the ECU_p muscle fibres, and the proximal muscle fibres of the digastric ECU_L have the same displacements. If the ECU_L would be independent of the deep flexor fibres, they would merely act as a digastric interosseus (Leijnse and Kalker, 1995). Anatomically, a sure way to realise the condition of equal displacements is by closely mixing the ECU_L and ECU_p at their origins, so that in any collection of intermediate ECU_L tendon fibres also a substantial amount of ECU_p end tendon fibres is present, and further by interconnecting such assemblies with connective tissue. These conditions would ensure that no substantial groups of ECU_L fibres can develop into independent digastric bodies. Nevertheless, tendon fibre collections in which the intermediate lumbrical tendon fibres are a majority can be easily imagined. As modelled in the above, the tendon fibres in the forearm may fuse in different ways. Homogeneous tendons result when all ECU_p and ECU_L are basically parallel. When the ECU_p slightly crisscross, and with them also the ECU_L , individualised tendon fibre strands are formed. These strands assemble to a varying degree into tendinous entities reflecting the lay-out of the FDP tendons. The lumbrical muscle fibres arise from the intermediate ECU_L tendon fibres within these tendons or tendon fibre strand assemblies. The variability in the lumbrical origins modelwise results from: (i) the degree of crisscrossing of the intermediate ECU_L tendon fibres with respect to the lumbrical end tendon in which their muscle fibres insert, and (ii) the degree of fusion of the tendon fibre strands into true FDP-FPL end tendons. In fig.2, some realistic configurations are generated.

1) Assume that all ECU_p and the ECU_L are strictly parallel, and that all intermediate lumbrical tendon fibres fuse with the nearest radial ECU_p end tendon. Then five independent FDP-FPL muscle bellies are obtained with four unipennate, mono-insertional lumbrical muscles (fig.2.a).

2) Assume that all intermediate lumbrical tendon fibres are fused in more or less equal proportions with the nearest ulnar and radial FDP tendons. Then lumbrical muscles with bitendinous origins are obtained (fig.2.b).

3) Assume that not all tendon fibre strands are fused with the main FDP tendon bodies, and that some lumbrical dominated tendon fibre strands run independently in the forearm. Then the lumbrical muscle bellies will arise partly from the FDP-FPL tendons, and partly from these independent tendon fibre strands (fig.2.c). At the level of the lumbrical origins these strands will dissociate, as the ECU_p tendon fibres must join the main FDP-FPL tendons, while the intermediate ECU_L fibres will continue straight-on to give rise to lumbrical muscle fibres (dissection examples: figs. 11-16).

4) Assume that only a minor part of the intermediate lumbrical fibres are fused with the FDP end tendons, both radially and ulnarly, and that the non-fused lumbrical dominated tendon fibre collections are evenly distributed in between these deep flexor tendons so that they form a

A generic model of the FDP-FPL-LU complex

thin continuous sheet. Then the lumbrical origins will span as a continuous structure the space between the radial and ulnar FDP tendons of origin (fig.2.d) (figs. 8, 9, 13 (4)).

5) Assume a distribution of ECU_L in the flexor group origin so that all ECU_L are positioned between the five ECU_P assemblies which insert into the respective FDP-FPL tendons. Then, when all the intermediate ECU_L tendon fibres fuse with the FDP tendons, the lumbrical muscles will seem to arise pronouncedly from the sides of the FDP end tendons. However, when the ECU_L are distributed randomly among the ECU_P origins, the fused intermediate ECU_L tendon fibres will be evenly distributed over the mass of the FDP end tendons. Then, the lumbrical muscle fibres are likely to emerge from these FDP tendons from the entire surface of the FDP tendons.

6) Assume that the degree of crisscrossing of the intermediate ECU_L tendon fibres is large. Then it is possible that intermediate tendon fibres arrive at the lumbrical origins at the side of the FDP opposite to the side from which normally the lumbrical arises. Then a lumbrical muscle is created of which a part crosses over from the opposite side of the FDP tendon (fig.2,c and d) (fig.11). Even, intermediate ECU_L tendon fibres can be imagined to cross over to the degree that they join a FDP tendon adjacent to the proper FDP tendon of origin. Then a lumbrical muscle results which derives part of its origin from the tendon adjacent to its normal tendons of origin. Modelwise, the occurrence of such variants depends on the chance of severe crisscrossing to occur, which should decrease sharply with the amount of crisscrossing.

Model applications

Tendinous connections between the FPL and FDP₂; bitendinous lumbricals in disguise?

Connections between the FPL and FDP₂ are not infrequent, and they are generally directed from proximal the FPL to distal the FDP₂ (Lindburg and Comstock, 1979; Rico Aguado and del Pino Paredes, 1988; and our own dissection results). In the terms of the model, this prevailing direction may be explained by the assumption that these connections are caused by: (i) ECU_L originating in the FPL origin area, and/or (ii) ECU_P originating in the FPL origin area, but included in the FDP₂ tendon with the partitioning of the FDP-FPL end tendon plate (i.e., the FDP₂ origin overlaps with the FPL origin). From these assumptions the following situations may result (fig.3).

(i) At the one extreme, the intermediate tendon fibres of the ECU_L arising from the FPL origin may be fully fused with the FPL tendon, until they give rise to lumbrical muscle fibres. This will result in a first lumbrical LU₁ with (part of) its origin at the FPL tendon (fig.3.a). Moreover, when the FDP₂ origin overlaps with the FPL origin, an additional tendinous connection will run from the FPL to the FDP₂. This connection consists of the ECU_P fibres which arise from the FPL origin, and which are proximally fused with the FPL tendon, until they cross over to join the FDP₂ tendon (fig.3.a).

(ii) At the other extreme, the ECU_{L1} and ECU_{P2} arising from the FPL origin may form a proximal muscle belly independent of the FPL, and of which the tendon in the forearm runs independently from both the FDP₂ and FPL, until the intermediate ECU_{L1} fibres become part of the LU₁ origin, and the remaining ECU_{P2} end tendon fibres insert into the FDP₂ tendon (fig.3.b). A dissection example of an independent muscle-tendon body arising from the FPL origin area, but

inserting into the FDP₂ tendon before the origin of the first lumbrical is given in fig.19.

(iii) Within these two extremes are the cases in which the ECU_{L1} and ECU_{P2} are proximally fused with the FPL tendon, of which they separate well before the lumbrical origins, to cross over to the FDP₂ tendon with which they may or may not completely fuse before the lumbrical arises. When their fusion with the FDP₂ tendon is complete, a normal unipennate first lumbrical arises, and an isolated tendinous interconnection is found between the FPL and FDP₂ (fig.3.c). Close dissection of the specimen in fig. 19 revealed that a small tendon strand of the tendinous crossover effectively gave rise to lumbrical muscles (see results). Other examples are figs. 7 and 16-18.

In model-embryological terms, the prevailing direction of the FPL-FDP₂ connection is motivated by the fact that ECU_{L1} fibres originating from the FPL area constitute an oblique path directed from the FPL origin towards the origin of the first lumbrical, which generally coincides with the FDP₂ end tendon. As a result, when the FDP-FPL tendon plate is partitioned, the chance that tendon fibres originating from the FPL origin area end up in the FDP₂ tendon is greater than the chance that fibres from the FDP₂ origin area are included into the FPL end tendon. However, the latter possibility is modelwise not excluded, and should therefore be expected to occasionally occur.

Lumbrical origins from the synovial membranes: dissolved intermediate ECU_L tendon fibres

Within the carpal tunnel, the flexor tendons are enwrapped in synovial sheaths. At the dissection table, individual unfused tendon strands between the main tendons in the carpal tunnel can be frequently seen to dissolve in the synovial sheaths (figs. 12, 13, and 15). On the other hand, lumbrical muscle fibres frequently seem to arise from the synovial sheaths themselves (LU₄ in fig. 13 (4), and LU₃, LU₄ in fig.14). The phenomenon of "disappearance" of tendon fibres and "origination" of lumbrical muscle fibres from the synovial membranes can be explained from the above model, and the model of the synovial membranes in the carpal tunnel presented in Leijnse^b et al. (1996). The latter model states that synovial sheaths will individually enwrap any individually identifiable tendinous structure in the carpal tunnel, however minute it may be. Consider now, proximal to the lumbricals, a lumbrical dominated tendon strand not fused with the main tendons. Modelwise, this strand will consist of both ECU_P end tendon fibres and ECU_L intermediate tendon fibres. The ECU_P end tendon fibres must insert into a FDP end tendon, while the intermediate ECU_L tendon fibres must give rise to lumbrical muscle fibres. Therefore, as the tendon strand approaches the level of the lumbrical origins, it must dissociate: the ECU_P tendon fibres it contains must run towards an FDP tendon, while the ECU_L intermediate tendon fibres should continue straight-on distally to give rise to lumbrical muscle fibres, because there is no reason why they should change direction towards a FDP end tendon first. Figs. 12, 13 and 15 show that this dissociation can be quite abrupt, with tendon strands ending in diffuse masses of minute, even microscopic, tendon fibres. Within the mass of the synovial membranes these tendon fibres cannot be macroscopically detected anymore, but nevertheless continue until they give rise to their lumbrical muscle fibres. These lumbrical fibres then seem to arise from the synovial membranes themselves. The opposite may also happen, as is demonstrated in fig.12, where a

clearly defined lumbrical tendon of origin seems to arise from the synovial membranes. However, close inspection shows that this tendon is gradually assembled from clouds of minute tendon fibres which diffuse from the main FDP tendon, or which even derive from another dissociating tendon strand (see results).

Interconnecting synovial membranes reinforced by dissolved ECU_p and ECU_L tendon fibres

The figs.12 and 15 show that when the small independent tendon strands dissociate into ECU_p and ECU_L tendon fibres, the ECU_p tendon fibres may run quite obliquely, even transversely to the main FDP end tendons. In doing so, they reinforce the connections formed by the synovial membranes. Fig.12 also shows that such tendon strands may insert in both adjacent FDP tendons, so that these dissociated ECU_p fibres form a connective tendon fibre matrix within the connective synovial membranes. Fig.13 further shows that also from the main FDP tendons ECU_L tendon fibres may dissociate well before the lumbrical origins. Such independent minute tendon fibres provide additional occasion for adhesion and reinforcement of the interconnective synovial membranes. Further connections between the main FDP-FPL tendon are formed by the ECU_p end tendon fibres, which may directly and substantially crisscross at level of the lumbrical origins, as is shown in fig.9.

Connective synovial membranes between the FPL and the FDP

In Leijnse^b et al. (1996) it is shown that the synovial membranes may cause strong interconnections between tendons in the carpal tunnel, by firmly adhering to the tendons. It is hypothesised that these membranes only adhere to tendons which are distinctly fibrous of character, and that they do not tend to adhere to tendons with a smooth surface. In Stern (1990) it is noted that such connective membranes are often found in conjunction with intertendinous connections, but also without them. The latter finding would contradict the hypothesis of Leijnse^b et al. (1996), because the FPL tendon usually is of a rather smooth surface, to which the synovial membranes should not easily adhere. The following argument is therefore proposed. Tendon fibres crossing over from the FPL to the FDP₂ locally break the smooth tendon surface of the FPL, and as such provide a cause for adhesion of the synovial membranes, while these membranes, of course, will also adhere to the tendinous crossovers themselves. Even small quantities of fibres crossing from the FPL to the FDP₂ should increase the chance of such adhesions. Such thinly spread-out overcrossing tendon fibres may well go macroscopically undetected in the thick synovial membranes, in the same way as individual tendon strands between the FDP tendons may dissolve into the synovial membranes (see previous section). Therefore, even if no obvious tendinous FPL-FDP₂ cross-overs are present, it may well be that minute quantities of crossing fibres provide an actual cause for stronger than expected synovial membrane adhesion to the FPL tendon. This phenomenon is illustrated by the figs. 16 and 17. Fig. 16 shows a thin but strong synovial membrane interconnecting the FPL and the FDP₂, and continuing into the mass of the synovial membranes of the other flexor tendons. In this membrane, no tendinous connection is apparent, although a diffuse mass with an oblique direction can be distinguished. However, fig. 17 shows that at the backside of the FPL tendon a clearly identifiable tendon strand leaves the

tendon, to spread out into the membrane. These spread-out fibres recombine into a thin tendon sheet and insert into the FDP₂ tendon at the level of the first lumbrical origin (fig.17). This insertion cannot be caused by the synovial membranes themselves, since these grow in transversely and around the tendon strands, and do not joint the tendon itself. Similar synovial interconnections are shown in figs. 7 and 19.

DISSECTION RESULTS

Independent muscle bellies

Figs. 4-7 illustrate the model of fig.1, which correlates independence of muscle bellies to the parallelism of elementary muscle-tendon fibre units. The two presented specimens show from radial to ulnar a decreasing independence of the deep flexors.

Fig. 4 shows the muscle bellies of the FPL (upper tendon), FDP₂, FDP₃..FDP₅. The muscle bellies of the FPL and FDP₂ were well separable from each other and from the FDP₃. They present with regularly arranged muscle fibres. The FDP₃..FDP₅ are much less independent.

Fig. 5 shows the muscle bellies of the FDP₂..FDP₅ of the specimen of fig.4. These FDP₃..FDP₅ muscle bellies are clearly less orderly constructed than the FDP₂ and FPL in fig.4, although the main muscle bodies are grossly separable.

Fig. 6 (same specimen) shows that in contrast to the FDP₂ and FDP₃ tendons, tendon fibre strands crisscross between the ulnar three FDP tendons, especially between the FDP₃ and FDP₄. This correlates to the disordered structure of the muscle bellies, as can be seen at the right-hand side of the picture. The third lumbrical inserts in the third, instead of in the fourth finger.

Fig. 7 shows a similar case. The FPL and FDP₂ tendons are well shaped, while the FDP₃..FDP₅ tendons consist of disordered tendon strands. A tendinous-synovial connection exists the FPL and the FDP₂, which inserts in the FDP₂ at the base of the first lumbrical. The third lumbrical inserts into both the third and fourth finger.

Tendinous crossovers and malinserting lumbricals

Figs. 8-10 illustrate the model figures of fig.2.c,d.

Fig. 8 shows a firmly interconnected FPL-LU complex comprising the ulnar three FDP tendons. The third lumbrical inserts into both the medius and ring finger, with the stronger insertion in the medius. The FDP₃ tendon (3) and the FDP₄ tendon are strongly interconnected by synovial membranes. Half of the fourth lumbrical arises from an independent tendon strand which runs between the FDP₄ and FDP₅ (5) tendons, and which inserts in both the lumbrical, and in the FDP₄ tendon. The third lumbrical derives its muscle fibres from tendon fibres distributed over the entire width of the FDP₄ tendon. The second lumbrical derives its muscle fibres from tendon strands running more laterally in the FDP₃ tendon (cfr. fig.2.c).

Fig. 9 shows FDP₃..FDP₅ tendons with so many minute tendon fibres crisscrossing at the lumbrical origins, in addition to the synovial connective membranes, that the main tendons are interconnected into a tendinous plate. The tendon fibres of origin of the second lumbrical have been followed up as far as macroscopically possible. Some tendon fibres could be followed up to the FDP muscle belly (upper fibre strand), others disappeared rather chaotically deep into the

A generic model of the FDP-FPL-LU complex

main tendon. The third lumbrical inserts into two fingers, with only a very small insertion in the fourth finger.

Fig. 10 shows FDP₂-FDP₅ tendons. LU₃ inserts in the third finger. The origin of LU₃ has been partly removed from FDP₄ (arrow), which reveals the cut ends of the tendons of origin of this lumbrical, and the fact that as the lumbrical arises the FDP₄ tendon grows thinner, because tendon fibre material disappears in the lumbrical muscle fibres.

Lumbrical tendons of origin, tendon strands dissolving in synovial sheaths

Figs. 11-16 illustrate the hypothesis that the ECU_p and ECU_L are densely mixed, i.e. that any tendon strand containing intermediate ECU_L fibres will also contain ECU_p fibres, which at the lumbrical origins must be sorted out. They also illustrate that the lumbrical origins may overlap, which modelwise results from the crisscrossing of the intermediate ECU_L fibres.

Fig.11. FDP₃-FDP₄-LU complex. The origins of LU₂ and LU₃ arise partly from a tendon strand which inserts in both FDP₃ and FDP₄. The origins from this strand overlap in a crisscross pattern of minute tendon fibres of LU₂ and LU₃ origin, which illustrates the lumbrical origins of fig.2, (c) and (d).

Fig. 12 shows lumbrical muscle fibres arising from the FDP tendons, and independent tendon strands. The synovial membranes have been wetted to make them transparent. Upper tendon: FDP₂, lower tendon: FDP₅. The tendon strand (1) is similar to fig.11, but being much thinner, it shows more clearly how such tendon strands sort themselves out. The strand dissolves into three kinds of fibres: (i) fibres joining the FDP₂ tendon; (ii) fibres which continue straight-on as the origins of the thin radial head of the second lumbrical; (iii) some fibres which continue along the FDP₂ tendon to give rise to the first lumbrical. The tendon strand (2) seems to end abruptly halfway into the picture. Close inspection shows that this tendon strand dissolves into minute tendon fibres which spread out in opposite directions to join both the FDP₂ and the FDP₃, while some fibres continue distally to give rise to some lumbrical muscle fibres. The exact opposite happens in the tendon strand above (3): it seems to originate abruptly from nowhere, and contains only tendon fibres of lumbrical origin. Close inspection shows that this strand is gradually assembled in its distal course from minute tendon fibres leaving the FDP₃ tendon, and probably also from tendon fibres dissipated from the tendon strand (2). Modelwise, the minute tendon fibres leaving the FDP₃ tendon are intermediate ECU_L tendon fibres which dissociate from the ECU_p fibres in the FDP₃ tendon, to recombine into a tendon strand consisting exclusively of tendon fibres of lumbrical origin. Above the tendon strand of (3) a more conventional lumbrical tendon of origin separates from the FDP₃ tendon.

Fig. 13 presents the ulnar three tendons of the specimen of fig.12 with somewhat dryer synovial membranes. It shows a fourth lumbrical of which a substantial part arises from a mass of minute tendon fibres (4) which dissociates from the FDP₅ tendon well before lumbrical muscle fibres originate, thus producing a lumbrical with a continuous origin from the FDP₄ to the FDP₅ tendon.

Fig. 14 shows a tendon strand (1) which contains almost exclusively tendon fibres of lumbrical origin, and which arrives straight-on from the muscle bellies. Nevertheless, a mass of

tendon fibres (distal to (1)) dissociates to join the FDP₂ tendon, and smaller masses of tendon fibres dissociate to join the FDP₃ tendon (arrows). This corresponds to the model assumption that the ECU_L and ECU_P are closely mixed, and that therefore any sizeable tendon strand would contain a quantity of both, if only a minute one.

Fig. 15 (1) shows the opposite of fig. 14, i.e. an isolated tendon strand which contains almost exclusively FDP tendon fibres. The strand ends abruptly proximal to the lumbrical origins. The synovial membranes have been carefully removed, exposing the masses of small tendon fibres which dissociate from the tendon strand near its end to join the main tendons. The majority of these tendon fibres joins the lower tendon (FDP₄), but at the end some join the middle tendon (FDP₃), while a small remainder of fibres continue as lumbrical origins. A similar situation can be observed in the tendon strand (2). The majority of the tendon fibres joins the upper tendon (FDP₂), but a good deal runs downwards to the FDP₃, to insert in this tendon, or to give rise to lumbrical muscle fibres just above the tendon.

FPL-FDP interconnections

The figs. 16-19 show adhesions of synovial membranes to the FPL tendons which are provoked by tendinous crossovers from the FPL to the FDP₂ tendon.

Fig.16 shows a mass of synovial membranes interconnecting the FPL tendon (1) with the FDP₂ (2) (same specimen as in fig.7, left hand side is proximal). Within the mass of the membranes a density of tendon fibres leaving the FDP tendon can be distinguished.

Fig.17 presents the FPL tendon from the other side (left-hand-side is distal), and shows a clearly distinguishable strand of tendon fibres at the bottom of the FPL tendon (arrow). In addition, a small strand originating from the most distal muscle fibres crosses over the top of the FPL tendon, to disappear into the synovial membranes at the other side of the tendon. In fig.7 the synovial membranes have been wetted to make them transparent, which reveals the fibrous tendon strand.

Fig.18 shows the stretching of the connection of fig.16. All force in the FPL is taken up by the FDP₂ tendon, while the FPL tendon distal to the connections is slack.

Fig.19 shows a connection between the FPL and FDP₂ as modelled in fig.3.b. An independent muscle belly and end tendon develops from the origin area of the FPL, but joins the FDP₂ tendon before the lumbrical arises. Close dissection showed that within the FDP₂ tendon the main insertion of the tendinous connection separated in different strands which followed different routes within the tendon. A small strand of these fibres ran obliquely to the main direction of the fibres to the deep side of the tendon, where it spread out into minute tendon fibres. These gave rise to minute lumbrical muscle fibres, together with masses of similar minute tendon fibres dividing from the main FDP₂ tendon strands. The specimen of fig.15 had no traceable insertions in the lumbricals.

DISCUSSION

The validity of the model

The model assumptions are not contradicted by the dissection results. Parallelism of tendon fibres corresponds to independent tendons and motors, and deviations from it correspond to fibrous tendons with crisscrossing muscle fibre insertions and tendon strands. Within the carpal tunnel, lumbrical origins are created by extensive rearrangements of fibrous material. In this rearrangement a principle of conservation of tendon fibre mass seems to hold, as tendon fibres can be seen to diffuse in the synovial sheaths, but also to reassemble in tendon strands or give rise to lumbrical muscle fibres. This principle of conservation of tendon fibre mass is incorporated in the model by the assumption that end tendons fibres of elementary muscle fibres continue as entities all the way to their insertion. The sorting out of ECU_p and ECU_L in the carpal tunnel interferes with the function of the synovial membranes. The dissociating tendon fibres are causes of adhesions of these membranes, in addition to the ingrowing in the membranes in the FDP tendons as described in Leijnse et al. (1996). Moreover, synovial membranes and interconnecting masses of tendon fibres may reinforce each other mutually to form strong FDP tendon interconnections. Although the model materials (ECU_p, ECU_L fibres) and assumptions (distally splitting up of the end tendon plates, statistical crisscrossing, and the ECU_p and ECU_L mixing assumption) are simple, they allow to interpret the actual, and to imagine the possible anatomic findings. The model indicates that the FDP, FPL and LU should be seen as a single complex, in which the independence of the muscles to the individual fingers statistically decreases from radial to ulnar, but in which clear chances exist for variations which also limit the independence of the radial motors.

The variability in the insertions of the lumbricals

In the classic anatomic model lumbrical insertions at the ulnar side of the finger are considered anomalous. However, at the dissection table the frequency of lumbricals inserting with both a radial and ulnar tendon is high, and regularly only an ulnarly inserting tendon is present. Perkins and Hast (1993) report, in a sample of 80, 50% of anomalously inserting lumbricals, with 34% of double insertions of the third lumbrical, and 5% ulnar insertions instead of radial insertions of the ulnar two lumbricals. Therefore, a statistical distribution of the insertions of the second and third lumbrical into two end tendons is a realistic anatomic concept.

Bi-insertional lumbricals and finger independence in the hand of the musician

Lumbricals inserting with two end tendons into adjacent fingers can be interpreted in two ways: (i) as two independent lumbricals: one ulnar, and one radial lumbrical; (ii) as one single lumbrical with two insertions. When the muscle bellies of the different insertions can be separately activated, the first view is the realistic one; when they cannot be separately activated, the second view must be accepted. With the bi-insertional lumbricals of our specimen, at the core of the muscle belly the muscle fibres were usually highly interconnected by connective tissue, which indicates that no independent movement of muscle fibres takes place within the main muscle body, although their distal muscle bellies ran independently. This suggests that such a lumbrical muscle

is activated as a unit, i.e. that the force in the insertions cannot be individually controlled. This would mean that with lumbrical activation, a force proportional to the inserting number of muscle fibres is present in each insertion. Such a situation results in a dynamic coupling of finger movement, which may hamper fast finger control in movements in which the lumbricals are highly active.

Independence of muscle bellies and the shape of the area of origin

The FPL and the FDP₂ have generally the most independent of all muscle bellies of the deep flexor group. Functionally this seems evident: in the human hand their independence is most important. In the above the independence of individual deep flexor muscle bellies was correlated to the geometric condition of parallelism of muscle-tendon fibre units in the original tendon fibre plate. Presently this reasoning is stretched (possibly a little far) to point out a correlation between the shape of the deep flexor origin area and the degree of interdependence of the FDP-FPL muscle bellies. The origins of the FPL, FDP₂ and the radial part of the FDP₃ are the volar surface of the radius, the volar surface of the membrana interossea, and the volar surface of the ulna. These origins form (in the supinated position) an almost flat surface. Such a regular geometry of the origin area should facilitate the parallelism of the elementary muscle-tendon fibre units, and hence the independence of the FPL-FDP₂ muscle bellies. In contrast, the muscle mass of the ulnar three deep flexors originates from the volar and ulnar surface of the ulna and the fascia antebrachii. This surface is sharply concave, with the trough where the fascia antebrachii arises from the ulna along a dorsal-ulnar line on the ulna (Leijnse^a et al., 1996). The fact that these muscle fibres arise from different depths, i.e. volar-dorsal levels of origin, and eventually join an end tendon plate which basically lies in a single plane means that they cannot be strictly parallel in the volar-dorsal direction. Therefore, the chances that they will not run exactly parallel in the ulnar-radial direction as well can be assumed greater than with the FPL-FDP₂ fibres. This disturbed parallelism correlates to the greater connectivity of the ulnar three muscle bellies of the FDP. Far from implying a causal link, the issue is raised to warrant that where independence may be correlated to a geometrical condition (of all-over muscle-tendon fibre parallelism), the successful implementation of this geometric condition may be affected by the geometric boundary conditions.

Embryological implications

Fundamental to the present model, as well as to the anatomical model studies of Leijnse^{e,f} (1996) is the assumption that a muscle can be modelled as an assembly of elementary contractile units, consisting of a tendon fibre, a muscle fibre, and a tendon fibre in series; multigastric contractile units being such units in series. This basic assumption allows for simple, yet comprehensive "generic descriptions" of highly specific morphological phenomena, be it muscle shape (Leijnse^e, 1996), perforations of aponeuroses by nerves or vessels and the morphology of anomalous muscle bellies (Leijnse^f, 1996), or the anatomic variability of a complex muscle group as the FDP-FPL-LU complex. This raises the question to what degree muscle fibres indeed grow as basic units together with their individual tendon fibres of origin and insertion.

ACKNOWLEDGEMENTS

The author cordially thanks Dr. E.T. Walbeehm, Dr. J. Zguricas and Dr. D. Nio for their assistance in dissections; and Dr. C.W. Spoor, Prof. Emer. Dr. J.M.F. Landsmeer, Dr. G.J. Sonneveld, Dr. S.E.R. Hovius, Prof. Dr. Ir. C.J. Snijders, Prof. Emer. Dr. J.C. Van der Meulen, and Prof. Dr. J. Voogd, for the discussion of the material; and the custodians of the dissection theatre C. Entius, J. Velkers, and the photographers, E. Dalm and P. Smaal for their kind support.

REFERENCES

- Fahrer, M. (1975) Considérations sur les insertions d'origines des muscles lombricaux: les systèmes digastriques de la main. *Ann. Chir.* 29, 979-982.
- Goldberg S. (1970) The origin of the lumbrical muscles in the hand of the south african native. *The hand* 2, 168-171.
- Leijnse^a, J.N.A.L., Walbeehm, E.T., Sonneveld, G.J., Hovius, S.E.R. (1996) Anatomical interconnections within the flexor digitorum profundus. Submitted to *Anatomical Record*, 1995.
- Leijnse^b, J.N.A.L., Walbeehm, E.T., Sonneveld, G.J., Hovius, S.E.R. (1996) Intertendinous connections between the deep flexor tendons formed by the synovial sheaths in the carpal tunnel. Submitted *anatomical record* 1995
- Leijnse, J.N.A.L., and Kalker, J.J. (1995) A two dimensional model of the lumbrical in the human finger. *J. Biomech.* 28, 237-239.
- Leijnse^a, J.N.A.L. (1996) Why the lumbrical should not be bigger - a synergistic force model of the lumbrical in the human finger. Accepted *J. Biomechanics*.
- Leijnse^b, J.N.A.L. (1996) Measuring anatomical interconnections in the deep flexors of the musicians' hand: theoretical analysis, clinical examples. Submitted *J. Biomech.* 1995.
- Leijnse^c, J.N.A.L. (1996) Measuring anatomical interconnections in the deep flexors of the musician's hand - device and systematic measuring errors. Accepted *J. Biomechanics*, 1995.
- Leijnse^d, J.N.A.L. (1996) Anatomical factors predisposing to focal dystonia in the musician's hand - principles, theoretical examples, clinical significance. Resubmitted to *J. Biomech*, 1995.
- Leijnse^e, J.N.A.L. (1996) A generic model of a muscle group - application to the muscles of the forearm, resubmitted to *Anatomical Record*.
- Leijnse^f, J.N.A.L. (1996) The morphology of the perforations of aponeuroses by nerves or vessels at the medial epicondyle of the elbow. Submitted to *Anatomical Record*, 1995.
- Linburg, R.M. and Comstock, B.E. (1979) Anomalous tendon slips from the flexor pollicis longus to the digitorum profundus. *Am. J. Hand Surg.* 4, 79-83.
- Malerich, M.M., Baird, R.A., McMaster, W., and Erickson, J.M. (1987) Permissible limits of flexor digitorum profundus tendon advancement - an anatomic study. *Am. J. Hand Surg.* 12A, 30-33.
- Perkins, R.E., and Hast, M.H. (1993) Common variations in muscles and tendons of the human hand. *Clinical Anatomy* 6, 226-231.
- Rico Aguado, A. and del Pino Paredes, V. (1988) Flexor digitorum profundus common to thumb and index finger, associated with a post-traumatic distal adherence of both tendons. *J. Hand Surg.* 13-B, 72-74
- Stern P.J. (1990) Tendinitis, overuse syndromes, and tendon injuries, *Hand Clinics* 6, 467-476.

FIGURES

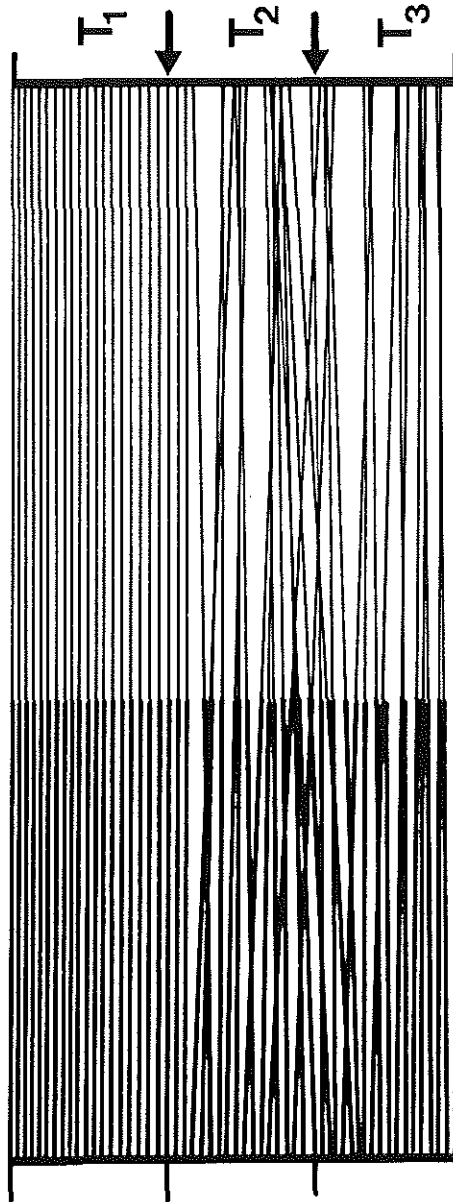


Figure 1 Tendon plate formed by the ECU_p of three FDP tendons. Bold lines: muscle fibres (proximal), thin lines: end tendon fibres. The plate is split up starting at the distal side (arrows). The strictly parallel ECU_p fibres of T₁ will give rise to a completely independent muscle belly and a homogeneous, smooth surfaced end tendon. However, the splitting up of the tendons T₁ and T₂ with crisscrossing ECU_p will result in overlapping origin areas. The crisscrossing of the tendon fibres results in fibre clusters, which should facilitate the formation of individualised tendon fibre strands, rather than smooth compact tendons.

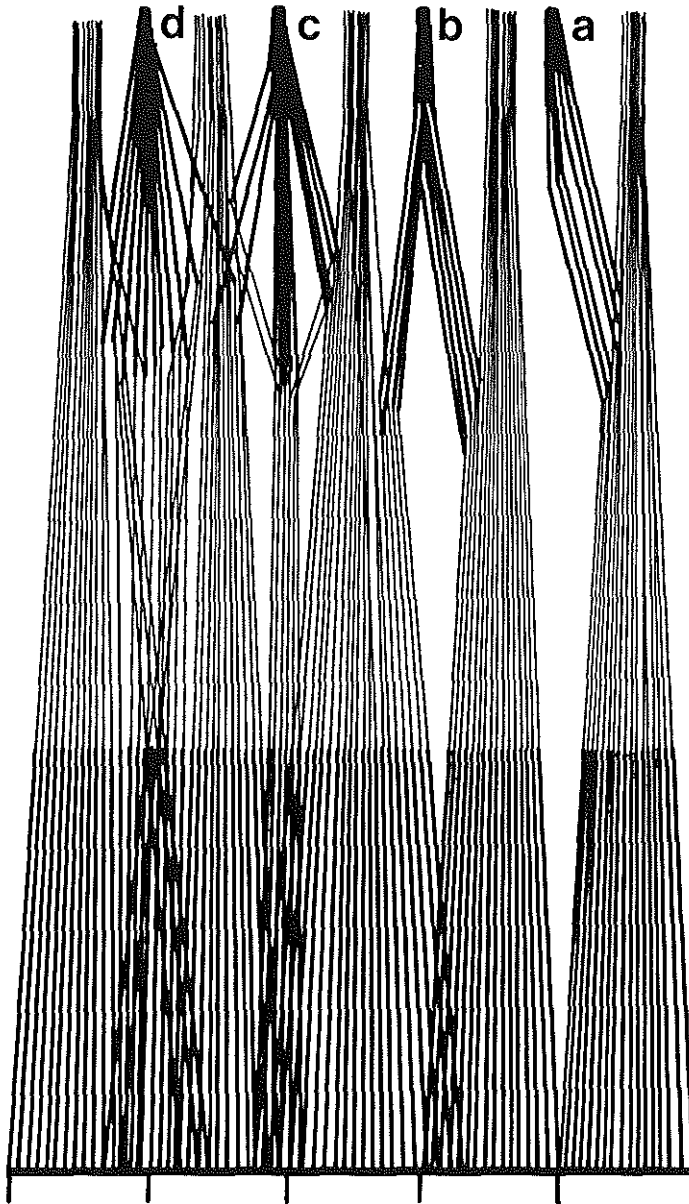


Figure 2 Different FDP-LU muscle morphologies. a) Independent FDP muscle with unipennate lumbrical. b) bitendinous lumbrical muscle. c) lumbrical muscle arising bitendinously from the main FDP tendons, but also from an independent tendon strand. The strand splits up into ECU_L from which lumbrical muscle fibres will arise, and ECU_p tendon fibres which in this case join both tendons. d) Lumbrical muscle arising with a continuous origin spanning the space between the radial and ulnar tendons of origin, and with a muscle part arising well outside the "normal" origin area. In b, c, and d crisscrossing of ECU_p/ECU_L leads to interdependent muscle bellies, and crosswise interconnected FDP tendons (c and d).

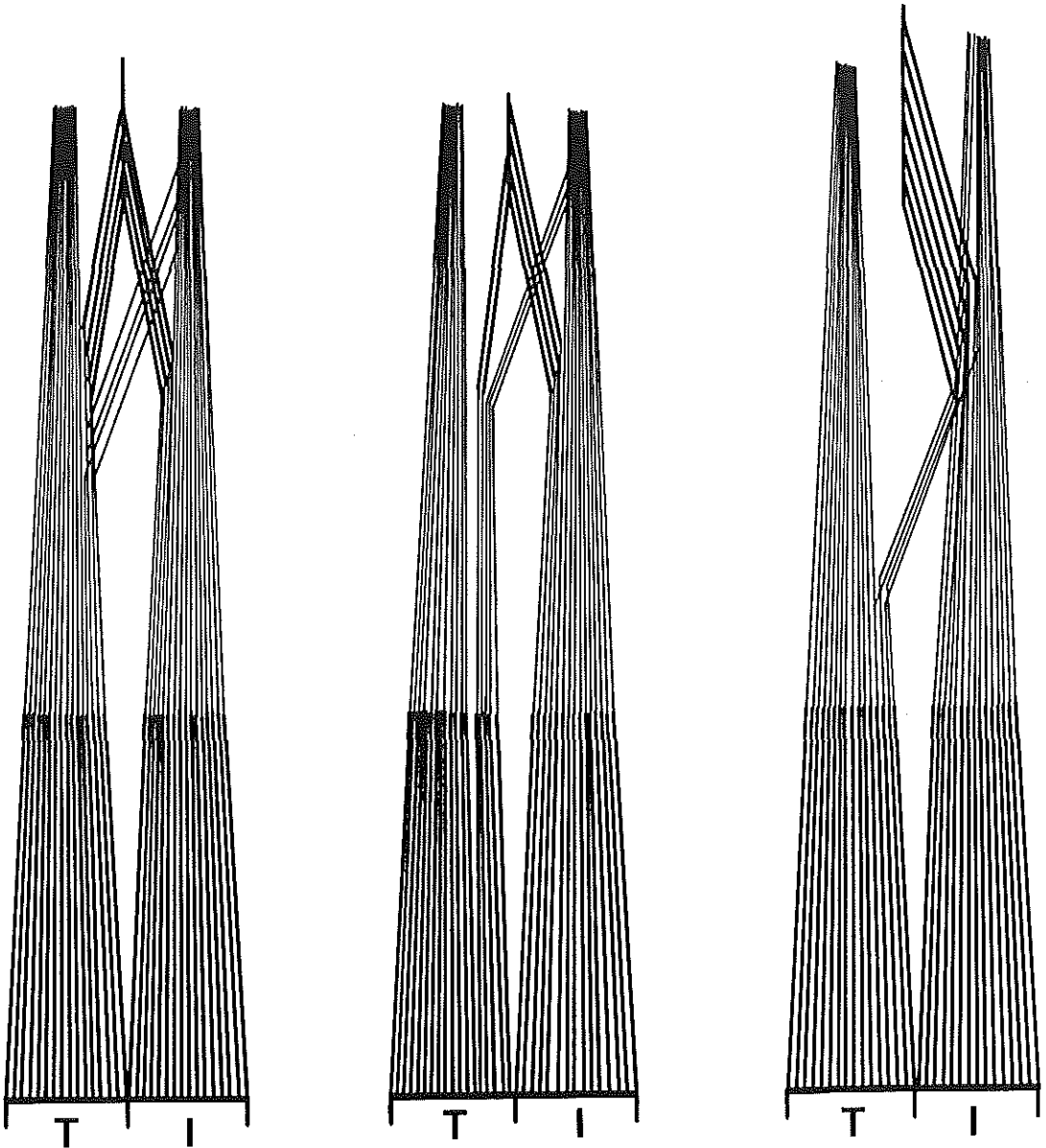


Figure 3 a,b,c Connections running from the FPL tendon to the FDP₂ tendon. a) ECU_L arise from the FPL origin and run with the FPL tendon until giving rise to lumbrical fibres: a bitendinous lumbrical results. A tendinous interconnection is also present, consisting of ECU_p from the FPL origin area, but included with the FDP₂ tendon when the end tendon plate was partitioned. b) The ECU_L and ECU_p arising from the FPL origin form a small intermediate tendon strand. The ECU_L end in lumbrical muscle fibres, the ECU_p continue in the FDP₂ end tendon. c) The ECU_L and ECU_p tendon fibres fuse proximally with the FPL tendon, but separate to join the FDP₂ tendon before the lumbrical arises. The ECU_L give rise to lumbrical muscle fibres, the ECU_p continue with the FDP₂ tendon.

A generic model of the FDP-FPL-LU complex

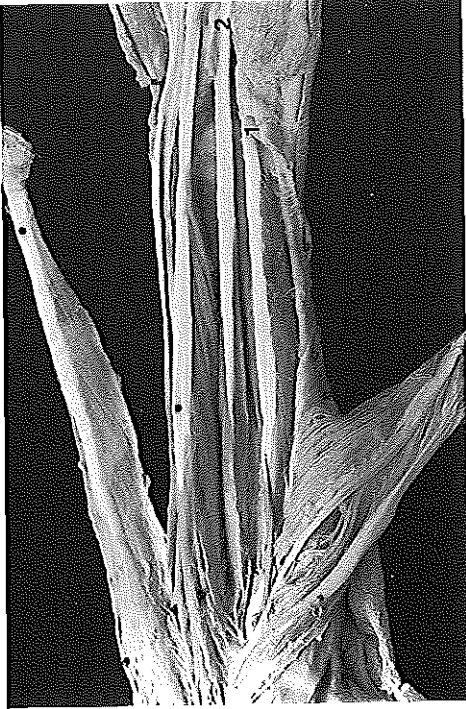


Figure 4

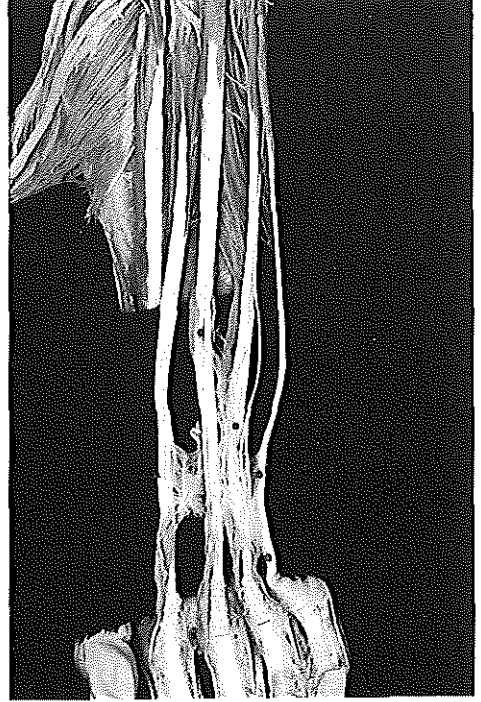


Figure 5

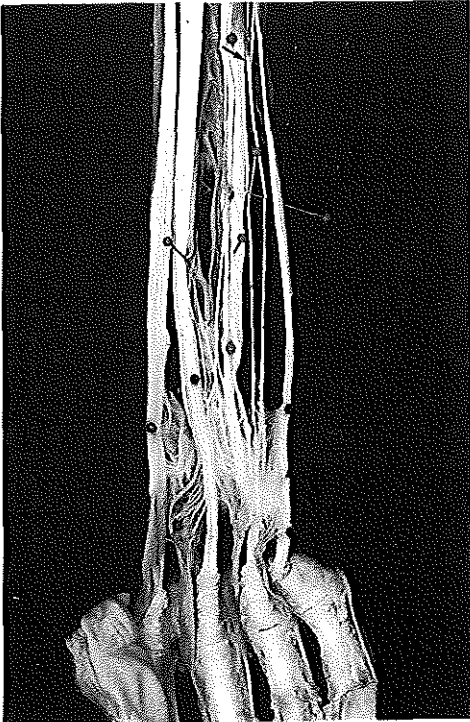


Figure 6

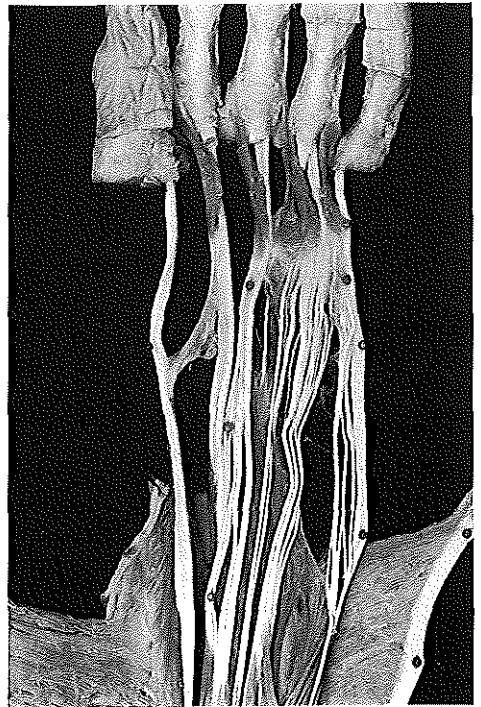


Figure 7

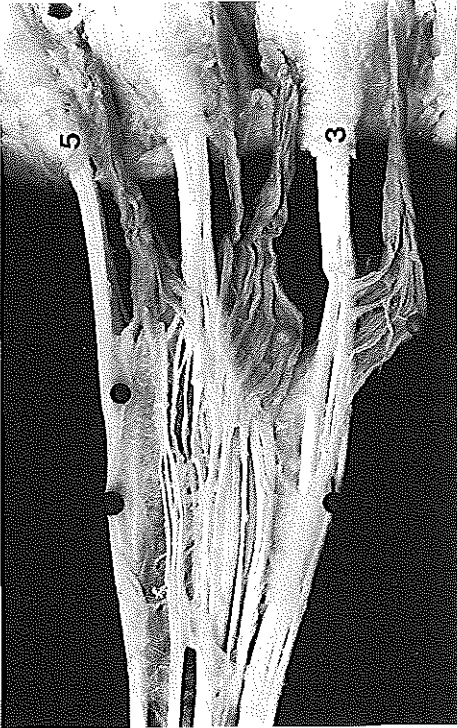


Figure 8

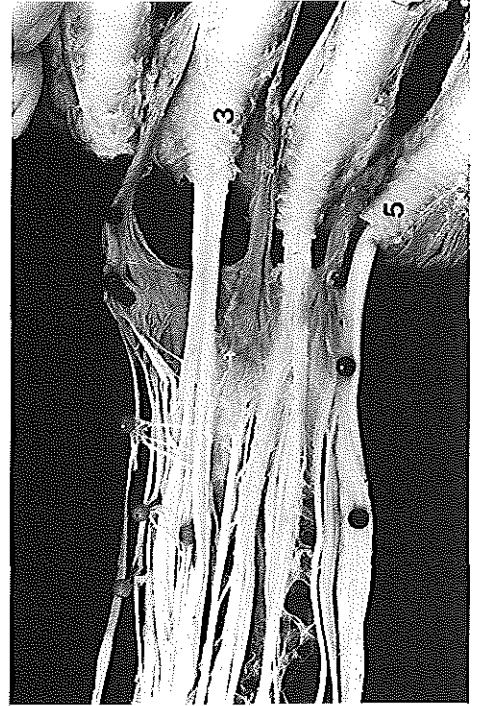


Figure 9



Figure 10

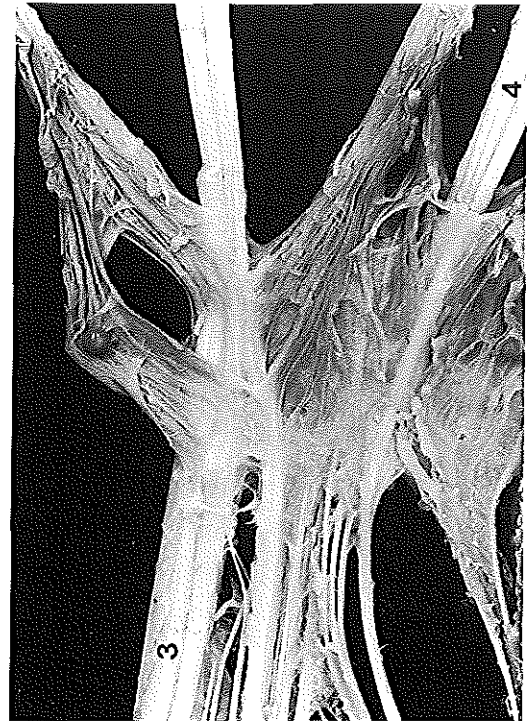


Figure 11

A generic model of the FDP-FPL-LU complex



Figure 12



Figure 13

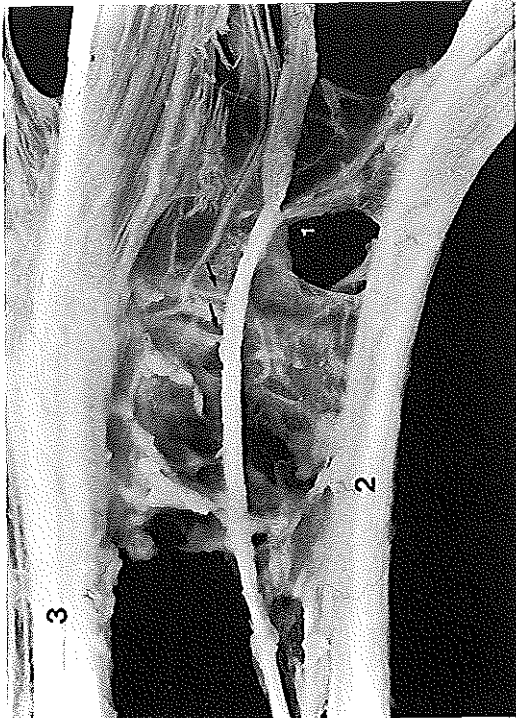


Figure 14

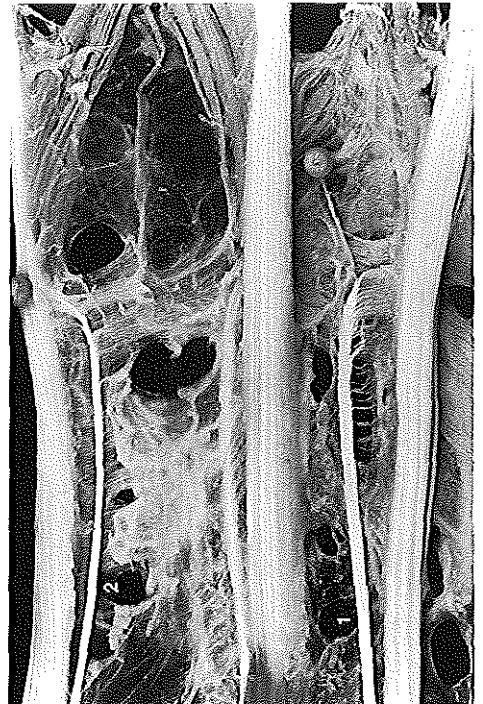


Figure 15



Figure 16

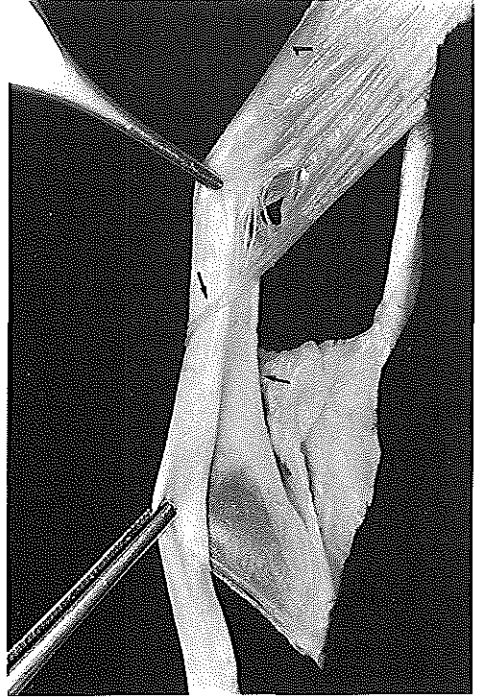


Figure 17



Figure 18

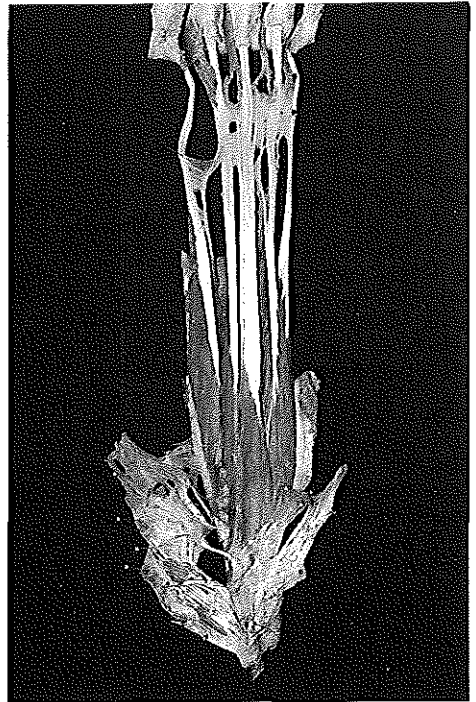


Figure 19

Captions with the figures 4-19

Figure 4 Independent FPL (1) and FDP₂ (2) muscle bellies, showing a very regular structure of tendons and muscle fibres, easily separable by blunt dissection.

Figure 5 FDP₂-FDP₅ of the specimen in fig.4 (top is radial). The muscle bellies of the FDP₃-FDP₅ are not completely separable by blunt dissection, and have muscle fibres and tendon strands crossing over between the main tendons. Note that the dissection of such muscle bellies can only be achieved from distally to proximally, conform to the model of the splitting up of the common end tendon plate.

Figure 6 FDP₂-FDP₅ tendons of the specimen of fig.4, with crisscrossing tendon strands and distal muscle bellies. The arrow (right) points to crisscross inserting muscle fibres, conform to the model of fig.1.

Figure 7 Volar of a FDP-FPL-LU muscle-tendon complex, with the FDP₃-FDP₅ consisting of numerous fibrous strands (top is radial). Bi-insertional third lumbrical, and a synovial-tendinous FPL-FDP₂ connection.

Figure 8 FDP₃-FDP₅-LU complex. Strong connecting synovial membranes. LU₂ originates from tendon fibres running quite radially in the FDP₃ tendon; LU₃ is mono-tendinous of origin but bi-insertional, and originates from tendon fibres distributed all over the FDP₄ tendon, in contrast to LU₂. LU₄ originates mainly from FDP₄, and a thick independent tendon strand between FDP₄ and FDP₅, as in fig.2.c. This strand further inserts in FDP₄.

Figure 9 FDP₃-FDP₅ tendons interconnected by crisscrossing tendon fibres into a single tendinous unit. LU₃ is bi-insertional, with a very thin insertion in the fourth finger.

Figure 10 FDP₂-FDP₅-LU complex with LU₃ partly removed from FDP₄, showing the cut ends of the tendon fibres of lumbrical origin (arrow), and the decrease in thickness of the FDP₄ tendon. LU₃ inserts in the third finger. LU₄ is absent.

Figure 11 FDP₃-FDP₄-LU complex. LU₂ and LU₃ originate from an overlapping area of origin on a tendon strand which inserts both in FDP₃ and FDP₄.

Figure 12 FDP₂-FDP₅-LU complex showing independent tendon strands dissolving into and assembling from minute tendon fibres in the synovial membranes. 1: tendon strand of origin of both LU₁ and LU₂, 2: tendon strand dissolving into tendon fibres inserting in both FDP₂ and FDP₃ and LU₃, 3: tendon strand assembled from tendon fibres splitting up from FDP₂ and from tendon strand 2.

Figure 13 Same specimen as fig.12. 2 and 3 as in fig.12. 4: tendon fibre mass separating from FDP₅ well in advance to LU₄.

Figure 14 FDP₂-FDP₅-LU complex. 1: Lumbrical dominated tendon strand of origin, with a small insertion in FDP₂ (distal to 1), and even smaller insertions in FDP₃ (arrows).

Chapter VI.iii

Figure 15 FDP₂-FDP₄-LU complex. 1: tendon strand dissolving into minute tendon strands which join the FDP₄ tendon; some strands which join the FDP₃ tendon; and a remainder which inserts in LU₃. 2: tendon strand which partly inserts into FDP₂, and at the opposite side dissolves in a mass of tendon fibres which run down to FDP₃ to give rise to some lumbrical tendon fibres, just above FDP₃.

Figure 16 Tendinous-synovial membrane connection between the FPL (1) and the FDP₂ (2) tendons.

Figure 17 Reverse side of the FPL tendon of fig.16. The arrows indicate two tendon strands crossing over to FDP₂, one small strand running above, and a bigger strand running beneath the FPL tendon.

Figure 18 The proximal displacement (to the left) of the FPL tendon (top) tautens both the synovial membranes and the tendinous connections. The distal FPL tendon remains slack, the distal FDP₂ tendon is tautened.

Figure 19 FDP-FPL-LU complex with an independent muscle belly which arises from the FPL origin and inserts into the FDP₂ tendon proximal to the LU₂ origin. Illustration of fig.3.b.

CHAPTER VII

SURGICAL CLEARANCE OF INTERTENDINOUS CONNECTIONS - A CASE STUDY

**Total surgical clearance of intertendinous connections in a musician's hands,
including cleavage of bitendinous lumbrical origins - a case study**

J.N.A.L. Leijnse, and J.E. Bonte

TOTAL SURGICAL CLEARANCE OF INTERTENDINOUS CONNECTIONS IN A MUSICIAN'S HANDS, INCLUDING CLEAVAGE OF BITENDINOUS LUMBRICAL ORIGINS - A CASE STUDY

J.N.A.L. Leijnse[§] and J.E. Bonte[¶]

[§]Dept. of Plastic and Reconstructive Surgery, Erasmus University Rotterdam, The Netherlands;

[¶]Emmanuel Hospital, Wetteren, Belgium.

ABSTRACT

A case is presented of total clearance of intertendinous connections in the extensors, superficial and deep flexors, and lumbricals in both hands of a musician with overuse problems. In addition, tightly interconnected bi-tendinous origins of bipennate lumbricals were released. A remarkable finger independence resulted, without functional loss of force or control. The results of surgery are demonstrated by the post-operatively measured force transfers between the deep flexors of adjacent fingers. The case shows that surgical clearance of intertendinous connections between the extrinsics is feasible and that it may greatly improve finger mobility and resolve overuse symptoms, but also that it will not relieve force transfers due to co-activation of the muscle bellies. Surgical complications are also discussed.

INTRODUCTION

The present case study discusses the results of the removal of all congenital non-pathological intertendinous connections between all extrinsic tendons and the lumbricals in both hands in a violin player with finger coordination problems. The complaint involved problems with finger coordination in playing, and, in a later career, with hand writing. The idea of solving problems with instrumental technique due to a lack of finger independence by severing intertendinous connections is not new. Already in 1885 Forbes (Editors note in *Medical problems of performing artists*, March 1991) advocated the surgical removal of the juncturae tendinum between the extensors in musicians. Apparently, he even operated about 300 hands, but such practice did not persist into the twentieth century. Recently, McGregor and Glover (1988) reported a successful case of the removal of the juncturae tendinum in a pianist with a well-defined finger extension problem. Beneficial effects on hand function of the clearance of other intertendinous connections have been reported, e.g. of connections between the long thumb flexor and the deep flexor of the index (Lombardi et al., 1988). To our knowledge, however, no case has been presented of the clearance of all connections between all extrinsic tendons, and between adjacent lumbricals. The aim of the present case report is to demonstrate (i) that intertendinous connections between the extrinsic tendons may cause hand problems, both in instrumental playing and in normal hand function, (ii) that these connections can be removed without functional impairments if proper care is taken to prevent collateral damage, (iii) that their removal may relieve symptoms, and further (iv) to present quantitative evidence about the functional outcome of such surgery. To this end photographic evidence is presented, while also the post-operative force transfers between the deep flexor tendons are measured by a special measuring device (Leijnse^b, 1996). Unfortunately, no

Total clearance of intertendinous connections

pre-operative measurements are available, as the device was only recently designed. However, a measuring result of another musician is provided as representative for the general force transfer characteristics between strongly interconnected deep flexor tendons. The present case initiated the model studies of Leijnse et al. (1992, 1993), and Leijnse^{a,c} (1996), which present a biomechanical analysis of the effects of intertendinous connections on finger movements and finger motor load, and the anatomical studies of the interconnections in the deep flexor group of Leijnse^{a,b} et al. (1996), and Leijnse^d (1996). Interconnections between the extensor tendons (juncturae tendinum) are discussed in von Schroeder et al. (1990). Reports on hand problems in musicians due to anatomical interconnections in the hand were presented by, amongst others, Markison (1990), and Stern (1990). General reports about hand problems in musicians, and focal dystonias, are presented by e.g. Fry^{a,b} (1986); Cohen et al. (1989); Lockwood (1989); Amadio and Rusotti (1990); Hochberg et al. (1990).

MATERIAL AND METHODS

The patient is the first author, the narrative will therefore be in the first person. I first developed finger control problems in the left hand as a violin student. The initial complaint was increasing difficulties with playing scales and fast passages regularly. To investigate this problem, during eight months I exercised a set of elementary finger movement combinations, which I considered basic to the violin playing, for three to four hours a day, with intermediate periods of rest. After this period I couldn't play a note in tune anymore. No pain was present, but a feeling of weakness and discontrol in the fingers. Moreover, a similar problem had become manifest in the right hand with bowing. Since a violonistic career seemed excluded, I went on to study graphic arts but after a year developed similar problems in the right hand. The complaint was a loss of fine motor control with drawing and engraving. More accurately, the "resolution" of the voluntary positioning of a line, and the control of its thickness and curvature decreased from highly accurate to inaccurate. No sign of tremor or nervous disorder was present, but there was a constant feeling of "stiffness" in the hand. I quit this career to study civil engineering, with a major in mathematics. However, handwriting soon became a problem, with symptoms similar as with drawing. In the writing of mathematical expressions, this led to a double impairment. First, the individual characters themselves were badly readable; second, it was impossible to arrange them into an orderly layout, making it difficult to recognise a written expression as a mathematical concept. This proved a severe handicap, which resulted in many formula manipulation errors. A vicious circle ensued: bad handwriting forced errors which needed to be corrected, which implied more hand writing. With no evidence of nervous disorder, and ample earlier proof of an above average motoric ability, I became convinced that the cause of these complaints was within the mechanics of the hand itself. The only difference with "normal" hands I could initially observe were the very strong juncturae tendinum between the extensor tendons. However, after their removal it became apparent that all other finger tendons (superficial flexors, deep flexors and lumbricals) were highly interconnected too. All these connections were removed in different stages by the same surgeon (second author). The aim of the surgery was twofold. In the left hand, it was

Chapter VII

to regain virtuose playing skills. The assumption was that the violinistic problems resulted from the lack of finger independence caused by the intertendinous connections, which motivated their removal. In the right hand, the aim was to restore basic hand skills such as writing and drawing. Assumed was that the right-hand "stiffness" was due to similar intertendinous connections, and that a generally increased hand/finger mobility would eliminate these problems also. Both assumptions turned out to be basically correct. In the surgery, the left (non-dominant) hand served as a model for the right hand, in which the same surgical procedures were implemented at a later stage, with the benefit of the left hand experience. The rehabilitation was carried out vigorously and despite the large number of operations unimpaired tendon mobility was obtained, albeit that regular mobilisation exercises are required up to this day to maintain this optimal result. The removal of the connections improved the kinematic finger independence to above normal ranges, and resolved all original symptoms of dysfunction. In the four fingers of both hands no loss of finger strength resulted. In both thumbs, however, the opposition was weakened by the repeated cleavage of the retinaculum flexorum, which did not regenerate due to vigorous post-operative mobilisation of the flexor tendons. Ironically, although the surgery had removed the original symptoms, this weakness of the thenar muscles eventually resulted in a full-blown focal dystonia in the thenar group muscles due to hand writing, involving muscle pain and discontrol. This problem was resolved by the reconstruction of the flexor retinacula, which, by improving the mechanical effectiveness of the thenar muscles, restored the basic thumb strength. Although the thumb never regained its full previous strength, in normal tasks no pain or sensible weakness remains. In the following a systematic overview of the surgery and results per muscle group is given. Both hands received similar treatment with similar results, therefore, the comments hold for both hands unless indicated otherwise.

Chronologic review of surgical procedures and findings

The first operation was in 1979, the last in 1990. The follow-up of the final extensor surgery is 14 years in the left hand, and 12 in the right hand. The follow-up of the surgery on the FDS is 14 years, left, and 12 years for the FDS, right. For surgery on the FDP, including cleavage of the lumbrical origins: 8 years left, and right. Reconstruction of the flexor retinaculum: 7 years, left, and 6 years, right.

Removal of the juncturae tendinum in the M. extensor digitorum communis (EDC)

First, all juncturae tendinum between the EDC tendons were removed. The left hand was treated first. Three operations were required, since after the first two the connections grew back, despite vigorous mobilisation. At the third operation, a long incision was made to allow full exposure, connective tissue was carefully removed from the tendon edges, and the exposed surfaces strongly coagulated. At the right hand one operation with the latter procedure proved sufficient. Post-operatively, the EDC₅ tendon to the little finger proved common to the EDC₄ tendon to the ring finger in both hands. This still limited independent D₄ extension with D₅ flexion. During one of the later flexor operations the EDC₅ tendons in both hands were transposed to the EDC₄ tendons. This was achieved by obliquely cutting the EDC₅ tendon at midcarpal level, and suturing the

Total clearance of intertendinous connections

proximal end to the EDC₄ tendon, and the distal end to the extensor digiti minimi.

Results. The overall result of the removal of the juncturae tendinum was an increase to above normal ranges of the active extensor independence between all fingers (fig.1). Moreover, there was a greatly increased mobility of the ulnar two metacarpals, which improved the feeling of suppleness of the hand, and a marked improvement of grip function because of the increased ability to mould the hand around the grasped objects. No dislocation of the extensor tendons at the MCP joints ensued. However, violin playing did not substantially improve, and it became apparent that similar interconnections existed between the flexor tendons.

Removal of connections between the superficial flexor tendons (FDS)

The superficial flexors were inspected. Within the carpal tunnel, in both hands adhesions were found between the tendons, presumably due to the synovial sheaths. These adhesions were severed, including the connections between the FDS₄ and FDS₅ tendons. Such connections have been reported by Baker et al. (1981), and Austin et al. (1989). The muscle bellies of the FDS extended quite distally, up to the carpal tunnel. Connective tissue was removed between the FDS muscle bellies from distal to proximal as far as the surgeon considered feasible. No traces of tenosynovitis were present.

Results. The procedure increased the independence of the superficial flexors to the maximal physiological ranges allowed by the joint movements, except between the little and ring fingers. The ring finger can be flexed with active FDS without affecting the little finger. However, flexion of the little finger with active FDS will still transfer some force to the FDS₄ tendons, although this force is not sufficient to limit the greatly increased range of independence (fig.2). Despite these considerable increases in EDC and FDS independence, many violinistic movements still proved kinematically impossible. This was due to strong interconnections between the deep flexors, which were subsequently inspected.

Removal of connections between the deep flexor tendons (FDP)

The exploration of the deep flexors revealed in both hands strong interconnecting synovial membranes, as investigated in Leijnse^{a,b} et al. (1996), and Leijnse^d (1996). The deep flexor tendons were separated from each other by cutting these interconnections distally up to the lumbrical origins, and proximally as far as considered feasible. The synovial sheaths themselves were not excised.

Results. The result was a clearly increased "feeling" of finger independence, i.e. the fingers felt more "loose". However, the increase in the actual kinematic range of the independence of the deep flexors was very limited. This range can be tested by keeping one finger in a flexed position with active deep flexor (i.e. with flexed DIP joint), and passively extending the adjacent finger(s) by pulling them by their fingertips. Connections between the deep flexors would prevent such extension. However, at the time of surgery, the surgeon had noted that all lumbricals, except the first (of the index), had bi-tendinous origins (i.e. from both their ulnar and radial FDP tendon) which were tightly interconnected by connective membranes. Obviously, such interconnected bi-tendinous origins also limited independent FDP tendon displacements.

The cleavage of the lumbrical origins

For the removal of the restrictions on the relative FDP tendon displacements caused by the lumbrical origins two options were considered. The first was to separate the ulnar and radial heads of origin of the lumbricals as far distally as feasible (fig.4), to allow the V shape of the origins to open up when the FDP tendons displace in opposite directions. The nerves and vessels are likely to enter and interconnect these muscle bellies halfway their length, so that the separation of the radial and ulnar heads would distally be limited to somewhat less than half the lumbrical fibre length ($L_{LU}/2$). This would allow a relative FDP displacement equal to the lumbrical fibre length (L_{LU}), at which the V of the origins would be fully stretched. Since $L_{LU} > 5\text{cm}$ (Brand, 1985), this is more than the maximal *physiologically* possible opposite FDP tendon displacement, which is less than 5 cm, being equal to the FDP excursion from full finger extension to full finger flexion. Therefore, the procedure seemed theoretically safe, as the nerves and vessels interconnecting the radial and ulnar heads could not be strained to the point of harm by the opposite displacements of the deep flexor tendons. Nevertheless, this procedure would still leave a *dynamic coupling* of the FDP tendons by the lumbrical muscles, as the lumbrical muscle force would pull both flexor tendons of origin in proportion to the relative cross section of the attached heads. Therefore, as a second option the uni-tendification of the lumbrical origins was considered, i.e. the transposition of the radial head from the radial tendon to the ulnar tendon of origin. Hereby the radial lumbrical origin would be harvested from the radial tendon on a thin strip of FDP tendon fibres, which was to be sutured on the ulnar FDP tendon. At surgery the first option was pursued, because in all bi-tendinous lumbricals the radial and ulnar muscle parts were clearly outlined (as in fig.7), so that maximal tendon mobility could be obtained with minimal risk by merely cutting the strong synovial-tendinous membranes which interconnected the lumbrical origins.

Results. The cleavage of the connective tissue between the bi-tendinous lumbrical origins resulted in an immediate, marked increase in the independence of the deep flexors. Moreover, with vigorous mobilisation of the flexors in opposite directions, this range increased daily for more than a month, until about the maximal physiological range of deep flexor independence was achieved. No pain or loss of extension strength in the fingers whatsoever resulted from the lumbrical surgery; nor did any sensible loss of the flexor strength become manifest. The figs.3 show the result today: all fingers can be completely flexed with strongly active FDP while the adjacent fingers remain extended. In the photographs, the activity of the FDP in the flexed fingers is guaranteed by the firm pressing, with flexed DIP joints, of a pen against the palm of the hand. "Normal" subjects would press the pencil by using the superficial flexors, of which the tendons are usually far less interconnected than the FDP. This would leave the DIP joints hyperextended.

Despite the dramatic improvements obtained so far in the independence of all tendons in both hands, many violinistic or pianistic movements still proved difficult, especially in the left hand (- I learned some piano playing to validate the effect of the surgery. In piano playing all fingers have basically identical playing positions, so that their actions can be easily compared. In the violin playing the left hand finger positions differ greatly between fingers, which complicates comparative movement analysis). It could be verified that a remaining problem in the left hand was a strong interaction of the deep flexor-lumbrical complexes of adjacent fingers. Hereby the

Total clearance of intertendinous connections

strong activation of the deep flexor-lumbrical complex in one finger would "stiffen" the adjacent finger into a swan-neck like position, which obviously resulted from the fact that both the extensor assembly and the deep flexor tendon of the passive finger were simultaneously proximally pulled. These coupling effects could not be caused by bi-tendinous lumbrical origins, or by mal-insertions of the lumbrical muscles, because the activation of the index would particularly strongly affect the passive medius, while the lumbrical of the index was mono-tendinous of origin, well formed, and well inserted.

A strong fascia interconnecting the lumbrical muscle bellies

The lumbricals in the left hand were explored distal to their origins. It was found that all lumbrical muscle bellies, including the lumbrical of the index, were interconnected by a strong fascia, to which the muscle bellies strongly adhered.

Results. The resection of this fascia nearly fully removed these dynamic finger coupling effects. A slight coupling remained, but diminished over the years. This may be due to the fact that a part of the connective fascia remained in situ, e.g. at the dorsal side of the lumbricals which is difficult to reach surgically, but has gradually been mobilised by exercise. The stiffening of passive fingers with the activation of adjacent fingers can be explained from these surgical findings. The co-active force transfers in the deep flexors would tense the deep flexors in the passive fingers, while the lumbrical activity would tense the interconnecting fascia and with it the lumbrical of the adjacent finger. This would produce the typical pre-op symptoms: a passive finger which would tend to flex in the DIP while simultaneously hyperextending in the PIP, i.e. which would stiffen between a tautened deep flexor and a tautened dorsal aponeurosis into a swan-neck-like position.

By now an above normal active finger independence was obtained with fully mobilised tendons, and many instrumental movements previously infeasible had become feasible. Nevertheless, the full use of the deep flexors in instrumental playing was still compromised. Three causes could be hypothesised. (i) Malinserting lumbrical muscles. (ii) Co-activation of FDP muscle bellies. (iii) Dynamic coupling of deep flexors by the bi-tendinous lumbrical origins. Only recently, after the design of the measuring device presented in Leijnse^b (1996), the co-activation of the FDP muscle bellies could be verified (fig.5, see further). At that time, however, it was decided that during the reconstruction of the flexor retinaculum in the right hand, the lumbricals should be checked for anomalous insertions, to exclude possibility (i), and an uni-tendification by transposition of the radial heads should be attempted, to exclude possibility (iii).

Further surgical evidence of lumbrical function

At operation, no fascia between the lumbrical muscle bellies was found in the right hand, nor any evidence of anomalous insertions. The surgeon decided that uni-tendification of the origins of the ulnar two lumbricals would create a local muscle bulk which could interfere with the carpal ligament reconstruction. Therefore, the two ulnar lumbricals were not further modified (the radial and ulnar heads had been released in a previous operation). However, the second lumbrical (to the medius) derived only a minute radial head from the index flexor tendon. This origin was severed not by transposition, but, because of its minuteness, by cutting the muscle fibres close to the

tendon, leaving them hanging free. Immediately post-operatively, there was a slight but noticeable difference in the resting position of the PIP of the medius, with some slight sensation of PIP discontrol. These symptoms disappeared in the following weeks. Only when I type very quickly for extreme periods of time with "strongly deep flexor controlled" movements a slight reminder of this feeling may develop. Clearly, the sacrifice of lumbrical muscle fibres in a musician's hand is disadvised. However, a lasting beneficial effect was a marked improvement of the "dynamic independence" of the right hand index and medius in the piano playing, e.g. thrills could be played more regularly and controlled. This shows that bi-tendinous lumbrical origins do subtly affect dynamic finger independence.

DISCUSSION

Surgical results

Kinematic finger independence is restricted by intertendinous connections, rather than by common muscle bellies

Kaplan (1965) reports an experiment in which he resects the juncturae tendinum between the extensor tendons, and electrically stimulates the muscle bellies, only to note that the independence of the tendons, as pulled by the stimulated muscles, is not greatly increased. From this he concludes that the real cause of the kinematic finger interdependence is within the muscle bellies, and not the juncturae tendinum. The present results, however, contradict these findings. Both the juncturae tendinum and the connections between the deep flexors were so stiff and tight that they limited almost any independent tendon displacements within these muscle groups, including the tendons of index and medius. Therefore, it can be reasonably assumed that also the muscle bellies to the different fingers were heavily interconnected by connective tissue, resulting in what Kaplan calls "a common muscle mass". Nevertheless, after clearance of the connections, in both hands between all tendons active opposite displacements became possible basically equal to the maximal ranges allowed by the joint displacements. This increase in finger independence was not immediate. Especially in the deep flexors of medius, ring and little finger, the actual range of independence only resulted after vigorous mobilisation for a period of a month or more. Clearly, the opposite displacements of the muscle bellies required the prolonged mobilisation of connective tissue which had never before been stretched, and possibly of nerves and vessels criss-crossing in between the different muscle parts as well (Leijnse^a et al. 1996). The present case, of course, does not exclude that in other cases cross-insertions of muscle fibres in different tendons and connective tissue within muscle bellies may present more severe limitations on independent movement.

Force transfers within the deep flexors

In Leijnse^a (1996) the general force transfers in the deep flexor were modelled, and experimentally validated by a measuring device presented in Leijnse^b (1996). In these studies it is shown that force transfers result from (i) the stretching of intertendinous interconnections, and (ii) co-activation of muscle bellies to different end tendons. These can be distinguished by the fact that co-activation of muscle bellies is in first order independent of the finger position, while passive

Total clearance of intertendinous connections

interconnections only become stretched and transfer force when the FDP tendons are pulled in opposite directions. Fig.5 presents the post-operative force transfers between the deep flexors measured with the mentioned device. The pre-operative results would have been similar to the reference result of fig.6, which presents the force transfers between two deep flexors which are highly interconnected. The results of fig.5 show that no strong passive interconnections are present between the deep flexor tendons of any two fingers. However, minor passive interconnections become manifest with greater opposite deep flexor tendon displacements, as quantified by the PIP rotations. These force transfers are to all probability caused by the stretching of connective tissue between the muscle parts moving in opposite directions (one part contracting, the other part pulled by its end tendon). From these results, and the figs. 1, 2 and 3, it can be concluded that *kinematic finger independence* (large ranges of independent tendon displacements) does not necessarily result in *dynamic finger independence*. Hereby the question remains whether the co-active contraction patterns within the muscle group can be altered by training.

Juncturae tendinum and extensor subluxation at the MCP joints

The juncturae tendinum have been generally thought of as structures which help to prevent the subluxation of the extensor tendons at the MCP joints. In present case (two hands) their removal has not resulted in extensor subluxation (follow-up of 14 and 12 years). It therefore seems that the risk of subluxation is small when (i) the extensor tendons are well positioned at the MCP joints, and (ii) the transverse laminae (Zancolli, 1968) which at the MCP run from the extensor tendons collaterally to the volar plates and which keep the extensor tendons in position at the MCP are well formed. Nevertheless, it remains a point of concern.

Do connections between the deep flexor tendons have a functional significance?

Functionally, little significance can be ascribed to the connections between the deep flexor tendons in the carpal tunnel. In Leijnse^b et al. (1996), and Leijnse^d (1996), these connections were investigated and it was hypothesised that they result from the trapping of the synovial membranes within the rough fibrouslike tendons of the deep flexors in the carpal tunnel, rather than being the implementation of a functional design. The present case shows that these connections are not present to protect lumbricals with bi-tendinous origins from being torn apart. Rather, it can be assumed that when the deep flexor tendons of origin of bi-tendinous lumbricals are unconnected, the lumbricals will develop fully mobilised and independent radial and ulnar heads of origin (fig.7), as have in the present case been surgically created without functional harm. In practice, the clearance of connections between the deep flexor tendons is far from obvious, since the synovial membranes, crisscrossing tendon fibres, and the lumbrical origins may form an unentangled entity (Leijnse^d, 1996).

Lumbrical origins can be separated without harmful effect on finger function

The results show that it is feasible to separate the origins of the lumbricals to allow greater freedom of FDP tendons without harm to their function. In present case all bi-tendinous lumbrical origins had distinctly delineated radial and ulnar heads, which allowed their easy separation.

Chapter VII

However, as the lumbrical to the little finger in fig.7 shows, when the tendons are highly interconnected the delineation of the radial and ulnar heads is not always present, and without this the surgical separation of the lumbrical heads at their origins is not obvious. In these cases, it seems more obvious to create independent FDP tendons by the uni-tendification of the lumbrical origins, i.e. by transposing the radial origin to the ulnar tendon - if the lumbrical insertion is anatomically correct. The case-study presents some evidence that bi-tendinous lumbricals, even with fully mobilised radial and ulnar heads, do constitute dynamic couplings between the deep flexor tendons which may subtly affect playing movements. Therefore, with respect to the creation of dynamic finger independence, uni-tendification seems the ideal option of lumbrical origin modification.

Sectioning of the flexor retinaculum is contraindicated

Considering the serious functional sequelae, such as thumb weakness by the loss of mechanical effectiveness of the thenar muscles, the complete sectioning of the flexor retinaculum is strongly contraindicated. If the ligament is transected, the hand should be splinted with the wrist in extension such that flexor tendon mobilisation does not interfere with the proper regeneration of the flexor retinaculum.

Tendinous interconnections can affect normal hand functions such as hand writing

The results indicate that tendinous interconnections may hamper normal hand function, such as writing. Initial problems disappeared after the removal of the connections. The biomechanical analysis of these phenomena is beyond the scope of the present paper.

Hand problems in musicians

Even with fully independent extrinsic tendons, playing difficulties may arise due to anomalies in the lumbricals

The results show that even with fully kinematically independent flexor and extensor tendons, playing difficulties may arise when the lumbricals are malformed or interactive. In the present case, with lumbrical muscle bellies interconnected by an adhesive fascia in the left hand, it was impossible to execute regular alternating fast finger movements, notably in playing thrills with index and medius at the piano, or similar movements involving combinations of movements of these fingers. This diagnosis was unambiguous. After clearance of the extrinsic connections the hand was well exercised for 1.5 years without improvement of these coordination difficulties. The symptoms were greatly relieved immediately post-operatively after the sectioning of the adhesive fascia. By inference, similar problems can be expected from mal-inserting (bi-insertional) lumbricals. Hereby holds that mal-inserting lumbricals not rare (Perkins and Hast, 1993; Leijnse^d, 1996).

The weakness in the pianist's fourth finger

In the biomechanical explanation of coordination difficulties in the musician's hand, the juncturae tendinum have always been highlighted as possible causes. Clearly, they can severely limit

Total clearance of intertendinous connections

extensor displacements, and therefore hamper finger independence in playing. The fact that the practice of excising them, as already advocated by Forbes (1885), has not prevailed indicates that this procedure did not meet the expected results, which motivated the idea that interdependencies within the extensor muscle bellies themselves were the main cause of the restrictions (Kaplan, 1965). The present case shows that although the clearance of the juncturae greatly improved the extensor independence, this independence was of little functional value in actual playing, because of all the connections - and possibly also the co-activations in the extensors - which remained. This concurs with the results of Leijnse et al. (1992, 1993), which theoretically show that connections between the extensors and between the flexors produce kinematically similar effects. In the present case, the greatest improvement in playing abilities was obtained by the removal of the deep flexor connections, including the cleavage of the lumbrical origins, and the lumbrical interconnections. This does not mean that the restrictions caused by the juncturae in the extensors would be unimportant. If the flexor tendons would have been cleared first, the final benefit of surgery may have been obtained only after the resection of the juncturae. Therefore, in the analysis of a hand problem, all limitations on movement must be considered. From this it can be concluded that the well-known weakness in the fourth finger of the pianist does not have a single anatomical cause, but results from the combined effects of interconnections between the extensor tendons, superficial flexor tendons (FDS₄ and FDS₅), deep flexor tendons, co-activations of the muscle bellies, and possibly anomalous lumbricals. Apart from the effects of these connections on movement kinematics, the juncturae will transfer force to other extensors which must be balanced by excess flexor forces; the flexor connections will transfer force to other flexors which must be balanced by excess extensor forces; and anomalous lumbricals may introduce further couplings of motor forces and weaknesses in the extensor apparatus (Leijnse^c, 1996). As such, a situations can be imagined in which no independent movements are executable except by the forceful stretching of least some of the connections, which with daily repetition may lead to clinical complaints.

Results of the case with respect to the original coordination problems

Apart from the mentioned negative sequellae of the thumb, the results of the clearance of the connections have been entirely beneficial. The feeling of "stiffness" in the hands has completely disappeared. The hands greatly increased in "user friendliness", as a result of improved grip function and manipulative capabilities. Fast typing for long periods of time became feasible, even pleasant. The violin playing was abandoned, primordially because the thumb weakness in the right hand prevented the relaxed manipulation of the violin bow for more than an hour (the thumb is the pivot in the gripping of the bow). Nevertheless, even without this complaint, the severe co-activation of the FDP₅ with the FDP₄ in the left hand could still have been problematic. When the fourth finger plays a note, its active deep flexor pulls the fifth finger with it. The fifth finger's extensors must balance this flexion force, which results in a sensible stiffening of the ulnar side of the hand. In piano playing, finger mobility and coordination improved greatly, but the co-activations in the deep flexors prevent the full implementation of these improvements in the technique.

A focal dystonia on laboratory scale

The original complaints of the case never involved true focal dystonia symptoms, such as fingers "cramping" into flexion, although accurate finger control was impaired and worsening at the time when violin playing was abandoned. Lately, however, I have been able to witness in my own hands true focal dystonia symptoms, in circumstances which support the hypothesis of Leijnse^c (1996). About a year ago I had to process a great many data in a spreadsheet, in which I habitually use the keyboard instead of the mouse to position the cursor. This results in tapping the cursor keys with frantic speed for hours on end. After some days I developed pain in the interossei of the ulnar three fingers of the right hand, which controls the cursor keys, but since the work needed finishing I continued until I could literally feel the onset of a flexion cramp in the fourth finger. Put as accurately as possible, there was a distinct tension radially at the extensor side of the PIP joint, i.e. in the radial slip of the extensor aponeurosis, while it felt as if the distal joints had to be extended against an "elastic" force too great to overcome. In the model study of Leijnse^c (1996), it was indicated that such cramp should be caused by an above normal loading of the extensor or intrinsics, leading to their functional degeneration and a subsequent inability to balance normal flexor forces, resulting in the compulsory flexing of fingers. These excess loads in the extensors or intrinsics can result from the following causes: (i) the stretching of intertendinous connections, e.g. between the flexors, in the typing movements; (ii) co-active force transfers, e.g. between the flexors, ; (iii) increased viscous gliding between tendons and their environment; (iv) movements in which the interossei are especially active, such as movements with zero displacements of the flexors. Cause (i) could be excluded, as no connections remained. The co-activations (cause (ii)) shown in fig. 5 43R, and 45R are certainly an aggravating factor, but can hardly be the only cause as the symptoms were most outspoken in the fourth finger, which was most intensely used (the cursor is statistically positioned from the left to the right on the screen; the corresponding cursor key is controlled by the fourth finger). If co-activation would be causal, it would likely affect the adjacent fingers. In considering cause (iii), I found the gliding of the flexor tendons sensibly restricted at their end ranges, which can be assumed symptomatic for a generally increased gliding viscosity, and I vigorously exercised them for a few days, while reducing the typing load. This resulted in the complete disappearance of the symptoms. On one or two occasions since, similar interosseus pain has occurred, which responded to the same treatment. From these results the cause of the focal dystonia symptoms can be hypothetically reconstructed. Although the flexor tendons are fully mobilised, the internal scars caused by the repeated surgery in the carpal tunnel remain alive even after six or more years, and will increase the "viscosity" of the flexor tendon gliding in the carpal tunnel when the hands are not regularly exercised. However, if all goes well, one tends to forget these exercises. Such increased flexor viscosity results in an increased load of the muscles of the extensor assembly when the finger is lifted and the flexor tendons are pulled distalwards, while these load increases should also increase with movement speed. To decrease these viscous power losses, the body subconsciously tends to minimize the displacements of the flexors, so that the typing movements evolve into movements with very small displacements of the flexors. In such movements, the downstroke of the keystroke is powered by almost exclusively the interossei, which expend in this movement a high power per

Total clearance of intertendinous connections

volume because of their short fibre length (Leijnse^o, 1996) (I could observe such movements at the keyboard). Therefore, the fast repetitive execution of such keystroke movements should strain especially the interossei in the downstroke, which should explain the pain in these muscle groups. It must be suspected that in these movements also the lumbrical was strained, since with difficulties in keeping the interphalangeal joints extended one would anticipate the involvement of both the interossei and the lumbrical.

CONCLUSIONS

A case study is reported of a violinist in whose both hands all intertendinous connections were removed between the tendons of the extrinsic muscle groups, i.e. the *M. extensor digitorum communis*, the *M. flexor digitorum superficialis*, and the *M. flexor digitorum profundus*. In addition, interconnected bi-tendinous lumbrical origins were successfully released from each other to allow greater relative FDP tendon displacements. The sequential sectioning of the intertendinous connections per muscle group gradually relieved the initial symptoms of dysfunction of the hand, and allowed to analyse the effect of the different intertendinous connections on hand function. It is concluded that these surgical procedures can be safely executed when some anatomic conditions are satisfied (e.g. regarding the position of the extensors at the MCP joints); that they effectively improve kinematic finger independence, but that in the musician this independence may be compromised by the co-activations of the muscle bellies; that malformed lumbricals may hamper virtuose playing movements; and that if surgery in the carpal tunnel is performed, the *retinaculum flexorum* must be handled carefully, since in the present case its repeated sectioning resulted in thumb weakness, which required a later reconstruction of the ligament.

ACKNOWLEDGEMENTS

The first author cordially thanks the second author for his excellent surgery and care, his friendship grown over the years, his financial support of the research project which ensued from this case, and the hospitality of his wife, Marguerite.

REFERENCES

- Amadio, P.C., Rusotti, G.M. (1990) Evaluation and treatment of hand and wrist disorders in musicians. *Hand Clinics* 6, 405-416.
- Austin, G.J., Leslie, B.M., Ruby, L.K. (1989) Variations of the flexor digitorum superficialis of the small finger. *Am. J. Hand Surg.* 14, 262-267.
- Baker, D.S., Gaul, J.S.Jr., Williams, V.K. and Graves M. (1981) The little finger superficialis - clinical investigations and functional shortcomings. *Am. J. Hand Surg.* 6, 374-378.
- Blair, W.F., and Omer, G.E. Jr. (1981) Anomalous insertion of the flexor pollicis longus. *Am. J. Hand Surg.* 5, 548-549.
- Brand, P.W. (1985) *Clinical mechanics of the hand.* pp. 194. The C.V. Mosby Company, St. Louis, USA.
- Cohen, L.G., Halett, M., Geller, B., Hochberg, F. (1989) Treatment of focal dystonias of the hand with botulinum injections. *J. Neurology, Neurosurgery, and Psychiatry* 52, 355-363.
- Fahrer, M. (1971) Considérations sur l'anatomie fonctionnelle du muscle fléchisseur commun profond des doigts. *Ann. Chir.* 25, 945-950.

Chapter VII

- Forbes, W.S. (1991) Liberating the ring finger. Editors note. *Medical Problems of Performing Artists*. March, 28-30.
- Fry^a, H.J.H. (1986) Overuse syndrome in musicians: prevention and management. *The Lancet*, sept 27, 728-731.
- Fry^b, H.J.H. (1986) Overuse syndrome in musicians 100 years ago - an historical review. *The Medical J. of Australia* 145, 620-624.
- Hochberg, F.H., Harris, S.U., Blattert, T.R. (1990) Occupational hand cramps: professional disorders of motor control. *Hand Clinics* 6, 417-428.
- Kaplan, E.B. (1965) *Functional and surgical anatomy of the hand* (2nd Edn). pp. 99-100. Pitman Medical Publishing, London.
- Leijnse, J.N.A.L., Bonte, J.E., Landsmeer, J.M.F., Kalker, J.J., van der Meulen, J.C., Snijders, C.J. (1992) Biomechanics of the finger with anatomical restrictions - the significance for the exercising hand of the musician. *J.Biomechanics* 25, 1253-1264.
- Leijnse, J.N.A.L., Snijders, C.J., Landsmeer, J.M.F., Bonte, J.E., van der Meulen, J.C., Sonneveld, G.J., Hovius, S.E.R. (1993), The hand of the musician - the biomechanics of the bidigital finger system with anatomical restrictions. *J. Biomechanics* 26, 1169-1179.
- Leijnse^a, J.N.A.L. (1996) Measuring anatomical interconnections in the deep flexors of the musician's hand: theoretical analysis, clinical examples. Submitted *J. Biomechanics*, aug. 1995.
- Leijnse^b, J.N.A.L. (1996) Measuring anatomical interconnections in the deep flexor of the musicians' hand - device and systematic measuring errors. Accepted *J. Biomechanics*, oct. 1995.
- Leijnse^c, J.N.A.L. (1996) Anatomical factors predisposing to focal dystonia in the musician's hand - principles, theoretical examples, clinical significance. Resubmitted to *J. Biomech*, 1995.
- Leijnse^d, J.N.A.L. (1996) A generic model of the anatomic variability in the M. flexor digitorum profundus, M. flexor pollicis longus and MM. Lumbricales complex - the significance for the hand of the musician. Submitted to *Anatomical Record*, 1995.
- Leijnse, J.N.A.L., Walbeehm, E.T., Sonneveld, G.J., Hovius S.E.R. (1996) Anatomical interconnections within the flexor digitorum profundus - the significance for the hand of the musician. Submitted to the *Anatomical Record*.
- Leijnse^b, J.N.A.L., Walbeehm, E.T., Sonneveld, G.J., Hovius, S.E.R. (1996) Intertendinous connections between the deep flexor tendons formed by the synovial sheaths in the carpal tunnel. Submitted anatomical record 1995.
- Lockwood, A.H. (1989) Medical problems in musicians. *The New England J. Medicine* 320, 221-227.
- Lombardi, R.M., Wood, M.B., Linscheid, R.L. (1988) Symptomatic restrictive thumb-index finger flexor tenosynovitis: incidence of musculotendinous anomalies and results of treatment. *J. Hand Surg.* 13A, 337-340.
- Markison, R.E. (1990) Treatment of musical hands: redesign of the interface. *Hand Clinics* 6, 525-544.
- McGregor, I.A., and Glover, L. (1988) The E-flat hand. *Am. J. Hand Surg.* 13A, 692-693
- Perkins, R.E., and Hast, M.H. (1993) Common variations in muscles and tendons of the human hand. *Clinical Anatomy* 6, 226-231.
- Stern, P.J. (1990) Tendinitis, overuse syndromes, and tendon injuries. *Hand Clinics* 6, 467-476.
- von Schroeder, H.P., Botte, M.J., Gellman, H. (1990) Anatomy of the juncturae tendinum in the hand. *Am. J. Hand Surg* 15, 595-602.
- Zancolli, E. (1968) *Structural and dynamic bases of hand surgery*. pp. 1-9. Pitman Medical Publishing Co.,

FIGURES

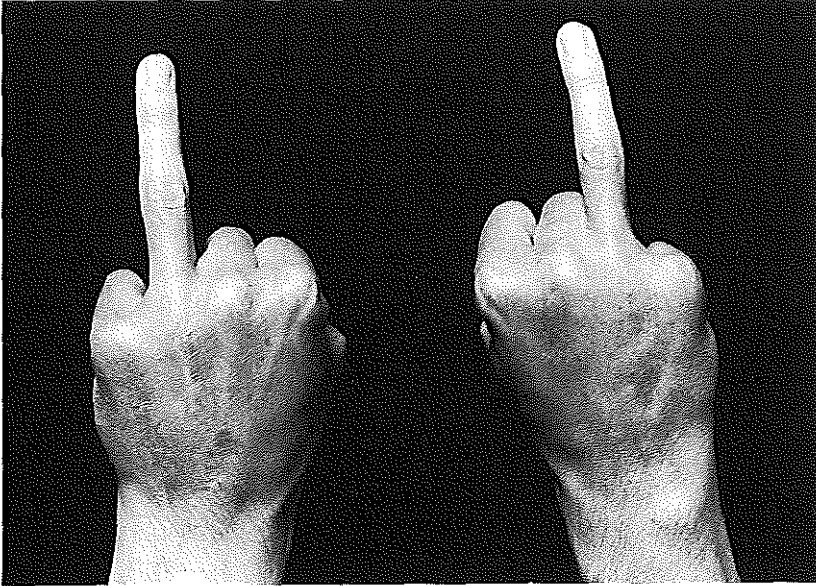


Figure 1 Post-operative active independent extension range of the fourth fingers in both hands. The third and fifth fingers are almost maximally flexed, the fourth fingers are almost maximally extended. The maximal passive extension range is not much larger than in the picture.

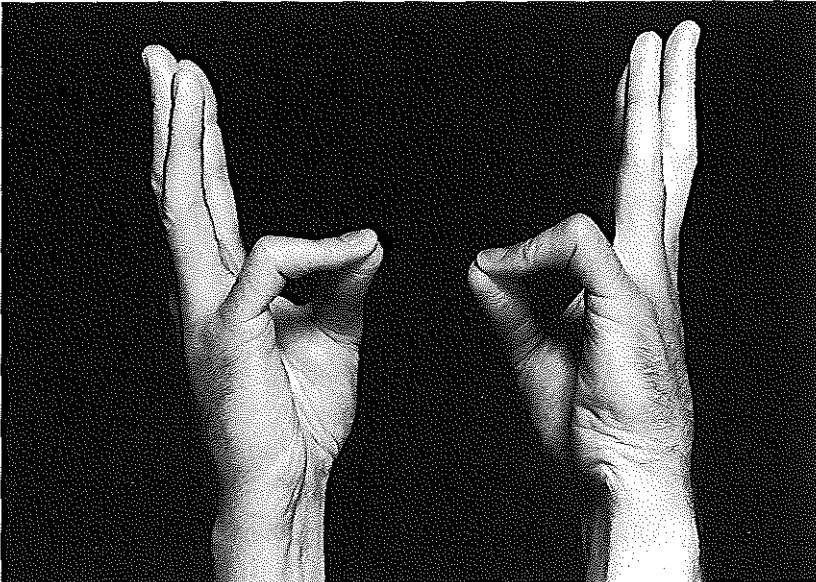


Figure 2 Post-operative range of extension of the fourth fingers with the fifth fingers flexed with active FDS, after removal of the FDS₄-FDS₅ connections. Pre-operatively, the fourth fingers could not be extended further than the fifth fingers.

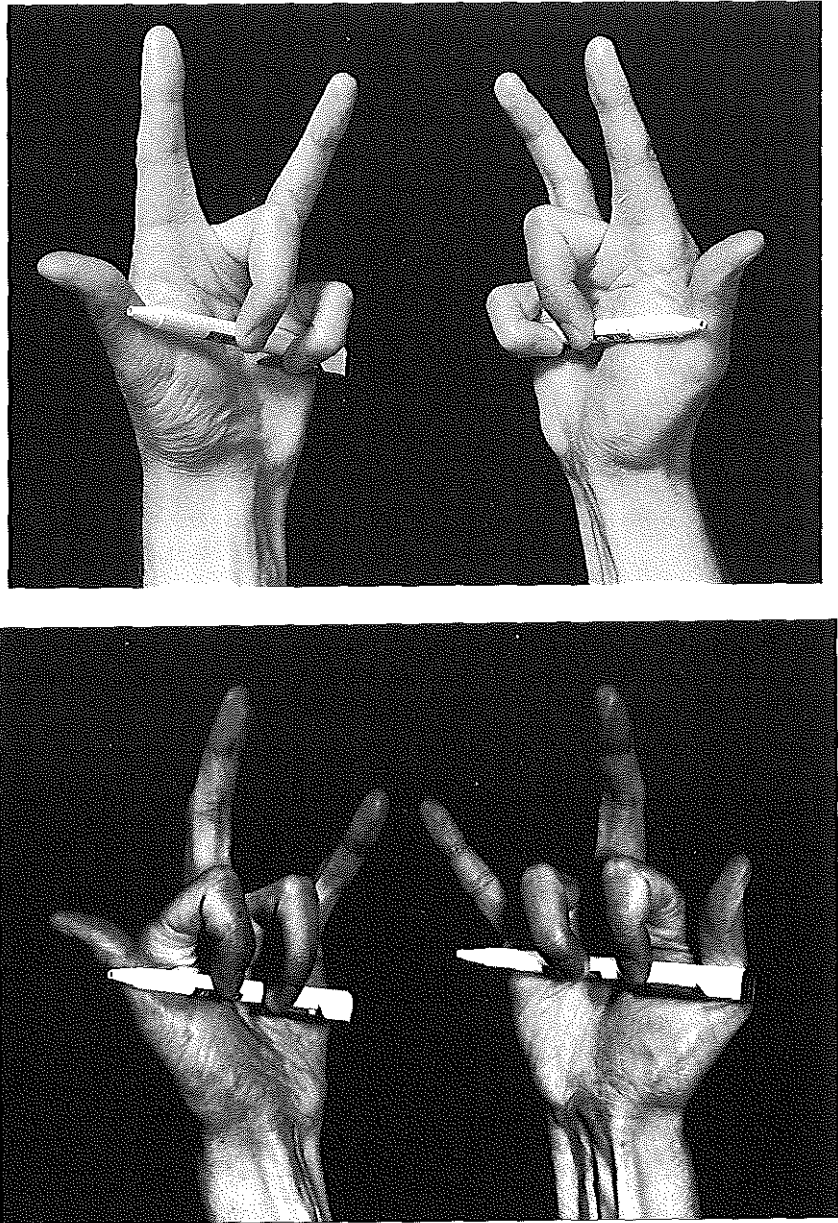


Figure 3 a,b Post-operative active independent flexion ranges of different fingers after the clearance of the passive connections in the FDS and FDP, the cleavage of the bi-tendinous origins of the lumbricals, and the removal of the connective fascia between the lumbrical muscles in the left hand. The maximal ranges of finger independence physiologically allowed by the joint rotations can be actively reached. The pencils are forcefully pressed, which can be seen by the white discoloration of the finger pads at the points of contact. The flexed DIP joints guarantee active FDP.

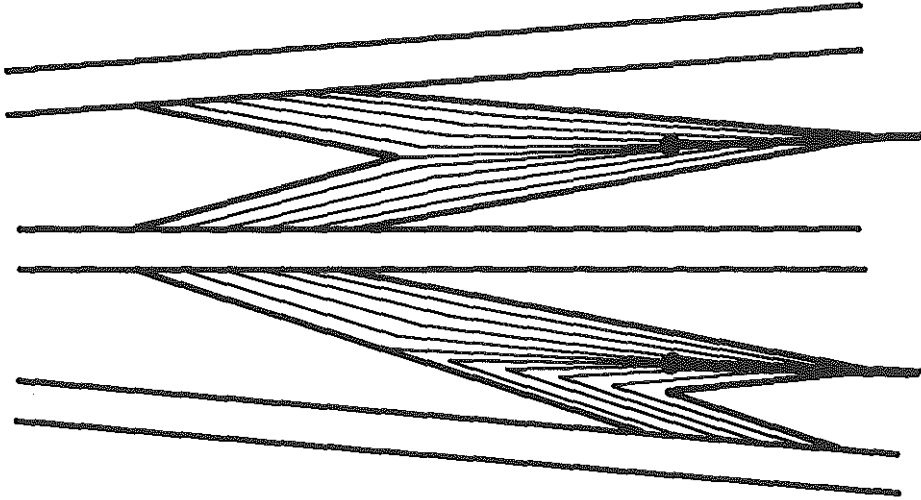


Figure 4 FDP tendon displacements when the bi-tendinous lumbrical origins are independent for about half the lumbrical muscle fibre length. The black dot indicates the beginning of the end tendon. Notice that at maximal opposite displacement of the tendons of origin the muscle fibres in the distally displaced head of origin are likely to be active insufficient.

Figure 5 (see next page) Post operative force transfers between the deep flexor tendons. 5.a: left hand, 5.b: right hand. For measurement procedures and device, see Leijnse^{a,b}, 1996. Two fingers are measured at the same time. Upper half of the graphs: forces of load cells at the finger tips. Lower half of graphs: PIP angles, which quantify the relative displacements of the deep flexor tendons. All other joints are fixed in correspondingly identical positions. Numbering: e.g. 23R: first digit: active deep flexor, in this case of the index (2). Second digit: inactive deep flexor, in this case of the medius (3). The measurements show to what degree the deep flexor tendon of the inactive motor is pulled by the active deep flexor, as a function of their relative contraction length.

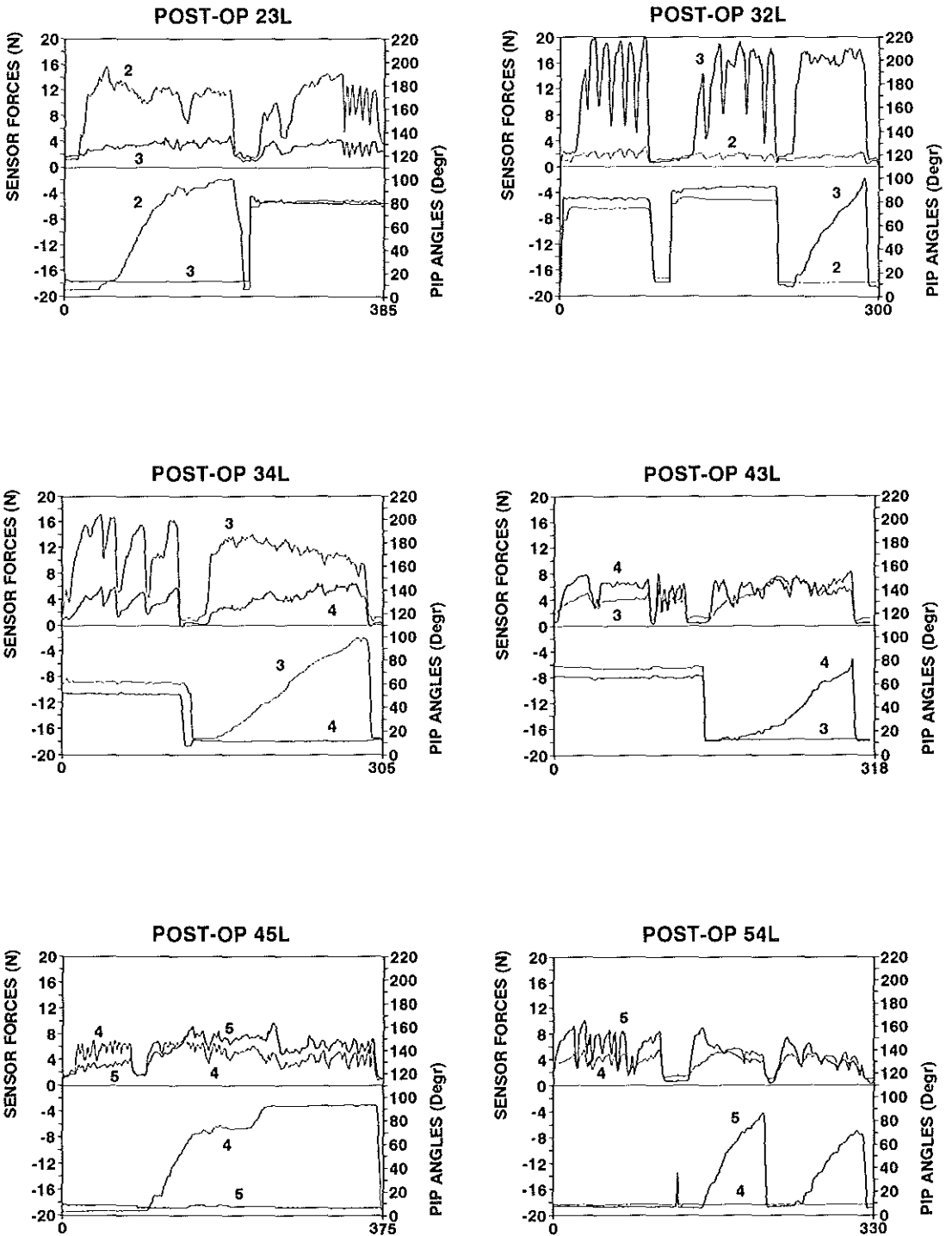


Figure 5 a Force transfers between the deep flexors of the left hand.

Total clearance of intertendinous connections

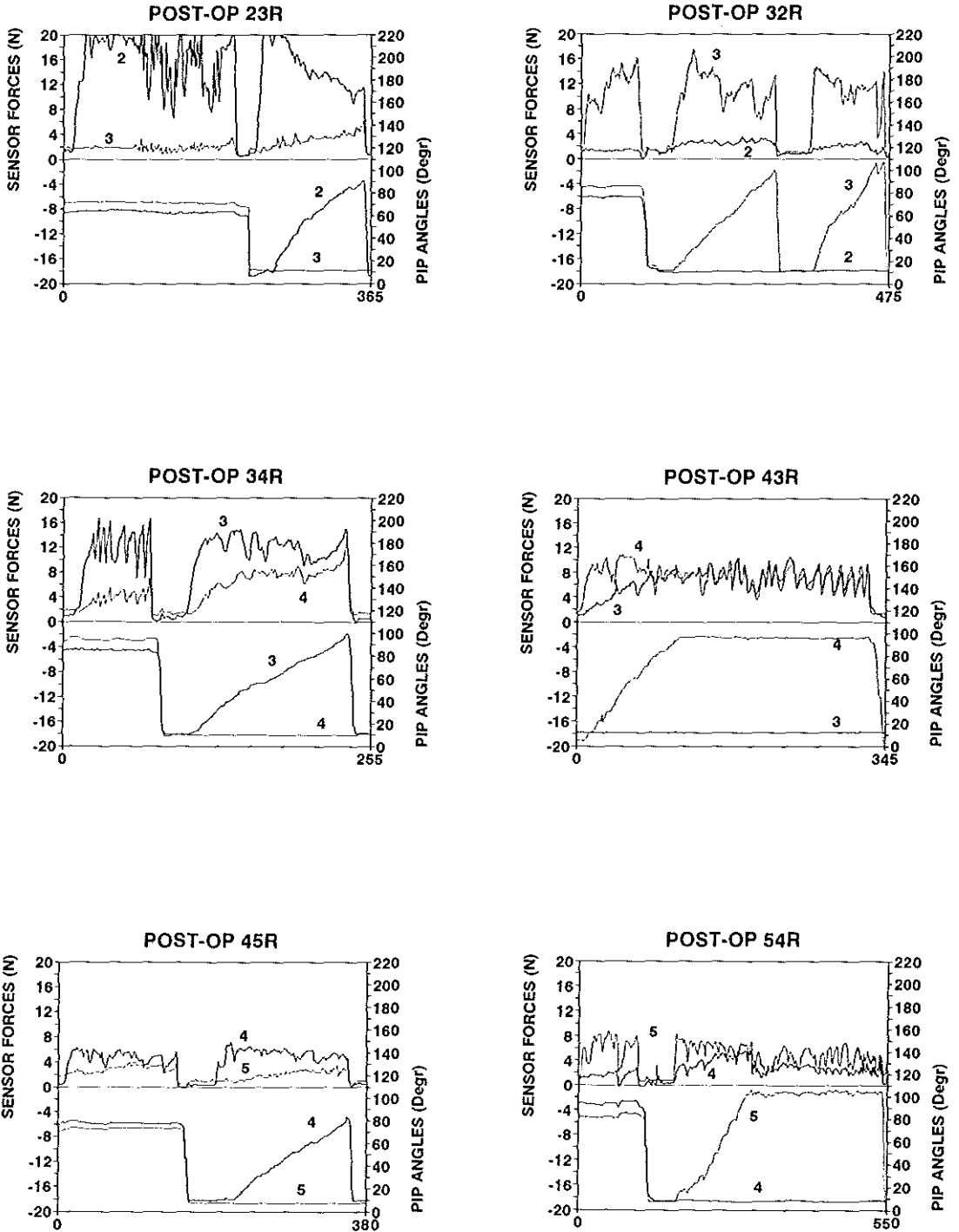


Figure 5 b Force transfers between the deep flexors of the right hand.

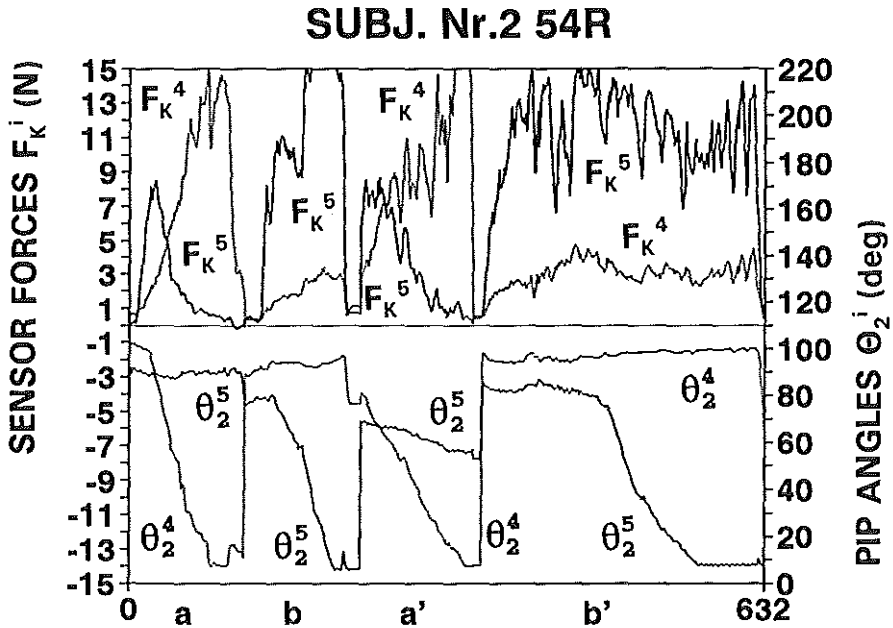


Figure 6 Example of force transfers with strongly interconnected FDP tendons. Passive connections show up in the tests (a) and (a'). The little finger deep flexor is active. Both little and ring finger are in flexed position. As the ring finger is extended, the passive connections between the deep flexor tendons get tautened, and all force from the little finger deep flexor (F_K^5) is transferred to the deep flexor tendon of the ring finger (F_K^4). The passive pre-operative force transfers between the FDP₃, FDP₄, FDP₅ in both hands of the case-study were of equal stiffness, if not stronger, while the relative displacements between the FDP₂ and FDP₃ tendons were also very limited. The tests (b) and (b') are auto-coactivation tests, explained in Leijnse* (1996).

Figure 7 (see next page) Picture of bi-tendinous lumbrical origins. The second and third lumbrical have clearly delineated radial and ulnar origins, from which the interconnecting synovial membranes have been resected. The connections between the tendons have been preserved. The fourth lumbrical has no clearly delineated radial and ulnar origins. 2: FDP₂, 5: FDP₅.

Figure 8 (see next page) Picture of bi-tendinous lumbrical origins. Although strongly interconnected by synovial membranes, of which some layers are removed, in all lumbricals the ulnar and radial heads can be clearly distinguished, even in LU₄ (little finger), this in contrast to LU₄ in fig.7. Also are visible the remains of nerves and vessels entering the lumbrical muscle bodies at the middle.

Total clearance of intertendinous connections

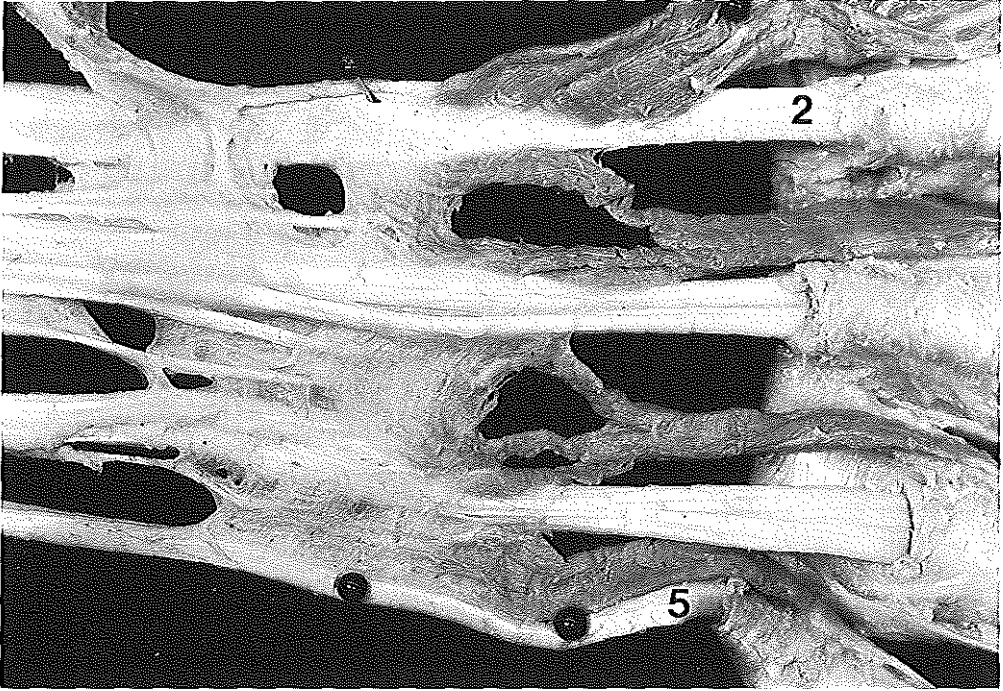


Figure 7

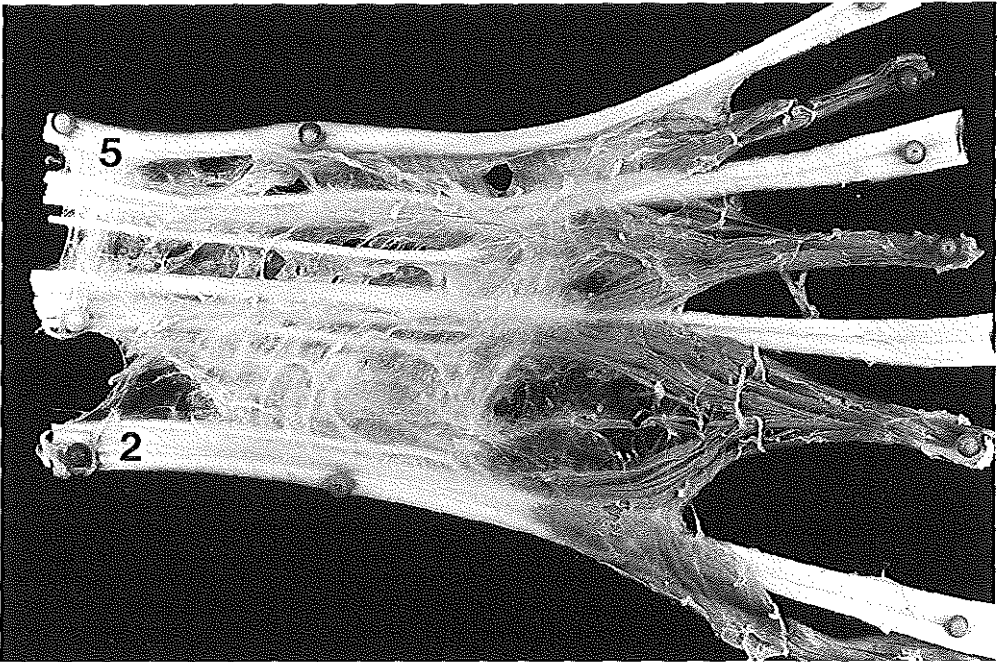


Figure 8

CHAPTER VIII

SUMMARY AND CONCLUSIONS

SAMENVATTING EN CONCLUSIES

SUMMARY AND CONCLUSIONS

Biomechanics of finger exercises with anatomical constraints

This work investigated the interdependencies between the muscles of different fingers as causes of problems in the musician's hand. These problems may involve the instrumental technique, but also clinical complaints. A typical example of the latter is focal dystonia, which is the dysfunction of specific muscle groups in specific playing movements. The view defended is that these complaints arise due to chronic overload of the affected muscles, and that these excess loads may be caused by anatomic limitations in the hand, or co-activation of muscles to different fingers. Important anatomic limitations are the restrictions of the relative tendon displacements by frequent and individually variable anatomical intertendinous connections. The following arguments are proposed.

i) First, in an anatomic section (Chapter VI), it is demonstrated that large differences exist in the individual anatomic independence of important finger motors, such as the *M. flexor digitorum profundus* (FDP) and *Mm. lumbricales* (the *M. extensor digitorum* and *M. flexor digitorum superficialis* (FDS) have been well documented in the literature). These differences are illustrated by dissection examples, and models are proposed to describe the systematic nature of these phenomena.

ii) A device was designed to measure *in vivo* the effects of the anatomic interconnections in the FDP (Chapters III). The results demonstrate the interindividual differences in the functioning of this muscle group and, by inference, of all interconnected muscle groups. These results concur with those obtained by dissection.

iii) Implicit in this thesis is that complaints, such as focal dystonia, occur only after the hand has exhausted all means to satisfy the instrumental demands with less stressful movements. Hereby, a subconscious tendency to minimize load can be assumed, while conscious learning will of course greatly influence the outcome of these processes. To avoid excess muscle loading, the subject, either consciously or subconsciously, makes use of the indeterminates which exist in the hand-instrument system. Therefore, the analysis of hand problems in musicians methodologically starts with the study of these indeterminates, which include the systematic indeterminates in motor function of the fingers or hand, and the kinematic freedom to determine alternative playing movements. This kinematic freedom is determined by the geometry and playing requirements of the instrument, and the movements anatomically feasible in the hand. Anatomic intertendinous connections limit these movements. This is investigated in Chapter I in a pianistic setting. Chapter I.i considers a single finger with tendons fixed to the environment (tenodised); Chapter I.ii investigates a bidigital system with interdigitally connected tendons. Both studies show that intertendinous connections, even when inextensible and of zero length, do not completely exclude movements. However, they drastically reduce the feasible finger trajectories and, by the limitation of this choice, severely diminish the exercisability of the hand. Moreover, the feasible movements may be inefficient with respect to the instrumental demands (Chapter IV).

iv) Chapter II addresses the systematic indeterminates in muscle function in the unconnected normal finger. These indeterminates are due to the mutual substitutability of the

Summary and conclusions

superficial and deep flexors, and of the interossei and lumbrical (intrinsic). The intrinsic indeterminates are kinematically studied in a two-dimensional model in Chapter I.iii, and in Chapter II.iii in a force model with bi-axial MCP joint. In the latter model, which contains all structural degrees of freedom of the finger, the interossei may completely substitute the lumbrical, but not inversely. This correlates with the fact that the lumbrical escapes voluntary control. In contrast, the finger flexors are both individually controllable. This results in the possibility of using one flexor when the other flexor is anatomically too strongly interconnected (disconnecting movements, Chapters I.ii and IV). However, the substitutability of the flexors is incomplete. The sole use of the superficial flexor leaves the DIP uncontrolled, although protected from hyperextension by the volar plate. The sole use of the deep flexor leaves the PIP weak in the loaded finger. In instrumental playing, the free phases of finger movements are important, as they serve to position the fingers for the loaded phases. The flexor substitutability then raises the question which flexor is most efficient in unloaded finger control, apart from the effect on the DIP joint. This is investigated in Chapter II.ii. It is demonstrated that the finger presents two specific anatomical constructions, the chiasma tendinum and the PIP-DIP coupling mechanism, which make it better controllable by the FP and by the FS. To properly present this proposition, an introduction to the controllability of the loaded and unloaded bi-articular chain is provided in Chapter II.i.

v) In addition to the kinematics allowed by the anatomic connections, the stresses they cause in the finger motors must also be known, if only qualitatively. In Chapter II.iii a muscle stress model of the static unloaded finger is presented, to be used for further analysis.

vi) In Chapter IV the general effects on muscle loading of the stretching of connections or co-activation of muscle bellies are summarised. These conclusions are illustrated by an example of a pianist's hand with a long thumb flexor anatomically interconnected with the deep index flexor. This example should provide a global picture of the phenomena to which anatomic constraints may give rise. First, the muscle stresses resulting from the straightforward stretching of the connections are calculated, from the model of Chapter II.iii. Second, basic kinematic properties and muscle stresses in movements which avoid the stretching of connections are discussed. Third, the possible mutual aggravation of simultaneous constraints is demonstrated. Fourth, compensatory movements are discussed. These may be necessitated by dynamic or kinematic impairments. In the first case the feasible finger movements are inefficient, e.g. lacking in force or speed; in the second case they are incompatible with the geometry of the instrument. The general view presented is that complaints are unavoidable when the anatomic possibilities of the hand exclude satisfactory instrumental movements with sufficiently low muscle stress and energy expenditure, in concurrence with a sufficiently severe exercise load. This leads to the clear options for treatment discussed in Chapter IV.

Structural analysis of anatomical variability

The aim of the anatomy section (Chapters V and VI) is firstly to supplement established knowledge of anatomic variations as relevant to the musician. However, an underlying aim is to investigate the possibility of surgical improvement of finger independence. To this end a

Chapter VIII

morphological understanding of anatomic variability is useful. Therefore, in the following a maximal effort is made to determine, rather than statistically describe, anatomic variability. This approach may be called "generic anatomy", as it considers the individual anatomy as the value of a parametric model, i.e. the result of the variations of a limited number of elementary anatomic structures and a set of morphological principles which describes their mutual interference. These elementary anatomic components, and their rules of interference are the true object of these studies.

i) In Chapter V.i, a simple muscle model is proposed which addresses a most basic question: how to attach a muscular apparatus to a skeleton with limited surface. This model demonstrates the structural importance of aponeurosis of origin, and provides a methodological background for the subsequent models. In Chapter V.ii, this model is further expanded into a systematic description of the anatomic variability in the region of the human elbow, as caused by the perforations of structurally present aponeurosis of origin by nerves or vessels. Although this paper does not specifically relate to musician's problems, it is included to demonstrate the value of the method of approach, and to familiarise the reader with the anatomic structure of the human forearm. Moreover, it may clarify the nature of clinical problems, such as nerve compression, which also occurs in musicians.

ii) In Chapter VI.i, a general overview is presented of the systematic anatomic interdependencies in the deep flexor group, including the long thumb flexor. Anatomic causes of co-activation of muscle bellies are motivated, and the synovial membranes in the carpal tunnel are shown to be the main causes of anatomic intertendinous connections. Further, the large variability in the origins and insertions of the lumbricals is discussed.

iii) Chapter VI.ii analyses the synovial sheaths in the carpal tunnel as systematic causes of intertendinous connections, and correlates their affinity to interconnect tendons to the degree of "fibrousness" (as opposed to "smoothness" and "compactness") of these tendons.

iv) Chapter VI.iii presents a generic model of the anatomical variations in the deep flexor-lumbrical complex, including the long thumb flexor. The flexor group is modelled as consisting of two elementary contractile elements, a monogastric for the deep flexor and FPL, and a digastric for the lumbrical, which are distributed along the origins of the FDP and FPL. The individual variations then correspond to possible distributions of these elementary contractile elements over the FDP, FPL and lumbrical end tendons. The model allows to generate the variants in the literature, and in our own dissections. The model also outlines the systematic problems with the surgical clearance of the connections between the deep flexors.

Clinical application: a case study

To illustrate the above results, in Chapter VII a case study is presented of an overuse patient in which all intertendinous connections were surgically removed in both hands. The post-operative force transfer characteristic of the deep flexors as measured by the device presented in Chapter III, and the outcome with respect to instrumental playing and general hand performance are discussed. The results support the biomechanical and anatomical analyses, but also illustrate the limitations on the benefit of such surgery.

CONCLUSIONS

Based on the results of this work, it can be concluded that intertendinous connections or co-active force transfers may severely hamper hand function in the musician's hand. They may result in finger coordination difficulties in playing, such as: difficulties in playing fast and regularly, e.g. thrills, scales, etc., as the trajectories of fingers become jerky by their mutual interference; the need for extended studying before a satisfactory result is achieved; the need for compensatory movements. Moreover, the presence of connections may increase focal load in hand muscles during playing, which can lead to clinical problems. Intertendinous connections can be surgically removed, but co-activations of muscle bellies generally not. Success of surgical clearance of connections will therefore depend on the level of the co-activations, and the required tasks. Conservative therapy aims at removing these focal excess loads by changes in technique or instrument, and its success will depend on the degree to which the hand-instrument interface can be adapted to the limited anatomic possibilities of the hand.

SAMENVATTING EN CONCLUSIES

Voorliggend werk onderzoekt anatomische afhankelijkheden tussen de spieren en pezen van de vingers als oorzaken van handproblemen bij musici. Deze handproblemen variëren van problemen met de instrumentele techniek tot klinische klachten. Een typisch voorbeeld van deze laatste is "focal dystonia", het fenomeen van oncontroleerbaarheid van specifieke spiergroepen bij specifieke bewegingen, terwijl deze spieren in normale taken normaal functioneren. De hypothese hier verdedigd is dat deze symptomen worden veroorzaakt door chronische overbelasting van de aangedane spieren, en dat deze belastingen het gevolg kunnen zijn van anatomische beperkingen in het bewegingsapparaat van de hand. Belangrijke anatomische beperkingen zijn de in elke hand in min of meerdere mate aanwezige verbindingen tussen de pezen van aangrenzende vingers. De hypothese wordt onderbouwd met volgende argumenten.

i) Vooreerst wordt anatomisch aangetoond dat een grote individuele variatie bestaat in de onderlinge afhankelijkheid van de *M. flexor digitorum profundus* spieren (afhankelijkheden in de *M. extensor digitorum*, en in de *M. flexor digitorum superficialis* zijn gedocumenteerd in de literatuur). Deze individuele variatie wordt geïllustreerd door dissectieresultaten, en morphologische modellen worden voorgesteld ter verklaring (Hoofdstukken V en VI).

ii) Een meetinstrument werd ontworpen om de krachtoverdrachten tussen pezen van de *M. flexor digitorum profundus* in vivo te meten (Hoofdstuk III). De resultaten tonen de interindividuele verschillen in het functioneren van deze spiergroep duidelijk aan, dit in overeenstemming met de dissectie resultaten, en dienen als voorbeeld voor gelijkaardige verschijnselen in andere spiergroepen.

iii) In dit proefschrift wordt impliciet vooropgesteld dat klachten als focal dystonia pas ontstaan nadat de hand alle middelen heeft uitgeput om aan de instrumentale eisen te voldoen met minder belastende bewegingen. Hierbij kan redelijkerwijze worden ondersteld dat de hand, onafhankelijk van de wil, poogt de belastingen te minimaliseren, waarbij het bewust richten van dit proces het resultaat natuurlijk aanzienlijk kan beïnvloeden. Om belastingen te ontwijken wordt, bewust of onbewust, gebruik gemaakt van de onbepaaldheden in het hand-instrument systeem. Een onderzoek van handklachten begint daarom noodzakelijkerwijze met de analyse van deze onbepaaldheden. Deze omvatten o.a. de systematische onbepaaldheden in de werking van de hand zelf, en de kinematische vrijheid om alternatieve spelbewegingen te kiezen. De kinematische vrijheid wordt bepaald door de geometrie en speeleisen van het instrument, en door de anatomische bewegingsmogelijkheden van de hand. Anatomische verbindingen tussen spieren of pezen kunnen deze bewegingsmogelijkheden aanzienlijk beperken. Dit wordt gemodelleerd in Hoofdstuk I, voor een hand aan de piano. Hoofdstuk I.i beschouwt één enkele vinger met pezen onwrikbaar verbonden aan een vaste omgeving (tenodese); Hoofdstuk I.ii onderzoekt een tweevinger model met onrekbare verbindingen tussen pezen van de twee vingers onderling. Deze studies tonen aan dat dergelijke verbindingen, zelfs wanneer onreikbaar en van zero lengte (verkleefde pezen), vingerbewegingen niet volledig uitsluiten. Echter, zij verminderen de mogelijke bewegingen drastisch, en door de beperking van deze bewegingskeuze de oefenbaarheid van de hand. Daarenboven zijn de nog mogelijke bewegingen niet noodzakelijk geschikt voor het

bespelen van het instrument.

iv) In Hoofdstuk II worden de systematische onbepaaldheden van de vingerspierfunctie in de normale, onbepaalde vinger zelf geanalyseerd. Deze onbepaaldheden bestaan uit de wederkerige substitueerbaarheid van de *M. flexor digitorum profundus* (FDP) en de *M. flexor digitorum superficialis* (FDS), en van de *Mm. interossei* en de *Mm. lumbricales* (de intrinsieke handspiers). De intrinsieke onbepaaldheden worden onderzocht in Hoofdstuk I.iii in een twee-dimensionaal kinematisch vingermodel, en in Hoofdstuk II.iii in een krachtmodel met een bi-axiaal MCP gewricht. Uit dit laatste model, dat alle controleerbare vrijheidsgraden van de vinger omvat, volgt dat de *interossei* de *lumbricalis* volledig kunnen substitueren, maar niet omgekeerd. Dit correleert met het feit dat de *lumbricalis-interosseus* substitutie niet willekeurig kan worden gecontroleerd. De FDP en FDS, daarentegen, zijn wel onafhankelijk controleerbaar. Dit schept de mogelijkheid om wanneer een van de flexoren anatomisch te zeer afhankelijk is, deze te desactiveren en de vinger te buigen met de resterende flexor. Dit wordt in de tekst "bewegingsontkoppeling" genoemd (disconnecting movements, Hoofdstukken I.ii en IV). De wederzijdse substitueerbaarheid van de FDP en FDS is functioneel echter niet volledig. In de vinger met inactive FDP blijft het distaal interphalangeaal (DIP) gewricht zonder controle, hoewel behoed voor hyperextensie door de palmaire gewrichtsligamenten. In de belaste vinger met inactive FDS zal het proximaal interphalangeaal (PIP) gewricht neigen naar hyperextensie. In het instrumentaal spel is de goede controleerbaarheid van onbelaste vingerbewegingen van groot belang. De wederkerige substitueerbaarheid van de FDP en FDS roept dan de vraag op welke flexor het meest geschikt is voor de controle van de onbelaste vinger, afgezien van hun invloed op het DIP gewricht. In Hoofdstuk II.ii wordt aangetoond dat de vinger twee specifieke anatomische constructies bevat, het chiasma tendinum en het PIP-DIP coördinatie mechanisme, die hem beter controleerbaar maken met de FDP dan met de FDS. De bewijsvoering maakt gebruik van concepten betreffende de controleerbaarheid van bi-articulare ketens, die worden geïntroduceerd in Hoofdstuk II.i.

v) Voor een diagnose moeten niet alleen de anatomisch mogelijke bewegingen gekend zijn, maar ook de belastingen welke zij in de spieren veroorzaken, zij het alleen in verhouding tot de andere spieren. Daartoe wordt in Hoofdstuk II.iii een krachtmodel van de statische, onbelaste vinger geïntroduceerd, waarvan de resultaten in Hoofdstuk IV worden toegepast.

vi) In Hoofdstuk IV worden de boven-normale belastingen veroorzaakt door verbindingen tussen pezen of co-activatie van spieren algemeen besproken, en verder uitgewerkt voor het partikuliere geval van een peesverbinding tussen de *M. flexor pollicis longus* en de *M. flexor digitorum profundus* van de wijsvinger bij een pianist. Hierbij worden aan de hand van eenvoudige voorbeelden onderscheiden aspecten belicht die bij de probleemanalyse van belang kunnen zijn. Deze zijn: (i) de spierbelastingen bij het uitrekken van de peesverbinding. (ii) De spierbelastingen bij bewegingen waarbij de peesverbinding niet wordt uitgerekt. (iii) De wederzijdse versterking van de effecten van meerdere gelijktijdig aanwezige beperkingen. (iv) De noodzaak van compensatoire bewegingen. Deze laatste kunnen nodig zijn om dynamische of kinematische beperkingen te compenseren. In het eerste geval zijn de mogelijke vingerbewegingen inefficiënt, bijvoorbeeld te zwak of te traag; in het tweede geval zijn de mogelijke vingerbewegingen onverenigbaar met de kinematische speelseisen van het instrument. Een

algemene hypothese betreffende het ontstaan van handklachten van musici wordt geformuleerd. Deze is dat handklachten onvermijdelijk zijn wanneer de instrumentale eisen in samenspel met de anatomische beperkingen in de hand alle spelbewegingen uitsluiten die aan de instrumentale eisen kunnen voldoen met voldoende lage spierbelastingen. Deze hypothese laat een systematische indeling van de therapeutische mogelijkheden toe. Hierbij wordt een therapie niet beschouwd als een "genezen", maar als het elimineren van de onverenigbaarheden in het hand-instrument systeem.

Structurele analyse van anatomische variabiliteit

Het doel van de anatomische studies (Hoofdstukken V en VI) is in de eerste plaats de huidige kennis betreffende anatomische variaties als van belang voor de musicus verder uit te breiden. De onderliggende vraag is in welke mate deze anatomische bewegingsbeperkingen chirurgisch kunnen worden verwijderd. Hierbij is een inzicht in de morfologische "aard" van deze beperkingen nuttig. Daarom is in de eerste plaats gepoogd deze structuren morfologisch te duiden, eerder dan hun voorkomen statistisch aan te tonen. De gekozen benadering kan worden beschreven als "generische anatomie", omdat ze de individuele anatomie beschouwt als de "waarde" van een geparametriseerd model, i.e. het resultaat van de individuele vorm van een beperkt aantal anatomische basisstructuren, en een geheel van morfologische regels die hun onderlinge verhouding bepalen. Deze anatomische basiskomponenten, en hun morfologische samenstellingsregels zijn het eigenlijke object van deze studies.

i) Ter methodologische inleiding wordt in Hoofdstuk V.i een eenvoudig spiermodel ontwikkeld als antwoord op de vraag: hoe een spierstelsel te konstrueren met als basis een skelet met veel te weinig oppervlak om alle spieren plaats te bieden. Dit model illustreert het structureel belang van oorsprongsaponeurosen voor spieren, en wordt verder gebruikt om een aantal vorm-eigenaardigheden van de spieren in de onderarm te duiden. In Hoofdstuk V.ii wordt dit model uitgewerkt tot een systematische beschrijving van de anatomische variabiliteit in de regio van de mediale epicondyl van de elleboog, als veroorzaakt door de perforaties van de oorsprongsaponeurosen van de elleboogspieren door vaten en zenuwen. Deze bijdragen hebben geen betrekking op musici, maar zijn toegevoegd om de lezer enigszins vertrouwd te maken met de aanpak van de verder behandelde morfologische vraagstukken, en met de globale anatomische structuur van de spieren van de onderarm. Verder illustreert Hoofdstuk V.ii hoe zenuwen of vaten anatomisch beklemd kunnen raken, een trauma dat ook bij musici voorkomt (pronator-syndroom).

ii) Hoofdstuk VI.i geeft een algemeen overzicht van de systematische anatomische afhankelijkheden in de *M. flexor digitorum profundus* (FDP), met inbegrip van de *M. flexor pollicis longus* (FPL). Aange-toond worden anatomische oorzaken van co-aktivatie van spieren, en verder dat de voornaamste systematische bewegingsbeperkende verbindingen tussen de flexorpezen worden gevormd door de synoviale schedes in de carpale tunnel. Ook de variabiliteit van de origo's en inserties van de *Mm. lumbricales* wordt geïllustreerd.

iii) Hoofdstuk VI.ii behandelt de volgende paradox: hoe kunnen de synoviale schedes verbindingen vormen tussen de diepe flexorpezen, waar hun specifieke taak is deze onafhankelijk van hun omgeving te laten glijden? Waarom zijn deze verbindingen dan ook niet aanwezig tussen

de pezen van de oppervlakkige flexoren? De hypothese wordt verdedigd dat de synoviale schedes verstrikt raken in de vezelachtige pezen van de diepe flexor, maar dat ze zonder problemen rond de gladde pezen van de oppervlakkige flexor heen kunnen groeien.

iv) In Hoofdstuk VI.iii wordt een generisch model voorgesteld dat de anatomische variaties in het *M. flexor digitorum profundus*-*M. flexor pollicis longus*-*Mm. lumbricales* complex beschrijft. Deze verzameling spieren wordt opgebouwd uit twee elementaire contractiele elementen, een monogastrisch element voor de FDP en FPL, en een digastrisch element voor de *Mm. lumbricales*. Deze elementjes worden in een geëigende proportie over de origo's van de diepe flexorgroep verdeeld. De anatomische variaties stemmen overeen met de mogelijke samenstellingen van de eindpeesjes en intermediaire peesjes van deze contractiele elementen tot de verschillende eindpezen van de FDP, FPL, en *lumbricalis* spieren. Het model laat toe alle beschreven en bij de dissecties gevonden varianten te genereren, en illustreert ook de principiële problemen met het chirurgisch verwijderen van de verbindingen tussen de diepe flexorpezen.

Klinische toepassingen: een case-study

In Hoofdstuk VII worden de bovengenoemde resultaten geïllustreerd aan de hand van een case-study van een overuse patiënt bij wie in beide handen alle verbindingen tussen alle vingerpezen werden verwijderd. De post-operatieve krachtoverdrachts-karakteristiek van de diepe flexoren werd gemeten met het meetapparaat van Hoofdstuk III, en de resultaten worden geëvalueerd met betrekking tot het instrumentale spel en de algemene handfunctie. Deze resultaten bevestigen de modelmatige conclusies, en illustreren ook de grenzen van de chirurgische verbeterbaarheid van de hand.

CONCLUSIES

Op basis van de resultaten van voorliggend werk kan worden geconcludeerd dat verbindingen tussen vingerpezen en co-aktivaties van spieren de handfunctie van de musicus in sterke mate nadelig kunnen beïnvloeden. Dit kan resulteren in vingercoördinatieproblemen, zoals: moeilijkheden met snelle en regelmatige uitvoering van trillers, toonladders, etc., doordat de vingertrajectories elkaar wederkerig storen, hetgeen resulteert in "jerkiness" (schokkerigheid) van de bewegingen; de noodzaak tot onevenredig lang oefenen voor een middelmatig resultaat; en de noodzaak tot compensatoire bewegingen. Verder kunnen anatomische beperkingen aanleiding geven tot sterk verhoogde spierbelastingen, welke kunnen resulteren in klinische klachten. Anatomische beperkingen tussen pezen kunnen chirurgisch worden verwijderd, maar spiercoactivaties in het algemeen niet. Deze laatste zullen daarom het best haalbare resultaat van het verwijderen van de peesverbindingen bepalen. Conservatieve therapie moet gericht zijn op het verminderen van het niveau van spierbelasting. Middelen daartoe zijn aanpassingen van de instrumentele techniek en/of van het instrument. Het resultaat wordt dan bepaald door de mate waarin de hand-instrument interface kan worden aangepast aan de anatomische mogelijkheden van de hand.

ACKNOWLEDGEMENTS

My first thanks are to my parents, and my brother and sisters, who supported me throughout three career attempts. Also, I am greatly indebted to my violin teacher, Andre Lazslo, a devoted and charismatic man who awakened in me a talent I ignored. Most sincere gratitude is due to my surgeon, Dr. J.E. Bonte. Over the years a friendship grew, and a great deal of the little I know of hand surgery is due to his kindness in answering my questions on this topic. Most sincere gratitude also goes to those, too many to enumerate, who supported me with their company and services over many long years. Especially remembered are Prof. J. Clarijs, and staff, of the Dept. of Anatomy of the Free University of Brussels, where I spent eight months preparing the reconstruction of my flexor retinacula. At the Erasmus University, Prof. J.C. van der Meulen, now retired head of the Dept. of Plastic and Reconstructive Surgery, was a driving force in establishing this project, and eventually managed to secure a proper research position, which was fundamental to the realisation of this work. Prof. Snijders, head of the Dept. of Biomedical Technology, where I have my desk, equally provided substantial financial and infrastructural support. Moreover, by his cheerful temperament and diplomatic talents many problems were easily resolved. During the past six years, Prof. Landsmeer, who stood with me throughout my application, has been a lucid opponent and a wise counselor. In this opposition Prof. J.J. Kalker, whose contributions are mentioned in the introduction, occasionally joined. Dr. C.W. Spoor close-read most of the papers with great determination; without his efforts the manuscript could hardly have been finished in time. At the anatomy department, Dr. Eric Walbeehm and Dr. Julia Zguricas, now themselves preparing their PhD, assisted extensively in dissections, and initiated many interesting discussions. Many thanks go to the custodians of the dissection theatre, C. Entius and J. Velkers, who tolerated the permanent storage of the dissection material in a corner of the dissection room for many months. There Dr. S.E.R. Hovius, now head of the Department of Plastic Surgery, was a regular visitor, who I thank for his stimulating questions. Dr. G.J. Sonneveld, who I thank for his collegiality, has turned a vision into reality by establishing a proper hand clinic for musicians. Prof. J. Voogd, head of the Dept. of Antomy, is thanked for his continuing support of the anatomic work. Prof. J.M.G. Kauer, of the Dept. of Anatomy in Nijmegen, is remembered for his hospitality, the discussion of the material, and the marvellous cross sections of wrists shown in Chapter VI.ii. Also in Nijmegen, Prof. R. Huiskes is thanked for his interest and personal advise. Further thanks are due to Drs. L. de Beukelaar, our manager, and Mrs. L. de Wit from the personnel's office, for their support. Equal appreciation goes to my colleges at the different departments, Cor Goedegebuur who beautifully built the mechanical demonstration models, the photographers E. Dalm and P. Smaal, for their advise and help, and our secretaries, Ria of the Dept. of Biomedical Technology, Edith of the Dept. of Anatomy, and Yvonne, Caroline, and others of the Dept. of Plastic Surgery. Last but not least, I thank the Erasmus University for accepting this PhD-thesis in exceptional conditions, in this decision reflecting the spirit in which it came into existence.

CURRICULUM VITAE

Joris Leijnse was born on October 27, 1956, in Aalst, Belgium. As a violin student he attended a special high school for musicians, the Lemmens Institute, Louvain (Belgium), where he graduated in 1974. The next two years he studied at the conservatory of Brussels with A. Gertler, but was forced to give up a violinistic career because of hand problems. From 1976 to 1978 he studied graphic arts in Ghent (Belgium). In 1978 he took a prep year of mathematics, and subsequently studied four years of Civil Engineering (applied mathematics) at the University of Louvain. He spent one year as a free researcher at the Dept. of Anatomy at the Free University of Brussels (VUB) (1989), and was in 1990 accepted as a researcher in the biomechanics of hands at the Dept. of Reconstructive and Plastic Surgery, and the Dept. of Biomechanical Physics and Technology, Erasmus University Rotterdam, where he has been working up to the present day.

